ISSN NO. : 2964-1802
VOLUME 29, 2025

HIMPUNAN AHLI TEKNIK TANAH INDONESIA (HATTI)
Indonesian Society for Geotechnical Engineering (ISGE)
Member Society of International Society for Soil Mechanics and Geotechnical Engineering (INA-ISSMGE)

Proceedings

29th Annual International Conference on Geotechnical Engineering

"Geotechnical Engineering for Sustainable Infrastructure: Driving Resilience and Innovation"

Jakarta, 10-12 November 2025

Supported by :

Proceedings

29th Annual International Conference on Geotechnical Engineering

Jakarta, 10-12 November 2025

Theme :

"Geotechnical Engineering for Sustainable Infrastructure: Driving Resilience and Innovation"

HIMPUNAN AHLI TEKNIK TANAH INDONESIA
INDONESIAN SOCIETY FOR GEOTECHNICAL ENGINEERING (ISGE)
GRAHA HATTI, JOR TB Simatupang, Jalan Asmin No. 45
Jakarta Timur 13750 – INDONESIA

Proceedings
29th Annual International Conference on Geotechnical Engineering
Jakarta, 10 - 12 November 2025

Editorial Team

Chief Editor : Dr. Fathiyah Hakim Sagitaningrum

Reviewer : Prof. Ir. Nurly Gofar, MSCE, Ph.D
Aswin Lim, Ph.D
Dayu Apoji, Ph.D
Dr. Fathin Andriati, ST., MT.
Dr. James Jatmiko Oetomo ST., MT., MSc.
Yuamar Immarazan Basarah, Ph.D
Dr. Eng. Lutfian R. Daryono
Dr. Ir. Budijanto Widjaja, MT.
Ir. Ignatius Tommy Pratama, ST., MSc.
Aflizal Arafianto, ST., MT.
Andreas Erdian Wijaya, ST., MT.
Lingga Ekaputra Lucky Suryajaya, ST., MT.

Editors : Yunan Halim, ST., MT.
Ir. Dandung S. Harninto, ST. MT.
Dwi Nandya, ST., MT.
Ariani Chitra Lestari, ST., MT.
Ir. Kirana Rongsadi, ST, MT.
Ir. Stefani Sugiarto, ST., MT.
Albert Johan, ST., MT.

HIMPUNAN AHLI TEKNIK TANAH INDONESIA
INDONESIAN SOCIETY FOR GEOTECHNICAL ENGINEERING (ISGE)
GRAHA HATTI, JOR TB Simatupang, Jalan Asmin No. 45
Jakarta Timur 13750 – INDONESIA

Proceedings *29th Annual International Conference on Geotechnical Engineering*
Jakarta, 10 - 12 November 2025

Theme :

"Geotechnical Engineering for Sustainable Infrastructure: Driving Resilience and Innovation"

ORGANIZING COMMITTEE

Penasehat	:	Prof. Ir. Widjojo Adi Prakoso, MSc, Ph.D
Steering Committee	:	Prof. Ir. Chaidir Anwar Makarim, MSCE, Ph.D Ir. Bigman M. Hutapea, MSc, Ph.D Prof. Ir. Masyhur Irsyam, MSE, Ph.D Dewan Penasehat
Chairman	:	Ir. Andi KS. Kartawiria, S.T., M.T.
Vice Chairman	:	Dr. Ir. Anthony Gunawan Dr. Ir. Pintor Tua Simatupang, MT
Secretary	:	Ir. Jefry Rory Paath, ST. MT Ir. Ali Iskandar, S.T., M.T.
Treasurer	:	Ir. Idrus M. Alatas. M.Sc. Ph.D Ir. Budiantari HL., M.Sc
Team Reviewer	:	Dr. Ir. Aksan Kawanda, ST. MT. Dr. Yustian Heri Suprapto, S.T., MSc Prof. Ir. Agus Setyo Muntohar, S.T., M.Eng.Sc., Ph.D. Prof. Ir. Teuku Faisal Fathani, S.T., M.T., Ph.D., IPU Prof. Dr. Ir. Tri Harianto, MSc Ir. Dr. Eng. Ardy Arsyad, S.T., M.Eng.Sc Prof. Ir. Nurly Gofar, MSCE, Ph.D Dr. Ir. Didiek Djarwadi, M.Sc Ir. Hendra Jitno, MASc, Ph.D Dr. Martin Wijaya Dr. James Jatmiko Oetomo S.T., M.T., M.Sc. Anthony Gunawan, Ph.D. Erly Bahsan, S.T., M.Kom. Dr. Yudhi Lastiasih, S.T., M.T. Dr. Ir. Nurindahsih Setionegoro, M.Sc

		Dr. Ir. Budijanto Widjaja, M.T. Dr. Heriansyah Putra, S.,T. M.T. Dr. Ir. Herwan Darmawan, S.,T. M.T. Dr. Luky Handoko, S.,T. M.T. Dr. Ir. Hendriyawan, S.T., M.T. Ir. Agus Himawan, ST. MT.
Editing	:	Yunan Halim, S.T., M.T. Stephen Gunawan Handoko, S.T., M.T. Dwi Nandya, S.T., M.T. Vinna Fransiska Chou, S.T., M.T. Tatag Yufitra Rus, S.T., M.Sc Muhammad Rifky Fakhrurozy, S.T., M.T. Ir. Reguel Mikhail, S.T., M.T.
Events	:	Dr. Ir. Aksan Kawanda, ST., MT. IPU Dr. Ir. Edwin L. Hendrikus, ST. MT. Dr. Yustian Heri Suprapto, ST. MT. Rara Dwi Noviarti, S.T., M.T Ir. Dolok H. Panjaitan, ST. Nugraha Seftian Jody, ST. Ir. Wahyuning Aila, ST, MSc. David Wibisono Setiabudi, ST., MT. Amalia Susanto, ST. MT. Serkandi, ST. Nurfaiz Rakhi Paramananda, ST. Richky Ardianto, ST. Pio Kefas, ST.
Sponsorship & equipment	:	Ir. Yasin Widodo, ST., MM. Ir. Marcello Djunaidy, ST, MT. Aditya Candra Y., ST. Fani Elmah Gari, ST. Achmad Faisal Amri, ST. Rizky Satria Putra, ST. MT. KM Abuhuroyroh. ST. MT.
Secretariat	:	Sugino, SE Budi Suryanto, ST. Sya'bani Wahyu Septiandi

Publisher : Himpunan Ahli Teknik Tanah Indonesia
(Indonesian Society for Geotechnical Engineering)

Address : Graha HATTI
JOR TB Simatupang, Jalan Asmin No. 45
RT.008 RW. 03 Susukan, Ciracas - Jakarta 13750
Telp. : 021 - 220900009
Email : sekretariat@hatti.or.id; hattipusat@yahoo.com
Website : http://www.hatti.or.id

ISSN No. : 2964-1802

Volume 29, 2025

FOREWORDS

The XXIX Annual International Conference on Geotechnical Engineering (PIT HATTI XXIX) was special because it coincides with the 50th anniversary of the founding of the Indonesian Society for Geotechnical Engineering (ISGE/HATTI). This event was organized by the National Board of the Indonesian Society for Geotechnical Engineering (ISGE/HATTI) in Jakarta on November 10–12, 2025. It is my great honor to return as the chairman of the committee.

The conference offers a valuable and expansive forum for the presentation of the most recent research as well as the discussion and sharing of ideas regarding research findings in geotechnical engineering. The success of this conference was reflected in the large number of participants involved, consisting of 9 keynote speakers, 38 speakers, and more than 800 participants. This proceeding is a compilation of the accepted papers and represents the vast and ever-growing knowledge in geotechnical field.

I would like to extend my gratitude to the organizing committee and to the sponsors, as without their support, PIT HATTI XXIX 2025 would not have been successfully organized. I sincerely hope that PIT HATTI XXIX 2025 will be a forum for excellent discussion that will put forward new ideas and promote collaborative research. We are sure that the proceedings will serve as an important research source of reference and knowledge, which will lead to not only scientific and engineering progress but also other new products and processes.

Jakarta, 10 November 2025

Ir. Andi KS Kartawiria, ST., MT
Chairman of the Committee

PRESIDENT OF ISGE ADDRESS

Assalamu'alaikum Wr. Wb. Salam Sejahtera bagi kita semua.

The Minister of Public Works, the Chairman of the Indonesian Academy of Science, Distinguished Keynote Speakers and Special Guests, Ladies and Gentlemen, on behalf of the National Board of Indonesian Society for Geotechnical Engineering (ISGE / HATTI), we would like to welcome you all to the XXIX Annual International Conference on Geotechnical Engineering (PIT HATTI XXIX).

The PIT HATTI XXIX is a special one, as we are celebrating the 50th Anniversary of ISGE / HATTI. We respect deeply our visionary founding fathers, as well as our dedicated past leaders, for their great commitment to ISGE / HATTI.

Dear Indonesian Society members, the theme of this conference is "Geotechnical Engineering for Sustainable Infrastructure: Driving Resilience and Innovation". We have a range of different topics from prominent geotechnical experts from Asia and Europe, as well as a number of technical paper contributors. We also have several interesting technical presentations from the geotechnical engineering companies.

We extend my sincere gratitude to all participants and all sponsors, particularly the Gold Sponsors : PT Geotekindo, PT Nittoc Construction Indonesia, PT Oriental Castle Group, PT Promisco Sinergi Indonesia, as well as the Silver Sponsors : Daehan – Menard, PT Bauer Pratama Indonesia, PT Oriental Castle Group, PT Keller Ground Indonesia, and PT Geoforce Indonesia.

We wish you a very enlightening and successful conference. Thank you very much.

Wassalamu'alaikum Wr. Wb.
Jakarta, 10 November 2025

Prof. Ir. Widjojo A. Prakoso, MSc., Ph.D
President of ISGE

TABLE OF CONTENTS

Editorial Team

Organizing Committee

Preface Committee Chairman …….. i

Message From President Of Indonesian Society For Geotechnical Engineering (ISGE) iii

Table of Contents v

Keynote Abstracts/Extended Abstracts :

ID	Keynote Speakers & Keynote Title	Page No.
2.	Ir. Hendra Jitno, MASc., Ph.D. - *Current Practice of Static and Seismic Stability of Embankment - A Critical Review*	1-4
3.	Dr. Shi Chao - Sparse Data-Enabled Underground Digital Twin for Infrastructure Development	5-8
4.	Prof. Ir. Indra Djati Sidi, M.Sc., Ph.D. - *Analisis Faktor Keamanan dan Reliabilitas dalam Rekayasa Geoteknik*	9-10
5.	Assoc. Prof. Dr. Suttisak Soralump - *Natural Vs Engineering Disaster-Risk Assessment in Geotechnical Perspective*	11-14
6.	Prof. Lyesse Laloui - *From Micro-Scale Mechanisms to Field Applications: Advancing Bio-Based Ground Improvement with MICP*	15-18
7.	Dr. Karsten Beckhaus - *The European Approach to standardize Geotechnical Works for Diaphragm Walls and Bored Piles*	19-20
8.	Prof. Dr.-Ing. habil. Christian Moormann - *Investigations into a dramatic collapse due to a diaphragm wall excavation - Consequences for quality assurance and risk management in ground engineering*	21-32
10.	Prof. Ir. Widjojo Adi Prakoso, MSc, Ph.D - *Do We Really Understand Our Deep Shear-Wave Velocity Profile? Case of Depok Campus of Universitas Indonesia*	33-34

Papers:

ID	Paper Title	Page No.
001	Comparison of Cast-in-Situ Diaphragm Wall for Deep Basements in Indonesia: Continuous Water Stop (CWS) System and Continuous System *(Juse Roejanto)*	35-42
002	Perubahan Nilai Kepadatan Relatif Tanah Pasir Akibat Variasi Percepatan Maksimum Gempa *(Muhammad Yunus)*	43-52
003	Evaluation of Toll Road Embankment Stability on Clay Soil Using 2 m Soil Replacement and Woven Geotextile *(Yani Putri Agustina)*	53-66
005	Design Review of Pile Cap Excavation Reinforcement System at the IC3 Interchange of the Patimban Access Toll Road Project, Indonesia *(Bobby Novialdi Saputra)*	67-80
006	Multi-Model Assessment of Anchor Pile Spacing Effects in Axial Load Testing: Mitigating Interaction-Induced Settlement Distortion *(Muhamad Fauzi Ahad)*	81-92
007	Water Retention Curve of Soil at Simpang Meo Region South Sumatra *(Nurly Gofar)*	93-94
008	Analysis of Seepage and Contaminant Transport to a Water Body Considering Waste Pile Distance and Impermeable Layer Presence *(Melisa Saferman)*	95-106
009	Determination of Bentonite's Flow Limit Using Cylinder Strength Test and Suspension Settling Model *(Budijanto Widjaja)*	107-120
010	Analysis and Design of a High-Risk Tiered Retaining Wall Using a Geosynthetic Reinforcement System *(Valdy Kosalim)*	121-122
011	Numerical analysis of rainfall-induced slope failure in Gumay Ulu, Lahat, South Sumatra *(Nurly Gofar)*	123-134
012	Stabilized Expansive Soils with High Alumina Cement at Longer Curing Time *(Arlyn Aristo Cikmit)*	135-148
013	Stabilization of Patimban Marine Soft Clay with Portland Composite Cement: The Effect of Initial Water Content Variations on Soil Bearing Strength *(Arlyn Aristo Cikmit)*	149-150
014	Stabilization of Patimban Marine Clay with Wide Range of Sand Content using Portland Composite Cement *(Arlyn Aristo Cikmit)*	151-164
015	Microbial Enzyme Extract Evaluation for Calcium Carbonate Biocementation: Implications for Ground Improvement *(Lutfian R Daryono)*	165-166

ID	Paper Title	Page No.
016	Use of CO_2 Nanobubble-Treated Alkaline Wastewater in Developing Low-Carbon Materials *(Sugeng Wahyudi)*	167-180
017	Influence of Underconsolidating Soil on Effective Stress Path in Deep Excavation Case *(Aswin Lim)*	181-182
018	An Overview of Different Types of TBM for the Construction of Subway Tunnels in Indonesia *(Simon Heru Prassetyo)*	183-184
021	Sub-Surface Movement Detection in a Tailings Storage Facility: Evaluating Inclinometer Real-Time Monitoring and Design Specification (Case Study: Martabe Gold Mine) *(Syavira Indah Utami)*	185-198
022	Comparative Analysis of Pile Driving Analyzer (PDA), Pile Driving Formula, and Standard Penetration Test (SPT) Data for Assessing the Reliability of Bearing Capacity Estimates in Pontianak Soft Soil *(Vivi Bachtiar)*	199-214
023	Utilization of Red Brick Waste for Soil Stabilization: Experimental Research on The Base Layer of the Jogja-Solo Toll Road *(Pradyta Galuh Oktafiani)*	215-228
025	Stabilization Behavior of Sepaku Clay Shale Using Bacillus Subtilis *(Yuswal Subhy)*	229-250
027	Comparative Site Classification Using Conventional Penetration Testing (SPT) and Microtremor Array Measurement (MAM): Case Study of Three Industrial Estates in Karawang, Indonesia *(Ayu Wijayanti Kurnia Dewi)*	251-266
028	Stability Assessment of Homogeneous Embankment Dam under Variable Drawdown Rates Using Unsaturated Soil Parameters *(Muhammad Adi Ibrahim)*	267-268
029	Mitigating Reclamation-Induced Settlement Using Rigid Inclusions: A Ground Improvement Case from Ahmad Yani Airport, Indonesia *(Ryan Rahmat Setiaji)*	269-282
030	Settlement Fitting of Soil Improvement on Toll Road Project in Northern Jakarta *(Muhammad Amhar Wajdi Yanreginata)*	283-294
031	Performance Evaluation of Freestanding Soldier Pile System for a 9-m Excavation in Clayshale Formation at IKN Using the Hardening Soil Model *(Ir. Muhammad Risyad Alditio, S.T.)*	295-304
033	Underwater Subsurface Imaging of the North Java Sea using Marine Resistivity Tomography *(Bagus Endar B. Nurhandoko)*	305-312
034	Adhesion Factor (α) of Drilled Piles in Clay Shale with Static and Dynamic Load (*Eddy Triyanto Sudjatmiko)*	313-314

ID	Paper Title	Page No.
035	Evaluasi Performa Penurunan Konsolidasi Jangka Panjang Dengan Metode CMC Pada Konstruksi Runway Studi Kasus Bandara Rendani *(Azliny Azreen)*	315-330
036	Development Distributed Acoustic Wave Sensing with Fiber Optics for Vibration and Structural Monitoring *(Bagus Endar B. Nurhandoko)*	331-338
037	The Effect of Fly Ash Addition on Clay Stabilization Using Clean Set Cement *(Efan Tifani)*	339-352
038	Ground Improvement of High-Organic Clay Using Sand Columns: Settlement and Stability Analysis *(Luthfi Amri Wicaksono)*	353-364
039	Interpretasi Bidang Gelincir Lereng Menggunakan Kombinasi Uji Geoteknik dan Geofisika *(Metta Devi Hartadi)*	365-374
040	Performance of Ground Improvement with Preloading and PVD on the Serang–Panimbang Toll Road: Analytical and Numerical Verification *(Agus Himawan)*	375-390
041	Characterization and Shear Strength Evaluation of Sensitive Volcanic Residual Soils in West Java *(Mirna Dwi Lestari S)*	391-392
042	Rasio Kecepatan Longsor Berdasarkan Data Gradient Modulus Young dan Strain pada Uji Ucs untuk Setting Alarm pada Slope Stability Radar *(Alam Tronics)*	393-404
043	Recommendation of Ground Surface Design-Spectra Through Site-Specific Response Analysis (SSRA) Considering Effect of Various Depth of Bedrock, Case Study of Jakarta *(Det Komerdevi)*	405-414
045	Penggunaan GI-Tube Berbahan Non Woven Dua Lapis Produksi Dalam Negeri untuk Tanggul Laut Studi Kasus Proyek Jalan Tol Semarang–Demak, Jawa Tengah *(Puji Kristianingsih)*	415-422
046	Implementation of Sludge-Filled Geotextile Tubes as a Sustainable Coastal Protection Measure in Muddy Coastline *(Nastiti Tiasundari)*	423

Papers Sorted by Topics & Parallel Room

Topic 1: Fundamental Soil Properties & Soil Investigation (Birawa Ballroom)

ID	Paper Title	Page No.
002	Perubahan Nilai Kepadatan Relatif Tanah Pasir Akibat Variasi Percepatan Maksimum Gempa *(Muhammad Yunus)*	35-42
007	Water Retention Curve of Soil at Simpang Meo Region South Sumatra *(Nurly Gofar)*	93-94
009	Determination of Bentonite's Flow Limit Using Cylinder Strength Test and Suspension Settling Model *(Budijanto Widjaja)*	107-120
027	Comparative Site Classification Using Conventional Penetration Testing (SPT) and Microtremor Array Measurement (MAM): Case Study of Three Industrial Estates in Karawang, Indonesia *(Ayu Wijayanti Kurnia Dewi)*	251-266
033	Underwater Subsurface Imaging of the North Java Sea using Marine Resistivity Tomography *(Bagus Endar B. Nurhandoko)*	305-312
041	Characterization and Shear Strength Evaluation of Sensitive Volcanic Residual Soils in West Java (Mirna Dwi Lestari S)	391-392
043	Recommendation of Ground Surface Design-Spectra Through Site-Specific Response Analysis (SSRA) Considering Effect of Various Depth of Bedrock, Case Study of Jakarta (Det Komerdevi)	405-414

Topic 2: Retaining Systems (Birawa Ballroom)

ID	Paper Title	Page No.
001	Comparison of Cast-in-Situ Diaphragm Wall for Deep Basements in Indonesia: Continuous Water Stop (CWS) System and Continuous System *(Juse Roejanto)*	35-42
005	Design Review of Pile Cap Excavation Reinforcement System at the IC3 Interchange of the Patimban Access Toll Road Project, Indonesia *(Bobby Novialdi Saputra)*	67-80
010	Analysis and Design of a High-Risk Tiered Retaining Wall Using a Geosynthetic Reinforcement System *(Valdy Kosalim)*	121-122
017	Influence of Underconsolidating Soil on Effective Stress Path in Deep Excavation Case *(Aswin Lim)*	181-182
031	Performance Evaluation of Freestanding Soldier Pile System for a 9-m Excavation in Clayshale Formation at IKN Using the Hardening Soil Model *(Ir. Muhammad Risyad Alditio, S.T.)*	295-304
045	Penggunaan GI-Tube Berbahan Non Woven Dua Lapis Produksi Dalam Negeri untuk Tanggul Laut Studi Kasus Proyek Jalan Tol Semarang–Demak, Jawa Tengah *(Puji Kristianingsih)*	415-422
046	Implementation of Sludge-Filled Geotextile Tubes as a Sustainable Coastal Protection Measure in Muddy Coastline *(Nastiti Tiasundari)*	423

Topic 3: Soil Bio- & Chemical- Treatment & Stabilization (Subadra Ballroom)

ID	Paper Title	Page No.
012	Stabilized Expansive soils with High Alumina Cement at Longer Curing Time *(Arlyn Aristo Cikmit)*	135-148
013	Stabilization of Patimban Marine Soft Clay with Portland Composite Cement: The Effect of Initial Water Content Variations on Soil Bearing Strength *(Arlyn Aristo Cikmit)*	149-150
014	Stabilization of Patimban Marine Clay with Wide Range of Sand Content using Portland Composite Cement *(Arlyn Aristo Cikmit)*	151-164
015	Microbial Enzyme Extract Evaluation for Calcium Carbonate Biocementation: Implications for Ground Improvement *(Lutfian R Daryono)*	165-166
016	Use of CO_2 Nanobubble-Treated Alkaline Wastewater in Developing Low-Carbon Materials *(Sugeng Wahyudi)*	167-180
025	Stabilization Behavior of Sepaku Clay Shale Using Bacillus Subtilis *(Yuswal Subhy)*	229-250
037	The Effect of Fly Ash Addition on Clay Stabilization Using Clean Set Cement *(Efan Tifani)*	339-352

Topic 4: Slope Stability & Monitoring System (Subadra Ballroom)

ID	Paper Title	Page No.
003	Evaluation of Toll Road Embankment Stability on Clay Soil Using 2 m Soil Replacement and Woven Geotextile *(Yani Putri Agustina)*	53-66
011	Numerical analysis of rainfall-induced slope failure in Gumay Ulu, Lahat, South Sumatra *(Nurly Gofar)*	123-134
021	Sub-Surface Movement Detection in a Tailings Storage Facility: Evaluating Inclinometer Real-Time Monitoring and Design Specification (Case Study: Martabe Gold Mine) *(Syavira Indah Utami)*	185-198
028	Stability Assessment of Homogeneous Embankment Dam under Variable Drawdown Rates Using Unsaturated Soil Parameters *(Muhammad Adi Ibrahim)*	267-268
039	Interpretasi Bidang Gelincir Lereng Menggunakan Kombinasi Uji Geoteknik dan Geofisika *(Metta Devi Hartadi)*	365-374
042	Rasio Kecepatan Longsor Berdasarkan Data Gradient Modulus Young dan Strain pada Uji Ucs untuk Setting Alarm pada Slope Stability Radar *(Alam Tronics)*	393-404

Topic 5: Ground Improvement & Soft Soil (Utari Ballroom)

ID	Paper Title	Page No.
023	Utilization of Red Brick Waste for Soil Stabilization: Experimental Research on The Base Layer of the Jogja-Solo Toll Road *(Pradyta Galuh Oktafiani)*	215-228
029	Mitigating Reclamation-Induced Settlement Using Rigid Inclusions: A Ground Improvement Case from Ahmad Yani Airport, Indonesia *(Ryan Rahmat Setiaji)*	269-282
030	Settlement Fitting of Soil Improvement on Toll Road Project in Northern Jakarta *(Muhammad Amhar Wajdi Yanreginata)*	283-294
035	Evaluasi Performa Penurunan Konsolidasi Jangka Panjang Dengan Metode CMC Pada Konstruksi Runway Studi Kasus Bandara Rendani *(Azliny Azreen)*	315-330
038	Ground Improvement of High-Organic Clay Using Sand Columns: Settlement and Stability Analysis *(Luthfi Amri Wicaksono)*	353-364
040	Performance of Ground Improvement with Preloading and PVD on the Serang–Panimbang Toll Road: Analytical and Numerical Verification *(Agus Himawan)*	375-390

Topic 6: Deep Foundation, Tunnelling, Instrumentationm & Environmental Protection (Utari Ballroom)

ID	Paper Title	Page No.
006	Multi-Model Assessment of Anchor Pile Spacing Effects in Axial Load Testing: Mitigating Interaction-Induced Settlement Distortion *(Muhamad Fauzi Ahad)*	81-92
008	Analysis of Seepage and Contaminant Transport to a Water Body Considering Waste Pile Distance and Impermeable Layer Presence *(Melisa Saferman)*	95-106
018	An Overview of Different Types of TBM for the Construction of Subway Tunnels in Indonesia *(Simon Heru Prassetyo)*	183-184
022	Comparative Analysis of Pile Driving Analyzer (PDA), Pile Driving Formula, and Standard Penetration Test (SPT) Data for Assessing the Reliability of Bearing Capacity Estimates in Pontianak Soft Soil *(Vivi Bachtiar)*	199-214
034	Adhesion Factor (α) of Drilled Piles in Clay Shale with Static and Dynamic Load *(Eddy Triyanto Sudjatmiko)*	313-314
036	Development Distributed Acoustic Wave Sensing with Fiber Optics for Vibration and Structural Monitoring *(Bagus Endar B. Nurhandoko)*	331-338

Current Practice of Static and Seismic Stability of Embankment - A Critical Review

Hendra Jitno [1,2]
[1]Department of Civil Engineering, National Institute of Technology, Bandung, Indonesia, 40211
[2]PT Solusi Geotek Optima, Bandung, Indonesia, 40293.
hjitno@itenas.ac.id; hendra.jitno@ptsgo.id

EXTENDED ABSTRACT

Current practice of static and seismic stability of embankments relies fundamentally on the concept of the Factor of Safety (FoS), which serves as a key measure for evaluating the stability and reliability of earth structures such as slopes, foundations, embankments, and dams under various loading conditions. Conceptually, the FoS is defined as the ratio between the resisting forces or moments that prevent failure and the driving forces or moments that tend to cause it:

$$FOS = \frac{\text{Resisting Forces}}{\text{Driving Forces}}$$

A value greater than unity indicates that the structure is theoretically stable, whereas a value less than one indicates potential failure. In practice, engineers adopt minimum target FoS values (typically between 1.3 and 1.5 for static conditions) to ensure an adequate margin of safety against uncertainties in soil properties, loading conditions, and construction quality.

Although this concept has served the profession well for over a century, misinterpretations and oversimplifications of the FoS remain common. Many engineers tend to equate FoS directly with reliability, overlooking other critical factors such as the variability of soil parameters, construction practices, or the behavior of complex materials under different stress paths. As a result, structures may be assigned seemingly acceptable FoS values but still experience instability or failure. This extended abstract discusses the major misconceptions related to FoS and highlights the importance of proper data quality, material characterization, and analytical judgment in achieving true geotechnical safety.

A widespread misunderstanding in geotechnical practice is that increasing the FoS automatically results in a safer design. In reality, the actual probability of failure depends not only on the numerical FoS but also on the quality of data, the competence of design engineers, and the standards of construction and operation.

Silva et al. (2008) classified geotechnical projects into four quality categories:

- Category I – high-quality projects using state-of-the-practice methods (e.g., large dams and critical structures)
- Category II – standard engineering practice
- Category III – substandard or temporary works
- Category IV – little or no engineering control

For example, a slope or dam with FoS = 1.5 may correspond to an annual probability of failure of 10^{-4} for Category I projects, but up to 10^{-1} for Category IV projects. This large variation demonstrates that FoS alone is not a consistent measure of safety; it must be evaluated in conjunction with data quality and professional judgment.

Another misconception is that all geotechnical data are equally valid once field and laboratory testing is completed. In practice, data quality and representativeness strongly influence the reliability of computed FoS. Poorly executed sampling, inadequate test numbers, or inappropriate interpretation can produce misleading strength parameters. When variability is high, the computed average FoS may appear satisfactory, but the actual probability of failure increases. As shown conceptually in reliability analyses, even when the mean FoS remains constant, poor-quality data (with high standard deviation) produce a much larger area where the resisting forces are lower than the driving forces, signifying a higher chance of failure. Hence, proper site investigation, laboratory control, and data validation are critical to ensure that the computed FoS reflects real stability conditions.

The same numerical FoS can correspond to very different risk levels depending on the stress–strain characteristics of the materials involved.

- Strain-softening materials, such as overconsolidated clays or cemented loose sands, lose strength with increasing deformation.
- Dilative materials gain strength as shear strain increases.

Structures built on strain-softening soils may therefore fail suddenly even when the computed FoS exceeds the design criterion. The 1998 Aznalcollar tailings dam failure in Spain is a well-known example, where design analyses showed FoS between 1.17 and 1.31, but the foundation clay exhibited strain-softening behavior that was not recognized during design (Olalla and Cuellar, 2001). Similarly, the Brumadinho dam failure in Brazil (Robertson et al., 2019) occurred due to brittle, cemented tailings that lost strength abruptly under shear. These examples highlight the danger of interpreting FoS without considering material behavior.

Engineers commonly assume that long-term stability corresponds to drained conditions, while short-term stability corresponds to undrained conditions. However, many historical dam failures occurred long after construction, under undrained conditions. The assumption that pore pressures fully dissipate over time is not always valid, especially in low-permeability materials or when slow loading rates are involved. Analyses must therefore consider both drained and undrained parameters when evaluating long-term performance.

Overconsolidated (OC) soils are often assumed to retain their higher strength characteristics permanently. In reality, if a soil element is reloaded beyond its preconsolidation pressure, it behaves as Normally Consolidated (NC) and loses the additional cohesion and stiffness associated with its OC state. Consequently, adopting a constant high-strength envelope for all stress levels can significantly overestimate stability. Correct interpretation of the Mohr–Coulomb envelope and understanding of effective stress paths are essential to avoid this error. A classical example of dam failure due to this misunderstanding is the Mount Polley dam failure (Independent Expert Panel, 2015).

For excavated slopes, the short-term stability is often greater than the long-term stability due to stress relaxation, weathering, and degradation of clay minerals. Laboratory data show that clay shales may lose strength rapidly upon exposure—sometimes within days. This progressive deterioration must be accounted for in design and monitoring.

Traditional slope stability analyses are based on two-dimensional (2D) assumptions, which neglect the contribution of side resistance and spatial geometry. Modern numerical methods allow more realistic three-dimensional (3D) modeling, which typically yields FoS values 10–20% higher than 2D results for the same slope. However, this does not imply a greater safety level; rather, it reflects the inclusion of additional resisting forces. Therefore, 3D FoS values cannot be directly compared to 2D design criteria (e.g., FoS = 1.5). To maintain consistency, slightly higher FoS thresholds should be adopted for 3D analyses.

Using undrained strength values obtained from triaxial compression (TC) tests for all parts of an embankment is another common mistake. Different zones within an embankment experience different stress paths (Figure 1):

- Beneath the crest: triaxial compression mode
- Near the toe: direct simple shear (DSS) mode
- In front of the toe: triaxial extension (TE) mode

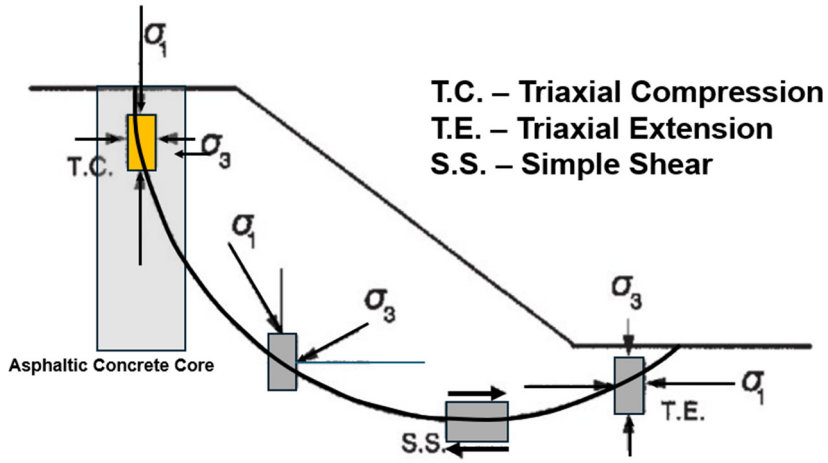

Figure 1. Different failure mechanisms under the embankment (adapted from Ladd, 1991).

The undrained strength ratio from TC tests is typically 1.5–2.0 times higher than those from DSS or TE tests. Therefore, applying TC results universally can lead to unconservative FoS and unsafe designs. Strength selection should correspond to the expected failure mechanism at each location.

Seismic stability is commonly evaluated using the pseudo-static method, a simple and widely adopted approach that applies a horizontal seismic coefficient—representing the ratio of earthquake acceleration to gravity—in limit equilibrium analysis. While convenient, this method assumes a constant, unidirectional force and neglects the cyclic, multi-directional, and time-dependent characteristics of actual earthquake loading. As a result:

- A computed FoS < 1.0 does not always mean slope collapse; it may only represent temporary displacement.
- A FoS > 1.0 does not guarantee post-earthquake stability, especially when materials experience strength loss due to cyclic loading or liquefaction.
- The method is also sensitive to the chosen seismic coefficient; using the Peak Ground Acceleration (PGA) directly is overly conservative.

Because of these limitations, pseudo-static results should be used only as a screening tool to determine whether more advanced dynamic or deformation analyses are necessary (ANCOLD, 2019).

The critical review of the static and seismic stability of embankment demonstrates that the Factor of Safety should never be interpreted in isolation. While FoS provides a useful measure of equilibrium between driving and resisting forces, it does not inherently account for uncertainty, variability, or the quality of engineering judgment. True reliability in geotechnical design arises from:

- High-quality field and laboratory data, collected and interpreted properly.
- Understanding of soil behavior under various loading and drainage conditions.
- Appropriate selection of strength parameters based on expected failure mechanisms.
- Consideration of three-dimensional effects and time-dependent degradation.
- Recognition of method limitations, particularly for simplified analyses such as pseudo-static or 2D limit equilibrium.

The Factor of Safety remains an essential tool in geotechnical engineering, but its value is meaningful only when combined with a proper understanding of soil mechanics, data reliability, and construction quality. The belief that higher FoS alone ensures safety is misleading and can result in a false sense of security. Instead, engineers should focus on improving data quality, parameter selection, and analysis realism.

Historical dam failures such as Aznalcollar, Brumadinho, and Mount Polley remind us that even apparently "stable" designs can fail when underlying assumptions are flawed. Therefore, the profession must move toward a more holistic approach, where FoS is complemented by probabilistic assessments, performance-based evaluations, and robust quality assurance throughout investigation, design, and construction.

Ultimately, the reliability of a geotechnical structure is determined not by the numerical FoS alone, but by the engineering judgment, data integrity, and understanding of soil behavior that underpin its calculation.

KEYWORDS: Slope Stability; Factor of Safety; Geotechnical Data Quality; Material Uncertainty; Strain-Softening Behavior.

ACKNOWLEDGEMENTS

I wish to acknowledge the support and encouragement of my former teacher in ITB, late Professor Aziz Jayaputra, and also my colleague Professor Masyhur Irsyam for all interesting discussions and for posing me with thought-provoking questions.

REFERENCES:

ANCOLD (2019), "Guidelines for Design of Dams for Earthquakes".

Independent Expert Engineering Investigation and Review Panel (2015). Report on Mount Polley Tailings Storage Facility Breach. Victoria, BC: Government of British Columbia

Ladd, C.C (1991). Stability Evaluation During Staged Construction, J. Geotech. Engrg. 1991.117:540-615.

Olalla, C. & Cue´llar, V. (2001). Failure mechanism of the Aznalco´llar Dam, Seville, Spain. Geotechnique 51, No. 5, 399–406.

Robertson, P.K. Melo, L.M, Williams, D.J., and Wilson, G.W (2019). Report of the Expert Panel on the Technical Causes of the Failure of Feijão Dam I, December 2019.

Silva, F., Lambe, T.W and Marr, W.A. (2008). Probability and Risk of Slope Failure, Journal of Geotechnical and Geoenvironmental Engineering, Vol. 134, No. 12.

Sparse Data-Enabled Underground Digital Twin for Infrastructure Development

Chao Shi[1*]
[1]**School of Civil and Environmental Engineering, Nanyang Technological University, Singapore, 639798; chao.shi@ntu.edu.sg**

EXTENDED ABSTRACT

Underground urbanization offers a sustainable pathway to relieve surface congestion, optimize limited land resources, and strengthen the resilience of modern cities (Shi and Wang, 2022). As urban functions, such as transportation, utilities, and storage increasingly extend underground, the complexity of subsurface environments, shaped by variable geological conditions and dense infrastructure networks, poses significant management challenges. In this context, underground digital twins are transformative, serving as dynamic, data-driven virtual replicas that continuously integrate information from sensors, surveys, and monitoring systems. This data-driven process bridges the physical and digital domains, enhancing situational awareness, improving safety, and optimizing the design, construction, and maintenance of underground spaces. Different from above-ground digital twin models, where the dimensions and engineering properties of various components can be reasonably accurately measured or tested, underground digital twins rely on limited site-specific measurements (e.g., boreholes) retrieved from scattered points. Figure 1 illustrates an underground digital twin paradigm for streamlining infrastructure design and analysis. The traditional workflow from geotechnical site investigation to geological modeling and engineering design can be viewed as a process of data and information flow. To automate the whole process, it is imperative to develop a data-driven tool that can accurately interpret and construct an underground digital twin from sparse data before subsequent engineering design and analysis can be carried out.

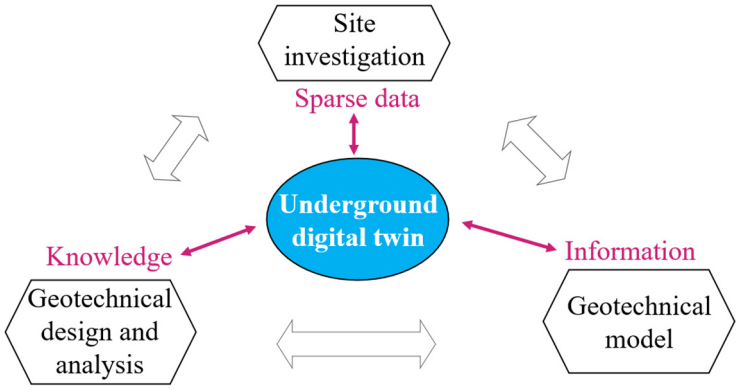

Figure 1. An underground digital twin paradigm for underground infrastructure development

Apart from data sparsity, subsurface heterogeneity is another challenge impeding the development of underground digital twins. Geotechnical engineering deals with natural materials (e.g., rocks and soils), and the accurate characterization of subsurface ground conditions is an essential task in geotechnical design and analysis. A false interpretation of subsurface conditions can lead to significant variations in engineering design schemes and construction costs. Previous studies conducted by Clayton (2001) identified key factors contributing to construction budget overruns in the UK. As shown in Figure 2, the two dominant factors are related to the interpretation of soil boundaries (i.e., 22%) and soil properties (i.e., 20%). The spatial prediction of stratigraphic boundaries and soil properties constitutes a key component of geotechnical site characterization.

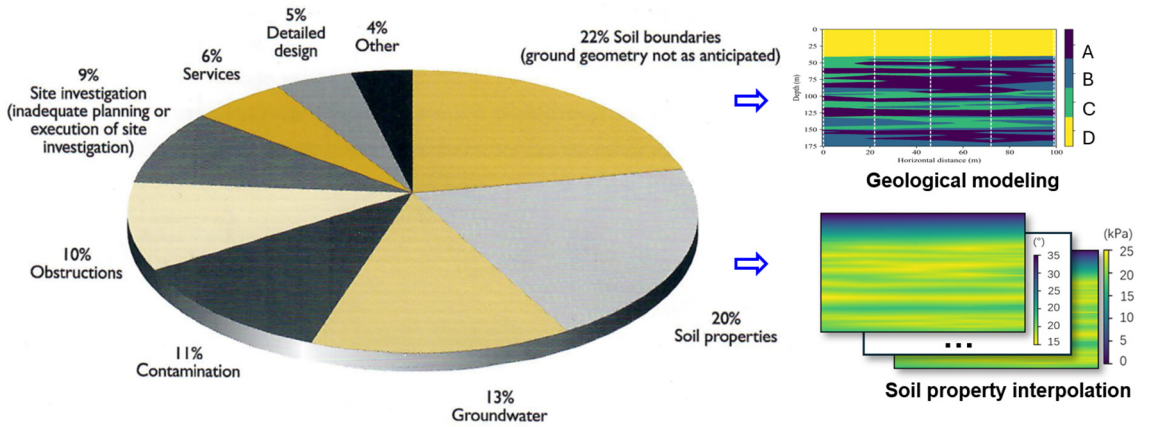

Figure 2. Challenges associated with geotechnical infrastructure development (modified from Clayton 2001)

In practice, it is challenging to reliably characterize subsurface ground conditions. As a result, engineers often rely on prior knowledge of local geology or engineering judgment to determine stratigraphic boundaries and the spatial variability of soil properties. For example, geological cross-sections are commonly developed using linear interpolation based on limited borehole logs. However, this simplified approach is subjective and may encounter difficulties when interbedded strata are present. To explicitly address this challenge, various machine learning and other data-driven methods have been proposed over the past decade to develop geological models from sparse data. Traditional parametric models, such as Markov-based models, and image-based simulations (e.g., multiple-point statistics), treat geological modeling as a classification problem, aiming to infer spatial stratigraphic connectivity among sparse categorical soil data revealed by boreholes. Nevertheless, it remains challenging to establish reliable correlations between the same soil types at multiple borehole locations due to limited data availability for specific sites and insufficient feature extraction and representation from borehole stratigraphy.

To address this challenge, an implicit feature learning approach (Qian et al., 2024) was developed to extract high-dimensional stratigraphic patterns from low-dimensional categorical soil variables for subsequent stochastic stratigraphic modeling. The soil stratigraphy along boreholes is transformed into continuous variables using a signed distance function (SDF), which enables flexible representations of spatial stratigraphic connectivity. Subsequently, the spatial distribution of signed distance fields for each soil type is inferred from signed distances at borehole locations using conventional spatial interpolators, such as Bayesian compressive sensing (BCS). The obtained signed distance fields for all soil types are then combined and converted back into geological cross-sections for statistical analysis. The performance of the proposed feature learning approach was demonstrated through a real case study (Shi and Wang, 2022). Figure 3 shows borehole logs retrieved from a land reclamation site, where subsurface ground conditions must be accurately characterized before tunnel design and construction. The ground consists of six different soil types, namely fill, disturbed marine deposit (DMD), marine deposit (MD), alluvial sand (Alls), alluvial clay (Allc), and completely decomposed granite (CDG). The spatial distribution of fine-grained materials (i.e., MD and Allc) significantly affects long-term ground settlement and tunnel segment performance. While it may be straightforward to determine the boundaries between fill, DMD, and MD using straight lines connecting strata of the same soil type, it is challenging to delineate the spatial distribution of interbedded Alls and Allc layers due to their inconsistent numbers and elevations between adjacent boreholes. Figure 4 presents the prediction results from the proposed SDF–BCS method, showing that a three-dimensional (3D) geological model can be automatically developed from limited borehole data in a data-driven manner. Cross-validation was conducted to evaluate the prediction accuracy, and the results indicate an accuracy of approximately 89%. More importantly, the proposed method not only provides the best estimate of the 3D geological model but also explicitly quantifies the associated stratigraphic uncertainty, offering a quantitative indicator for subsequent risk-

informed engineering design and analysis. The above illustrative example highlights the importance of data-driven tools to characterize subsurface heterogeneities for building underground digital twins and streamlining engineering design and analysis.

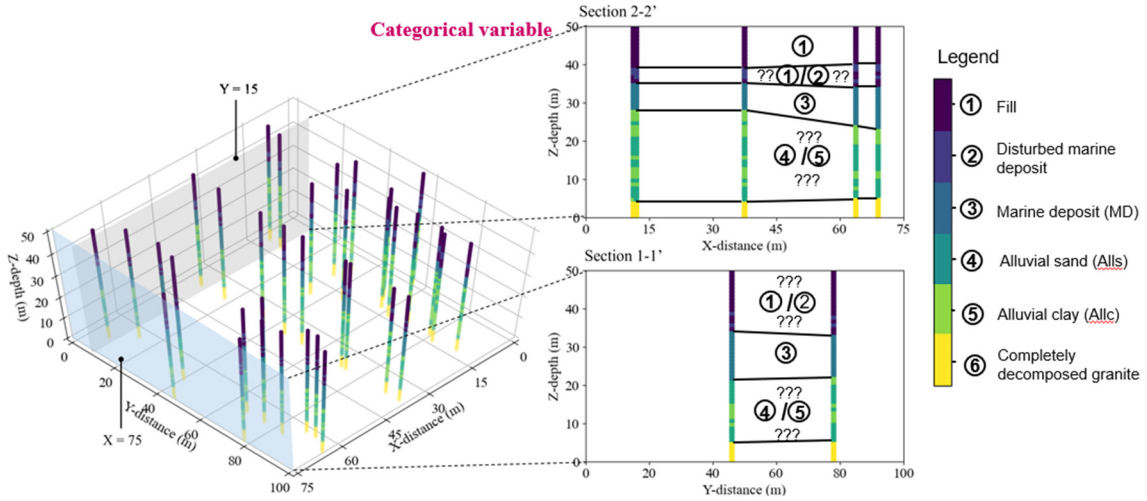

Figure 3. Illustration of a geological modelling challenge for a tunnelling site in Hong Kong (modified from Shi and Wang (2022))

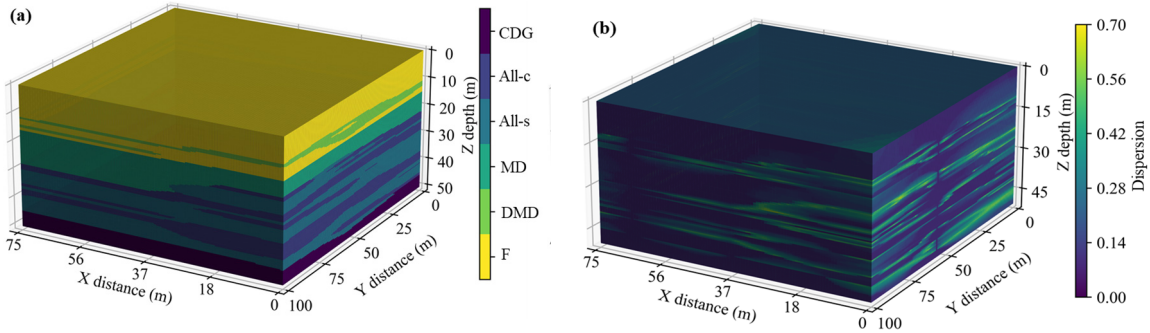

Figure 4. Prediction of three-dimensional geological models with quantified uncertainty

ACKNOWLEDGMENTS

research was supported by the Ministry of Education, Singapore, under its Academic Research Fund (AcRF) Tier 1 Seed Funding Grant (Project no. RS03/23), AcRF regular Tier 1 Grant (Project nos. RG69/23 and RG86/25), Cities of Tomorrow (CoT) grant (Project no. CoT-V3-2024-2), and the Start-Up Grant from Nanyang Technological University. The financial support is gratefully acknowledged.

REFERENCES

Clayton, C. R. 2001. Managing geotechnical risk: improving productivity in UK building and construction. Thomas Telford, London

Qian, Z. and Shi, C., 2025. Large language model-empowered paradigm for automated geotechnical site planning and geological characterization. *Automation in Construction*, *173*, p.106103.

Qian, Z.H., Shi, C., Wang, Y. and Cao, Z.J., 2024. Nonparametric and continuous variable-based stratigraphic modelling from sparse boreholes using signed distance function and Bayesian compressive sensing. *Canadian Geotechnical Journal*, *62*, pp.1-23.

Shi, C. and Wang, Y., 2022. Data-driven construction of Three-dimensional subsurface geological models from limited Site-specific boreholes and prior geological knowledge for underground digital twin. *Tunnelling and underground space technology*, *126*, p.104493.

Shi, C. and Wang, Y., 2022. Machine learning of three-dimensional subsurface geological model for a reclamation site in Hong Kong. *Bulletin of Engineering Geology and the Environment*, *81*(12), p.504

Analisis Faktor Keamanan dan Reliabilitas dalam Rekayasa Geoteknik

Indra Djati Sidi, Ph.D.[1]

Dosen Purna Tugas[1], Departemen Teknik Sipil, Kelompok Struktur, Institut Teknologi Bandung

Dalam perencanaan dan desain rekayasa geoteknik, memastikan keamanan struktur seperti pondasi tiang bor, pondasi dangkal, dinding penahan tanah, dan lereng sangat penting selama umur layan yang ditentukan. Secara tradisional, hal ini dicapai dengan menerapkan faktor keamanan tunggal, yang merupakan rasio antara ketahanan nominal dan beban nominal. Namun, penggunaan faktor keamanan tunggal mungkin tidak memberikan rasa keamanan yang setara karena variabilitas inheren parameter tanah dan kesalahan epistemik dalam akurasi formula yang digunakan. Selain itu, setiap perencana mungkin memiliki tingkat kepercayaan yang berbeda dalam memilih faktor keamanan yang tepat. Namun perlu dicatat bahwa penggunaan angka keamanan tunggal telah menorehkan sejarah keberhasilan perencanaan struktur geoteknik di Indonesia.

Untuk mengatasi keterbatasan ini, pendekatan faktor keamanan berbasis risiko dapat digunakan. Ini melibatkan penggunaan analisis probabilitas dan menerapkan prinsip reliabilitas untuk memodelkan ketidakpastian secara konseptual dan sistematis. Oleh karena itu, data tentang variabilitas parameter2 tanah harus disediakan atau diukur.

Makalah ini menunjukkan manfaat menerapkan pendekatan probabilistik atau reliabilitas dalam perencanaan dan desain struktur geoteknik. Dengan memperlakukan beban permanen dan sementara secara berbeda sesuai dengan karakteristik statistiknya, maka penilaian kinerja struktur dalam bentuk reliabilitas dapat diperoleh. Nilai ini akan dibandingkan dengan tingkat reliabilitas yang dapat diterima secara universal.

Khususnya, dalam perencanaan pondasi dalam, tingkat reliabilitas yang lebih tinggi dapat dinyatakan secara eksplisit untuk dibandingkan dengan struktur atas, dalam model perencanaan dua tahap. Selain itu, pendekatan probabilistik memungkinkan evaluasi komprehensif problema interaksi tanah-struktur.

Pendekatan Bayesian juga disorot, yang memungkinkan kombinasi sistematis data pengukuran baru, seperti uji beban, dengan nilai prediksi awal, untuk memperbarui penilaian keamanan dan reliabilitas yang bersangkutan.

This page is intentionally left blank

Natural Vs Engineering Disaster-Risk Assessment in Geotechnical Perspective

Suttisak Soralump[1]
[1] Department of Civil Engineering, Faculty of Engineering, Kasetsart University, Bangkok, Thailand, 10900 1;
soralump_s@yahoo.com

EXTENDED ABSTRACT

Dealing with engineering inherently involves managing uncertainty. In civil engineering, this uncertainty is particularly pronounced in load assessment. Every structure is designed to manage this variability through the principle of reliability, often formalized using the Capacity-Demand Model. This model ensures that the structural capacity (C) which is highly influenced by uncertain material and in-situ soil properties exceeds the structural demand (D), which includes variable load conditions. For typical construction, the primary source of uncertainty is usually associated with soil properties. However, for more complex infrastructural projects including tunnels, dams, and high-rise buildings uncertainty stems not only from subsurface conditions but also from the potential for unexpected load conditions or extreme events (e.g., earthquakes, mega-floods). The critical response to this inherent variability is the implementation of proper risk assessment, which serves as an essential tool for uncertainty management. Three case studies will be presented to demonstrate the utility of risk assessment in addressing complex civil engineering challenges.

The first case study is the collapse of the high-rise building in Bangkok soft clay in March 2025. On March 28, 2025, a powerful magnitude 7.7 earthquake struck the Sagaing Region of Myanmar, with its epicenter near the city of Mandalay. Despite being over 1,000 kilometers (about 620 miles) from the epicenter, Bangkok experienced significant shaking. This was primarily due to the earthquake's rupture characteristics and the city's soft soil, which amplified the seismic energy. A 33-story high-rise building intended for the State Audit Office collapsed in Bangkok's Chatuchak district (Figure 1). The structure was still under construction at the time, although it had already topped out. Notably, this was the only building completely destroyed by the earthquake in Thailand. The collapse tragically resulted in dozens of confirmed deaths and numerous injuries among the workers on site. The fact that a building in Bangkok collapsed from a far-field earthquake immediately sparked an intensive investigation into the cause, with authorities probing for issues such as sub-standard building materials or construction flaws. Arrest warrants were subsequently issued for several individuals involved in the construction.

The second case study details a dramatic road collapse in the Bangkok soft clay in September 2025. The failure occurred on September 24, 2025, on Samsen Road in the Dusit district of Bangkok, situated directly in front of Vajira Hospital and the Samsen Police Station (Figure 2). The road surface suddenly gave way, resulting in a massive sinkhole initially estimated to be approximately 30 meters wide and up to 50 meters deep. The collapse caused significant damage, including the loss of multiple vehicles (such as a police tow truck) and utility poles, and completely severed the main road. Fortunately, no casualties or injuries were reported, but the incident necessitated the evacuation of the adjacent Samsen Police Station and the temporary precautionary closure of outpatient services at Vajira Hospital. The Bangkok Governor and officials quickly attributed the failure to the ongoing construction of an underground subway tunnel (part of the MRT Purple Line). The direct cause was hypothesized to stem from an unexpected factor not considered during the project's design, with initial assumptions pointing toward either human error or significant soil erosion around the unfinished underground tunnel and station site. Emergency response efforts involved pouring thousands of tonnes of concrete into the massive void for stabilization. However, the repair was

complicated when concrete began leaking into the subway tunnel below, requiring a temporary halt to re-evaluate the stabilization plan. Samsen Road remains closed indefinitely as the extensive and complex recovery operation continues.

The preceding failures of Case 1 and Case 2 suggest that, had a comprehensive risk assessment been conducted and its findings implemented during the design and construction phases, the damage and overall project risk could have been significantly minimized. The third case study will illustrate the application of risk assessment concepts to a dam engineering project in Thailand. The risk assessment process comprehensively incorporated both internal factors, such as potential material degradation and structural deficiencies, and external factors, including extreme events like seismic activity and flood loading. Utilizing these rigorous parameters, the assessment quantified the risk in terms of the probability of failure and established a specific tolerable risk threshold aligned with international dam safety guidelines. This final example will specifically demonstrate how an initial risk assessment is used not only to quantify the potential for loss of life and infrastructure but also to systematically guide the implementation of cost-effective and targeted risk reduction measures.

1.1 Figures

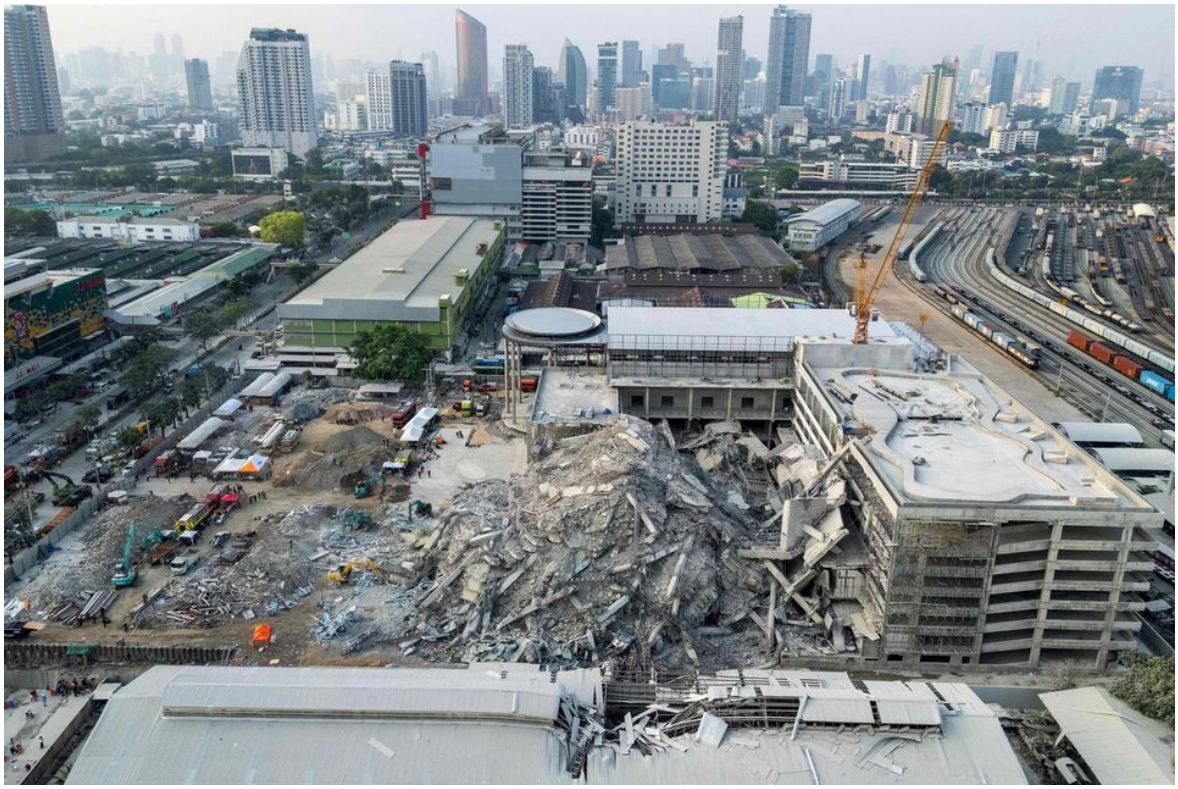

Figure 1. The under-construction State Audit Office building collapsed on March 28 due to the impact of an 8.2-magnitude earthquake near Mandalay, Myanmar. (Source: straittimes.com, Photo: AFP)

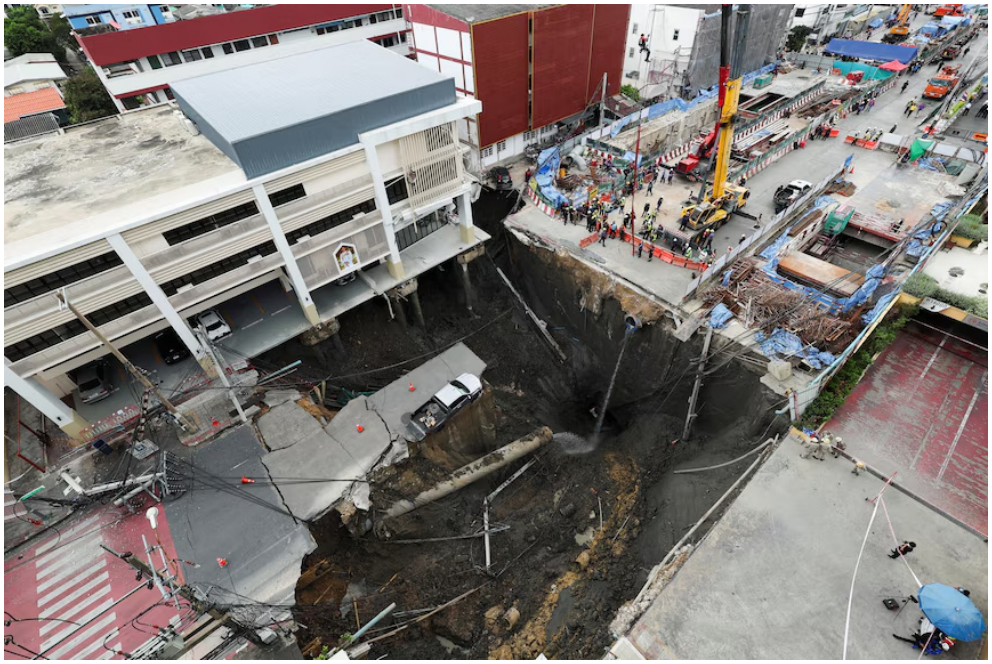

Figure 2. A massive sinkhole opened on Samsen Road near Vajira Hospital in central Bangkok. (Source: Reuters.com: Chalinee Thirasupa)

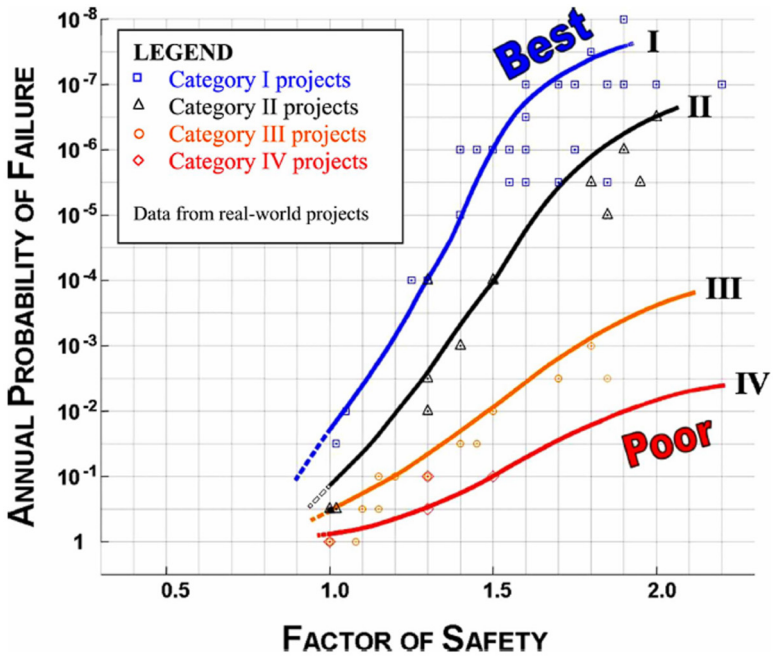

1. Category I—facilities designed, built, and operated with state-of-the-practice engineering. Generally these facilities have high failure consequences;
2. Category II—facilities designed, built, and operated using standard engineering practice. Many ordinary facilities fall into this category;
3. Category III—facilities without site-specific design and sub-standard construction or operation. Temporary facilities and those with low failure consequences often fall into this category; and
4. Category IV—facilities with little or no engineering.

Figure 3. Probability of Failure vs. Factor of Safety (Silva et al., 2008)

REFERENCES

Silva, F., Lambe, T.W. and Marr, W.A., 2008. Probability and risk of slope failure. *Journal of geotechnical and geoenvironmental engineering*, 134(12), pp.1691-1699.

From Micro-Scale Mechanisms to Field Applications: Advancing Bio-Based Ground Improvement with MICP

Lyesse Laloui[1]
Laboratory of Soil Mechanics, Swiss Federal Institute of Technology, (EPFL), Lausanne, Switzerland; lyesse.laloui@epfl.ch

EXTENDED ABSTRACT

Ground improvement is a fundamental challenge in geotechnical engineering, as natural soils often lack the strength, stiffness, and durability required for safe and resilient infrastructure. Failures of foundations, slope instabilities, and soil liquefaction or erosion in seismic and coastal environments illustrate the importance of enhancing soil performance.

Conventional improvement methods have long been used, but they depend on heavy machinery, high injection pressures, and significant energy input, leading to high costs and environmental impacts. These limitations highlight the urgent need for sustainable alternatives.

Microbially Induced Calcite Precipitation (MICP) has emerged as one such approach. By inducing calcium carbonate precipitation through urea hydrolysis, soil particles are bound together, resulting in improved stiffness and strength. Unlike conventional methods, MICP can be applied with low-pressure injection and highly fluid solutions, reducing equipment requirements and environmental footprint.

The key objective of this research is how MICP can be optimized and scaled from pore-scale processes to field-scale applications while ensuring homogeneous treatment, sustainability, and engineering reliability. To address this, the research carried out at EPFL follows MICP across multiple scales; from micro-scale mechanisms to laboratory testing, large-scale validation, numerical modeling, and finally, technology transfer to pilot applications.

1.1. Micro-scale investigations

Understanding the process at the particle scale was a prerequisite for the reliable application of MICP in engineering practice. Initial microscopic observations revealed the morphology of $CaCO_3$ crystals and their direct attachment to sand grain surfaces, confirming the coexistence of pore-filling and contact-bridging mechanisms. These findings provided visual evidence of how mineralization develops at grain boundaries and within pores.

To complement these observations, specially designed microfluidic cells were employed and calcite precipitation was monitored using X-ray μCT scanning (Elmaloglou et al., 2022). Two-dimensional cross-sections and three-dimensional reconstructions confirmed the formation of a well-distributed $CaCO_3$ network bridging soil grains. These results offered direct insight into the coupled processes of solute transport and biochemical reaction, and demonstrated how flow regimes govern the spatial distribution of urea hydrolysis and subsequent $CaCO_3$ deposition.

Together, microscopic and μCT analyses consistently identified two distinct bonding mechanisms: passive bonds, characterized by pore filling and grain coating, and active bonds, formed by calcite bridges at particle contacts that contribute directly to load transfer. Recognition of this dual bonding behavior was fundamental for interpreting the macroscopic mechanical response observed in subsequent laboratory and large-scale experiments.

1.2. Mechanical performance

The influence of calcite bonding on engineering behavior was assessed through a comprehensive series of laboratory tests (Harran et al., 2022). Specimens treated to different cementation levels were subjected to oedometer compression, direct shear (Figure 1), drained triaxial compression, and cyclic simple shear tests. Results indicated that compressibility decreased in oedometer tests, while stability was maintained under cyclic loading. In triaxial tests, the friction angle increased from 37–38° to 45–46°, and cohesion rose from 0 kPa to 371 kPa. Furthermore, cyclic shear tests demonstrated a significant enhancement in liquefaction resistance, as evidenced by the reduction in pore pressure buildup.

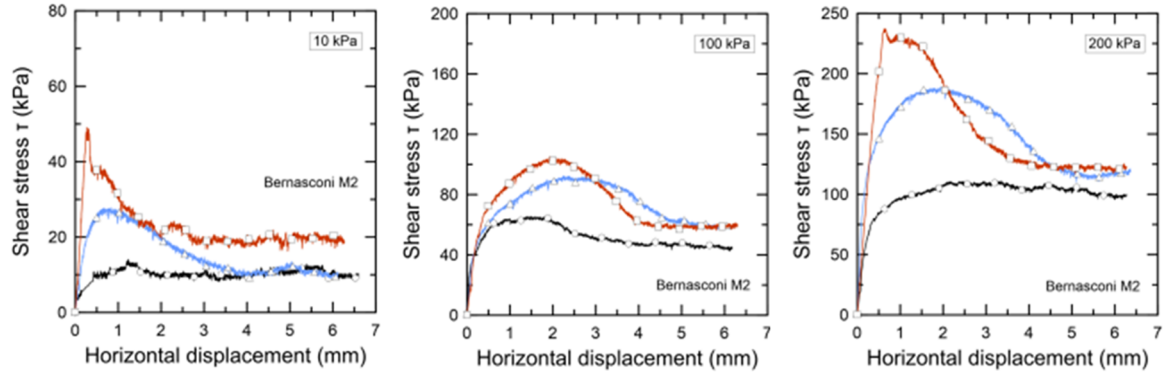

Figure 1. Direct shear test stress-deformation results for medium grained sand.

1.3. Large-scale experiments

In order to better represent field conditions, large-scale tests were performed in a custom-built concrete tank. Three trials were performed in an 80 m³ reinforced concrete tank (8.0 × 10.0 × 2.5 m) filled with 125 tonnes of poorly graded sand (0–4 mm, porosity ~32%). The setup included a gravel drainage layer with 18 perforated PVC tubes and a geotextile filter, enabling both saturated and unsaturated hydraulic regimes.

Two hydrolysis pathways were tested: ex-situ hydrolysis, where carbonate-rich solutions were prepared in a bioreactor and ammonium was removed before injection, and in-situ hydrolysis, where ureolysis occurred directly in the soil matrix. Various injection designs were employed and operated with incremental lifting. Flow rate, injected volume, and cycle number were systematically varied, while injection pressures and effluent chemistry were continuously monitored.

Results from ex-situ hydrolysis in saturated soil showed precipitation efficiencies above 80% and strength improvements from 0.5–1 MPa (untreated) to 2–4.5 MPa (treated), though heterogeneity due to preferential flow remained (Harran et al., 2023). In unsaturated conditions, ex-situ hydrolysis reached higher peak strengths (up to 7 MPa) with reduced injection volumes (~0.7 pore volumes), demonstrating improved reactant distribution but also increased risks of clogging and bioslurry formation. In Figure 2, the in-situ hydrolysis tests revealed the critical role of injection configuration: high flow rates and multiple cycles produced localized strengths up to 20 MPa (Büyüklü et al., 2023).

Overall, the experiments confirm that MICP can be scaled to field-representative volumes when injection strategies and hydraulic regimes are optimized. Ex-situ hydrolysis provides a sustainable advantage through ammonium removal prior to injection.

1.4. Constitutive and mathematical modeling

Since experimental results alone are not sufficient to generalize the variability of field conditions, it has been necessary to develop mathematical tools capable of linking micro-scale processes with macro-scale soil behavior. In this context, early studies on biogrout propagation proposed a comprehensive bio-hydro-mechanical model that incorporates bacterial growth and decay,

attachment and detachment processes, as well as porosity changes and biologically induced stresses, and validated it through numerical simulations of injection tests (Fauriel and Laloui, 2011). Building on this foundation, a multiphysical modelling framework was developed in COMSOL Multiphysics to replicate the large-scale ex-situ MICP hydrolysis experiment (Bosch et al., 2023). This framework integrates fluid flow, solute transport, and calcite precipitation, while dynamically updating porosity and hydraulic conductivity as functions of precipitation. Both 2D and 3D finite element models were applied: the 2D model reproduced general injection pressure trends, whereas the 3D model captured well-to-well interactions and provided a more realistic representation of precipitation patterns. Comparisons with experimental results confirmed that the models successfully reproduced observed injection pressures and qualitatively matched penetration resistance profiles, thereby demonstrating their capacity to predict the evolution of calcite precipitation and its impact on soil behavior. In parallel, a comprehensive bio-chemo-hydro-mechanical (BCHM) framework was developed and calibrated against experimental data (Bosch et al., 2024). This model couples fluid flow, solute transport, urea hydrolysis, and calcite precipitation with an elasto-plastic soil constitutive law based on the Mohr–Coulomb criterion, enabling the simulation of consolidation, bonding induced by calcite precipitation, and subsequent debonding. In this way, the BCHM framework captures not only the coupled chemo-hydraulic processes but also the strength and deformation response of bio-cemented soils.

Figure 2. Exhumation of columns after bio-cementation

1.5. Technology transfer and applications

The transition from laboratory findings to practical field applications necessitated the development of deployable technologies. In this context, Medusoil, an EPFL start up, developed the process, a patented ex-situ hydrolysis approach. Laboratory measurements confirmed that the solution has a viscosity nearly identical to water, allowing it to be injected using low-pressure pumps and small-diameter pipes. The process eliminates the need for bacterial injection and prevents ammonium by-products, delivering a carbonate-rich, nitrogen-free solution to the soil, where it reacts with calcium to precipitate calcite and cement the grains.

Beyond laboratory validation, Medusoil has already implemented the process in pilot field applications. These include liquefaction mitigation trials in seismic areas, erosion protection along riverbanks, and slope stabilization works (Terzis et al., 2020). The field tests confirmed that low-pressure injection with the proposed solution can be carried out using conventional site equipment, and demonstrated measurable improvements in soil stiffness and resistance under realistic boundary conditions. These early applications provide confidence in scaling up bio-based ground improvement to full engineering practice.

Complementary patents, including electrode-based consolidation systems and geosynthetic elements for bio-improvement, illustrate the pathway from EPFL laboratory research to field-scale implementation.

1.6. Conclusions and future work

The research demonstrates that MICP has advanced considerably along the pathway from scientific curiosity to engineering application. Micro-scale investigations clarified cementation mechanisms,

mechanical testing revealed significant gains in strength and stiffness, large-scale experiments validated feasibility under near-field conditions, mathematical modeling laid the groundwork for predictive tools, and patented technologies enabled field implementation.

Nevertheless, further steps are required for full maturity of the method:

- Applications in unsaturated soil conditions to better reflect real field environments.
- Optimization of injection parameters and methods to ensure homogeneous treatment across various soil types.
- Development of reliable databases linking laboratory, large-scale, and field-scale results.

MICP is a clear example of how bio-based ground improvement can evolve from fundamental science into patented, field-ready technologies. This approach not only responds to the demand for sustainable engineering practices but also provides a vision of how organically inspired methods may transform the future of geotechnical practice.

ACKNOWLEDGMENTS

The author wish to acknowledge the financial support provided by the Swiss State Secretariat for Education, Research and Innovation (SERI) (Contract No.: 23.00426). This work is also supported by the European Innovation Council and SMEs Executive Agency (EISMEA) under the European Union's HORIZON-EIC-2022-TRANSITION-01 research and innovation program (Grant Agreement No.: 101113081)

REFERENCES

Bosch, J.A., Terzis, D., and Laloui, L., 2024. A Bio-Chemo-Hydro-Mechanical Model of Transport, Strength and Deformation for Bio-Cementation Applications. *Acta Geotechnica* 19(5): 2805–21. doi:10.1007/s11440-023-02172-0.

Büyüklü, M., Terzis, D., and Laloui, L., 2023. On The effect of Injection Parameters and Techniques Towards, Achieving Homogenous Soil Bio-improvement: Insights From a Large Scale Experiment. *Proceedings of the 9. Geotechnical Symposium*, Istanbul, Turkiye. doi:10.5505/2023geoteknik.SS-07.

Elmaloglou, A., Terzis, D., Pietro, A., and Laloui, L., 2022. 'Microfluidic Study in a Meter-Long Reactive Path Reveals How the Medium's Structural Heterogeneity Shapes MICP-Induced Biocementation'. *Scientific Reports* 12(1): 19553. doi:10.1038/s41598-022-24124-6.

Fauriel, S., and L. Laloui. 2011. 'A Bio-Hydro-Mechanical Model for Propagation of Biogrout in Soils'. In *Geo-Frontiers 2011*, Dallas, Texas, United States: American Society of Civil Engineers, 4041–48. doi:10.1061/41165(397)413.

Harran, R., Terzis, D., and Laloui, L., 2023. Addressing the Challenges of Homogeneity, Quality Control and Waste Handling in Soil Bio-Cementation: A Large-Scale Experiment. *Soils and Foundations* 63, no. 4, 101332. https://doi.org/10.1016/j.sandf.2023.101332.

Terzis, D., Laloui, L., 2019. A Decade of Progress and Turning Points in the Understanding of Bio-Improved Soils: A Review. *Geomechanics for Energy and the Environment*, 19, 100116. https://doi.org/10.1016/j.gete.2019.03.001.

Terzis, D., Laloui, L., Dornberger, S., and Harran, R., 2020. A Full-Scale Application of Slope Stabilization via Calcite Bio-Mineralization Followed by Long-Term GIS Surveillance. In *Geo-Congress 2020*, Minneapolis, Minnesota: American Society of Civil Engineers, 65–73. doi:10.1061/9780784482834.008.

The European Approach to standardize Geotechnical Works for Diaphragm Walls and Bored Piles

Dr. Karsten Beckhaus[1]

ABSTRACT

In Europe, the design, the execution and the testing of geotechnical works such as deep foundations, are standardized through a combination of European Norms (EN). These are authorized by the European Committee for Standardisation (CEN), having passed a systematic and formal process ensuring a broad consensus of all interested parties in the respective construction community.

Guidelines, specific Technical Contract Conditions or other "regulations" from individual parties, like the Recommendations on Piling by the German Geotechnical Society, may complement these general norms. These often comprise more detailed information, reflect individual or local experiences, or just support with additional expert advice. A valuable contribution made by the organisations EFFC and DFI is the Guide to Tremie Concrete for deep foundations (3rd Ed, 2024).

The structural and geotechnical design of piled foundations or retaining walls is standardized in EN 1992 and EN 1997, also known as Eurocodes EC2 and EC7. A series of EN's covers the relevant executions aspects, distinguished by the working methods applied, like jet grouting, deep mixing, or ground anchors, and separated in 13 norms in total, plus a 14th for ground freezing (new work item in progress).

The respective norms for Bored Piles and Diaphragm Walls are EN 1536 and EN 1538 are presently under revision, and the author of this paper is the chairman of the respective working group.

All execution standards shall follow a uniform structure: based on a clear scope (1), respective normative references (2) and defined terms relevant for the norm (3), the following chapters cover the Information needed for the execution of the work (4), Geotechnical investigation (5) and Materials and products (6).

Chapter 7 reveals specific Considerations related to design which are deemed essential to respect for the specific design of a bored pile (including walls) or a diaphragm wall (including barrettes), i.e. expanding the general design rules given in EC2 or EC7. For example, these considerations will comprise --in their revised version-- a classification for the necessary watertightness of a diaphragm wall, or a minimum concrete cover and a minimum clear spacing of the reinforcement to allow complete filling of the excavation and full embedment of all bars in concrete.

„Execution“ is obviously the core of the execution standards, and this chapter 8 covers specific aspects such as tolerances, and basic requirements to be regulated during the actual execution, starting from working platforms, over excavation and cleaning, installation of any reinforcement or others, concreting, until trimming.

Concluding chapters deal with Supervision, Testing and Monitoring, with Records and with Measurements. For future revisions of execution norms, it is envisaged to add a new and specific chapter on Sustainability.

The revision of EN 1536 and EN 2538 has come close to an end by now. Highlights of the future Execution Standard on Bored Oiles and Diaphragm Walls will be presented and set into the context of the principal need for perfectly harmonised and interlinked standards. In turn, if the "combined"

requirements set by European Norms have been respected and implemented in practice, a sufficient quality and integrity of completed geotechnical works must be assumed.

Investigations into a dramatic collapse due to a diaphragm wall excavation - Consequences for quality assurance and risk management in ground engineering

Christian Moormann[1]
[1]Institute of Geotechnical, Engineering, University of Stuttgart, Stuttgart, Germany; christian.moormann@igs.uni-stuttgart.de
[2]Prof. Moormann Geotechnical Consult · MGC, Stuttgart · Cologne, Germany; christian.moormann@moormann-geotechnik.de

EXTENDED ABSTRACT

In the field of geotechnical engineering, risks that materialise can have a significant impact on the serviceability and stability of a geotechnical structure, as well as its construction timeline. Additionally, these risks can potentially affect the surrounding environment. Those risks arise not alone from variable and complex characteristics of the subsoil and groundwater, as well as from design and modelling of the soil-structure interaction, but also from execution process. Hence, risk management must identify various sources of risk and conduct risk analyses to assess the probability and consequences of undesirable events. Risk control and mitigation measures should cover all stages of ground investigation, geotechnical interpretation, design and construction.

These aspects are explored and reflected on the collapse of the Historical Archive of the city of Cologne as an example for a deep diaphragm wall box excavation. On March 3rd, 2009, the collapse of the archive and adjacent buildings occurred during the construction of the new North-South metro line. This incident caused significant damage to the city of Cologne, but also affected the underground construction sector in general. With a total damage sum of around 1.3 billion euros, it stands as the most severe accident on a German construction site to date. The investigation of the damage evidence was a technically challenging task that lasted more than twelve years. It involved numerous steps, including the construction of a 34 m deep investigation shaft. Based on these experiences the consequences for the independent checking of design and execution, for the quality assurance of underground works and their supervision, but also the need for a risk prevention based on communication and partnership between all parties involved in the construction process will be reflected, whereby a special focus will be set on execution and quality assurance for diaphragm walls.

2 RISK ASSESSMENT IN GROUND ENGINEERING

Dealing with uncertainties and risks is an omnipresent task in structural and geotechnical engineering. The key features distinguishing geotechnical and structural engineering are the natural origin of the ground and the lack of sufficient data to characterize the ground using the more familiar frequentist interpretation of probability (Chwala et al., 2022). Therefore, especially for the design of geotechnical structures an appropriate consideration of uncertainties and risks is essential for all engineering stages - from soil investigation, field and laboratory testing, specification of subsoil models and evaluation of soil/ rock properties to calculation with adequate empirical, analytical or numerical models, execution and supervision. The motivation to elaborate risk management and assessment is first and foremost the avoidance of danger to people and property but unquestionable also the elimination of financial and societal consequences a severe failure like the collapse of the historical archive in Cologne can produce.

Sowers (1993) performed a comprehensive analysis of over 500 case studies of reported civil engineering failures (Fig. 1a). The author identifies three main causes of failure: absence, ignorance, and rejection of current technologies. Absence of knowledge or current technology denotes the cause of 12 % of failures (Fig. 1b). This includes lack of data, i.e. the magnitude of a 1000 year return

period extreme weather event. It is argued that “blindly” relying on an estimation, based on the observed time period is ignorance or rejection. Ignorance is encountered by the author often in shape of a “know-it-all” attitude of engineers, who are often not properly qualified or experienced enough for specialized and complex problems. This cause is linked to 33 % of failures. Over 55 % of failures are classified in the rejection category, which includes several different aspects. The major ones that lead to rejection are faulty communications, pressures on the engineer like time, economical or ecological constraints. Thus, 88 % of failures can be appointed to human error. Some of the proposed mitigating measures are persisting engineering education, recognition of limitations and “resisting the unbalanced pressures that thwart good engineering” (Sowers, 1993).

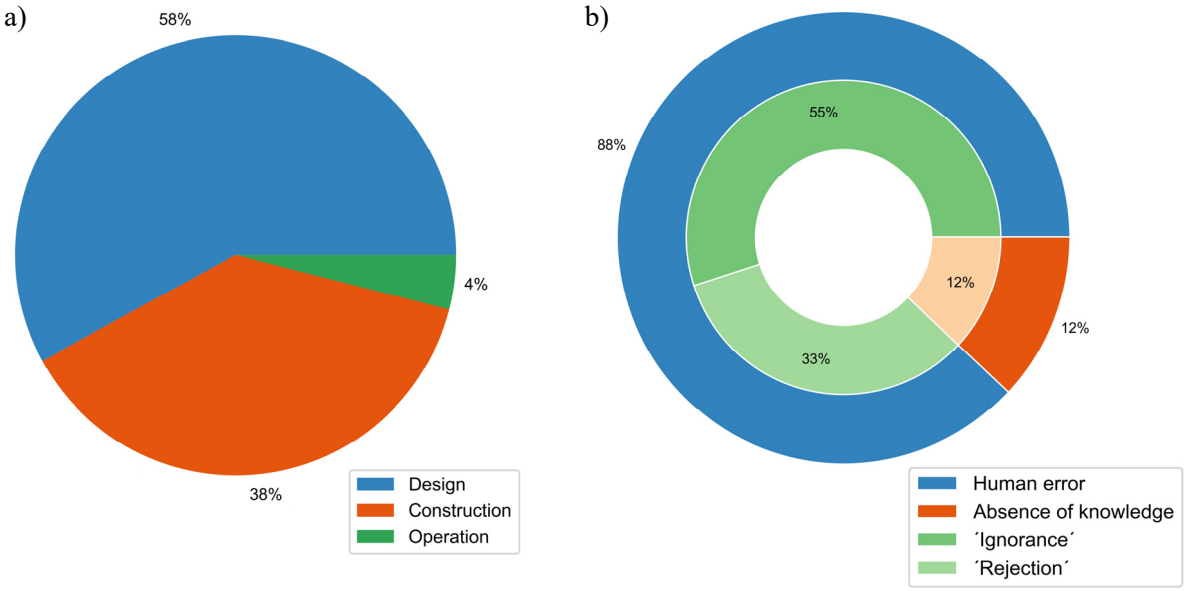

Figure 1. Analysis of over 500 case studies of reported civil engineering failures by Sowers (1993): a) Origin of civil engineering failure; b) Causes of civil engineering failure.

Bea (2006) extends this discussion by reflecting the advances made in the field of quantifying uncertainty due to natural variation or model uncertainty even though these sources account for only 12 % of failures compared to the 88% influenced by human errors. The author introduced a framework that aims to include human, organisational, and knowledge related factors with existing reliability-based techniques.

3 COLLAPSE OF THE HISTORICAL ARCHIVE IN COLOGNE

3.1 Deep excavation ´GWB´

On March 3rd, 2009 the Historical Archive of the City of Cologne, Germany, and adjacent residential buildings collapsed (Fig. 2). These buildings were located at the square ´Waidmarkt´ in the immediate neighbourhood to the deep excavation ´GWB´ which was part of the construction work for a new 4.3 km long north-south underground line in Cologne. At the time of the accident the final excavation level had just been reached around 26.6 m below ground level. The collapse was a dramatic loss for Cologne's urban society but has also a severe impact on other underground and infrastructure construction activities. With a damage amount evaluated to ~1.3 billion euros it was the most serious accident on a German construction site to date (Moormann & Effenberger 2024).

The excavation pit ´GWB´ was constructed with diaphragm walls with wall thicknesses of 1.0 m and 1.5 m. To stabilise against hydraulic ground failure the diaphragm walls were embedded up to 45 m below ground level, i.e. a lower wall edge of 2.8 m above sea level (a.s.l.) in the corner areas and 6.25 m a.s.l. on the long sides of the walls considering the higher hydraulic gradients resulting from the spatial inflow at the corners of the excavation. The retaining walls were anchored in the upper

part and braced by two reinforced concrete slabs constructed during excavation at 10.0 m and 17.3 m below ground level (Fig. 3a).

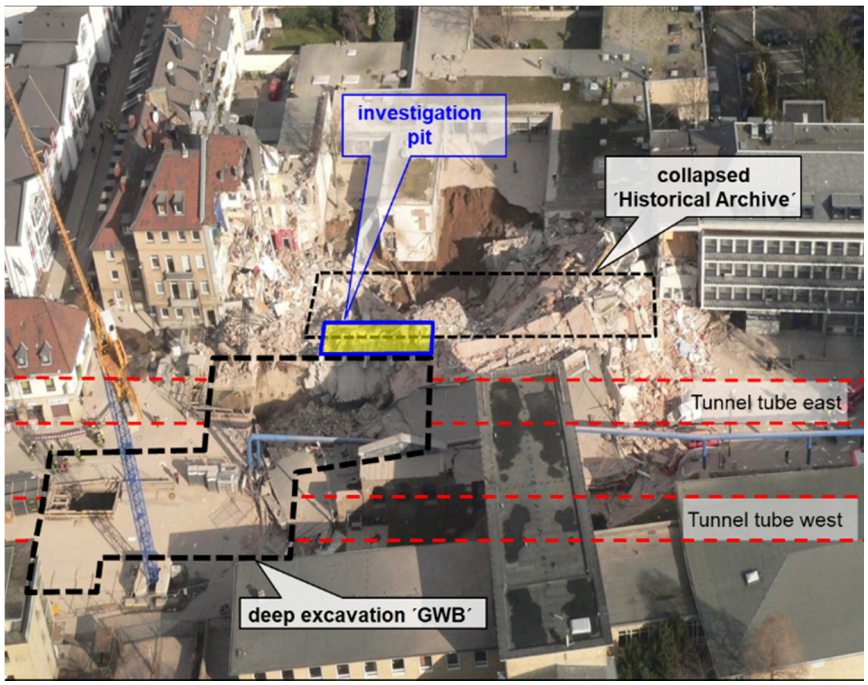

Figure 2. Aerial view of the collapsed Historical Archive and neighbouring residential buildings on Cologne's Waidmarkt immediately after the accident on March 3rd, 2009.

The dewatering in the 'GWB' pit was carried out via wells arranged in the footprint of the excavation pit and filtered in the quaternary and/or tertiary, which led to a lowering of the free groundwater level in the quaternary and a (partial) relaxation of the tertiary aquifer. Within the diaphragm wall enclosure the groundwater level in the quaternary layers was lowered by open dewatering.

a) Before collapse b) After collapse

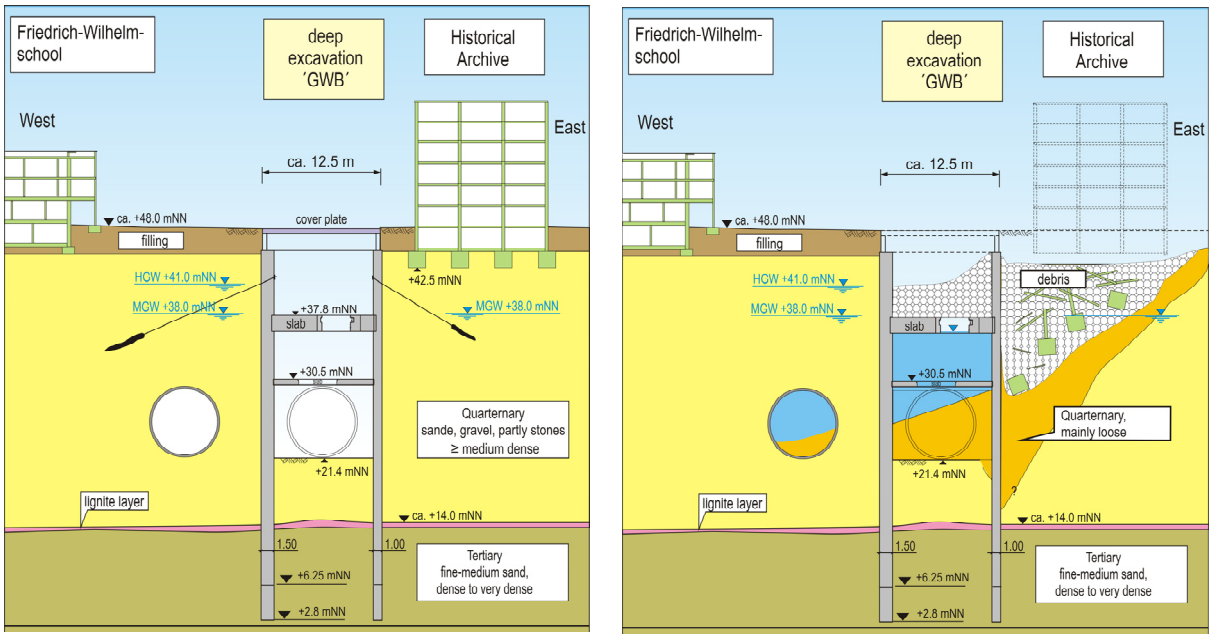

Figure 3. East-west section through the deep excavation 'GWB' with neighbouring buildings and subsoil situation (position of section corresponds to section 1-1 in Fig. 4a).

The subsoil conditions at the ´Waidmarkt´ site are illustrated for an east-west section in Figure 3a. Below street level and up to 6 m thick fillings Pleistocene terrace deposits (Quaternary) down to a depth of around 14 m a.s.l. which consist of terrace gravels and sands of the Rhine of varying grain size and composition. The surface of an Oligocene lignite layer is reached at approx. 14.0 m a.s.l. which was explored in predominantly continuous thicknesses of 0.7 m to 1.8 m, but is also exposed locally. The lignite is underlain by tertiary dense to very dense fine-medium sands which were exposed as a largely uniform layer with a thickness of approx. 48 m down to a depth of -35 m a.s.l. Concerning the groundwater situation, two aquifers have to be considered, a quaternary and a tertiary aquifer. The groundwater levels in the Quaternary follow the water levels of the Rhine, which is located approx. 400 m east from ´Waidmarkt´, with a slight attenuation and generally fluctuate between approx. 36.5 and 40 m a.s.l.

The diaphragm wall was already constructed in 2005 using the conventional two-phase method. As joint system lost flat steel profiles were used which had a smooth surface on the side of the subsequent panel. When excavating the neighbouring panel, the tool used for cleaning the joint and removing concrete that has flowed in behind the joint profiles was therefore not guided by the joint construction. In fact, the cleaning of the diaphragm wall joints resp. stop ends was only partially successful, so that in the course of the excavation leaks occurred in several places at the joints, which required sealing measures to stop local water inflow.

An analysis of the execution records of the diaphragm wall carried out after the accident shows that obstacles were encountered during the production of panels #10 and #11 (for location of panels see Figs. 4b and 5) of the eastern diaphragm wall. During the construction of bite #10.3, obstacles were encountered at a depth of approx. 25 m (21.8-22.8 m a.s.l.) which made the use of a chisel necessary. The problems were even more severe during the following construction of the neighbouring panel #11, which was planned as a 3.4 m wide single bite closing panel being the last panel to be executed for the whole ´GWB´ pit. Massive obstructions were encountered in this panel at a depth of approx. 23 m (23.2-22.8 m a.s.l.), which caused a damage to the grab shells used. This obstruction could not be removed even with the use of chisels. In consequence, the grab shell was changed from 3.4 m to 2.8 m wide and the excavation of panel #11 was continued to the final level. An evaluation of the recorded concrete consumption shows a lower additional consumption for panel #11 compared to the theoretical concrete consumption than for the other panels. It was not possible to precisely analyse the increase or decrease in concrete consumption over the height due to the small number of measuring points; however, a decrease in concrete consumption up to the height of the obstacles encountered is recognisable.

3.2 Collapse of March 3rd, 2009

On March 3rd, 2009, an accident occurred in the deep excavation ´GWB´ during which about 5,000 m³ of sand and gravel flowed into the excavation pit, causing the collapse of the adjacent ´Historical Archive´ of the City of Cologne, a massive 7-storey reinforced concrete skeleton building, immediately adjacent to the excavation pit to the east, as well as of parts of the adjacent multi-storey residential buildings on both sides (Fig. 2). The spread foundation of the Historical Archive, consisting of single and strip foundations founded in the quaternary sands and gravels, sank into the ground (Fig. 3b); foundations were later recovered from a depth of up to 20 m below ground level. This sudden “loss of foundation” caused the building to tilt towards the street, then to completely collapse, thereby partly falling into the excavation pit, breaking through its covering. The soil inflow at the lowest level of the excavation pit resulted in the formation of a cone of debris up to 7 m high consisting of quaternary sands and gravels, the foothills of which reached into the four tunnel tubes (Fig. 4a) and whose greatest height was directly in front of the eastern diaphragm wall (Fig. 3b). Although the workers fleeing from the final excavation level of the ´GWB´ pit who had noticed a rapidly increasing water and then soil ingress during final excavation and construction of a pump sump in front of the eastern diaphragm wall, warned visitors to the Historical Archive and residents of the neighbouring residential buildings of the impending accident at the proverbial last minute, two young residents died in the subsequent collapse of the residential buildings. At that moment, around 30 linear kilometres of archives from 1,200 years of Cologne´s regional history, the

city's memory that has grown over the centuries, seemed to have been destroyed within seconds and lost forever.

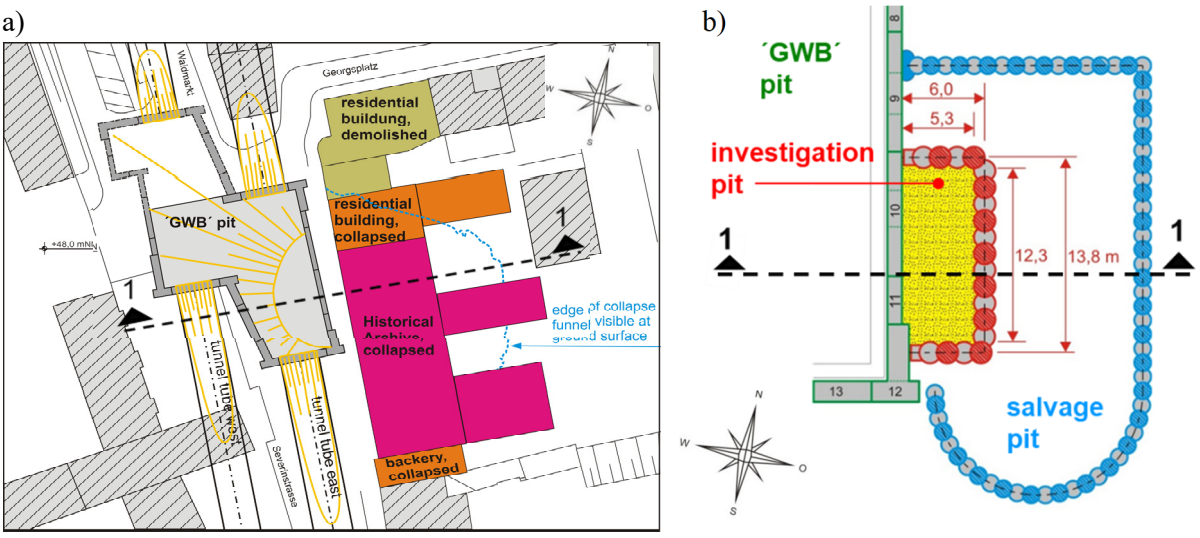

Figure 4. Site plan of the deep excavation ´GWB´ at ´Waidmarkt´ square in Cologne, a) at the time of the collapse, b) southeastern corner of the excavation ´GWB´ with salvage pit and investigation pit.

After phases of immediate stabilisation, salvage and an initial survey, the cause of the damage was investigated through a technically highly demanding investigation of evidence lasting more than twelve years, during which, among others, a 34 m deep inspection shaft was executed in direct neighbourhood to the potentially damaged diaphragm wall of the deep excavation ´GWB´.

3.3 Indirect investigations

Immediately after the collapse subsoil investigations were carried out to clarify the subsoil conditions and to examine the stability of the excavation pit and of the surrounding buildings including several public secondary schools. These investigations already formed a dense grid, including a total of 113 core drillings, 260 heavy dynamic probing tests (DPH), 186 borehole dynamic probing tests (BDP) and 18 cone penetration tests (CPT). These investigations made it possible to identify the centre of the damage to a tightly confined area in the vicinity of panel #11 in the eastern part of the diaphragm wall of the ´GBW´ pit (see Fig. 4b).

The core drillings being modified to monitoring wells were used to investigate the integrity of the eastern diaphragm wall of the ´GWB´ excavation pit by applying indirect methods. In particular, seismic cross-hole tomography was successfully used to check the presence, quality and integrity of the diaphragm wall panels. The planned geometric embedment of the diaphragm wall panels could be verified, but at the same time, in the area of the joint between the adjacent panels #10 and #11 at a depth of approx. 16 m to 23 m a.s.l., i.e. between the final excavation level down to the quaternary base, significantly reduced local wave velocities were clearly recognisable identifying anomalies (Fig. 5). Supplementary thermographic investigations by fibre-optical temperature measurements in combination with the heat pulse method showed significant temperature anomalies in the groundwater flow and thus clear indications of hydraulic pathways in the area of the joint between the diaphragm wall panels #10 and #11 in a depth range of approx. 13 m to 20 m a.s.l. (Fig. 5).

In accordance with anomalies identified during the construction of diaphragm wall panel #11, the results of the investigation gave rise to the suspicion that the accident was probably due to one - or possibly several - defects in the joint area of the eastern diaphragm wall, in particular in the joint area between panels #10 and #11 at a level between the final excavation level and the lignite layer (Fig. 5), while a hydraulic ground failure was largely ruled out as the cause of the failure.

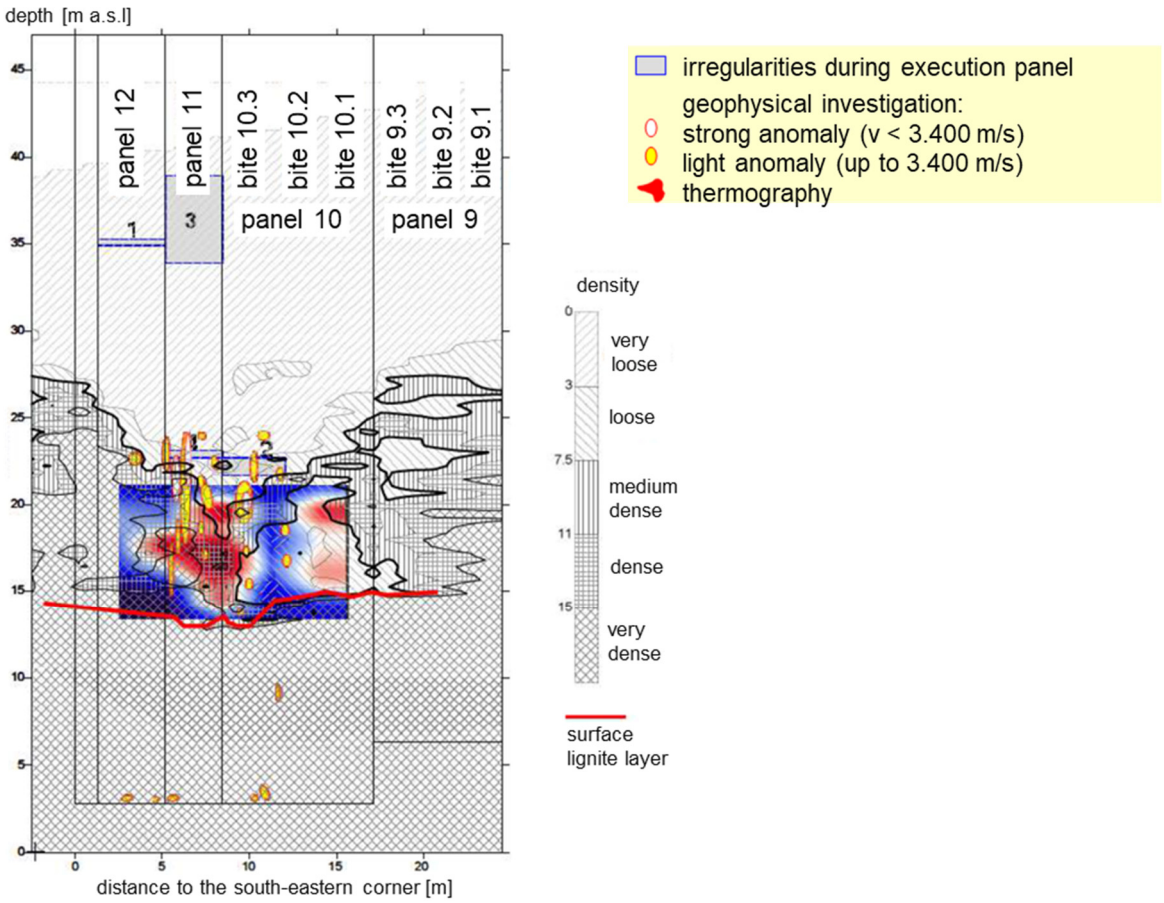

Figure 5. View of the eastern diaphragm wall of the ´GWB´ pit (looking west) with compilation of the results of all indirect exploration measures (source: expert report by Prof. Kempfert (2011-2020), modified).

3.4 Investigation pit

While the numerous indirect investigations had already provided reliable indications of the cause of the damage related to "Suspected area of diaphragm wall quality", a direct visual inspection of the suspected areas was required to dispel the last possible doubts regarding the cause of the damage. This investigation pit, located in the centre of the collapse funnel in front of the diaphragm wall panels #10, #11 and #12 of ´GWB´ pit, had comparatively small ground plan dimensions of around 5.3 m x 12.3 m (clear internal dimensions, see Fig. 4b) and was intended to allow inspection of both the diaphragm wall and - layer by layer - the subsoil conditions down to the surface of the lignite layer, which was expected at 14.0 m to 14.8 m a.s.l. in the construction area of the investigation pit, i.e. at a depth of 34 m below street level. The investigation pit was designed for underwater excavation and inspection by divers. In a second stage, it was considered as a supplementary option, to deballast the inspection pit using compressed air, what was finally not realized. The investigation pit was braced by steel bracing frames in a total of eight levels (Fig. 6). This bracing solution ensured that the eastern diaphragm wall of the ´GWB´ pit was supported almost over its entire surface. To stabilise the diaphragm wall joints, a frozen ground body was arranged on the inside of ´GWB´ pit, i.e. to the west of the eastern diaphragm wall, within the soil volume deposited in this area ('cone of debris') in the course of the accident and in the quaternary sands and gravels between the former final excavation level in the ´GWB´ pit the lignite layer in the area of the two diaphragm wall joints of panels #10 and #11 and of panels #11 and #12 to be inspected (Fig. 6).

The excavation and exploration of evidence in the inspection pit began in January 2014 and was completed in July 2020 with the excavation of the surface of the lignite. All of the work had to be carried out by divers at increasingly great depths, which was a key boundary condition.

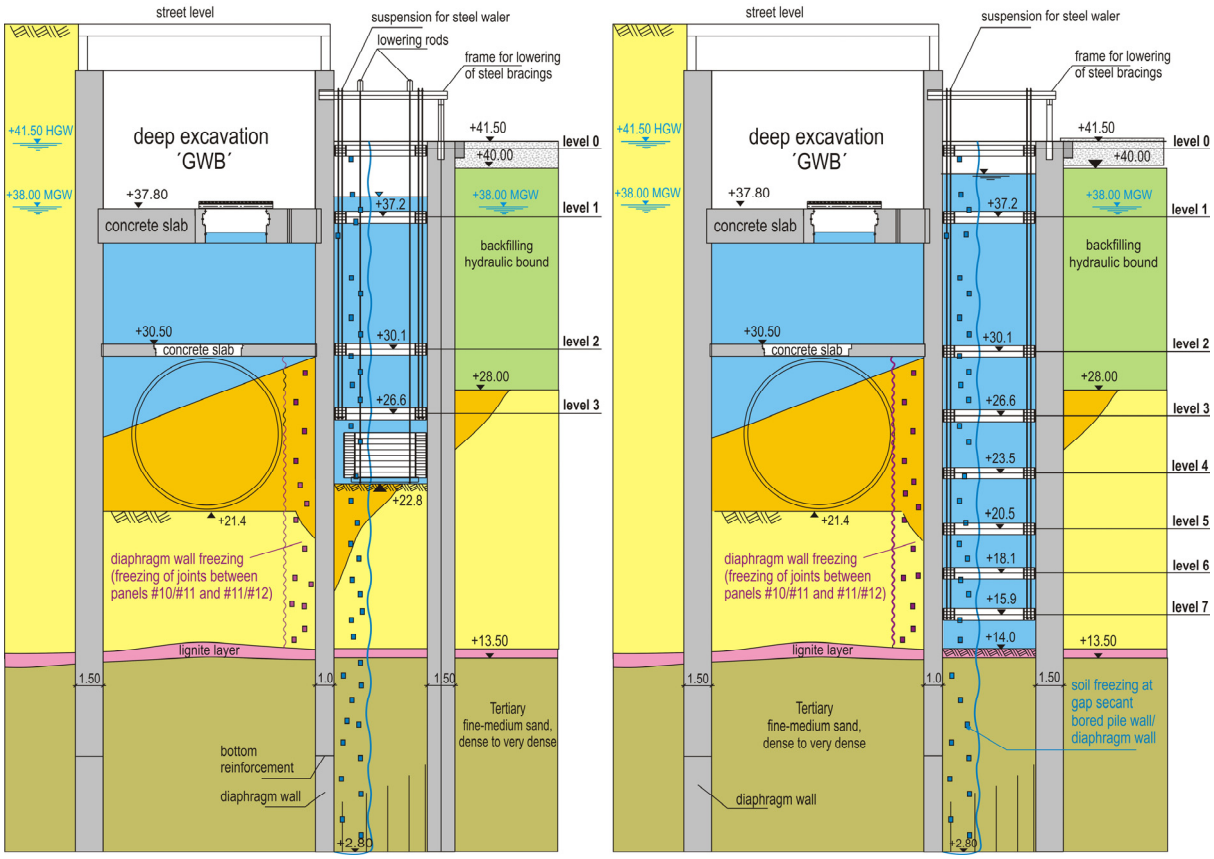

Figure 6. Construction sequence of the inspection pit (west-east section, selected stages).

During the successive excavation of the investigation pit, not only the detailed documentation of the excavated soil material was carried out as described, but also a comprehensive survey of the diaphragm wall surface. The underwater recording consisted of several elements that were applied in each 0.5 m excavation step: In addition to an initial video recording by the diver´s helmet camera, a) a recording with a high-resolution video, b) a recording with an underwater laser scanner and c) a manual-electronic measurement of the geometry of the diaphragm wall surface (only in the case of anomalies) were carried out geometrically referenced by a guide construction. In addition, the diaphragm wall surface was recorded with a sonar device. As a result of these recordings, the expert and his divers were able to provide a complete graphic-visual and photogrammetric documentation of the diaphragm wall surface down to a depth of 34 m below street level in outstanding quality. The area of the joints between panels #10 and #11 as well as between panels #11 and #12 was examined with particular care. When joint fillings and defects were encountered, the joint or void material was completely collected in special trays and the joint/ defect geometry was documented using the afore-mentioned methods and with the additional use of smaller GoPro cameras for the interior and flanks of the joints/defects.

3.5 Cause of the collapse

In the course of the exploration carried out in this way, in the area of the joint between panels #10 #11, from a depth of approx. 25.2 m a.s.l. on, concrete increasing in width by depth was detected, which extended from panel #10 into panel #11 (Fig. 7) and reached a width of around 600 mm at a depth of approx. 23.0 m a.s.l. A large natural boulder was encountered beneath this concrete from panel #10 at a depth of 22.1-21.4 m a.s.l. and thus directly at or below the final excavation level in the ´GWB´ excavation pit to the south of the panels #10/#11 joint, i.e. in the cross-sectional area of panel #11 (Figs. 7 and 8). The trachyte boulder with a diameter of around 600 mm and a length of

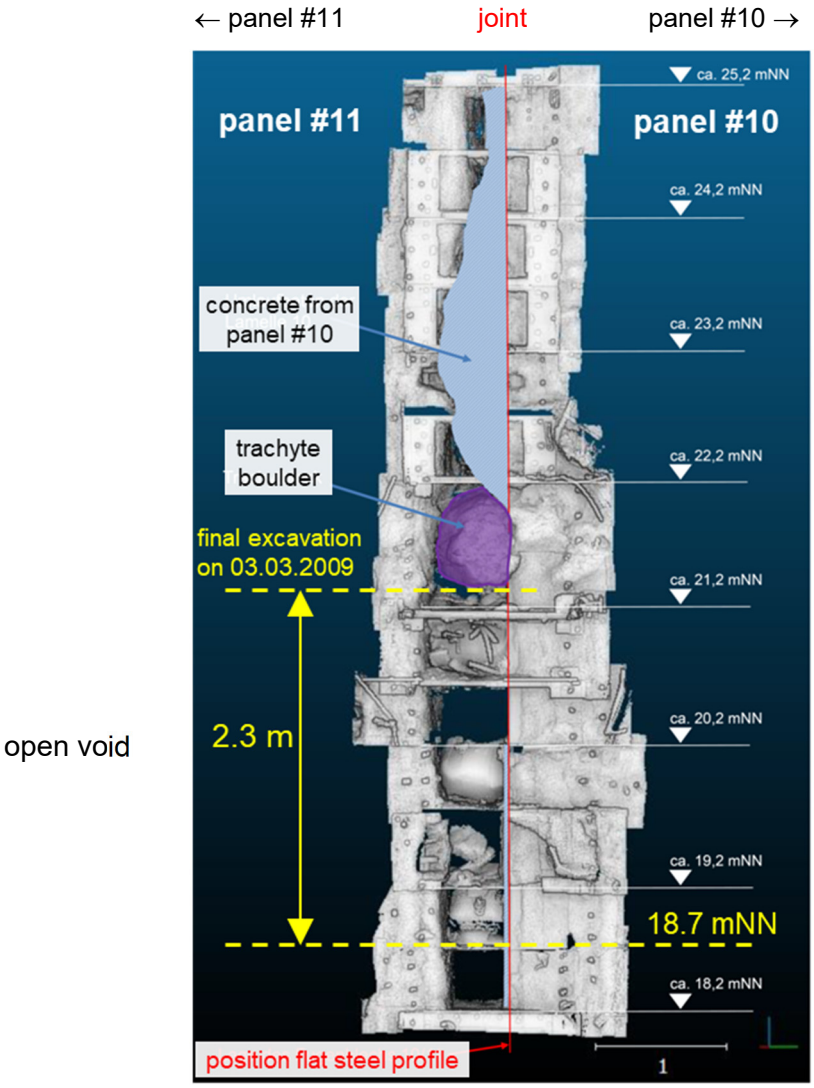

Figure 7. Compiled visualisation of the explored situation in the joint area of the diaphragm wall panels #10/#11 (evaluation of the underwater laser scans based on Kempfert (2011-2022)).

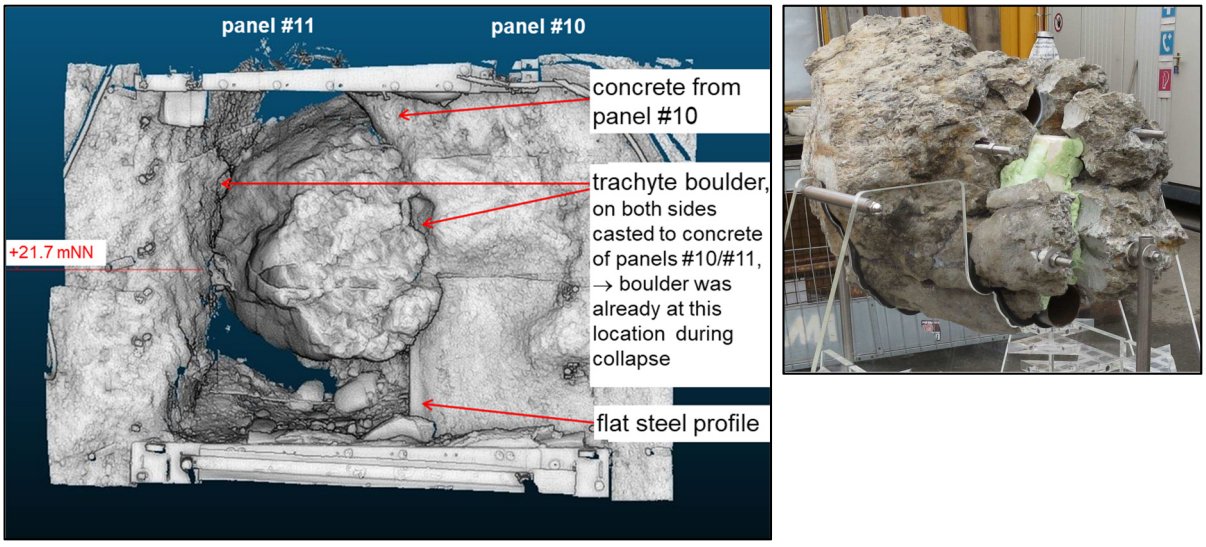

Figure 8. Natural boulder (trachyte) from the joint between panels #10 and #11, a) underwater laser scan in situ, b) recovered and assembled block (basis: Kempfert (2011-2022), modified).

around 1.20 m was first extensively documented in situ. It was then divided into two half-shells with the help of guided overcut horizontal drillings, which were carried out with an underwater drilling template approximately in the centre of the block, and recovered from the joint using anchors. In dry conditions, the boulder was reassembled and examined (Fig. 8b). Traces of the teeth of diaphragm wall grabs were found on both the northern and southern sides of the boulder; traces from the reinforcement cage of panel #11 were also found on the southern side. These traces prove that the natural boulder was already in the position encountered during the exploration of the evidence when panel #11 was executed (Fig. 9). In conjunction with the triangularly growing concrete from panel #10 found above it, it can be concluded that the natural boulder was encountered in the course of the execution of panel #10 and was displaced into the ground section of the later panel #11 during the attempt to salvage it, without the salvage being successful (Fig. 9). During the construction of panel #11, the boulder was then not removed from under the overlying concrete; after the change from the 3.4 m to the 2.8 m wide grab shells, the teeth of the diaphragm wall grab merely "scraped" along the natural boulder (Fig. 9). Under the trachyte boulder, a continuously open void up to 600 mm wide and filled with quaternary material was encountered in the further excavation over the depth, which, although only explored up to the surface of the lignite, is expected to be open to the lower edge of the diaphragm wall. Based on the distribution of anthropogenic findings, colour changes of the in-situ soil material and other indicators such as the erosion/ presence of the filter cake in the joint surfaces, it was possible to identify and to prove that the base of the "moving" masses (collapse funnel) in the void lies at a level of around 18.7 m a.s.l. In consequence it can be concluded that the area of the void through which around 5,000 m³ of quaternary material flowed in the course of the accident is only around 2.3 m high and about 600 mm wide and therefore has an area of only approx. 1.5 m² in total.

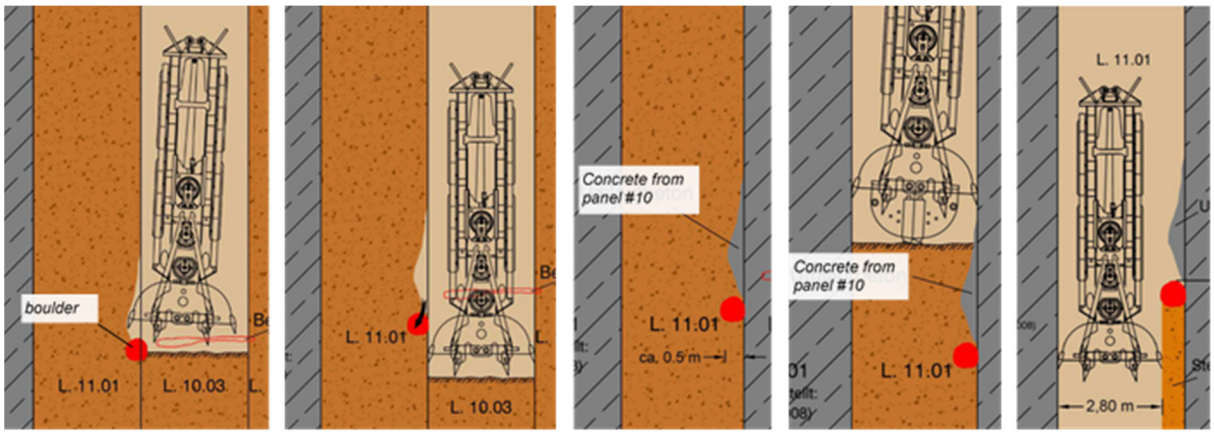

Figure 9. Construction sequence of the panels #10 and #11 of the eastern diaphragm wall with the natural boulder (trachyte, marked in red) encountered during execution of both panels.

3.6 Conclusions

As a result of the highly complex preservation of evidence procedure and investigations it was possible to clarify the cause of the damage clearly and beyond doubt. As a result of the investigations carried out from 2009 to 2020, the accident on March 3rd, 2009 can be attributed solely, i.e. mono-causally, to a defect that remained in the joint area between two panels during the construction of the diaphragm wall. In the area of the joint between the panels #10 and #11 an approximately 600 mm wide void was found below approx. 21.7 m a.s.l., i.e. at about the level of the final excavation of the ´GWB´ pit downwards. This defect results from the fact that the existing soil material in this area had not been excavated and replaced by concrete during the construction of diaphragm panel #11.

The cause of the damage can therefore be traced back to an execution issue respectively to the fact that suitable countermeasures were not taken in response to the difficulties encountered during the execution of panel #11 of the diaphragm wall in 2005. The obstacles encountered during excavation of this panel and the failure to remove these obstacles, finally the change of the grab shells from

3.40 m to 2.80 m wide for excavation of the 3.4 m wide, single bite panel #11 were an unambiguous evidence that the panel #11 was not executed in a regular way and that from the depth where the grab shells were changed most probably a 600 mm wide void filled with quaternary sand and gravels was left.

Technically, it would have been possible to reliably seal the remaining defect in panel #11, for example with one or two columns executed using the jet grouting method.

Against the background of these results of the investigation of the evidence, the City of Cologne and the construction JV, which still assumed an alternative course of events, reached an out-of-court agreement in a moderated procedure to settle the financial loss incurred by the City of Cologne and concluded finally on a settlement in June 2020. According to this settlement the construction JV paid 600 million euros in damages to the City of Cologne and committed themselves to reconstruct the damaged ´GWB´ excavation pit and to finalize this structure at its own expense and under its own responsibility.

Currently it is expected that the very challenging reconstruction activities will last until about 2032, what means that it will have taken nearly 25 years from the occurrence of the damage to its removal and to the moment the first metro train will have run through the ´GWB´ underground structure at the ´Waidmarkt.

4 RISK PREVENTION AND MITIGATION

Risk prevention and risk mitigation are important tasks in order to avoid collapses and damages. Based on experiences from damages consequences for the independent checking of design and execution, for the quality assurance of underground works and their supervision, but also the need for a risk prevention based on communication and partnership between all parties involved in the construction process needs to be implemented especially but not solely for major projects and especially in ground engineering including diaphragm wall excavations.

Besides measures and approaches for risk management and assessment during design the successful realisation of geotechnical structures in engineering practice requests the following additional measures especially related to checking and quality assurance:

1. An independent structural and geotechnical checking is essential and must include both,
   a. the checking of the design and all verifications and
   b. the supervision and monitoring of the execution.
2. For all stages of soil investigation, design, execution, checking and supervision geotechnical expertise and experience is required; therefore it is mandatory to involve an independent geotechnical checking engineer at least for structures of the Geotechnical Category 3 according to EN 1997-1.
3. The (independent) supervision of execution of special geotechnical works like e.g. piling, diaphragm walls, ground improvement and injections has to be carried out by qualified and experienced experts on site.
4. A risk prevention in partnership needs to be established and practiced in all phases of planning and realisation. In this context a regular communication on technical level between client, contractors, designers and the independent checking engineer is essential. Such a regular communication, e.g. organisationally to be implemented by jour fixes, allows also to identify and discuss any irregularities and anomalies occurred during execution.

All of the above measures are relevant and needs to be established but especially a regular technical communication between all parties is considered to be an essential tool for risk prevention and mitigation during the execution.

In this regard the presented case study of the collapse of the ´Historical Archive´ at the Waidmarkt in the city of Cologne is an example where irregularities during execution of the diaphragm wall were observed and documented but were subsequently not pursued further neither internally inside the construction companies nor in communication with the owner´s independent supervision and by the owner itself. As shown in this paper human factors have been identified as main cause for failure on site and one of the major impacts are faulty communications as well as pressures on the involved people like time, economical or ecological constraints. In this regard, an open-minded communication focused on technical aspects and a partnership-based approach are considered to be effective mitigating measures for risks in geotechnical engineering and execution.

REFERENCES

Bea, R. 2006. Reliability and human factors in geotechnical engineering. J. of Geotech. And Geoenviron. Eng. Vol. 132(5), pp. 631-643. doi.org/10.1061/(ASCE)1090-0241(2006)132:5(631)

Chwala, M., Phoon, K.-K., Uzielli, M., Zhang, J., Zhang, L., Ching, J. 2022. Time capsule for geotechnical risk and reliability. *Georisk: Assessment and Management of Risk for Engineered Systems and Geohazards*, 17:3, pp. 439-466. doi.org/10.1080/17499518.2022.2136717

Kempfert, H.-G. (2011-2020): Beweisverfahren KVB und Stadt Köln ./. Arge Nord-Süd Stadtbahn Köln, Los Süd u.a. (Einsturz des Historischen Archivs der Stadt Köln). Landgericht Köln 5 OH 1/10. Sachverständigengutachten Teil I bis X, (in German, not published).

Moormann, Ch. & Effenberger, M.J.P. 2024. Risk analysis and mitigation in geotechnical engineering – Lessons learned from the collapse of the historical archive in Cologne due to underground construction. Keynote Lecture, *Proc. XVIIIth European Conf. on Soil Mechanics and Geotechnical Engineering*, ECMGE 2024, 26-30 August 2024, Lisbon, Portugal, CRC Press, Taylor & Francis Group, Balkema, pp. 45-71. DOI: 10.1201/9781003431749-03

Moormann, Ch. 2025. Collapse of the historical archive of the city of Cologne due to underground construction – Damage analysis and conclusions for quality assurance and risk management in geotechnical engineering. *Proc. 2nd South African Geotechnical Conference*, SAGC 2025, 29-30 May 2025, Durban, KwaZulu-Natal, South Africa, S.W. Jacobsz (ed.), pp. 3-18.

Sowers, G. 1993. Human factor in civil and geotechnical engineering failures. *J. Geotech. Eng*., Vol. 119(2), pp. 238-256.

This page is intentionally left blank

Do We Really Understand Our Deep Shear-Wave Velocity Profile? Case of Depok Campus of Universitas Indonesia

Widjojo A. Prakoso[1], Lingga E.L. Suryajaya[1], Sigit Pramono[2]
[1] Universitas Indonesia, [2] Badan Meteorologi, Klimatologi, Geofisika
(e-mail: wprakoso@eng.ui.ac.id)

Many parts of Indonesia are seismically active, and the Depok Campus of Universitas Indonesia is one of those areas with high seismic risks. Within the Depok Campus, there are three accelerometers installed by the Indonesian Agency for Meteorological, Climatological and Geophysics, including one accelerometer installed at a depth of 300m paired with a surface accelerometer. The geotechnical characteristics of the location have been surveyed using geotechnical and geophysical methods. One of the seismic events recorded by these accelerometers was the 14 January 2022, M=6.6 Banten earthquake; this event was located about 210 km from the Depok Campus and consequently a low-strain event. The recorded ground motions are subsequently used to evaluate the deep shear-wave velocity profiles of the location using the site response analysis program DEEPSOIL. Different profiles are generated in an attempt to match the peak acceleration of the event ground motion records and simultaneously to match the corresponding response spectra. Based on this experience, a critical discussion on our understanding of the deep shear-wave velocity profiles is offered.

This page is intentionally left blank

Comparison of Cast-in-Situ Diaphragm Wall for Deep Basements in Indonesia: Continuous Water Stop (CWS) System and Continuous System

Juse Roejanto[1], Harianto Hardjasaputra[2]
[1]Graha Pondasi Semesta, Jakarta, Indonesia, 14240; roejanto68@gmail.com
[1]Civil Engineering Departement, Faculty Engineering, Pelita Bangsa University, Cikarang, Indonesia, 17530; roejanto68@gmail.com
[2]Civil Engineering Department, Faculty Engineering, Pembangunan Jaya University, Tangerang, Indonesia, 15413; hardja@yahoo.com
*Correspondence: roejanto68@gmail.com

ABSTRACT The increasing development of tall buildings are being developed with deep underground basements, it is essential to carry out reliable underground planning and select appropriate construction methods. A key and early consideration in underground construction is the design of earth-retaining walls and how it will be constructed. Various types of retaining walls are available, and one widely used method is the cast-in-situ diaphragm wall. The construction of diaphragm walls can generally be classified into two systems, the continuous water stop (CWS) System and the Continuous System. Both systems are recommended for buildings designed with more than three basement levels, or for other structures with deep excavations, such as MRT stations or power houses in power plant facilities. This research is based on qualitative method, used data collected from foundation contractors, field observations, and interviews with site managers and supervisors of foundation contractor with period time from 2005 until 2020. During panel excavation, both diaphragm wall systems utilize a slurry stabilizer (bentonite or polymer), prepared with the specified mix design to prevent the panel collapse. The CWS System applies a CWS form and rubber waterstop, with the joint removed using a chisel when excavating the adjacent panel. The Continuous System begins with excavation of the female panel, followed by the male panel. The waterstop in this system uses an endplate installed simultaneously with the fabrication of the reinforcement cage. In the CWS System, reinforcement between panels is discontinuous, In the Continuous System, the reinforcement is continuous across adjacent panels. In the CWS system, there are levels of implementation difficulties such as removing the CWS Form and in the continuous system, implementation difficulties such as inserting the male panel steel cages into the female panel, and all systems need to be strengthened to prevent horizontal movement during basement excavation according to the structural planner's design.

KEYWORDS Diaphragm Wall; Cast in Situ; CWS System; Continuous System

1 INTRODUCTION

With increasingly limited land, especially in major cities, and with the increasingly massive development of tall buildings planned to have deep basements, it is necessary to have a proper and accountable basement plan both technically and in terms of construction methods. According to (Chew Yit Lin, 2025) the Council on Tall Buildings and Habitat (CTBUH), tall buildings are divided into tall categories (height ≥ 50 m), supertall (height ≥ 300 m) and megatall (height ≥ 600 m). Planning a basement for a tall building requires accurate calculations of retaining walls, especially to withstand very large horizontal forces during basement excavation. There are many types of retaining walls that can be used, as shown in Figure 1. Classification of retaining walls according to (O'Rourke, 1990). Cast-in-situ retaining wall systems such as soldier piles (bored piles), cement-bentonite walls, secant pile walls, and diaphragm walls, are widely utilized as structural basement walls in deep excavations.

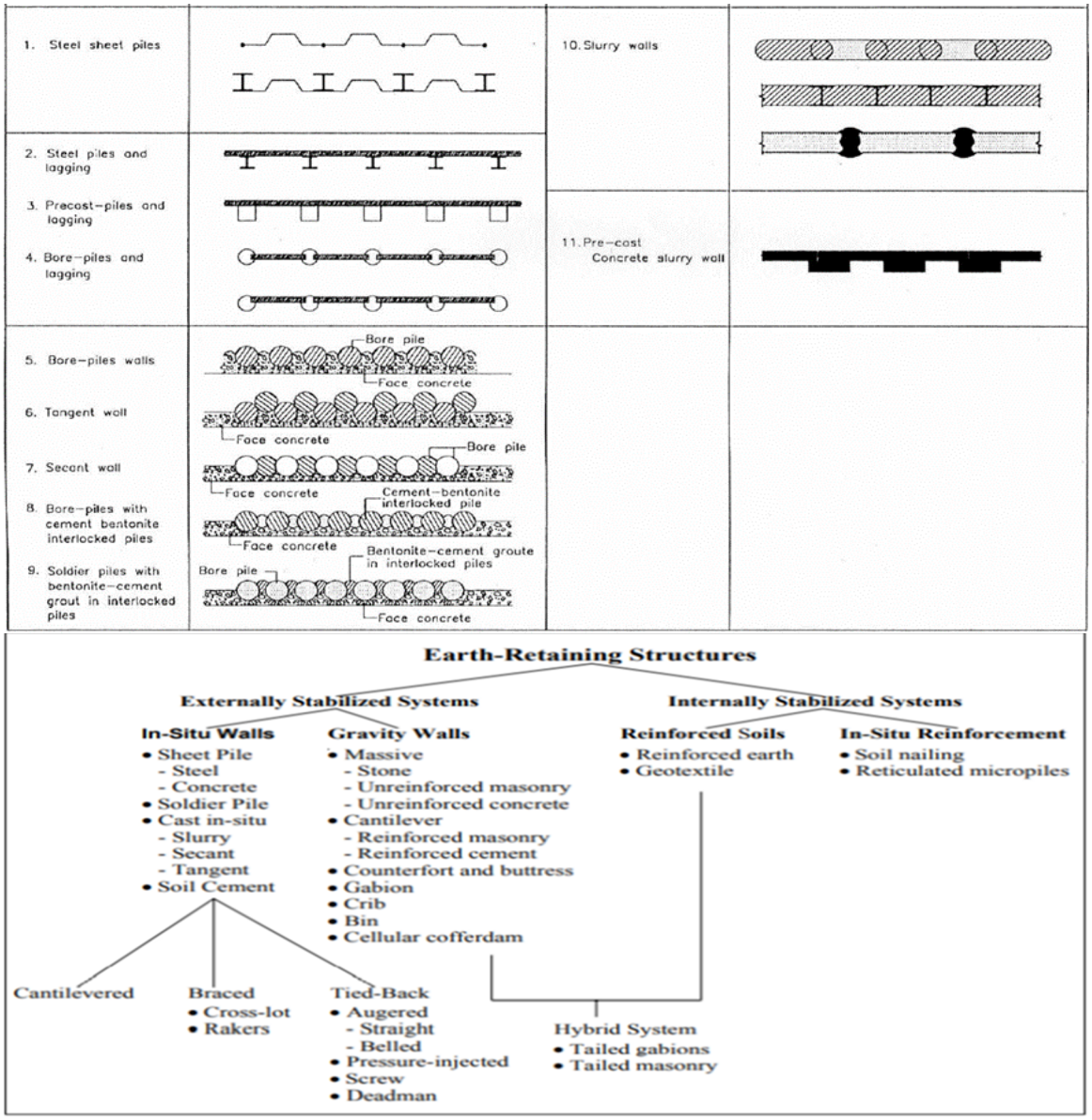

Figure 1. Earth Retaining Structure Classification

With the rapid advancement of technology, in situ earth-retaining wall systems have undergone significant development. Various types of in situ earth-retaining walls can be seen in Figure 2.

Figure 2. Type of Retaining Structure in Situ Walls

Nowadays, many tall building basement designs utilize diaphragm walls cast in situ. For basement levels exceeding three, it is recommended to use diaphragm walls (Hardjasaputra, 2014). A diaphragm wall is a type of earth-retaining wall that also serves as the structural basement wall in buildings with deep basements. In practice, cast in place diaphragm walls can be constructed using two systems: the continuous Water Stop (CWS) system and the continuous system. Both systems are applicable to all soil types, including fine-grained and coarse-grained soils.

The Main equipment for working on diaphragm wall excavation is a grabber mounted on a crawler crane, the types of grabbers can be seen in Figure 3.

Figure 3. Type of Grabber for Excavation

During the excavation of planned diaphragm wall panels, grabbers are used in conjunction with the introduction of slurry stabilizers such as bentonite or polymer (Arun Kumar, 2024) to ensure panel stability and prevent collapse. Diaphragm walls belong to the category of embedded walls (Nasional, 2017). Horizontal support systems are required once basement excavation begins to withstand lateral earth pressures. These supports can include strutting, ground anchors (J.Josifovski, 2011) or selected basement floors acting as king posts, particularly when the top-down method is used. In Indonesia, cast-in-situ diaphragm walls have been widely implemented in tall buildings such as Plaza Indonesia, BII Plaza, Pasar Tanah Abang Blocks A & B, Grand Indonesia, Thamrin Nine (Autograph Tower), JW Marriott Hotel Medan, Sahid Lifestyle Yogyakarta, Indonesia One, and other buildings also in several “underground MRT Jakarta stations”.

1.1. Diaphragm Wall Continuous Water Stop (CWS) System

Field execution begins with the construction of guide walls, which are tailored to match the thickness of the diaphragm wall, along with the installation of the slurry plant. Once preparations are complete, the initial stage involves excavating the primary panel using grabbers. During this excavation process, a slurry stabilizer either bentonite or polymer is simultaneously introduced into the excavation trench, as illustrated in Figure 4.

The excavation process follows the width of the grabber used. For instance, if the panel width is six meters, the excavation is carried out in three stages: first the side sections (left and right), followed by the remaining central section, continuing down to the planned depth. Next, the CWS form, pre-installed with rubber waterstops on both sides is positioned. The prepared reinforcement cage is then lowered into the panel using a service crane. Afterward, the tremie pipe is inserted, and concrete casting can commence once a sufficient supply of ready-mix concrete is available. Upon completion of the casting process, the CWS form (Arun Kumar, 2024) is removed from the adjacent panel side that will be excavated next. This sequence continues repetitively until all panels are completed. The construction method is illustrated in Figure 5.

Figure 4. Panel Excavation & filling slurry stabilizer

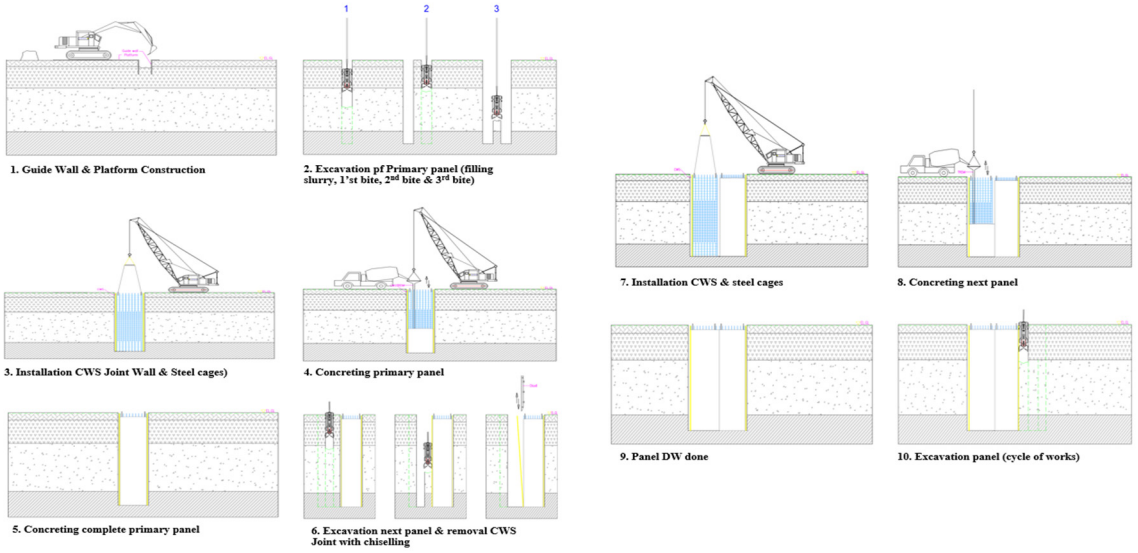

Figure 5. Method of Work Continuous Water Stop (CWS) System

The characteristic of this system is the use of a prefabricated formwork that must be prepared beforehand, which also serves as the housing for the waterstop. The waterstop material used is rubber. The reinforcement between panels is discontinuous, leaving a gap of approximately 30 cm between adjacent panels where no reinforcement is placed. To remove the CWS form, a chisel may be dropped freely along the guide rail of the CWS form or alternatively, the form can be detached using a grabber with an installed release mechanism. An example of the CWS form can be seen in Figure 6, while various CWS form types and rubber waterstop samples are illustrated in Figure 7.

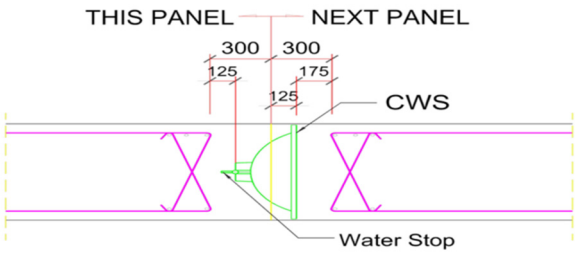

Figure 6. CWS Form

Figure 7. CWS Form & rubber waterstop

The reinforcement details of the panels, along with the specifications of the rubber waterstop, are illustrated in Figure 8.

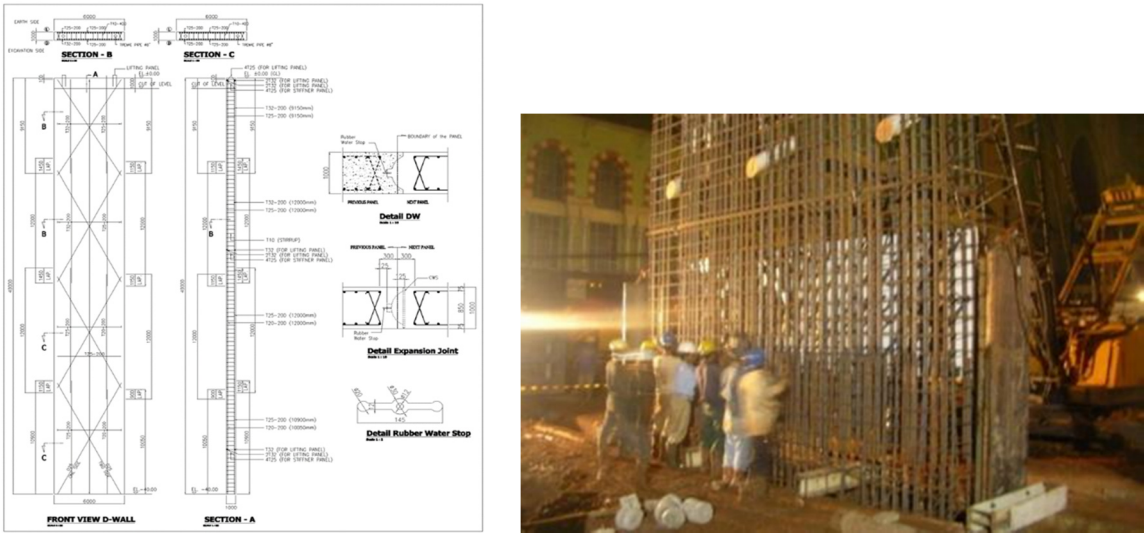

Figure 8. Reinforcement CWS System & Detail Rubber Waterstop.

In the reinforcement layout, provisions for ground anchor sleeves and block-outs for floor and slab penetrations can be added according to the elevation and the number of layers, especially if the design includes ground anchors as horizontal support during basement excavation. To remove the CWS form, the chiseling method may be employed, as illustrated in Figure 9.

Figure 9. Pullout CWS Form with Chiselling

1.2. Diaphragm Wall “Continuous” System

The execution of this system generally follows the same procedure as the CWS system, beginning with the construction of guide walls, installation of the slurry plant, and division of panels according to the basement layout. The construction sequence for this system must start with the excavation of the female panel, followed by the excavation of the male panel, and so on.

For the reinforcement of the female panel, a plastic sheet is placed over it to prevent intrusion by ready-mix concrete during the casting process. The difference between this system and CWS system is the use of continuous reinforcement across panels, as illustrated in Figure 10.

The joint detail and waterstop used in this system incorporate an end plate that is continuously installed along the reinforcement of the diaphragm wall, (El-Razek, 1999) as illustrated in Figure 11.

The reinforcement in the female panel is covered with a plastic sheet, as illustrated in Figure 12.

During the casting of ready-mix concrete in the female panel, if any concrete leaks into the male panel, a cleaning box is required to remove the leaked material from the joint between the two panels, as illustrated in Figure 13.

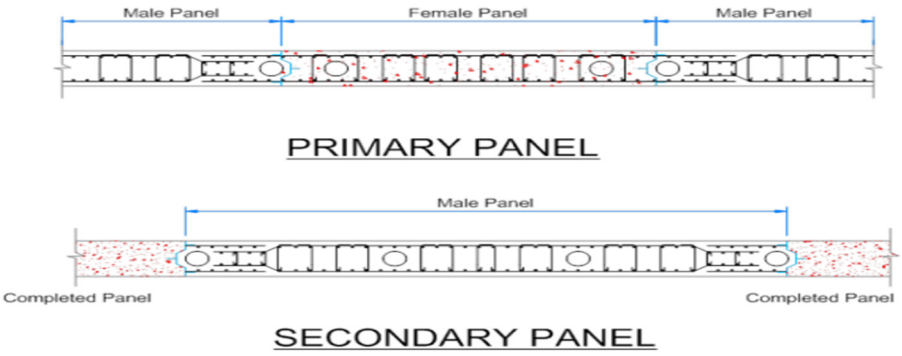

Figure 10. Reinforcement Continuous System

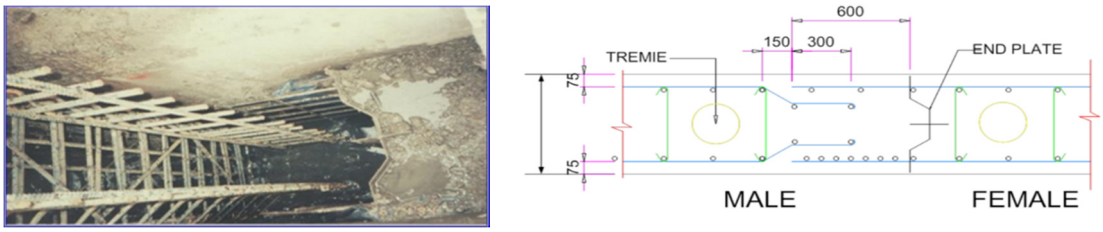

Figure 11. Joint Detail & Waterstop Continuous System

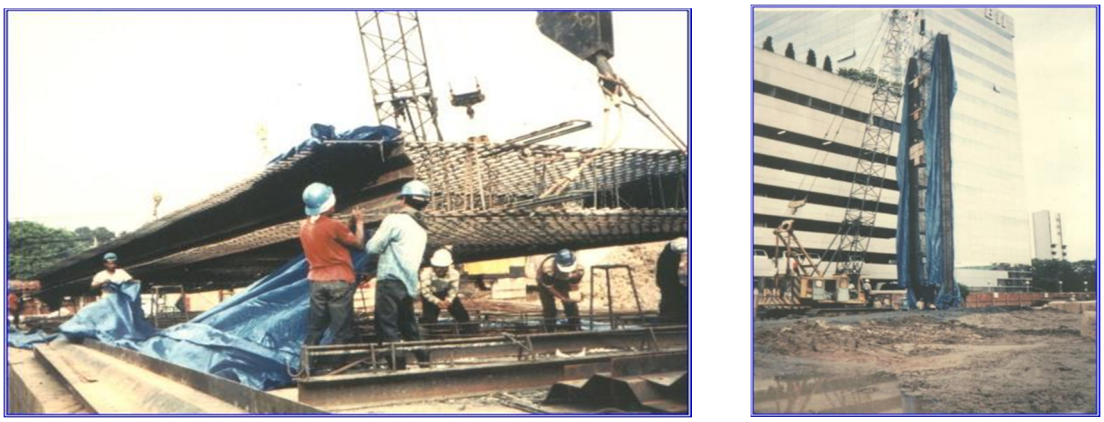

Figure 12. Steel cages & plastic sheet on female panel

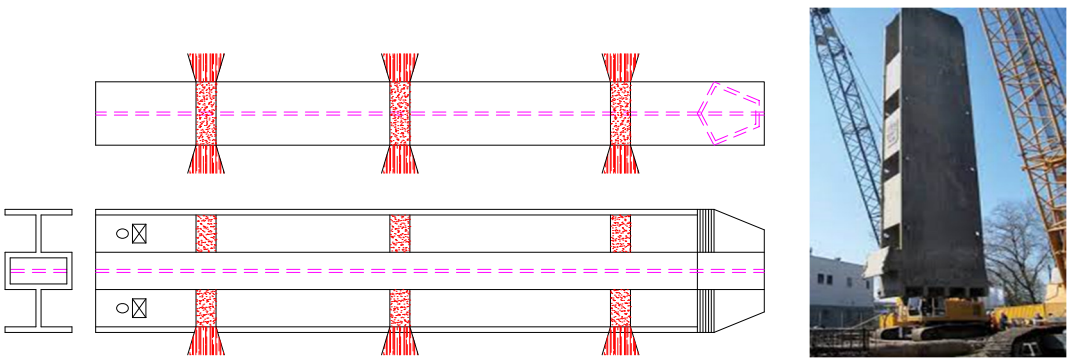

Figure 13. Special cleaning box to remove leaked material

2 METHODS

This research uses qualitative methods, used data collection from foundation contractor PT. Acset Indonusa and direct observation during the implementation of work as well as direct question to site managers and supervisors in the field. Data collection from foundation contractor from projects in Indonesia, and research period since 2005 to 2020.

3 RESULTS

This diaphragm wall solution is highly suitable for deep basement construction, with horizontal support systems such as ground anchors or strutting implemented during excavation. It may also be combined with the king post method when employing a top-down excavation approach. In panel excavation using grabbers, both systems consistently require the use of slurry stabilizers (bentonite or polymer) to maintain trench stability. A comparison of construction methodologies between the two systems is presented in Table 1.

Table 1. Comparison between CWS System with Continuous System

NO	ACTIVITY / ITEM of WORKS	"CWS" SYSTEM	"CONTINUOUS" SYSTEM
1	Sequence of excavation	Unbound excavation	The sequence of bound excavation begins with the female panel
2	Water Stop	Rubber + Water stop Joint	End plate, install in steel cages
3	Length of Water stop	Installed at least one meter below the basement bottom elevation	Installed along the panel reinforcement
4	Panel reinforcement	Not continuous	Continuous
5	Plastic sheet	No need	Installed in Female Panel
6	Difficulty	High Difficulty in Pull Out CWS Form	High Difficulty when inserting Steelcages the male panel to female panel
7	Rigidity	Less Rigid	More Rigid
8	Cost of Works	More Competitive	Less Competitive

4 DISCUSSION

For the implementation of the CWS system, materials for the CWS form may also be considered beyond steel, such as PVC. In addition, the geometry of the CWS form can be modified to suit specific project conditions. Further research is recommended to evaluate the production rate between the two systems.

5 CONCLUSION

Diaphragm wall CWS system or continuous can be selected as retaining walls for buildings with deep basement. Each system has a level implementation difficulty such as removing CWS Form in the CWS System and insert steel cages male panel to female panel in the continuous system. All Diaphragm wall system need to be reinforced to prevent horizontal movement during basement excavation according to the design structural planner (ground anchor, strutting or with king post).

DISCLAIMER

The authors declare no conflict of interest.

AVAILABILITY OF DATA AND MATERIALS

All data are available from the author.

ACKNOWLEDGMENTS

The Authors would like to thank Mr. Irawan Firmansyah as the principal of Geotechnical Consultant from PT. IFP Pratama Design who often interacted in the past, also PT. Acset Indonusa as a foundation Contractor

REFERENCES

Akhilesh Kumar Sharma, D. N. G. M., 2023. Construction and Challanges of The Diaphragm Wall in Fine Sandy Soil. *International Advance Research Journal in Science Engineering and Technology,* 10(9 september 2023, ISSN (O) 2393-8021, ISSN (P) 2394-1588).

Arun Kumar, P. K. Y., 2024. Construction of Diaphragm Wall for Underground Works. *International Journal of Creative Research Thoughts (IJRT),* 12(ISSN), pp. 2320-2882.

C.Y.Ou, L., 2011. Observed Performance of Diaphragm Wall Construction. *Geotechnical Engineering of The SEAGS & AGSSEA,* 42 No.3(ISSN 0046-5828).

Chew Yit Lin, M., 2025. *Construction Technology for Tall Buildings.* 6th ed. s.l.:World Scientific Publishing Co. Pte.Ltd.

Clayton, C., 1992. *Retaining Structures.* s.l.:Institution of Civil Engineers, Thomas Telford.

Comodromos E.M, P. M. G., 2013. *Effect on Adjacent Buildings of Diaphragm Wall Installation.* Paris, Procceedings 18th International Conference on Soil Mechanics and Geotechnical Engineering. p1951-1954.

Dong, Y., 2024. Effect of Diaphragm wall Construction Process on the Performance of Braced Excavation. *Geotechnical Aspects of Underground Construction in Soft Ground,* 978-1-032(ISBN), pp. 53812-9.

El-Razek, M. E. A., 1999. New Method for Construction of Diaphragm Walls. *Journal of Contruction Engineering and Management,* 125 No.4(ISSN 0733-9634/99/0004-0233-0241).

Geotechnical Engineering Office, C. E. a. D. D. C. E. a. D. B., 2023. *Deep Excavation Design and Construction.* 1st ed. s.l.:THE Government of The Hongkong Special Administrative Region.

Hardjasaputra, H., 2014. *Construction Engineering of Deep Basement.* s.l.:s.n.

Hsii Sheng Hsieh, L. H. W. T. M. L. J. C. C. W. T. H., 2011. Performance of T-Shaped Diaphragm Wall in A Large Scale Excavation. *Journal of GeoEngineering,* Volume 6 No.3, pp. 135-144.

J.Josifovski, S. M. J., 2011. *Deep Excavation With Multi Anchored Diaphragm wall.* s.l., Proceedings of the 15th European Conference on Soil Mechanics and Geotechnical Engineering A. Anagnostopoulos et al. (Eds), doi: 10.3233/978-1-60750-801-4-1485, IOS Press.

John, E., 2020. *Deep Excavations in Soils.* 1st ed. s.l.:CRC Press, Taylor & Francis Group.

Michael Carter, S. P. B., 2016. *Soil Properties and Their Correlations.* 2nd ed. s.l.:John Willey & Sons,Ltd.

Nasional, B. S., 2017. *SNI 8460: 2017 Persyaratan Perancangan Geoteknik.* Jakarta: BSN.

O'Rourke, T. &. J., 1990. Overview of Earth Retention Systems: 1970-1990, In Design and Performance of Earth Retaining Structures. Issue New York: Geotechnical Special Publication 25, Amirican Society of Civil Engineers, pp. 22-51.

Salgado, R., 2022. *The Engineering of Foundations, Slope and Retaining Structures.* 2nd ed. s.l.:CRC Press, Taylor & Francis Group.

Perubahan Nilai Kepadatan Relatif Tanah Pasir Akibat Variasi Percepatan Maksimum Gempa

Muhammad Yunus[1,*], Achmad Bakri Muhiddin[2], Tri Harianto[3], Ardy Arsyad[3]
[1]Mahasiswa Doktoral, Departemen Teknik Sipil, Fakultas Teknik Universitas Hasanuddin, Kabupaten Gowa, 92171; yunusm22d@student.unhas.ac.id
[2]Profesor, Departemen Teknik Sipil, Fakultas Teknik Universitas Hasanuddin, Kabupaten Gowa, 92171, bakrim@unhas.ac.id
[3]Profesor, Departemen Teknik Sipil, Fakultas Teknik Universitas Hasanuddin, Kabupaten Gowa, 92171, triharianto@unhas.ac.id
[4]Associate Profesor, Departemen Teknik Sipil, Fakultas Teknik
Universitas Hasanuddin, Kabupaten Gowa, 92171; ardyarsyad@unhas.ac.id

*Correspondence: yunusm22d@student.unhas.ac.id

ABSTRAK Gempa bumi sering kali menyebabkan perubahan sifat fisik tanah, termasuk perubahan nilai kepadatan relatif (*relative density*). Kepadatan relatif tanah merupakan parameter penting yang menentukan kekuatan geser tanah, ketahanan terhadap likuifaksi, dan stabilitas tanah saat menerima beban dinamis. Penelitian ini bertujuan untuk mengevaluasi perubahan nilai kepadatan relatif tanah akibat variasi percepatan beban gempa. Penelitian dilakukan dengan metode eksperimental menggunakan alat uji shaking table di laboratorium. Nilai kepadatan relatif tanah pasir diambil sebesar 40%, percepatan beban gempa divariasikan 0,3g; 0,4g; dan 0,5g. Alat Hand Cone Penetrometer digunakan untuk menentukan tahanan penetrasi konus (q_c) dan melakukan evaluasi hubungan antara percepatan beban gempa, dan kepadatan relatif (D_r) tanah. Hasil penelitian menunjukkan nilai kepadatan relatif (D_r) yang diperoleh tidak seragam pada tiap kedalaman lapisan tanah akibat variasi percepatan maksimum gempa *(Peak Ground Acceleration/PGA)* yang diberikan, sehingga menginduksi aliran air dari bawah ke atas yang membuat lapisan tanah pada bagian atas (dangkal) rentan mengalami likuifaksi.

KATA KUNCI : Kepadatan relatif, tahanan penetrasi, shaking table, percepatan maksimum gempa

1 PENDAHULUAN

Di wilayah dengan resiko gempa yang tinggi, seperti Indonesia yang berada di jalur cincin api Pasifik (Suyadi et al., 2023), studi mengenai perubahan sifat fisik tanah akibat gempa menjadi sangat penting. Fenomena likuifaksi tanah dan deformasi yang menyertainya selama terjadinya gempa bumi merupakan salah satu ancaman utama terhadap stabilitas infrastruktur. Peristiwa gempa bumi berulang di masa lalu, seperti gempa Aceh 2004 (Aksa et al., 2020), gempa Padang 2009 (Rusnardi & Kiyono, 2011), gempa Palu 2018 (Hazarika et al., 2021), dan gempa Majene 2021 (Arsyad et al., 2024) melaporkan kejadian likuifaksi tanah yang disertai dengan penurunan tanah dan kegagalan fondasi.

Salah satu dampak utama gempa bumi terhadap tanah adalah perubahan struktur internalnya, termasuk redistribusi partikel tanah yang dapat mengubah sifat fisik dan mekaniknya. Salah satu parameter tanah yang sangat dipengaruhi oleh gempa adalah kepadatan relatif tanah (*relative density*), yang merupakan indikator tingkat kekompakan atau kerapatan tanah dibandingkan dengan kondisi tanah yang paling longgar/lepas dan paling padat.

Kepadatan relatif tanah memainkan peran penting dalam menentukan stabilitas tanah, kekuatan geser, dan ketahanan terhadap fenomena seperti likuifaksi. Likuifaksi sering kali terjadi pada tanah granular, terutama pasir yang jenuh air, ketika tanah kehilangan kekuatannya akibat tekanan air pori yang meningkat selama gempa bumi. Variasi percepatan maksimum gempa *(Peak Ground Acceleration/PGA)* dapat mempercepat redistribusi partikel tanah dan memicu perubahan drastis pada nilai kepadatan relatif, sehingga memengaruhi daya dukung tanah dan kestabilannya.

Penelitian mengenai efek dari pembebanan gempa bumi, khususnya pada saat terjadi likuifaksi dan hubungannya dengan nilai tahanan penetrasi konus (q_c) serta kepadatan relatif tanah menjadi topik bahasan yang menarik khususnya dalam mempelajari studi kasus kejadian likuifaksi di lapangan seperti yang dilakukan oleh beberapa peneliti (Darby et al., 2017; Gu et al., 2022; Ha et al., 2011; Jamiolkowski et al., 2003a; Padmanabhan & Shanmugam, 2022; Sharp et al., 2010; Varghese & Madhavi Latha, 2014). Sebagian besar catatan kasus kejadian likuifaksi dalam basis data pemicu terjadinya likuifaksi hanya mencakup data hasil uji penetrasi kerucut (*Cone Penetration Test* / CPT) yang dikumpulkan setelah terjadinya peristiwa likuifaksi, sehingga memunculkan pertanyaan mengenai sejauh mana data tersebut dapat merepresentasikan kondisi tanah sebelum kejadian (Darby et al., 2017).

Tujuan dari penelitian ini adalah untuk menentukan tahanan penetrasi konus (q_c) dari tanah yang diberikan variasi percepatan maksimum gempa (PGA), serta mengevaluasi perubahan nilai kepadatan relatif tanah dan hubungannya dengan nilai tahanan penetrasi konus (q_c). Alat shaking table yang dipasang dengan bak pengujian transparan digunakan untuk melakukan pengujian. Tanah pasir dalam kondisi jenuh dengan kepadatan relatif 40% disiapkan dan diuji berulang dengan variasi PGA 0.3g, 0.4g, dan 0.5g dengan durasi waktu selama 60 detik.

2 METODE

2.1 Pasir yang digunakan

Jenis tanah pasir yang digunakan dalam penelitian ini berupa jenis pasir lokal yang diperoleh di sekitar daerah pantai Galesong, Kabupaten Takalar, Provinsi Sulawesi Selatan. Hasil pengujian indeks properties pasir Galesong disajikan pada Tabel 1 dan distribusi ukuran butiran pasir ditunjukkan pada Gambar 1. Untuk metode pengujian berat isi kering minimum dan maksimum, serta angka pori minimum dan maksimum mengacu ke (ASTM 4253 - 16, 2016).

Jenis pasir Galesong termasuk ke dalam kategori pasir besi (hitam) yang mengandung mineral berat berupa magnetit sehingga memiliki berat jenis > 2.70. Pasir jenis ini biasanya ditemukan di sekitaran pantai atau endapan alluvial dengan kandungan mineral berat tinggi. Distribusi ukuran butir pasir Galesong menunjukkan pasir termasuk kategori bergradasi seragam *(uniformly graded)* dengan nilai koefisien keseragaman ($C_u = 2.21 < 4$), dan nilai koefisien gradasi $C_c = 1.02$.

Tabel 2. Indeks properties pasir Galesong

No.	Jenis Pengujian	Satuan	Nilai
1.	Berat jenis (G_s)	-	3.17
2.	Ukuran butiran		
	a. D_{10}	mm	0.120
	b. D_{30}	mm	0.180
	c. D_{60}	mm	0.265
	d. Koefisien keseragaman (c_u)	-	2.21
	e. Koefisien gradasi (c_c)	-	1.02
3.	Berat isi kering		
	a. Berat isi kering minimum ($\gamma_{dmin.}$)	kN/m^3	18.25
	b. Berat isi kering maksimum ($\gamma_{dmax.}$)	kN/m^3	20.21
4.	Angka pori (e)		
	a. Angka pori minimum ($e_{min.}$)	-	0.65
	b. Angka Pori maksimum ($e_{max.}$)	-	0.86

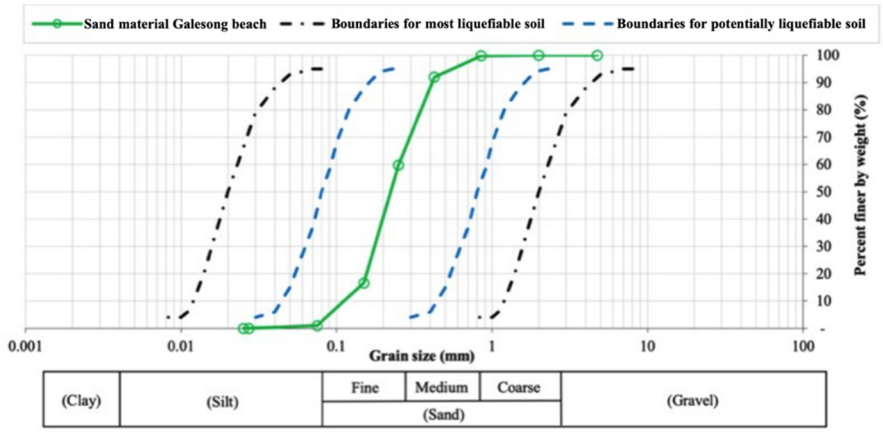

Gambar 1. Distribusi ukuran butiran pasir Galesong yang rentang terlikuifaksi (Tsuchida, 1970)

2.2 Shaking table

Pengujian laboratorium dilakukan menggunakan shaking table yang tersedia di Laboratorium Geoteknik dan Geoenviromental, Departemen Teknik Sipil Fakultas Teknik Universitas Hasanuddin. Dimensi unit shaking table adalah 1,2 m x 1,2 m dengan kapasitas 3 T. Gerakan horizontal meja dapat dibentuk dengan menggunakan aktuator servo-hidrolik yang dipasang di atas shaking table, seperti ditunjukkan pada Gambar 2. Kecepatan puncak maksimum, panjang langkah maksimum, frekuensi operasi, dan rentang akselerasi masing-masing adalah 1 m/s, perpindahan maksimum 400 mm, 0,01-50 Hz, dan 0,001-1g. Frekuensi akselerasi dan beban dinamis dapat dipilih sesuai dengan kondisi pengujian menggunakan akuisisi data yang dikontrol secara digital.

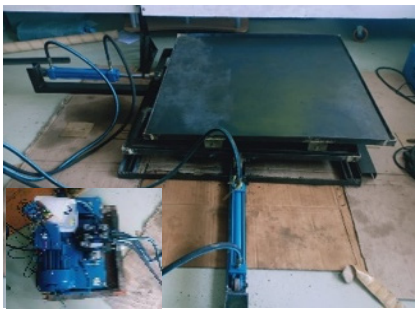

Gambar 2. Shaking table

2.3 Persiapan model fisik

Dalam pengujian eksperimental ini, model bak pengujian transparan berukuran 120 cm x 100 cm x 80 cm (panjang x lebar x tinggi) dibuat khusus dan digunakan dalam penelitian ini. Kaca acrylic yang digunakan untuk membuat model bak memiliki ketebalan 10 mm, dan diikat dengan aman menggunakan braket baja yang diikat ke rangka baja. Karena kekakuan wadah dapat menimbulkan efek batas pada sampel tanah (Lee et al., 2012), maka untuk meminimalkan efek batas ini, di bagian samping dari dinding bak pengujian dipasang papan busa *(foam board)* berupa busa polyurethane. Papan busa ini berfungsi untuk mereduksi pengaruh gelombang yang dipantulkan dari dinding samping bak pengujian yang kaku (Lombardi & Bhattacharya, 2012); (Lombardi et al., 2015); (Ghorbani et al., 2023).

Pembuatan model fisik di laboratorium dilakukan untuk menentukan tahanan penetrasi konus dan mengevaluasi perubahan nilai kepadatan relatif di bawah pengaruh percepatan pembebanan berulang Model fisik di laboratorium disiapkan dengan menggunakan metode *sand bed saturation*. Lapisan pasir kering dengan ketebalan 600 mm dan tingkat kepadatan relatif sebesar 40% disiapkan. Lapisan pasir dibagi ke dalam enam lapisan untuk menjaga keseragaman nilai kepadatan relatif yang direncanakan. Metode pembobotan digunakan untuk mengestimasi berat pasir yang dibutuhkan

sesuai dengan berat isi kering pasir (γ_d) dan volume bak pengujian. Dalam pengujian eksperimental ini, berat pasir yang digunakan per lapisan (100 mm) sebesar 194,52 kg, sehingga untuk enam lapisan yang direncanakan dibutuhkan total berat pasir kering sebesar 1.167,12 kg. Pasir kering yang telah ditimbang sesuai berat tiap lapisan kemudian dituangkan ke dalam bak pengujian. Proses penuangan pasir ke dalam bak pengujian dilakukan secara seragam dan dijaga tinggi jatuh (*fall height*) minimum agar nilai kepadatan relatif 40% dari pasir dapat dicapai. Untuk penelitian ini, tinggi jatuh (*fall height*) penuangan pasir ke bak pengujian sebesar 20 cm (Padmanabhan & Shanmugam, 2024) . Setelah proses penuangan pasir selesai dilakukan, tahapan selanjutnya adalah proses penjenuhan sampel pasir dengan cara memasukkan air secara perlahan ke dalam bak pengujian. Perubahan ketinggian air di dalam bak pengujian diamati melalui dinding kaca acrylic dari bak pengujian. Aliran air dihentikan ketika ketinggian air melewati permukaan lapisan pasir setinggi 1 cm. Lapisan pasir yang telah diisi air kemudian didiamkan selama 24 jam agar air dapat meresap dan redistribusi air pori tercapai sehingga lapisan pasir dapat dalam kondisi jenuh sempurna.

Tahap berikutnya adalah pembuatan model *embankment* yang akan ditempatkan di bagian atas lapisan pasir yang telah jenuh. Model *embankment* dibuat dari tanah lempung dengan sudut sebesar 60^0 menggunakan cetakan (*mold*) yang terbuat dari rangka besi dan dipadatkan di luar bak pengujian. Setelah proses pemadatan selesai dilakukan, model *embankment* kemudian diangkat ke dalam bak pengujian yang telah terisi pasir jenuh dan ditempatkan sesuai dengan rencana pengujian model fisik yang ditunjukkan pada Gambar 3.

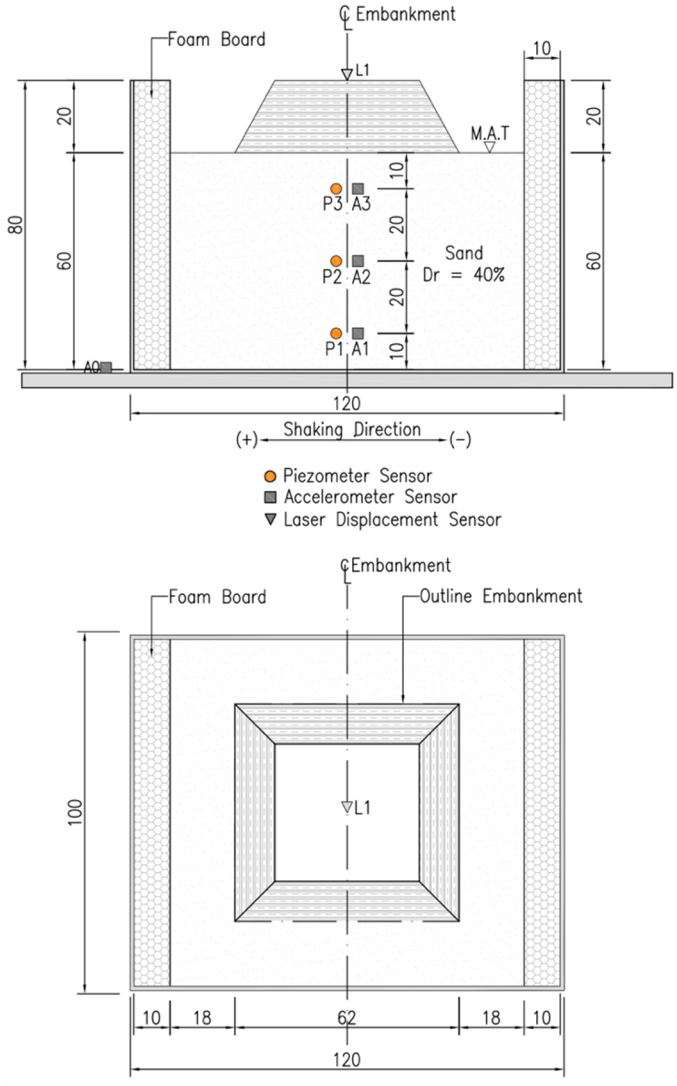

Gambar 3. Rencana model fisik pengujian

2.4 Evaluasi Kepadatan Relatif

Kepadatan tanah yang telah disiapkan diuji dengan menggunakan *Hand Cone Penetrometer* (HCP). Penetrometer kerucut ini terdiri dari konus penggerak yang memiliki sudut kerucut 60° dengan luas penampang 6,45 cm^2, batang penyambung, dan proving ring yang terpasang dial beban. Untuk evaluasi kepadatan, konus penggerak didorong secara vertikal ke dalam tanah yang telah disiapkan dengan kecepatan 10 mm/detik merujuk ke (SNI 2827:2008, 2008) dan (ASTM D 3441 - 16, 2016), nilai resistensi penetrasi yang sesuai pada setiap penetrasi 100 mm dicatat. Lokasi titik pengujian HCP dilakukan pada tiap sisi dari model embankment yang dimodelkan seperti ditunjukkan pada Gambar 4. Dari nilai tahanan penetrasi kerucut yang diperoleh, kepadatan relatif lapisan pasir pada kedalaman yang berbeda diestimasi dengan menggunakan Persamaan 1 yang diusulkan oleh (Jamiolkowski et al., 2003b).

$$Dr = 100\left[0{,}268\ x\ ln\left(\frac{{}^{q_c}/_{\sigma_{atm}}}{\sqrt{{}^{\sigma'_{vo}}/_{\sigma_{atm}}}}\right) - 0{,}675\right] \quad (1)$$

Dimana D_r adalah nilai kepadatan relatif (%), q_c adalah nilai tahanan penetrasi konus hasil pengujian HCP (kPa), σ'_{v0} adalah nilai tekanan overburden efektif (kPa), dan σ_{atm} adalah tekanan atmosfir (atm).

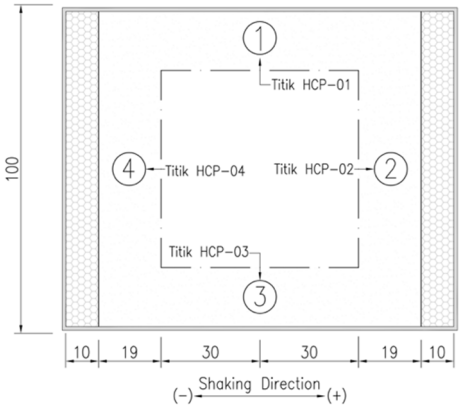

Gambar 4. Titik pengujian HCP

2.5 Tahap Pengujian Model

Tujuan dari penelitian ini adalah untuk mengevaluasi perubahan kepadatan relatif tanah pasir dalam kondisi jenuh yang mengalami guncangan berulang. Oleh karena itu, variasi percepatan maksimum gempa (*PGA)* dipilih. Untuk studi eksperimental, gelombang sinusoidal dengan PGA 0.3g, 0.4g, dan 0.5g pada frekuensi konstan dipilih dengan durasi waktu getaran selama 60 detik. Matriks pengujian yang dilaksanakan di laboratorium disajikan pada Tabel 2. Untuk kondisi model fisik sebelum dan setelah pengujian ditunjukkan pada Gambar 5.

Tabel 2. Matriks pengujian model fisik

Kode	Dr (%)	Akselerasi (g)	Waktu (detik)
PGA 0.3g	40	0.3	60
PGA 0.4g	40	0.4	60
PGA 0.5g	40	0.5	60

(a) (b)

Gambar 5. Kondisi model fisik, (a) sebelum pengujian, (b) setelah pengujian

3 HASIL DAN PEMBAHASAN

3.1 Tegangan overburden yang bekerja

Tegangan overburden tanah adalah tekanan vertikal yang bekerja pada suatu lapisan tanah akibat berat tanah yang berada di atasnya. Jenis tegangan overburden yang biasa bekerja pada lapisan tanah terdiri atas, tegangan overburden total (σ_v), tekaan ai pori (u), dan tegangan overburden efektif (σ'_v). Untuk besaran nilai tegangan overburden lapisan tanah pasir pada model fisik yang diuji ditunjukkan pada Tabel 2 dan Gambar 6.

Tabel 2. Analisis tegangan overburden yang bekerja

No.	Kedalaman (m)	γ (kN/m^3)	γ_w (kN/m^3)	σ_{v0} (kPa)	u (kPa)	σ'_{v0} (kPa)
1.	0,00	22,51	9,81	0,00	0,00	0,00
2.	0,10	22,51	9,81	2,25	0,98	1,27
3.	0,20	22,51	9,81	4,50	1,96	2,54
4.	0,30	22,51	9,81	6,75	2,94	3,81
5.	0,40	22,51	9,81	9,00	3,92	5,08
6.	0,50	22,51	9,81	11,25	4,91	6,35

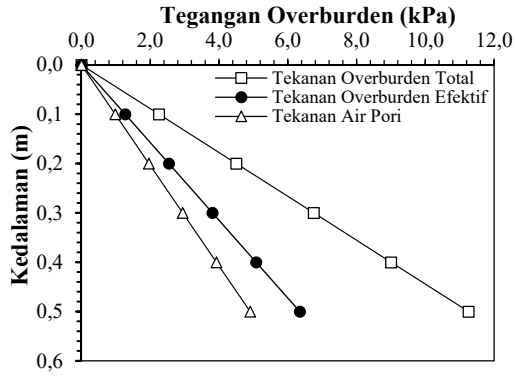

Gambar 6. Tegangan overburden yang bekerja

3.2 Tahanan penetrasi konus (q_c)

Nilai tahanan penetrasi konus (q_c) yang diperoleh dari hasil pengujian HCP pada tiap kedalaman lapisan tanah dibahas pada bagian ini. Nilai tahanan penetrasi konus (q_c) setiap kedalaman lapisan

tanah dengan nilai kepadatan relatif sebesar 40% pada tiap titik pengujian HCP yang mengalami guncangan akibat variasi percepatan beban gempa yang diberikan ditunjukkan pada Gambar 7.

Gambar 7 menunjukkan perbedaan nilai tahanan penetrasi konus (q_c) yang diperoleh pada tiap titik pengujian, dimana pada titik HCP-02 dan titik HCP-04 yang sejajar arah guncangan memiliki nilai q_c yang lebih kecil dibandingkan dengan nilai q_c pada titik HCP-01 dan titik HCP-03 yang tegak lurus arah guncangan. Hal ini disebabkan pengujian titik HCP-01 dan titik HCP-03 mengalami proses densifikasi tanah yang lebih cepat dibandingkan titik HCP-02 dan titik HCP-04. Gambar 5 juga menunjukkan peningkatan nilai q_c sesuai dengan nilai percepatan beban gempa yang diberikan, namun peningkatan nilai q_c yang diperoleh tidak linier dengan kedalaman tanah yang menunjukkan proses densifikasi tidak seragam dengan kedalaman.

3.3 Perubahan kepadatan relatif (D_r)

Dari hasil analisis nilai tahanan penetrasi konus (q_c), maka selanjutnya dilakukan evaluasi nilai kepadatan relatif tanah dengan menggunakan Persamaan 1. Hasil evaluasi nilai kepadatan relatif tanah yang mengalami guncangan akibat variasi percepatan gempa *(Peak Ground Acceleration/PGA)* ditunjukkan pada Gambar 8. Untuk perbandingan yang lebih baik, maka nilai kepadatan relatif tanah pada kondisi awal diplot pada Gambar 8 yang sama.

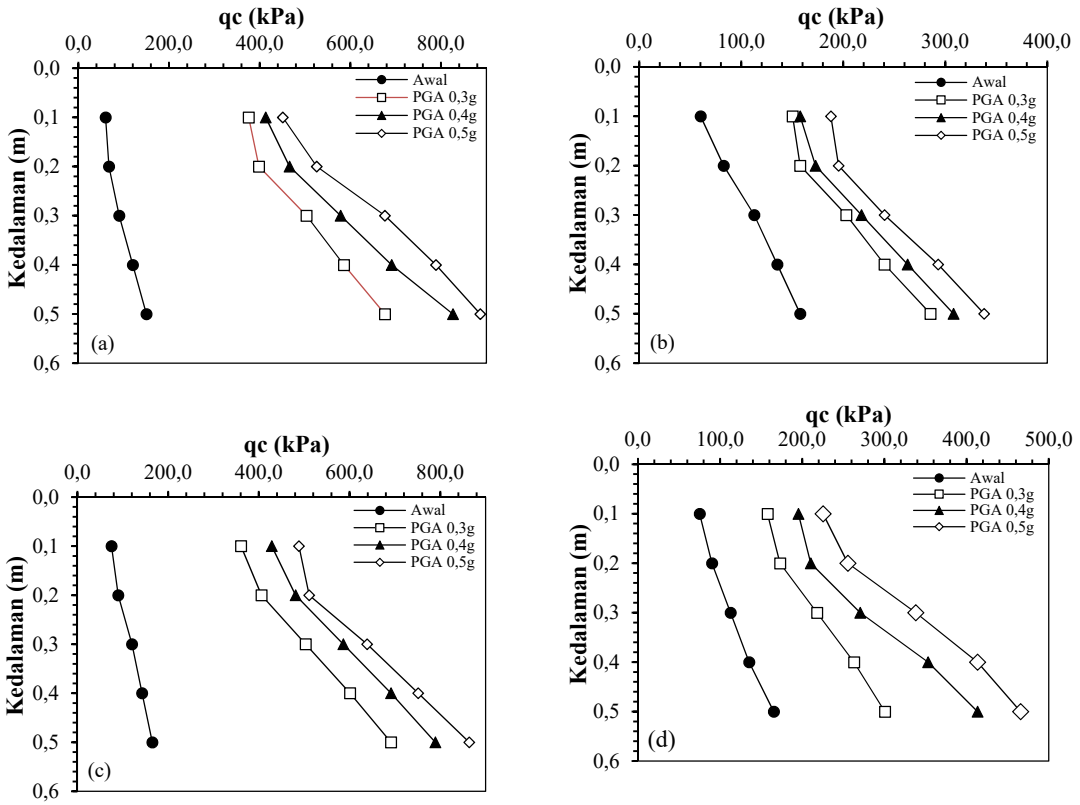

Gambar 7. Nilai tahanan penetrasi konus (q_c), (a) Titik HCP-01; (b) Titik HCP-02; (c) Titik HCP-03; (d) Titik HCP-04

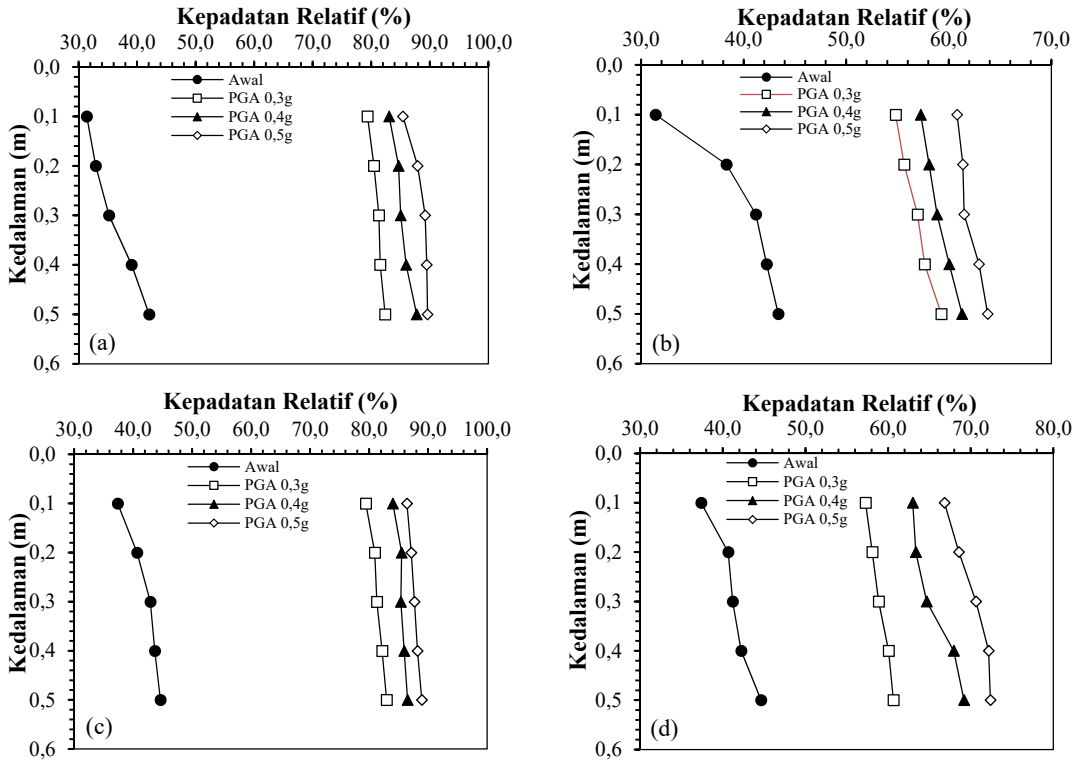

Gambar 8. Nilai kepadatan relatif (*Dr*), (a) Titik HCP-01; (b) Titik HCP-02; (c) Titik HCP-03; (d) Titik HCP-04

Gambar 8 menunjukkan peningkatan nilai kepadatan relatif tanah yang tidak linier pada tiap lapisan kedalaman tanah dan peningkatan nilai kepadatan relatif ditemukan bervariasi dari lapisan atas ke lapisan bawah. Pada kondisi awal diperoleh peningkatan nilai kepadatan relatif sekitar 8% hingga 12%, setelah PGA 0.3g diperoleh nilai peningkatan kepadatan relatif sebesar 4% hingga 5%, setelah PGA 0.4g diperoleh peningkatan nilai kepadatan relatif sebesar 3% hingga 6%, dan setelah PGA 0.5g diperoleh peningkatan nilai kepadatan relatif sebesar 1% hingga 3%.

Peningkatan nilai kepadatan relatif yang signifikan mayoritas terjadi pada lapisan bagian bawah dibandingkan pada bagian atas. Hasil pengujian ini menvalidasi bahwa variasi kepadatan tanah salah satunya disebabkan oleh pengaruh drainase ke atas selama guncangan berlangsung dan setelah terjadi guncangan (Darby et al., 2017); (Padmanabhan & Shanmugam, 2022). Meskipun proses densifikasi tanah terjadi setiap peningkatan pembebanan, akan tetapi peningkatan nilai kepadatan relatif yang signifikan terjadi pada PGA sebesar 0.3g, dimana pada kondisi PGA 0.3g ini terjadi likuifaksi pada tanah. Hal ini disebabkan oleh variasi kepadatan yang memiliki kepadatan yang lebih tinggi di bagian bawah daripada di bagian atas yang secara terus menerus menginduksi drainase ke atas yang menyebabkan timbulnya tekanan air pori yang berlebih dengan cepat. Selanjutnya pada PGA 0.4g dan PGA 0.5g dimana nilai kepadatan relatif tetap mengalami peningkatan tapi tidak menyebabkan re-likufaksi (likufaksi berulang) karena tekanan air pori yang berlebih tadi telah terdisipasi sepenuhnya

4 KESIMPULAN

Dari hasil pengujian dan evaluasi yang telah dilakukan, maka dapat dituliskan kesimpulan sebagai berikut:

a. Distribusi ukuran butir pasir Galesong menunjukkan pasir termasuk kategori bergradasi seragam *(uniformly graded)* dengan nilai koefisien keseragaman (C_u = 2.21 < 4), dan nilai koefisien gradasi C_c = 1.02. Pasir dengan kategori bergradasi seragam memiliki stabilitas yang rendah dan kurang baik untuk konstruksi fondasi karena mudah mengalami penurunan *(settlement)* dan terlikuifaksi jika dalam kondisi jenuh dan mengalami guncangan gempa.

b. Terjadi peningkatan nilai tahanan penetrasi konus (q_c) seiring dengan bertambahnya percepatan maksimum gempa yang diberikan. Peningkatan nilai q_c pada tiap kedalaman lapisan tanah tidak seragam, dimana lapisan bagian bawah memiliki nilai q_c lebih besar dibandingkan lapisan bagian atas. Lapisan tanah pasir yang awalnya dalam kondisi lepas mengalami peningkatan nilai tahanan penetrasi konus (q_c) hampir tiga kali lipat.
c. Nilai kepadatan relatif (D_r) yang diperoleh tidak seragam pada tiap kedalaman lapisan tanah akibat percepatan maksimum gempa yang diberikan, sehingga menginduksi aliran air dari bawah ke atas yang membuat lapisan tanah pada bagian atas (dangkal) rentan mengalami likuifaksi. Untuk mereduksi hal tersebut, disarankan agar substruktur yang terletak di kedalaman tanah dangkal pada daerah rawan gempa harus diperkuat dengan pemilihan metode perbaikan tanah yang sesuai agar dapat meminimalisir tekanan air pori yang berlebih selama kejadian gempa berlangsung.

UCAPAN TERIMA KASIH

Penulis mengucapkan terima kasih yang sebesar-besarnya atas dukungan dan pembiayaan Beasiswa Pendidikan Indonesia (BPI) dari Pusat Pembiayaan dan Asesmen Pendidikan Tinggi (PPAPT) Kementerian Pendidikan Tinggi, Sains, dan Teknologi (Kemendiktisaintek), dan Lembaga Pengelola Dana Pendidikan (LPDP) Pemerintah Republik Indonesia.

DAFTAR PUSTAKA

Aksa, F. I., Utaya, S., Bachri, S., & Handoyo, B. (2020). Investigating the Role of Geography Education in Enhancing Earthquake Preparedness: Evidence from Aceh, Indonesia. *International Journal of GEOMATE*, *19*(76), 9–16. https://doi.org/10.21660/2020.76.90006

Arsyad, A., Syamsuddin, E., Azmi, M., Asyhari, M., & Wiryadiputra Suryadi, R. (2024). A site-specific earthquake ground response analysis and relations to collapsing buildings in the 2021 Mw. 6.2 Mamuju-Majene Earthquake Sulawesi Indonesia. *Japanese Geotechnical Society Special Publication*, *10*(26), v10.OS-15-03. https://doi.org/10.3208/jgssp.v10.OS-15-03

ASTM 4253 - 16. (2016). *Standard Test Methods for Maximum Index Density and Unit Weight of Soils Using a Vibratory Table*. ASTM International. https://doi.org/10.1520/D4253-16E01

ASTM D 3441 - 16. (2016). *Test Method for Mechanical Cone Penetration Testing of Soils*. ASTM International. https://doi.org/10.1520/D3441-16

Darby, K. M., Boulanger, R. W., & Dejong, J. T. (2017). Effect of multiple shaking events on cone penetration resistances in saturated sand. In M. Taieb (Ed.), *In Proc., 3rd Int. Conf. on Performance-based Design in Earthquake Geotechnical Engineering, PBDIII*.

Ghorbani, A., Hasanzadehshooiili, H., Somti Foumani, M. A., Medzvieckas, J., & Kliukas, R. (2023). Liquefaction Potential of Saturated Sand Reinforced by Cement-Grouted Micropiles: An Evolutionary Approach Based on Shaking Table Tests. *Materials*, *16*(6), 2194. https://doi.org/10.3390/ma16062194

Gu, L., Zheng, W., Zhu, W., Wang, Z., Ling, X., & Zhang, F. (2022). Liquefaction-induced damage evaluation of earth embankment and corresponding countermeasure. *Frontiers of Structural and Civil Engineering*, *16*(9), 1183–1195. https://doi.org/10.1007/s11709-022-0848-7

Ha, I. S., Olson, S. M., Seo, M. W., & Kim, M. M. (2011). Evaluation of reliquefaction resistance using shaking table tests. *Soil Dynamics and Earthquake Engineering*, *31*(4), 682–691. https://doi.org/10.1016/j.soildyn.2010.12.008

Hazarika, H., Rohit, D., Pasha, S. M. K., Maeda, T., Masyhur, I., Arsyad, A., & Nurdin, S. (2021). Large distance flow-slide at Jono-Oge due to the 2018 Sulawesi Earthquake, Indonesia. *Soils and Foundations*, *61*(1), 239–255. https://doi.org/10.1016/j.sandf.2020.10.007

Jamiolkowski, M., Lo Presti, D. C. F., & Manassero, M. (2003a). *Evaluation of Relative Density and Shear Strength of Sands from CPT and DMT*. 201–238. https://doi.org/10.1061/40659(2003)7

Jamiolkowski, M., Lo Presti, D. C. F., & Manassero, M. (2003b). Evaluation of Relative Density and Shear Strength of Sands from CPT and DMT. *Soil Behavior and Soft Ground Construction*, 201–238. https://doi.org/10.1061/40659(2003)7

Lee, C. J., Wei, Y. C., & Kuo, Y. C. (2012). Boundary effects of a laminar container in centrifuge shaking table tests. *Soil Dynamics and Earthquake Engineering*, *34*(1), 37–51. https://doi.org/10.1016/j.soildyn.2011.10.011

Lombardi, D., & Bhattacharya, S. (2012). Shaking table tests on rigid soil container with absorbing boundaries. *15th World Conference on Earthquake Engineering 2012 (15WCEE)*.

Lombardi, D., Bhattacharya, S., Scarpa, F., & Bianchi, M. (2015). Dynamic response of a geotechnical rigid model container with absorbing boundaries. *Soil Dynamics and Earthquake Engineering*, *69*, 46–56. https://doi.org/10.1016/j.soildyn.2014.09.008

Padmanabhan, G., & Shanmugam, G. K. (2022). Reliquefaction Assessment Studies on Saturated Sand Deposits under Repeated Acceleration Loading Using 1-g Shaking Table Experiments. *Journal of Earthquake Engineering*, *26*(6), 2888–2910. https://doi.org/10.1080/13632469.2020.1778588

Padmanabhan, G., & Shanmugam, G. K. (2024). Performance assessment of prefabricated vertical drains in mitigating soil reliquefaction subjected to repeated seismic events using shaking table experiments. *Frontiers of Structural and Civil Engineering*, *18*(3), 411–427. https://doi.org/10.1007/s11709-024-1057-3

Rusnardi, R., & Kiyono, J. (2011). Estimation of Earthquake Ground Motion in Padang, Indonesia. *International Journal of GEOMATE*, *1*(1), 71–77.

Sharp, M. K., Dobry, R., & Phillips, R. (2010). CPT-Based Evaluation of Liquefaction and Lateral Spreading in Centrifuge. *Journal of Geotechnical and Geoenvironmental Engineering*, *136*(10), 1334–1346. https://doi.org/10.1061/(ASCE)GT.1943-5606.0000338

SNI 2827:2008. (2008). *Cara uji penetrasi lapangan dengan alat sondir*. Badan Standarisasi Nasional.

Suyadi, Harianto, T., Muhiddin, A. B., & Arsyad, A. (2023). Soil Reinforcement Model Test Using Timber Pile at Liquefaction Area. *Civil Engineering Journal (Iran)*, *9*(6), 1509–1521. https://doi.org/10.28991/CEJ-2023-09-06-016

Tsuchida, H. (1970). Prediction and Countermeasure against Liquefaction in Sand Deposits. *Abstract of the Seminar of the Port and Harbour Research Institute*, *1*(3), 1–3.

Varghese, R. M., & Madhavi Latha, G. (2014). Shaking table tests to investigate the influence of various factors on the liquefaction resistance of sands. *Natural Hazards*, *73*(3), 1337–1351. https://doi.org/10.1007/s11069-014-1142-3

Evaluation of Toll Road Embankment Stability on Clay Soil Using 2 m Soil Replacement and Woven Geotextile

Yani Putri Agustina[1,*], Fitriana Sarifah[2]
[1,2]Department of Civil Engineering, Faculty of Engineering, Siliwangi University, Tasikmalaya, Indonesia, 46115;
[1]yaniputriagustina@gmail.com [2]fitriana.sarifah@unsil.ac.id
*Correspondence: yaniputriagustina@gmail.com

ABSTRACT This study examines the slope stability and settlement behavior of a 6-meter-high embankment built on medium clay soil at borehole point DD-08, part of the Subang Toll Road national strategic project. The area is characterized by saturated clay layers with low shear strength and high compressibility, making it highly vulnerable to slope failure and excessive settlement under load. The evaluation used a quantitative-descriptive approach with the Limit Equilibrium Method to assess the Safety Factor (SF) at six loading stages: during embankment construction, under seismic loading during construction, during pavement installation, under seismic loading during installation, during operation, and under seismic loading during operation. Before improvement, the safety factor values were below the minimum stability threshold, recorded as 1.24 during embankment, 0.84 under seismic loading during embankment, 1.34 during pavement installation, 0.95 under seismic loading during pavement, 1.38 during operation, and 0.97 under seismic loading during operation. Ground improvement involved replacing 2 meters of soil and installing woven geotextile with a tensile strength of 75 kN/m². After enhancement, the safety factors increased to 1.55 during embankment, 1.13 under seismic loading, 1.57 during pavement installation, 1.15 under seismic loading during pavement, 1.63 during operation, and 1.21 under seismic loading during operation. Settlement analysis revealed a vertical deformation of 0.01 m and a settlement rate of 0.01 m/year, within acceptable design limits. These results show that combining soil replacement with woven geotextile effectively improves slope stability and controls embankment settlement on medium clay soils in earthquake-prone areas.

KEYWORDS Slope Stability; Settlement; Embankment; Soil Replacement; Woven Geotextile

1 GENERAL INFORMATION

2 INTRODUCTION

Subang Regency, located on the northern coast of West Java Province, is characterized by complex geological conditions. According to the Regional Geological Map (Thahir et al., 2024) The area consists of young alluvial deposits of clay and water-saturated silt, as well as loose and unconsolidated sand. These conditions classify the soil as compressible ground with low bearing capacity, high compressibility, and very low permeability. (Gusnadi et al., 2023). Furthermore, Subang is classified as an earthquake-prone zone. (Pustlitbang PUPR, 2017), with a peak ground acceleration (PGA) of 0.15g and soil type SE (Soft Soil). This combination makes the region highly vulnerable to settlement and slope failure, particularly in large-scale infrastructure development.

Geotechnical challenges are commonly encountered in toll road construction projects in Indonesia, especially in areas dominated by clay soils with relatively low shear strength, significant compressibility, and low permeability. These conditions result in insufficient bearing capacity and a high risk of failure or excessive settlement if no proper ground improvement is applied. This aligns with (Hamonangan & Syahputra, 2023), who reported that soil replacement can effectively reduce compressible layer thickness and enhance embankment stability at the Subang Toll Road site.

One of Indonesia's strategic infrastructure projects is the 37.7 km Subang Toll Road, which connects the Cikopo–Palimanan (Cipali) Toll Road to Patimban Port. The project plays a vital role in strengthening the national logistics system, accelerating goods distribution, and improving

connectivity among industrial zones in northern West Java. Consequently, embankments constructed over medium clay soil must ensure sufficient load-bearing capacity, long-term stability, and resistance to seismic forces.

Previous studies by (Agustina et al., 2024) The DD-03 borehole demonstrated that soil replacement to a depth of 2.5 m combined with 75 kN/m² woven geotextile reinforcement significantly improved the Safety Factor (SF). However, such methods must be tailored to other sites with different geotechnical conditions. One critical location that has not been thoroughly investigated is borehole DD-08, where the planned embankment height reaches 6 m. This elevation was determined not only to adjust to the existing contour but also to prevent surface water accumulation in low-lying areas, a primary consideration in road geometric design for basin areas (SNI 8460, 2017).

At DD-08, the embankment was also designed to act as a preload to accelerate the consolidation of the compressible subgrade, which consists of saturated clay with low cohesion and high compressibility. To optimize this preloading effect, a temporary surcharge of 1.8 m was added, resulting in a total construction height of 7.8 m. This surcharge was intended to accelerate the dissipation of pore water pressure and increase effective vertical stress, thereby improving the shear strength of the subgrade and reducing the risk of excessive settlement during operation (Gusnadi et al., 2023). The preloading was not accompanied by Prefabricated Vertical Drains (PVD), as soil investigation revealed a soft clay layer of approximately 5 m, and after a 2 m soil replacement, the remaining compressible layer was only about ±2 m. In such conditions, PVD installation was deemed unnecessary, consistent with (SNI 8460, 2017), which notes that PVD is less effective for relatively thin compressible layers.

It should be noted that although the subgrade at DD-08 is classified as medium stiff clay based on NSPT values (≈5), its engineering behavior—characterized by low shear strength and high compressibility—still poses risks similar to those of soft clay. Therefore, in this study, the term compressible soil is adopted consistently, while acknowledging that the problematic layer can also be considered “soft” in the context of embankment settlement and stability analysis. (SNI 8460, 2017).

This study, therefore, introduces a new soil improvement approach: shallow soil replacement to a depth of 2 m combined with 75 kN/m² woven geotextile reinforcement. The 2 m depth was selected as a cost-efficient construction strategy without compromising safety. To date, no study has specifically evaluated the performance of this improvement combination on a six m-high embankment constructed over clay soil with compressible characteristics under staged loading, including seismic conditions. Accordingly, this research aims to analyze slope stability and settlement behaviour at borehole DD-08, both before and after soil improvement with 2 m soil replacement and woven geotextile reinforcement. The analysis was conducted using the Limit Equilibrium Method (LEM) to evaluate the Safety Factor under six scenarios: during embankment construction, embankment under seismic loading, pavement installation, pavement under seismic loading, operational period with traffic load, and operational period under seismic loading. In addition, settlement analysis was carried out after soil improvement to ensure that vertical deformation remained within design tolerances.

Several previous studies have reported the effectiveness of soil replacement combined with geosynthetic reinforcement. e.g., (Muntohar et al., 2021); (Indraratna et al., 2024); (Agustina et al., 2024). However, most of these studies focused on clay deposits with medium clay soil characteristics or were conducted under controlled laboratory or pilot-scale conditions. In contrast, the present study investigates explicitly the performance of a six m-high toll road embankment with shallow soil replacement of only 2 m combined with woven geotextile reinforcement, under real-field staged loading and seismic conditions. The findings are expected to provide technical updates on clay soil improvement methods, enrich geotechnical design references based on real-field case studies, and serve as a basis for decision-making in the development of similar infrastructure across various regions of Indonesia.

3 METHODS

This study employs a quantitative-descriptive approach with geotechnical analysis methods to evaluate slope stability and settlement of embankments on medium clay soil. The analysis focused on borehole DD-08, located along the Subang Toll Road construction route, with a planned embankment height of 6 meters. Two scenarios were analyzed: (i) without soil improvement, and (ii) with soil improvement using a 2 m soil replacement combined with woven geotextile reinforcement placed horizontally at the embankment base. The analysis was conducted using the Geo5 Demo Version software (Slope Stability and Settlement modules), which supports safety factor calculations and settlement analysis based on Terzaghi's consolidation theory.

The geotextile used is a woven type (TenCate Geolon® PET 200) with a maximum tensile strength (T_{ult}) of 200 kN/m in the machine direction (MD) and 50 kN/m in the cross direction (CD). The allowable tensile strength (T_{all}) is calculated based on reduction factors consisting of the reduction factor due to installation (RF_{ID}), the reduction factor due to long-term conditions (RF_{CR}), and the reduction factor due to chemical and biological conditions (RF_{CBD}). The calculation of the allowable tensile strength is formulated as follows, referring to (Koerner, 2005). The calculation yielded an allowable tensile strength of approximately 75 kN/m, which was used as an input parameter in Geo5 to represent the long-term reinforcement capacity. In terms of deformation characteristics, the geotextile exhibits an elongation of about 10% at ultimate tensile strength, while the tensile strength at 5% strain is approximately 100 kN/m. These properties confirm that the geotextile provides sufficient reinforcement capacity at relatively small working strains, making it highly suitable as basal reinforcement for embankments constructed on medium clay soil. Nevertheless, it should be noted that the Limit Equilibrium Method (LEM) does not account for the stress–strain behavior of geotextiles, and thus the analysis results should be interpreted with this limitation in mind.

The primary data used comes from field soil investigations and laboratory tests. The soil parameters analyzed include the average NSPT value, soil bulk density, and effective cohesion (c_{ef}), effective internal friction angle (φ_{ef}) And elastic modulus. Drilling results indicate the groundwater table is approximately 2 meters below the ground surface. Secondary data from (Pustlitbang PUPR, 2017) It was used to determine soil classification and the maximum ground acceleration (PGA) value of 0.15g.

Slope stability analysis was conducted using the Limit Equilibrium Method (LEM), which includes short-term, long-term, and earthquake conditions. The horizontal earthquake coefficient (k_h) was calculated based on the approach of the response spectrum acceleration (PSA) value, using the equation referred to in (SNI 1726, 2019).

Based on (SNI 8460, 2017) The toll road is classified as Class I with a traffic load of 15 kN/m². The pavement load is calculated according to (Badan Penelitian dan Pengembangan Pekerjaan Umum, 2012), with a result of 11.82 kN/m².

The research location is at borehole DD-08 in Subang Regency, with coordinates Easting 0801943 m and Northing 9295974 m, based on the UTM Zone 48M projection system. This location was chosen because it represents the geotechnical conditions for the detailed design of the toll road alignment. The research location can be seen in Figure 1.

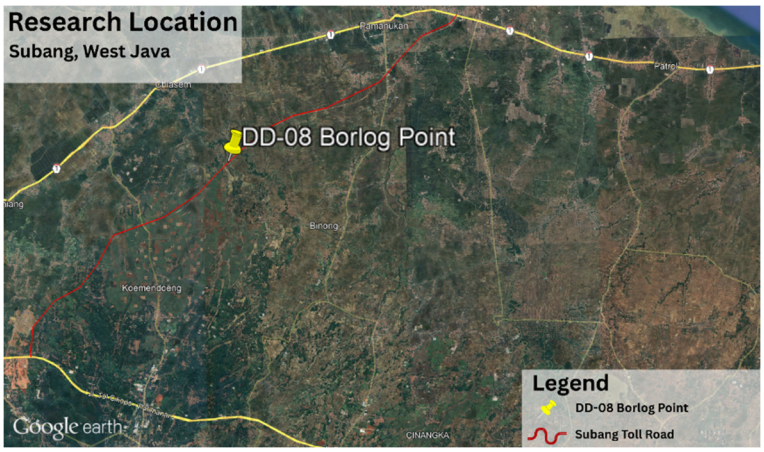

Figure 1. Research location (Source: Google Earth, 2025)

Technical criteria referring to applicable national standards were used to assess the safety and performance aspects of the site's embankment structure. Table 1 below presents the requirements for analyzing embankment stability and ground subsidence.

Table 1. Embankment stability and settlement analysis criteria

Stability			
Parameter	Load type	Term	Source
Short term	Embankment load	SF > 1.4	Road class I: (Departemen Permukiman dan Prasarana Wilayah, 2002)
	Pavement load	SF > 1.5	(SNI 8460, 2017)
Long term	Traffic load	SF > 1.5	(SNI 8460, 2017)
	Earthquake load	SF > 1.1	(SNI 8460, 2017)
Settlement			
Parameter	Term		Source
Total settlement after the operation	≤ 0.10 m		(Manual Desain Perkerasan Jalan No. 02/M/BM/2017, 2017)
Settlement rate	< 0.02 m/year		Road class I: (Departemen Permukiman dan Prasarana Wilayah, 2002)

4 RESULTS

4.1 Subgrade Soil Parameters

Table 2 presents a recapitulation of subgrade soil parameters. The parameters input into the Geo5 program to analyze slope stability in the short term are total parameters (c_u). Total parameters are used because, in the short term, after the load is applied, the soil has not had sufficient time to drain water out or into its pores, so the pore water pressure remains high. The formula for calculating undrained shear strength was adopted from (Ameratunga et al., 2016).

Meanwhile, the parameters used to analyze slope stability in the long term are effective parameters, such as effective cohesion (c') and effective internal friction angle (φ'). These parameters are applied after the soil has reached equilibrium with the applied load, typically after several months or years, when pore water pressure has dissipated and effective stress conditions prevail. The effective soil parameters were not obtained from CU or CD triaxial tests but were instead estimated indirectly using empirical correlations as recommended by (Hardiyatmo, 2002). Specifically, φ' was correlated with NSPT values, while c' was estimated based on the relationship between undrained shear strength (c_u) and SPT-based correlations for soft clay. This approach ensures that the effective soil parameters used in the analysis remain consistent with field investigation data and accepted empirical practices.

The parameters required for settlement analysis are the deformation modulus (E_{ref}), Poisson's ratio (v), and the permeability coefficient (k). In this study, the deformation modulus was estimated empirically based on correlations with NSPT values obtained from field tests.

It should be clarified that this empirical equation provides an approximation of the soil deformation modulus (E), which in this study is adopted as the reference stiffness modulus (E_{ref}) in the Geo5 software. In the analysis, E_{ref} is considered stress-dependent, with the reference stress corresponding to the vertical effective stress ($\sigma' v$) at the mid-depth of each soil layer. Although this approach represents a simplification, it has been widely applied in practice and is considered acceptable for preliminary embankment design on medium clay soil. Unlike many previous studies that assume a constant stiffness modulus, this research applies a depth- and stress-dependent reference modulus (E_{ref}), which more accurately represents field conditions and improves the reliability of settlement predictions.

The values of Poisson's ratio (v) and the permeability coefficient (k) were obtained from empirical correlations recommended by (Ameratunga et al., 2016), which are widely adopted in geotechnical engineering practice. The adopted subgrade soil parameters are summarized in Table 2.

Table 2. Recapitulation of subgrade soil parameters

Layer (Depth)	NSPT	Soil Type	Consistency /Density	γ/γ_{sat} (kN/m^3)	φ' (°)	c' (kPa)	c_u (kPa)	E_{ref} (MPa)	v	k (m/day)
1 (0.00 – 4.00)	5	Silty CLAY	Medium	13.45 /16.80	17.50	0.31	35.91	6.38	0.30	0.0864
2 (4.00 – 7.00)	10	Silty CLAY	Stiff	13.36 /15.70	27.14	1.90	71.82	14.00	0.30	0.0864
3 (7.00 – 10.00)	44	SAND STONE	Dense	17.50 /21.00	36.40	3.50	-	66.00	0.20	8.64
4 (10.00 – 13.50)	32	Silty CLAY	Hard	14.01 /17.18	26.27	0.44	191.52	47.00	0.35	0.0864
5 (13.50 – 14.50)	51	SAND STONE	Very Dense	19.00 /21.50	38.00	10.00	-	76.50	0.35	86.40
6 (14.50 – 22.00)	27	Silty CLAY	Very Stiff	14.45 /17.47	30.45	7.42	191.52	39.19	0.35	0.0864
7 (22.00 – 24.50)	34	Sandy CLAY	Hard	20.00 /20.00	26.70	0.58	191.52	50.25	0.35	0.8640
8 (24.50 – 27.00)	32	Silty CLAY	Hard	20.00 /20.00	26.33	0.56	191.52	47.50	0.35	0.0864
9 (27.00 – 29.00)	44	Silty SAND	Dense	19.00 /21.50	35.50	3.50	-	66.00	0.35	8.64
10 (29.00 – 30.00)	51	Silty SAND	Very Dense	19.00 /21.50	38.00	10.00	-	76.50	0.35	86.40
11 (30.00 – 33.00)	30	Silty CLAY	Hard	20.00 /20.00	30.00	5.00	191.52	45.00	0.35	0.0864
12 (33.00 – 35.00)	51	SAND STONE	Very Dense	17.50 /21.00	38.00	10.00	-	76.50	0.20	86.40
13 (35.00 – 36.00)	36	Silty CLAY	Hard	20.00 /20.00	30.00	5.00	191.52	54.00	0.35	0.0864
14 (36.00 – 39.00)	51	SAND STONE	Very Dense	17.50 /21.00	38.00	10.00	-	76.50	0.20	86.40
15 (39.00 – 40.00)	51	Silty CLAY	Hard	20.00 /20.00	30.00	5.00	191.52	76.50	0.35	0.0864

4.2 Embankment Planning

Staged construction was essential for the embankment due to the presence of compressible soils with low shear strength and high compressibility. The embankment was constructed in layers of 0.3 m before and 0.2 m after compaction. (SNI 1742, 2008). A rate of one layer per day (≈5 days/m) was adopted up to a height of 5 m to reach the critical elevation. Beyond this stage, a minimum preloading period of 30 days was applied to allow excess pore water pressure dissipation and strength gain. Subsequently, a surcharge of approximately 1.8 m was added to accelerate primary consolidation. The overall staged construction sequence is illustrated in Figure 2.

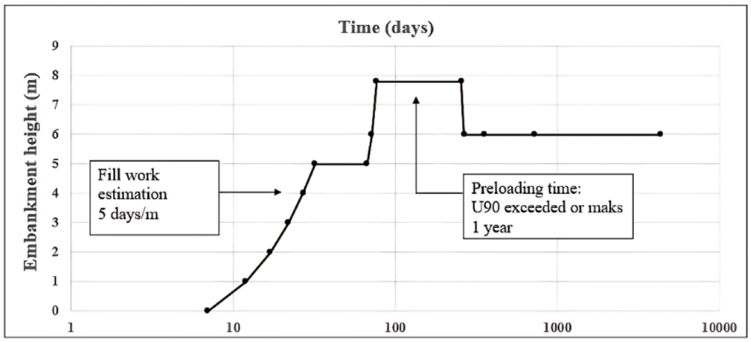

Figure 2. Stages for Embankment Work

4.3 Embankment Data and Soil Replacement Data

The selection of fill materials and soil replacement methods is based on the guidelines contained in the reference. (Departemen Permukiman dan Prasarana Wilayah, 2002)The parameters used in the planning are presented in detail in Table 3.

Table 3. Parameters for embankment design and soil replacement

	γ/γ_{sat} (kN/m^3)	φ' (°)	c' (kPa)	E_{ref} (MPa)	v	k (m/day)
Embankment	17.00/17.00	20.00	5.00	3.00	0.40	0.000864
Soil Replacement	17.00/21.00	36.00	0.50	76.50	0.25	8640

4.4 Results

4.4.1 Embankment Stability Analysis without Improvement

A stability analysis of the embankment was conducted to evaluate slope stability under existing conditions without soil improvement, considering embankment, pavement, traffic, and earthquake load combinations. The following figure shows the contour of potential failure and the safety factor values for each load case. The application setting limited the analysis boundary; however, the critical sliding surface and safety factors were still adequately captured. Thus, the adopted boundary is considered sufficient. Figure 3 presents the embankment conditions without improvement under two types of loading: embankment load alone and embankment load plus earthquake load.

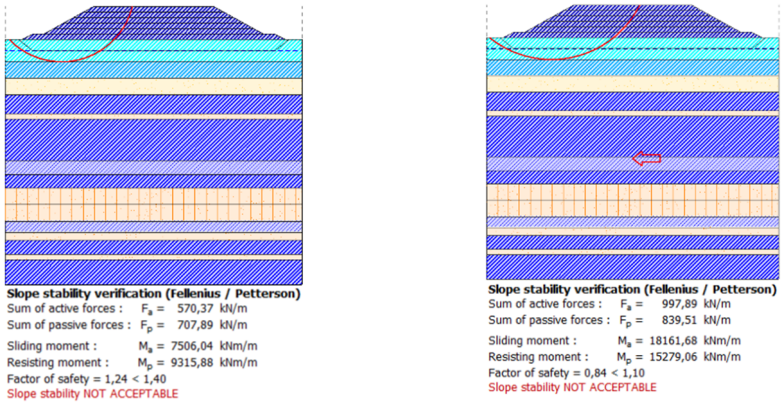

(a) (b)

Figure 3. a. Embankment Load without Improvement, b. Embankment Load Plus Earthquake Load without Improvement.

Meanwhile, Figure 4 illustrates the conditions when the embankment has been installed, with only pavement load added, and pavement load plus earthquake load added.

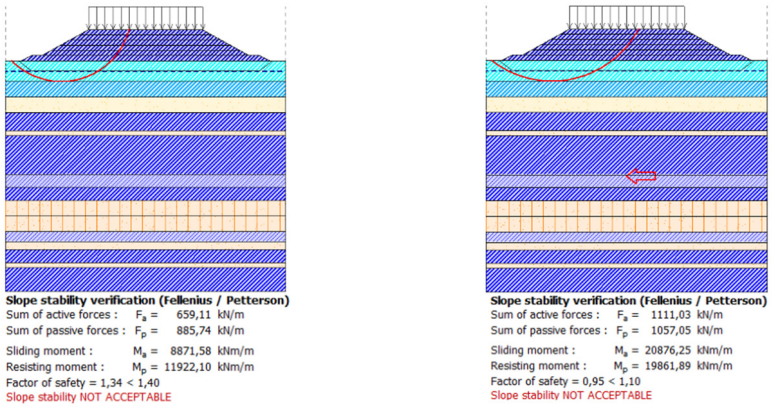

(a) (b)

Figure 4. Pavement Installation without Improvement, b. Pavement Installation Plus Earthquake Load without Improvement

Furthermore, Figure 5 shows the conditions during the operational period, i.e., after the pavement layer and traffic load have been applied. The analysis was conducted only for pavement and traffic load conditions with additional earthquake load.

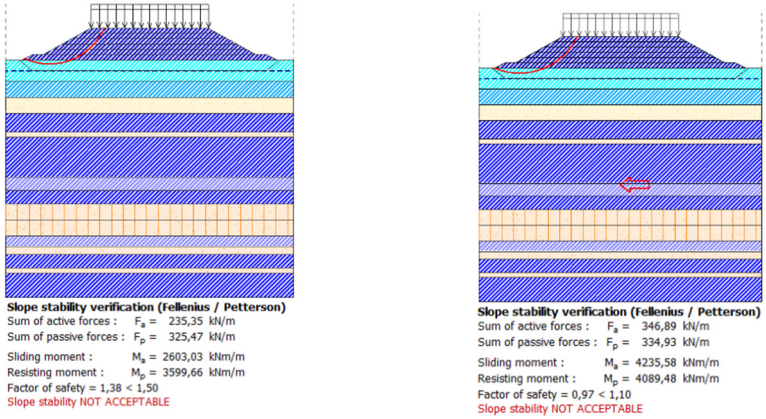

(a) (b)

Figure 5. Operational Period without Improvement, b. Operational Period Plus Earthquake Load without Improvement

The figure's visual and numerical analysis results show that the safety factor values under all conditions do not meet the minimum stability requirements, indicating that the embankment structure in this condition is still unstable and requires soil improvement or other stabilization methods.

4.4.2 Soil Improvement Method

A soil improvement and embankment reinforcement approach was adopted to address the geotechnical problems at the study site, considering the medium clay soil characteristics identified at borehole DD-08. Based on the analysis results and referring to (Koerner, 2005) and (Departemen Permukiman dan Prasarana Wilayah, 2002)A combination of soil replacement and basal geosynthetic reinforcement was selected as the most efficient technical solution.

The soil improvement works were carried out through soil replacement up to a depth of 2 meters to reduce the thickness of the compressible clay layer and increase the bearing capacity. To further improve slope stability and resist shear forces within the soft layer, a woven geotextile with a long-term tensile strength of 75 kN/m² was installed horizontally at the base of the embankment. The horizontal placement of woven geotextile at the embankment base provides lateral reinforcement to the medium clay soil, particularly in the zone of maximum shear stress, which is critical to potential failure under the embankment load. According to (Koerner, 2005), geosynthetics placed at the

embankment base function as tensile elements that enhance slope stability, reduce lateral deformation, and increase the safety factor under both static and seismic conditions.

Although (Das & Sobhan, 2014) Note that basal reinforcement can be combined with preloading or vertical drains to accelerate consolidation. In this project, the applied method was limited to soil replacement and basal geosynthetic reinforcement. This selection was based on both technical and economic considerations, aiming to reduce residual settlement, improve slope stability, and achieve an adequate factor of safety without requiring additional ground improvement measures.

4.4.3 Embankment Stability Analysis with Improvement

Stability analysis of the embankment after soil improvement was conducted to evaluate the effectiveness of the reinforcement method applied, namely a combination of soil replacement to a depth of 2 meters and the installation of horizontally laid woven geotextile at the base of the embankment. According to the previously established stability criteria, the evaluation included loading conditions due to the embankment, pavement, traffic loads, and seismic effects. Figure 6 shows the analysis results of the embankment conditions after soil improvement under two load conditions: embankment load alone and embankment load plus earthquake load. The distribution of failure zones and safety factor values is displayed to demonstrate the improved performance of the embankment structure.

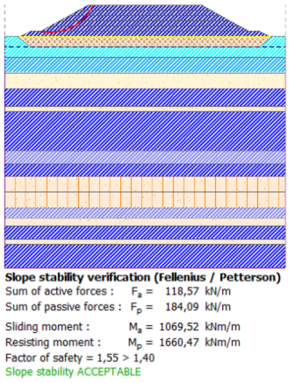

(a)

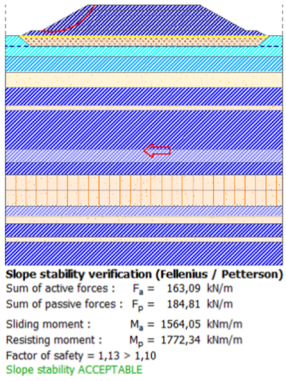

(b)

Figure 6. Embankment Load with Improvement, b. Embankment Load Plus Earthquake Load with Improvement.

Meanwhile, Figure 7 shows the condition of the embankment after the installation of the pavement layer, which was analyzed under two types of loading, namely pavement load alone and pavement load combined with seismic load.

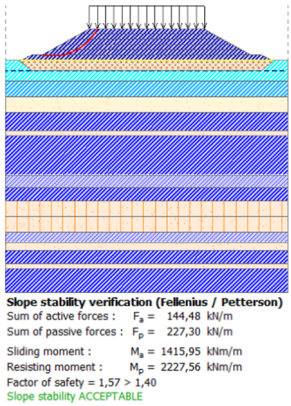

(a)

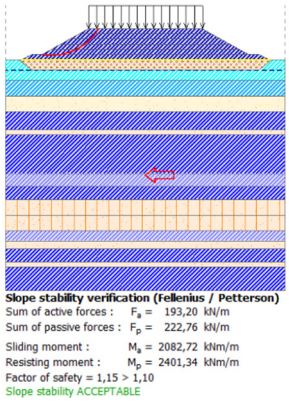

(b)

Figure 7. Pavement Installation with Improvement, b. Pavement Installation Plus Earthquake Load with Improvement.

Furthermore, Figure 8 shows the conditions during operation, i.e., after the pavement layer and traffic load are fully operational. The analysis was conducted for two conditions: pavement load and traffic load alone, and pavement load, traffic load, and earthquake. The analysis results show that the safety factor value increased significantly after applying the soil improvement method.

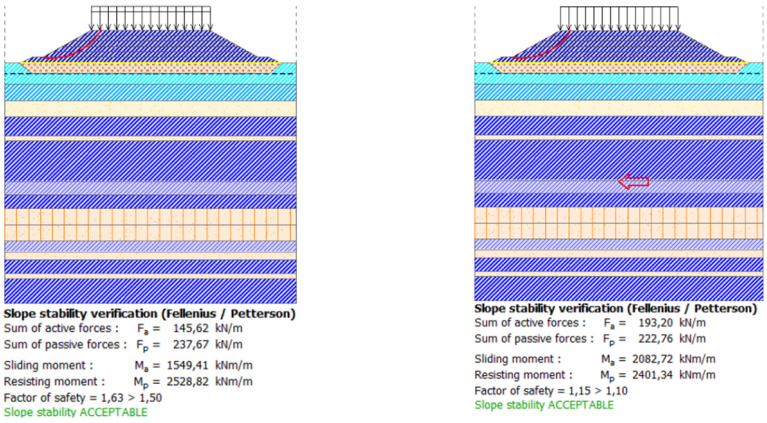

(a) (b)

Figure 8. Operational Period with Improvement, b. Operational Period Plus Earthquake Load with Improvement

After soil improvement was carried out using a combination of soil replacement and geotextile installation methods, visual and numerical analysis showed that the safety factor values under all load conditions met the minimum required limits. This indicates that the embankment structure is stable and safe under both static and dynamic (earthquake) loads, making it suitable to proceed to the operational stage.

4.4.4 Settlement Analysis

A settlement analysis was conducted to predict the magnitude and rate of settlement of the embankment during the construction and operational periods, especially since the embankment was built on highly compressible medium clay soil. Uncontrolled settlement can damage the road structure and endanger users' safety. Therefore, the construction stages and their timing must be accurately modelled to obtain precise settlement estimates. (Chen et al., 2024). Table 4 presents the construction work stages and their cumulative execution times, which are used as input data in the settlement analysis modelling process.

Table 4. Construction stages for settlement analysis in the program

Number	Construction Stages	Cumulative Road Construction Time (days)
1	Excavation and soil replacement	7
2	Embankment 1 m	12
3	Embankment 2 m	17
4	Embankment 3 m	22
5	Embankment 4 m	27
6	Embankment 5 m	32
7	Rest period (30 days)	67
8	Embankment 6 m	72
9	Installation surcharge load (1,8 m)	77
10	Preloading (4 months)	257
11	Unloading surcharge	267
12	Installation pavement	357
13	1-year consolidation	722
14	10-year consolidation	4372

Based on the modelling software analysis results, Figure 9 presents a graph of the relationship between settlement and time, and Figure 10 shows the degree of consolidation over time.

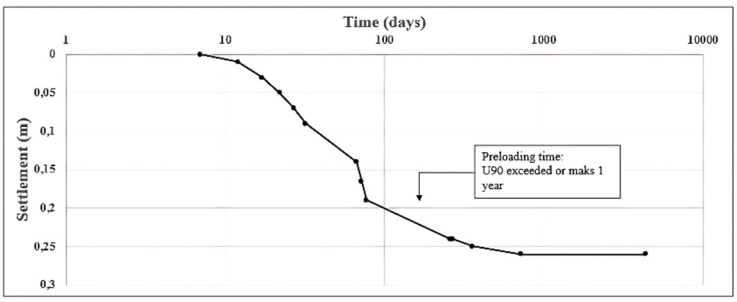

Figure 9. Graph of settlement over time

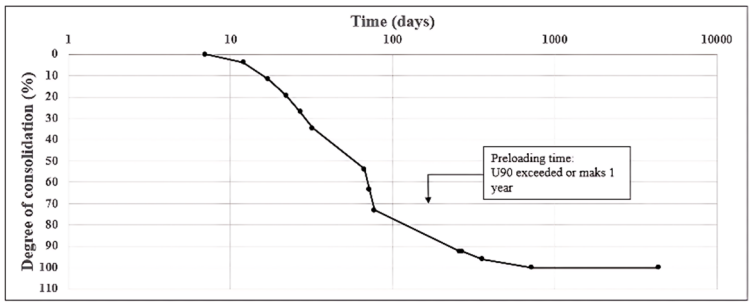

Figure 10. Graph of the degree of consolidation over time

Figure 9 shows the graph of settlement over time, where at the end of the preloading stage, the degree of consolidation had reached more than 90%, indicating that primary consolidation had been achieved. Meanwhile, Figure 10 presents the graph of the degree of consolidation over time. The total settlement during the operational period of 0.01 m is within the permitted limit of ≤ 0.10 m according to (Departemen Permukiman dan Prasarana Wilayah, 2002). Additionally, the settlement rate of 0.01 m/year is also below the maximum limit of < 0.02 m/year, thus meeting the criteria set by (Manual Desain Perkerasan Jalan No. 02/M/BM/2017, 2017).

4.4.5 Recapitulation of Analysis Results

Table 5 below provides a summary of the results of the evaluation of pile stability and settlement analysis.

Table 5. Recapitulation of the Results of the Embankment Stability and Settlement Analysis

Embankment Stability				
Condition		Construction Stages and SF Term	SF Value	Description
Without improvement	Short term	Embankment, SF > 1.4	1.24	Collapse
		Embankment plus earthquake load, SF > 1.1	0.84	Collapse
		Pavement installation, SF > 1.4	1.34	Collapse
		Pavement installation plus earthquake load, SF > 1.1	0.95	Collapse
	Long term	Operational period, SF > 1.5	1.38	Collapse
		Operational period plus earthquake load, SF > 1.1	0.97	Collapse
With improvement	Short term	Embankment, SF > 1.4	1.55	Safe
		Embankment plus earthquake load, SF > 1.1	1.13	Safe
		Pavement installation, SF > 1.4	1.57	Safe
		Pavement installation plus earthquake load, SF > 1.1	1.15	Safe
	Long term	Operational period, SF > 1.5	1.63	Safe
		Operational period plus earthquake load, SF > 1.1	1.21	Safe
Settlement				
Total settlement after the operational period			0.01 m ≤ 0.10 m	
Settlement rate			0.01 m/year < 0.02 m/year	

5 DISCUSSION

Based on the analysis results, the dominant collapse zone is identified as the water-saturated clay layer at a depth of 1–5 meters, classified as medium clay with relatively low strength. This condition confirms that slope collapse occurs in medium clay soil, not deeper and denser soil layers. This

finding is in line with (Gusnadi et al., 2023), which states that soft clay in Subang has high compressibility and low cohesion, making it highly susceptible to collapse when subjected to vertical loads from embankments.

The parameter most influencing slope stability is the bulk density of the fill material (γ). The sand used as fill has high density, exerting significant additional pressure on the underlying soil. In the short term, pore water pressure has not yet dissipated, and the soil's shear strength depends only on undrained cohesion, resulting in a low SF. However, in the long term, after primary consolidation, the soil experiences an increase in adequate shear strength, contributing to the rise in the SF value. (Chen et al., 2024).

The safety factor increased significantly after improvements were made using a combination of soil replacement to a depth of 2 meters and the installation of woven geotextile with a strength of 75 kN/m². This improvement was evident throughout all loading stages, including during backfilling, compaction, and operational conditions, both without and with seismic loads ($k_h = 0.16g$). The effectiveness of this improvement is also confirmed by (Agustina et al., 2024), who found that horizontal reinforcement with woven geotextile can resist lateral deformation and substantially increase the shear strength of the subgrade soil.

The following is a visualization of the results summarized in Table 5, which presents two comparison graphs of safety factor values. Figure 12 compares SF values between the condition without improvement and with improvement under static conditions. Meanwhile, Figure 13 compares SF values for earthquake loading conditions, both without improvement and with improvement.

The following figures present the results from Table 5. Figure 11 shows a comparison of SF values under earthquake load, both without and with improvement, while Figure 12 presents a similar comparison for SF values under other loading conditions.

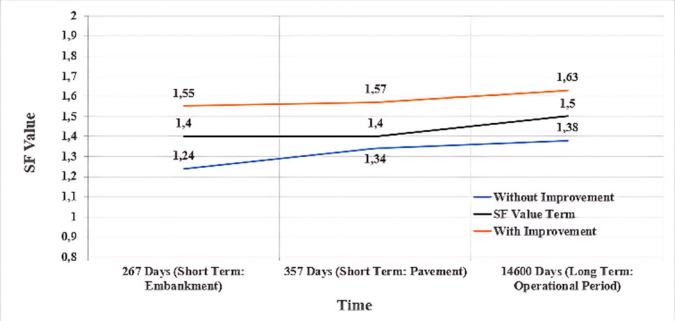

Figure 11. Comparison Graph of SF Value without Improvement and with Improvement

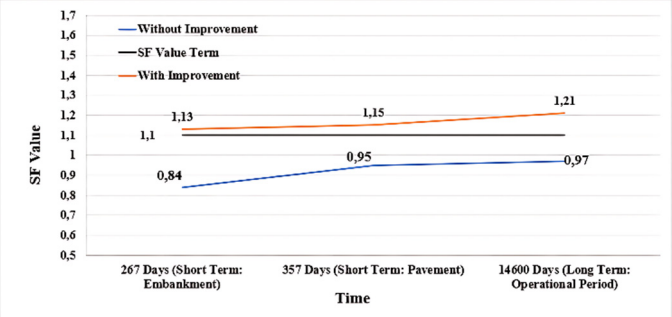

Figure 12. Comparison Graph of SF Values of Earthquake Load without Improvement and with Improvement

Figure 11 shows the trend of increasing safety factor values over time for two conditions: without repair and with repair. Under the no-repair condition, the SF value starts at 1.24 during the embankment phase (267 days), increases to 1.34 during the pavement phase (357 days), and reaches 1.38 during the operational phase (14,600 days). Although there is an increase, this value does not yet meet the established safety threshold of 1.4 for the long term. Conversely, in the condition with

improvements, the SF value was already above the stability threshold from the start, at 1.55 during the embankment phase, increasing to 1.57 during the paving phase, and reaching 1.63 during the operational phase. This indicates that the improvement methods (soil replacement and woven geotextile) successfully created slope stability from the early stages of construction. Additionally, Figure 12 shows the Safety Factor (SF) trend over time under earthquake load conditions for two conditions: without improvement and with improvement. Under the no-remediation condition, the SF value remained below the safe threshold throughout the analysis period. The SF value was recorded at 0.84 during the embankment phase (267 days), increased to 0.95 during the paving phase (357 days), and only reached 0.97 during the operational phase (14,600 days). This condition indicates that the embankment structure is highly susceptible to collapse when subjected to dynamic loads, particularly during long-term service. This improvement suggests that the repair method, which combines soil replacement to a depth of 2 meters and the installation of woven geotextile with a strength of 75 kN/m², effectively enhances slope stability against seismic loads from the initial stage through the operational period. Furthermore, the settlement analysis results show a total vertical deformation of 0.01 m with a settlement rate of 0.01 m/year, well below the national threshold (≤ 0.10 m and < 0.02 m/year). These results reinforce the conclusion that phased construction planning, preloading loads, and geotextiles can accelerate consolidation and control long-term deformation in embankments on medium clay soil (Chen et al., 2024)..

6 CONCLUSION

Based on the analysis results, it can be concluded that the combination of soil replacement to a depth of 2 meters, installation of woven geotextile with a tensile strength of 75 kN/m², and a four-month preloading stage effectively improves slope stability and controls the settlement of a 6-meter-high embankment constructed on medium clay soil. After the improvement, all safety factor values under six loading conditions increased significantly and met the minimum stability criteria. The predicted vertical deformation of about 0.01 m and a settlement rate of 0.01 m/year are within acceptable design limits. This combined method has proven suitable for application in embankment projects on clay soil, particularly in earthquake-prone areas.

REFERENCES

Agustina, Y. P., Handiman, I., Sarifah, F., Hamonangan, E. K., Irawan, P., & Gusnadi, Z. (2024). Analysis of Soil Replacement and Woven Geotextile Reinforcement on Embankment Stability. *INVOTEK: Jurnal Inovasi Vokasional Dan Teknologi*, *24*(1), 53–66. https://doi.org/10.24036/invotek.v24i1.1168

Ameratunga, J., Sivakugan, N., & Das, B. M. (2016). *Correlations of Soil and Rock Properties in Geotechnical Engineering* (B. M. Das & Henderson (eds.)). Springer. https://doi.org/10.1007/978-81-322-2629-1

Badan Penelitian dan Pengembangan Pekerjaan Umum. (2012). Pedoman Analis Harga Satuan Pekerjaan (AHSP) Bidang Pekerjaan Umum. In *simantu.pu.go.id*.

Chen, D., Wu, Y., Liu, J., Wu, H., & Ren, Y. (2024). Field Observation and Settlement Prediction Study of a Soft Soil Embankment under Rolling Dynamic Compaction. *Applied Sciences (Switzerland)*, *14*(15). https://doi.org/10.3390/app14156454

Das, B. M., & Sobhan, K. (2014). *Principles of Geotechnical Engineering* (H. Gowans (ed.)). Global Engineering.

Departemen Permukiman dan Prasarana Wilayah. (2002). *Pedoman Kimpraswil No: Pt T-10-2002-B Panduan Geoteknik 4 Desain dan Konstruksi Timbunan Jalan pada Tanah Lunak*. Departemen Permukiman dan Prasarana Wilayah.

Gusnadi, Z., Handiman, I., & Sarifah, F. (2023). Analisa Perbaikan Tanah Lunak Menggunakan Controlled Modulus Columns (CMC) pada Konstruksi Timbunan Jalan. *Akselerasi : Jurnal*

Ilmiah Teknik Sipil, *4*(2), 11–16. https://doi.org/10.37058/aks.v4i2.5670

Hamonangan, E. K., & Syahputra, M. Y. (2023). Perbandingan Hasil Analisis Finite Element Untuk Stabilitas Dan Penurunan Timbunan Dengan Beberapa Soil Model Di Lokasi Rencana Pembangunan Jalan Tol Subang. *Jurnal HPJI*, *9*(1), 1–8. https://doi.org/10.26593/jhpji.v9i1.6434.1-8

Hardiyatmo, H. C. (2002). *Mekanika Tanah 1*. Gadjah Mada University Press.

Indraratna, B., Atapattu, S., Rujikiatkamjorn, C., Arivalagan, J., & Jing, N. (2024). Soft Soil Improvement by Geosynthetics for Enhanced Performance of Transport Infrastructure. *Geotechnical Engineering*, *55*(1), 1–10. https://doi.org/10.14456/seagj.2024.1

Koerner, R. M. (2005). Designing with Geosynthetics. In *Designing With Geosynthetics*. Pearson Education, Inc.

Manual Desain Perkerasan Jalan No. 02/M/BM/2017 (Issue 02). (2017). Kementerian Pekerjaan Umum dan Perumahan Rakyat Direktorat Jenderal Bina Marga.

Muntohar, A. S., Hartono, E., Diana, W., & Rahmawati, A. (2021). Effect of Cement Replacement with Carbide Waste on the Strength of Stabilized Clay Subgrade. *Civil Engineering Dimension*, *18*(1), 8–15. https://doi.org/10.9744/ced.18.1.8-15

Pustlitbang PUPR. (2017). *Peta Sumber dan Bahaya Gempa Indonesia Tahun 2017*.

SNI 1726. (2019). *Tata Cara Perencanaan Ketahanan Gempa untuk Struktur Bangunan Gedung dan Non Gedung*. Badan Standarisasi Indonesia.

SNI 1742. (2008). Cara Uji Kepadatan Ringan Untuk Tanah. In *Badan Standardisasi Nasional*.

SNI 8460. (2017). *Persyaratan Perancangan Geoteknik*. Badan Standarisasi Nasional.

Thahir, L., Barkah, M. N., Sophian, R. I., Firmansyah, Y., Sunarie, C. Y., Hadian, M. S. D., & Kevin, A. M. (2024). Sumber Daya Geologi Dan Tantangan Bencana Alam Di Kecamatan Cijambe Dan Cibogo, Kabupaten Subang, Provinsi Jawa Barat. *Padjadjaran Geoscience Journal*, *8*(4). https://jurnal.unpad.ac.id/geoscience/article/view/61661

This page is intentionally left blank

HIMPUNAN AHLI TEKNIK TANAH INDONESIA - HATTI
Indonesian Society for Geotechnical Engineering - ISGE
PIT HATTI XXIX
10-12 November 2025

Design Review of Pile Cap Excavation Reinforcement System at the IC3 Interchange of the Patimban Access Toll Road Project, Indonesia

Bobby Novialdi Saputra[1, *]
[1]PT Wijaya Karya (Persero) Tbk, Infrastructure 1 Division, Jakarta, Indonesia, Postal Code 13340; bobby.novialdi@gmail.com
*Correspondence: bobby.novialdi@novialdi@gmail.com

ABSTRACT This paper presents a design review of the pile cap excavation reinforcement system at the IC3 Interchange of the Patimban Access Toll Road Project, Package 4. The original design relied on a steel sheet pile (SSP) wall as the retaining structure, which was found to be inadequate in meeting stability requirements. To address this issue, the design was reviewed by adding strut and waler reinforcement using H-Beam 350x350 mm and 400x400 mm sections. The analysis was based on the soil investigation data from CB.04-26 and construction drawings at location P-8. Numerical analysis was performed using Plaxis 2D for geotechnical modeling and SAP2000 for structural verification. The results indicated that the reinforcement system achieved a global factor of safety of 1.64 and limited wall deformation to 4.9 cm, both satisfying the minimum requirements of SNI 8460:2017. The results showed that the reviewed system achieved a global factor of safety of 1.64 and limited wall deformation to 4.9 cm, both of which satisfied the minimum requirements of SNI 8460:2017. Structural analysis confirmed that he P–M ratios of the H-beam struts and walers were below the allowable limit, although additional diagonal struts were required to ensure structural adequacy. This study demonstrates the effectiveness of integrating geotechnical and structural modeling for excavation design, particularly for complex conditions near active roadways. The findings contribute to practical knowledge on excavation reinforcement systems and provide a methodological reference for similar infrastructure projects.

KEYWORDS steel sheet pile; strut and waler; excavation; PLAXIS 2D; SAP 2000

1 INTRODUCTION

The Patimban Access Toll Road Project is a national strategic project designed to improve connectivity between Patimban Port in Subang, West Java, and the Trans-Java Toll Road network, especially the Cikopo–Palimanan (Cipali) section. The project extends for 37.05 km and is divided into five construction packages. Package 4, executed by the WIKA–ADHI joint operation, covers a 3.55 km segment between STA 33+500 and STA 37+050. Within this package, Interchange 3 is located at STA 35+900, spanning 337 m and supported by bored pile foundations with a diameter of 1.0 m grouped into pile caps. Several pile caps are situated adjacent to the active Pantura highway, creating additional safety challenges due to traffic loads and the potential impact on excavation stability. Under these conditions, excavation support systems play a critical role in ensuring safe construction practices and minimizing adverse effects on nearby infrastructure.

Excavation support structures are widely applied in geotechnical engineering to stabilize soil masses and control deformation during construction. Retaining walls such as steel sheet piles (SSP), struts, walers, and diaphragm walls are commonly selected based on soil conditions and project requirements [Han, 2015; Duncan et al., 2014; Das, 2010]. Numerical modeling has become an essential tool for the design and evaluation of these systems, particularly through finite element methods. The Hardening Soil Model (HSM) is often adopted for its ability to capture nonlinear stress–strain behavior, stress-path dependency, and realistic soil–structure interaction compared to traditional limit equilibrium methods [Carter & Bentley, 2016; Bui et al., 2024]. This approach enables more reliable prediction of wall deflection, ground deformation, and internal forces.

Previous studies have demonstrated the effectiveness of strut-supported excavation systems in controlling excavation stability. Goh et al. (2018) analyzed strut responses under failure scenarios, while Zhang et al. (2019) and Nguyễn & Le (2023) examined strut force estimation through numerical analysis and field data. Case studies in Jakarta have further demonstrated the benefits of reinforced systems, such as double-wall retaining structures, in reducing soil movement during deep excavations [Anthony et al., 2024]. However, these investigations primarily focus on deep urban excavations for metro stations or basement structures, with limited attention to shallower but equally critical applications, such as pile cap excavations adjacent to major highways.

In this project, the original design for the pile cap excavation at Interchange 3 used a steel sheet pile wall. Preliminary analysis indicated that this design was insufficient to meet the required safety factor and deformation limits. A revised design was proposed by adding struts and walers using H-Beam 350 × 350 mm and 400 × 400 mm sections. To evaluate this system, geotechnical modeling was performed using PLAXIS 2D, while structural verification was carried out in SAP2000. The combination of these tools enabled comprehensive analysis of both soil–structure interaction and member capacity under axial and bending effects. The objective of this study is to assess the capacity of the reinforcement system and to demonstrate the importance of integrating geotechnical and structural modeling in excavation design. The findings are expected to contribute to practical knowledge on safe excavation practices near heavily trafficked infrastructure and serve as a methodologoical reference for similar geotechnical projects in Indonesia.

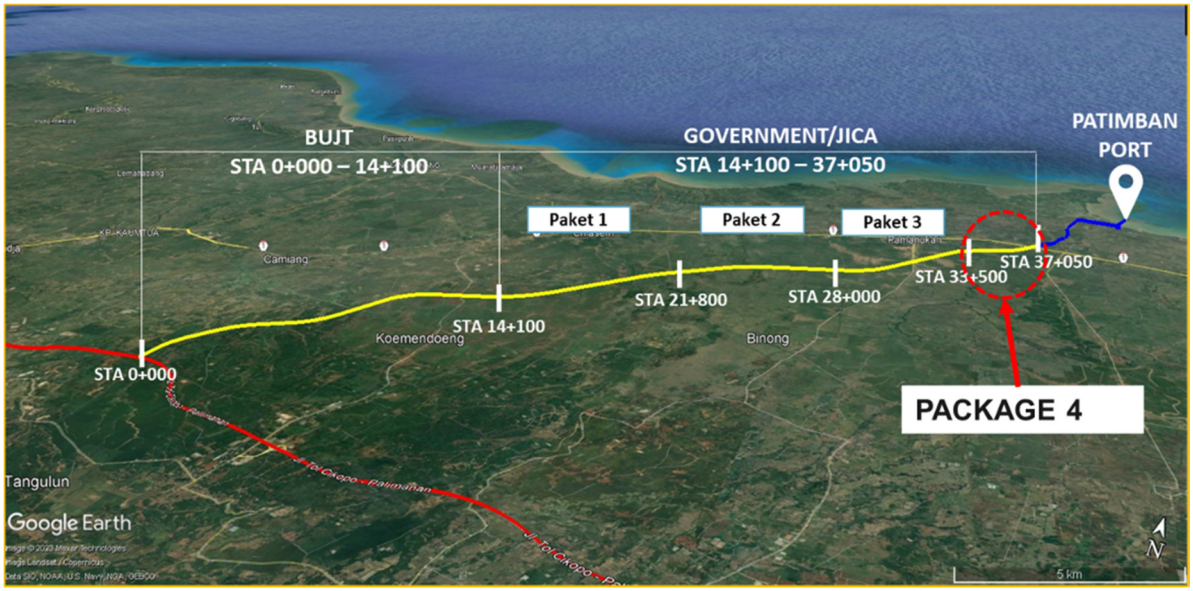

Figure 2. Location of Patimban Access Toll Road Project

Table 2. Maximum Allowable Lateral Deformation for Retaining Walls

Batas maksimum deformasi lateral pada dinding Keterangan: x = jarak dari batas galian, H = Kedalaman galian, δw = defleksi dinding	**Lokasi gedung dan infrastruktur eksisting terdekat**			
	Zona 1 (x/H < 1)	Zona 2 (1≤ x/H ≤ 2)	Zona 3(x/H > 2)	
			Tanah Tipe A	Tanah Tipe B
Batas izin maksimum deformasi (δw/H)	0,5%	0,7%	0,7%	1,0%

Keterangan:

a) Tanah Tipe A meliputi: tanah lempung dan lanau *overconsolidated* (*over-consolidated stiff clays dan silts*), tanah residual (*residual soils*), dan tanah pasir dengan kepadatan sedang sampai dengan padat (*medium to dense sands*).

b) Tipe Tanah B meliputi: tanah lempung dan lanau lunak (*soft clays, silts*), tanah organik (*organic soils*) dan tanah timbunan tidak terpadatkan (*loose fills*).

2 PROJECT DATA AND ANALYSIS METHODS

2.1 Project Data

The excavation for the IC3 pile caps required substantial earthworks due to the large foundation dimensions and depth. For this study, the pile cap at Pier 8 (P8) was selected as the representative case. The excavation depth typically range from 6 to 7 m, with plan dimensions of approximately 12 m × 20 m, depending on the pile cap configuration (Figure 3). The original design employed a steel sheet pile (SSP) retaining wall using Type III and Type IV sections (Figure 4). Considering the excavation geometry, subsurface conditions, and groundwater table, slope stability and lateral wall deformation were identified as the primary design concerns requiring further review.

2.2 Subsurface Conditions

Subsurface conditions were characterized from Borehole CB.04-26 (Patimban, 2024), which is the closest investigation point to the IC3 pile cap (Figure 5). The soil profile generally consists of soft to stiff clays with occasional silty and sandy layers. The upper 2.0 m is dominated by soft silty clay (CH–OH), which is highly compressible, weak, and contains shallow groundwater, posing critical challenges for excavation stability. Below this, the soil transitions into medium stiff to stiff high-plasticity clays (CH) extending to about 6.0 m depth, followed by a mixed zone of low-plasticity clays (CL) and silty soils (ML) down to around 12.0 m. These intermediate layers increase the risk of water seepage due to higher permeability.

At depths greater than 12.0 m, the soil profile is dominated by stiff high-plasticity clays (CH) with occasional sand seams, providing higher undrained strength, and further down transitions into dense silty clays (MH/CL) that serve as a competent bearing stratum. Overall, the soil conditions indicate potential stability and deformation issues in the upper soft clay layers, justifying the need of a reinforced excavation system with steel sheet piles and additional struts and walers to control lateral movement and achieve global stability.

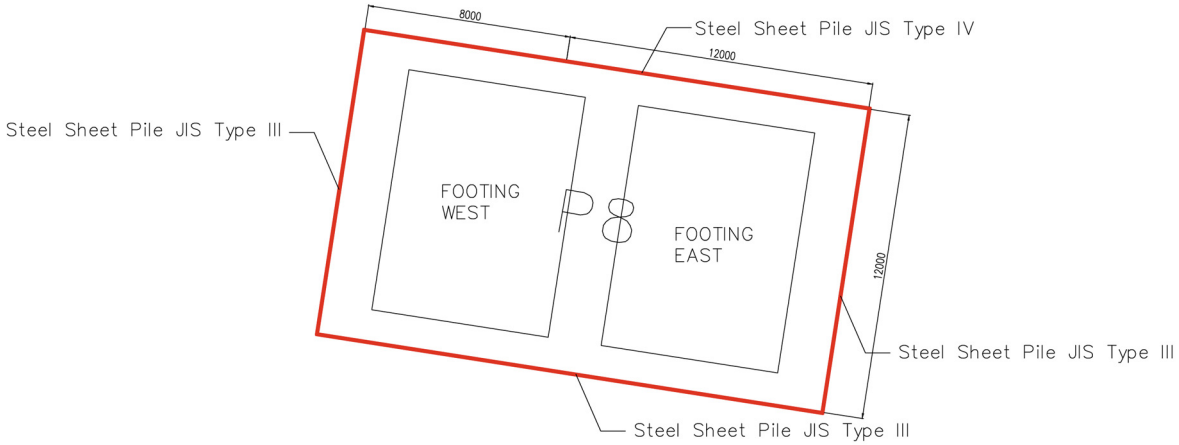

Figure 3. Pile cap excavation layout (P8)

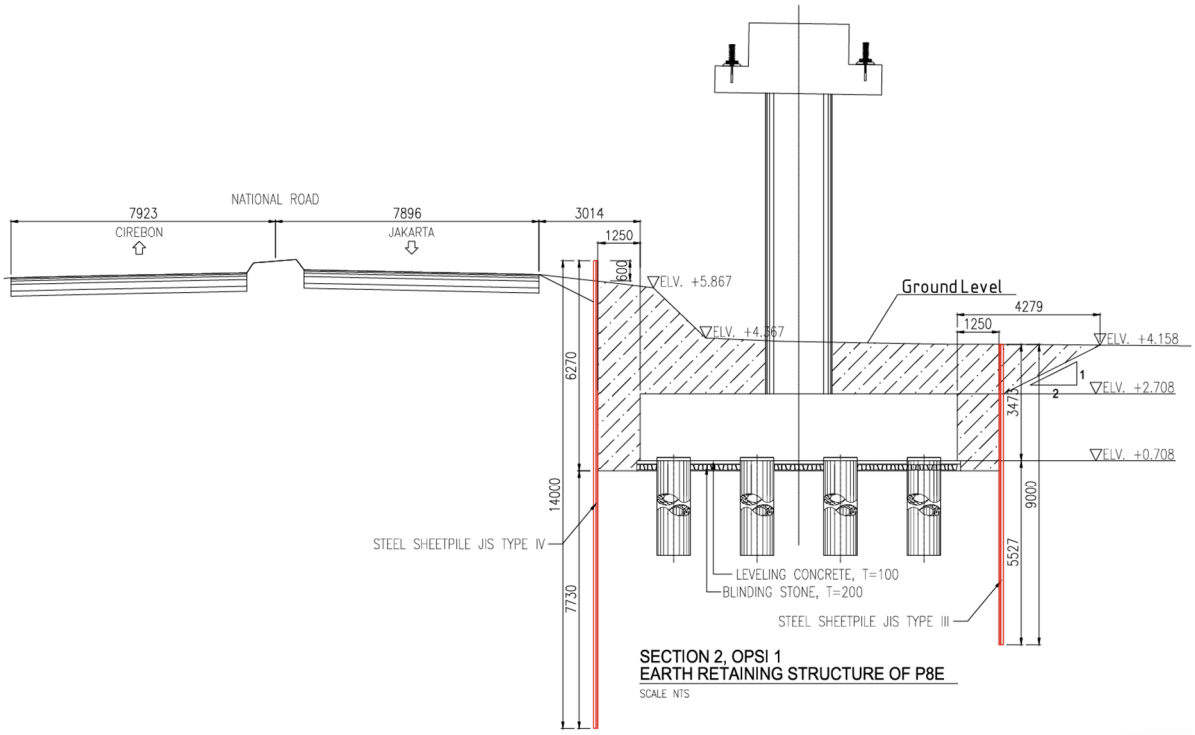

Figure 4. Cross section of pile cap excavation (P8)

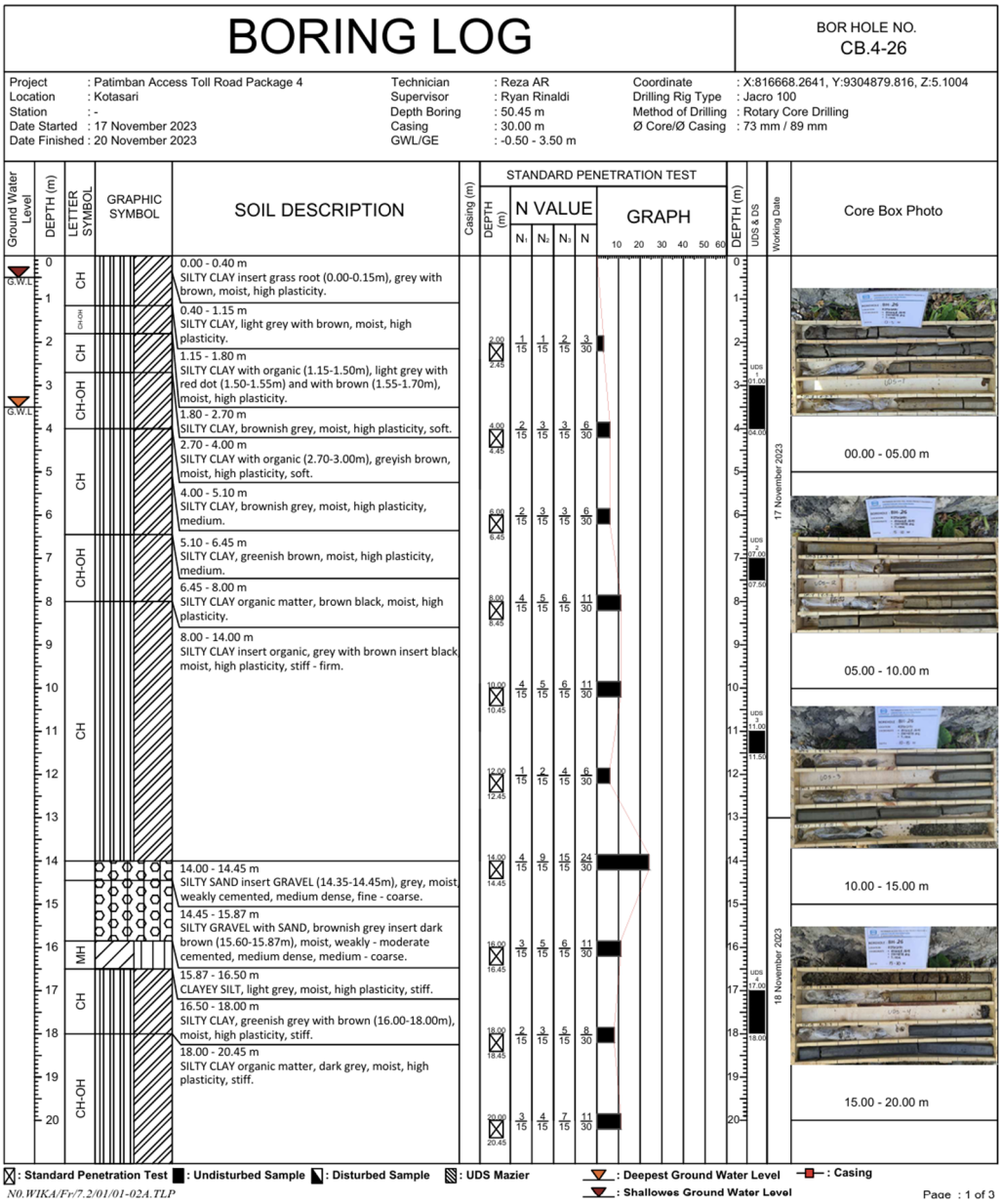

Figure 5. Soil investigation data (CB.04-26) (1/2)

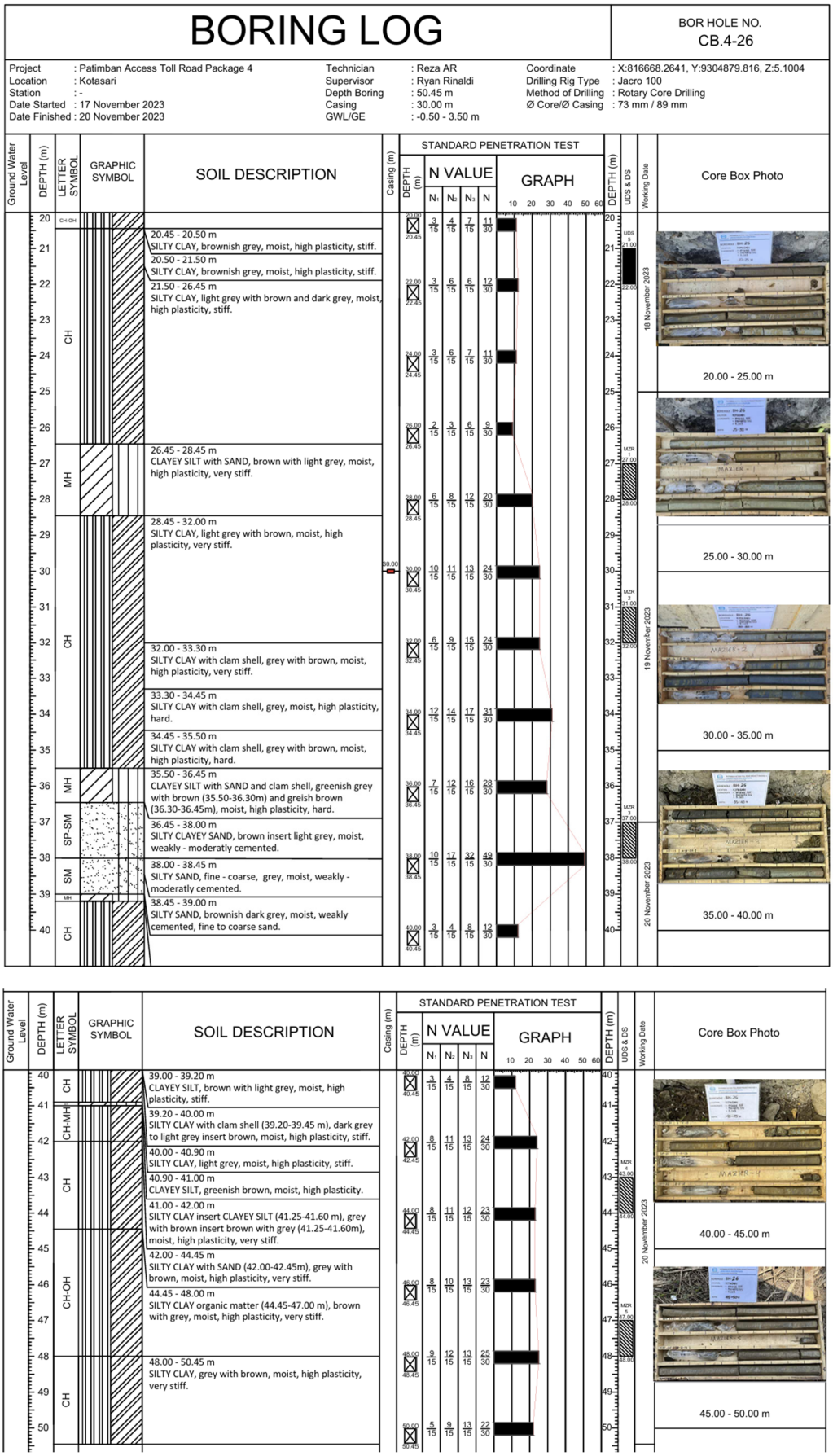

Figure 6. Soil investigation data (CB.04-26) (2/2)

Table 3. Laboratory test result of CB.04-26

NO	TITIK BOR	KODE SAMPEL DEPTH (m)	KLASIFIKASI (USCS)	SIFAK FISIK (INDEX PROPERTIES)												SIFAT KETEKNIKAN (ENGINEERING PROPERTIES)												
				WC	ATTERBERG (%)			ANALISA SARINGAN (%)				BERAT JENIS (gr/cm³)	ACTIFITY	BERAT ISI TANAH		TRIAXIAL UU		DS		UCS		CONSOLIDATION TEST						
				%	LL	PL	PI	CLAY	SILT	SAND	GRAVEL			w	d	c (kg/cm²)	(ϕ) °	c (kg/cm²)	(ϕ) °	Qu (kg/cm²)	Sr	Po (kg/cm²)	Pc (kg/cm²)	OCR	Cc	Cr	Cv (cm²/year)	Mv (cm²/kg)
1	BH 26	UDS-1 (3.00-4.00 m)	CH-OH	39,88	66,706	23,844	42,863	51,38	45,60	3,03	-	2,508	0,834	1,772	1,250	0,22	34,26	-	-	0,36	0,89	0,332	0,071	0,212	0,167	0,013	14,910	1,E-02
2	BH 26	UDS-2 (7.00-7.50 m)	CH-OH	32,43	64,175	27,892	36,283	53,09	44,21	2,70	-	2,553	0,683	1,905	1,443	0,67	20,75	-	-	1,59	1,09	0,279	0,114	0,409	0,195	0,014	20,105	1,E-02
3	BH 26	UDS-3 (11.00-11.50 m)	CH-OH	52,63	92,739	37,059	55,680	51,96	47,37	0,67	-	2,539	1,072	1,771	1,229	0,42	17,87	-	-	-	-	0,389	0,190	0,489	0,259	0,019	16,424	1,E-02
4	BH 26	UDS-4 (17.00-18.00 m)	CH-OH	46,08	81,857	32,601	49,256	51,37	48,00	0,64	-	2,587	0,959	1,692	1,119	0,45	31,05	-	-	1,50	1,36	0,267	0,041	0,155	0,228	0,036	16,157	2,E-02
5	BH 26	UDS-5 (21.00 - 22.00 m)	CH-OH	36,82	69,121	25,592	43,529	52,76	41,97	5,05	0,21	2,663	0,825	1,855	1,392	0,18	32,79	-	-	0,31	1,65	0,498	0,173	0,348	0,179	0,058	16,615	1,E-02
6	BH-26	MAZIER-1 (27.00-28.00 m)	CH-OH	38,80	57,791	21,160	36,631	45,81	36,12	1,50	16,57	2,679	0,800	1,827	1,316	0,09	0,91	-	-	0,38	1,18	-	-	-	-	-	-	-
7	BH-26	MAZIER-2 (31.00-32.00 m)	CH-OH	37,20	71,646	29,221	42,425	76,28	22,87	0,85	-	2,469	0,556	1,795	1,309	0,17	5,27	-	-	2,05	1,69	-	-	-	-	-	-	-
8	BH-26	MAZIER-3 (37.00-38.00 m)	CH-OH	41,33	91,618	36,392	55,225	81,23	18,29	0,48	-	2,553	0,680	1,871	1,326	0,0013	3,14	-	-	-	-	-	-	-	-	-	-	-
9	BH-25	MAZIER-1 (25.00-26.00 m)	CH-OH	31,02	83,212	29,762	53,450	81,65	18,25	0,11	-	2,620	0,655	1,840	1,410	0,05	1,61	-	-	1,53	1,79	-	-	-	-	-	-	-
10	BH-26	MAZIER-5 (47.00-48.00 m)	CH-OH	37,86	72,631	20,262	52,369	91,49	7,03	-	1,48	2,532	0,572	1,843	1,338	0,87	0,57	-	-	2,63	1,74	-	-	-	-	-	-	-

2.3 Soil Properties

The development of soil properties for numerical modeling in PLAXIS 2D was carried out by correlating field and laboratory test results with empirical relationships. Subsurface data from CB.04-26 were interpreted to identify representative soil layers, supported by soil classification, Atterberg limits, and grain size distribution. Engineering parameters such as unit weight (γ), cohesion (c), friction angle (φ), and stiffness (E) were obtained from laboratory test results and Standard Penetration Test (SPT) correlations. These correlations were cross-checked with published references [Das, 2010 & Carter et al, 2016] to ensure the reliability and representativeness of the soil input parameters used for finite element modeling.

For numerical analysis, the Hardening Soil Model (HSM) was selected as the constitutive model in PLAXIS 2D. Unlike the conventional Mohr–Coulomb model, which assumes constant stiffness, the HSM accounts for stress-dependent stiffness, plasticity, and stress-path dependency, making it more suitable for simulating the behavior of soft clays and granular soils under excavation loading. The model requires three reference stiffness moduli—secant stiffness in standard drained triaxial tests (E50), tangent stiffness for primary oedometer loading (Eoed), and unloading/reloading stiffness (Eur)—in addition to the conventional shear strength parameters. By adopting the HSM, the numerical simulation can better capture the nonlinear stress–strain response and deformation characteristics of the soil, thus providing more realistic predictions of excavation stability and wall deformation.

Among these parameters, the secant stiffness in standard drained triaxial tests (E50) is one of the key input parameters in the Hardening Soil Model (HSM) of PLAXIS 2D. It represents the soil stiffness corresponding to 50% of the maximum deviatoric stress obtained from a drained triaxial test, reflecting the soil's deformation behavior under primary loading. Unlike the elastic modulus in the Mohr–Coulomb model, E50 accounts for the nonlinear stress–strain response of soils, making it more realistic for predicting ground movements in geotechnical problems such as deep excavations. In practice, E50 is often estimated from triaxial laboratory test results or correlated with the Standard Penetration Test (SPT). E50 can also be correlated to SPT 'N' values. As proposed by Hsiung (2018) and Yong (2015), E50 is estimated to be 4'N' (MPa) for clay and 2'N' for sand. The Architectural Institute of Japan (2001) recommends a correlation of E50 = 2.8'N' for all types of soil. Table 4 presents the detailed information about soil parameters which used in PLAXIS 2D analysis.

Table 4. Soil parameters in FEM model

No	Parameter Desain	Code	Unit	Layer 1	Layer 2	Layer 3	Layer 4	Layer 5
0	Depth		m	0-6	6-26	26-36	36-39	39-50
1	Material type	-	-	HS	HS	HS	HS	HS
2	Code material	-	-	C	C	C	S	C
3	Drainage type	-	-	Undrained	Undrained	Undrained	Undrained	Undrained
4	Nilai SPT	NSPT	-	5.00	11.00	25.00	49.00	21.00
5	Unsaturated weight volume	γ_{unsat}	kN/m³	12.50	13.00	13.00	13.50	13.00
6	Saturated weight volume	γ_{sat}	kN/m³	17.00	18.00	18.00	18.50	18.00
7	Total cohession	cu	kN/m²	30	66	150	-	126
8	Effective cohession	c'	kN/m²	3	6.6	15	5	12.6
9	Total friction angle	ϕu	°	5.00	5.00	10.00	44.25	10.00
10	Effective friction angle	ϕ'	°	20.0	25.0	30.0	30.0	30.0
11	Permeability coff.	k	m/s	-	-	-	-	-
12	Permeability coff.	k	m/day	-	-	-	-	-
13	Modulus Young	Eu	kN/m²	15000	19800	52500	66000	44100
14	Modulus Young Efektif	E'	kN/m²	13500	17160	45500	57200	38220
15	Modulus Young 50%	E_{50}	kN/m²	13500	17160	45500	57200	38220
16	Modulus Young Oedometer	E_{oed}	kN/m²	13500	17160	45500	57200	38220
17	Modulus Young Reloading	E_{ur}	kN/m²	40500	51480	136500	171600	114660
18	Poisson ratio	v	-	0.35	0.3	0.3	0.3	0.3
19	Void Ratio	e0	-	0.5	0.5	0.5	0.5	0.5

For the structural analysis of the excavation reinforcement system, the struts and walers were modeled using the material properties of structural steel in PLAXIS 2D. The input parameters included steel sheet pile parameter, the cross-sectional dimensions of H-beam 350 × 350 mm and H-beam 400 × 400 mm, with their respective geometric properties such as area, moment of inertia, and section modulus taken from standard steel profiles. The material strength was defined by the yield stress (fy = 240 MPa) and modulus of elasticity (E = 200,000 MPa). These properties allowed the numerical model to evaluate axial forces between axial element and soils under excavation loads (

No	Section	Dimensions			Sectional Area		Mass		Moment of Inertia	Modulus of Section	Modulus Elasticity
		Width	Height	Thickness			Pile	Wall			
		(b) m	(h) m	t (m)	m2/pile	m2/m	kg/m	kg/m2	m4/m	m3/m	kN/m2
1	NS-SP-IV	0.4	0.17	0.0155	0.009699	0.02425	76.1	190	0.000386	0.00227	2.00E+08
2	NS-SP-III	0.4	0.125	0.013	0.007642	0.0191	60	150	0.000168	0.00134	2.00E+08

Table 6).

Table 5. Steel sheet pile parameters

No	Section	Dimensions			Sectional Area		Mass		Moment of Inertia	Modulus of Section	Modulus Elasticity
		Width	Height	Thickness			Pile	Wall			
		(b) m	(h) m	t (m)	m2/pile	m2/m	kg/m	kg/m2	m4/m	m3/m	kN/m2
1	NS-SP-IV	0.4	0.17	0.0155	0.009699	0.02425	76.1	190	0.000386	0.00227	2.00E+08
2	NS-SP-III	0.4	0.125	0.013	0.007642	0.0191	60	150	0.000168	0.00134	2.00E+08

Table 6. Strut (node-to-node anchor) parameters

No	Section	Dimensions						
		t1	t2	r	A	Ix	Iy	E
1	HB-350x350	12	19	20	0.01739	0.000403	0.000136	2E+08
2	HB-400x400	13	21	22	0.02187	0.000666	0.000224	2E+08

2.4 Geotechnical and Structural Analysis

The analysis procedure was carried out in sequential steps both geotechnical and structural analysis. In the first stage, the original design using a steel sheet pile was simulated in PLAXIS 2D to evaluate global stability (Figure 7). Then, the design was modified by adding a strut and waler system. The reviewed design was a trial error process for resulting an effective and efficient sections (Figure 8).

From these geotechnical models, critical outputs such as global factor of safety, soil and structural deformation, internal forces in steel sheet pile, and axial loads in the strut (modeled as node-to-node anchor) were obtained.

In the second stage, the geotechnical results especially strut axial loads were imported into SAP2000 software for structural verification. The strut and waler system were modeled in three dimensions as shown in Figure 9. The axial forces from PLAXIS 2D were applied as distributed loads on the H-Beam members to represent soil-structure interaction. The structural analysis was performed without load combinations, but the evaluation of H-Beam members followed the Allowable Strength Design (ASD) method, which requires a minimum safety factor of 1.67. This integrated approach ensured that the reinforcement system not only met geotechnical requirements but also the structural strength criteria under excavation conditions.

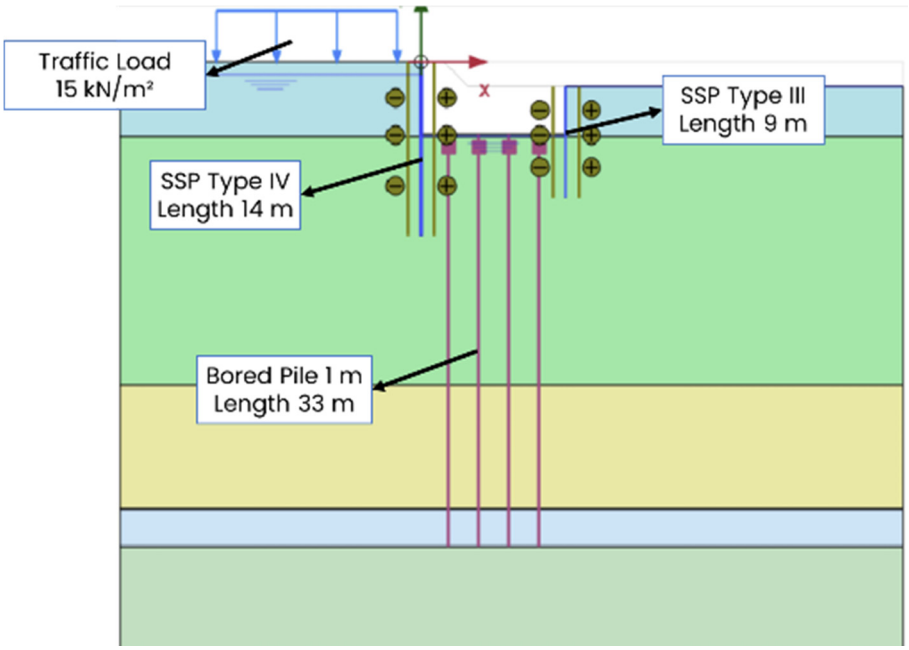

Figure 7. PLAXIS 2D model for pile cap excavation original design

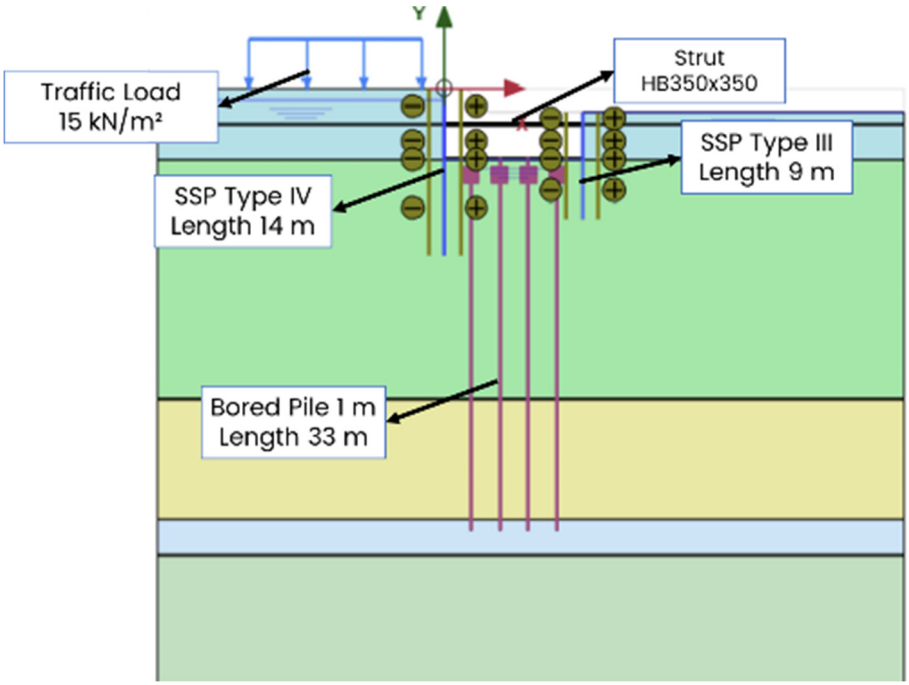

Figure 8. PLAXIS 2D model for pile cap excavation reviewed design

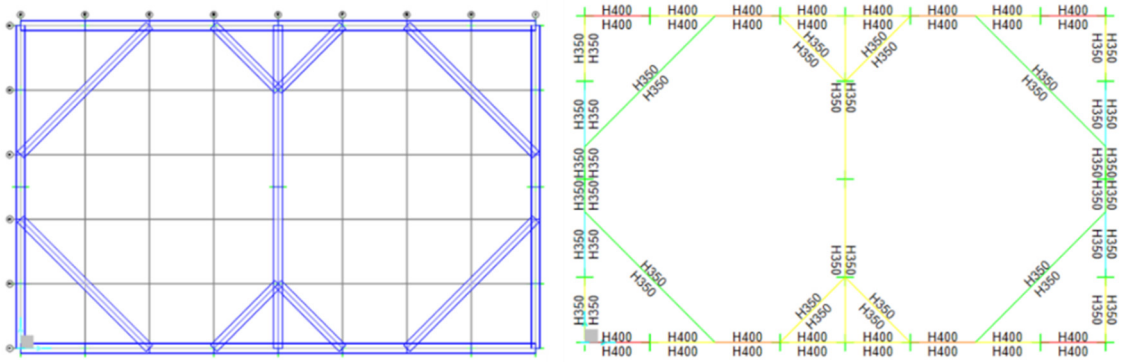

Figure 9. Strut and Waler Structural Analysis in SAP2000

3 RESULTS

3.1 Geotechnical Result

The geotechnical analysis of the original excavation retaining wall design without reinforcement indicated insufficient stability. The factor of safety was less than 1.0, confirming that the initial steel sheet pile could not ensure safe excavation. Excessive lateral displacement was also observed, as shown in Figure 10. Consequently, a design review of the excavation reinforcement system is necessary to ensure safety and compliance with geotechnical design standards.

The reviewed design was developed by adding one layer of struts and walers using H-Beam 350x350 mm and H-Beam 400x400 mm sections. According the analysis result, the global factor of safety increased to 1.64, which exceeds the minimum requirement (Figure 11). The maximum lateral deformation of steel sheet pile wall was reduced to 4.9 cm, which is below the allowable serviceability limit of 6 cm. The corresponding wall deformation patterns, internal forces, and bending moment are illustrated in Figure 12 and Figure 13.

In addition, the PLAXIS 2D output indicated that the strut element carried an axial force of approximately 1478 kN (Table 7). Since the strut was modeled as node-to-node anchor in the PLAXIS 2D, the axial force was converted into a distributed load to be applied to the H-Beam sections in the structural analysis software (SAP2000).

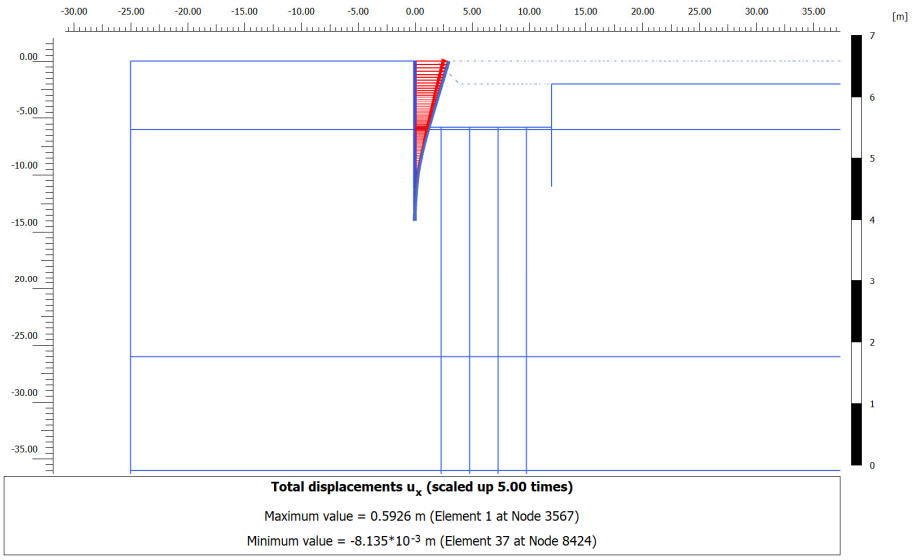

Figure 10. Excessive lateral displacement due to pile cap excavation failure

Reached total time	0.000 day
CSP - Relative stiffness	-1.416E-12
ForceX - Reached total force X	0.000 kN/m
ForceY - Reached total force Y	0.000 kN/m
Pmax - Reached max pp	279.6 kN/m²
ΣM_{stage} - Reached phase proportion	0.000
ΣM_{weight} - Reached weight proportion	1.000
ΣM_{sf} - Reached safety factor	1.639

Figure 11. Factor of Safety of pile cap excavation reinforcement system design

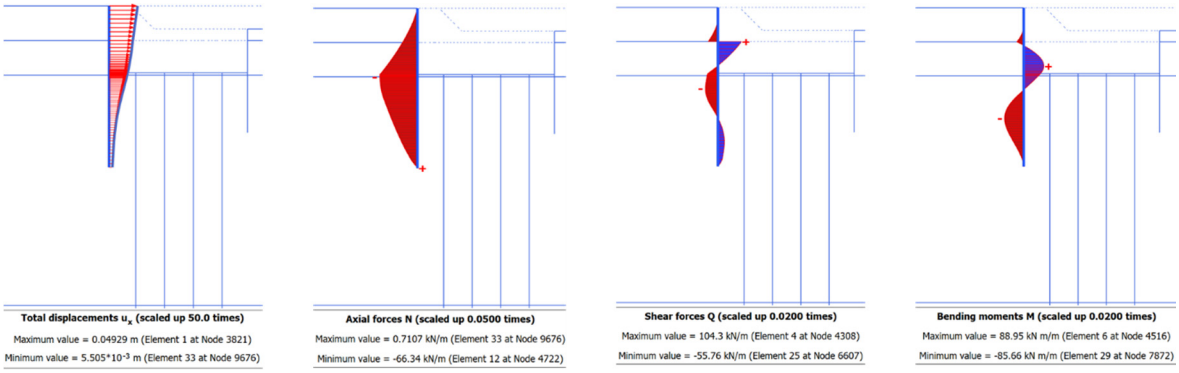

Figure 12. Deformation and forces of steel sheet pile type IV

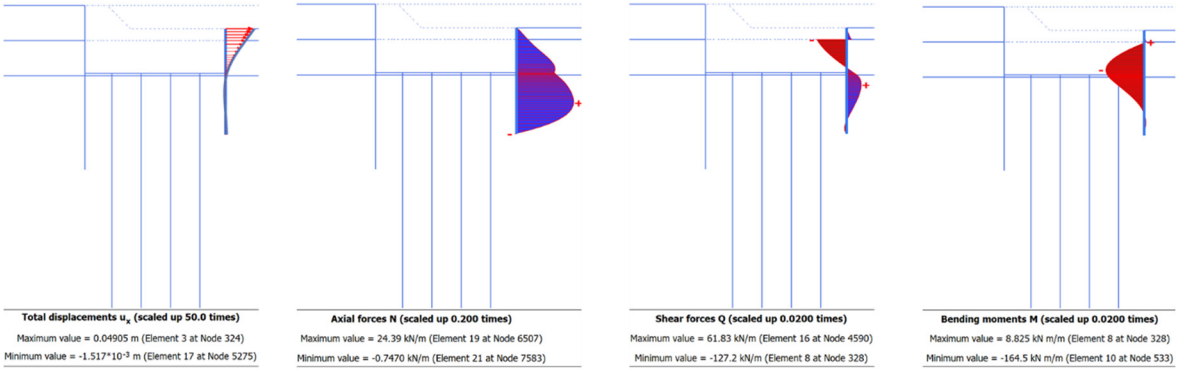

Figure 13. Deformation and forces of steel sheet pile type III

Table 7. Axial force in strut element for structural analysis

Structural element	Node	Local number	X [m]	Y [m]	N [kN]	N_{min} [kN]	N_{max} [kN]
NodeToNodeAnchor_1_1	4308	1	0.000	-3.000	-1478.345	-1478.345	0.000
Element 1-1 (Node-to-node anchor)	328	2	12.000	-3.000	-1478.345	-1478.345	0.000

3.2 Structural Result

The structural verification of the excavation reinforcement system was performed using SAP2000. The analysis results showed that the P-M Ratio for the H-Beam 400×400 section was 0.807, while the H-Beam 350×350 section was 0.88. Both values are below the structural design limit (P-M < 1), confirming that the strut and waler members remained within allowable strength limits under the applied loads. The corresponding structural responses of the reinforced excavation system are presented in the following figures.

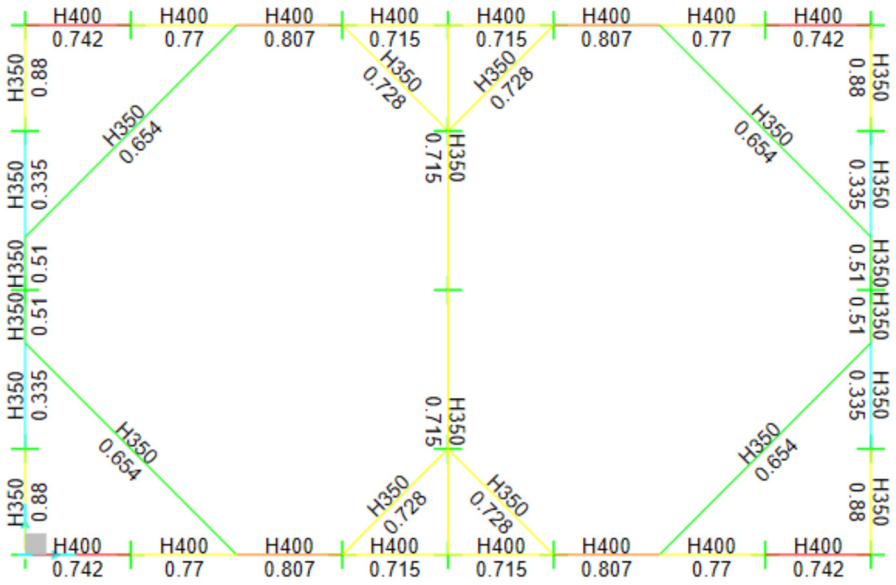

Figure 14. P-M ratio output of pile cap excavation reinforcement system design

4 DISCUSSION

The comparison between the original and the reviewed design highlights a significant improvement in both safety and serviceability. The initial configuration, which relied solely on a steel sheet pile wall, did not achieve the minimum factor of safety required by SNI 8460:2017 and exhibited excessive wall deformation under excavation loading. In contrast, the reviewed design, incorporating struts and walers with H-Beam 350 × 350 and H-Beam 400 × 400 sections, improved the global factor of safety to 1.64 and reduced lateral wall deformation to 4.9, which is below the allowable limit of 6 cm. These results demonstrate that the additional reinforcement system effectively enhanced excavation stability and met geotechnical performance requirements.

For the structural verification, the internal forces obtained from PLAXIS 2D were imported into SAP2000 for capacity checks. The axial forces from the geotechnical model were applied as distributed loads along the H-Beam elements. The analysis was conducted using the Allowable Stress Design (ASD) method with a minimum safety factor of 1.67. While the Plaxis model simulated axial linear soil-structure interaction, the SAP2000 results indicated the necessary of diagonal struts to reduce bending moments and maintain the P-M ratio below limit (Figure 14). Although these additional struts were not modeled in PLAXIS 2D, they were added into structural analysis to ensure overall the structural safety requirements.

Table 8 Comparison between original and reviewed design

No	Type of Design	Safety Factor	Deformation (cm)
1	Original design (steel sheet pile)	1.64	4.9
2	Reviewed design (steel sheet pile with strut & waler system)	<1	59.2

Table 9 P-M ratio of reinforcement structure

No	Structure Profile	P-M Ratio	SF
1	H-Beam 400 x 400	0.807	2.1
2	H-Beam 350 x 350	0.88	1.9

When compared with existing studies, the findings of this paper are consistent with prior research. Goh et al. (2018), Zhang et al. (2019), and Nguyễn & Le (2023) highlighted the critical role of strut forces and their redistribution in maintaining excavation stability. Similarly, Anthony et al. (2024) also demonstrated that reinforced retaining wall systems effectively reduce wall deformation in deep excavation. Furthermore, the application of the Hardening Soil Model in this study aligns with Bui et al. (2024), who verified its realibility for predicting wall deflections under complex soil-structure interactions. Thus, the outcomes of this study are well supported by existing literature, while extending their application to the novel context of pile excavation adjacent to an active highway.

A new insight from this study lies in the integration of PLAXIS 2D and SAP2000 as complementary tools. While PLAXIS 2D provided a reliable estimation of soil deformation and soil-structure interaction, SAP2000 ensured that the reinforcement members meet structural strength requirements. This collaboration workflow highlights a practical approach for addressing excavation problems where geotechnical and structural concerns must be reconciled. The presented method could serve as a reference for future case studies, particularly for evaluating the effectiveness of different bracing configurations.

Overall, this study contributes to both academic literature and practical engineering practice by demonstrating a systematic design review process for pile cap excavation reinforcement system. It not only verifies compliance with geotechnical aspects but also ensures structural adequacy through capacity checks. These findings highlight the importance of integrating field investigation, numerical modeling, and structural verification to achieve safe, effective, and efficient excavation support system in large infrastructure projects.

5 CONCLUSION

In this case study, the effectiveness of a pile cap excavation reinforcement system was evaluated by adding one layer of struts and walers using H-Beam 350 × 350 mm and 400 × 400 mm sections. Numerical modeling with PLAXIS 2D was performed to asses soil deformation, wall behavior, and strut forces, while SAP2000 was used for structural verification. The reviewed design successfully increased the factor of safety and reduced wall deformation compared to the original design. However, additional diagonal struts were required to satisfy structural strength requirements, highlighting that geotechnical analysis alone is not sufficient without complementary structural verification. These findings align with previous studies that emphasize the importance of strut configuration in excavation stability, while also introducing a practical workflow by integrating PLAXIS and SAP2000 for more reliable design. Considering that the study was based on project-specific conditions and simplified assumptions, further research is recommended to validate the results through field monitoring and to explore the application of this combined approach in different soil and structural systems.

DISCLAIMER

The authors declare no conflict of interest.

AVAILABILITY OF DATA AND MATERIALS

All data are available from the author.

ACKNOWLEDGMENTS

The author would like to express sincere gratitude to the Patimban Access Toll Road Project Package 4, particularly Mr. Yasir Arrofiq, Project Manager, for granting permission to use this project as the subject of this geotechnical paper. Special thanks are also extended to Mr. Romi Ramadhan, the author's direct supervisor, for his guidance and valuable input in the completion of the design review of the pile cap excavation system in this project.

REFERENCES

A.T.C. Goh., Zhang Fan., Liu Hanlong., Zhang Wengang., & Zhou Dong, 2018. *Numerical Analysis on Strut Responses Due to One-Strut Failure for Braced Excavation in Clays*. Proceedings of the 2nd International Symposium on Asia Urban Geoengineering

Anthony, Anthony & Wahyuningtyas, Indah & Farkhantiansyah, Aggie, 2024. *Case Study of Double-Wall Retaining Wall System for Deep Excavation in Jakarta, Indonesia*. Indonesian Geotechnical Journal. 3. 1-16.

Badan Standardisasi Nasional, 2017. *SNI 8460:2017 Persyaratan Perancangan Geoteknik*. Jakarta

Bui, L.M., Wu, L., Cheng, Y., & Dong, D.J., 2024. Evaluation of using Hardening Soil Model for Predicting Wall Deflections caused by Deep Excavation: A Case Study at the Ho Chi Minh Metro Line 1, Vietnam. Archives of Civil Engineering, LXX, pp. 357-373.

Carter, M., & Bentley, S., P., 2016. *Soil Properties and Their Correlations*. United Kingdom: John Wiley & Sons, Inc

Das, B. M., 2010. *Principles of Geotechnical Engineering, 7th ed.* Stamford: Cengage Learning

Das, B. M., 2011. *Principles of Foundation Engineering, 7th ed.* Stamford: Cengage Learning

Duncan., J., M., Wright, S., G., Brandon, T., L., 2014. *Soil Strength and Slope Stability*. United Kingdom: John Wiley & Sons, Inc

Han, J., 2015. *Principles and Practice of Ground Improvement*. United Kingdom: John Wiley & Sons, Inc

Zhang et al., 2019. *Estimation of Strut Forces for Braced Excavation in Granular Soils from Numerical Analysis and Case Histories.* Journal Computers and Geotechnics.

Patimban Access Toll Project Package 4, 2024. *Dokumen Penyelidikan Tanah*. Jakarta, PT Wijaya Karya

Tổng, Nguyễn & Le, Phuong, 2023. *A Numerical Method for Estimating Strut Forces in Multi-Braced Excavation Systems*. Journal of Technical Education Science. 78-87.

HIMPUNAN AHLI TEKNIK TANAH INDONESIA - HATTI
Indonesian Society for Geotechnical Engineering - ISGE
PIT HATTI XXIX
10-12 November 2025

Multi-Model Assessment of Anchor Pile Spacing Effects in Axial Load Testing: Mitigating Interaction-Induced Settlement Distortion

Muhamad Fauzi Ahad
PT Anugerah Fondasi Indonesia, Tangerang, Banten, Indonesia, 15560, anugerahfondasiindonesia@gmail.com
Correspondence: fauziahad@gmail.com

ABSTRACT
Anchor pile systems are widely adopted in axial compression load testing, but their accuracy depends critically on the spacing between test and reaction piles. ASTM D1143 specifies a minimum clear distance of ≥5D or 2.5 m, whichever is greater, to ensure mechanical isolation. However, in practice particularly in Indonesia anchor piles are often improvised by reusing production piles within pile caps, where spacing is typically only 2.5–3D. This divergence from the standard creates stress overlap that can distort load–settlement curves and misrepresent true pile capacity. To evaluate these effects, this study applies a multi-model theoretical framework integrating Pile Group Efficiency, Elastic Interaction, Stress Influence Zone, Mindlin's Elastic Solution and the Load Transfer Method. Representative soil parameters derived from SPT data were used to analyze spacing scenarios of 2D, 3D, 4D, and 6D. The baseline isolated pile settlement of 91.94 mm was established as a reference. Results demonstrate severe distortion at 2D ($\eta = 0.65$, $R \approx 196\%$, $\sigma_z = 10.82$ kPa), partial overlap at 3D, convergence toward isolation at 4D, and negligible influence at 6D. The findings further show that shallow soft clay layers govern interaction despite deeper stiff soils, and that bored piles, being non-displacement elements, are more vulnerable to stress diffusion. These insights do not contradict ASTM D1143 but reinforce its intent, offering engineers analytical justification for exercising discretion to adopt ≥6D in compressible soils, maintain ≥5D as standard practice, and allow 4D only under constraints with strict safeguards such as creep checks and unload–reload cycles.

KEYWORDS Anchor pile load test; Axial compression; Pile spacing; Pile-soil interaction; Group efficiency; Elastic interaction theory; Stress influence zone; Mindlin's solution; Load transfer method (t–z); ASTM D1143; Settlement distortion

1 INTRODUCTION

Axial compression load tests are essential in evaluating the capacity and settlement behavior of deep foundations. Among test configurations, top-down loading using reaction piles (anchor piles) is widely adopted due to its practicality in constrained sites (Cherian, 2021; Smith et al., 2020). However, these setups assume that anchor piles provide passive resistance without influencing the test pile, a premise that becomes questionable when anchors are spaced too closely, particularly in soft soils with broad stress diffusion (Poulos and Davis, 1980).

In principle, ASTM D1143 specifies that the minimum clear distance between the test pile and any reaction pile shall be not less than 5 times the diameter of the largest pile (test or anchor), but not less than 2.5 m, whichever is greater. This rule is intended to ensure mechanical isolation between the test and anchor systems. However, in practice especially in Indonesia this requirement is often not followed. Anchor systems are frequently improvised by reusing existing production piles in a pile cap, where typical pile spacing is only 2.5–3D center-to-center (Coduto, 2001; Das, 2010). This means that even before the load test begins, the anchor pile spacing is inherently less than the ASTM requirement. Such practice creates a critical gap between specification and implementation and has direct implications on the reliability of interpreted load–settlement curves.

The effect of insufficient spacing is not trivial. When anchors are too close, overlapping stress zones can induce additional displacements in the test pile, reduce apparent capacity, or conversely give a misleadingly high resistance depending on soil stratigraphy. This behavior mirrors the efficiency loss seen in pile groups, were close spacing lowers overall performance. If production piles are used as anchors without additional clearance, the resulting test no longer represents an isolated pile response but a distorted group effect, potentially leading to unsafe design assumptions in practice.

This study examines the influence of anchor pile spacing on test pile behavior using a purely theoretical approach grounded in five frameworks:

- **Pile Group Efficiency Theory,** to conceptualize performance loss from pile proximity (Terzaghi and Peck, 1948; Randolph and Wroth, 1978).
- **Elastic Interaction Theory,** to quantify induced displacements through interaction factor (α_{ij}) between piles (Poulos and Davis, 1980).
- **Stress Influence Zone Theory,** to visualize stress overlap using classical elasticity (Boussinesq, 1885; Das, 2010).
- **Mindlin's Elastic Solution,** to refine modelling by applying closed-form stress and displacement formulations (Mindlin, 1936; Poulos and Davis, 1980).
- **Load Transfer Method (t–z Method),** to provide a baseline settlement of a single isolated pile (Fleming et al., 1992; Randolph and Wroth, 1978).

The analysis is based on representative soil stratigraphy derived from SPT data and evaluates interaction for anchor spacings of 2D, 3D, 4D, and 6D. While the approach is theoretical and does not involve field test benchmarking or finite element modelling, it serves an important role in providing engineers with a systematic guideline for interpreting or adjusting ASTM spacing requirements, especially in contexts where site constraints or local practices lead to deviations. By decoupling interaction effects from total settlement, the study contributes a decision-support framework for ensuring reliable interpretation of pile load tests.

2 LITERATURE REVIEW AND THEORETICAL BACKGROUND

To evaluate this practice gap, classical theoretical models of pile–soil–pile interaction can be adapted to the context of anchor piles. Each framework offers a distinct lens for understanding how closely spaced anchors may influence the response of the test pile and together they form the analytical foundation of this study.

2.1 Pile Group Efficiency Theory

Pile group efficiency quantifies the reduction in capacity when piles are placed too closely under vertical loads. For anchor pile setups, this analogy is relevant because closely spaced reaction piles may cause the test pile to experience the same efficiency loss observed in working groups. The efficiency factor (η) serves as a quick indicator of how much performance is lost when anchors are located at 2D–3D compared to the theoretical isolation at ≥5D (Terzaghi and Peck, 1948; Randolph and Wroth, 1978). While originally developed for permanent groups, it provides an empirical starting point for evaluating anchor interaction.

2.2 Elastic Interaction Theory

Elastic Interaction Theory directly models how a load applied to one pile induces settlement in an adjacent pile. In load testing, this framework is critical because it treats the test pile and anchor piles as an elastic system within the same soil medium. The interaction factor (α_{ij}) quantifies additional settlement transferred from anchor to test pile and decreases logarithmically with spacing. This makes it particularly suited to evaluate the danger of anchors placed at 2D–3D, where interaction can distort load–displacement curves (Poulos and Davis, 1980).

2.3 Stress Influence Zone Theory

Axial pile loading creates a stress bulb around the shaft and tip, the extent of which depends on soil stiffness and pile geometry. When the bulbs of anchor piles overlap with the test pile, mechanical isolation is lost. Applying this theory to anchor setups allows visualization of whether 2D–3D spacing leads to stress overlap in soft clays or sands. It is a conceptual but powerful tool to explain why ASTM's ≥5D recommendation exists, and why deviations increase risk (Boussinesq, 1885; Das, 2010).

2.4 Mindlin's Elastic Solution

Mindlin's closed-form elastic solution refines stress predictions by considering point loads at depth, making it applicable to embedded piles. For anchor pile systems, Mindlin's equations can quantify how stresses propagate laterally and vertically from anchors into the test pile zone, particularly in stratified soils. This enhances the understanding gained from stress bulb diagrams and provides a more precise estimate of stress overlap (Mindlin, 1936; Poulos and Davis, 1980).

2.5 Load Transfer Method (t–z Method)

The Load Transfer Method simulates the settlement of a single pile by discretizing it into segments and mobilizing shaft and base resistance progressively. Although it does not model pile–pile interaction directly, it provides the baseline isolated pile settlement against which all interaction effects are measured. In anchor pile analysis, this baseline serves as the reference to determine how much additional displacement is induced by closer anchor spacing (Randolph and Wroth, 1978; Fleming et al., 1992).

Taken together, these five frameworks create a multi-model approach where efficiency provides capacity loss, elastic interaction gives displacement transfer, stress influence and Mindlin define stress overlap, and the load transfer method sets the baseline. By integrating them, the present study establishes a structured theoretical basis to evaluate anchor pile spacing from 2D to 6D under stratified soil conditions. This combined framework forms the foundation for the modelling and analysis presented in the following sections.

3 METHODOLOGY, MODELLING AND FRAMEWORK

This study is deliberately limited to closed-form analytical models rather than numerical simulations or field load tests. The purpose is not to replace experimental validation, but to establish a transparent theoretical benchmark that can guide engineers when interpreting or adjusting ASTM D1143 spacing requirements, especially in contexts where practice deviates from the standard. Representative soil parameters from SPT data are used to provide realistic calibration, but the analysis remains a theoretical desk study.

3.1 Analytical Basis for Theoretical Modelling

This study adopts a multi-theoretical framework to assess the effect of anchor pile spacing on axial compression load test outcomes. Five models are integrated: Pile Group Efficiency Theory, Elastic Interaction Theory, Stress Influence Zone Theory, Mindlin's Elastic Solution and Load Transfer Method. Each theory contributes a distinct analytical lens ranging from conceptual efficiency loss to precise displacement estimation and stress field evaluation.

The analysis assumes a uniform pile geometry embedded in stratified cohesive soils, using site-based SPT data for parameter calibration. Spacing scenarios of 2D, 3D, 4D, and 6D are evaluated to reflect field constraints. Efficiency factors (η), interaction coefficients (α_{ij}), stress bulb overlaps, t–z behavior and elastic half-space responses are computed accordingly. This integrated modelling approach forms the foundation for interpreting how anchor proximity alters load–settlement behavior and test validity.

3.2 Pile Group Efficiency Theory

Pile group efficiency quantifies the reduction in capacity when piles are placed closely under vertical loads. Isolated piles have additive capacities but overlapping stress zones especially in compressible soils like clay, reduce total capacity. The efficiency factor (η) measures deviation from ideal independent behavior:

$$\eta = \frac{Q_{group}}{n \cdot Q_{single}} \quad (1)$$

Where Q_{group} = total bearing capacity of the pile group; Q_{single} = capacity of a single pile; n = number of piles

This theory is relevant for soft to medium clays where limited lateral stress dissipation causes significant overlap in load transfer zones (Terzaghi and Peck, 1948; Randolph and Wroth, 1978). Empirical η values for typical spacing and soil types are shown in Table 1.

Table 1. Summarizes Typical η Values Based on Pile Spacing and Soil Type

Pile Spacing	Efficiency Factor η – Clay	Efficiency Factor η – Sand	Remarks
2D	0.6 – 0.7	0.5 – 0.7	Strong interaction (unsafe)
3D	0.7 – 0.8	0.6 – 0.8	Moderate interaction
4D	0.8 – 0.9	0.8 – 1.0	Acceptable in most field tests
≥ 5D	≈ 1.0	≈ 1.0	Safe distance (negligible overlap)

Source: Terzaghi and Peck (1948); Prakash and Sharma (1990); Coduto (2001); Das (2010)

3.3 Elastic Interaction Theory

Poulos and Davis (1980) describe how a load on one pile affects adjacent piles through deformation of the surrounding soil, assuming a linear-elastic, homogeneous, isotropic half-space. The theory is key for modelling pile–pile interaction under elastic conditions, including static load testing with anchor piles or dense pile groups.

The interaction factor (α_{ij}) quantifies additional settlement in pile *i* from a load Q_j on pile *j*, governed by pile spacing (s_{ij}), pile length (L), and soil modulus (E_s). It is calculated as:

$$\alpha_{ij} = \frac{1}{\pi E_s}\left[\ln\left(\frac{4L}{s_{ij}}\right)\right] + k \quad (2)$$

Where E_s = soil elastic modulus (MPa); L = embedded length of the pile (m); s_{ij} = spacing between test pile and anchor pile (m); k = empirical correction factor (commonly taken as 1.0 for conservative design).

α_{ij} decreases logarithmically with spacing; at ≤ 2D, significant interaction can distort load–displacement results, violating isolation assumptions. This framework supports analytical justification for spacing rather than relying solely on empirical rules.

In pile group design, α_{ij} forms the basis for stiffness/influence matrices used in predicting load sharing and deformation compatibility. For load testing, it ensures that nearby anchors do not compromise measured performance. ASTM D1143 recommends a minimum 5D or 2.5 m clear spacing, though site limits often lead to deviations.

3.4 Stress Influence Zone Theory

Axial pile loading produces a 3D stress zone extending vertically and laterally, influenced by pile diameter (D), length (L), applied load (Q), and soil stiffness (Coduto, 2001; Poulos and Davis, 1980). In compression, the stress zone typically spans 2D–4D laterally and up to 1.5L vertically. If the test

pile's zone overlaps with anchor piles, isolation is lost, potentially distorting settlement and load–displacement readings.

The radial extent (r_i) can be estimated as:

$$r_i = n \, . D \tag{3}$$

Where r_i = radial extent of stress influence; D = pile diameter; n = empirical factor ranging from 2 to 6, depending on soil type and stiffness.

Soft to medium clays (n ≈ 4–6) have larger influence zones due to higher compressibility, while dense sands or stiff soils (n ≈ 2–3) confine stress more tightly (Das, 2010; Randolph, 2003).

Vertical stress beneath a pile can be estimated using Boussinesq's solution:

$$\sigma_z = \frac{3Q}{2\pi z^2} \times cos^3(\theta) \tag{4}$$

Where σ_z = vertical stress at depth z; Q = applied load; θ = angle from vertical axis to point of interest in the soil.

This theory confirms stress effects can extend several diameters from the load point, especially in low-modulus soils. Anchor piles closer than 3D risk intruding into the test pile's zone, altering load transfer and compromising test interpretation. While common in pile group design, its application in load test planning improves assessment of mechanical isolation.

3.5 Mindlin's Elastic Solution

Mindlin (1936) provides a closed-form elastic solution for stress and displacement within a semi-infinite solid due to a point load applied at depth. Unlike Boussinesq's surface-load formulation, it models subsurface loads, making it suitable for embedded piles.

The vertical stress σ_z at a point due to a vertical point load Q at depth d is given by:

$$\sigma_z = \frac{3Q}{2\pi} \times \frac{z^3}{(r^2 + z^2)^{5/2}} \tag{5}$$

Where Q = point load (kN); z = vertical distance from load point to observation point (m); r = radial distance from load axis to observation point (m).

In this study, Mindlin's solution estimates stress overlap between test and anchor piles by superimposing stress fields for different spacings (2D–6D). This quantifies potential interference in elastic media, capturing effects of load propagation beyond the shaft.

Mindlin's model complements Elastic Interaction Theory by refining stress field estimation, especially in stratified profiles, and helps identify spacing thresholds where anchor influence becomes negligible.

3.6 Load Transfer Method (t-z Method) – Baseline Settlement

The Load Transfer Method simulates the non-linear load–settlement behavior of a single pile under axial load by discretizing the pile into segments, each with distinct shaft (t-z) and base (q-z) load–displacement relationships. This method captures progressive mobilization of shaft friction (t) and base resistance (q), accommodating layered soil profiles and variable geotechnical parameters.

Originally formalized by Randolph and Wroth (1978) and extended by Fleming et al. (1992), it assumes total load is resisted by shaft friction along the pile–soil interface and base resistance at the tip. Mobilization is typically expressed as:

$$\left[t\,(z) = t_{max} \times \left(\frac{z}{z_{50}+z}\right)\right],\ \left[q\,(z) = q_{max} \times \left(\frac{z}{z_{b50}+z}\right)\right] \quad (6,7)$$

Where $t\,(z)$ = mobilized shaft resistance at displacement z (kPa); t_{max} = ultimate shaft resistance (kPa); z = local vertical displacement (mm); z_{50} = displacement at 50% mobilization; $q\,(z)$ = mobilized base stress at displacement z (kPa); q_{max} = ultimate base resistance (kPa); z_{50b} = displacement at 50% of q_{max} mobilisation (typically 5-10mm).

For linear-elastic mobilization (simplified case), the shear force in each segment can be expressed as:

$$\left[F_{s,i} = t_i \times A_{s,i}\right],\ \left[k_{s,i} = \frac{E_{s,i} \times A_{s,i}}{\Delta z_i}\right],\ \delta_{s,i} = \frac{F_{s,i}}{k_{s,i}} \quad (8,9,10)$$

Where $E_{s,i}$ = surface area of pile shaft segment i; Δz_i = thickness of segment i; $A_{s,i}$ = elastic modulus of surrounding soil.

The total base resistance force is then:

$$F_b = q(z) \times A_b \quad (11)$$

Where A_b is cross-sectional area of the pile base

The pile is discretised into *n* segments and the total settlement Δ at pile head is computed by summing displacements of all shaft segments and the base:

$$\left[\Delta_{total} = \sum_{i=1}^{n} \delta_{s,i} + \delta_b\right],\ \left[\delta_b = \frac{F_b \times L}{A_b \times E_p}\right] \quad (12,13)$$

Where $\delta_{s,i}$ = local settlement due to shaft friction at segment i; δ_b = settlement due to base resistance b.

3.7 Soil, Pile and Modelling – Characterization, Geometry and Test Setup

Table 2. Soil, Pile and Load Data

Category	Parameter	Description / Value
Soil Properties	Layer 1: 0–2m; SPT-N = 7	Soft Clay; fs = 20 kPa; fb = 300 kPa
	Layer 2: 2–6m; SPT-N = 22	Stiff Clay; fs = 50 kPa; fb = 650 kPa
	Layer 3: 6–30m; SPT-N > 60	Dense Sand; fs = 150 kPa; fb = 1,500 kPa
	Soil Elastic Modulus, Es	10–130 MPa; Es1 = 15, Es2 = 25, Es3 = 45
	Poisson's Ratio (Soil), νs	0.45
Pile Properties	Pile Diameter, D	1,000 mm
	Pile Embedment Length, L	30.0 m
	Elastic Modulus (Pile), Ep	30,000 MPa
	Pile Type / Material	Bored-pile Reinforced Concrete
	Pile Group	5 pile (2:1:2); Spacing 2D, 3D, 4D, 6D
Load Parameter	Applied Load (Q)	10,000 kN
	Anchor Load (4 nos)	2,500 kN

fs = unit shaft friction / fb = unit base resistance

3.8 Baseline Modelling of Isolated Single Pile Settlement

To establish a theoretical reference, the settlement of a single isolated pile was computed using the Load Transfer Method. This approach incorporates non-linear mobilisation of shaft and base

resistance via t–z and q–z curves and accounts for elastic shortening of the pile. Soil parameters, including unit skin friction *(f_s)*, end bearing *(f_b)*, and elastic modulus *(E_s)*, were derived from SPT-N correlations based on the site's stratigraphy and test pile design.

The resulting settlement value *(S_o)* serves as a benchmark to evaluate deviations caused by pile–pile interaction in configurations with varying anchor pile spacing (2D to 6D). This baseline enables consistent comparison across all theoretical frameworks applied in this study.

4 RESULT AND ANALYSIS

4.1 Modelling of Isolated Single Pile Settlement

Table 3. Calculation of Baseline Modelling Single Pile Settlement

Settlement Type	Formula	Calculation	S, (mm)
Elastic Shortening / Elastic Settlement Pile	$S_e = \frac{Q\ .\ L}{A\ .\ E_p}$	$S_e = \frac{10^7\ .\ 30}{0.785\ .\ 3\ \times 10^7}$	12.74
Settlement in Soil –	$S_{1i} = \frac{q_i}{A_p} \times \frac{H_i}{E_{si}}$		
Layer 1: fs = 20 kPa		E_{s1} = 15 MPa	0.16
Layer 2: fs = 50 kPa		E_{s2} = 25 MPa	0.37
Layer 3: fs = 150 kPa		E_{s3} = 45 MPa	4.43
	TOTAL		17.7

4.2 Group Efficiency Theory – Modelling and Analytic

Table 4. Pile Group Capacity after Factor of Efficiency

Pile spacing	Efficiency Factor, η	Ideal group capacity, (kN)	Est. Group capacity, (kN)
2D	0.65	$Q_{ideal} = n \times Q_{single}$	32,500
3D	0.75	Take Q_{single} = 10,000 kN, n = 5	37,500
4D	0.85	$Q_{ideal} = 5 \times 10{,}000$	42,500
6D	1.00	$= 50{,}000\ kN$	50,000

4.3 Group Efficiency Theory – Modelling and Analytic

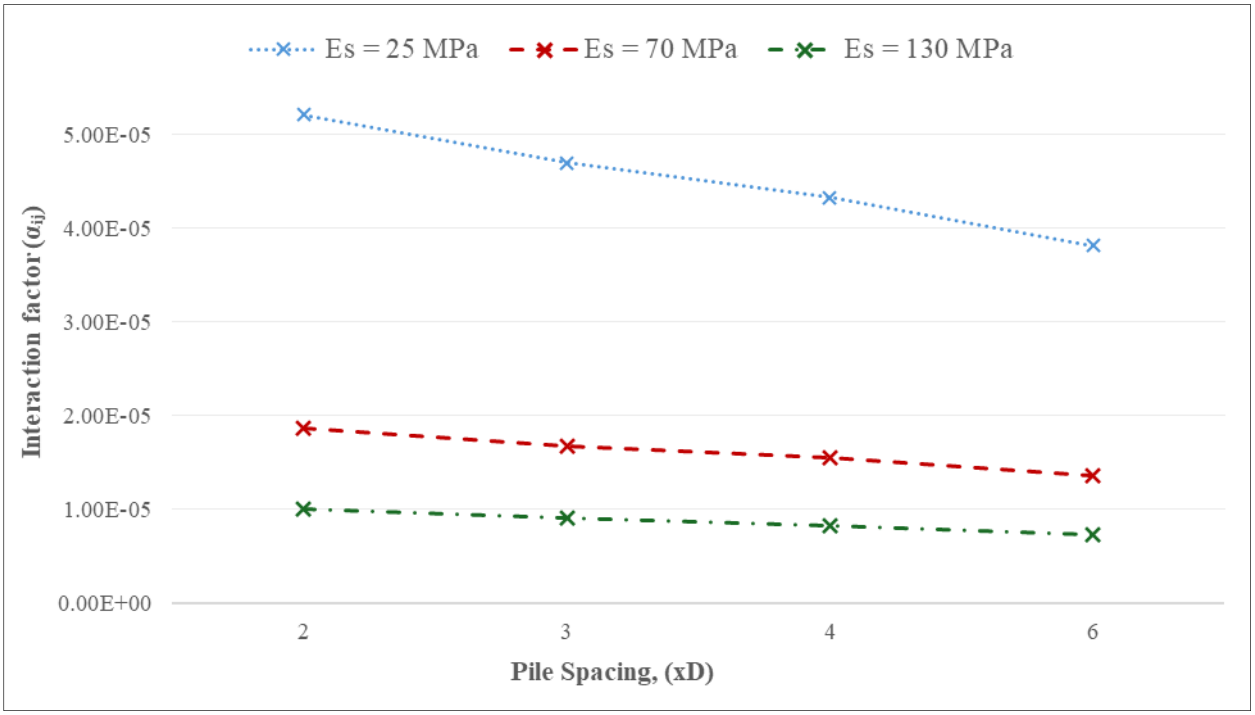

Figure 1. Pile Spacing Versus Interaction Factor (α_{ij})

4.4 Stress Influence Zone Theory – Modelling and Analytic

Table 5. Stress Influence Radius Zone

Soil Layer	Empirical Factor (n)	Pile Diameter, D (m)	Stress Influence Radius, r_i (m)
Soft Clay (0–2 m)	4.0	1.0	4.0
Stiff Clay (2–6 m)	4.0	1.0	4.0
Dense Sand (6–30 m)	2.5	1.0	2.5

Table 6. Stress Influence Overlap Zone

Spacing (D)	Radial distance (m)	Soft/stiff clay, (r < 4.0 m)	Dense sand, (r < 2.5 m)
2	2.0	Yes	Yes
3	3.0	Yes	No
4	4.0	No	No
6	6.0	No	No

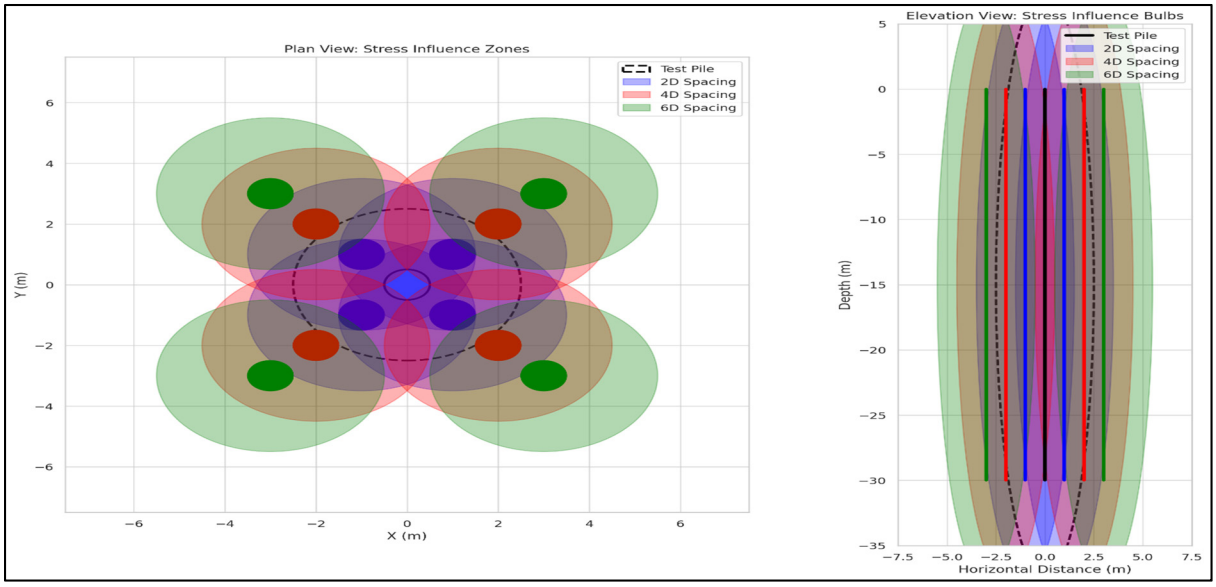

Figure 2. Plan View and Elevation View of Stress Influence Zone

4.5 Mindlin's Elastic Solution – Modelling and Analytic

Table 7. Mindlin's Vertical Stress Calculation

Spacing (D)	Radial Distance, r (m)	Vertical Stress, σ_z (kPa)
2	2.0	10.8218
3	3.0	9.6231
4	4.0	8.2364
6	6.0	5.5339

4.6 Load Transfer Method (t–z Method) – Baseline Settlement

Table 8. Calculation Settlement using Load Transfer Method (t-z Method)

Segment	Δz (m)	Area (m²)	F_{shaft} (kN)	Stiffness, k (kN/m)	Settlement (mm)
Segment 1	2.0	6.28	125.7	47,100.0	2.67
Segment 2	4.0	12.57	628.3	78,562.5	8.00
Segment 3	24.0	75.40	11,309.7	141,374.6	80.00
Base Resistance	-	0.785	-	-	1.27
		TOTAL			91.94

4.7 Analysis on Relative Effect of Pile Spacing

Table 9. Relative Effects of Pile Spacing on Efficiency, Interaction and Vertical Stress (Baseline = 6D)

Spacing	Group Effiecency		Interaction Index		Vertical Stress	
(D)	η (–)	η (% of 6D)	R (–)	R (% of 6D)	σ^z (kPa)	σ^z (% of 6D)
2	0.65	65%	5.21	137%	10.82	196%
3	0.75	75%	4.70	123%	9.62	174%
4	0.85	85%	4.33	114%	8.24	149%
6	1.00	100%	3.81	100%	5.53	100%

NOTE: *6D spacing is taken as the reference baseline (100%). Interaction index, R, is a relative measure of interaction effects compared to the 6D case; higher values indicate greater interference.*

5 DISCUSSION

The integrated use of five theoretical models of Pile Group Efficiency, Elastic Interaction, Stress Influence Zone, Mindlin's Elastic Solution, and the Load Transfer Method demonstrates consistent trends on anchor pile spacing in axial compression load tests. The baseline settlement of 91.94 mm (Table 8) represents the isolated single-pile response and serves as the reference benchmark. Any increase beyond this value in the 2D–4D cases indicates distortion caused by anchor interaction rather than intrinsic pile capacity.

At 2D spacing, interaction was most severe: efficiency (η) fell to 0.65 (Table 4), the interaction index R rose to 5.21 (196% of the 6D baseline in Table 9), and Mindlin's vertical stress reached 10.82 kPa (196% in Table 7). At 3D, η improved to 0.75, R = 4.70 (174%), and stress overlap persisted in clay layers (Table 6). From 4D onward, $\eta \geq 0.85$, $R \leq 149\%$, and stress overlap disappeared across all layers at 6D, baseline conditions were essentially restored, confirming it as the spacing of negligible interaction. These results are consistent with recent numerical evaluations of pile group effects, which also showed severe efficiency reduction when spacing is below 4D (Zhou, 2018).

The soil stratigraphy explains these outcomes. Although Table 2 lists stiff clay and dense sand at depth, the upper 0–2 m soft clay (SPT-N = 7, Es = 15 MPa) governs interaction. Stress Influence Zone analysis (Table 5) gave a radius of 4D in clay, while Mindlin's solution confirmed elevated stresses at shallow depth, causing overlap at 2D–3D. Thus, recommending 6D in compressible soils is not contradictory but reflects governing-layer control. This finding aligns with field test observations in soft clays, where load–settlement responses were strongly influenced by shallow strata even when deeper layers were stiff (Lanyi-Bennett, 2019).

Pile type also influences behavior. The study focused on bored piles (non-displacement), which do not densify surrounding soils make stress bulbs therefore remain wider than for driven piles, especially in clay. This makes the recommendations conservative for bored piles where the dominant system in Indonesia while interaction effects may be less severe for driven piles in dense sands. Comparable outcomes have also been noted for pile groups in layered anisotropic soils, where governing effects consistently arise from weaker upper layers (Ai et al., 2024).

The practical implications are significant. In Indonesia, anchor piles are often improvised by reusing production piles within pile caps, typically spaced only 2.5–3D. This practice violates ASTM D1143's requirement of ≥5D or 2.5 m and means the load test no longer reflects isolated capacity but a distorted group effect. The consequence is ambiguous settlement curves and unsafe or uneconomical designs.

Overall, the models converge on a clear message: spacings ≤3D compromise test validity, ≥4D provides a conditional minimum, and 6D remains the benchmark of negligible interference. These findings do not contradict ASTM D1143, but they reinforce its intent. ASTM permits engineer discretion in adjusting spacing and this study provides analytical justification how increase to 6D in compressible soils, maintain ≥5D in standard conditions and consider 4D only under constraints with safeguards such as creep checks and unload–reload cycles.

It must also be recognized that this study is limited to closed-form models and does not include installation effects or 3D numerical benchmarking. Nevertheless, by synthesizing multiple classical and recent approaches, it offers engineers a practical tool for decision-making. While the Indonesian context illustrates the urgency, the issue is relevant internationally wherever shortcuts in anchor installation occur. By reinforcing ASTM practice with analytical clarity, this study transforms theory into actionable guidance.

6 CONCLUSION

This study examined the influence of anchor pile spacing on axial compression load tests using five classical theoretical models. The baseline settlement of 91.94 mm provided a reference for evaluating distortions induced by close anchor spacing. The results converge on a consistent message that

anchor spacings ≤3D significantly distort test outcomes, ≥4D provides a conditional minimum, and 6D represents negligible interaction. Although the stratigraphy included stiff clay and dense sand at depth, the shallow soft clay layer governed stress diffusion, explaining why overlap persists at 2D–3D. This finding resolves the apparent contradiction with Table 2. The analysis also emphasizes that bored piles, as non-displacement elements, are more susceptible to interaction, making the recommendations conservative for Indonesian practice. These findings do not conflict with ASTM D1143 that they reinforce its intent. ASTM requires ≥5D or 2.5 m spacing and permits engineer discretion in adjustment. The framework presented here provides the analytical justification for such decisions how to increase to 6D in compressible soils, maintain ≥5D in standard conditions and consider 4D only under constraints with strict safeguards. While limited to closed-form models, this study highlights a critical gap between specification and practice. By linking theory to observed field habits, it offers engineers an evidence-based guideline to ensure pile load tests remain reliable and safe.

DISCLAIMER

The authors declare no conflict of interest.

AVAILABILITY OF DATA AND MATERIALS

All data are available from the author.

REFERENCES

Book

Coduto, D.P., 2001. *Foundation design: Principles and practices*. 2nd ed. Upper Saddle River, NJ: Prentice Hall.

Das, B.M., 2010. *Principles of foundation engineering*. 7th ed. Stamford, CT: Cengage Learning.

Fleming, W.G.K., Weltman, A.J., Randolph, M.F. & Elson, W.K., 1992. *Piling engineering*. 2nd ed. London: Taylor & Francis.

Poulos, H.G. & Davis, E.H., 1980. *Pile foundation analysis and design*. New York: John Wiley & Sons.

Smith, I.M., Griffiths, D.V. & Margetts, L., 2020. *Programming the finite element method*. 6th ed. Hoboken, NJ: Wiley.

Terzaghi, K. & Peck, R.B., 1967. *Soil mechanics in engineering practice*. 2nd ed. New York: John Wiley & Sons.

Journal

Ai, Z.Y., et al., 2024. Interaction analysis of energy pile groups and layered transversely isotropic soils under vertical loading. *Marine Georesources & Geotechnology*, 42(7), pp.458–472.

Broms, B.B., 1981. Lateral resistance of piles in cohesionless soils. *Journal of the Geotechnical Engineering Division, ASCE*, 107(3), pp.123–136.

Fellenius, B.H., 2001. From strain measurements to load in piles. *Geotechnical News*, 19(1), pp.35–38.

Lanyi-Bennett, S.A., 2019. Axial load testing of helical pile groups in glaciolacustrine clays. *Canadian Geotechnical Journal*, 56(4), pp.607–619.

Liang, R. & Zhang, J., 2019. Review of pile load testing practice and interpretation methods. *Journal of GeoEngineering*, 14(2), pp.87–102.

Mindlin, R.D., 1936. Force at a point in the interior of a semi-infinite solid. *Physics*, 7(5), pp.195–202.

Poulos, H.G., 2001. Piles subjected to cyclic loading: Literature review and design guidance. *Ground Engineering*, 34(9), pp.28–37.

Randolph, M.F. & Wroth, C.P., 1978. Analysis of deformation of vertically loaded piles. *Journal of the Geotechnical Engineering Division, ASCE*, 104(GT12), pp.1465–1488.

Zhang, L. & Small, J.C., 2000. Analysis of pile groups subjected to vertical and horizontal loads. *Computers and Geotechnics*, 26(2), pp.169–192.

Zhou, Y., 2018. Numerical evaluation of pile group effects in composite foundations. *Soil Dynamics and Earthquake Engineering*, 110, pp.31–42.

Report

ASTM International, 2013. *ASTM D1143/D1143M-07: Standard test methods for deep foundations under static axial compressive load*. West Conshohocken, PA: ASTM International.

HIMPUNAN AHLI TEKNIK TANAH INDONESIA - HATTI
Indonesian Society for Geotechnical Engineering - ISGE
PIT HATTI XXIX
10-12 November 2025

Water Retention Curve of Soil at Simpang Meo Region South Sumatra

Purnamawati[1)], Herdian Gumay[2], Nurly Gofar[3*)]
[1,3] Department of Civil Engineering, Graduate Program, Universitas Bina Darma, Jalan Jend. A. Yani No 3, Palembang, 30111, Indonesia,
[2]Doctoral Program, Department of Civil Engineering, Universitas Hasanuddin Jalan Poros Malino Km.6, Gowa, 92171, Indonesia.

**) corresponding author*: nurly_gofar@binadarma.ac.id

ABSTRACT: Steep slopes are typically formed on residual soil with deep groundwater levels; hence, the slopes are in the unsaturated zone. Therefore, in analyzing the stability of steep slopes, it is necessary to consider the properties of unsaturated soil. The main property of unsaturated soil is the Water Retention Curve (SWCC), which describes the relationship between matric suction and soil moisture content. Many methods are available to determine the SWCC of a soil, such as laboratory and field tests, as well as empirical equations. Laboratory testing is considered the best method for determining the SWCC. However, the laboratory work involved in the determination of SWCC is tedious; thus, several models have been developed by researchers to obtain SWCC. This study compares SWCC obtained based on the results of laboratory testing using an Osmotic Tensiometer assisted by soil shrinkage measurements using a 3-D scanner, and the SWCC obtained using the empirical equation proposed by Zapata for plastic soil based on the percentage of particles passing the No. 200 sieve and the soil plasticity index. The soil samples were retrieved from a location in the Simpang Meo region in South Sumatra. Air entry value for the SWCC was obtained both graphically and deterministically. Both methods resulted in a lower air entry value (AEV) for the Zapata equation as compared to the osmotic tensiometer test. A lower AEV indicates that lower suction is required for water to enter the soil pores. Therefore, analysis of rainfall infiltration and slope stability using SWCC curves estimated from the Zapata equation could result in later saturation of soil, hence a slightly higher factor of safety.

KEYWORD Unsaturated soil, Soil water characteristic curve, osmotic tensiometer, Zapata equation,

This paper is published in the Indonesian Geotechnical Journal Vol. 4 Issue 2:

https://www.indonesian-geotechnical-journal.org/index.php/IGJ/article/view/122

This page is intentionally left blank

HIMPUNAN AHLI TEKNIK TANAH INDONESIA - HATTI
Indonesian Society for Geotechnical Engineering - ISGE
PIT HATTI XXIX
10-12 November 2025

Analysis of Seepage and Contaminant Transport to Water Body Considering Waste Pile Distance and Impermeable Layer Presence

Melisa Saferman[1*], Fathiyah Hakim Sagitaningrum[1], Widjojo Adi Prakoso[1], Lingga Ekaputra Lucky Suryajaya[2]

[1]Department of Civil and Environmental Engineering, Faculty of Engineering, Universitas Indonesia, Depok, Indonesia, 16424; melisa.saferman@gmail.com

[2]Department of Civil and Environmental Engineering, Faculty of Engineering, The Hong Kong University of Science and Technology, Kowloon, Hong Kong SAR, China; lelsuryajaya@connect.ust.hk

*Correspondence: melisa.saferman@gmail.com

ABSTRACT

Open dumping at final disposal sites (landfills) in Indonesia often results in untreated leachate infiltration into surrounding soil and water bodies. At Cipayung Landfill, Depok, excess waste volume has led to leachate migration into the nearby river. This study focuses on two factors affecting leachate seepage and contaminant migration: (1) the distance between waste piles and the water body, and (2) the presence of an impermeable layer at a depth of 30 m. Field surveys and laboratory data were combined with numerical simulations using SEEP/W and CTRAN/W modules in GeoStudio. Boundary conditions and soil parameters were derived from permeability tests and secondary data for leachate composition. The simulations were conducted for multiple waste-water distances with and without an impermeable layer. Darcy's law was applied to model seepage, while contaminant transport was calculated using the advection-dispersion equation with retardation. Results showed that shorter wastewater distances significantly reduced travel time of contaminants to the river, with concentration peaks occurring earlier. The presence of an impermeable layer decreased contaminant concentration at the riverbed due to retardation and diversion of flow paths, with the most substantial effect observed in the shortest-distance scenario. These findings highlight the importance of strategic waste placement and engineered barriers to reduce groundwater and surface water contamination.

Keywords: landfill, leachate, seepage, impermeable layer, contaminant transport

1 INTRODUCTION

Leachate migration from landfills poses a significant environmental risk, especially when waste is disposed without engineered containment systems. In Indonesia, many landfills still operate using open dumping methods, resulting in untreated leachate infiltrating surrounding soil and potentially contaminating nearby surface and groundwater. At Cipayung Landfill in Depok, West Java, the absence of a proper liner system and the proximity of the waste piles to a river increase the likelihood of contaminant transport into the aquatic environment. Cipayung Landfill in Depok, West Java, has been in operation since 1984 and is now overcapacity, receiving approximately 750 tonnes of waste per day (DLHK Depok, 2023).

Two factors critically influence the migration of leachate from a landfill to a water body: the distance between the waste to the water body and the presence of an impermeable layer within the subsurface profile. Shorter distances reduce the travel time of contaminants, while impermeable layers can act as hydraulic barriers, increase retardation and alter seepage patterns.

Previous studies have examined general leachate migration mechanisms, but quantitative assessments of how these two factors interact under local site conditions in Cipayung are limited.

This study aims to fill this gap by numerically modelling seepage and contaminant transport for various wastewater distances, both with and without an impermeable layer at 30 m depth.

This study models seepage and contaminant transport at Cipayung Landfill using SEEP/W and CTRAN/W, focusing on the effects of varying wastewater distances and the presence of an impermeable layer at a depth of 30 m. The research aims to quantify how these factors influence breakthrough times, peak concentrations, and equilibrium conditions at the river boundary, providing insights for landfill design and leachate management strategies.

2 METHODS

2.1 STUDY AREA

The study was conducted at Cipayung Landfill in Depok, West Java, Indonesia. This landfill is the only final disposal site serving the city and is located adjacent to a river that acts as a potential receptor of leachate contamination. The site has a tropical climate with distinct wet and dry seasons, and receives high annual rainfall, increasing leachate production. Overcapacity at the landfill has led to waste being piled without engineered liners or adequate leachate collection systems.

To model the seepage and contaminant transport of leachate through soil, 2D analysis was performed using GeoStudio SEEP/W and CTRAN/W. The model consists of the waste landfill on the left side and potential seepage face and riverbed along the right side. Also, there are two models with and without an impermeable layer at 30 m depth.

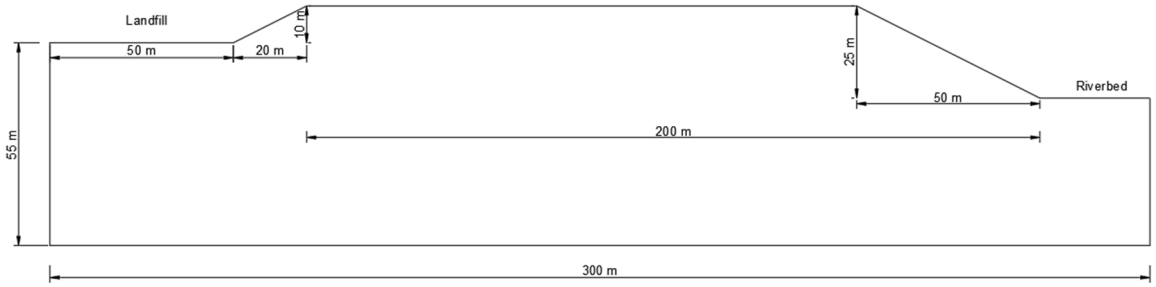

Figure 1. Cross Section View of the Landfill without Impermeable Layer.

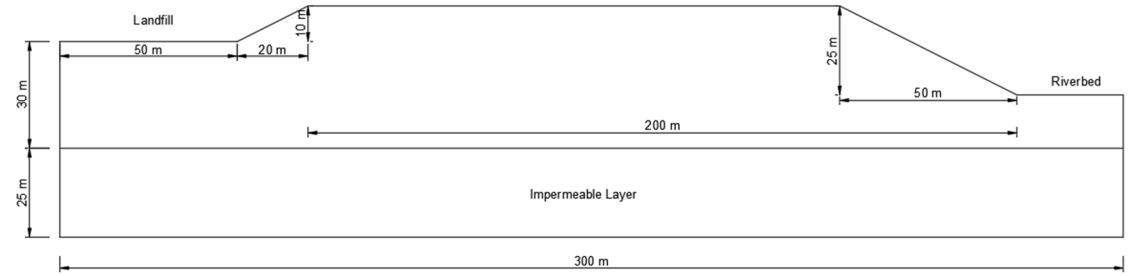

Figure 2. Cross Section View of the Landfill with Impermeable Layer.

2.2 BOUNDARY CONDITIONS

For the seepage analysis, material properties (saturated and unsaturated hydraulic conductivity functions, SWCC curves) were assigned to each layer. Boundary conditions included rainfall infiltration on the landfill surface and constant head at the river boundary. Parent analysis used a steady-state simulation to establish the initial hydraulic conditions, followed by transient analysis to simulate infiltration events.

For the advection-dispersion analysis, using the pore-water velocity output from SEEP/W, contaminant transport was simulated based on advection–dispersion processes. Leachate contaminant input concentrations were assigned at the landfill base, with transport towards the river boundary.

2.3 MODEL GEOMETRY AND VARIATIONS

The numerical modelling domain represented a 2D cross-section from the waste pile to the adjacent river. The base geometry included the landfill waste layer, underlying sandy soil, and river boundary. Two primary variables were altered:

a) **Distance between waste pile and river**: Four scenarios were defined.
b) **Presence of an impermeable layer at 30 m depth**: Two conditions were modelled for each distance, with and without the impermeable layer.

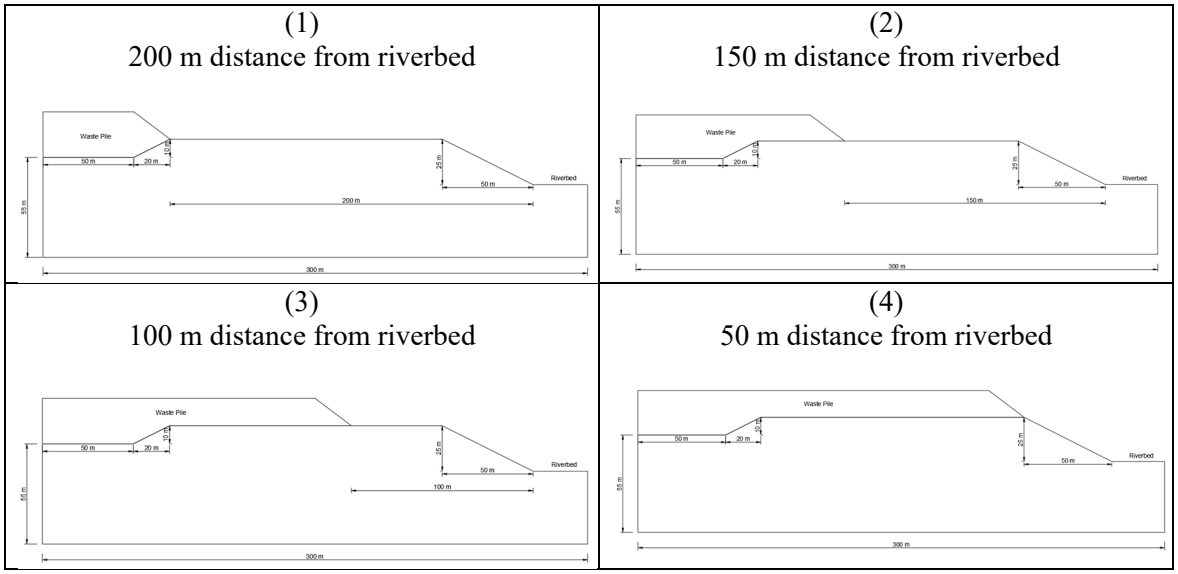

Figure 3. Cross Section of Studied Cases for Models without Impermeable Layer.

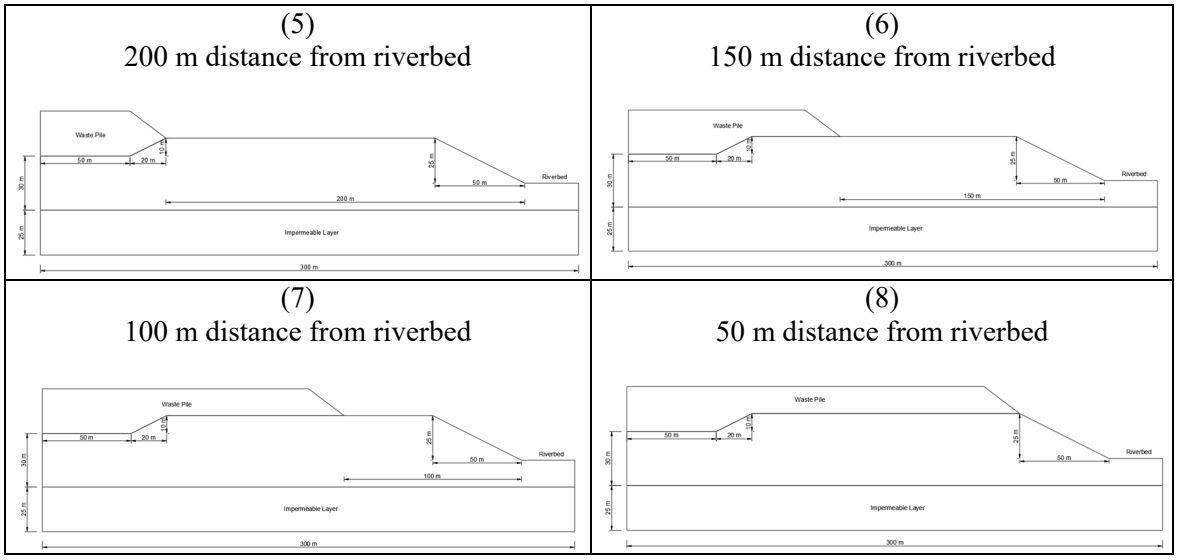

Figure 4. Cross Section of Studied Cases for Models with Impermeable Layer.

To illustrate the impact of distance of waste piles and the presence of impermeable layer in the depth of 30 m, the cases shown in table 1 are studied.

Table 1. Studied Cases

Cases	Description
Case 1	Waste piles distance from riverbed = 200 m without impermeable layer in depth 30 m
Case 2	Waste piles distance from riverbed = 150 m without impermeable layer in depth 30 m
Case 3	Waste piles distance from riverbed = 100 m without impermeable layer in depth 30 m
Case 4	Waste piles distance from riverbed = 50 m without impermeable layer in depth 30 m
Case 5	Waste piles distance from riverbed = 200 m with impermeable layer in depth 30 m
Case 6	Waste piles distance from riverbed = 150 m with impermeable layer in depth 30 m
Case 7	Waste piles distance from riverbed = 100 m with impermeable layer in depth 30 m
Case 8	Waste piles distance from riverbed = 50 m with impermeable layer in depth 30 m

To identify the contaminants contained in leachate at the Cipayung landfill site, tests were conducted to determine the concentrations of heavy metals, namely Cu, Zn, Pb, and Cd, in soil samples taken at a depth of approximately 30 to 50 cm. The laboratory analysis revealed that Zn exhibited the highest concentration among the tested metals. The following table presents the results of the heavy metal content analysis in the soil at the Cipayung landfill.

Table 2. Results of Laboratory Analysis of Heavy Metal Content in Soil Samples

Lab No.	Field No.	IKM-ITSL-33		IKM-ITSL-34	
		HNO_3:$HClO_4$		HNO_3:$HClO_4$	
		Cu	Zn	Pb	Cd
		….(ppm)….		….(ppm)….	
BJ 0316	KTL Soil	40.2	87.6	21.8	tr
BJ 0317	TPA-01 Soil	26.5	71.1	21.1	tr
BJ 0318	TPA-02 Soil	31.5	80.8	22.6	tr

One type of contaminant concentration Zinc (80.8 ppm) was chosen to be studied in this research since it's the highest contaminant contain in Cipayung landfill soil. The diffusion coefficient used for Zn through soil is assumed to be $D^* = 4.1 \times 10^{-11}$ m/s^2 (Shackerlford, 1991). The diffusion coefficient is used to represent how contaminants spread due to molecular diffusion in porous media. It quantifies the rate at which solute particles move from areas of higher concentration to areas of lower concentration.

The type of soil that is used in this case is sandy soil which contains 70% of sand and 30% of clay, this soil is tested in laboratory to get hydraulic conductivity value. The parameters used in the numerical model are summarized in table 3, table 4, and table 5 respectively for soil, waste, and impermeable layer.

Table 3. Considered Parameters for Soil in The Numerical Model

Parameters	Value	Unit
Water Content	0.2	
Ksat	1.364×10^{-4}	m/s
Contaminant Concentration	0	g/m^3
Diffusion Coeff.	4.1×10^{-11}	m/s^2
Longitudinal Dispersivity	30	m
Transversal Dispersivity	6	m

Table 4. Considered Parameters for Waste in The Numerical Model

Parameters	Value	Unit
Water Content	0.512	
Ksat	4.50×10^{-3}	m/s
Contaminant Concentration	80	g/m^3
Diffusion Coeff.	4.1×10^{-11}	m/s^2
Longitudinal Dispersivity	5	m
Transversal Dispersivity	1	m

Table 5. Considered Parameters for Impermeable Layer in The Numerical Model

Parameters	Value	Unit
Water Content	0.10	
Ksat	4.98×10^{-7}	m/s
Contaminant Concentration	0	g/m^3
Diffusion Coeff.	4.1×10^{-11}	m/s^2
Longitudinal Dispersivity	30	m
Transversal Dispersivity	6	m

Dispersion in the direction of the water flow is usually higher than dispersion perpendicular to the flow direction. Two dispersivity values are therefore required to define the spreading process. Dispersivities in the flow directions are designated as the longitudinal dispersivity α_L and the transverse dispersivity α_T (GEO-SLOPE International Ltd., 2012). Dispersivity is the ratio of the hydrodynamic dispersion coefficient (d) divided by the pore water velocity (v); thus a = d/v and has units of length. Typically, the dispersivity varies from 0.1 to 100 m however field and laboratory tests have indicated that dispersivity varies with the scale of the test. Large scale tests have higher dispersivity than small lab column tests. An approximate value for dispersivity is 0.1 times the scale of the system (Fetter, 1999). If simulating contaminant transport in a 1 m long laboratory column, then dispersivity ~ 0.1 m. However, if simulating transport in a large aquifer greater than 1 km in extent, then use dispersivity ~ 100 m (GEO-SLOPE International Ltd., 2012).

3 RESULTS

The SEEP/W and CTRAN/W simulations produced spatial distributions of total head and contaminant concentration for each time step. The breakthrough time, defined as the time required for the contaminant concentration at the riverbed to exceed 0.2 g/m³, was 10 days for Case 1, 5 days for Case 2, 2 days for Case 3, and 1 day for Case 4. Figures 5–8 present graphical outputs of the seepage and advection–dispersion analyses of leachate migration through the soil profile. The contour plots illustrate the different concentration of leachate throughout the simulation period.

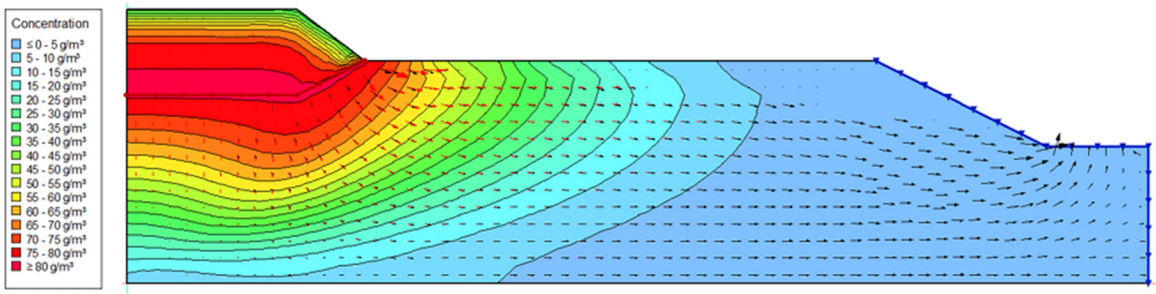

Figure 5. Modelling Analysis for Case 1 after 10 days

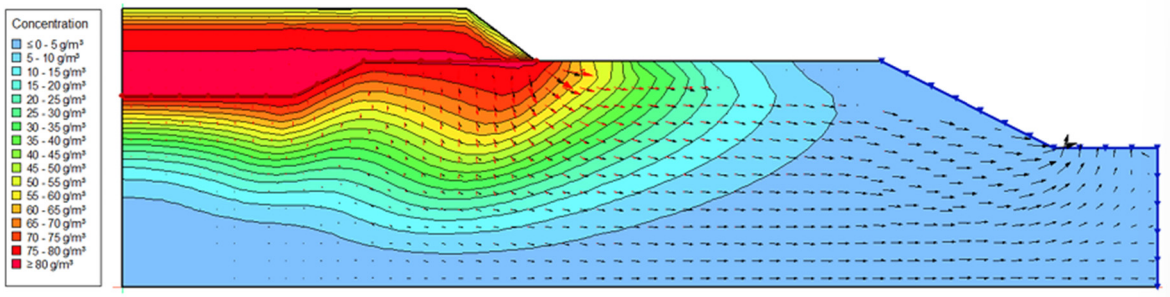

Figure 6. Modelling Analysis for Case 2 after 5 days

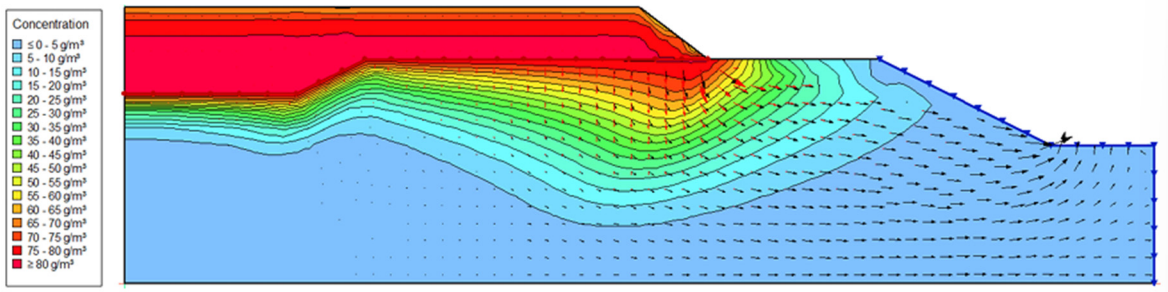

Figure 7. Modelling Analysis for Case 3 after 2 days

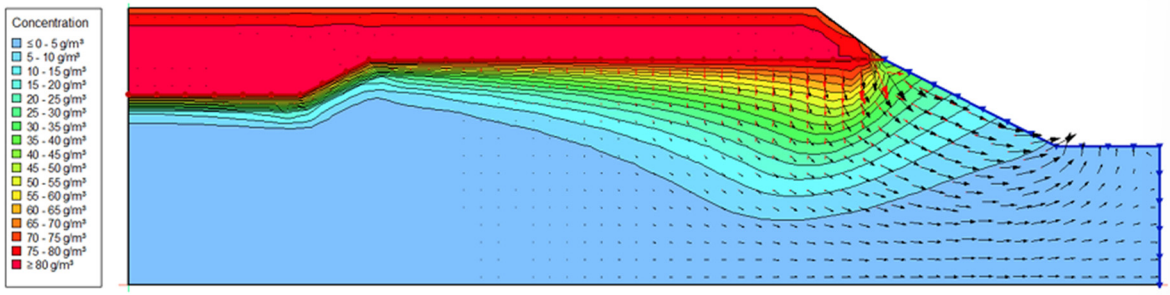

Figure 8. Modelling Analysis for Case 4 after 1 day

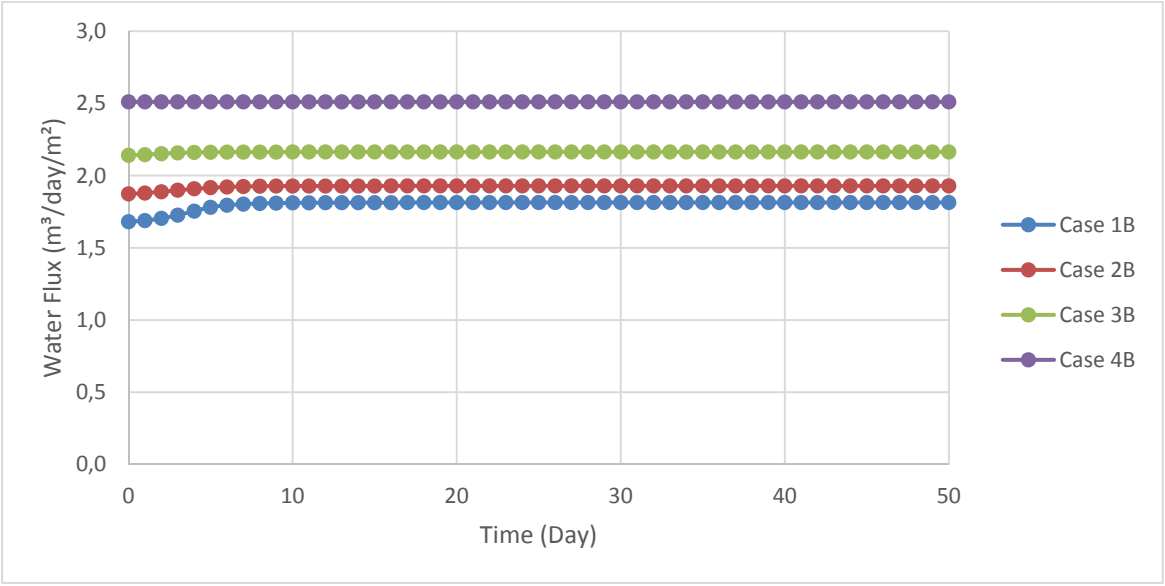

Figure 9. Water Flux at the Riverbed for Different Distance of Waste Pile in Model without Impermeable Layer

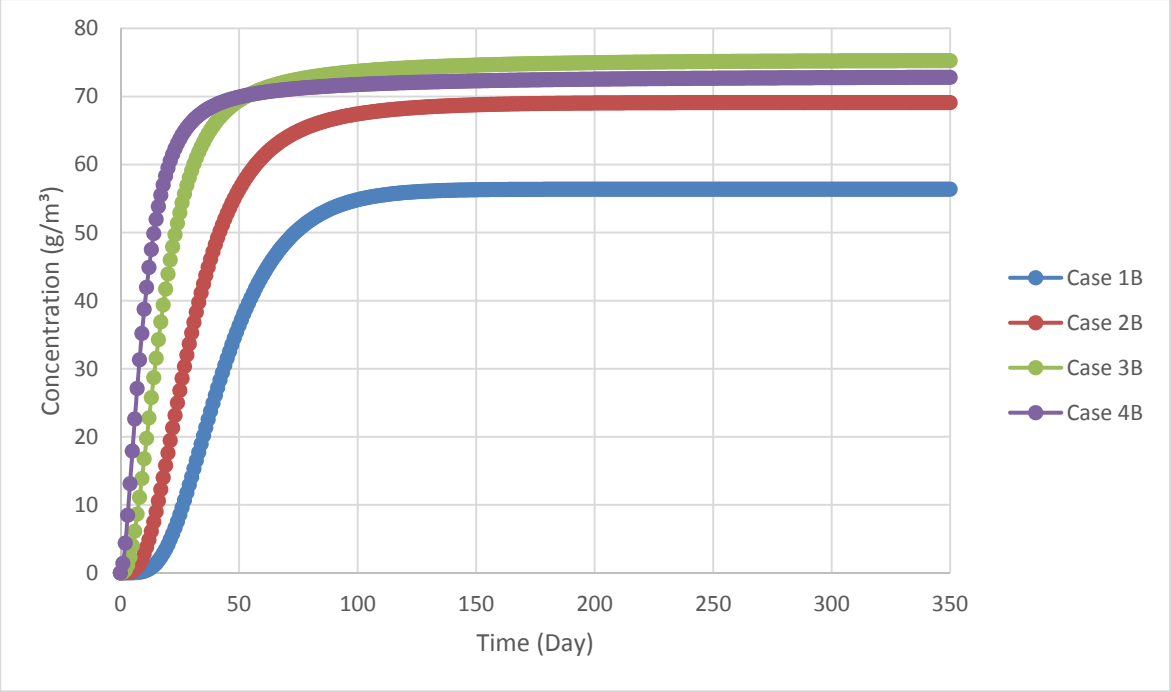

Figure 10. Concentration of Leachate at the Riverbed for Different Distance of Waste Pile in Model without Impermeable Layer

Results of the model showed that waste piles with the furthest distance will take more time to reach riverbed and will have lower peak concentrations, but there is an exception in Case 3 and Case 4. In figure 10, Case 4 begins with a very rapid increase in concentration, but also fast in reaching the equilibrium point. Meanwhile, in Case 3 also started rapidly in increasing concentration but not as rapid as case 4. Although the increase in concentration is not as fast as in Case 4 in the beginning, the equilibrium point reached takes much longer, which results in peak concentration points in Case 3 being much higher than in Case 4.

Furthermore, Figures 11-14 shows the result of the model with impermeable layer at 30 m depth. Time taken for each distance is still the same as the models without impermeable layers but have lower contaminant concentration values in riverbed.

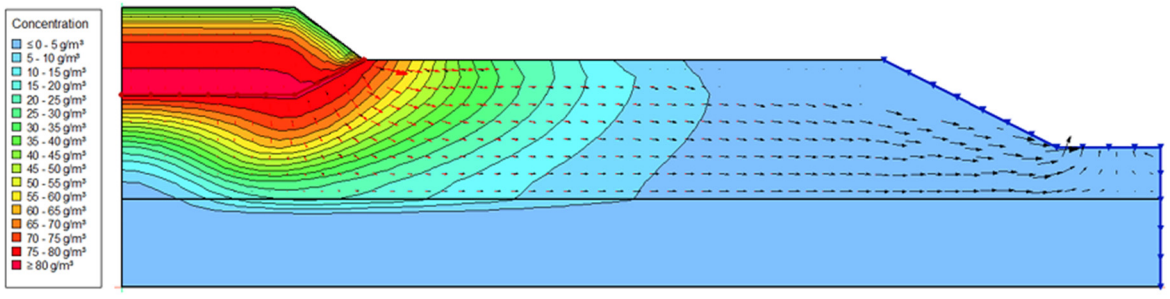

Figure 11. Modelling Analysis for Case 5 after 10 days

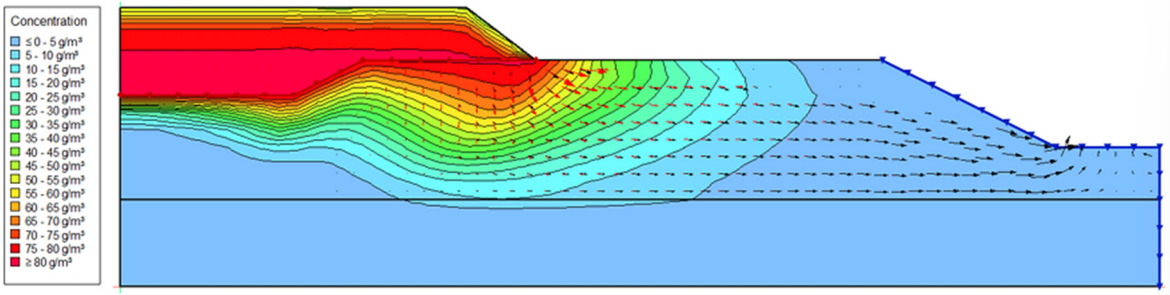

Figure 12. Modelling Analysis for Case 6 after 5 days

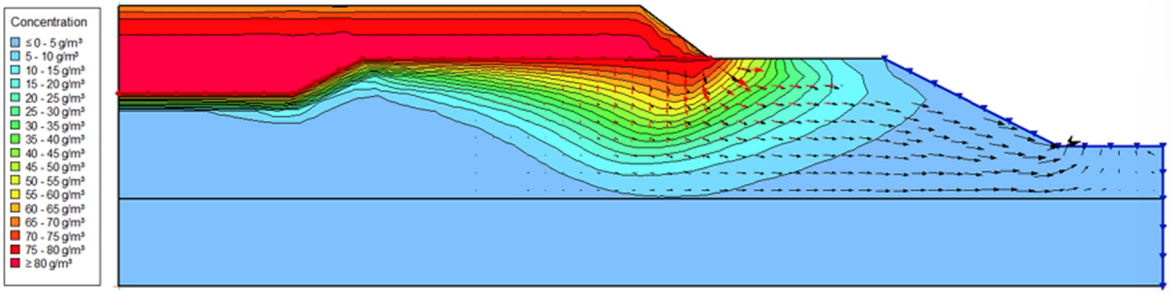

Figure 13. Modelling Analysis for Case 7 after 2 days

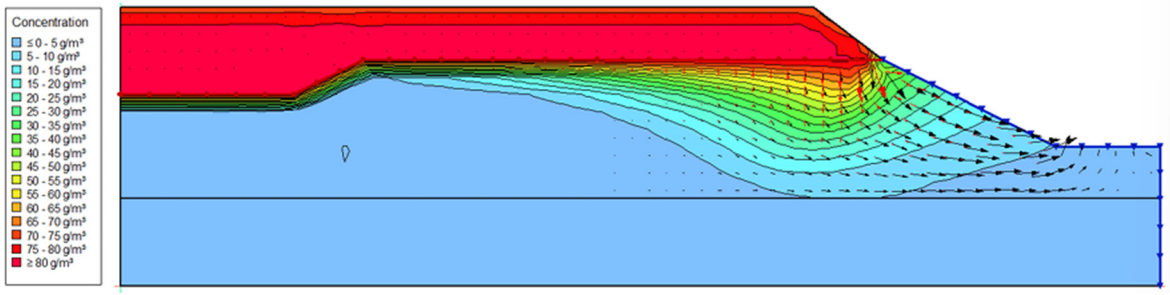

Figure 14. Modelling Analysis for Case 8 after 1 day

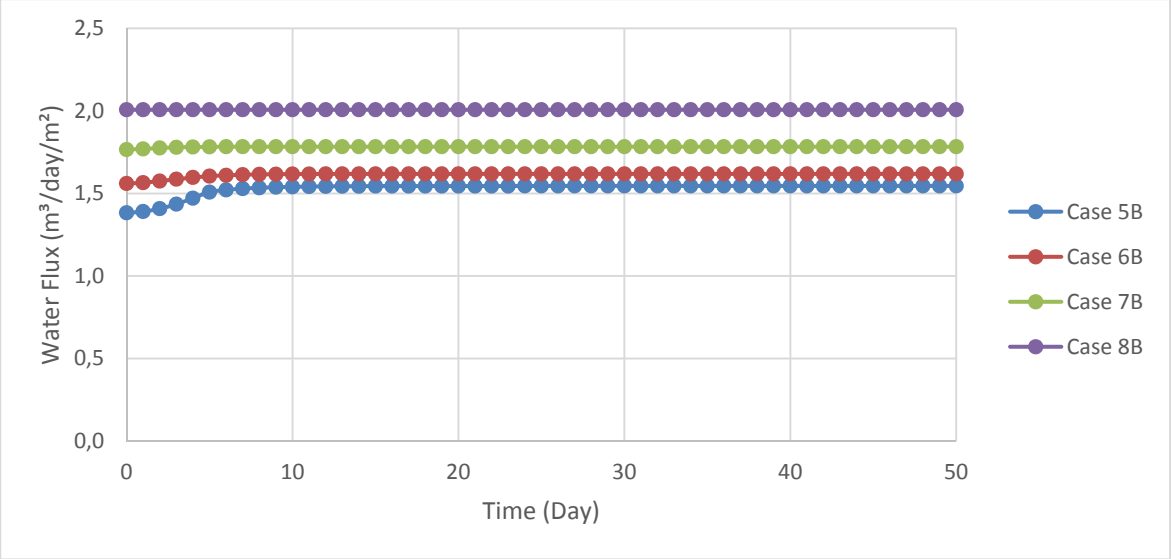

Figure 15. Water Flux at the Riverbed for Different Distance of Waste Pile in Model with Impermeable Layer

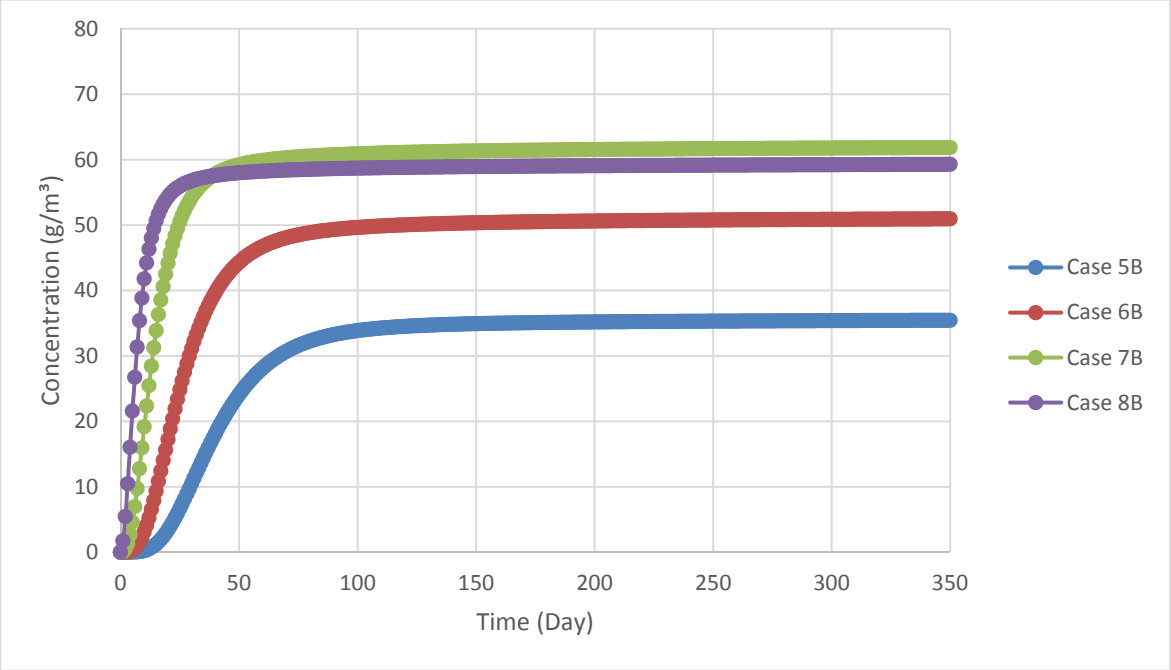

Figure 16. Concentration of Leachate at the Riverbed for Different Distance of Waste Pile in Model with Impermeable Layer

A brief visual comparison of Figures 10 and 16 shows that the overall shapes of the graphs are quite similar. However, differences become evident when examining concentration values. As illustrated in Figure 17, the concentration in models without an impermeable layer is nearly twice that observed in models incorporating an impermeable layer.

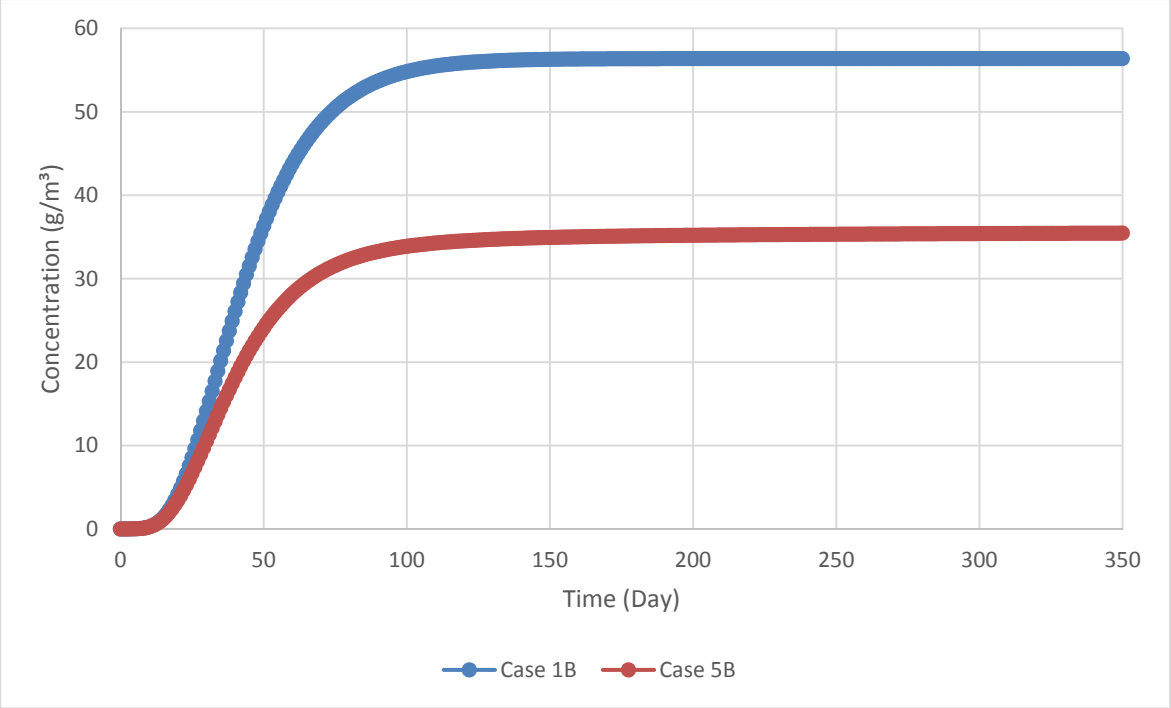

Figure 17. Comparison Concentration of Leachate at the Riverbed for Cases 1 and 5, with and without Impermeable Layer

4 DISCUSSION

The simulation results reveal that the waste–water distance strongly influences contaminant travel time and concentration, but with notable exceptions observed between Case 3 and Case 4. In general, waste piles located at the furthest distance required more time for contaminants to reach the riverbed and exhibited lower peak concentrations, consistent with the principles of advection-dispersion and natural attenuation. This is explained by Darcy's Law, which states that seepage flow occurs from areas of higher total head to areas of lower total head, with the velocity proportional to the hydraulic gradient and the soil's hydraulic conductivity. In the landfill context, the total head difference between the waste pile and the river, combined with gravitational forces, drives water and contaminants downslope through the subsurface.

However, in Figure 10, Case 4 displayed a distinct behavior, with an initial rapid rise in concentration followed by a quick approach to equilibrium. This pattern suggests a high initial advective flux towards the river, potentially driven by a steeper hydraulic gradient or reduced dispersion along the shorter path, leading to a faster flushing of contaminants.

In contrast, Case 3 also began with a rapid concentration increase, but not as pronounced as Case 4. Despite the slower initial rise, the time taken to reach equilibrium was significantly longer, allowing more mass to accumulate in the system and resulting in a higher peak concentration compared to Case 4. This phenomenon indicates that intermediate distances can sometimes produce higher concentration peaks than shorter distances if the flow path characteristics, dispersion rates, and storage effects in the subsurface favor prolonged contaminant release.

These findings highlight that while increasing the wastewater distance is generally effective in delaying breakthrough and lowering peak concentrations, the relationship is not strictly linear. The hydraulic and transport properties of the intervening media, as well as the presence or absence of impermeable barriers, can lead to exceptions. This underscores the need for site-specific modelling rather than relying solely on general distance-based guidelines when designing landfill layouts or leachate control measures.

5 CONCLUSION

This study examined how waste–water distance and subsurface conditions affect leachate transport from Cipayung Landfill to a nearby river. Results showed that greater distances generally delayed breakthroughs and reduced peak concentrations, though exceptions occurred, with Case 3 producing higher peaks than the shorter-distance Case 4 due to longer equilibrium times. These findings indicate that distance alone does not determine impact, and flow path characteristics, dispersion, and barrier presence must be considered in landfill design. Future work should include 3D modelling, heterogeneous soil conditions, and field validation to improve predictive accuracy.

DISCLAIMER

The authors declare no conflict of interest.

AVAILABILITY OF DATA AND MATERIALS

All data are available from the author.

ACKNOWLEDGMENTS

The authors thank the Cipayung Landfill management for site access and the Soil Mechanics Laboratory at Universitas Indonesia for technical support.

REFERENCES

Das, B. M., 1995. *Principles of Geotechnical Engineering, Third Edition.* Boston: PWS Publishing Company.

Eltarabily, M. G. A. &. N. A. M., 2015. Numerical simulation of fertilizers movement in sand and controlling. *International Journal of Environmental Science and Development,* p. 559.

Fetter, C. W., 1999. *Contaminant hydrogeology (2nd ed.).* s.l.:Prentice Hall.

Fredlund, D., 1996. *The Emergence of Unsaturated Soil Mechanics.* Canada: The Fouth Spencer J. Buchanan Lecturer, College Station, Texas, A & M University Press.

Freeze, R. A. & Cherry, J. A., 1979. *Groundwater.* s.l.:Prentice Hall.

George, M. & Beena, K., 2011. *Geotechnical Characteristics of Leachate-Contaminated Lateratic Soil.* Kochi: Indian Geotechnical Society.

GEO-SLOPE International Ltd., 2012. *Contaminant Modelling with CTRAN/W.* Calgary: GEO-SLOPE International Ltd..

Ibrahim, M., Saufan, L. O. & Bende, L. O. S., 2023. Analisis Persebaran Lindi Tempat Pemerosesan Akhir (TPA) Puuwatu. *Jurnal Perencanaan Wilayah,* pp. 69-79.

Laboratorium Mekanika Tanah Departemen Teknik Sipil, 2017. *Buku Panduan Praktikum Mekanika Tanah.* Depok: Fakultas Teknik Universitas Indonesia.

PT Arkonin EMP, 2019. *Detailed Engineering Drawing (DED) Revitalisasi TPA Cipayung,* s.l.: s.n.

Rahardjo, H., Yongmin, K. & Satyanaga, A., 2019. *Role of Unsaturated Soil Mechanics in Geotechnical Engineering.* Singapore: International Journal of Geo-Engineering.

Shackerlford, C., 1991. Laboratory Diffusion Testing For Waste Disposal - A Review. *Journal of Contaminant Hydrology, 7,* pp. 177-217.

Siracusa, G., La Rosa, A., Musumeci, L. & Maiolino, G., 2007. Modelling of Contaminant Migration in Unsaturated Soils. *Sustainable Development and Planning III,* pp. 455-465.

Wang, V. W., 2021. *Analysis of seepage, contaminant transport, compaction and safety of the Zhaoli ditch dam, a tailing reservoir,* Villavagen: Department of Earth Science, Air, Water and Landscape Science, Uppsala University.

HIMPUNAN AHLI TEKNIK TANAH INDONESIA - HATTI
Indonesian Society for Geotechnical Engineering - ISGE
PIT HATTI XXIX
10-12 November 2025

Determination of Bentonite's Flow Limit Using Cylinder Strength Test and Suspension Settling Model

Samuel Jemmy Setiadjie[1], Budijanto Widjaja[2*], Mayolus Musa Putra[3], Atharayhan Anandito[4]

[1]Center for Geo-Hazard, Parahyangan Catholic University, Bandung, Indonesia, 40141;samuel.setiadjie@unpar.ac.id
[2]Center for Geo-Hazard, Parahyangan Catholic University, Bandung, Indonesia, 40141;widjaja@unpar.ac.id
[3]Department of Civil Engineering, Faculty of Engineering, Parahyangan Catholic University, Bandung, Indonesia, 40141; 6102001024@student.unpar.ac.id
[4]Department of Civil Engineering, Faculty of Engineering, Parahyangan Catholic University, Bandung, Indonesia, 40141; alle.atharayhan@gmail.com
*Correspondence: widjaja@unpar.ac.id

ABSTRACT Cohesive soils exhibit complex behavior characterized by distinct transitional boundaries between different states. One of the boundaries is the flow limit (FL), which is the transition between the viscous liquid and suspension states. Currently, there are no specific standard tests to determine the flow limit. Most previous studies have used the undrained shear strength (c_u) value to determine the FL value. This study employed two different approaches to obtain the FL value: first, using the cylinder strength test (CST), which approaches from the viscous state, and second, using the suspension settling model, which approaches from the suspension state. There are five variations of samples for each test: 100% bentonite, 90% bentonite and 10% sand, 80% bentonite and 20% sand, 70% bentonite and 30% sand, and 60% bentonite and 40% sand. The cylinder test was conducted with three different cylinder diameters: 30 mm, 40 mm, and 50 mm. For the suspension settling model, five solid concentrations were used, namely 0.5%, 0.4%, 0.3%, 0.2%, and 0.1%, for each sample. The results show that the CST for bentonite suspension gave higher results than the other; meanwhile, the suspension settling model is the most conservative. The FL value from the CST test ranges from 3.33 to 4.9 times higher than the liquid limit (LL); the suspension settling model yielded values of 1.9 to 2.6 times higher than LL. The results are higher than those in previous studies, which can be attributed to differences in apparatus capacities used to determine the c_u value, variations in bentonite mineral compositions, and different estimation approaches. Although in this research the range of FL values is still vast, this study has provided insights from two different approaches. This research still has various development opportunities, such as mineralogy effect and new method development to divine the FL value.

KEYWORDS Cylinder Strength Test, Flow Limit, Suspension Settling Model, Suspension State, Viscous Liquid State

1 INTRODUCTION

Cohesive soils have several virtual boundaries that indicate the transitions between states. The state can be divided into solid state, semi-solid state, plastic state, viscous liquid state, and suspension state. Slurry materials are composed of cohesive soils between the viscous liquid and suspension states. Gary *et al*. (1977) stated that the suspension state occurs when soil particles are dispersed or separated from water particles. However, in the viscous liquid state, the soil and water particles are usually in a single phase or blended into a single material.

Atterberg (1911) proposed six limits, but most people are familiar with only the plastic limit (PL), the liquid limit (LL), and the shrinkage limit (SL). The SL shows the transition point between the solid state and semi-solid state, PL is between the semi-solid state and the plastic state, and LL is between the plastic state and the viscous liquid state. However, there is no clear limit that separates the suspension state from the viscous liquid state for slurry materials.

Casagrande (1932), Germaine and Germaine (2009), and Park and Nong (2013) proposed a new limit that separates the suspension state from the viscous liquid state, known as the flow limit. The flow

limit is not yet considered an international standard due to a lack of research, and there is no standardized test to define it. However, understanding the flow limit is essential to comprehending the soil behavior during the transition from a viscous liquid state to a suspension state. This condition can be identified through the hydrometer test, desludging process, tailing pumping, flow landslides, and tunneling excavation using a TBM, which transports the excavated material with a pump to the storage facility (O'Brien, 2003; Widjaja, 2019).

This study aims to determine the FL value using two different approaches. The first is the Cylinder Strength Test (CST), which estimates FL from the viscous liquid side. The second is the suspension settling model, which approaches FL from the suspension side. This study focused on bentonite samples due to their exceptionally high water absorption capacity, which enables better suspension (Bain, 2009). This study involved five gradation variations of sand, combined with five additional variations of solid concentration for the suspension settling model, and three different cylinder diameters. This study aims to estimate the FL value using various approaches to determine the intersection range, thereby providing a more accurate understanding and a more reliable test for determining the value of FL.

2 LITERATURE REVIEW

2.1 Flow Limit (FL)

According to Germain and Germain (2009), the FL is the boundary between fluid and suspension states, where in the suspension state, solid and fluid particles have no contact forces, resulting in no effective stress within the material. Park and Nong (2013) define the FL as the point at which the undrained shear strength (c_u) reaches a value of zero. Typically, the flow limit is 1.5 to 2 times higher than the liquid limit value. Shen and Tsai (2024) offer an alternative perspective for flow landslide cases, defining FL as the moisture content at which the soil starts to flow at a certain inclination angle.

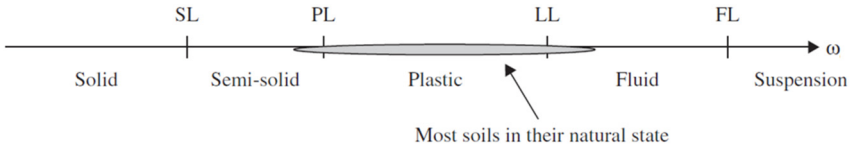

Figure 1. Flow Limit and Other Atterberg's Limits (Germain & Germain, 2009)

Some previous studies have employed various methods to determine the FL. Park and Nong (2013) used torvane (portable vane shear) to determine the FL value, which shows that FL is around 1.5 to 2.21 times higher than the LL. Widjaja and Florentini (2020) used the Fall Cone Penetrometer Test to determine the FL value, employing both the standard cone and a modified cone with a 4 g weight. It was found that FL is 1.5 to 1.6 times higher than the liquid limit. Shen and Tsai (2024) used the Atterberg liquid limit and flow limit instrument; they found that the FL is dependent on the slope angle for flow landslide cases, and the FL values are around 1.5 to 2 times higher than the LL values.

2.2 Cylinder Strength Test (CST)

Slurry material is a very weak material that sags under its own weight. Therefore, slurry samples cannot be tested with conventional shear strength tests, including vane shear or torvane, which cannot measure very low undrained shear strengths (c_u). Vallejo and Scovazzo (2003) proposed a new test using a cylinder, based on Sokolovski's theory (1995), that calculates the indentation pressures developed by Tresca plastic when the cylinder penetrates it. This method consists of slowly lowering a cylinder of known dimensions and weight into a mud sample. From the penetration, the c_u value can be defined using the bearing capacity principle and the buoyancy effect, as shown in Figure 2. Equations 1 and 2 show how to calculate the c_u value.

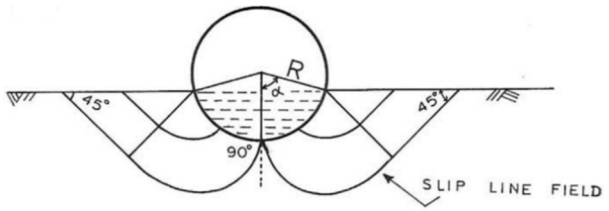

Figure 2. Cylinder Strength Test Principle (Vallejo, 2019)

$$c_u = \frac{R\left[\pi\,\gamma_c - \left(\alpha - \sin\alpha\,\cos\alpha\right)\gamma_f\right]}{2\left[\left(\pi+2\right)\sin\alpha + 2(1-\cos\alpha-\alpha\sin\alpha)\right]} \quad (1)$$

$$\alpha = \cos^{-1}\left(\frac{R-h}{R}\right) \quad (2)$$

where R is the radius of the cylinder, γ_c is the cylinder unit weight, γ_f is the mud unit weight, and h is the immersed cylinder height.

2.3 Suspension Settling Model

The suspension settling model is a model that helps us understand the sedimentation process of soil particles, which has been used since the Stone Age (Concha, 2014). This test utilized the extension of Stokes' equation or empirical modelling (Egolf & McCabe, 1937). Mishler (1912) and Coe and Clevenger (1916) recognized that the settling of a homogeneous flocculent suspension has four settling zones. The four settling zones, namely clear water (zone A), initial concentration (zone B), transition zone (zone C), and compression zone (zone D), are illustrated in Figure 3.

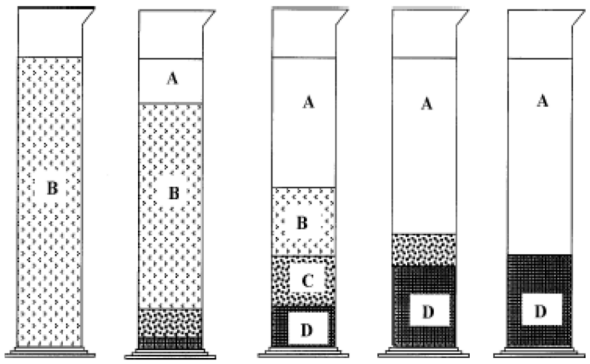

Figure 3. Suspension Settling Model (after Coe & Clevenger, 1916)

Figure 4 shows the settling cycle of a suspension based on Kynch's (1952) theory, where the sedimentation velocity only depends on particle concentrations. There are mudlines and sludge lines, where the mudline indicates where the suspension behaves like mud, and the sludge line marks the boundary between suspension and sedimentation. The critical sedimentation velocity (v_c) can be calculated using Equation 3, where v_c is determined by the completion of sedimentation and indicates the limit at which the sample has reached equilibrium, corresponding to the viscous liquid state limit.

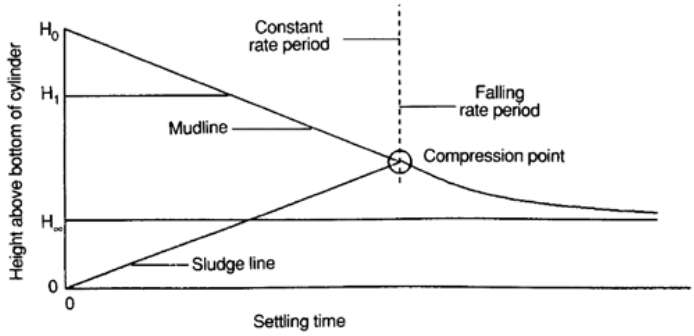

Figure 4. Settling Cycle of a Suspension (El-Shall *et al.*, 1993)

$$v_c = \left(\frac{H_1 - H_c}{t_c} \right) \tag{3}$$

where H_1 is the constant suspension height, H_c is the critical suspension height, and t_c is the critical time.

The conclusion of the sedimentation process is recognized when the sedimentation velocity diminishes below a specified critical threshold, as denoted by an exceedingly low critical velocity, thereby indicating the completion of the process (Kynch, 1952). Essential parameters, including the critical suspension height (H_c) and critical time (t_c), delineate the transition to a viscous liquid state as well as the point at which the sediment achieves full compaction at the base. The ultimate sedimentation height is determined by subtracting the critical height from the initial suspension height and comparing it to empirical observational data. To verify the viscous liquid condition at the base of the sample, assessments such as water content and index properties are undertaken, encompassing the LI and FL, which demonstrate that the soil maintains shear strength despite its viscous state.

Conca (2014) states that the phase before the critical condition still undergoes the sedimentation process, where each particle has no force to interact with other particles. However, when the condition after the sample passes through the critical point, the sample is undergoing compression. In this case, compression means that the sample can interact with each other but cannot hold its weight and starts to be compressed; in other words, this condition indicates that the sample already has an effective stress.

Zhang *et al.* (2025) found that, during the compression phase, the van der Waals force was the first to dominate the particles' interaction. In the next phase, the particles undergo a densification process dominated by double-layer interaction. In the rarefaction phase, the yield stress is the dominant force to govern the interactions (Figure 5). Wesley (2009) gave a similar opinion. However, with a different perspective, where the deposition process (compression) stage is the first stage, where the stress of the soil is neglected, due to the high void and very soft consistency, while the soil volume is increasing at deposition area the stress will increase and start to compress it self by it own weight that increasing the strength and reduces the void (Figure 6).

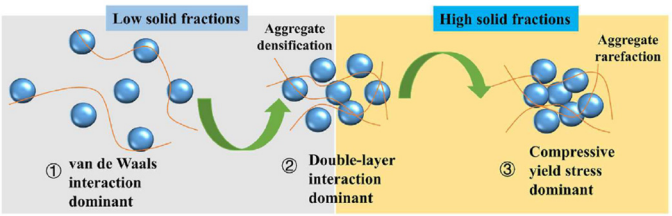

Figure 5. Illustration of Particle Interaction with Force Domination for each Phase (Zhang *et al.*, 2025)

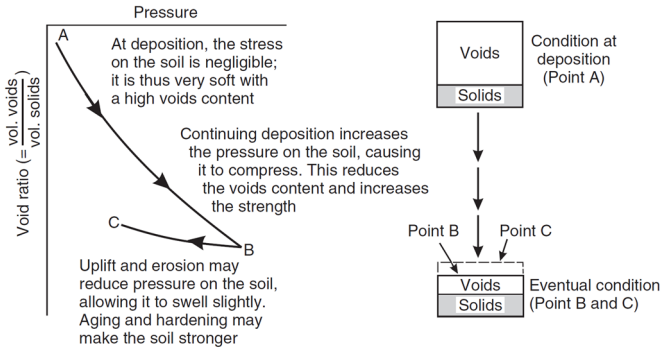

Figure 6. Sedimentary Soils Formation (Wesley, 2009)

3 METHODS

This study was done with five gradation variations of sand mixing (100% bentonite, 90% bentonite and 10% sand, 80% bentonite and 20% sand, 70% bentonite and 30% sand, and 60% bentonite and 40% sand). In the suspension settling model, there are five additional variations of solid concentration: 0.5% (50 g soil), 0.4% (40 g soil), 0.3% (30 g soil), 0.2% (20 g soil), and 0.1% (10 g soil). For the CST test, the cylinder diameter was varied to 30 mm, 40 mm, and 50 mm. In this study, water content is presented as the liquidity index (LI) to normalize the water content values, accounting for sample variations.

The CST was conducted in an aquarium filled with bentonite mud using an acrylic cylinder. The cylinder was placed on the mud and allowed to sink under its own weight until it came to rest. The depth of the submerged part of the cylinder was then measured. The CST is performed by increasing the water content until the cylinder is fully submerged. The increase in water content is calculated by determining the water needed for a specific LI value, mixing the soil and water with a mixer until it is homogeneous, and then placing the bentonite back into the aquarium to the same level. To measure the cylinder, the submerged height was first measured by removing it from the aquarium and using a caliper to measure the height covered by the bentonite. The CST process is illustrated in Figure 7, featuring the sample preparation, CST with three different cylinder diameters, and submerged height measurement.

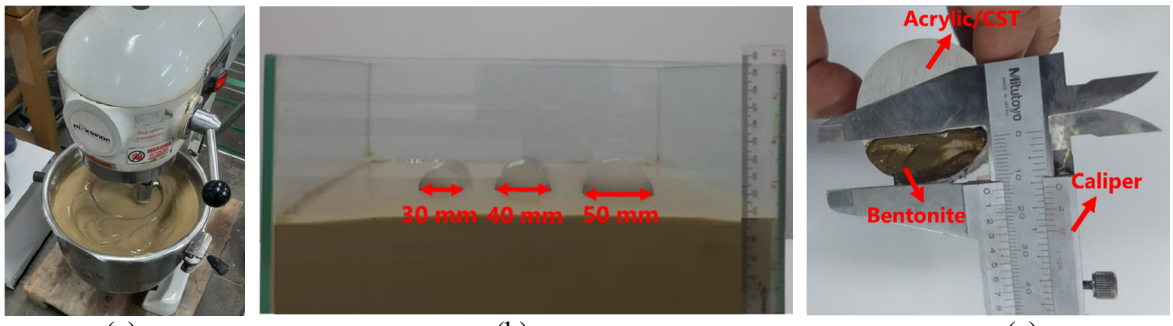

(a) (b) (c)

Figure 7. (a) Sample Preparation; (b) CST Illustration for Three Diameters; (c) Cylinder Submerged Height Measurement Using Caliper.

For the suspension settling model, which utilized approximately 1000 ml sedimentation cylinders, the bentonite sample was mixed with 20 ml of dispersing agent (water glass), dissolved in 80 ml of water, and then mixed using a mixer until it became homogeneous. Next, the slurry is transferred to the sedimentation cylinders and diluted with water until a total volume of 1000 ml is reached. After that, the slurry is mixed by an agitator for 1 minute. Observe the slurry as it settles at 1-minute intervals during the initial phase. When the sediment height increases by around 20 ml, the observation is conducted, and the test is stopped after five days. The illustration of the suspension settling model is shown in Figure 8.

After performing the suspension settling model simulation, the aqueous phase that separates from the bentonite sediment is removed. To validate the results, a CST was performed on the bentonite sediment using a 6 mm diameter and 40 mm length plexiglass cylinder. A metal clamp was used to drop the cylinder onto the sediment, and the submerged part was measured to obtain the c_u value. Figure 9 shows the CST process.

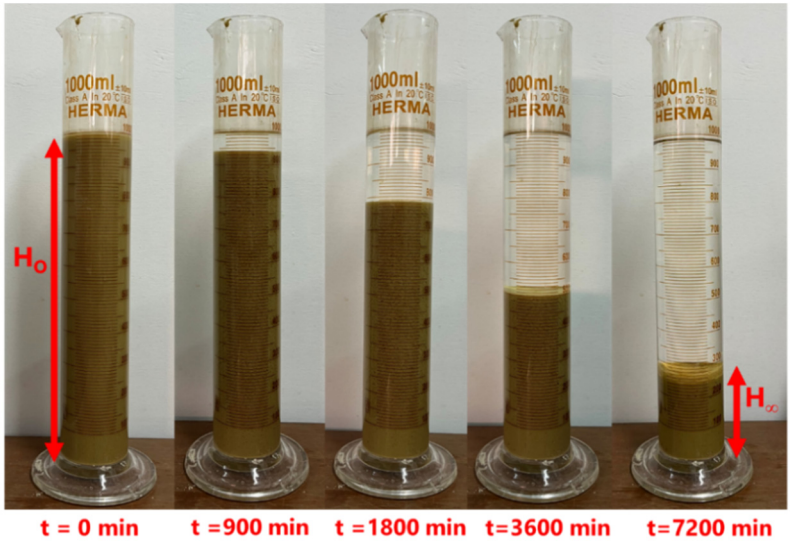

Figure 8. Suspension Settling Model Simulation for Bentonite Sample

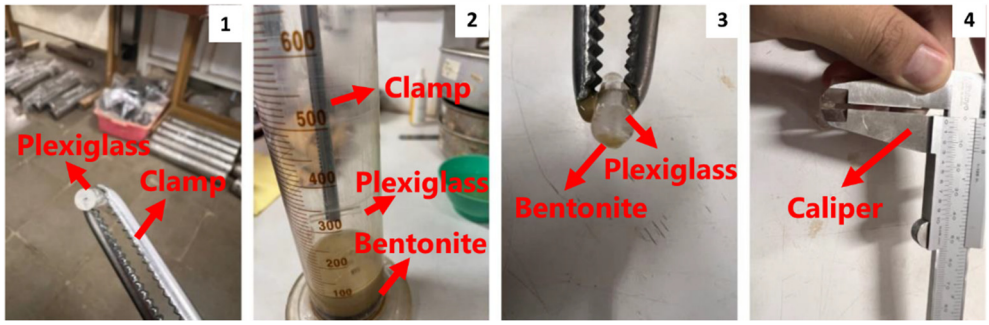

Figure 9. CST for the Bentonite Suspension Sediment Process

4 RESULTS AND DISCUSSION

4.1 Samples Index Properties

Before all those tests began, the index properties test was conducted first, namely the liquid limit (LL) and plastic limit (PL), using the fall cone penetrometer test and specific gravity test. From the results (Table 1), it is evident that as the sand percentage increases, the LL and PL values decrease, while the G_s value increases. The grain size analysis (Figure 10) shows that all bentonite variations are dominated by clay (more than 50%). In contrast, the behavior as indicated by Casagrande's plasticity chart (Figure 11) classifies all samples as MH (silt with high plasticity). The sand used in this study is dominated by medium sand (Figure 10) with a G_s value of 2.68.

Table 1. Samples Index Properties

Paramaters	Bentonite 100%	Bentonite 90% + Sand 10%	Bentonite 80% + Sand 20%	Bentonite 70% + Sand 20%	Bentonite 60% + Sand 40%
Liquid Limit (LL)	430	320	300	260	210
Plastic Limit (PL)	148	125	110	100	70
Specific Gravity (G_s)	2.67	2.68	2.69	2.73	2.76
Plasticity Index (PI)	282	195	190	160	140
Soil Classification	MH	MH	MH	MH	MH

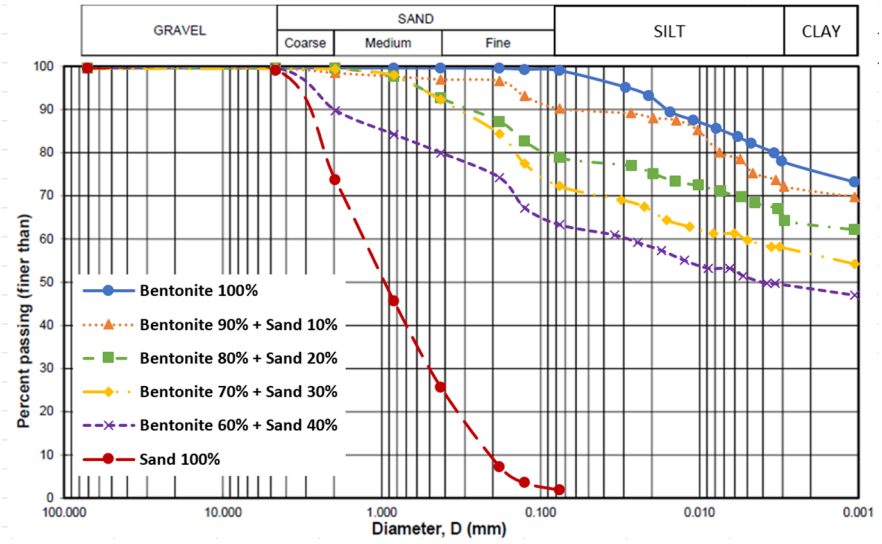

Figure 10. Samples Grain Size Distribution

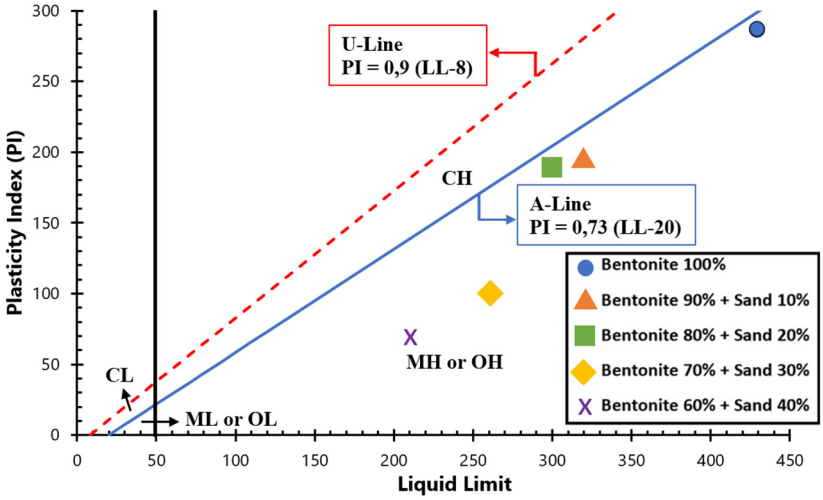

Figure 11. Cassagrande Plasticity Chart with Sample Conditions

4.2 Suspension Settling Model Results

The suspension settling model provides a relationship between settling time and slurry height, allowing for the determination of the critical height and time to estimate the boundary between suspension and viscous liquid states. The result (Figure 12) shows that the concentration controlled the settling rate; the higher the concentration, the faster the sediment settled. Figure 13 illustrates the method for determining critical time and height, using the tangent line and sludge line.

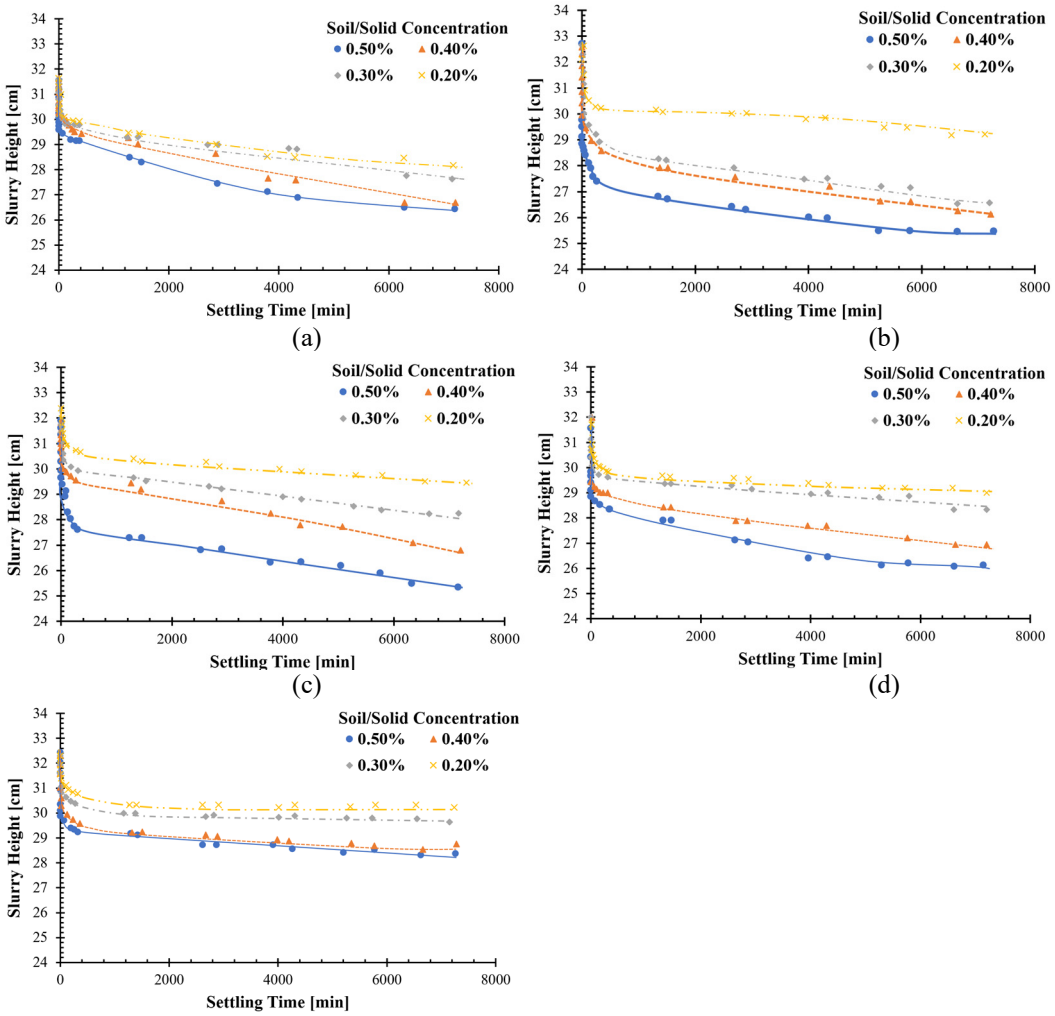

Figure 12. Suspension Settling Model Observation Result for Each Concentration and Sample Variation (a) 100% Bentonite, (b) 90% Bentonite 10% Sand, (c) 80% Bentonite 20% Sand, (d) 70% Bentonite 30% Sand, and (e) 60% Bentonite 40% Sand

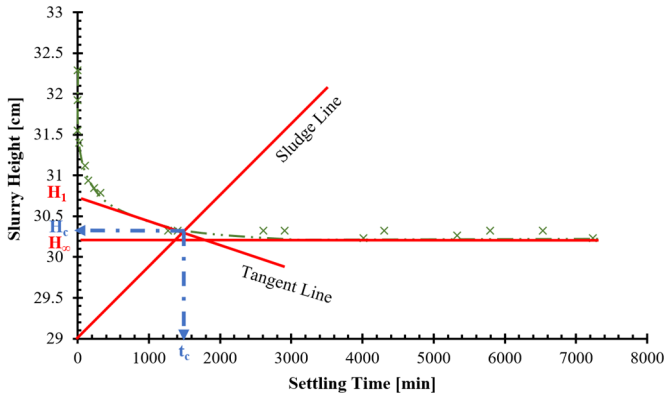

Figure 13. Illustration of Define H_1, H_∞, H_c, and t_c in Suspension Settling Model for Bentonite 60% Sand 40% for 20 g Concentration

From the data above, the critical settling rate (v_c) for each variation in Table 2. The results show that sand and sample concentrations are not impacting the v_c and H_c values. The results (Table 2) show that bentonite has a very slow settling rate (v_c), so the smaller the number, the longer it takes to reach the critical condition.

Table 2. The Critical Sedimentation Velocity

Samples	Samples Concentration [g]	H_0 [cm]	H_1 [cm]	H_c [cm]	t_c [min]	v_c [cm/s]
100% Bentonite	50	31.5	28.5	27.2	3300	3.9×10^{-4}
	40	31.5	29.8	29	1440	5.6×10^{-4}
	30	31	29.8	29	2300	3.5×10^{-4}
	20	31.3	29.7	28.6	4500	2.4×10^{-4}
90% Bentonite +	50	32.5	28.8	27.8	2600	3.8×10^{-4}
10 % Sand	40	32.2	28.1	27.8	2400	1.3×10^{-4}
	30	31.5	28.0	27.4	3500	1.7×10^{-4}
	20	32	30.0	29.6	3800	1.1×10^{-4}
80% Bentonite +	50	31.8	27.8	25.9	4600	4.1×10^{-4}
20% Sand	40	31.7	29.5	28	4300	3.5×10^{-4}
	30	31.6	29.5	28.5	5300	1.9×10^{-4}
	20	32.3	30.5	30.2	3500	9.0×10^{-5}
70% Bentonite +	50	31.5	28.0	27	3200	3.1×10^{-4}
30% Sand	40	31	28.8	27.9	4100	2.2×10^{-4}
	30	32	29.2	29	5500	4.0×10^{-5}
	20	31.7	31.1	29.55	1900	8.2×10^{-4}
60% Bentonite +	50	32.2	29.1	28.75	5600	6.0×10^{-5}
40% Sand	40	31.7	29.0	28.7	4400	7.0×10^{-5}
	30	32.3	30.3	29.9	2500	1.6×10^{-4}
	20	32.3	30.8	30.3	1500	3.0×10^{-4}

4.3 Cylinder Test Results

The CST can be performed within an LI range of 1.4 to 2.9. Beyond LI 2.9, the cylinder sinks completely due to its weight exceeding the undrained shear strength (c_u) and the buoyant force acting on its entire volume. The data trend (Figure 14) shows an exponential relationship between LI and c_u, where the c_u value reduces while the LI value increases. The increase in sand amount causes the c_u value to increase for the initial water content.

The cylinder diameter also influences the determination of c_u values. Figure 14 illustrates the influence of changing the cylinder diameter, which leads to a change in its weight and contact surface. The results show that the highest c_u value was obtained with a 50 mm cylinder diameter, and the smallest value was obtained with a 30 mm CST diameter. At the initial LI, the c_u value for each diameter shows quite significant gaps, but when the LI exceeds 2.4, the gaps become tighter.

The CST was conducted on the bentonite sediment to determine the c_u value and verify whether the sample had passed the critical condition. The CST results shown in Figure 15 indicate that the trend is quite different, with the c_u of bentonite being the highest at all conditions, as observed in the results of the previous section.

4.4 Estimating the Flow Limit Value

From the CST and suspension settling model, the value of FL was obtained. Where the c_u values are zero for CST. Figure 16 shows the CST result for the bentonite sediment after the suspension settling mode. The results indicate that the trend is quite different, with the c_u of bentonite being the highest at all conditions, as observed in the results of the previous section.

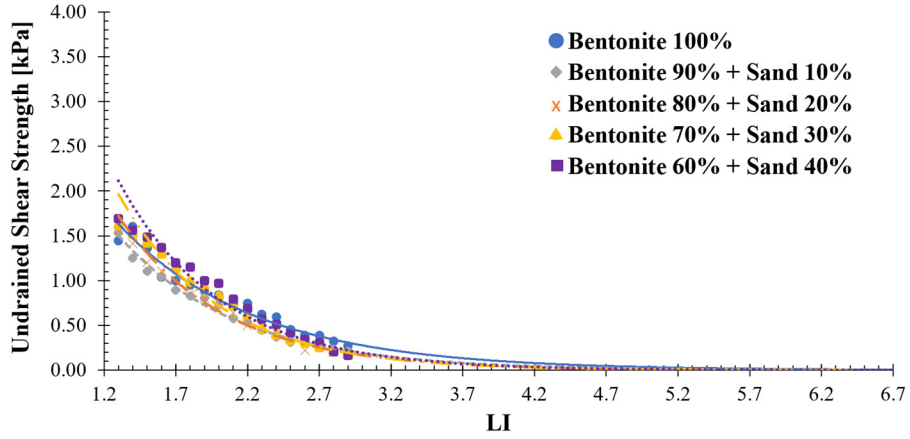

(a)

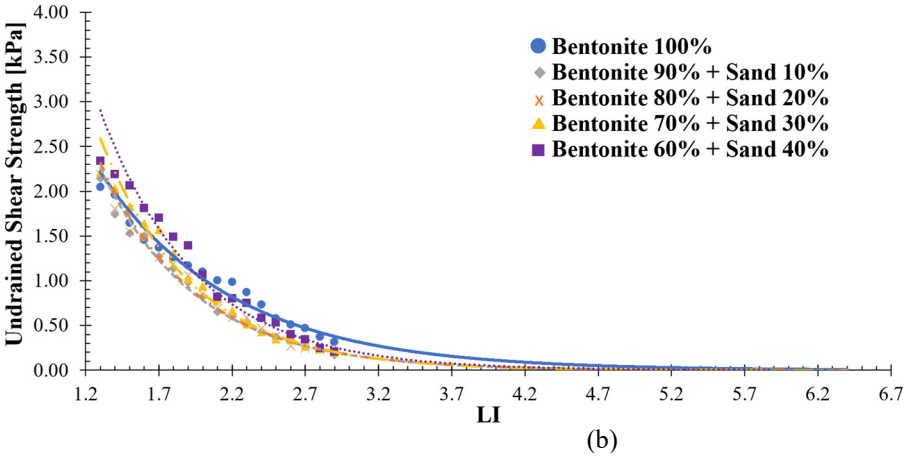

(b)

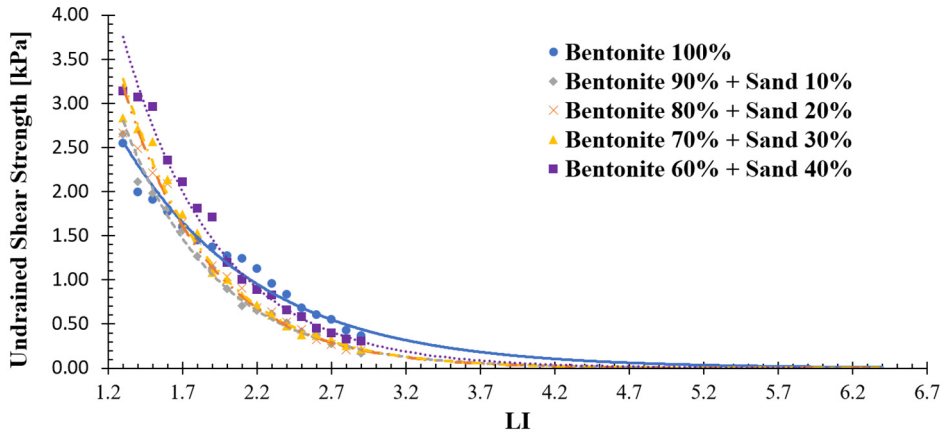

(c)

Figure 14. CST Result for Cylinder Diameter (a) 30 mm, (b) 40 mm, and (c) 50 mm.

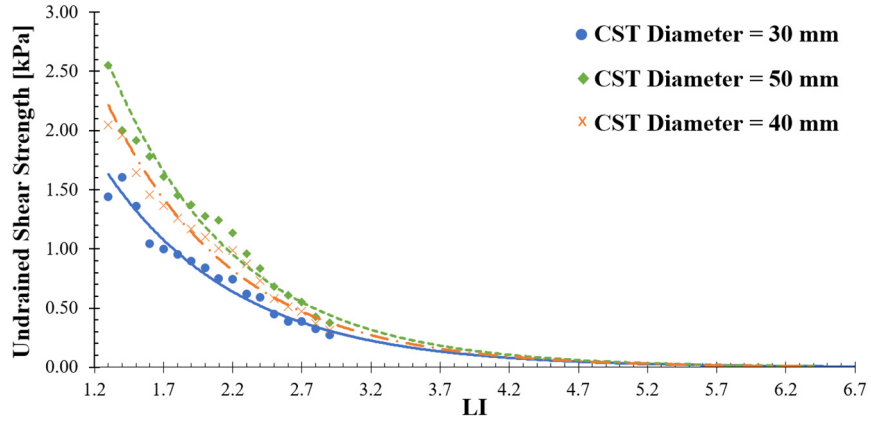

Figure 15. Comparison of CST Results for Different Cylinder Diameters with 100% Bentonite Sample

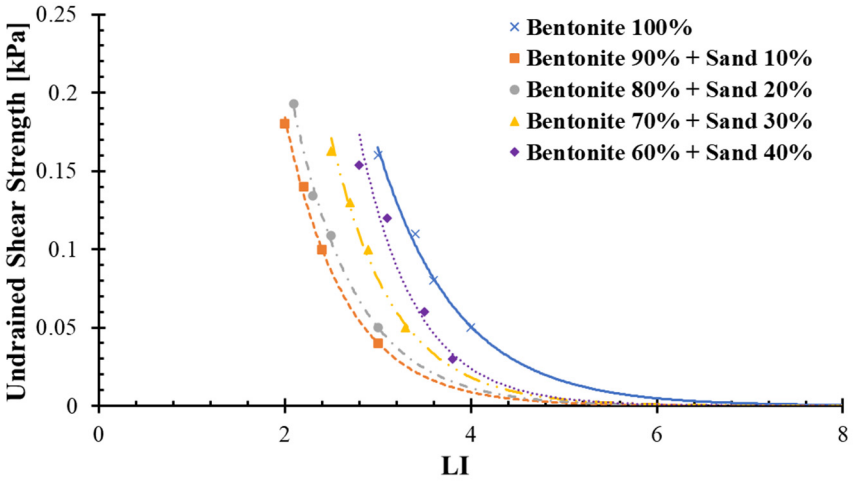

Figure 16. The CST Results from the Suspension Settling Samples

The CST shows the same FL value for each diameter variation (Figure 14), and the bentonite mixed with sand obtained the same LI value for all sand variations in LI, water content (w) and ratio of FL over LL (Table 3). Table 4 shows the results for the bentonite sediment FL value using CST. According to the suspension settling model, the FL value can be determined by subtracting the water content from sediment samples, assuming no changes in water content occur when clear water is removed. In this context, FL is considered the critical condition in the suspension model; the FL value is taken from the average of all variations of soil concentrations (Table 5).

Table 3. Flow Index Value CST

Samples	FL		
	LI	w (%)	FL/LL
Bentonite 100%	6	1840	4.28
Bentonite 90% + Sand 10%	4.8	1061	3.32
Bentonite 80% + Sand 20%	4.8	1022	3.41
Bentonite 70% + Sand 30%	4.8	868	3.33
Bentonite 60% + Sand 40%	4.8	742	3.53

Table 4. Flow Index Value CST after Suspension Settling Model Simulation

Samples	FL		
	LI	w (%)	FL/LL
Bentonite 100%	7	2122	4.9
Bentonite 90% + Sand 10%	6	1295	4
Bentonite 80% + Sand 20%	6	1250	4.2
Bentonite 70% + Sand 30%	5.2	932	3.6
Bentonite 60% + Sand 40%	5.2	798	3.8

Tables 3 and 4 show that the sand materials contribute to dragging down the FL value. Where the effect of adding sand to pure bentonite is quite significant on average, the value can drop by around 14 to 25%. However, uniquely, the increase in sand concentration when there is already sand in the sample has almost no effect on the FL value.

According to Tables 3, 4, and 5, different approaches lead to different results. Based on all the tests using the suspension settling model, the smallest FL value is yielded, while the bentonite sediment CST FL value is the largest. Many factors can influence the results, including the CST and the CST after suspension settling model. One of them is the boundary effect, where in the small concentration samples, the resulting slight sediment can lead to the failure plane from the CST not being fully developed, which affects the c_u values. The other aspect where the CST from the suspension settling model is not tested until the cylinder entirely drowns; additionally, the results fall within a narrow range of cu values, which can affect the trendlines.

Table 5. Flow Index Value from Suspension Settling Model Simulation

Samples	FL		
	LI	w (%)	FL/LL
Bentonite 100%	3.5	1135	2.6
Bentonite 90% + Sand 10%	2.4	593	1.9
Bentonite 80% + Sand 20%	2.5	585	2
Bentonite 70% + Sand 30%	2.9	564	2.2
Bentonite 60% + Sand 40%	3.3	532	2.5

The differences in the results of these three tests are due to the different approaches that use different principles. Each test has advantages and disadvantages. For example, CST can determine the magnitude of the c_u value to a relatively small value, but has difficulty in estimating when the c_u value will reach zero. The main difficulty in determining the FL value lies in its relative subjectivity when determining the critical suspension settling time. Although the suspension settling model has shortcomings in determining the FL value compared to CST, this model can at least provide an overview of the sedimentation process of soil suspension towards viscous liquid.

When the results were compared to those of the previous study by Park and Nong (2013), the FL/LL ratio ranged from 1.5 to 2.21, which is close enough to the results of the suspension settling model. A previous study by Widjaja and Florentini (2020) and Shen and Tsai (2024) reported an FL/LL ratio of around 1.5 to 2, which differs significantly from the results of this study.

The gap between this study's results and those of the previous study may be attributed to the differences in bentonite mineralogy (Chen, 1975). According to Widjaja *et al.* (2024), the CST can determine the c_u value much further than the other tests. Another aspect of the significant difference in the FL value is the regression; Park and Nong (2013) determined that the regression uses a sharp

angle to determine when c_u is 0, which may lead to subjective and inconsistent results. In this study, a regression was performed to make the regression smoother, thereby obtaining more objective and consistent results. The CST shows more consistent results for all conditions, as opposed to the suspension settling model, due to the latter having a higher degree of disturbance in water content determination, and the settling phase having already passed through the critical condition.

5 CONCLUSION

This study employed the CST and the suspension settling model to determine the FL value. Both methods use different approaches to determine the FL value. The samples in this study are composed of bentonite and a mixture of sands with five gradation variations. There are three additional diameter variations for CST, and five concentrations of samples in the suspension settling model. CST determines the FL from the viscous liquid state using c_u values. In contrast, the settling model determines it from the suspension state based on the critical condition when it starts behaving like a viscous liquid.

The results show that the suspension settling model yielded the smallest results for all variations, while CST at the bentonite sediment was the largest. All of the CST results show consistent results for all dimension variations. The amount of sand in the samples has no clear patterns to be concluded in the suspension settling model; on the other hand, the sand's effect on the increase of the c_u value in the early LI values makes the trendline steeper, and makes the FL value consistent for all samples that were mixed with sand. Although this study did not find a single FL value at the intersection of these two approaches, it provides an overview of the proposed FL values from different approaches.

The results of this study show higher FL values than those of previous studies, particularly in the CST results. This can occur due to the varying mineral composition of the bentonite samples, differences in test apparatus capacity, and varying approaches to estimating the FL value. Further studies should consider evaluating other soil types, especially natural soils, and utilize alternative apparatus to determine the FL value, such as the laboratory vane shear test. Another factor that needs to be considered is the soil's mineralogy, and proposes a new method that is more objective, which may help explain the results gaps for each soil sample.

DISCLAIMER

The authors declare no conflict of interest.

AVAILABILITY OF DATA AND MATERIALS

All data are available from the author.

ACKNOWLEDGMENTS

The authors acknowledge Parahyangan Catholic University for the opportunity to conduct this research.

REFERENCES

Atterberg, A., 1911. *Über die physikalische Bodenuntersuchung und über die Plastizität der Tone. Internationale Mitteilungen für Bodenkunde,* 1 (1911).

Bain, J. A., 2009. *Industrial Clays. Society for Mining, Metallurgy, and Exploration (SME)*

Casagrande, A., 1932. *Research on the Atterberg Limits of Soil*. *Public Roads,* 13:121-136

Chen, F. H., 1975. *Foundations on Expansive Soils. Elsevier.*

Conca, F., 2014. *Solid–Liquid Separation in the Mining Industry. Cham: Springer Switzerland*.

Coe, H.S., & Clevenger, G. H. 1916. *Methods for Determining the Capacity of Slime Settling*

Tanks. Transactions, AIME, 55,356-385.

Egolf, C. B., & McCabe, W. L., 1937. *Rate of sedimentation of flocculated particles*. *Transactions AIChE, 33, 620-640.*

El-Shall, H., Bogan, M., & Moudgil, B., 1993. *Mathematical Modelling of Settling of Solid Suspensions*. *Mining, Metallurgy and Exploration, 10, 57–61.*

Gary, M., McAfee, R. J., Wolf, C. L., 1977. *Glossary of Geology. American Geosciences Institute (AGI)*

Germaine, J. T., & Germaine, A.V., 2009. *Geotechnical Laboratory Measurements for Engineers.* New Jersey: Mc. Wiley & Sons, Inc.

Kynch, G. J., 1951. *A Theory of Sedimentation. Trans. Faraday Soc., 48, 166-176.*

Mishler, R. T., 1912. *Settling Slimes at the Tigre Mill. Eng. Min. Chem., 25(10):18-28.*

O'Brien, J.S., 2003. *Reasonable Assumption in Routing a Dam Break Mudflow. 3rd Conference on Mud and Debris Flows on Proceedings of Debris Flow Hazards Mitigation.*

Park, S., & Nong, Z., *2013. A Proposal of Flow Limit for Soils at Zero Undrained Shear Strength. Journal of the Korean Geotechnical Society, 29 (1), pp. 73-84.*

Shen, M., & Tsai, Y., 2024. *Application of Cohesive Soil Flow Limit and Slope Critical Flow Angle. Geotechnical Research 11 (2): 88-99.*

Vallejo, L. E., & Scovazzo, V. A., 2003. *Determination of the Shear Strength Parameters Associated with Mudflow. Soils and Foundations, 43 (2), 129-133.*

Vallejo, L. E., 2019. *The Measurement of the Undrained Shear Strength of Muds Using a Cylinder. Cancun, Geotechnical Engineering in the XXI Century: Lessons learned and future challenges*.

Wesley, L. D., 2009. *Fundamentals of Soil Mechanics for Sedimentary and Residual Soils. John Wiley & Sons, Inc.*

Widjaja, B., 2019. *Landslide and Mudflow Behavior Case Study in Indonesia: Rheology Approach. IPTEK Journal of Proceedings Series. 93:97*

Widjaja, B., & Florentini, F., 2020. *Determining Flow Limit Using Fall Cone Penetrometer Test. Jakarta, The 24th Annual National Conference on Geotechnical Engineering.*

Widjaja, B., Pratama, I. T., Hartono, I., & Limowa, B., 2024. *Laboratory Study on Vallejo and Scovazzo's Methods in Estimating the Rheology Parameters of Bentonite and Kaolinite Muds. Civil Engineering Dimension*, 26 (2), 51- 62

Zhang, L., Yang, K., Liu, F., *et al*. 2025. *An Approach to Determine Settling Properties of Flocculated Tailings Suspensions Based on a Single Batch Settling Test. Particuology, 102 (2025) 15-26*

HIMPUNAN AHLI TEKNIK TANAH INDONESIA - HATTI
Indonesian Society for Geotechnical Engineering - ISGE
PIT HATTI XXIX
10-12 November 2025

Analysis and Design of a High-Risk Tiered Retaining Wall Using a Geosynthetic Reinforcement System

Valdy Kosalim[1,*], Isparmo[2], Krisandi Saptyanto[3], Wira Rante Paganggi[4], Dwi Agrina[5]
[1]PT Multibangun Rekatama Patria, Jakarta, Indonesia, 12160;valdy@multibangunpatria.com
[2]PT Multibangun Rekatama Patria, Jakarta, Indonesia, 12160;isparmo@multibangunpatria.com
[3]PT Multibangun Rekatama Patria, Jakarta, Indonesia, 12160;sandi@multibangunpatria.com
[4]PT Multibangun Rekatama Patria, Jakarta, Indonesia, 12160;wira@multibangunpatria.com
[5]PT Multibangun Rekatama Patria, Jakarta, Indonesia, 12160;dwi@multibangunpatria.com
*Correspondence: valdy@multibangunpatria.com

ABSTRACT Infrastructure development in Indonesia often faces rugged terrain and high seismicity, requiring advanced geotechnical solutions. One of the challenges lies in ensuring that an embankment can effectively withstand heavy loading conditions. Mechanically stabilised earth (MSE) walls provide a safe and efficient option to address these challenges. This background motivates the study of modern reinforcement system applications for high reinforced retaining structures. The objective of this paper is to present a case study on the design and analysis of a tiered RSS with a total height of 26.95 meters based on a previous project. The structure is designed to withstand a large static surcharge load (up to 375 kPa) and a seismic load with a peak horizontal ground acceleration (kh) of 0.225g. The method employed is a limit equilibrium stability analysis using Janbu's simplified method of slices for non-circular failure surfaces, referring to the SNI 8460:2017 standard, and utilising TensarSlope software. The selected system is the SierraScape System, which combines high-strength uniaxial geogrid primary reinforcement with a flexible welded wire for facing. The analysis results show that the retaining wall design meets the required factors of safety for both static (FS = 1.301 > 1.30) and seismic (FS = 1.163 > 1.10) conditions. In conclusion, this case study demonstrates that the application of modern geosynthetic reinforcement systems is a reliable and effective solution for addressing geotechnical challenges in high-risk projects in Indonesia, contributing a design reference for similar conditions.

KEYWORDS MSE Wall; High Risk Tiered; Heavy Loading Conditions, Reinforced Retaining Structure; Geosynthetic Reinforcements

This paper will be published in the future issues of Indonesian Geotechnical Journal

This page is intentionally left blank

HIMPUNAN AHLI TEKNIK TANAH INDONESIA - HATTI
Indonesian Society for Geotechnical Engineering - ISGE
PIT HATTI XXIX
10-12 November 2025

Numerical Analysis of Rainfall-Induced Slope Failure in Gumay Ulu, Lahat, South Sumatra

Al Amirsyah[1], Yudi Harianto[2], Nurly Gofar[3*]
[1,3)]Civil Engineering Department, Graduate Program, Universitas Bina Darma, Palembang 30111, Indonesia[2]
CV. Geoteknik Pratama, Civil Engineering Laboratory, Palembang, Indonesia
*Correspondence: nurly_gofar@binadarma.ac.id

ABSTRACT: Many slope failures occurred after a heavy rainfall; thus, rainfall infiltration is identified as the triggering factor for the failures. Important factors influencing rainfall-induced slope instability include slope geometry, soil characteristics, and the duration and intensity of rainfall. A case study was performed using SEEP/W and SLOPE/W programs to investigate the mechanism of slope failure that occurred on March 13th, 2023, in Gumay Ulu, Lahat, South Sumatra, Indonesia. The geometry of the slope after failure was obtained using topographical measurements. The original geometry was reconstructed based on observation of the failed slope and the nearby slopes. Soil samples were collected and tested in the laboratory for index properties, shear strength parameters, SWCC, and saturated permeability. Rainfall data was collected from a nearby station. Medium and heavy rainfall for twelve days before slope failure was considered in the analysis. The cumulative rainfall on the day of failure was 216 mm. Seepage analysis shows that rainfall infiltration increases the pore water pressure in the soil and reduces the shear strength and hence slope stability. The factor of safety decreased from 1.884 on 1st of March to 1.166 on March 13th when the failure took place. A combination of regrading and terracing with slope protection from rainfall infiltration was proposed as a mitigation measure. The factor of safety of the improved slope is 2.146.
KEYWORDS: rainfall infiltration; matric suction; unsaturated soils; regrading & terracing, slope protection.

1 INTRODUCTION

Slope failure is a prevalent geohazard in tropical areas covered with residual soils (Rahardjo et al., 2005). The slip surface is usually shallow, ranging from one to three meters in depth, and it is aligned in a direction parallel to the slope surface (Matsutsi et al., 2006). The mechanism of the failures is usually attributed to the complete or partial dissipation of matric suction within the unsaturated zone during the process of rainfall infiltration. The reduction of matrix suction results in a decrease in the soil's shear strength which lead to failure (Lee et al, 2009).

The phenomenon of slope failure induced by rainfall infiltration has been investigated through a combination of field observations, laboratory experiments, and numerical modelling. The integration of computer programs facilitates the execution of seepage and infiltration analysis in unsaturated soil, as well as the assessment of slope stability. The computation of pore-water pressure in slopes subjected to rainfall in numerical analysis typically involves finite element analysis of water flow through unsaturated-saturated soils (SEEP/W). Additionally, the assessment of slope stability is commonly conducted through limit equilibrium methods (SLOPE/W). These methods are employed in the integrated Geostudio software application (Geoslope International, 2018) to evaluate the impact of rainfall infiltration on slope stability. The programs have been used extensively by researchers to evaluate the impacts of rainfall on slope stability.

Few studies have been conducted on the topic of rainfall-induced slope failures in South Sumatra (Gofar et al., 2006; Aisah & Gofar, 2022; Gofar et al., 2025). Gofar et al. studied the mechanism of slope failure at the dumping area in open pit mine in Tanjung Enim. Aisah and Gofar studied the causations of slope failures in jalan Lematang, Pagaralam. Gofar et al. (2025) evaluated the influence of several rainfall scenarios causing slope failures in Pagar Alam, South Sumatra. They concluded that the most critical rainfall pattern is the combination of low-intensity rainfall and heavy rain. The duration of low-intensity rainfall is inversely proportional to the slope angle.

Lahat district is located in the western part of South Sumatra Province. The district covers part of the Bukit Barisan Mountains, which are controlled by the main Sumatran Fault that forms hills and mountains in the northwest-southeast direction. The topography of the area is hilly and undulating, resulting in medium to steep slope inclinations.

Many slope failures occurred in this area. Based on slope inventory by the South Sumatra National Road Implementation Center (BBPJNSS) from 2018 to 2022, 85% slopes with high risk of landslide are located in the national road segment connecting Lahat – Pagar Alam – Tanjung Sakti – Border of Bengkulu Province (National Road segment No 15-036, 15-37, and 15-38) (Epianti et al., 2025). Landslide is the most dominant ground movement in this area, and rainfall is the most frequent triggering factor for the landslide (Erlangga et al., 2024). Furthermore, Fathoni et al. (2024) showed that the most common mitigation measures in this area are (a) by reducing the forces that cause movement at the toe and use of some types of anchors on the slope surface, as well as (b) increasing the resisting forces by controlling seepage or rainfall infiltration.

The first objective of this study was to evaluate the mechanism of slope failure in Jalan Gumay Ulu (coordinate location: 3°56'55" S;103°25'76" E), Lahat District, South Sumatra. The incident that occurred on March 13th, 2023, was thought to be caused by three days of continuous rainfall. The total amount of rainfall 12 days before failure was 216 mm. SEEP/W and SLOPE/W programs were utilized to evaluate the effect of rainfall on the slope failure. The second objective was to propose appropriate mitigation measures to protect the slope from future instability. The stability of the slope after treatment was evaluated using SLOPE/W.

2 RAINFALL-INDUCED SLOPE FAILURE

The study of suction distribution and water flow within the unsaturated zone is a prerequisite for understanding slope failure in unsaturated soil (Gofar et al., 2008). An unsaturated soil has water and air in its voids and possesses four phases: i.e., solid, water, air, and contractile skin. The pore water pressure is always negative relative to the pore air pressure (Fredlund, et al., 2012). The flow of water in unsaturated soils differs from that of saturated soils. In the former, the coefficient of permeability varies with matric suction or degree of saturation, and this function is assumed to be constant in the latter.

Rainfall infiltration induced a transient water flow in the soil forming the slope. The second type of flow is the transient state or time-dependent flow, whereas the flow is governed by Richards' equation (which takes care of the change of volumetric water content with time). This equation is given as:

$$\frac{\partial}{\partial x}\left(k_x \frac{\partial h}{\partial x}\right)+\frac{\partial}{\partial y}\left(k_y \frac{\partial h}{\partial y}\right)+q = m_w^2 \rho_w g \frac{\partial h}{\partial t} \quad (1)$$

where; θ_w is the volumetric water content, m_w^2 is the coefficient of volumetric water change with respect to a change in negative pore–water pressure ($u_a - u_w$) and is equal to the slope of the soil–water characteristic curve (SWCC), ρ_w is the density of water, and g is gravitational acceleration.

SWCC is the most important characteristic of unsaturated soil, which defines a sigmoidal relationship between the soil moisture content and the soil suction ($u_a - u_w$) in a semi-logarithmic

plot (Satyanaga et al., 2017). The greater the amount of water within these pores, the lower the soil suction and vice versa. Soil moisture affects the initial portion of the curve, while the soil grain size distribution controls the slope of the curve. The maximum amount of water that can enter the soil depends on the size of the soil pores (porosity). The SWCC also plays an important role in explaining the hydraulic and mechanical characteristics of unsaturated soil, including water storage capacity, permeability coefficient, and strength properties (Fredlund et al., 2012).

The stability of a slope is usually expressed in the form of a factor of safety (FOS), which is the ratio of the shear strength of the soil and the induced shear stress by loading.

$$FOS = \frac{\tau_f}{\tau_m} \quad (1)$$

Thus, the shear strength of soil is an important parameter for the slope stability analysis. The shear The shear strength of unsaturated soils is given by Fredlund et al. (1978) to take care of additional shear strength by matric suction and can be written as:

$$\tau_f = c' + (\sigma_n - u_a) \tan \phi' + (u_a - u_w) \tan \phi^b \quad (2)$$

where τ_f is the shear strength along the failure plane at the time of failure, while c' is effective cohesion, ϕ' is the effective frictional angle, $(\sigma_n - u_a)$ is net normal stress, u_a is pore-air pressure, u_w is pore-water pressure, $(u_a - u_w)$ is matric suction, ϕ^b is the internal friction angle due to matric suction, γ_t is the total unit weight of soil, z_w is vertical depth of saturated soil, and α is the slope angle.

The shape and location of the failure plane should be determined in advance before the slope stability analysis. For a circular failure plane, the most critical failure plane can be identified by considering a series of slip circles with the minimum factor of safety. Circular failure plane is the most commonly assumed in slope stability analysis. In SLOPE/W, the critical failure plane could be identified by assigning the locations of the center of rotation and different radii or by assigning the locations of entry and exit points along the crest, surface, and toe of the slope.

3 METHODS

3.1 Study Location

The study was conducted at Jalan Gumay Ulu Road, Lahat District (coordinate location: 3°56'55" S;103°25'76" E), Lahat District, South Sumatra. The slope failed on 13th March 2023 after three days of continuous heavy rainfall (more than 40 mm/day). The geographical map of the study area is shown in Figure 1 while the slope conditions after failure are given in Figure 2.

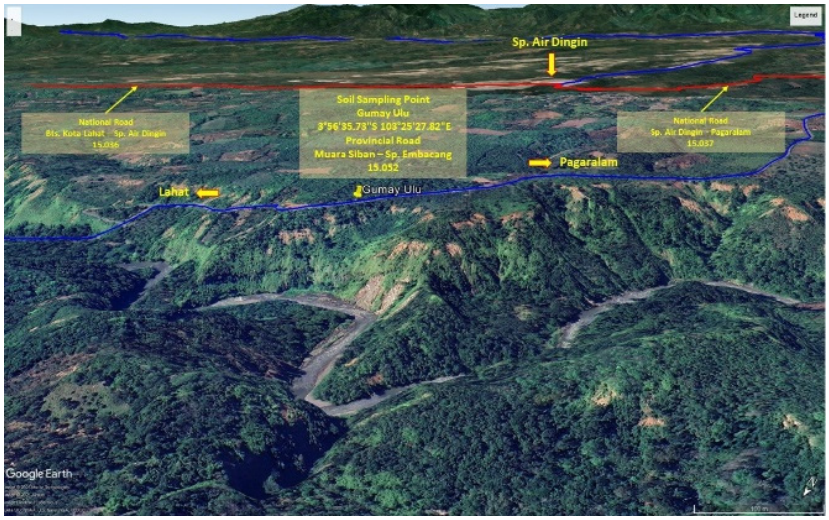

Figure 1. Study Location.

Figure 2. Slope condition after failure (a) on the crest (b) at the toe

The failed slope is part of several slopes on the hilly topography. The elevation of the crest is at 492.2 m above sea level. The height of the slope was 20 m, and the inclination of the individual slope is 47^{o}. A provincial road is located on both the crest and the toe of the slope, but the failure did not affect traffic on the road located at the crest because the slip surface was shallow. The failure affected the transportation on the road located at the toe due to the debris material. The sliding plane was almost parallel to the slope surface, and the average depth of the slip plane was about 2 – 3 meters. The slope geometry before failure was obtained from Google Earth data while topographical mapping was used to evaluate the geometry of the slope after failure.

3.2. Rainfall Records

Figure 3 presents the daily rainfall records before slope failure (1 – 12 March 2023), recoded by the nearby rainfall station (PTPN VII Pagar Alam). Medium and heavy rainfall lasted for twelve days before slope failure. The slope failure occurred in the early morning (at 02:00 on 13th March 2023). The cumulative rainfall at the time of failure was 216 mm.

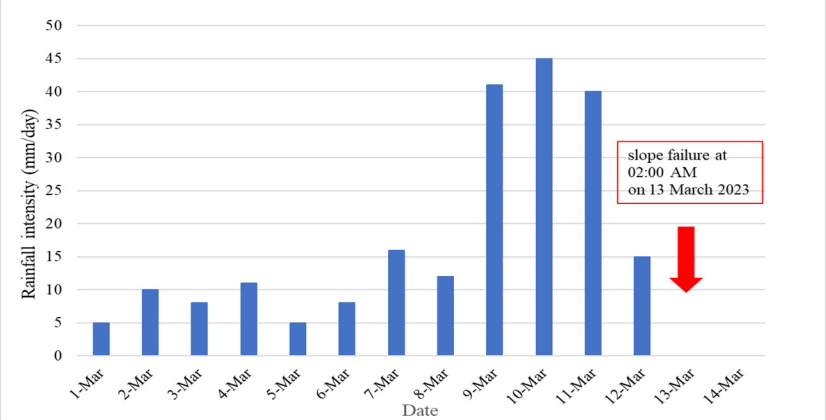

Figure 3. Daily rainfall records before slope failure.

3.2 Soil Properties

The basic soil properties were obtained from laboratory tests conducted on samples retrieved from the site. Disturbed samples, collected from a depth of 1.5 – 2m, were used for index properties tests including particle size distribution, Atterberg limits, and specific gravity tests, and soil classification. Samples were also collected for the determination of the soil water characteristic curve (SWCC) required for seepage analysis. Undisturbed samples were taken from a depth of 3 m for the determination of shear strength and coefficient of permeability. Drilling, sampling, and laboratory tests were conducted following relevant ASTM standards.

The saturated permeability coefficient (k_s), the SWCC, and the permeability function of the soil are required in the seepage analysis. The k_s was obtained from a falling head permeability test (D5084-16). The SWCC was tested in the laboratory using an osmotic tensiometer (Rahardjo et al, 2021). The data were corrected with a shrinkage curve to obtain the SWCC in terms of volumetric water content (Fredlund et al., 2002). The curve obtained from the laboratory was best fitted using Fredlund and Xing (1994) equation. Both the saturated permeability coefficient and SWCC were used to predict the permeability function using a statistical approach (Brooks and Courier, 1966).

Effective shear strength (c' and ϕ'), and the increase in shear strength due to suction (ϕ^b), are required for stability analysis. The effective shear strength was obtained using a direct shear test following ASTM D3080-04. The ϕ^b is estimated as 2/3 of ϕ' (Fredlund, et al. 2012).

The results of laboratory tests are summarized in Table 1, while the SWCC and the permeability function used for this study are presented in Figure 4.

Table 10: Index and strength properties of soil

Properties	Unit	Value
Moisture content	%	43.53
Specific gravity	-	2.55
Passing sieve No. 200	%	98.06
Percentage of clay (< 0.002 mm)	%	83.72
Liquid Limit	%	46.70
Plastic limit	%	35.30
Plasticity Index	%	11.40
Soil classification	USCS	CL
Unit weight	kN/m^3	17.30
Saturated unit weight	kN/m^3	18.70
Effective cohesion	kPa	27
Effective Friction Angle	Degree	38
Increase in friction angle with suction	Degree	27
Coefficient of permeability k_s	m/s	6.25 E-06

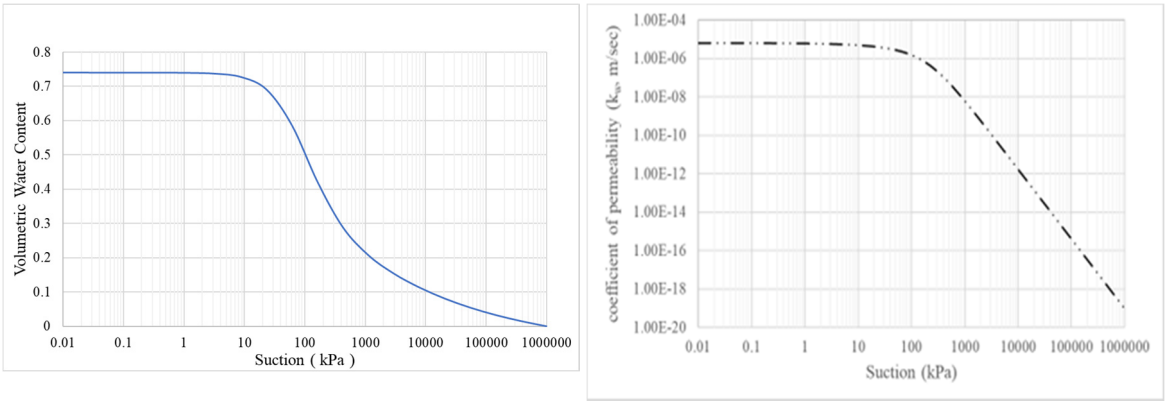

Figure 4. (a). Soil Water Characteristic Curve and (b) Permeability function.

3.3 Slope Geometry

The reconstruction of slope geometry and the slip plane based on data and pictures of slope failure is shown in Figure 5. The original slope is 20 m high and inclined at 47°. The failure started at about 3 m from the crest. This failure surface did not affect the road on the crest because the road was located 7 m from the slope edge. However, the ruins have caused road closure at the toe for about one day. The shape of the slip plane indicates that the slope failure was indeed caused by rainfall.

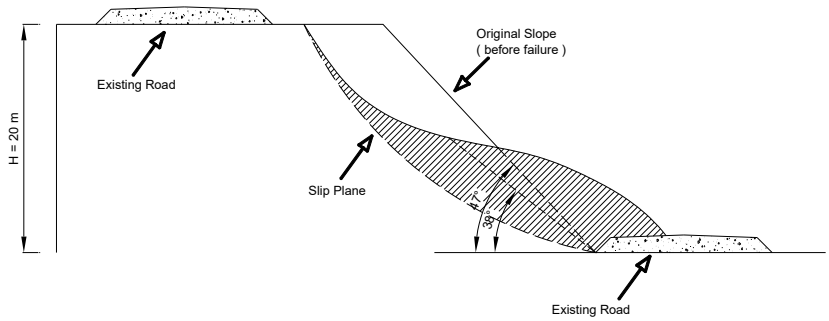

Figure 5. Reconstruction of Slope Geometry and Slip Plane.

3.4 Numerical Modelling

Numerical modelling was performed to investigate the stability of the slope before failure, and the effect of rainfall on the stability. The slope was assumed to be homogeneous with soil properties as summarized in Table 1 and Figure 4. The transient seepage analysis was conducted using the finite element tool SEEP/W to assess the pore water pressure change in soils due to rainfall infiltration. The slope stability at various points during rainfall was evaluated using the slope stability program SLOPE/W.

The slope was modelled with boundary conditions shown in Figure 6. The bottom boundary (light blue) was set to be impermeable. The left and right boundaries above the water table (light blue) were set as no-flow boundaries, while those below the groundwater table (red) were set as total head boundaries. The groundwater table was drawn in this analysis to set the initial suction at a reasonable value. Flux boundaries (blue) are set at the crest, slope surface, and the toe to represent the rainfall. The transient analysis was conducted for the rainfall data obtained from a nearby rainfall station (Figure 3). A uniformly distributed load of 12 kN/m^2 was applied over a 7-m-wide road on the crest.

Stability analysis was performed using the Simplified Bischop method with the exit-entry point as the basis for searching the critical slip surface. In this case, the entry point was set at the crest based on the reconstruction of slope geometry and slip plane, as shown in Figure 5, while the exit point is set at the toe.

The pore water pressure was identified at point A, located at a depth of 2 m in the middle of the crest. The pore-water pressure is recorded and plotted with the date. Stability analysis was also performed each day to evaluate the effect of rainfall on slope stability.

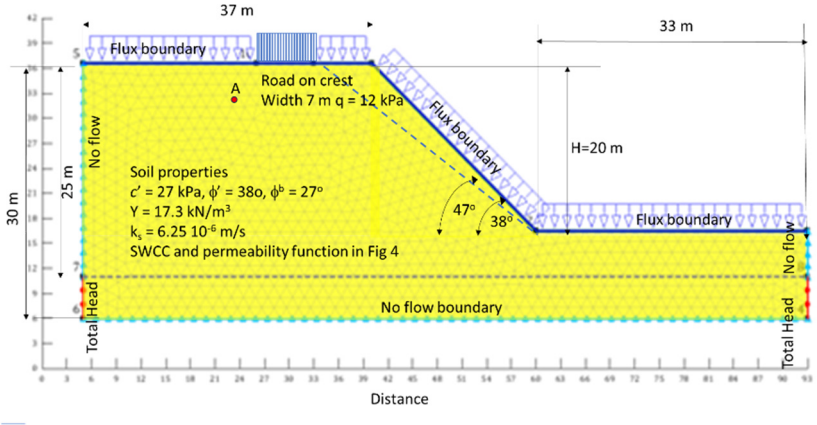

Figure 6. Slope model for Numerical analysis.

4 RESULTS AND DISCUSSION

The results of the transient seepage and slope stability analysis are presented as the variation of matric suction at point A and the factor of safety of the slope. In addition, the factor of safety was also evaluated for the proposed method of slope improvement.

4.1 Pore-Water Pressure Variation due to Rainfall Events

The variation of pore water pressure at point A as a result of rainfall infiltration is presented in Figure 7. Observation of Figure 7 indicates that the suction (negative pore-water pressure) at point A diminishes immediately after rainfall. The wetting front reached point A at 2 m depth on day 8, causing saturation. The pore water pressure becomes positive and stable at about 10 kPa before slope failure on March 13th.

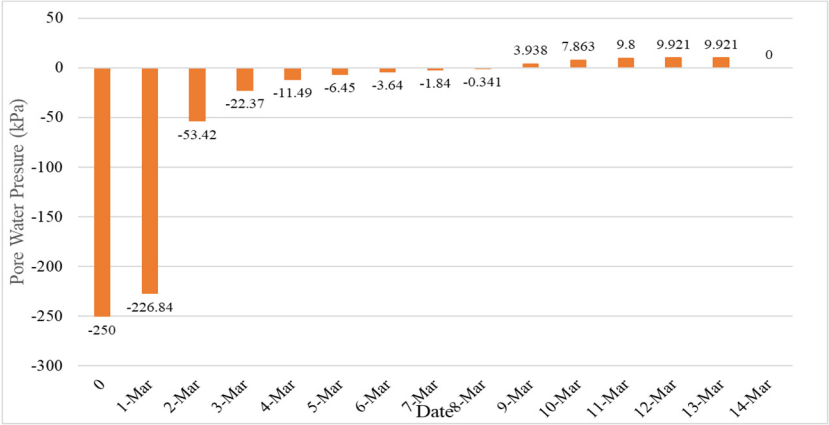

Figure 7. Pore-water pressure variation at point A.

4.2 Factor of Safety Variation due to Rainfall Events

The transient suction distribution from SEEP/W analyses was used as parent analysis of SLOPE/W for slope stability analyses. The results obtained are expressed in the form of FOS versus time and are presented in Figure 8. This Figure generally indicates how the changes in suction distribution due to rainfall infiltration affect the FOS of the slope. The initial FOS was 1.890. The FOS decreased significantly from day 2 to day 8, and became nearly constant afterwards. The FOS at the time of slope failure on March 13th was 1.164 with the failure plane as shown in Figure 9.

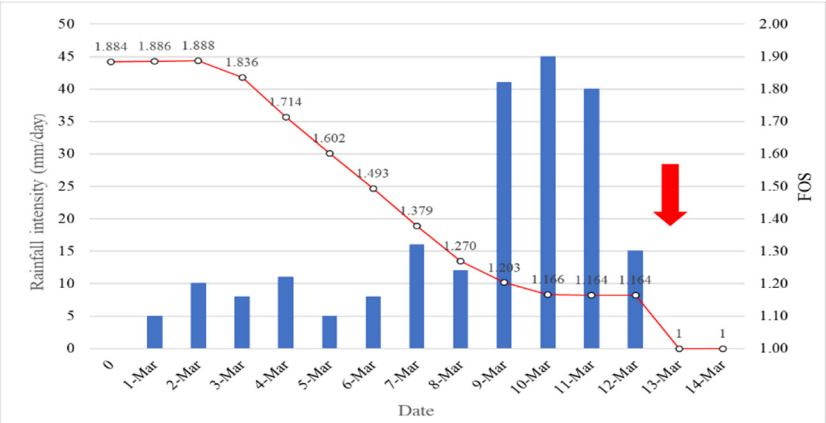

Figure 8 FOS variation with Rainfall

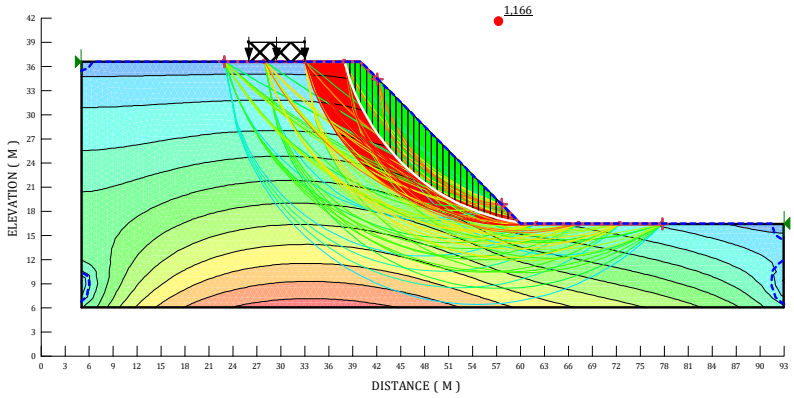

Figure 9 Critical failure plane and FOS at the time of slope failure

4.4. Slope Improvement

Slope regrading, terracing, and surface protection were proposed as a combined mitigation method based on the reconstruction of slope geometry and the slip plane obtained from numerical analysis. The method is expected to increase the slope stability and protect the soil from further reduction in shear strength (due to future rainfall infiltration). The proposed method is shown in Figure 10.

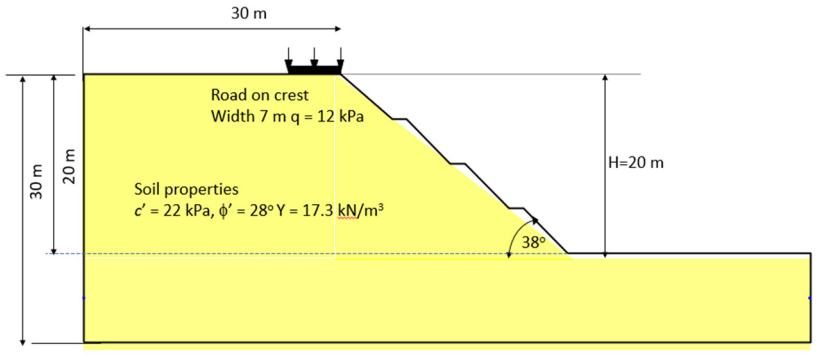

Figure 10 Geometry of the slope after regrading and slope protection

Slope stability analysis was performed for the slope shown in Figure 10. In this case, residual strength parameters from direct shear test were used, i.e. c' = 22 kPa and ϕ' = 28°. Since the slope is protected from rainfall infiltration, only the stability analysis using SLOPE/W was performed for the new slope. The result of the slope stability analysis is shown in Figure 11. The factor of safety increased to 2.146.

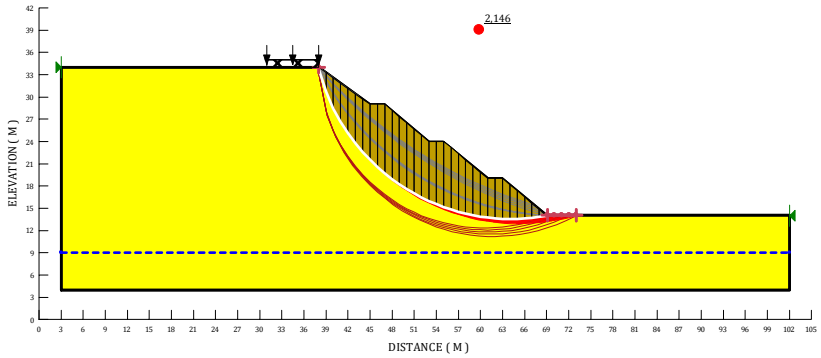

Figure 11 Critical failure plane and FOS for improved slope

5 CONCLUSION

This article discusses the results of numerical analyses on the effect of rainfall on the stability of soil slope related to the slope failure in Jalan Gumay Ulu, Lahat, South Sumatra. To achieve this, finite element analyses were carried out to simulate the transient flow of water through unsaturated-saturated soils using SEEP/W. Furthermore, slope stability was assessed by employing limit equilibrium method in SLOPE/W.

Based on the results obtained from the finite element analysis of transient water flow and slope stability, the following conclusions were drawn.:

1. Prolonged rainfall events with various intensities that last for 12 days critically reduce the stability and lead to slope failure. The inclination of the original slope was 47º. The factor of safety decreased from 1.890 to 1.166 due to rainfall, which is a 40% reduction. This reduction in the factor of safety is due to the decrease in matric suction, which contributes to the reduction in soil strength and factor of safety. The results support the initial prediction that the slope failure was induced by rainfall.

2. Slope regrading, terracing, and surface protection were proposed as a combined mitigation method. The slope was regraded and terraced to have an overall slope angle of 38°. Then, a type of slope protection was proposed to diminish the effect of rainfall on the slope. The factor of safety of the slope after improvement is 2.146. The FOS increased by 15% as compared to the original condition.

This study is limited to the proposal of alternative slope improvement, i.e. combination of slope regrading, terracing and slope protection. Many types of slope protection can be selected, such as vegetation, geosynthetics, rubble wall, shotcrete, or a capillary barrier system (CBS) (Gofar, 2011). Realignment of the road on the crest may be required due to slope regrading.

DISCLAIMER

The authors declare no conflict of interest.

AVAILABILITY OF DATA AND MATERIALS

All data are available from the author.

ACKNOWLEDGMENTS

The authors are grateful to Universitas Bina Darma for the licensed software for this study.

REFERENCES

Aisah, E. & Gofar, N., 2022. Studi Pengaruh Curah Hujan Terhadap Stabilitas Lereng Menggunakan Program PERISI. *Jurnal Rekayasa Sipil*. 18(2):133-147

Brooks, R.H. and Corey, A.T., 1966. Properties of porous media affecting fluid flow. *Journal of the irrigation and drainage division*, 92(2), pp.61-88.

Epianti, P., Fathoni, B., & Gofar, N., 2025. Evaluasi dan Pemetaan Tingkat Resiko Longsor di Sumatra Selatan. Paper Accepted *Cantilever Jurnal Penelitian dan Kajian Bidang Teknik Sipil*. 14(2), pp.

Erlangga, S., Fathoni, B. & Gofar, N., 2024. Mapping of Risk Levels and Types of Slope Failure in South Sumatra. *Rekayasa Sipil*. 18(1), pp. 66-71

Fathoni, B., Erlangga, S. & Gofar, N., 2024. Evaluasi Faktor Faktor Penyebab Longsor dan Kesesuaian Mitigasi. *Cantilever Jurnal Penelitian dan Kajian Bidang Teknik Sipil*. 13(1), pp.13-22.

Fredlund, D. G., Rahardjo, H., & Fredlund, M. D. (2012). *Unsaturated Soil Mechanics in Engineering Practice*. Hoboken, New Jersey: Wiley.

Fredlund, M. D., Wilson, G. W. & Fredlund, D. G. 2002. Representation and estimation of the shrinkage curve. *Proceedings 3rd International Conference on Unsaturated Soils (UNSAT 2002).* Recife, Brazil (Jucá, J.F.T., de Campos, T.M.P. and Marinho, F.A.M. Eds)

Fredlund, D. G., & Xing, A. (1994). Equations for the soil-water characteristic curve. *Canadian Geotechnical Journal*, 31(3), pp. 521 - 532.

Geoslope International Ltd. 2018. Seepage Modelling with SEEP/W. Calgary, Canada.

Geoslope International Ltd. 2018. Slope Stability Analysis with SLOPE/W. Calgary, Canada.

Gofar, N., Harianto, Y., & Dewi, APS., 2025. Identification of Rainfall Scenario Triggering Slope Failures in Pagar Alam and its Surrounding Area. *Media Komunikasi Teknik Sipil*, 30(2), pp. 256–264.

Gofar, N. (2011) Shotcrete Application for Slope Stabilization in Civil Infrastructure. Proceedings of National Seminar on Sustainable and Innovative concrete Technology and Infrastructure, Hotel Bintang Mulia Jember 22 December 2011. Universits Jember dan PT Holcim Indonesia

Gofar, N. Lee M.L and Asof, M. (2006) Transient Seepage and Slope Stability Analysis for Rainfall-Induced Landslide: A Case Study. Malaysian Journal of Civil Engineering. 18(1) 1-13.

Lee M.L. Gofar, N. & Rahardjo H., 2009. A Simple Model for Preliminary Evaluation of Rainfall-Induced Slope Instability. *Engineering Geology* 108(3–4) pp. 272-282.

Matsushi, Y., Hattanji, T., & Matsukura, Y., 2006. Mechanisms of shallow landslides on soil-mantled hillslopes with permeable and impermeable bedrocks in the Boso Peninsula, Japan, *Geomorphology*, 76(1–2), pp. 92–108.

Pamela, A.Y., Sadisun, I. & Kartiko, R.D. (2018) The Selective Causative Factors on Landslide Susceptibility Assessment: Case Study Takengon, Aceh, Indonesia, *AIP Conference Proceedings* 1987, 020089

Rahardjo, H., Shen, Y., Tsen-Tieng, D. L., Ramos-Rivera, J., Nong, X., & Hamdany, A. H., 2021. New Osmotic Tensiometer Development. *ASTM International. Geotechnical Testing Journal* 44(3), pp. 722–740.

Satyanaga, A., Zhai, Q., & Rahardjo, H., 2017. Estimation of Unimodal Water Characteristic Curve for Gap-graded Soil. *Soils and Foundations*, 57(5), pp. 789-801.

Sriwijaya Media, 2023. Kembali Longsor, Akses Jalan Alternatif Lahat-Pagaralam Lumpuh Total. [Online] Available at: https://sriwijayamedia.com/2023/03/kembali-longsor-akses-jalan-alternatiflahat-pagaralam-lumpuh-total/[Accessed 04 May 2023].

This page is intentionally left blank

HIMPUNAN AHLI TEKNIK TANAH INDONESIA - HATTI
Indonesian Society for Geotechnical Engineering - ISGE
PIT HATTI XXIX
10-12 November 2025

Stabilized Expansive soils with High Alumina Cement at Longer Curing Time

Khairani Ayuni Fitri[1], Arlyn Aristo Cikmit[1*], Sesan Henu Alfanoza[2] Rangga Adiprima Sudisman[3] Leong Sing Wong[4]
[1]Department of Civil Engineering, Faculty of Infrastructure Planning, Universitas Pertamina, Jakarta, Indonesia, Postal 12220
[2]Department of Construction, PT. Aneka Jaringan Indonesia, Jakarta, Indonesia 13920.
[3]Department of Civil Engineering, Institut Teknologi Bandung, Indonesia.
[4]College of Graduate Studies, Universiti Tenaga Nasional, Jalan Ikram-Uniten, 43000 Kajang, Selangor, Malaysia

*Correspondence: arlyn.aristo@universitaspertamina.ac.id

ABSTRACT Expansive soils present significant challenges in geotechnical engineering due to their high swelling potential, which leads to significant volume changes with moisture variation. These characteristics can cause severe damage to pavements, foundations, and lightweight structures if not properly treated. This study investigates the use of high alumina cement (HAC) as a chemical stabilizer for expansive soil obtained from Malingping, Banten, Indonesia. The primary objectives are to evaluate the effects of long-term curing periods (>28 days) on the unconfined compressive strength (UCS) and expansion index (EI), and to assess the applicability of the Japan Cement Association (JCA, 2007) estimation model in predicting UCS strength development. Samples were prepared with 7% and 15% HAC contents, and water-to-cement (w/C) ratios of 0.5, 1, 1.25, and 1.5. Curing times were set at 1, 3, 7, 14, 28, 34, 56, 90, and 120 days. Curing periods extended up to 120 days to capture the influence of hydration processes over time. The results indicated that long-term curing substantially reduced the expansion index (EI) of Malingping expansive soil stabilized with HAC, with the best performance achieved at 15% HAC content and a low w/C ratio on day 34, corresponding to optimal hydration reactions. However, by day 120, a slight increase in EI was observed, likely due to reduced hydration activity over time. The UCS values generally increased with curing time, though minor fluctuations occurred due to partial pre-hydration of the cement before mixing. Furthermore, the UCS estimation model by the Japan Cement Association (2007) showed strong agreement with experimental data when analyzed separately for each HAC content (R^2 = 0.96, A.N.D = 6% for 7% HAC; R^2 = 0.93, A.N.D = 9% for 15% HAC), but its accuracy decreased when all data were combined (R^2 = 0.72, A.N.D = 16%), suggesting the need for model refinement to better capture long-term stabilization behavior.

KEYWORDS Expansion index; Expansive soil stabilization; High alumina cement: Longer curing; Unconfined compressive strength

1 INTRODUCTION

As a tropical country with high rainfall intensity and warm temperatures, Indonesia frequently faces various challenges in infrastructure development caused by the complexity of its soil characteristics. One problematic soil type that is widely distributed in Indonesia, particularly on the island of Java, is expansive soil (Affandi, 2021). Expansive soil has complex physical and mechanical properties, characterized primarily by significant volume changes in response to variations in moisture content. If not properly managed, this soil type poses serious risks, such as damaging road pavements and compromising the stability of both light and heavy structures. Therefore, improvements are required to ensure this soil can safely be used in construction.

One method to address the problems associated with expansive soils is chemical stabilization. Chemical stabilization involves the addition of additives such as lime, fly ash, rice husk ash, and cement, which act as binding agents and fill voids within the soil, significantly improving its load-bearing capacity. Among these additives, Portland cement is the most used in chemical stabilization

due to its practicality and wide availability. However, research conducted by Chittoori et al. (2018) has shown that using conventional Portland cement as a stabilizing agent may lead to a decline in soil strength with increasing curing periods. This indicates the need for further examination of alternative types of cement, such as high alumina cement (HAC).

HAC, or high alumina cement, offers several advantages, including rapid strength development, resistance to temperature fluctuations, and enhanced abrasion durability (Newman and Choo, 2003). Recent investigations by Alfirdausi (2024), Sedayu (2024), and Alfanoza (2025) demonstrated that HAC effectively mitigates swelling–shrinkage behavior in expansive soils while improving both unconfined compressive strength and shear strength. However, these studies were limited to less than one month of curing periods. In practice, the duration of curing is a governing factor in the stabilization process, as it dictates the progression of hydration and pozzolanic reactions between the stabilizing agent and the soil matrix. Extended curing periods facilitate continued formation of cementitious compounds such as calcium silicate hydrate (C–S–H) and calcium aluminate hydrate (C–A–H), thereby enhancing interparticle bonding, strength, and durability (Firoozi et al., 2017).

Based on this background, the present study aims to analyze the effect of long-term curing on the expansion index (EI) and the unconfined compressive strength (UCS) of expansive soils stabilized with high alumina cement. EI and UCS were selected as key indicators because they represent the soil's volumetric stability and strength development. In addition, this study will evaluate the applicability of the Japan Cement Association (JCA, 2007) estimation model by comparing its predicted UCS values with experimental results to determine whether the model reliably reflects the behavior of HAC-stabilized expansive soils under long-term curing. The findings are expected to provide valuable insights for improving soil stabilization practices in Indonesia.

2 METHODS

2.1 Sample preparation

The present study adopts a quantitative experimental approach to evaluate the stabilization of expansive soil obtained from Jalan Nasional III, Malingping, Cikeusik District, Pandeglang Regency, Banten Province. Soil stabilization was performed using high alumina cement (HAC) with varying water-to-cement ratios, as summarized in Table 1. The experimental program was designed to assess the improvement in soil strength through unconfined compressive strength (UCS) testing and expansion index (EI) testing. Cylindrical specimens measuring 50 × 101 mm were prepared for UCS tests and subjected to curing periods of 0, 1, 3, 7, 14, 28, 34, 56, 90, and 120 days. For each curing period, three specimens were tested to minimize potential anomalies and ensure data reliability. The expansion index tests were carried out on specimens measuring 50 × 12 mm with curing durations of 1, 34, and 120 days. Testing for the other curing period times could not be performed due to laboratory equipment constraints.

Table 11. Mix design variations of test specimens

No.	HAC content, C	Water-to-cement ratio, w/C	Initial water content, w_0	UCS specimens	Curing time	EI specimens	Curing time
1	7%	0.50	34.83%	30	0, 1, 3, 7, 14, 28, 34, 56, 90, and 120 days	9	1, 34, and 120 days
2		1.00		30		9	
3		1.25		30		9	
4		1.50		30		9	
5	15%	0.50		30		9	
6		1.00		30		9	
7		1.25		30		9	
8		1.50		30		9	

2.2 Expansion index test method

The expansion index (EI) test was conducted in accordance with ASTM D 4829-95 using Oedometer. The soil specimen is subjected to a seating load of 6.9 kPa under compact conditions and subsequently saturated (Figure 1). The expansion index (EI) test using the direct method (Oedometer test) provides the most reliable assessment of soil expansivity, yet its application is often limited due to the difficulty of preparing specimens at the required degree of saturation. As a result, indirect approaches (e.g., plasticity index, liquid limit, clay fraction correlations) are frequently adopted, even though studies such as Cikmit et al. (2024) have shown that these methods are less accurate compared to the direct test. Furthermore, the ASTM D4829 standard specifies a target saturation of 50 ± 2% but does not provide detailed guidance on how to achieve this condition, particularly for stabilized expansive soils whose pore structure and water retention properties differ from untreated soils.

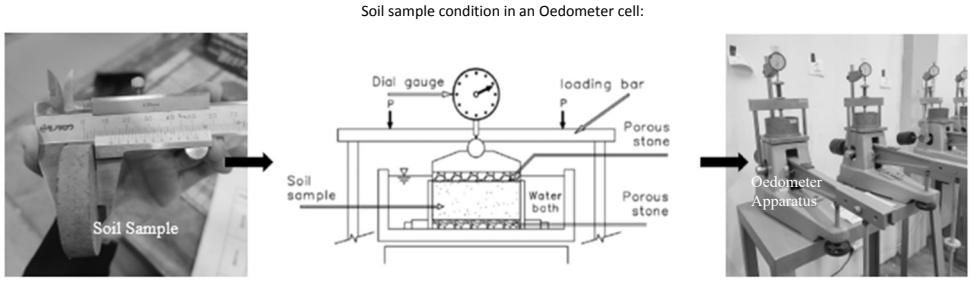

Figure 15. Expansion index setup using an Oedometer.

To overcome this limitation, the present study developed a trial-and-error procedure to determine an effective approach for adjusting the water content of stabilized samples. This protocol was designed to ensure reproducibility and compliance with the ASTM saturation requirement. The following procedures were carried out to adjust the water content of the samples in order to achieve a standard degree of saturation of 50±2% before conducting the Oedometer test:

1. A representative sample was selected from each variation.
2. The sample volume was measured, after which the sample was placed in an oven one day before testing to determine its moisture content.
3. The initial degree of saturation of the sample was calculated using Equation (1).
4. If the degree of saturation exceeded 50%, the water content was adjusted using Equation (3) by oven-drying the sample at 60°C until its weight was reduced to meet the target saturation level of 50 ± 2%.
5. If the degree of saturation was less than 50%, the water content of the specimen was gradually increased by carefully adding water droplets until the saturation level reached 50 ± 2%. The amount of water that needs to be add can be determined using Equation (3). After the adjustment, the specimens were left to stand for 24 hours before testing to ensure a uniform distribution of moisture within the sample.

$$S_{meas} = \frac{w\ x\ Gs\ x\ \Upsilon_d}{Gs\ x\ \Upsilon_w\ -\ \Upsilon_d} \quad \textbf{(1)}$$

$$w_{sr} = \frac{(Gs\ x\ \Upsilon_w\ -\Upsilon_d)x\ 0.5}{Gs\ x\ \Upsilon_d} \quad \textbf{(2)}$$

$$W_{add} = \ (w_{sr} - w\ \pm 0.2)\ x\ Wd \quad \textbf{(3)}$$

where w is moisture content (%), Gs is specific gravity, Υ_d is the dry unit weight (gr/cm^3), Υ_w is the unit weight of water (gr/cm^3), w_{sr} is the moisture content at 50% degree of saturation (%), and Wd is dry mass of the sample (gr). W_{add} (in grams) represents the amount of water adjustment required for the sample to reach 50% degree of saturation.

The initial saturation condition determined the appropriate equation for calculating the expansion index (EI). When the saturation level (S_{meas}) was within 50 ± 2%, the EI value was obtained using Equation (4), whereas for S_{meas} within the 40–60% range, the EI value was calculated using Equation (5).

$$EI_{meas} = \frac{\Delta H}{H_1}\, x\, 1000 \quad \textbf{(4)}$$

$$EI_{50} = EI_{meas} - (50 - S_{meas})\, x\, \frac{65 + EI_{meas}}{220 - S_{meas}} \quad \textbf{(5)}$$

where ΔH= D2 – D1 is the change in height (cm), H1 is the initial sample height (cm), D1 is the initial dial reading (cm), D2 is the final dial reading (cm), EI_{meas} is the expansion index, S_{meas} is the degree of saturation (%), and EI_{50} is the estimated expansion index.

Table 12. Expansion index value classification

Expansion index, EI	Potential expansion
0 - 20	Very Low
21 – 50	Low
51 – 90	Medium
91 – 130	High
>130	Very High

*ASTM D 4829-95

After conducting several trials of expansion index testing on expansive soils, several factors were identified as influencing the obtained results:

6. Sample drying temperature
   In this study, water content adjustment to achieve the target degree of saturation was carried out by oven-drying samples at 60 °C. This temperature was selected because the reduction in water content could be consistently controlled, with decreases of approximately 0.5–0.8 grams every 10 minutes, thereby enabling a more uniform reduction process. In contrast, oven-drying at 110 °C can potentially damage the soil structure, resulting in less valid expansion index values. Similar concerns were also highlighted by Owoyemi (2020) and Yoon et al. (2015), who found that repeated oven heating at 110 °C permanently altered soil index properties, such as Atterberg limits, liquid limit, plasticity index, and compaction/strength parameters demonstrating that high-temperature pre-treatment can modify fundamental soil behavior relevant to expansion assessments.

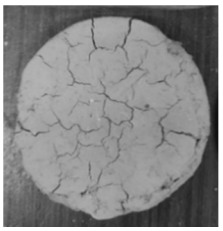

Figure 16. Samples oven-dried at 110°C.

7. Adjustment of water content to achieve initial saturation
   Proper water content adjustment to reach the target saturation condition is a critical step before testing. During the trial-and-error process, two approaches were employed: (a) partial oven-drying at 60 °C until the sample mass was reduced to correspond to a 50% degree of saturation, and (b) total oven-drying for 24 hours to reach 0% water content, followed by the reintroduction of water. The results demonstrated that the total-drying method rendered the samples brittle,

prone to disintegration, and weakened the interparticle bonds, reducing their suitability for testing. Consequently, partial drying was selected in this study as a more representative method for achieving the desired degree of saturation.

Figure 17. Adjustment of saturated water content using method (a).

Figure 18. Adjustment of saturated water content using method (b).

2.3 Unconfined compressive test method

The unconfined compression test (UCS) is a laboratory-scale test conducted to measure the axial load-carrying capacity of soil until particle detachment or specimen failure occurs (Anggraini and Saleh, 2021). In this test, cylindrical soil specimens with dimensions of 50 × 101 mm are subjected to axial loading at a constant strain rate. The loading continues until the axial strain reading on the apparatus reaches 15%, or until the soil specimen fails. The test was performed in accordance with ASTM D 2166, with the apparatus providing data on load and strain. The procedure for the unconfined compression test is as follows:

1. Place the soil specimen in the UCS apparatus, positioning it at the center (Figure 5a).
2. Install the dial gauge and load cell on the apparatus, then set them to zero.
3. Adjust the strain rate to 1.08 mm/min and initiate the software to begin the test (Figure 5b).
4. Terminate the test once the specimen undergoes failure (Figure 5c).

(a) (b) (c)

Figure 19. Unconfined compressive strength (UCS) testing procedure.

3 RESULTS AND DISCUSSION

3.1 Effect of curing time on the expansion index (EI) of stabilized soil

The expansion index (EI) testing in this study was conducted in accordance with ASTM D4829-95, wherein the degree of saturation of the sample was adjusted to 50±2%. Upon achieving the target saturation, an Oedometer test (direct method) revealed that the untreated Malingping soil's expansion index was classified as medium (EI = 76). This finding contrasts with the study conducted by Damayanti (2022), which examined soil from the same source and reported a very high expansion index (EI > 130). Such discrepancies may be attributed to differences in saturation adjustment methods, sample compaction, or potential human error during instrument readings. Variation in the water content required to achieve the standard degree of saturation may also play a role. Specifically, in Damayanti (2022) the required water content was 12%, whereas it was 16% in this study. A higher initial water content likely resulted in a more saturated condition at the outset, reducing the available pore space for additional water intake and, consequently, lowering the soil's expansion potential. This explains the lower expansion index observed in this study, as the soil already contained sufficient water before further wetting during testing.

Table 13. Comparison of the expansion index between untreated and treated soil

Expansion Index Value of Untreated Soil	Lowest Expansion Index Value of Soil Stabilized with 7% HAC	Lowest Expansion Index Value of Soil Stabilized with 15% HAC
76	8.03	1.59

Following stabilization with high alumina cement (HAC), the expansion index of the soil decreased significantly, reaching the low (EI < 50) and very low (EI < 20) categories across all curing periods. As shown in Table 3, adding 7% HAC reduced the expansion index by up to 90%, while 15% HAC achieved a maximum reduction of approximately 96% compared to the untreated soil. Figures 6 and 7 illustrate the decreasing trend in the expansion index with increasing HAC content. The influence of the water-to-cement (w/C) ratio was also evident. After one day of curing, a higher w/C ratio tended to produce lower expansion index values due to incomplete hydration reactions, which left water as the dominant factor influencing soil behavior. However, by day 34, the trend reversed: samples with lower w/C ratios exhibited lower expansion indices, reflecting the optimal progress of cementation, whereas higher w/C ratios resulted in increased expansion indices due to the development of excess pores that allowed water ingress and subsequent re-expansion.

At 120 days of curing, the expansion index values generally increased again, attributable to the weakening of HAC hydration, which released free water to be absorbed by clay particles. Nonetheless, an anomaly was observed in the w/C ratio 1.5 with 15% HAC, where the expansion index deviated substantially from the general trend, displaying markedly lower values. This anomaly was linked to significant variation between two tested samples, whose results were subsequently averaged. As only two samples were tested (with an additional sample allocated for saturation control), the researchers could not determine which measurement more accurately reflected soil behavior, given that both samples underwent identical preparation and testing procedures. For future studies, it is recommended that a minimum of three samples be tested for each variation of the expansion index to better identify and validate potential anomalies.

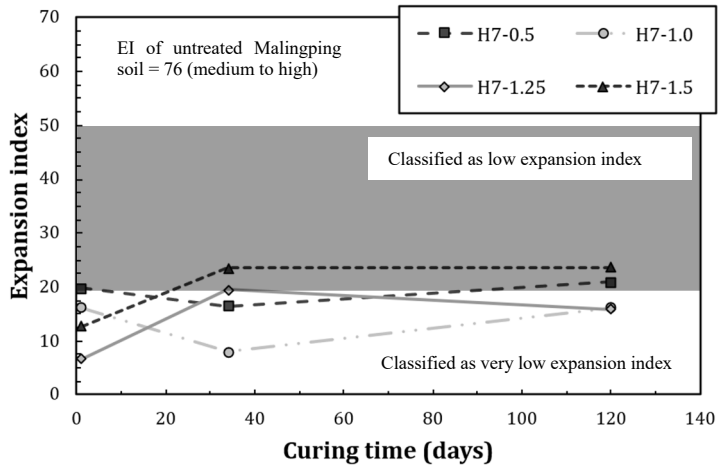

Figure 20. Relationship between curing time and EI of expansive soil stabilized with 7% HAC.

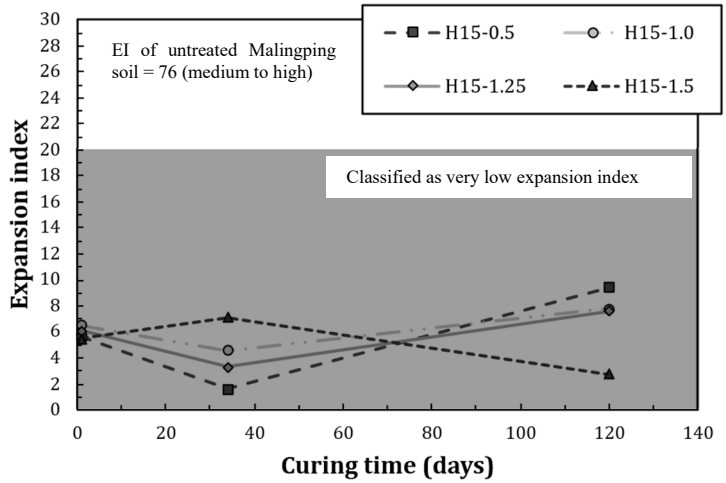

Figure 21. Relationship between curing time and EI of expansive soil stabilized with 15% HAC.

3.2 Stress–strain behavior of the stabilized soil

As illustrated in Figure 8 below, testing on untreated soil indicated ductile behaviour, characterized by the ability to undergo large deformations while sustaining relatively low stress. The specimen exhibited strain after failure exceeding 10% with a maximum stress of 123.33 kN/m². In contrast, stabilization with high alumina cement (HAC) significantly altered the soil behaviour, resulting in higher strength but increased brittleness. As shown in Figure 9, the stabilized specimens achieved maximum stresses exceeding 1000 kN/m², while the strain after failure was reduced to less than 4%.

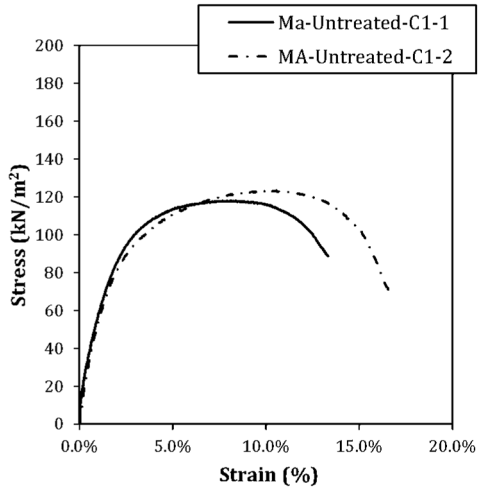

Figure 22. Stress–strain curve of specimens without stabilization (untreated).

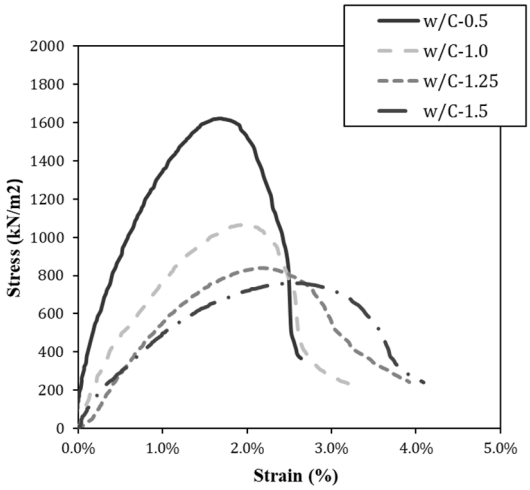

Figure 23. Stress–strain curve of specimens stabilized with 15% HAC at 120 days of curing.

The water-to-cement (w/C) ratio was also found to influence soil behaviour. Higher w/C ratios produced more ductile characteristics, with greater deformability, attributable to the increased water content in the mixture. This condition yielded a more flexible soil structure but reduced density, lowering strength. Conversely, lower w/C ratios produced denser and stronger soil structures, leading to higher compressive strength. However, these specimens became stiffer and more prone to sudden brittle failure.

3.3 Effect of curing time on the stabilization of expansive soil

High alumina cement (HAC) effectively enhanced the unconfined compressive strength (qu) of expansive soils, as illustrated in Figures 10 and 11. Both figures demonstrate a clear positive correlation between curing time and UCS, indicating that strength generally increases with longer

curing durations. This trend aligns with the progressive development of hydration products such as calcium silicate hydrate (C–S–H) and calcium aluminate hydrate (C–A–H), which densify the soil matrix and improve interparticle bonding over time (Firoozi et al., 2017).

Despite the overall trend, some fluctuations in strength were observed at intermediate curing periods, particularly in mixtures with low w/C ratios. For instance, the 7% HAC–0.5 mixture showed a sharp strength increase up to day 34, followed by a decline at day 56. A similar trend was also identified in other variations at different curing periods. This irregularity is likely due to non-uniform cement distribution during mixing and partial pre-hydration of the cement before use, which reduced reactivity in certain portions of the sample. Consequently, while the long-term curing process generally enhanced soil strength, variability in cement condition and mixing uniformity occasionally influenced the strength development pattern.

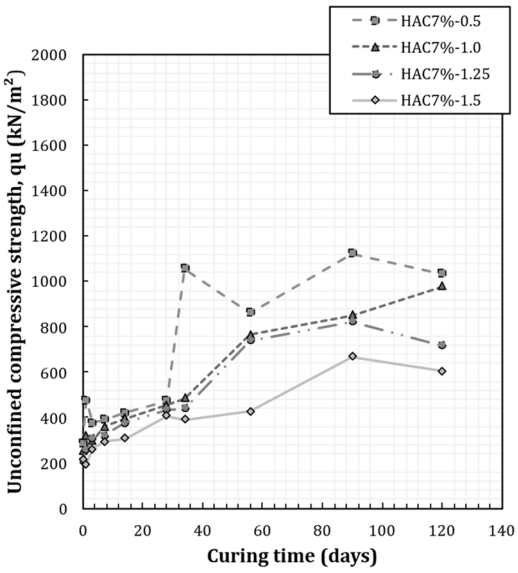

Figure 24. Relationship between qu and curing time in stabilization with 7% HAC.

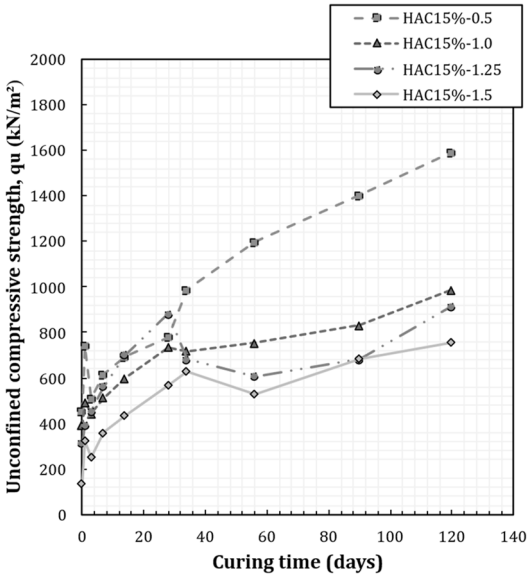

Figure 25. Relationship between qu and curing time in stabilization with 15% HAC.

Furthermore, the results presented in the graphs confirm that variations in the water-to-cement (w/C) ratio in the stabilization of expansive soils using high alumina cement (HAC) significantly influence the improvement of unconfined compressive strength. Mixtures with lower w/C ratios generally produced higher strength values compared to those with higher ratios. This is because excess water content promotes greater hydration of HAC within a given curing period, which directly affects strength development. Horpibulsuk et al. (2003) emphasized that the strength of soil stabilized with cementitious binders is more closely related to the ratio of the soil's initial water content to cement (wc/C), rather than the nominal w/C ratio added during mixing. In addition, variations in cement content also contributed to strength differences. At a constant w/C ratio, soils stabilized with 15% HAC consistently exhibited higher unconfined compressive strength than those stabilized with 7% HAC. This improvement can be attributed to the greater availability of reactive binding material in mixtures with higher HAC content. Consequently, the hydration products more effectively filled the pore spaces between soil particles, resulting in a denser and stronger stabilized soil structure.

3.4 Analysis of unconfined compressive strength estimation using the Japan Cement Association (2007) equation

The Japan Cement Association (2007) originally proposed an equation based on Abram's law, which emphasizes that a lower water-to-cement ratio (w/C) leads to higher composite strength. However, when applied to soil stabilization, this approach becomes less representative due to the unavoidable influence of natural soil water content on the hydration process. To overcome this limitation, Horpibulsuk et al. (2003) modified the parameter into wc/C, defined as the ratio of soil water content to cement weight, which better reflects the total water available for hydration. This modified

approach has proven effective in estimating the unconfined compressive strength (UCS) of stabilized soils, including those treated with high alumina cement (HAC) as in this study. The equation incorporates three constants (a, b, and x), were obtained through curve fitting using nonlinear power regression on data describing the relationship between unconfined compressive strength (qu-b) and the wc/C ratio.

$$q_u = \frac{a}{(w_c/C)^x} + b \quad (6)$$

where q_u is the unconfined compressive strength of cement-stabilized soil (kN/m²), is the w_c/C ratio of soil water content to cement mass, and a, b, and x are regression constants.

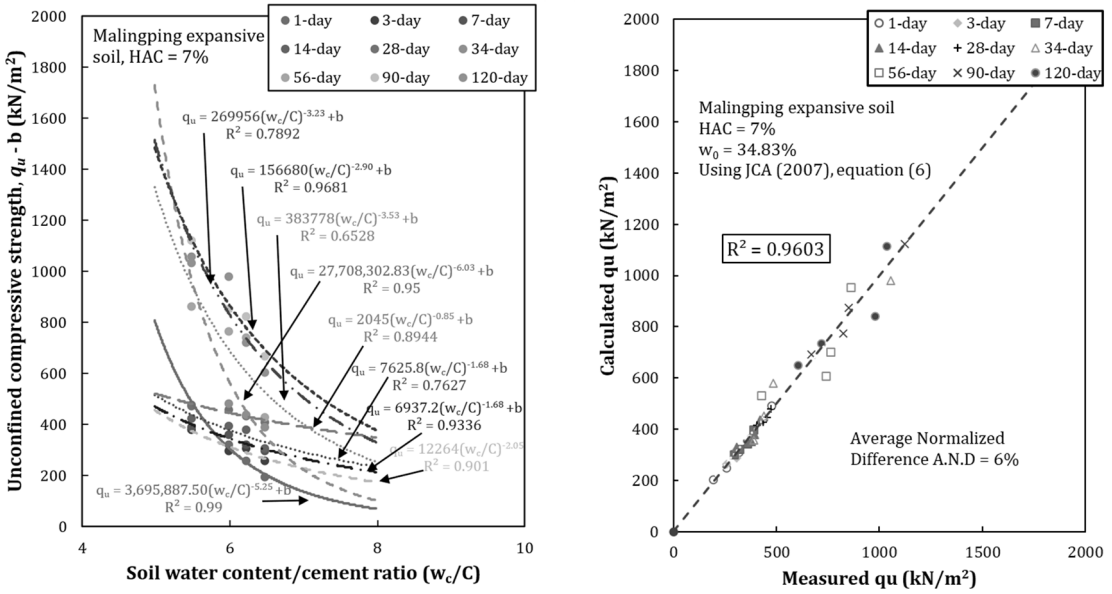

(a) Relation between (w_c/C) and q_u-b for HAC 7%. (b) Measured vs calculated qu for HAC 7%.

Figure 26. UCS estimation using JCA (2007) model for soil stabilized with 7% HAC.

The following equations were obtained from Figure 11 for each curing time:

$$\begin{aligned}
q_u &= 3{,}695{,}887.5(w_c/C)^{-5.25} && \text{(1 day)}\\
q_u &= 12{,}264(w_c/C)^{-2.05} + 0.35 && \text{(3 day)}\\
q_u &= 6937.2(w_c/C)^{-1.68} + 0.23 && \text{(7 day)}\\
q_u &= 7625.8(w_c/C)^{-1.68} + 0.35 && \text{(14 day)}\\
q_u &= 2045(w_c/C)^{-0.85} + 0.40 && \text{(28 day)}\\
q_u &= 27{,}708{,}302.83(w_c/C)^{-6.03} + 2.57 && \text{(34 day)}\\
q_u &= 383{,}778(w_c/C)^{-3.53} + 5.83 && \text{(56 day)}\\
q_u &= 156{,}680(w_c/C)^{-2.90} + 0.89 && \text{(90 day)}\\
q_u &= 269{,}956(w_c/C)^{-3.23} + 2.37 && \text{(120 day)}
\end{aligned} \quad (7)$$

Figure 12 presents the estimation of unconfined compressive strength (UCS) using the JCA equation for expansive soil stabilized with 7% HAC. The model achieved a coefficient of determination (R^2) of 0.96 and an average normalized difference (A.N.D) of 6%, indicating a very good level of accuracy between the estimated and measured values. Similarly, Figure 13 shows the estimation results for stabilization with 15% HAC, where the model also performed well with an R^2 of 0.93 and an A.N.D of 9%.

In contrast, when the datasets for 7% and 15% HAC were combined, the model performance declined. Figure 14(a) illustrates the relationship between wc/C and qu-b, where the constant a, derived as in Equation (9), fluctuated rather than following a consistent trend. The difference is

attributed to cement quality, as the cement used in this study had undergone partial hydration, reducing the strength development consistency. This observation aligns with Kumar (2016), who reported that binders subjected to partial hydration during storage may produce inconsistent strength over curing time.

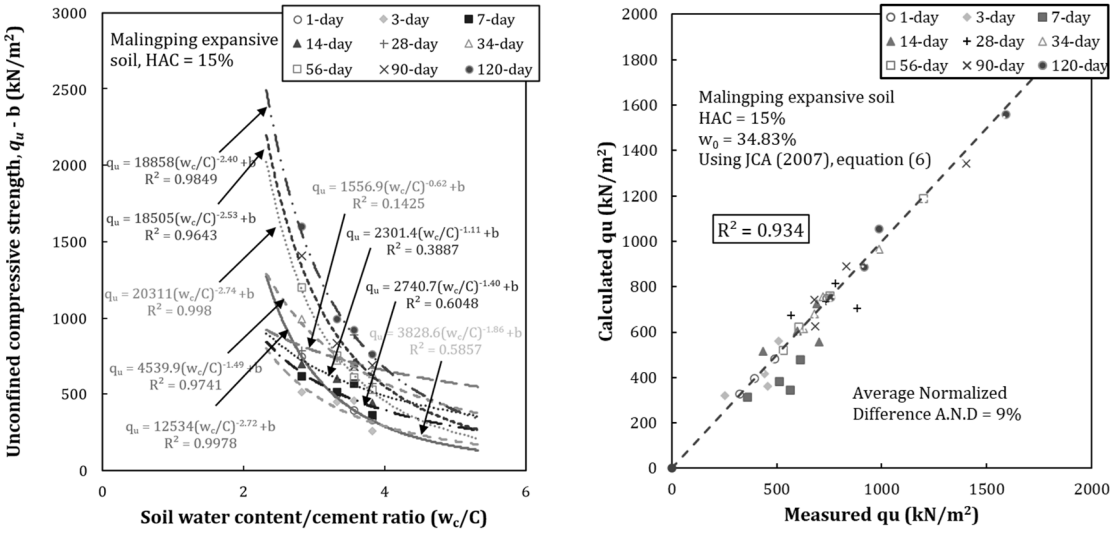

(a) Relation between (w_c/C) and q_u-b for HAC 15%. (b) Measured vs calculated qu for HAC 15%.

Figure 27. UCS estimation using JCA (2007) model for soil stabilized with 15% HAC.

The following equations were obtained from Figure 13 for each curing time:

$$
\begin{aligned}
q_u &= 12{,}534(w_c/C)^{-2.72} && \text{(1 day)}\\
q_u &= 3828.6(w_c/C)^{-1.86} + 4.35 && \text{(3 day)}\\
q_u &= 2040.7(w_c/C)^{-1.40} && \text{(7 day)}\\
q_u &= 2301.4(w_c/C)^{-1.11} && \text{(14 day)}\\
q_u &= 1556.9(w_c/C)^{-0.62} && \text{(28 day)}\\
q_u &= 4539.9(w_c/C)^{-1.49} + 0.74 && \text{(34 day)}\\
q_u &= 20{,}311(w_c/C)^{-2.74} + 0.62 && \text{(56 day)}\\
q_u &= 18{,}505(w_c/C)^{-2.53} + 3.73 && \text{(90 day)}\\
q_u &= 18{,}858(w_c/C)^{-2.40} + 1.20 && \text{(120 day)}
\end{aligned}
\qquad (8)
$$

Figure 14(b) compares the measured unconfined compressive strength with the estimated values calculated using the JCA (2007) equation. The coefficient of determination (R^2) was 0.72, indicating that approximately 72% of the variation in the data was explained by the model. The remaining 28% variation was not captured by the equation and may be attributed to factors such as material variability, non-uniform mixing, and complex chemical interactions in the mixture. The average normalized difference (A.N.D), as shown in Figure 13(b), was 16%, indicating the relative discrepancy between measured and estimated unconfined compressive strength values. Although compressive strength is theoretically expected to increase with curing time, decreases were observed in several sample variations. This outcome was seemingly attributed to the reduced hydration product due to partial hydration before use, inconsistencies during mixing, and the absence of temperature control during curing. As a result, the JCA (2007) equation applied in this study did not fully represent the actual behavior of unconfined compressive strength.

Since the accuracy of the combined model was not optimal, the dataset was separated based on HAC content, as shown in Figures 12 and 13. The analysis revealed that the coefficient of determination (R^2) and average normalized difference (A.N.D) from the segmented data demonstrated better

performance compared to the combined dataset. Therefore, a more comprehensive curve fitting analysis is necessary to refine the estimation model, enabling the identification of the most suitable mathematical relationship that can more reliably represent the stabilized soil behavior.

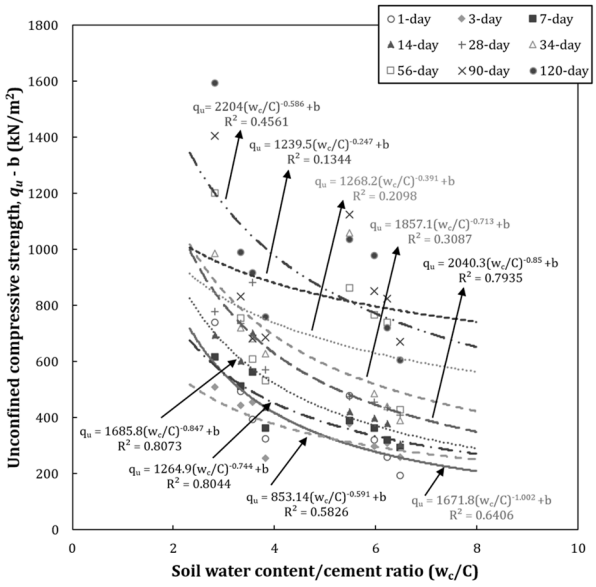

(a) Relationship between (w_c/C) and unconfined compressive strength, q_u-b.

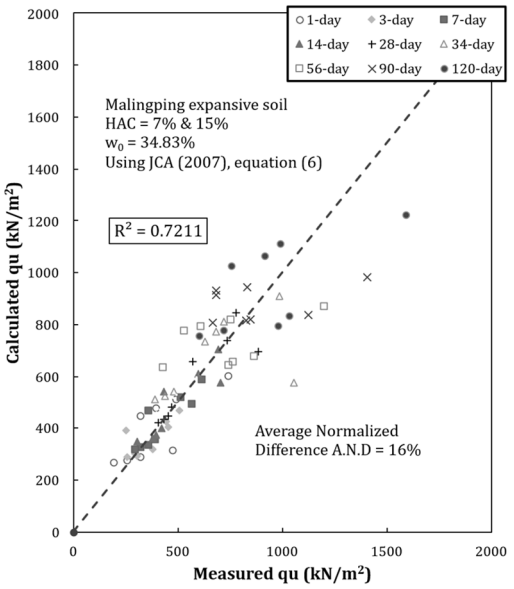

(b) Relationship between measured and calculated unconfined compressive strength (qu).

Figure 28. UCS estimation using JCA (2007) for HAC 7% and 15%.

The following equations were obtained from Figure 14 for each curing time:

$$
\begin{aligned}
q_u &= 1671.8(w_c/C)^{-1.00} + 11.42 \quad (1\text{ day})\\
q_u &= 853.14(w_c/C)^{-0.59} + 5.83 \quad (3\text{ day})\\
q_u &= 1264.9(w_c/C)^{-0.74} + 3.26 \quad (7\text{ day})\\
q_u &= 1685.8(w_c/C)^{-0.85} + 3.39 \quad (14\text{ day})\\
q_u &= 2040.3(w_c/C)^{-0.85} + 3.94 \quad (28\text{ day})\\
q_u &= 1857.1(w_c/C)^{-0.71} + 22.58 \quad (34\text{ day})\\
q_u &= 1268.2(w_c/C)^{-0.39} + 26.16 \quad (56\text{ day})\\
q_u &= 1239.5(w_c/C)^{-0,25} + 25.67 \quad (90\text{ day})\\
q_u &= 2204.0(w_c/C)^{-0.59} + 21.25 \quad (120\text{ day})
\end{aligned}
\qquad (9)
$$

4 CONCLUSION

Based on the findings, it can be concluded that long-term curing has a significant influence on reducing the expansion index of Malingping expansive soil stabilized with high alumina cement (HAC). A higher cement content (15%) proved more effective than 7%, while variations in the water-to-cement ratio also influenced stabilization performance across different curing periods. The unconfined compressive strength (UCS) generally tended to increase with longer curing duration, although fluctuations were observed due to the partial hydration of the cement used. Furthermore, the UCS estimation equation by JCA (2007) showed strong accuracy when applied separately to soils stabilized with 7% and 15% HAC, with high R^2 values (0.96 and 0.93) and low A.N.D (6% and 9%). However, when the datasets were combined, the model performance decreased, with R^2 dropping to 0.72 and A.N.D increasing to 16%. Therefore, a more comprehensive curve fitting analysis is necessary to refine the estimation model and identify a more reliable mathematical relationship for stabilized soil behavior.

DISCLAIMER

The authors declare no conflict of interest.

AVAILABILITY OF DATA AND MATERIALS

All data are available from the author.

ACKNOWLEDGMENTS

This work was supported by the collaboration research between Universitas Pertamina and Universiti Tenaga Nasional No. 0145/UP-R/SK/HK.01/VII/2023. The authors would like to sincerely thank the Soil Mechanics Laboratory, Universitas Pertamina, for providing the facilities and technical support essential to this research. Sincere appreciation is also extended to the laboratory staff, fellow students, and all individuals whose support and contributions, whether direct or indirect, greatly assisted in the successful execution and completion of this study.

REFERENCES

Affandi, D., 2021. Mapping Expansive Soil Characteristics on The National Road Segment in Java Island, in: Proceeding of 25th Annual National Conference on Geotechnical Engineering. pp. 361–372.

Alfanoza, S.H., 2025. Analisis Pengaruh Rasio Kadar Air Tanah/Semen Pada Stabilisasi Tanah Ekspansif Dengan Semen Alumina Tinggi Terhadap Nilai Kuat Tekan Bebas Tanah. Universitas Pertamina, Jakarta.

Alfirdausi, A.A., 2024. Pengaruh Penambahan High Alumina Cement dan Polyethylene Terephthalate Terhadap Kuat Tekan Bebas dan Nilai Expansion Index Tanah Ekspansif. Universitas Pertamina, Jakarta Selatan.

Anggraini, M., Saleh, A., 2021. Stabilisasi Tanah Lempung Dengan Abu Tandan Kosong Kelapa Sawit dan Semen Terhadap Kuat Tekan Bebas. Sainstek (e-Journal) 9, 108–115. https://doi.org/10.35583/js.v9i2.182

ASTM D 2166, 2006. Standard Test Method for Unconfined Compressive Strength of Cohesive Soil.

ASTM D 4829-95, 1997. Standard Test Method for Expansion Index of Soils.

Chittoori, B.C., Puppala, A.J., Pedarla, A., 2018. Addressing Clay Mineralogy Effects on Performance of Chemically Stabilized Expansive Soils Subjected to Seasonal Wetting and Drying. Journal of Geotechnical and Geoenvironmental Engineering 142.

Damayanti, A., 2022. Analisis Potensi Tanah Ekspansif dan Kekuatan Geser Tanah Berdasarkan Variasi Kadar Air Pemadatan (Studi Kasus Ruas Jalan Nasional III arah Malingping, Jalan Simpang Labuan-Cibaliung, Jalan Raya Saketi-Malingping, dan Jalan Tigaraksa Adiyasa, Provinsi Banten). Universitas Pertamina, Jakarta.

Firoozi, Ali Akbar, Guney Olgun, C., Firoozi, Ali Asghar, Baghini, M.S., 2017. Fundamentals of soil stabilization. International Journal of Geo-Engineering 8. https://doi.org/10.1186/s40703-017-0064-9

Horpibulsuk, S., Miura, N., Nagaraj, T.S., 2003. Assessment of Strength Development in Cement-Admixed High Water Content Clays with Abram's Law as A Basis. Geotechnique 53 (4), 439–444.

Japan Cement Association, 2007. Ground Improvement Manual Using Cement-based Solidification Material. JCA: Chiyoda-Ku, Japan 3, 43–44.

Newman, J., Choo, B.S., 2003. Advanced concrete technology: constituent materials. Butterworth-Heinemann.

Owoyemi, O.O., Afolagboye, L.O., 2020. Effect of cyclic heating on some engineering characteristics of some soils from Ilorin, Nigeria. SN Appl 2.

Sedayu, H.A., 2024. Estimasi Kekuatan Tanah Lempung dengan Ekspansivitas Tinggi Menggunakan Campuran High Alumina Cement dan Polyethylene Terephthalate. Universitas Pertamina, Jakarta Selatan.

Yoon, T.C., Yunus, Z.M., Marto, A., Hezmi, M.A., Jusoh, S.N., Ahmad, K., 2015. Comparison of Soil Index Properties Value for Different Pre-Drying Conditions on Clayey Soil. J Teknol 76.

This page is intentionally left blank

HIMPUNAN AHLI TEKNIK TANAH INDONESIA - HATTI
Indonesian Society for Geotechnical Engineering - ISGE
PIT HATTI XXIX
10-12 November 2025

Stabilization of Patimban Marine Soft Clay with Portland Composite Cement: The Effectof Initial Water Content Variations on Soil Bearing Strength

Yosse Triade Pandiangan[1], Arlyn Aristo Cikmit[1*], Listya Diah Anindita[1], Takashi Tsuchida[2]
[1]Department of Civil Engineering, Faculty of Infrastructure Planning, Universitas Pertamina, Jakarta, Indonesia, 12220.
[2]Hiroshima University Resilience Research Center, Hiroshima University, Kagamiyama 1-4-1, Hiroshima, Japan 739-8527.
*Correspondence: arlyn.aristo@unversitaspertamina.ac.id

ABSTRACT Marine clay soil generally has poor physical and mechanical properties, such as high plasticity, low bearing capacity, and excessive settlement under pressure. Soil improvement efforts are needed to enhance the characteristics of the soil, such as cement stabilization. This study aims to investigate the effect of the ratio of soil water content to cement content (w_c/C) and variation of curing times on unconfined compressive strength (q_u) on Patimban dredged marine soil stabilized with Portland Composite Cement. The experimental method involved laboratory testing with variations in ratio of initial water content to its liquid limit (w_0/LL), i.e., 1, 1.25, 1.5, and 2, as well as variations in cement content of 20% and 30% of the soil dry mass. Unconfined compressive strength (UCS) test was carried out at curing periods of 1, 3, 7, 28, and 56 days. It is observed that the most effective cement hydration process occurred in the first 7 days and began to slow down after day 28. The results showed that w_c/C ratio had a negative relationship to the unconfined compressive strength of the soil, where an increase in the w_c/C ratio caused a decrease in the q_u value. The high-water content resulted in large voids between cement-soil particles, weakening the strength of the binder. The relationship between the w_c/C ratio and the q_u value indicated a good match yielded an R^2 value of 0.88-0.94. Further, the unconfined compressive strength of the soil continued to develop with the increasing *curing* time of 1-56 days. The Average Normalized Difference (A.N.D) value obtained from the relationship between the measured and the estimated compressive strength value is low (11.40%), meaning the estimation equation can be effectively used to estimate the compressive strength of marine clay soil stabilized with *Portland* Composite Cement at various curing times.

KEYWORDS Cement; Curing Time; Initial Water Content; Marine Clay; Unconfined Compressive Strength

This paper will be published in the future issues of Indonesian Geotechnical Journal

This page is intentionally left blank

HIMPUNAN AHLI TEKNIK TANAH INDONESIA - HATTI
Indonesian Society for Geotechnical Engineering - ISGE
PIT HATTI XXIX
10-12 November 2025

Stabilization of Patimban Marine Clay with Wide Range of Sand Content using Portland Composite Cement

Listya Diah Anindita[1], Arlyn Aristo Cikmit[1*], Yosse Triade Pandiangan[1], Takashi Tsuchida[2], Tatsuru Aoyama[3], Leong Sing Wong[4]
[1]Department of Civil Engineering, Faculty of Infrastructure Planning, Universitas Pertamina, Jakarta, Indonesia, 12220.
[2]Hiroshima University Resilience Research Center, Hiroshima University, Kagamiyama 1-4-1, Hiroshima, Japan 739-8527.
[3]FUKKEN CO., Ltd. 2-10-11 Hikarimachi, Higashi-ku, Hiroshima, 732-0052 Japan.
[4]College of Graduate Studies, Universiti Tenaga Nasional, Jalan Ikram-Uniten, 43000 Kajang, Selangor, Malaysia
*Correspondence: arlyn.aristo@universitaspertamina.ac.id

ABSTRACT Patimban Port is one of Indonesia's National Strategic Projects and generates a large volume of dredged soil materials. Most of the dredged soil is disposed of at sea, despite its potential for reuse as fill material. However, marine clay dredged from the seabed typically has high-water content, low shear strength, and high compressibility, making stabilization necessary before utilization. One commonly used stabilization method is soil mixing with cement. The effectiveness of this method is highly influenced by the physical properties of the soil, particularly its sand content. This study aims to examine the effect of varying cement and sand content on the undrained shear strength of marine clay from Patimban stabilized with Portland Composite Cement (PCC), and to compare the results of unconfined compressive strength (UCS) tests with strength estimations obtained using equations proposed by Japan Cement Association (JCA) and Yamashita. The results indicate that increasing the cement content and curing time enhances the shear strength of the soil. Sand content variation does not significantly affect the strength as long as the ratio of cement to fine particles (cf*) is maintained. The JCA equation offers a more accurate estimation (R^2 = 0.95; *A.N.D.* = 13.17%) compared to Yamashita' equation, suggesting that the water–cement ratio (wc/c) plays a more critical role in developing strength in cement-stabilized soils than the primary variables in Yamashita's equation, namely the ratio of cement mass to fine fraction (cf*) and the ratio of fine solids volume to total mixture volume (Yf*).

KEYWORDS Strength Estimation; Shear Strength; Sand; Cement; Marine Clay

1 INTRODUCTION

The construction of Patimban Port is one of Indonesia's National Strategic Projects, aimed at strengthening the national logistics system and supporting economic growth. As part of its development, soil dredging was required to deepen the navigation channel and construct port facilities. According to the Ministry of Environment and Forestry (2017) the total dredged volume reached approximately 26.05 million m³. However, most of this material was disposed of offshore, posing significant environmental concerns. Reusing dredged soils represents a more sustainable alternative to direct marine disposal. Nevertheless, the direct utilization of marine clay as reclamation or fill material presents substantial technical challenges. Dredging activities drastically increase the water content of the clay, resulting in reduced shear strength, high compressibility, and potential for excessive settlement. These geotechnical limitations prevent the immediate application of the dredged soils in construction without prior improvement.

Soil stabilization with cement has been extensively investigated as an effective method to improve the mechanical properties of soft and marine clays. Previous studies have demonstrated the efficacy of cement stabilization under varying conditions, including the effects of sand content (Yamashita et al., 2020; Chian et al., 2017), initial water content (Tsuchida & Tang, 2015), and mixing techniques (Suksiripattanapong et al., 2022). Furthermore, Alfanoza et al. (2024) examined the expansivity and strength behavior of expansive clay mixed with high-alumina cement and polyethylene terephthalate (PET), confirming that specific material combinations can significantly enhance soil performance.

These findings suggest that soil characteristics, particularly water content and sand fraction, strongly influence stabilization effectiveness.

This article aims to investigate the reuse of dredged soils from Patimban Port, Indonesia through cement stabilization. It focuses on the effect of varying sand content on the mechanical strength of stabilized marine clay and evaluates the predictive accuracy of two unconfined compressive strength estimation models, those proposed by the Cement Association (2007) and Yamashita et al. (2020).

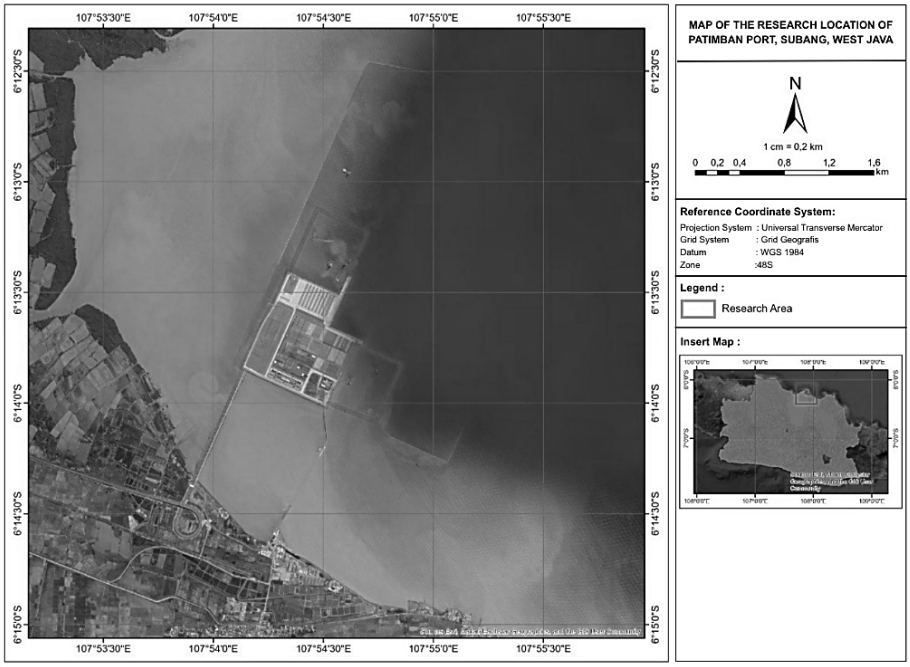

Figure 29. Location of soil sampling at Patimban Port

2 OUTLINE OF EXPERIMENT

This study was designed as a laboratory-based experimental investigation to improve the engineering properties of dredged marine clay obtained from the Patimban Port area. Soil stabilization was conducted using Portland Composite Cement (PCC) as the primary chemical additive. The experimental program was structured to evaluate the influence of cement content, sand content, and curing time on the mechanical performance of the stabilized soil. The principal parameter assessed was the unconfined compressive strength (UCS), which was an indicator of soil strength improvement under different stabilization conditions.

2.1 Materials

The primary materials utilized in this study were Patimban marine clay, Bangka sand, and Portland Composite Cement (PCC). The Patimban marine clay was obtained through dredging operations at Patimban Port using a grab dredger. This clay is characterized by a dark gray, soft and plastic texture, and a slightly saline odor indicative of its marine depositional environment, as shown in Figure 30. In contrast, Bangka sand exhibits a light brown to whitish color, a medium to coarse granular texture, and no distinctive odor, as illustrated in Figure 31. The cement employed in this study was commercially available Portland Composite Cement (PCC), which served as the binder in the soil stabilization mixtures. The particle size distribution of Patimban marine clay and Bangka sand is presented in Figure 31, while the physical properties of the materials are summarized in Table 14, Table 15, and Table 16.

Table 14. Specific gravity of marine clay and sand

Materials	Specific Gravity
Marine Clay Patimban	2.70
Bangka Sand	2.66

Table 15. Physical properties of the Patimban marine clay

Sand Content, *S*	Liquid Limit, *LL*	Plastic Limit, *PL*	Plasticity Index, *PI*
0%	85.38%	43.31%	42.07%
10%	76.81%	40.23%	36.58%
30%	57.53%	31.97%	25.56%
50%	39.58%	24.73%	14.85%
70%	26.30%	15.07%	11.23%

Table 16. Composition of Portland Composite Cement according to Uddin et al. (2013)

Chemical compound	Mass percentage (%)
SiO_2	20.60
Al_2O_3	4.74
Fe_2O_3	3.28
CaO	64.82
MgO	1.84
SO_3	2.4
Na_2O	0.21
K_2O	0.38
Loss of Ignition, *LOI*	1.73

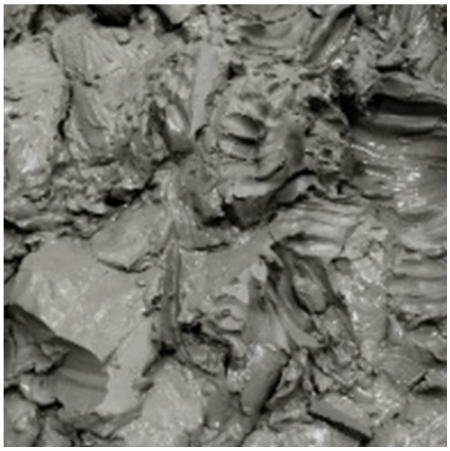

Figure 30. Patimban Marine Clay

Figure 31. Bangka Sand

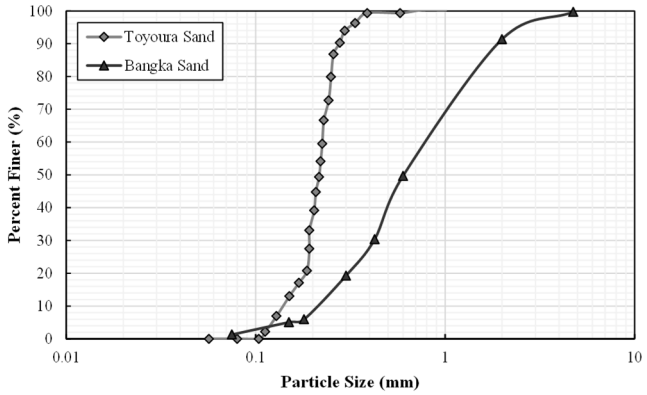

Figure 32. Particle size distribution of Patimban marine clay and Bangka sand

2.2 Preparation of samples

The marine clay obtained from Patimban Port was sieved through a No. 200 sieve to remove coarse particles such as sand, shell fragments, and coral debris. A similar sieving process was applied to the Portland Composite Cement (PCC), passing through a No. 100 sieve to ensure uniform particle size per the required standards. Bangka sand was also sieved using a series of progressively finer sieves

(No. 4, No. 10, No. 30, No. 40, No. 50, No. 80, No. 100, and No. 200). For this study, the sand fraction used ranged between 2 mm and 0.075 mm, corresponding to particles passing through the No. 10 sieve and retained on the No. 200 sieve, consistent with AASHTO specifications. Specimen preparation began with cooling the marine clay and mixing water to 2°C in order to retard the cement hydration reaction during mixing. The cement was blended with water to form a slurry, which was then combined with the clay, sand, and additional water. The mixture was homogenized using a hand mixer for 15 minutes. The prepared mixture was subsequently placed into cylindrical molds measuring 50 mm in diameter and 100 mm in height. Light tapping was applied to the molds to remove entrapped air bubbles. Curing was performed by submerging the specimens in water maintained at 25°C. After 24 hours, the acrylic molds were removed, and the specimens were wrapped with perforated plastic film before being returned to the curing tank at 25 °C for the designated curing periods. Unconfined compressive strength (UCS) tests were conducted on the specimens after curing durations of 1, 3, 7, 28, and 56 days.

2.3 Method and cases of strength tests

Unconfined compressive strength (UCS) tests were performed on the specimens after curing periods of 1, 3, 7, 28, and 56 days. The mix combinations used in the study are presented in Table 17. The cement content (c^*) was calculated using the equation proposed by Tsuchida and Tang (2015), while the sand content (S) and the cement factor, defined as the mass ratio of cement to the fine fraction (clay and silt) (cf^*), were determined using the equations proposed by Yamashita et al. (2020). The equations for calculating cement content (c^*), sand content (S), and cement factor (cf^*) are as follows:

$$c^* = \frac{m_{semen}}{m_{fine} + m_{pasir} + m_{semen}} \times 100 \quad (1)$$

$$S = \frac{m_{pasir}}{m_{fine} + m_{pasir}} \times 100 \quad (2)$$

$$c_f^* = \frac{m_{semen}}{m_{fine} + m_{semen}} \times 100 \quad (3)$$

Table 17. Experiment cases

Case	c^* (%)	S (%)	cf^* (%)	Initial Water Content	Curing Time
1	10	70	27	1.5 LL (%)	1, 3, 7, 28, 56, and 90 (days)
2	20	30	26.3		
3	20	50	33.3		
4	20	70	45.5		
5	30	0	30		
6	30	10	32.3		
7	30	50	46.2		
8	30	70	58.8		
9	45	0	45		
10	60	0	60		

3 RESULT AND DISCUSSION

3.1 Effect of Curing Time on the Moisture Content of UCS Specimens

The influence of curing time on the post-test moisture content of UCS specimens is presented in Figure 33. The results indicate that curing duration did not significantly affect the final moisture content of the samples, as all curing was performed under water-submerged conditions. This environment maintained high moisture levels throughout the curing period, thereby minimizing variations in water content. These findings are consistent with those of Chen (2024), who reported that the volumetric water content of cement-treated soils remained stable for up to 90 days of curing due to a continuous external water supply that preserved sample saturation. Although moisture content remained relatively stable regarding curing time, differences in material composition led to variations among specimens.

Mixtures with higher sand exhibited lower final moisture content, as sand is non-plastic and has limited water retention capacity. This observation is further supported by the Atterberg limits results presented in Table 15, which show a decrease in liquid limit (LL) with increasing sand content, reflecting a reduced ability of the soil to retain water.

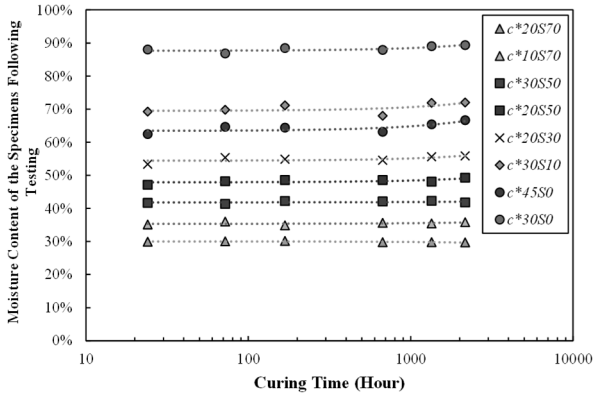

Figure 33. Effect of Curing Time on Post-Test Moisture Content

3.2 Stress–Strain Behavior of Marine Clay after Stabilization

Unconfined compressive strength (UCS) testing was conducted on marine clay stabilized with Portland Composite Cement (PCC) under varying cement factors (c*) and sand contents (S). The resulting stress–strain responses demonstrated distinct patterns depending on the mixture composition. Figure 34a illustrates the stress–strain behavior of marine clay stabilized with varying cement contents (30–60%) in the absence of sand. The results indicate that increasing cement content increases peak stresses, reflecting enhanced compressive strength. However, the strain at failure remained nearly constant at approximately 1%, suggesting that cement addition alone does not significantly influence the deformability of clay-dominated mixtures. This phenomenon is attributed to the fine-grained matrix, where plasticity and cohesion govern the mechanical response.

Figure 34b presents the mixtures' stress–strain behavior with constant sand content (70%) and varying cement contents. In this case, peak stress and stiffness increased with higher cement content, while the strain at failure decreased. This behavior indicates a transition toward a more brittle response, caused by forming a rigid matrix due to the combined effects of high cement and sand contents. The increase in c* reflects a higher cement mass relative to clay and sand, enhancing interparticle bonding through cement hydration and reducing the mixture's deformability. These findings are consistent with Wei et al. (2021), who reported that high cement–sand combinations result in brittle failure characteristics.

Figure 34c shows the effect of sand content variation (0–70%) at a constant cement content of 30%. Increasing sand content from 0% to 50% improved peak stress and strain at failure, indicating enhanced strength and ductility. However, further increasing sand content to 70% led to a sharp reduction in strain at failure despite continued strength gains. This suggests that the mixture becomes excessively granular beyond an optimal sand proportion (approximately 40–55%), reducing cohesion and promoting brittle fracture. These results align with Yao et al. (2019), who identified an optimal sand range for soil–cement mixtures that maximizes strength and deformability.

3.3 Effect of Portland Composite Cement (PCC) Content on the Undrained Shear Strength of Patimban Marine Clay

The variation in Portland Composite Cement (PCC) content significantly influenced the enhancement of the undrained shear strength of Patimban marine clay. Laboratory test results, as illustrated in Figure **35**, demonstrated that increasing PCC content contributed to progressive shear strength development with more extended curing periods. At a PCC content of 60%, the shear strength increased substantially, reaching 2424.79 kN/m² after 2160 hours of curing. In comparison, 45% and 30% PCC contents yielded shear strengths of 1591.28 kN/m² and 970.7 kN/m², respectively.

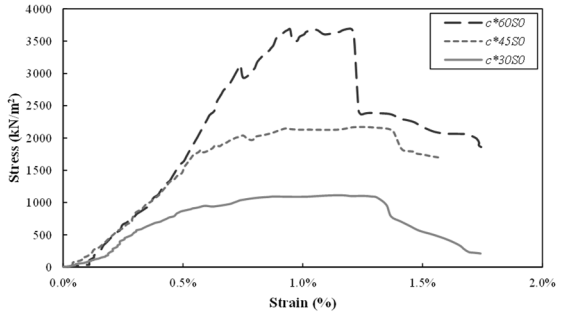

(a) Stress–Strain Behavior of Mixtures *at c* = 30–60% with S = 0%*

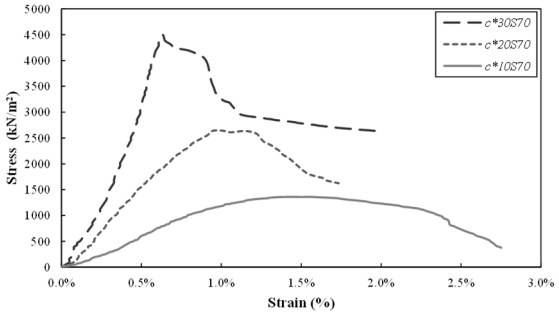

(b) Stress–Strain Behavior of Mixtures *at c* = 10–30% with S = 70%**

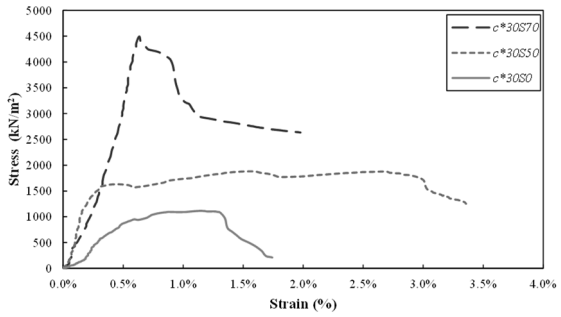

(c) Stress–Strain Behavior of Mixtures *at* c^* = 30% with S = 0–70%

Figure 34. Stress–Strain Response of Stabilized Soil

The observed trend indicates that higher cement contents enhance the hydration process, generating greater amounts of hydration products that reinforce the interparticle bonding within the soil matrix. This phenomenon is consistent with the findings of Tsuchida and Tang (2015), who reported that cement addition at a constant water content effectively increases the strength of stabilized soils. In this context, higher PCC contents result in greater volumes of hydration products, particularly calcium silicate hydrate (C–S–H), which fill soil pores and contribute to the development of a denser and more cohesive microstructure.

These results align with the gel-space ratio theory proposed by Tsuchida and Tang (2015) which states that material strength is directly proportional to the gel-space ratio—the ratio of hydration product volume to the total volume of hydration products and pores in the mixture. Accordingly, cement directly increases the gel-space ratio, enhancing soil shear strength. The experimental findings on Patimban marine clay confirmed this relationship, demonstrating that higher PCC contents consistently produced greater shear strength throughout the curing period.

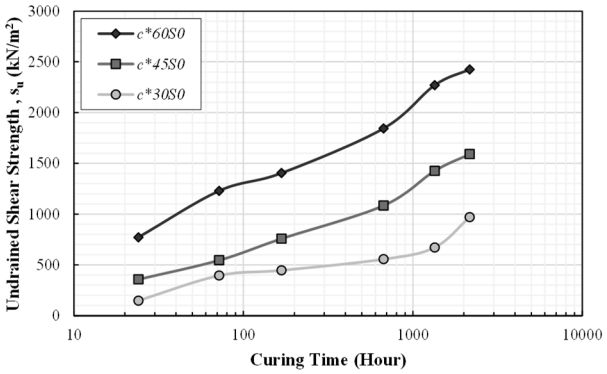

Figure 35. Relationship between undrained shear strength (S_u) and curing time

3.4 Effect of Sand Content and Cement Factor (*cf**) on the Undrained Shear Strength of PCC-Stabilized Soil

Figure 36 illustrates the influence of sand content variation on soil's undrained shear strength (Su) at a constant cement content. The results indicate that increasing sand content from 0% to 70% significantly improves Su. Although sand is inert and does not participate in cement hydration reactions, its addition reduces the proportion of fine soil within the mixture. Consequently, the ratio of cement to reactive soil mass increases, thereby elevating the cement factor (*cf**), as defined in Equation (3).

As expressed in Equation (3), when the clay fraction decreases due to sand replacement while cement content remains constant, the cement factor (*cf**) increases significantly. This mechanism explains why the c*30S70 mixture achieved higher shear strength than the c*30S0 mixture, despite both containing the exact cement dosage. The higher concentration of cement relative to clay particles enhances the formation of hydration products, such as calcium silicate hydrate (C–S—H), which strengthens interparticle bonding.

Figure 37 Figure 38 further supports this interpretation by presenting the relationship between the cement factor (*cf**) and shear strength at equivalent curing periods. The results show a proportional correlation, wherein a mixture with *c*20S70 and a cement factor (cf*)* of 45.5 exhibited higher shear strength compared to the *c*30S10 mixture, which had a cement factor (cf**) of 32.3, as shown in Figure 36. This finding suggests that the cement factor (*cf**) is more representative in describing the effectiveness of cement on soil strength than the total cement content (*c**).

This observation aligns with the empirical formulation developed by Yamashita et al. (2020)which asserts that the strength of cement–soil mixtures depends primarily on the ratio of cement to fine soil (*cf**) and the active solid volume ratio (*Yf**), rather than the sand content itself. Accordingly, although sand does not chemically react during hydration, its presence alters cement's mass balance and distribution, ultimately affecting the shear strength of stabilized soils.

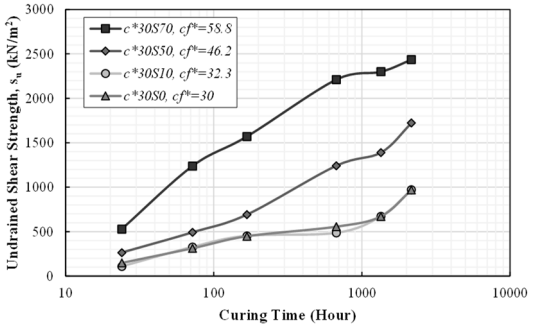

Figure 36. Relationship between curing time and undrained shear strength (S_u) with varying sand content

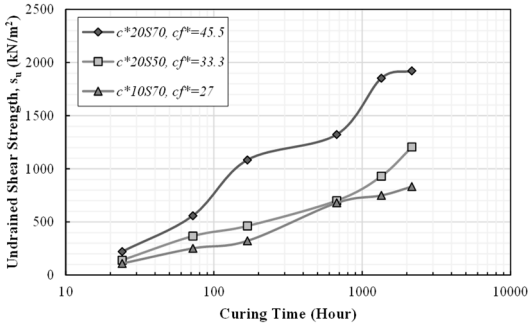

Figure 37. Relationship between curing time and shear strength with varying cement factor (*cf**)

3.5 Influence of Cement Factor (*cf**) on the Shear Strength of Stabilized Soil with Different Mix Compositions

The empirical formulation proposed by Yamashita et al. (2020) assumes that the shear strength of stabilized soil can be predicted as a function of the cement factor (*cf**) and curing time. To validate this approach, the present study evaluated several mix variations with differing cement and sand contents but with nearly equivalent *cf** values. As illustrated in Figure 38, an increase in curing time consistently resulted in higher shear strength across all mixtures. This trend is consistent with the cement hydration mechanism, in which hydration products such as calcium silicate hydrate (C–S–H) progressively develop over time, thereby strengthening the interparticle bonding.

Furthermore, Yamashita et al. (2020) demonstrated that shear strength increases linearly with (*cf** – *cf₀**) and logarithmically with curing time, a relationship that aligns with the patterns observed in this study. Despite initial compositional differences, mixtures with comparable cf* values exhibited nearly identical shear strengths. These findings suggest that when the ratio of cement to fine soil fraction is maintained constant, the influence of sand content becomes negligible. This supports the assertion of Yamashita et al. (2020) that the strength of stabilized soil is governed primarily by the interaction between cement and the fine soil fraction, rather than by the inert sand fraction. Consequently, design parameters such as *cf** and *Yf** should be determined solely based on the mass of cement and fine soil to represent their effective contribution to soil strength development accurately.

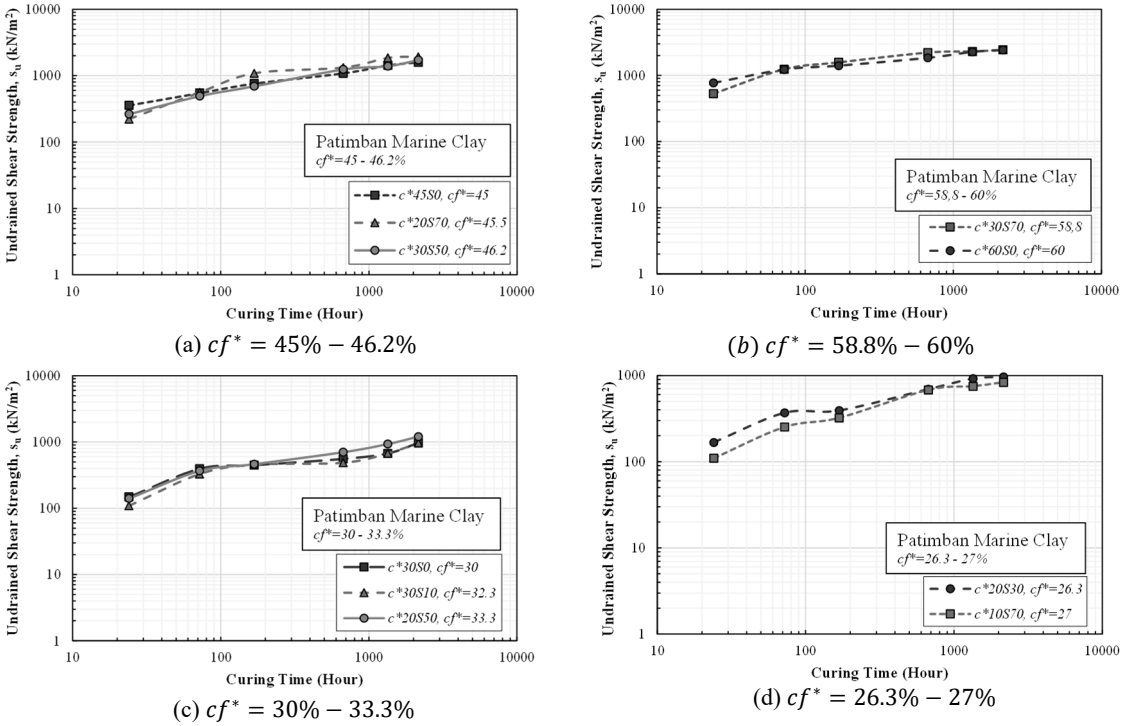

(a) $cf^* = 45\% - 46.2\%$ (b) $cf^* = 58.8\% - 60\%$

(c) $cf^* = 30\% - 33.3\%$ (d) $cf^* = 26.3\% - 27\%$

Figure 38. Relationship between undrained shear strength (S_u) and curing time at nearly identical cement factor (*cf**) values

3.6 Estimation of Unconfined Compressive Strength Based on Empirical Equations

The predictive accuracy of two empirical models for estimating the unconfined compressive strength (UCS) of cement-stabilized soils was evaluated against laboratory test results. The models examined were those proposed by the Japan Cement Association (2007) and Yamashita et al. (2020). Model predictions were compared with experimental UCS values, and the degree of agreement was quantified using the *Average Normalized Difference* (A.N.D), expressed as:

$$A.N.D = \frac{1}{n}\sum_{i=1}^{n}\left|\frac{A_i - B_i}{B_i}\right| \quad (4)$$

where A_i is the predicted UCS, B_i is the experimental UCS, n and is the number of observations.

This metric assessed model validity and identified the most suitable equation for the soil and materials investigated.

3.6.1 UCS Estimation Using the Japan Cement Association (2007) Equation

The predictive model for unconfined compressive strength (UCS) developed by the Japan Cement Association (2007) is based on an empirical relationship between the soil water-to-cement ratio and UCS. This approach fundamentally refers to Abrams' law, in which the strength of a mixture is governed by the ratio of water to binder. In soil stabilization with cement, the parameter w_c/c is employed as the principal predictor of UCS. Mathematically, the model is expressed as a nonlinear power regression with three parameters, namely the constants *a*, *b*, and the exponent *x*, as follows:

$$q_u = \frac{a}{\left(\frac{w_c}{C}\right)^x} + b \quad (5)$$

where q_u is the unconfined compressive strength of cement-stabilized soil (kN/m²), $\frac{w_c}{C}$ is the ratio of soil water content to cement mass, and a, b, and *x* are regression constants.

The relationship between unconfined compressive strength ($qu–b$) and the soil water-to-cement ratio (w_c/c) at curing periods of 1, 3, 7, 28, and 56 days are presented in Figure 39a. The parameters *a*, *b*, and *x* were determined through a curve-fitting procedure to obtain the best coefficient of determination (R^2). The fitted equations corresponding to each curing period are provided in the subsequent section.

$$\begin{aligned}
q_u &= 993.03(w_c/C)^{-1,31} + 19.46 \quad (1\ \text{day})\\
q_u &= 1882.77(w_c/C)^{-1,05} + 26.03 \quad (3\ \text{day})\\
\boldsymbol{q_u} &= \boldsymbol{2536.4(w_c/C)^{-1.1} + 23.67} \quad (7\ \text{day})\\
q_u &= 3472.9(w_c/C)^{-0,99} + 35.97 \quad (28\ \text{day})\\
q_u &= 4177.3(w_c/C)^{-0,94} + 25.8 \quad (56\ \text{day})\\
q_u &= 4549(w_c/C)^{-0,814} + 9.28 \quad (90\ \text{day})
\end{aligned} \quad (6)$$

The empirical model developed by the Japan Cement Association (2007) does not explicitly account for curing time within its formulation. Consequently, distinct regression parameters are required for each curing period to ensure the model represents actual conditions. Regression analysis in this study revealed that the constant *a* generally increased with longer curing durations. This trend reflects the progressive enhancement of the baseline strength of the stabilized soil, attributable to the ongoing cement hydration process that produces stronger interparticle bonds. In contrast, the exponent *x*, which governs the model's sensitivity to the soil water-to-cement ratio, exhibited a decreasing trend with increasing curing time. This pattern indicates that, during the early stages, the water-to-cement ratio exerts a dominant influence on strength development. However, this influence diminishes as the stabilized soil structure becomes increasingly consolidated and stable.

A comparison between the unconfined compressive strength values obtained from laboratory testing and those estimated using Equation (6) demonstrated strong agreement, yielding a coefficient of determination (R^2) of 0.95 and an Average Normalized Difference (A.N.D.) of 13.17%. These results confirm high consistency between the measured and predicted strength values. Figure 39b illustrates this relationship, highlighting the estimation model's ability to capture the data's distribution pattern. Accordingly, the unconfined compressive strength of Patimban marine clay with varying sand contents, stabilized using PCC, can be reliably predicted by Equation (6) for specified curing periods.

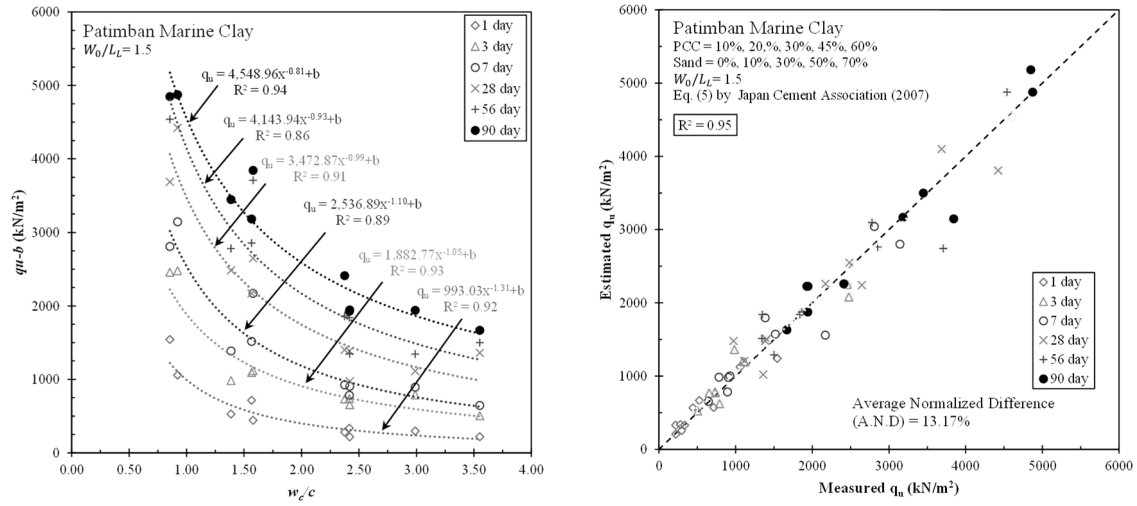

(a) Relationship between unconfined compressive strength (qu−b) and the soil water-to-cement ratio (wc/C)

(b) Comparison between estimated and measured unconfined compressive strength

Figure 39. Analysis of the application of the estimation model Equation (6)

3.6.2 UCS Estimation Using the Yamashita et al. (2020) Equation

The predictive model proposed by Yamashita et al. (2020) was developed in response to the limitations of earlier estimation approaches that did not account for variations in sand content and initial water content. This formulation aims to provide a more general and accurate method for predicting the unconfined compressive strength of marine clay stabilized with cement, particularly under field conditions characterized by diverse marine sediment properties. The model is expressed as follows:

$$q_u = (E^* + F^* lnD)\left(c_f^* - c_{f0}^*\right)\left(Y_f^*\right)^N \quad (7)$$

where q_u denotes the unconfined compressive strength, cf^* represents the cement content ratio relative to the mass of fine soil, $cf0^*$ is the minimum cement threshold, Yf^* denotes the volumetric ratio of solids excluding sand, N is the void parameter, and E^* and F^* are regression constants.

In this study, the Yamashita et al. (2020) model was applied to evaluate the unconfined compressive strength of Patimban marine clay. As shown in Figure 40a, a linear relationship was observed between $qu(Yf^*)^{-N}$ and cf^* with N=1.27. The parameter N is an experimental coefficient that reflects the dependency of compressive strength on the porosity of the cement-stabilized soil matrix. This coefficient was obtained by selecting the value that produced the highest coefficient of determination (R^2) across linear relationships at each curing period, and subsequently averaging the results to derive a representative value. Figure 40b presents the relationship between $qu(Yf^*)^{-N}$ and the corrected cement-to-fines ratio ($cf^*–cf0^*$), where $cf0^*$ represents the threshold cement content of 16.34%. Incorporating this correction yielded highly linear correlations across all curing periods, with R^2=1.0 in each case. Applying $cf0^*$ improved the predictive accuracy by demonstrating that strength development commences only once a minimum cement threshold is exceeded. Further, Figure 40c illustrates the relationship between kc^* and curing time (D), as expressed in Equation (8).

$$k_c^* = E^* + F^* lnD \quad (8)$$

where k_c^* denotes the strength gain coefficient, D is the curing period (days), and E^* and F^* are regression parameters obtained from curve fitting.

The results of the estimation, compared with laboratory test data, are presented in Figure 40d. The comparison demonstrated a reasonable level of agreement, with a coefficient of determination (R^2) of 0.85. However, the Average Normalized Difference (A.N.D.) was 25.43%, indicating a notable discrepancy between the measured laboratory strength and the model predictions.

3.6.3 Evaluation of Soil Strength Prediction Models

The predictive performance of two estimation models for saturated clayey soils was evaluated: the Japan Cement Association (2007) and the volumetric-based model proposed by Yamashita et al. (2020). Model accuracy was assessed using the coefficient of determination (R^2) and the average normalized deviation (A.N.D.). The Japan Cement Association model demonstrated superior accuracy (R^2 = 0.95; A.N.D. = 13.17%) compared to the Yamashita model (R^2 = 0.85; A.N.D. = 25.43%). This enhanced performance is attributed to the explicit consideration of the water-to-cement ratio (wc/c), which directly governs the hydration process and more accurately reflects the saturated soil conditions in the Patimban area.

In contrast, the Yamashita model relies on volumetric parameters (cf^* and Yf^*) and does not explicitly account for water content, resulting in reduced predictive accuracy. The observed A.N.D. in the present study is higher than the 9.4–22.1% range reported by Yamashita et al. (2020) for marine clays in Japan, a discrepancy is likely influenced by differences in sand characteristics. While Yamashita et al. utilized Toyoura sand with uniform gradation (Cu = 1.71; Cc = 1.07), the current study employed Bangka sand, which exhibits a broader particle size distribution (Cu = 3.3; Cc = 0.96). Improved gradation enhances mixture density and stability Wahyudi and Prihatin (2011), affecting estimation outcomes. Overall, models incorporating *wc/c* are considered more representative for predicting the strength of high-

moisture marine clay soils in Patimban, with sand type identified as a critical factor influencing model suitability.

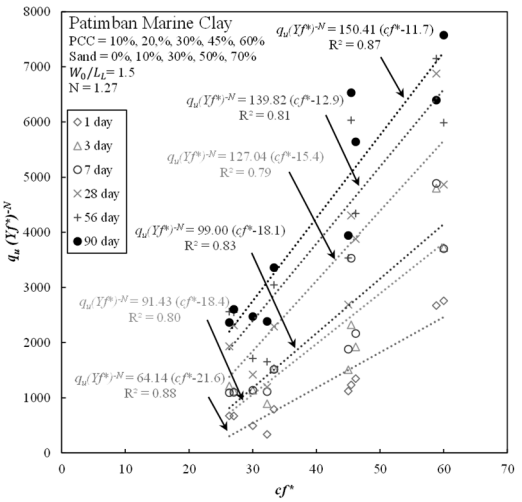

(a) Relationship between $qu(Yf^*)^{-N}$ and cf^*, N=1.27

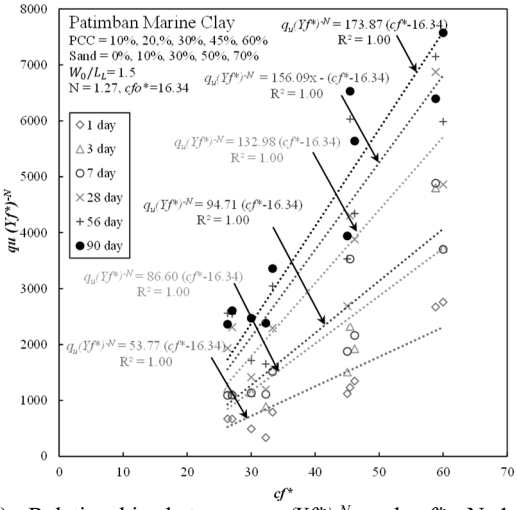

(b) Relationship between $qu(Yf^*)^{-N}$ and cf^*, N=1.27 cfo^*=16.34

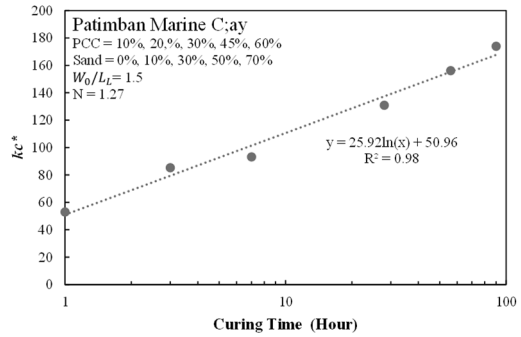

(c) Relationship between kc^* and curing time

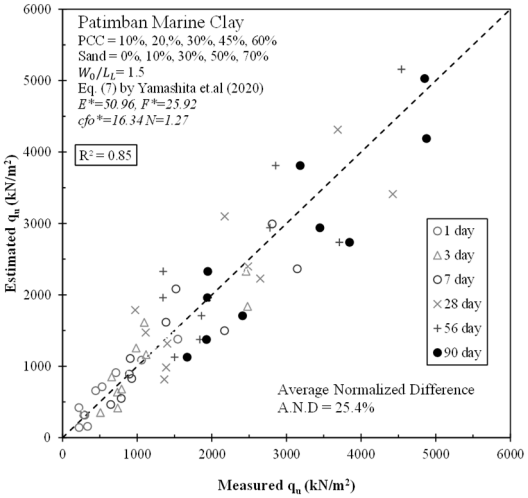

(d) Comparison between estimated and measured unconfined compressive strength

Figure 40. Analysis of the application of the estimation model Equation (7)

Table 18. Parameters *N, cf0*, kc*, E*,* and *F**in Eq. (7) for Patimban Marine Clay

Curing Time (days)	N	Average N	*Cfo** (%)	Average *Cfo** (%)	*Kc** (kN/m²)	*E** (kN/m²)	*F** (kN/m²/ln(days))
1	2.1	1.27	21.6	16.34	52.88	50.96	25.92
3	1.5		18.4		85.2		
7	1		18.1		93.18		
28	1		15.4		130.88		
56	1		12.9		156.09		
90	1		11.7		173.87		

4 CONCLUSIONS

Based on the results of the present study, it was found that the addition of Portland Composite Cement (PCC) significantly influenced the increase in undrained shear strength of Patimban marine clay. Higher PCC content, maintained at a consistent water-to-cement ratio, resulted in greater increases in shear strength. The effectiveness of PCC addition was also found to depend on the distribution of

cement relative to the fine soil fraction, with the cement factor (*cf**) providing a more representative measure of strength improvement than total cement content; mixtures with similar *cf** values exhibited comparable shear strength, even when sand compositions differed. Free unconfined compressive strength estimation was conducted using models from both the Japan Cement Association (JCA, 2007) and Yamashita et al. (2020). The JCA model demonstrated higher predictive accuracy (R^2 = 0.95; Average Normalized Difference, A.N.D. = 13.17%) than the Yamashita model (R^2 = 0.85; A.N.D. = 25.43%), indicating that the water-to-cement ratio (*wc/c*) more accurately reflects the effect of cement hydration on strength development of Patimban marine clay. Nevertheless, according to the Yamashita model, cement still plays a critical role in soil strength, highlighting the need for further investigation into the influence of sand characteristics on the mechanical behavior of stabilized clay soils.

DISCLAIMER

The authors declare that they have no conflict of interest.

AVAILABILITY OF DATA AND MATERIALS

All data are available from the author.

ACKNOWLEDGMENTS

This work was supported by the collaboration research between Universitas Pertamina and Universiti Tenaga Nasional No. 0145/UP-R/SK/HK.01/VII/2023. Authors would like to convey great gratitude to the Department of Civil Engineering, Universitas Pertamina. The authors would like to thank the Soil Mechanics Laboratory of Universitas Pertamina for providing research facilities and the Patimban local government for granting permission and assistance in marine clay soil sampling within their area.

REFERENCES

Alfanoza, S.H., Cikmit, A.A., Sudisman, R.A., Alfirdausi, A.A., Hariansyah, A.R., 2024. Expansivity and Strength Behaviors of Expansive Clay Soils mixed with High-Alumina Cement and Polyethylene Terephthalate.

Chen, Z., 2024. Experimental study on the evaluation in thermal-hydraulic-mechanical-chemical properties of cement-stabilized clay. PLoS One 19. https://doi.org/10.1371/journal.pone.0313760

Chian, S.C., Chim, Y.Q., Wong, J.W., 2017. Influence of sand impurities in cement-treated clays. Geotechnique 67, 31–41. https://doi.org/10.1680/jgeot.15.P.179

Japan Cement Association, 2007. Ground improvement manual using cement-based solidification material 3, 43–44.

Ministry of Environment and Forestry, 2017. Decree of the Minister of Environment and Forestry of the Republic of Indonesia Number SK 136/Menlhk/Setjen/PLA.4/2/2017 concerning the Environmental Permit for the Development of Patimban Port in Patimban Village, Kalentambo Village, Gompol Village, Kotasari Village, Pusakaratu Village, Pusakanagara Subdistrict, and Pusakajaya Village, Pusakajaya Subdistrict, Subang Regency, West Java Province.

Suksiripattanapong, C., Sakdinakorn, R., Tiyasangthong, S., Wonglakorn, N., Phetchuay, C., Tabyang, W., 2022. Properties of soft Bangkok clay stabilized with cement and fly ash geopolymer for deep mixing application. Case Studies in Construction Materials 16. https://doi.org/10.1016/j.cscm.2022.e01081

Tsuchida, T., Tang, Y.X., 2015. Estimation of compressive strength of cement-treated marine clays with different initial water contents. Soils and Foundations 55, 359–374. https://doi.org/10.1016/j.sandf.2015.02.011

Uddin, M.A., Jameel, M., Sobuz, H.R., Islam, M.S., Hasan, N.M.S., 2013. Experimental study on strength gaining characteristics of concrete using Portland Composite Cement. KSCE Journal of Civil Engineering 17, 789–796. https://doi.org/10.1007/s12205-013-0236-x

Wahyudi, H., Prihatin, K., 2011. Correlation of Material Gradation Coefficient with Density and Soil Shear Strength, © ITS JOURNAL OF CIVIL ENGINEERING.

Wei, R., Wang, B., Cai, H., Xiao, J., Wu, S., 2021. Increased sand content and its effect on the strength of cement-solidified soft clay, in: IOP Conference Series: Earth and Environmental Science. IOP Publishing Ltd. https://doi.org/10.1088/1755-1315/861/4/042076

Yamashita, E., Aristo Cikmit, A., Tsuchida, T., Hashimoto, R., 2020. Strength Estimation of Cement-Treated Marine Clay with Wide Ranges of Sand and Initial Water Contents. Soils and Foundations 60, 1065–1083. https://doi.org/10.1016/j.sandf.2020.05.002

Yao, X., Guan, J., Bai, W., 2019. Effects of soil grading and sand content on soil-cement properties, in: IOP Conference Series: Earth and Environmental Science. Institute of Physics Publishing. https://doi.org/10.1088/1755-1315/304/5/052038

This page is intentionally left blank

HIMPUNAN AHLI TEKNIK TANAH INDONESIA - HATTI
Indonesian Society for Geotechnical Engineering - ISGE
PIT HATTI XXIX
10-12 November 2025

Microbial Enzyme Extract Evaluation for Calcium Carbonate Biocementation: Implications for Ground Improvement

Lutfian R Daryono[1,*], M Akmal Putera[1], Tomohiko Abe[1], Aoi Ichinohe[2], Kazunori Nakashima[3], Satoru Kawasaki[3]

[1] Engineering and Development Divisions, NITTOC Construction Co., Ltd., JAPAN.
[2] Division of Sustainable Resources Engineering, Graduate School of Engineering, Hokkaido University, JAPAN.
[3] Division of Sustainable Resources Engineering, Faculty of Engineering, Hokkaido University, JAPAN.
*Correspondence: luthfian.daryono@gmail.com; lutfian.rusdi.daryono@nittoc.co.jp

ABSTRACT Microbially Induced Carbonate Precipitation (MICP) has emerged as a promising technique for slope surface stabilization or other ground improvements. However, its effectiveness in fine-grained soils is limited due to challenges associated with bacterial cell transport. This study explores the feasibility of an alternative approach Enzyme Induced Carbonate Precipitation (EICP) from microbial bacteria itself for stabilizing fine-grained slope soils. In this study, urease was extracted from whole-cell cultures of *Lysinibacillus xylanilyticus (LyXy)* which developed under Hokkaido University and using cyclic sonication. The extracted enzyme solution was then applied to a precipitation test using fine-grained sand and/or soil samples. The performance of enzyme extract was evaluated in comparison to traditional MICP with a focus on the adaptability to precipitate the fine-grained sand/soil and the effectiveness of the enzyme. Results indicated that the urease extract exhibited higher enzymatic activity than the original bacterial culture and maintained better stability at 15°C. The observation verified that the effectiveness of enzyme-induced and MICP would vary depending on the soil to be treated. The enzyme-induced resulted in unconfined compressive strength around 4 MPa and deeper cementation in the finest sand. Microscopic analysis revealed that while enzyme-induced produced smaller calcium carbonate crystals compared to MICP, it generated a significantly higher quantity of crystals, leading to enhanced particle bonding and improved soil stabilization.

KEYWORDS Microbial induced carbonate precipitation (MICP); Enzyme Induced Carbonate Precipitation (EICP), enzyme extract, soil stabilization, fine-grained.

This paper will be published in the future issues of Indonesian Geotechnical Journal

This page is intentionally left blank

HIMPUNAN AHLI TEKNIK TANAH INDONESIA - HATTI
Indonesian Society for Geotechnical Engineering - ISGE
PIT HATTI XXIX
10-12 November 2025

Use of CO_2 Nanobubble-Treated Alkaline Wastewater in Developing Low-Carbon Materials

Sugeng Wahyudi[1*], Akihiro Hamanaka[2], Muhammad Akmal Putera[3], Gde Pandhe Wisnu Suyantara[4], Tomohiko Abe[5], Hideki Shimada[6], Takashi Sasaoka[7]

[1]Engineering and Technology Development Division, Technology Center, NITTOC Construction Co., Ltd., Saitama, Japan, 349-0134; sugeng.wahyudi@nittoc.co.jp
[2]Department of Earth Resources Engineering, Faculty of Engineering, Kyushu University, Fukuoka, Japan, 819-0395; hamanaka@mine.kyushu-u.ac.jp
[3]Engineering and Technology Development Division, Technology Center, NITTOC Construction Co., Ltd., Saitama, Japan, 349-0134; muhammad.akmal.putera@nittoc.co.jp
[4]Department of Earth Resources Engineering, Faculty of Engineering, Kyushu University, Fukuoka, Japan, 819-0395; pandhe@mine.kyushu-u.ac.jp
[5]Engineering and Technology Development Division, Technology Center, NITTOC Construction Co., Ltd., Saitama, Japan, 349-0134; tomohiko.abe@nittoc.co.jp
[6]Department of Earth Resources Engineering, Faculty of Engineering, Kyushu University, Fukuoka, Japan, 819-0395; shimada@mine.kyushu-u.ac.jp
[7]Department of Earth Resources Engineering, Faculty of Engineering, Kyushu University, Fukuoka, Japan, 819-0395; sasaoka@mine.kyushu-u.ac.jp
*Correspondence: sugeng.wahyudi@nittoc.co.jp

ABSTRACT In response to the global challenge of reducing greenhouse gas emissions in construction industry, particularly in ground improvement works, this study explores the reuse of CO_2 nanobubble-treated alkaline wastewater ($nbCO_2$-NTAW) as sustainable mixing water for low-carbon materials (LCMs). Studies have shown that CO_2 nanobubbles ($nbCO_2$) enhance gas transfer efficiency and accelerate the formation of carbonic acid, enabling safe and environmentally friendly neutralization of alkaline wastewater. In this study, this $nbCO_2$-NTAW was used to prepare solidification materials composed of ordinary Portland cement (OPC) and blast furnace slag (BFS4000), aiming to reduce fresh water and OPC usage, and promote carbon sequestration. A series of tests, including viscosity, flow diameter, bleeding ratio and uniaxial compressive strength (UCS), were conducted to evaluate the performance of $nbCO_2$-NTAW in LCM. Results showed that up to 70% OPC replacement is feasible without compromising long-term UCS performance. This approach demonstrates a promising pathway for sustainable ground improvement technologies.

KEYWORDS CO_2 nanobubble; alkaline wastewater; low carbon material; circular economy; sustainable construction

1 INTRODUCTION

1.1 The use of CO_2 nanobubble ($nbCO_2$) Technology in Alkaline Wastewater Treatment

Recent studies have demonstrated that CO_2 nanobubbles ($nbCO_2$) significantly enhance gas transfer efficiency into liquids (Cerron et al., 2022). Building on this, Wahyudi et al. (2024) reported that, under the same CO_2 gas flow volume, the concentration of carbonic acid (H_2CO_3) formed from reaction between H_2O and CO_2 is approximately three times higher in $nbCO_2$ systems compared to microbubble CO_2 ($mbCO_2$), and substantially greater than achieved used conventional CO_2 gas. This finding highlights the strong potential of $nbCO_2$ for improving the neutralization of alkaline construction wastewater.

Furthermore, Wahyudi et al. (2024) found that $nbCO_2$-treated alkaline water ($nbCO_2$-NTAW) retains a higher concentration of CO_2 nanobubbles and maintains their stability in solution for a longer duration than CO_2 microbubble treated alkaline water (mb CO_2-NTAW). This enhanced retention is

hypothesized offers a promising opportunity for its use as mixing water in low-carbon materials (LCMs). The presence of stable CO_2 nanobubble is expected to accelerate the reaction between CO_2 and calcium ions (Ca^{2+}), promoting solidification and enhancing CO_2 capture in the material matrix. Based on this hypothesis, the present study investigates the application of the $nbCO_2$-NTAW as a mixing water in LCMs, aiming to advance CO_2 emission reduction strategies, reduce the use of freshwater and OPC.

Obviously, the $nbCO_2$-NTAW exhibits distinct chemical characteristics and components compared to alkaline wastewater (AW). The AW is defined by its high pH (>11) and strong reactivity, primarily containing calcium hydroxide ($Ca(OH)_2$) and hydroxide ions (OH^-). In contrast, $nbCO_2$-NTAW is characterized by a neutral pH, chemical stability (stable pH, stable CO_2 species, reduced reactivity, consistency over time), and enhanced CO_2 reactivity. Following treatment with $nbCO_2$ method, the water composition shifts significantly. The $nbCO_2$-NTAW contains $nbCO_2$, dissolved CO_2, H_2CO_3, calcium carbonate ($CaCO_3$), CO_3^{2-} and HCO_3^-. The presence of these CO_2-rich species in high concentration is expected to enhance carbonation and CO_2 fixation, promote solidification, and stabilize hydration reaction when used as mixing water in cement-based materials (CBMs). A detailed comparison of the water composition before and after CO_2 nanobubble treatment is provided in Table 1.

Table 1. Comparison of wastewater composition before and after treatment using nbCO2 technology

Category	Alkaline wastewater (AW)	CO_2 nanobubble treated alkaline water ($nbCO_2$-NTAW)
pH level	High (typically >11) due to $Ca(OH)_2$	Neutralized (approx. pH 7-8)
Main alkaline agent	$Ca(OH)_2$	Partially converted to $CaCO_3$
Hydroxide ions (OH^-)	High concentration	Reduced due to neutralization
CO_2 microbubble ($mbCO_2$) and CO_2 nanobubble ($nbCO_2$)	Not present	Introduced via nanobubble generator
Dissolved CO_2	Not present	Present in high concentration
Carbonic acid (H_2CO_3)	Not present	Formed from CO_2+H_2O
Calcium carbonate ($CaCO_3$)	Not present	Formed from $Ca(OH)_2$+ CO_2
Carbonate (CO_3^{2-}) and bicarbonate (HCO_3^-) ions	Minimal or absent	Generated during CO_2 dissolution and reaction

1.2 The use of CO_2 nanobubble ($nbCO_2$) Water and Alkaline Wastewater in Cement-based Materials (CBMs) and Low-carbon Materials (LCMs) Cementation

Several researchers have investigated the effect of CO_2 gas and $nbCO_2$ on the development of CBMs and LCMs. For example, Wahyudi and Abe (2022) explore the use of $nbCO_2$ water as curing water to accelerate the carbonation process of CBMs. Their findings revealed that after one day of water curing, the UCS of the samples increased by 31%, indicating effective early carbonation. However, this early improvement did not lead to significant long-term strength improvements. The increase in early UCS suggests that CO_2 was effectively captured in the form of $CaCO_3$ that is indicated by near-neutral pH (less than 9) of the $nbCO_2$ curing water during curing period which indicates less (OH^-) ions released into the curing water. The ions react with $nbCO_2$ form H_2CO_3, which contributes to the gradual reduction of pH of the curing water.

While research on utilizing CO_2 gas and $nbCO_2$ in the development of low-carbon materials (LCMs), particularly slag cement, have been reported by Moro et al. (2023) and Kawai, Hamanaka, Wahyudi et al. (2023), subsequently. Moro et al. (2023) found that CO_2 exposure enhanced early compressive strength by up to 12% in 7 days and improve long-term strength by approximately 8%. While Kawai, Hamanaka, Wahyudi et al. (2024) demonstrated that using the $nbCO_2$ water in OPC-BFS4000 mixture resulted in UCS improvement ranging from 10% to 20%, depending on the BFS4000-to-OPC ratio.

In parallel, growing interest has emerged in using alkaline construction wastewater as a replacement for conventional mixing water (Chen et al., 2022; Ha et al., 2025). Chen et al. (2022) reported that up to 50% substitution was feasible without compromising strength, depending on treatment and mix design. Ha et al. (2025) replaced 100% of tap water with simulated concrete wash water in cement pastes and mortars, observing faster hydration and reduced flowability, while maintaining comparable compressive strength at higher water-to-binder ratios (W/B=0.6). These findings support the potential of construction wastewater in sustainable construction. Despite its benefits, such as reduced freshwater usage, elimination of treatment costs, and accelerated early hydration in CBMs, alkaline construction wastewater poses safety risks due to its high pH and lacks environmental contributions like CO_2 fixation. Addressing these issues, this study introduces $nbCO_2$-NTAW, which stabilizes pH and enhances carbonation reactions.

2 MATERIALS AND METHODS

In this study, $nbCO_2$-NTAW refers to specialized treated water produced by neutralizing $Ca(OH)_2$ -based alkaline water with $nbCO_2$. The treatment process involved adjusting 25 liters of alkaline water, initially at pH 11.02, to a near-neutral range (approximately pH 7–8). This was accomplished using a microporous diffuser (model AZ-01500284, Anzai Kantetsu Co., Ltd.) within a batch-type recirculation system. As shown in Figure 1, the system consists of a storage chamber for the alkaline water, a pump that circulates the water through the diffuser, and a return line that feeds the treated water back into the chamber.

During circulation, CO_2 is introduced into the system through the microporous diffuser, forming micro- and nanobubbles that facilitate chemical reactions. CO_2 reacts with $Ca(OH)_2$ and H_2O in the water, resulting in the formation of H_2CO_3 and $CaCO_3$. Additionally, dissolved CO_2 enhances the carbonation process, further promoting the neutralization of the alkaline solution. This cycle is repeated until the water reaches the target near-neutral pH, and the final composition of the $nbCO_2$-NTAW includes CO_2 micro-nanobubbles, dissolved CO_2, $CaCO_3$, and H_2CO_3. The influence of these compounds on the carbonation and hydration processes is summarized in Table 2.

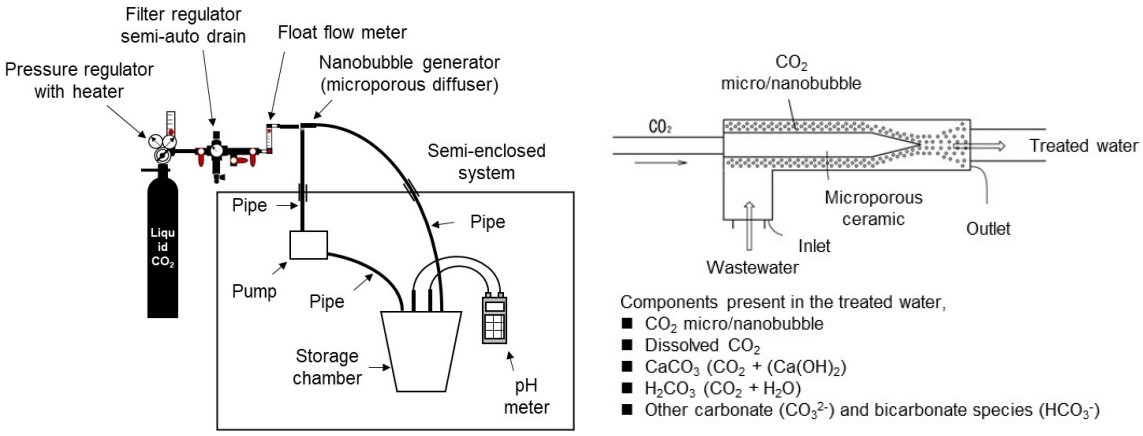

Figure 1. Schematic illustration of the preparation process for $nbCO_2$-NTAW.

To evaluate its impact on LCMs, $nbCO_2$-NTAW was utilized as mixing water in various blend ratios of OPC and BFS4000. BFS4000 refers to ground granulated blast furnace slag with a specific surface

area of approximately 4,000 cm²/g, classified under JIS A 6206:2024 (Japanese Industrial Standard, 2024). It is widely used as a supplementary cementitious material to enhance concrete durability, reduce the heat of hydration, and significantly lower CO_2 emissions by partially replacing OPC. The chemical composition of OPC-BFS4000, and specific mixing ratios of OPC and BFS4000 used in this study are presented in Table 3 and Table 4, subsequently.

In this study, four tests, UCS, flow, viscosity and bleeding tests, were conducted to evaluate the mechanical and fresh properties of LCMs. Specimen preparation followed standard procedures. Initially, the dry binder components were blended for 60 seconds to ensure uniformity, followed by mixing with nbCO_2-NTAW using a mechanical mixer for 3 minutes. After mixing, the resulting fresh mix LCM paste was divided for each test.

For UCS test, a modified version of JIS A 1132 (Japanese Industrial Standard, 2020) was used, adopted for dry curing without demolding. The fresh mix was cast into 50 mm in diameter and 100 mm in height of clean cylindrical molds. The specimens were then subjected to dry curing at temperature-controlled room with a constant temperature of 20 ± 2 °C for the entire curing period, 7 and 28 days, without being demolded. Just before UCS testing, the specimens were demolded, their dimensions and weights were measured, and compressive strength testing was performed in accordance with JIS A 1216 (Japanese Industrial Standard, 2020). The UCS test apparatus is shown in Figure 2.

The flow diameter test was conducted by placing the fresh mix into a cylindrical mold (80 mm diameter x 80 mm height, shown in Figure 3a. After lifting the mold, the horizontal spread of the material was measured to assess its workability (Figure 3b). Viscosity was evaluated using a viscometer TVB-15 at rotational speeds of 6, 12, 30, and 60 rpm to characterize the rheological behavior of the LCMs. The viscometer TVB-15 equipment used in this study is presented in Figure 4.

Table 2. Effects of nbCO_2-NTAW components on carbonation and hydration

Compound	Function	Merit	Demerit
CO_2 micro-nanobubbles	Improve CO_2 contact and reaction speed	Faster and more uniform carbonation	May affect pore structure
Dissolved CO_2	Boost carbonation reactions	Help form $CaCO_3$ and reduce pH	Too much can slow hydration
$CaCO_3$	Fills pores, improves durability	Strengthens material, reduce permeability	Excess may block hydration pathways
H_2CO_3	Lowers pH, promotes carbonation	Enable deeper carbonation	May destabilize hydration if pH too low

Table 3. Chemical component and composition of OPC and BFS4000

	Chemical composition, %					Density	Specific surface area
	CaO	SiO_2	Al_2O_3	Fe_2O_3	MgO	(g/cm^3)	(cm^2/g)
OPC	64.3	21.4	5.5	2.79	2.06	3.15	3310
BFS4000	43.4	34	14.4	0.83	6.51	2.9	4000

Table 4. Mixing proportions of OPC and BFS4000 for 1 m³ of LCM

Sample code	S0	S30	S50	S70	S100
OPC:BFS400 mixing ratio	100:0	70:30	50:50	30:70	0:100
OPC (g)	1223.3	847.43	601.15	358.23	0
BFS4000 (g)	0	363.18	601.15	835.87	1182
nbCO2-NTAW (g)	611.65	605.31	601.15	597.05	591
W/B (%)	50	50	50	50	50

The bleeding test was performed in accordance with Japan Society of Civil Engineering bleeding test procedure JSCE-F522 (2018). The freshly prepared mix was placed into a polyethylene bag (50 mm diameter x 200 mm length) up to the designated volume specified in the standard. After sealing the top of the bag, it was submerged in a graduated cylinder filled with water. Surface of the fresh mix inside the bag was aligned with the water surface in the cylinder recorded as the initial reference level. Measurements were taken after 1 hour to evaluate early-stage bleeding by re-aligning the water surface in the cylinder with the mix surface inside the bag, followed by recording of the alignment level. The bleeding rate was calculated by dividing the change in the mix surface level to the initial reference level and expressing the ratio as a percentage. The measurement setup is illustrated in Figure 5.

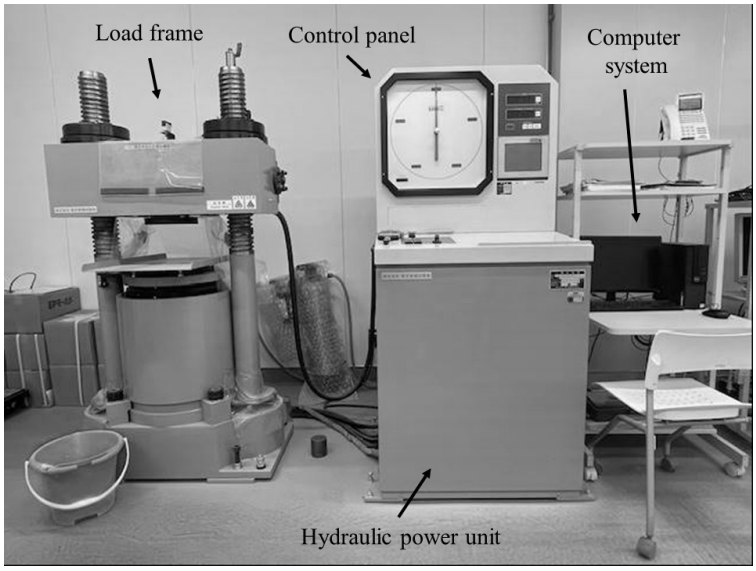

Figure 2. UCS test apparatus.

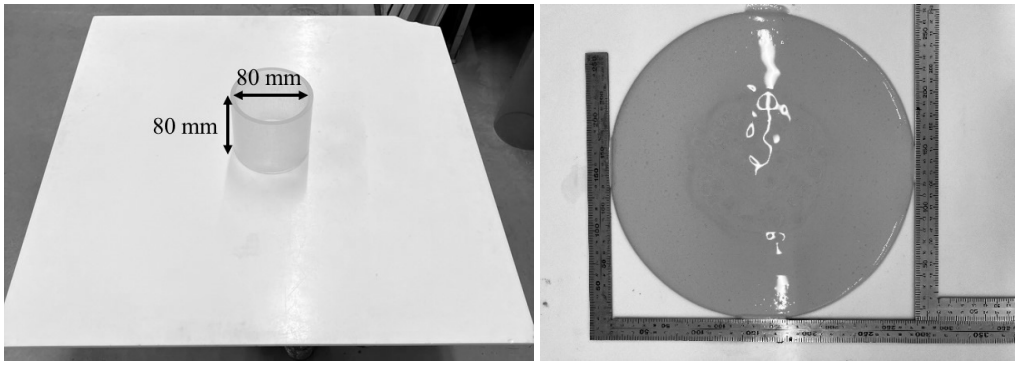

(a) (b)

Figure 3. (a) Flowability testing tools; (b) Flow diameter of 100% BFS4000 using freshwater as the mixing water.

Figure 4. Viscometer TVB-15.

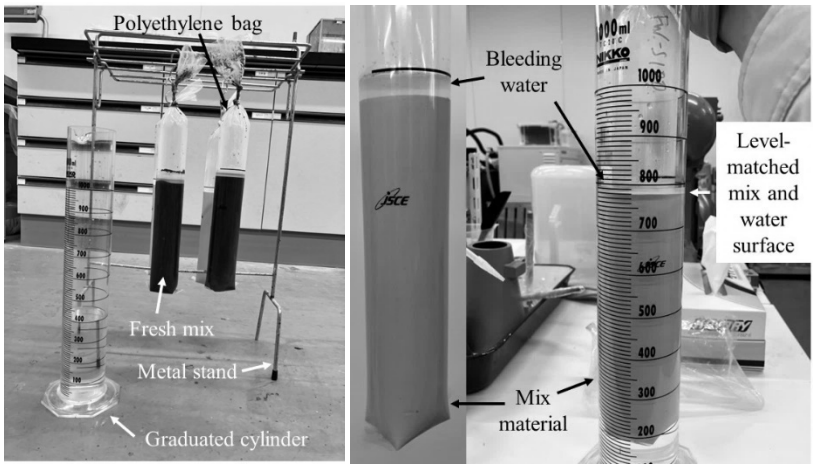

(a) (b)

Figure 5. Bleeding test setup following JSCE-F522 (Japanese Society of Civil Engineering, 2018).

3 EXPERIMENT RESULTS AND DISCUSSION

3.1 Influence of CO_2 Nanobubble-Treated Alkaline Water ($nbCO_2$-NTAW) on the Rheological Behavior of OPC (S0) and BFS4000 (S100)

Understanding the rheological behavior of 100% OPC (S0) and 100% BFS4000 (S100) when mixed with $nbCO_2$-NTAW, specifically how these materials flow and deform under stress, is an essential factor in evaluating the impact of this mixing water on development of LCMs. In cementitious systems, rheological properties such as yield stress, plastic viscosity and apparent viscosity directly affect workability, pumpability, and segregation resistance (Schmidt and Link, 2024). To thoroughly assess these effects, flow diameter and bleeding ratio parameters were also included in the analysis.

Figure 6 presents the rheological profile of OPC and BFS4000 pastes prepared with either freshwater (FW) or $nbCO_2$-NTAW. In general, BFS4000 shows higher viscosity than OPC, due to BFS4000 having a higher surface area (see Table 3). Higher surface area means more particle surface is exposed to water, that may absorb more water into its surface, reducing the amount of free water available for flow, resulting lower bleeding ratio as shown in Figure 7b. This leads to a thicker as described with smaller flow diameter as shown in Figure 7a, more viscous paste (see Figure 6). Moreover, finer BFS4000 particles tend to pack more densely, increasing interparticle friction. This friction contributes to higher yield stress and plastic viscosity as explained by Rajadurai and Kang (2021). Despite these differences, both materials demonstrate enhanced shear-thinning behavior when mixed with $nbCO_2$ water, indicating better handling performance under shear conditions.

Notably, the yield stress of OPC mixed with FW and $nbCO_2$-NTAW remains nearly identical at lower shear rate (below $7s^{-1}$). However, as shown in Figure 7, the OPC paste prepared with $nbCO_2$-NTAW exhibits a 17% smaller flow diameter (see Figure 7a) compared to the paste mixed with FW. This suggests that while the initial resistance to flow remains unchanged, the use of $nbCO_2$-NTAW promotes a more cohesive internal structure, likely due to early hydration without significantly affecting the yield stress. This analysis is further supported by a 50% reduction in bleeding ratio (see Figure 7b). When exposed to $nbCO_2$-NTAW, the surface of OPC particles interact more intensively with the dissolved CO_2 and ions in the treated wastewater, promoting early surface reactions. At higher shear rate (above $7s^{-1}$), the rheological behavior diverges. As illustrated in Figure 6 (left), $nbCO_2$-NTAW enhances the shear-thinning characteristics more prominently than FW, which only moderately influences the material's flow behavior.

Unlike the OPC case, the rheological behavior of BFS4000 paste mixed with $nbCO_2$-NTAW shows lower viscosity than when mixed with FW at low shear rates (below $3s^{-1}$) but becomes higher at elevated shear rates (above $3s^{-1}$) as depicted in Figure 6 (right). The lower viscosity at low shear rates is attributed to a reduction in yield stress. Interestingly, despite the reduced yield stress, the flow diameter is 6.85% smaller compared to BFS4000 paste mixed with FW. Like the OPC case, the bleeding ratio of BFS4000 paste mixed with $nbCO_2$-NTAW is lower than that of the FW mix (see Figure 7b), indicating that $nbCO_2$-NTAW promotes faster and denser gel formation in BFS4000 accordingly reduce the flow diameter (see Figure 7a). At Figure 6 (right), it is understood that the $nbCO_2$-NTAW at higher shear rate (above $3s^{-1}$) improve significantly the shear-thinning characteristics of BFS4000. The comparative analysis of rheological behavior of OPC and BFS4000 mixed with either FW or $nbCO_2$-NTAW is given in Table 5.

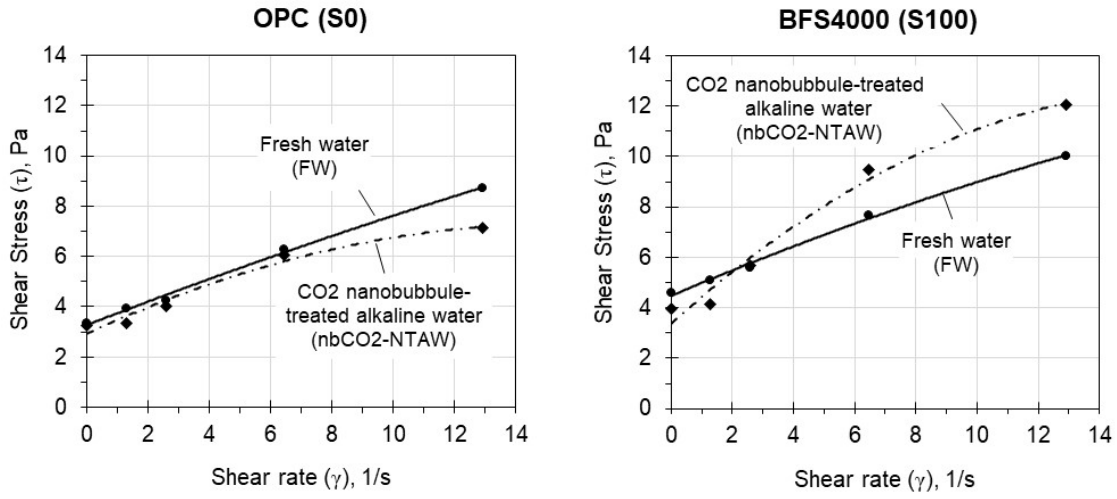

(a) OPC (b) BFS4000

Figure 6. Rheological behavior of OPC and BFS4000 when incorporating with freshwater (FW) and CO_2 nanobubble treated alkaline water nbCO_2-NTAW).

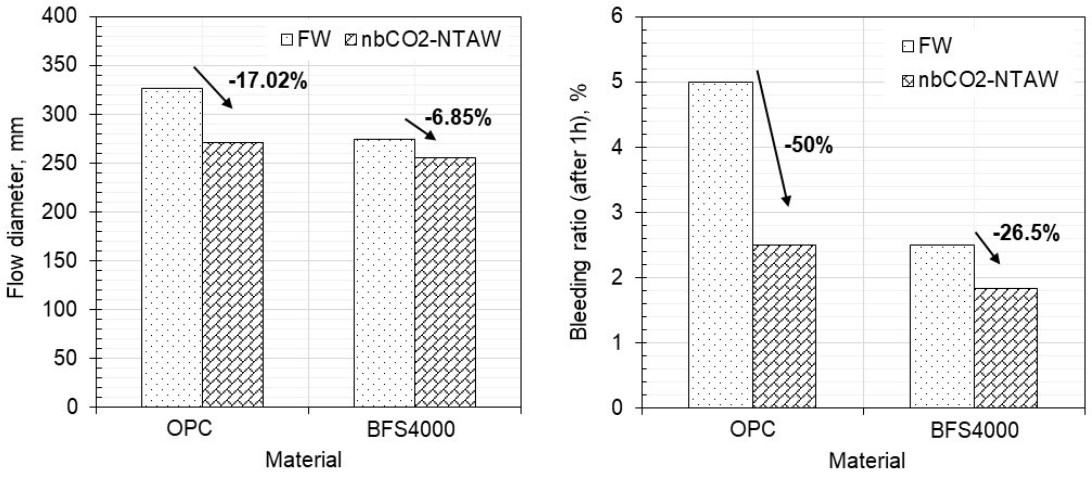

(a) Effect of mixing water type on flow diameter (b) Effect of mixing water type on bleeding ratio

Figure 7. Effect of mixing water type on flow diameter and bleeding ratio of OPC (S0) and BFS4000 (S100) pastes.

3.2 Effect on Low-Carbon Material Properties

In this study, the LCMs were developed by replacing OPC with BFS4000. The mixing proportions for OPC and BFS4000 for 1 m³ are detailed in Table 4. Key performance parameters relevant to ground improvement work such as viscosity, flow diameter, bleeding ratio, and UCS were evaluated. UCS tests were conducted on samples cured for 7 and 28 days. To specifically evaluate the influence of nbCO_2-NTAW on hydration behavior, a dry curing method was employed. This approach minimizes the external water contribution that would otherwise occur in conventional water curing, allowing for clearer assessment of the effects of nbCO_2-NTAW on the hydration process.

Table 5. Comparative summary of the rheological behavior of OPC (S0) and BFS4000 (S100) pastes mixed with either FW or $nbCO_2$-NTAW

Material	OPC (S0)		BFS4000 (S100)	
Mixing water	FW	$nbCO_2$-NTAW	FW	$nbCO_2$-NTAW
Yield stress	Nearly unchanged	Nearly unchanged	Higher	Lower
Plastic/apparent viscosity	Higher at higher shear rate	Lower at higher shear rate	Lower at higher shear rate	Higher at higher shear rate
Shear-thinning behavior	Moderate	Enhanced	Moderate	Strongly enhanced
Flow diameter	Larger	Smaller	Larger	Smaller
Bleeding ratio	Higher	Lower	Higher	Lower

3.2.1 Viscosity

Figure 6 shows the rheological profile of 100% OPC (S0) and 100% BFS4000 (S100) pastes prepared with either FW or $nbCO_2$-NTAW. Both S0 and S100 exhibit shear-thinning characteristics when mixed with $nbCO_2$-NTAW, as shown in Figure 6 and summarized at Table 5. This enhancement is more pronounced in S100, indicating that $nbCO_2$-NTAW has a stronger influence on the rheological properties of BFS4000 compared to OPC.

To assess the impact of $nbCO_2$-NTAW on the viscosity of LCMs, OPC was partially replaced with BFS4000 at 30% (S30), 50% (S50) and 70% (S70) replacement levels. The resulting viscosity measurement are presented in Figure 8.

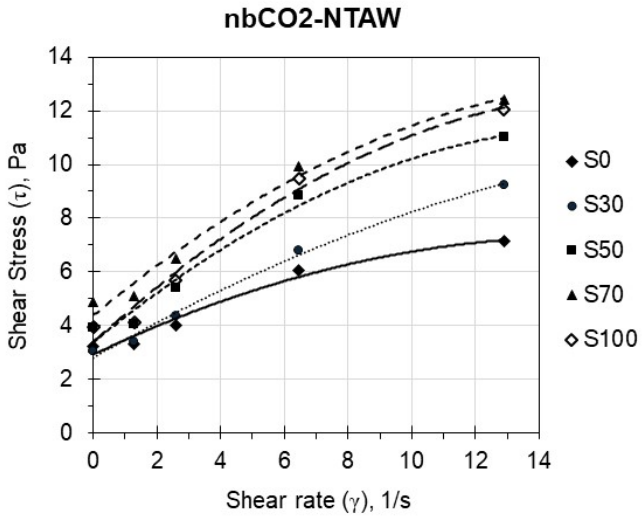

Figure 8. Rheological profile with varying BFS4000 replacement levels mixed with $nbCO_2$-NTAW.

Figure 8 shows that the viscosity of the LCM increases with higher BFS4000 content. This trend aligns with the rheological behavior observed in Figure 6b, when $nbCO_2$-NTAW promotes faster and denser gel formation in BFS4000, increasing cohesion and resistance to flow.

However, this trend does not extend to yield stress. As shown in Figure 8, the yield stress of the S30 remains nearly unchanged compared to S0. A slight increase is observed at S50, but a significant rise occurs at S70, suggesting a threshold effect where BFS4000 becomes dominant in influencing rheological behavior. Remarkably, when OPC is fully replaced by BFS4000 (S100), the yield stress

slightly decreases compared to S70, indicating small amount of OPC may enhance the activation and cohesion of BFS4000 more effectively than BFS4000 alone.

This behavior indicates that nbCO$_2$-NTAW has weaker influence on yield stress when OPC is dominant in the LCM (e.g. S30), as OPC governs the hydration process through its rapid and consistent reaction. In contrast, at higher BFS4000 content (S70), nbCO$_2$-NTAW acts as a chemical activator, accelerating the latent hydraulic reactivity of BFS4000. This leads to early gel formation, resulting in higher yield stress.

3.2.2 Flow diameter and bleeding ratio performance

Due to rapid hydration and enhanced cohesion internal structure promoted by nbCO$_2$-NTAW, the flow diameter of OPC mixed with nbCO$_2$-NTAW is approximately 17% lower than those mixed with FW, as shown in Figure 7a. Additionally, the finer particle size and larger surface area of BFS4000 contribute to a smaller flow diameter compared to OPC.

This trend is further detailed in Figure 9a, which shows the effect of BFS4000 replacement levels on the flow diameter of LCMs mixed with nbCO$_2$-NTAW. When nbCO$_2$-NTAW is used as mixing water, a significant reduction in flow diameter is observed. As the BFS4000 usage increases, the flow diameter continues to decrease, reaching its smallest flow diameter at 70% BFS4000 replacement (S70). Beyond this usage level (e.g. S100), a slight increase in flow diameter occurs, which aligns with the yield stress behavior described in Figure 8. This higher flow diameter observed in S100 is likely due to the retention of more free water, as confirmed by bleeding ratio, as described in Figure 9b.

Figure 9b shows that the bleeding ratio after 1 hour for the S70 mix is lower than that of other OPC and BFS4000 compositions. This suggests that the LCM formulation containing 30% OPC and 70% BFS4000 achieves a balanced combination of reactivity and water retention.

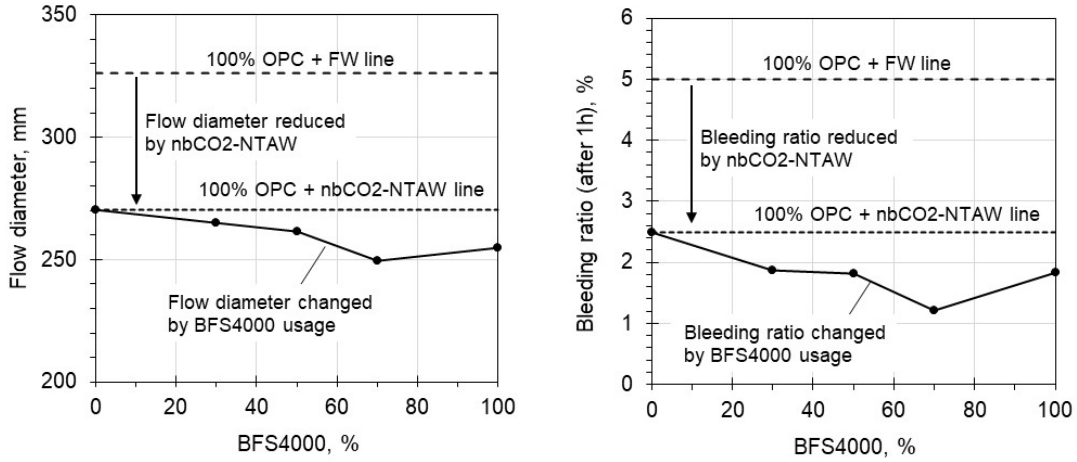

(a) Effect of BFS4000 usage on flow diameter (b) Effect of BFS4000 usage on bleeding ratio

Figure 9. Effect of BFS4000 replacement level on LCMs mixed with nbCO$_2$-NTAW.

3.2.3 Short and long-term UCS performance

The long-term UCS performance of LCMs incorporating nbCO$_2$-NTAW is closely linked to their fresh-state rheological properties. As shown in Figures 8 and 9, the use of nbCO$_2$-NTAW promotes early gel formation and enhances internal cohesion, as evidenced by high yield stress (Figure 8), reduced flow diameter (Figure 9a) and lower bleeding ratio (Figure 9b). These rheological characteristics indicate a stiffer and more cohesive paste, contributing to improved structural integrity during setting and curing. The increased resistance to flow reflects a denser particle network, which supports the development of higher UCS.

The variation in UCS with BFS4000 usage at 7 and 28 days is presented in Figure 10. At 7 days, only the S0 mix (100% OPC) achieves the designated σ_7 strength, due to the immediate and rapid hydration of OPC when mixed with nbCO_2-NTAW. As BFS4000 replaces OPC, the early strength (σ_7) decreases, which is attributed to the latent hydraulic nature of BFS4000, as it reacts more slowly than OPC and contributes less to early strength development.

In contrast, the 28-day strength (σ_{28}) remain stable and meets the designated target even when 70% of OPC is replaced by BFS4000 (S70). This is because BFS4000 mixed with nbCO_2-NTAW which improves the latent hydraulic reactivity efficiency, given sufficient curing time, undergoes hydration and contributes significantly to cementation and strength gain.

However, when the BFS4000 exceeds 70%, the system seems it may lack enough $Ca(OH)_2$ from OPC to activate the BFS4000 efficiently, even with nbCO_2-NTAW. Indicating the nbCO_2-NTAW works well when there is a sufficient mix of reactive components.

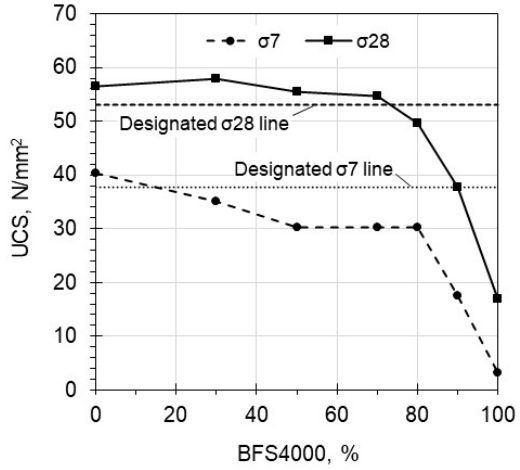

Figure 10. Variation of UCS with BFS4000 content at 7 and 28 days.

3.3 Environmental Impact Analysis

To estimate the amount of CO_2 captured in this study, the volume of CO_2 required to neutralize alkaline water from pH 11.02 to 8 was monitored. Experiment measurements conducted under various gas flow rates (36.38, 58.74, 84.34 and 123.6 mL/min.) showed that, on average, 0.596 L of CO_2 was needed to treat 25 liters of alkaline water using the nbCO_2 method. This result closely aligns with the theoretical calculation, which estimated 0.59 liters of CO_2 for the same pH reduction level (pH 11.02 to 8 of 25 liters of alkaline water), confirming the reliability of the measurement for further analysis.

In this study, the mixes were prepared at multiple BFS4000 replacement ratios (by mass of binder). Under these conditions, the 70% BFS4000 mixture exhibited a rheological profile (shear stress response) superior to the 50% and 100% BFS cases as shown in Figure 8. This indicates that nbCO2-NTAW likely acted as a chemical activator at 70% BFS, as explained in the previous discussion. Assuming that entire 25 liters of nbCO_2-NTAW contains 0.596 liters of CO_2 is used as mixing water, the CO_2 fixation of the S70 mix composition is estimated at 28.9 kg-CO_2 per 1000 m^3 LCM-S70. Although the amount of CO_2 fixation may appear modest compared to the CO_2 emitted during conventional cement production, its impact becomes significant when considered alongside other sustainable benefits. In the S70 mix design, where composed of 30% OPC and 70% BFS4000, the CO_2 emission is reduced up to 67%.

Moreover, this approach supports circular economy principles by eliminating the need for alkaline wastewater treatment, thereby reducing operational costs and environmental burden. The use of nbCO_2-NTAW as mixing water not only conserves freshwater resources in construction applications

but also contributes meaningfully to CO_2 emission reduction, reinforcing its potential as a sustainable solution for ground improvement technologies.

4 CONCLUSION

The nbCO_2-NTAW-based LCM-S70 material offers a sustainable alternative to conventional cementitious slurries used in ground improvement. Its enhanced rheological properties, such as shear-thinning behavior and reduced bleeding, make it ideal for methods like deep mixing and jet grouting. The material maintains sufficient long-term strength even with up to 70% OPC replacement by BFS4000, contributing to a 67% reduction in CO_2 emissions and enabling carbon sequestration of approximately 28.9 kg-CO_2 per 1000 m³ of LCM. Additionally, the use of neutralized alkaline wastewater promotes resource efficiency and environmental safety, making it a valuable innovation for eco-friendly geotechnical engineering.

These findings demonstrate a promising pathway for sustainable ground improvement technologies. Limitations include the need for further pumpability and long-term durability studies. Future research should focus on exploring the scalability of this approach in diverse geotechnical applications.

DISCLAIMER

The authors declare no conflict of interest.

AVAILABILITY OF DATA AND MATERIALS

All data are available from the author.

REFERENCES

Cerron-Calle, G.A., Magdaleno, A.L., Graf, J.C., Apul, O.G., 2022. Elucidating CO_2 nanobubble interfacial reactivity and impacts on water chemistry. *Journal of Colloid & Interface Science*, 607, pp. 720-728.

Feng, H., Lu, S., Guo, A. et al., 2025. Research progress on the water resistance of magnesium phosphate cement-based composites. *Journal of Materials Science*. https://doi.org/10.1007/s10853-025-11462-9

Ha, T.M., Dinh, H.B.T., Dao, T.V., *et al.*, 2025. Utilising Concrete Wash Water to Produce Cement Pastes and Mortars: Effect of Water-to-Binder Ratios. *Iranian Journal of Science and Technology, Transactions of Civil Engineering.* https://doi.org/10.1007/s40996-025-01950-y

Japanese Industrial Standard, 2020. *JIS A 1132:2020 – Method of making and curing concrete specimens.* Tokyo: Japanese Standards Association. First English edition published in 2020-11.

Japanese Industrial Standard, 2020. *JIS A 1216:2020 – Method of one-axis compression test for soils.* In Japanese.

Japanese Industrial Standard, 2024. *JIS A 6206:2024 – Ground granulated blast-furnace slag for concrete.* Tokyo: Japanese Standards Association. First English edition published in 2025-07.

Japan Society of Civil Engineers, 2018. *JSCE-F522-2018: Test Method for Bleeding Rate and Expansion Rate of Grouting Mortar for Prepacked Concrete (Polyethylene Bag Method)*. JSCE, Tokyo, Japan.

Kawai, R., Hamanaka, A., Wahyudi, S., Sasaoka, T., Shimada, H., Abe, T., 2024. *Development of low-carbon cement materials using CO_2 nanobubble.* The Mining and Materials Processing Institute of Japan (MMIJ) Spring Meeting 2024.

Moro, C., Grout, J. & Gonzalez, B., 2023. Effect of Dual CO2 Technologies on the Properties of Mortars with Slag Cement. *International Journal of Civil Engineering*, 21, pp. 1897-1909.

Rajadurai, S.R., Kang, S.T., 2021. Influence of Inter-Particle Distance on the Rheological Properties of Cementitious Suspensions. *Materials*, 14(24), 7869. https://doi.org/10.3390/ma14247869

Schmidt, W., Link, J., 2024. *Rheological Properties. In: Sonebi, M., Feys, D. (eds) Measuring Rheological Properties of Cement-based Materials*. RILEM State-of-the-Art Reports, vol 39. Springer, Cham. https://doi.org/10.1007/978-3-031-36743-4_2

Wahyudi, S., Abe, T., 2022. *Nanobubble Technology for Accelerating Carbonation on Cement-based Material.* Fukuoka, International Symposium on Earth Science and Technology 2022.

Wahyudi, S., Amarakoon., G.G.N.N., Abe, T., Putera, M.A., 2024. *Cement Wastewater Treatment Using CO_2 Nanobubble Technology*. Jakarta, The 28th Annual Scientific Meeting of the Indonesian Geotechnical Society.

Wu, T., Ng, T., Chen, J., 2025. Incorporating carbon capture and storage in decarbonizing China's cement sector. *Renewable and Sustainable Energy Reviews*, 209.

This page is intentionally left blank

HIMPUNAN AHLI TEKNIK TANAH INDONESIA - HATTI
Indonesian Society for Geotechnical Engineering - ISGE
PIT HATTI XXIX
10-12 November 2025

Influence of Underconsolidating Soil on Effective Stress Path in Deep Excavation Case

Albert Sebastian[1] , Aswin Lim[2,*]
[1]Department of Civil Engineering, Universitas Katolik Parahyangan, Bandung, Indonesia, 40141; 8102501017@student.unpar.ac.id
[2]Department of Civil Engineering, Universitas Katolik Parahyangan, Bandung, Indonesia, 40141; aswinlim@unpar.ac.id
*Correspondence: aswinlim@unpar.ac.id

ABSTRACT This study investigates the influence and impact of clay soil that is presumed to be undergoing an underconsolidating process on an unbraced shallow excavation system. The excavation geometry spans up to 160 meters with a maximum depth of 5.25 meters. A concrete sheet pile wall was installed at the front side of the excavation, supported by additional tie beams connected to square precast piles behind the wall. Based on soil investigation data, residual excess pore water pressures were identified within the underconsolidating clay layer at depths between 3 to 12 meters. These residual pore pressures contribute additional loading to the retaining wall system. A back analysis was conducted to obtain appropriate soil parameters for modeling using PLAXIS 2D. The finite element analysis results were compared with inclinometer data to validate the back analysis. Modeling of the underconsolidating condition was performed by manually inputting the pore water pressure into the initial condition. Results show that under underconsolidating conditions, the maximum wall deflection reached 190 mm, whereas under hydrostatic conditions, it was only 100 mm. Additionally, a parametric study was carried out to examine the correlation between the degree of consolidation and wall deflection. The findings indicate that a higher degree of consolidation leads to reduced wall deflection. To confirm the stress changes on the wall due to underconsolidating soil, a stress path analysis was performed to understand the stress history around the excavation. It was found that in underconsolidating conditions, the average effective stress tends to be lower and the deviatoric stress higher, resulting in a stress path that is closer to the failure line.

KEYWORDS Back Analysis; Excavation; FEM; Stress Path; Underconsolidating

This paper will be published in the future issues of Indonesian Geotechnical Journal

This page is intentionally left blank

HIMPUNAN AHLI TEKNIK TANAH INDONESIA - HATTI
Indonesian Society for Geotechnical Engineering - ISGE
PIT HATTI XXIX
10-12 November 2025

An Overview of Different Types of TBM for the Construction of Subway Tunnels in Indonesia

Simon Heru Prassetyo[1*], Dayu Apoji[2], and Visakhadevi Sutandhi[3]

[1]Mining Engineering, Faculty of Mining and Petroleum Engineering, Institut Teknologi Bandung, Bandung, Indonesia
[2]Civil Engineering, Faculty of Civil and Environmental Engineering, Institut Teknologi Bandung, Bandung, Indonesia
[3]Civil and Structure Section Head, PT. MRT Jakarta, Jakarta, Indonesia
*Correspondence: simon@itb.ac.id

ABSTRACT For millions of commuters in Jakarta, mass rapid transit (MRT) is an essential lifeline that offers convenience as they travel between destinations. Additionally, the development of modern urban MRT systems in other metropolitan areas of Indonesia, with their crucial use of subway tunnels, represents a significant advancement in public transportation and deserves our highest appreciation. Given the extensive length of subway tunnels and their presence in urban environments, the use of tunnel boring machines (TBMs) has emerged as the most effective and preferred approach. This fully mechanized excavation method has demonstrated substantial efficiency and safety throughout the construction process. The question that guides our study is: considering the various types of TBMs and ground conditions, which machine is most suitable for a specific subway tunnel project? In this paper, we will highlight various types of TBMs, discussing their primary components, applications, and notable examples of their implementation in subway tunnel construction. Furthermore, we will present two detailed case studies that illustrate the process of selecting an appropriate TBM for tunnelling in both soft ground and hard rock conditions, specifically in the context of a typical subway tunnel project in Indonesia.

KEYWORDS Mass rapid transit; subway tunnel; urban tunnel; TBM; soft ground tunnelling; hard rock tunnelling

This paper will be published in the future issues of Indonesian Geotechnical Journal

This page is intentionally left blank

Sub-Surface Movement Detection in a Tailings Storage Facility: Evaluating Inclinometer Real-Time Monitoring and Design Specification (Case Study: Martabe Gold Mine)

Syavira Indah Utami[1,*], Anggie Hardian[2], Zubeyir Siregar[3], Prianta Ginting[4], Titik Astiwi[5]
[1]Junior Engineer, PT Agincourt Resources, Indonesia, 22738; syavira.utami@agincourtresources.com
[2]Superintendent Engineering, Department TSF, PT Agincourt Resources, Indonesia, 22738; anggie.hardian@agincourtresources.com
[3] Engineer, Department TSF, PT Agincourt Resources, Indonesia, 22738; zubeyir.siregar@agincourtresources.com
[4] Manager, Department TSF, PT Agincourt Resources, Indonesia, 22738; prianta.ginting@agincourtresources.com
[5]Senior Engineer, Department TSF, PT Agincourt Resources, Indonesia, 22738; titik.astiwi@agincourtresources.com
*Correspondence: syavira.utami@agincourtresources.com

ABSTRACT

The Tailings Storage Facility (TSF) at Martabe Gold Mine, one of Indonesia's largest tailings dams, with a design capacity up to 80 million tonnes of tailings across 180 hectares, with a dam height of 117 meters and a length of 1.2 kilometers. Classified as an extreme consequence facility because of the potential risk to surrounding communities, the TSF requires precise design, construction, and continuous monitoring to maintain long-term stability and operational safety. This study evaluates how application of real-time inclinometer monitoring systems in detecting sub-surface movements at TSF Martabe and examines how the monitoring results compare with the original design specifications developed by the consultant, Knight Piésold. Automatic inclinometers installed at critical subsurface zones to continuously monitor deformation, allowing early detection of movement that could signal slope instability. The integration of real-time monitoring is linked to the Trigger Action Response Plan (TARP) thresholds, helping the site team to risk-based decision-making. Recorded displacements value remains within the design limits, with slightly higher movements observed in the upper embankment related to active area construction. In conclusion, the integration of inclinometer-based real-time monitoring with validated design criteria enhances slope stability management at Martabe's TSF. This approach enables proactive intervention before critical thresholds are exceeded, promotes safe and sustainable TSF operations in line with international standards such as the Global Industry Standard on Tailings Management (GISTM), and emphasizing the integration of innovative geotechnical engineering and field monitoring practices.

KEYWORDS: Tailings Storage Facility (TSF); Inclinometer Real-Time Monitoring; Sub-Surface Movement Detection, Slope Stability, Geotechnical Design Specifications

1 INTRODUCTION

The Martabe Gold Mine, located in South Tapanuli, North Sumatera, Indonesia, is operated by PT Agincourt Resources (PTAR), processed approximately 5.7 to 6.9 million tons of ore per year, producing more than 200,000 ounces of gold and 1-2 million ounces of silver annually, making it one of the largest gold mines in Indonesia. Ore is currently extracted from three active pits, namely Purnama, Barani, and Ramba Joring. A Tailings Storage Facility (TSF) at Martabe Gold Mine is designed to accommodate 77.8 million tonnages of tailings, with a planned crest elevation of 377 m above sea level, plays a crucial role by providing engineered containment structures for minewaste management to protect the environment and ensure operational safety.

Global concern for tailings dam safety monitoring has increased due to catastrophic failures of such dams caused by increasing tailings waste volumes and larger dam constructions. The integrity and

safety of a TSF relies on conservative designs, diligent operations, and continuous, cost-effective monitoring. Given the severe consequences of tailings dam failures, it is important to understand failure mechanisms and implement effective risk mitigation measures.

As summarized in Table 1, understanding failure modes and monitoring key parameters – such as pore-water pressure, surface, and sub-surface movements – is crucial for monitoring dam structural stability, ensuring compliance with safety standards, and selecting appropriate monitoring instruments. The behavior causing surface movement instability in TSFs typically involves weakening of materials due to changes in physical and mechanical properties of soil or waste, increased pore-water pressure which reduces shear strength, and environmental factors such as heavy rainfall and seismic activity. These factors can trigger cracking, deformation, and surface displacement that affect slope stability and embankment deformation.

Table 1. Failure modes and corresponding monitoring parameters

Failure Mode	Monitored Parameter and Behaviour
Slope instability	Displacement, rotation, settlement, pore pressure change, tension crack
Earthquake	Ground acceleration, pore pressure change, settlement
Overtopping	Freeboard change, pore pressure change, seepage flux
Seepage	Seepage quantity and quality, settlement/sloughing
Foundation	Displacement, rotation, tension crack
Structural	Displacement, tension crack, seepage (core failure)
Mine subsidence	Ground acceleration, settlement
Erosion	Effluent quantity and quality change, surface elevation changes

The purpose of this study is to evaluate the performance of real-time monitoring systems in detecting subsurface movement in response to mine waste deposition during the construction of the TSF Martabe and to compare the monitoring results with the original geotechnical design specifications prepared by the consultant, Knight Piesold. A major challenge in the mining sector is implementing monitoring systems for tailings dams that are both effective and efficient. Although TSFs are essential for large-scale mining operations, these facilities pose significant risks; failures or leakage events can cause serious harm to mining companies, nearby communities, and the environment. Therefore, continuous and adequate monitoring systems are crucial to reducing the likelihood of failures and minimizing their potential impacts.

The stability of a TSF depends not only on the engineering design and construction but also on continuous and accurate monitoring results that can identify deformation at an early stage. Real-time instrumentation, such as In-Place Inclinometers (IPIs) and Shape Array Accelerometers (SAAs), provide valuable data for understanding subsurface behavior during mine waste placement and for validating design assumptions under actual field conditions.

The study integrates real-time inclinometer monitoring data with geotechnical design spesiifications and Trigger Action Response Plan (TARP) thresholds to assess how observed movements align with the predicted deformation limits at the TSF. The findings aim to enhance slope stability management at TSF Martabe by improving early warning capability and supporting the team to risk-informed decision-making. This research contributes to the safe and sustainable operation of the facility and provides practical insights into other large-scale tailings storage facilities operating under similar conditions to minimizing environmental impact and ensuring compliance with regulatory standards.

2 METHODS

2.1 Instrumentation Overview

Tailings Storage Facilities (TSFs) require careful stability management because changes in the foundation conditions, staged embankment raises, and repetitive loading from tailings deposition may trigger subsurface deformation before visible signs appear at the surface. Geotechnical instrumentation provides a quantitative approach to monitor slope instability, detect early warning

signs, and track the progression slope behaviour. These instruments are essential throughout TSF design, construction, and monitoring phases and verify design assumptions, help monitor changing conditions during construction, and ensure TSF stability and safety.

Inclinometer systems – including manual probes, automated in-place inclinometers (IPIs), and shape arrays—are commonly used to detect lateral ground movement and identify potential shear zones that could affect slope stability. Installed within TSF embankments, these instruments monitor deep-seated displacement and assess their impact on embankment integrity. As the embankment is raised, inclinometers are extended accordingly. Each instrument is monitored at scheduled intervales defined in the monitoring program. Displacements exceeding trigger thresholds defined in the Trigger Action Response Plan (TARP) may indicate stability issues requiring investigation and potential remedial actions based on the findings.

At the TSF Martabe, there are two types of sub-surface movement monitoring tools are used to monitor subsurface movement such as In-Place Inclinometers (IPIs) and Shape Arrays (SAA). These instruments continuously collect displacement data used throughout the TSF lifecycle – from design verification to operational safety management. A summary comparative between the two types of instruments is also presented in Table 2. The following below is an overview of each monitoring tool's methodology and how the data align with the design requirements.

Table 2. Comparison between IPIs and SAA system

Specification	In-Place Inclinometer (IPIs)	Shape Array Accelerometer (SAA)
Measurement	Tilt sensor (biaxial MEMS)	MEMS array
Spatial Resolution	Sensor per-3 meters	Vertical sensor per-0.5 meters
Precision	Deformation accuracy ±2 mm for 30 m	Deformation accuracy ±1.5 mm for 32 m
Angle Accuracy	±1	±1
Sampling Frequency	1 – 4 hours	4 hours
Power and Communication	Depending on system, can be wired / data logger	Can be wired / data logger / wireless with PC
Installation	Requires special casing, more rigid	More flexible, using PVC casing
Resistance	Will not be able to install into damaged, deformed, or spiralized casing	Resistant to large deformations, can monitor large shifts

2.1.1 In Place Inclinometers (IPIs)

In-Place Inclinometers (IPIs) is designed installed permanently within boreholes, IPIs provide real-time measurements of lateral displacement at multiple depths. Data is collected at intervals ranging from 1 to 4 hours, enabling detection of deep-seated movements and shear zones that could threaten embankment stability. The system consists of a series of MEMS sensors connected by steel bay rods, each approximately 3 meters long. These sensors continuously measure angular displacement (tilt) at multiple depths, producing high-resolution subsurface lateral movement profiles. IPIs offer automated data logging, eliminating the need for manual probing, which facilitates continuous monitoring and timely identification of gradual or sudden ground deformations and potential slip surfaces within the embankment or foundation.

Figure 1. Field Installation of IPIs at TSF Martabe

2.1.2 Shape Array (SAA)

Shape Array inclinometers use flexible sensing cables inserted into protective casings within boreholes. The cables contain multiple inclinometer sensors spaced along their length, generating continuous displacement profiles as the cable bends or deforms. These systems provide high spatial resolution with sensors positioned every 0.5 meters vertically (or 1 meter horizontally), capturing detailed deformation and shape changes in subsurface soil or tailings. Data acquisition can be fully or semi-automated, enabling regular monitoring and early detection of slope movement and failure mechanisms.

Figure 2. Field Installation of SAA at TSF Martabe

2.2 Data Acquisition and Monitoring

Geotechnical instruments provide real-time data on TSF behavior, enabling engineers to detect and address issues before they become critical. The monitoring system utilizes Internet of Things (IoT) technology, illustrated by the topology on Figure 3, to achieve automated, continuous data acquisition from sensors to centralized data processing. Data from IPIs and SAAV are processed to identify trends, peak displacements, and rates of movement that are indicative of potential failures, facilitating prompts interventions to stabilize the structure.

These IoT-enabled monitoring frameworks integrate automated data logging, wireless communication, and cloud-based analytics, allowing seamless transformation of raw sensor signals into actionable risk assessments and response triggers. By providing real-time insights into subsurface movements and environmental conditions, the system supports proactive decision-making for risk mitigation and remediation, thereby enhancing TSF safety and operational resilience.

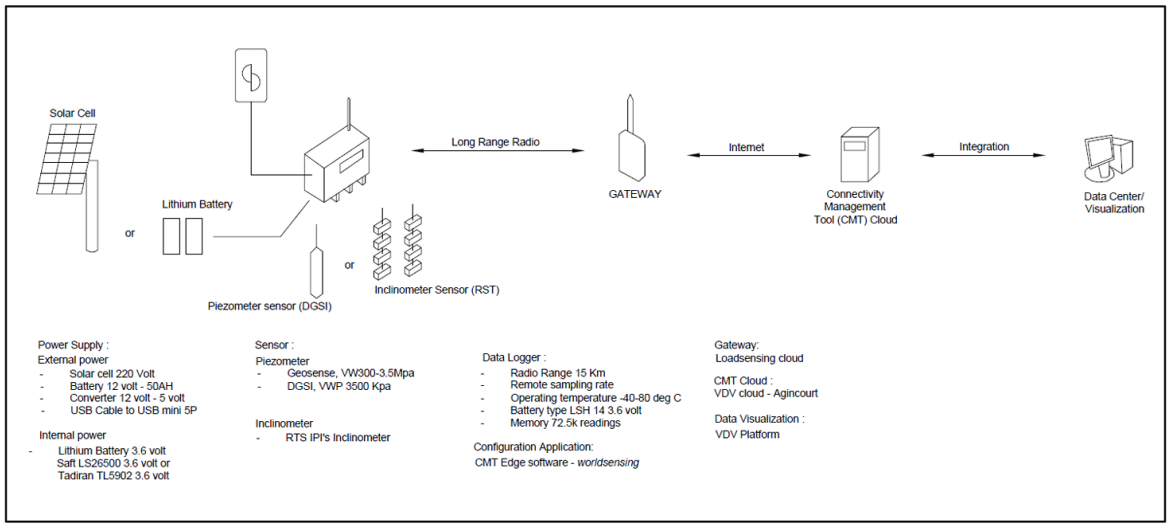

Figure 3. Topology of IoT-based for Instrumentation Monitoring at TSF Martabe Gold Mine.

2.3 Design Requirements of TSF Dam and Trigger Frameworks

The TSF dam design was developed using 3D finite element analysis via Plaxis 3D by the consulting firm, Knight Piesold, including stability, pore-water pressure, seismic, and deformation evaluations. The design of TSF Martabe Gold Mine follows the ANCOLD Standard to ensure safety and performance. Design consultants perform stability analyses based on minimum safety factors, from which operational deformation criteria are derived. These criteria guide the assessment of stability and deformation, as provided by the consultant, illustrated in Figure 4.

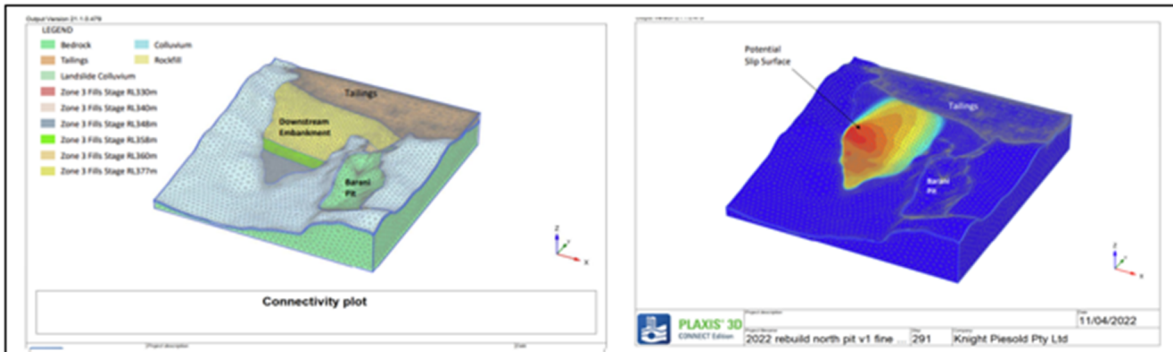

Figure 4. Stability and Design Analysis of TSF Embankment.

Table 3 presents the forecast for the horizontal embankment deformation rate during the RL373 m construction phase using Plaxis 3D finite element modelling.

Table 3. Forecast horizontal deformation

Embankment Location	Forecast deformation
Upper (>RL260 m)	Up to 35 mm / month
Middle	Up to 30 mm / month
Lower (<RL200 m)	Up to 10 mm / month

Trigger levels are established for various monitoring instruments to flag elevated or unexpected readings that require investigation. These trigger levels, documented in the Trigger Action Response Plan (TARP), are regularly updated to reflect ongoing construction and changing embankment geometry. Specifically, inclinometer movement triggers are as follows with the list and Table 4:

a) For the embankment fill, the trigger level is limited to 40 mm/month.
b) For the foundation zone, two different trigger levels are proposed, 20 mm/month within the landslide area, and 10 mm/month outside the landslide area.

Table 4. Summary of trigger level for existing inclinometers

Zone	ICN	Trigger Level (mm/month)	
		Embankment Fill	Foundation Zone
Outside Landslide Zone	ICN-08 ICN-11 ICN-14 ICN-22 ICN-23 ICN-24 ICN-26 ICN-27 ICN-28	40	15
Inside Landslide Zone	ICN-09 ICN-10 ICN-17 ICN-18 ICN-19 ICN-20 ICN-21 ICN-25 ICN-29	40	20

Displacements exceeding these trigger levels must be reported to the TSF embankment Engineer of Record (EoR) for review. Sudden or distinct deformation patterns should prompt repeated measurements and confirmation. Upon confirming exceedance or concerning deformation, the EoR must be consulted to recommend further actions.

3 RESULTS

3.1 Monitoring Results

Subsurface movement monitoring at Martabe Gold Mine is conducted in real-time using an IoT framework integrated with the online platform, Vista Data Vision, which issues immediate warning alerts to users for proactive response. Eighteen inclinometers (7 Shape Arrays and 11 In-Place Inclinometers) are strategically deployed across critical TSF embankment zones (Figure 5). These instruments record displacement data at intervals ranging from 1 to 4 hours, providing high-resolution, real-time insights into subsurface behavior.

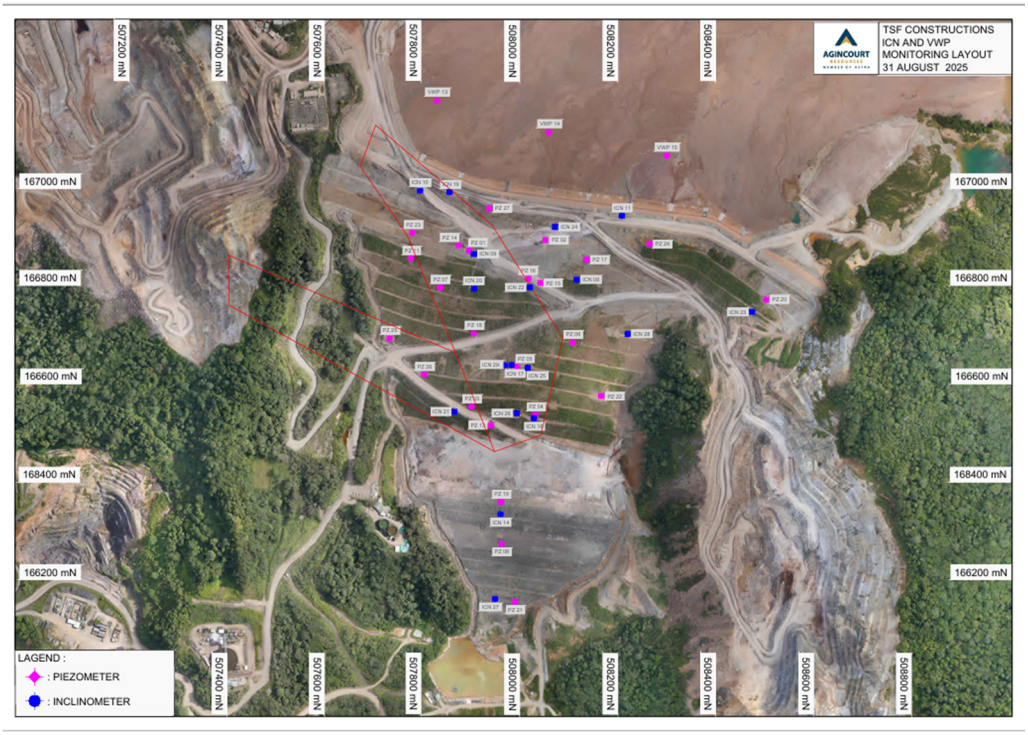

Figure 5. Sub-surface Movement Instrumentation Map TSF Layout.

Time-series analysis over six months indicates that lateral displacements are generally stable and consistent with expected staged construction and consolidation processes, rather than progressive shear failure. Maximum monthly lateral displacements by section are summarized in Table 5 as follows:

Table 5. Maximum monthly lateral displacements of inclinometers at TSF embankment.

Position	Inclinometer ID	ICN Type	Average Deformation/month (mm)		Average Deformation/month (mm)	
			Foundation	Embankment Fill	Foundation	Embankment Fill
			Per-station (mm/month)		Per-location (mm/month)	
Upper	ICN-08	IPIs	1.5	1	1	7
	ICN-09	SAA	1.5	6		
	ICN-10	SAA	1	10		
	ICN-11	SAA	1	1		
	ICN-23	IPIs	1	2.5		
	ICN-24	IPIs	1	7		
	ICN-19	IPIs	1	10		
	ICN-20	SAA	1	2		
	ICN-22	SAA	1	8		
Middle	ICN-17	IPIs	2.5	4	2	4
	ICN-18	IPIs	1	5		
	ICN-21	IPIs	2.5	3		
	ICN-25	SAA	1	3		
	ICN-26	IPIs	1.5	2.5		
	ICN-29	IPIs	3	4		
	ICN-28	IPIs	1	3.5		
Lower	ICN-14	SAA	1	4	1	3
	ICN-27	IPIs	1	2		

The upper fill zone exhibits the highest displacement rates (7 mm/month) due to active tailings deposition, while foundation movements remain minimal (1 mm/month), for example displacement graph data for ICN-22 using SAA system on Figure 6 and Figure 7. In the middle section, foundation movements (4 mm/month) slightly exceed fill rates, suggesting deeper subsurface redistribution along stratigraphic or construction interfaces. The lower section shows uniformly low displacements, reflecting limited placement activity and greater stiffness at depth, for example displacement graph of ICN-27 that uses IPIs system on Figure 8.

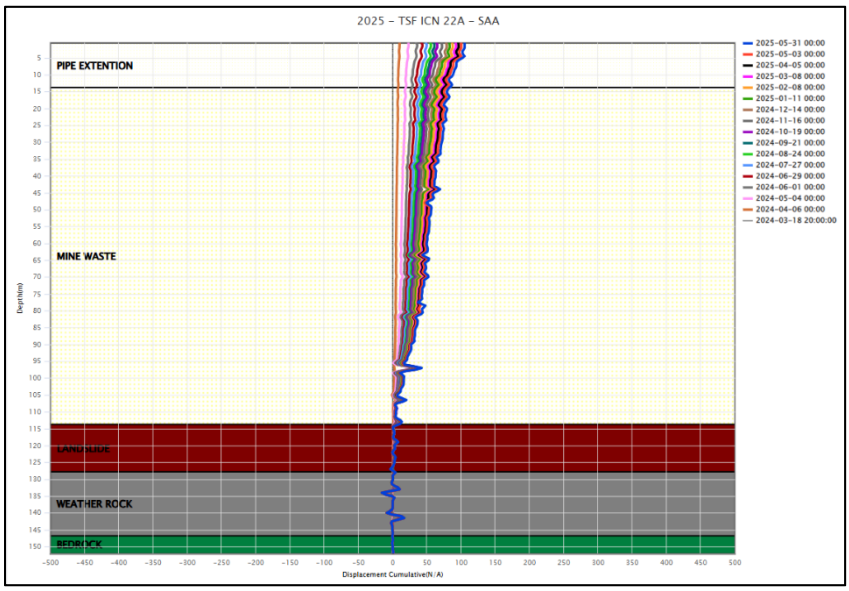

Figure 6. Cummulative Displacement Graph ICN-22 at Upper Embankment TSF using SAA.

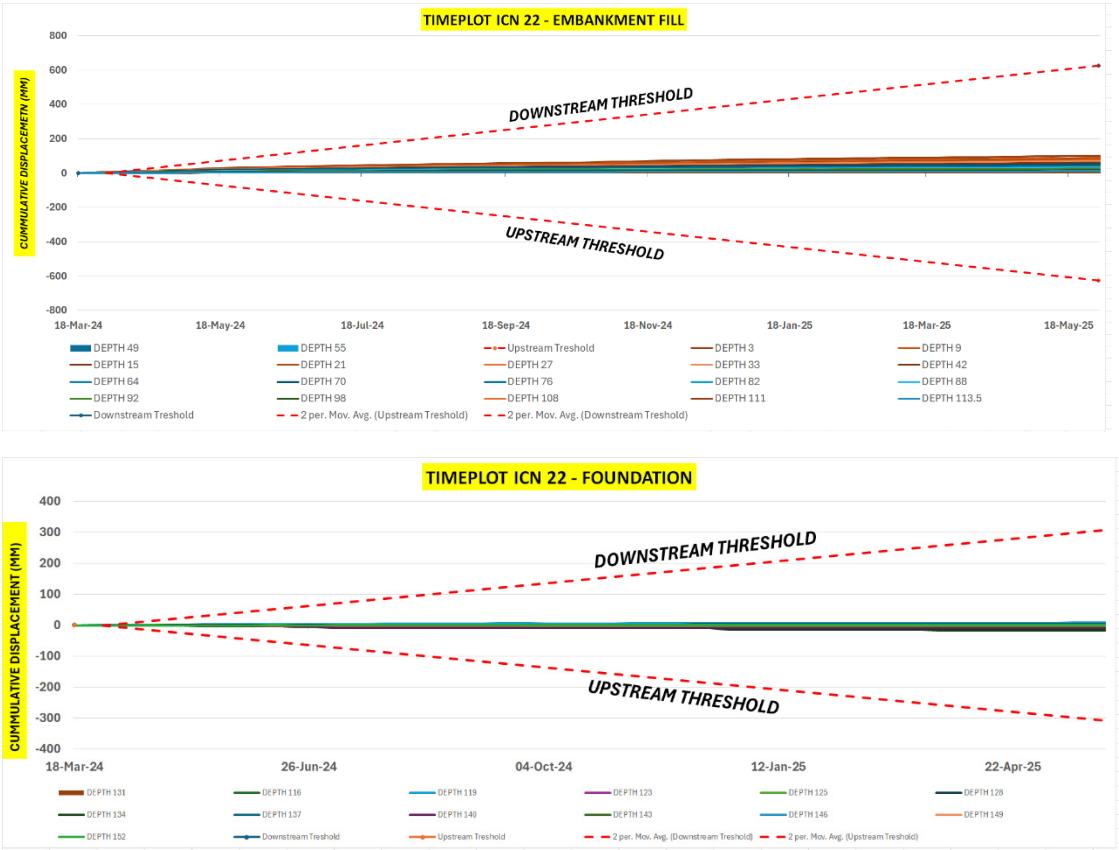

Figure 7. Timeplot Graph ICN-22 at Upper Embankment TSF using SAA.

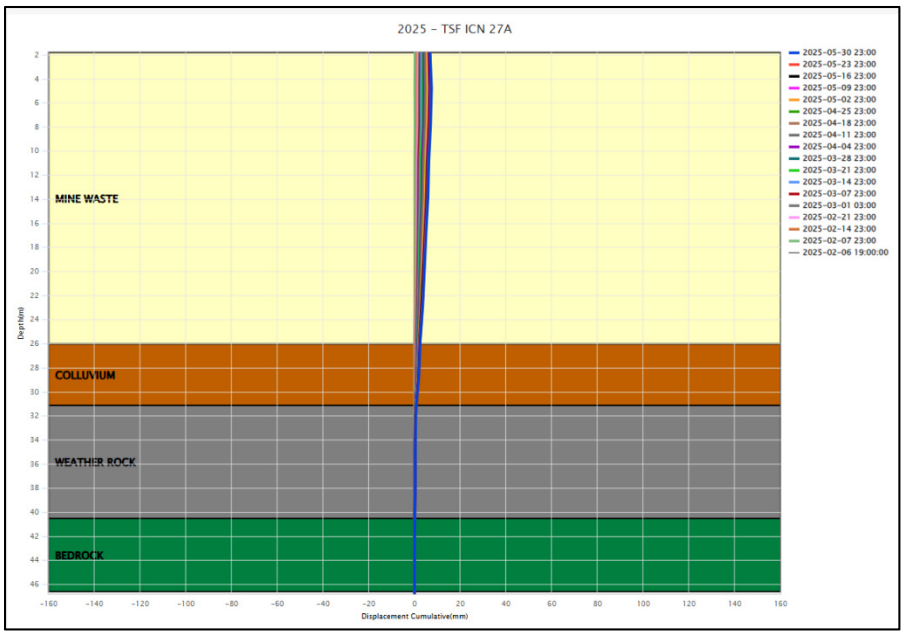

Figure 8. Cummulative Displacement Graph ICN-27 at Middle Embankment TSF using IPIs.

Figure 9. Cummulative Displacement Graph ICN-27 at Middle Embankment TSF using IPIs.

Both inclinometer types demonstrated consistent, reliable displacement trends without abrupt or accelerating movements, affirming measurement robustness across sensors. Data collected at frequent intervals enabled detection of transient displacement spikes, providing early-warning capability to mitigate potential stability risks. Overall, the integration of Shape Arrays and In-Place

Inclinometers with rapid data acquisition supports effective monitoring aligned with design trigger levels, promoting proactive slope stability management crucial for TSF safety.

3.2 Comparison of Sub-surface Monitoring with TSF Design Requirements

The sub-surface movement data collected at TSF Martabe were rigorously compared to the TSF design criteria and classified according to the Trigger Action Response Plan (conditions). Throughout the six-month monitoring period, no displacement exceeded the action or critical trigger levels, indicating that the TSF dam remains within the standard operation classification, as summarized in Table 6.

Table 6. Summary displacement of inclinometers at TSF embankment

Section	Zone	Displacement (mm/month)		Remarks
		Actual	Design Criteria	
Upper	Embankment	7	40	OK
	Foundation (Outside Landslide Zone)	1	15	OK
	Foundation (Inside Landslide Zone)	1	20	OK
Middle	Embankment	4	40	OK
	Foundation (Outside Landslide Zone)	2	15	OK
	Foundation (Inside Landslide Zone)	2	20	OK
Lower	Embankment	3	40	OK
	Foundation (Outside Landslide Zone)	1	20	OK

The design criteria define the maximum allowable displacements that correspond to embankment performance stability. Comparing real-time inclinometer data results with these trigger levels helps to ensure that the observed embankment behavior remains consistent with the design expectations. The TARP matrix, illustrated in Figure 8, serves as an practical decision-making framework that translates continuous monitoring results into actionable and clear operational actions. This study highlights the importance of a continuous feedback loop in which advanced subsurface monitoring directly supports both design validation and safety operational compliance. The strong correlation between real-time inclinometer readings and the predefined deformation limits confirms that the Martabe Gold Mine TSF maintains its structural integrity and operational safety in dynamic conditions.

Item		Standard Operation	Yellow Trigger	Yellow Action	Orange Trigger	Orange Action	Red Trigger	Red Action
Vibrating Wire Piezometers (Within embankment)		Fluctuates starting from negative to slightly positive reading depending on install depth.	Greater than set trigger levels	Remeasure to ensure reading correct. Highlight for checking in next reading.	Readings maintaining or increasing greater than the set trigger levels	Cease material placement or surcharge load within 100 m of trigger breached piezometer for at least two weeks. Assess overall phreatic surface and embankment stability. Inspect for obvious cracking, settlement, slumping, wet spots etc.	Readings maintaining or increasing greater than the set trigger levels	Conduct stability/deformation modelling. Prepare buttress works if required.
Standpipe Piezometers (Within embankment)		Fluctuates from dry to positive readings below ground level	Greater than natural ground in the vicinity of the standpipe	Remeasure to ensure reading correct. Highlight for checking in next reading.	Greater than 0.5 metre increase per month, or 6 metres per year	Cease material placement or surcharge load within 100 m of standpipe for at least two weeks. Assess overall phreatic surface and embankment stability. Inspect for obvious cracking, settlement, slumping, wet spots etc.	Greater than 1.0 metre increase per month, or 12 metres per year	Conduct stability/deformation modelling. Prepare buttress works if required.
Embankment Settlement Pins or Prisms (Within embankment)		Typical fluctuations in survey readings	Greater than 40 mm change from previous monthly reading	Remeasure to ensure reading correct. Check directional movement. Highlight for checking in next reading.	Greater than 80 mm change from previous 3 monthly readings	Check all for directional movement. Install additional settlement pins or prisms. Inspect for obvious cracking, settlement, slumping, wet spots etc.	Greater than 120 mm change from previous 3 monthly readings	Conduct stability/deformation modelling. Prepare buttress works if required.
Inclinometers (Within embankment, Fill Zone)		Typical fluctuations in readings	Greater than 40 mm change in a month or 200 mm in total / year	Remeasure to ensure reading correct. Check directional movement. Highlight for checking in next reading.	Greater than 80 mm change in a month or 400 mm in total / year	Check all for directional movement. Inspect for obvious cracking, settlement, slumping, wet spots etc.	Greater than 120 mm change in a month or 600 mm in total / year	Conduct stability/deformation modelling. Prepare buttress works if required.
Inclinometers (Within Embankment Foundation)	Outside Landslide Zone	Typical fluctuations in readings	Greater than 15 mm change in a month or 150 mm in total / year	Remeasure to ensure reading correct. Check directional movement. Highlight for checking in next reading.	Greater than 30 mm change in a month or 240 mm in total / year	Check all for directional movement. Inspect for obvious cracking, settlement, slumping, wet spots etc.	Greater than 45 mm change in a month or 450 mm in total / year	Conduct stability/deformation modelling. Prepare buttress works if required.
	Inside Landslide Zone		Greater than 20 mm change in a month or 200 mm in total / year		Greater than 40 mm change in a month or 400 mm in total / year		Greater than 60 mm change in a month or 600 mm in total / year	
Seismic Monitoring (Within embankment)		-	-	-	Modified Mercalli Intensity Scale V or less (Felt outdoors as well as indoors, liquid disturbed, small objects displaced, doors swing, pictures move)	Inspect pipelines for rupture or leakage. Inspect embankments and decants for obvious deformation or movement. Monitor all instrumentation immediately after the event and weekly thereafter until readings return to normal. If any damage or leakage is observed, immediately arrange for an inspection.	Modified Mercalli Intensity Scale VI or greater (Difficulty standing, hanging objects quiver, masonry cracks, waves on ponds, some minor injuries)	Immediately terminate deposition of tailings into the TSF and pumping from the decant. Immediate inspection of facility embankments and decants for obvious deformation or movement. Immediate inspection of all pipes including residue pipeline(s) for rupture or leakage. Arrange for immediate inspection and report of storage by a suitably qualified geotechnical engineer.

Figure 8. Trigger Action Response Plan (TARP) at Martabe TSF RL373 m Embankment

4 DISCUSSION

Both inclinometer instrumentations, the In-Place Inclinometers (IPIs) and Shape Array Inclinometers (SAA) have proven consistent and comparable performance in detecting subsurface movement trends in the TSF Martabe. The displacement data from both instrumentations show aligned patterns and respond predictably to nearby construction activities, indicating stable sensor performance and reliable data quality. The real-time monitoring results also consistent with the geotechnical design specifications developed by the consultant Knight Piesold through Plaxis 3D modeling, confirming that observed displacements remain well below the predicted deformation limits. This correlation validates that the implemented design measures and monitoring systems are effective in maintaining slope stability and providing early-warning detection of potential instability.

The monitoring system not only confirms design expectations but also plays a crucial role in identifying any unexpected or localized movements that could indicate early stage of instability. Real-time data integration with visualization and emergency alerts allows the team to respond promptly and enhancing operational safety. For future improvements, predictive analytics monitoring using anomaly detection algorithms is expected to further improve the ability to forecast and mitigate risks proactively, reducing potential impacts and operational costs.

Trigger Action Response Plans (TARPs) serves as the operational link between monitoring results and field actions. Effective TARPs depend on accurate and redundant data, achieved in this study through the combined use of IPIs and SAAs. This ensures reliable detection of critical displacements and supports timely escalation of alerts within the site's risk management framework. Continuous development in sensor technology, wireless communication, and integrated data analysis will further enhances TSF monitoring systems, contributing to safer and more sustainable tailings dam management at the Martabe Gold Mine.

5 CONCLUSION

This study evaluated and assessed subsurface movements behavior at the TSF Martabe by comparing real-time inclinometer monitoring data with the original geotechnical design spesifications by the consultant, Knight Piesold. The strong agreement between field observation and predicted

deformation limits confirms that the TSF is performing safely under current operational conditions. This validation highlights the critical role of integrated geotechnical monitoring in supporting sustainable infrastructure and driving resilience within tailings dam management. The results lead to the following conclusion:

a) Alignment with Design Spesifications
Data from the In-Place Inclinometers (IPIs) and Shape Array Accelerometers (SAAs) are consistent with the design criteria for the TSF. Recorded displacements remain well below the allowable deformation limits, validating both the design assumptions and construction quality.
b) Zone-Specific Movement Trends
Displacement rates vary across different zones of the TSF, with higher rates observed in actively constructed and filled upper sections. All zone-specific movements remain within and below thresholds, confirming that the staged construction and buttress design effectively control deformation.
c) Monitoring System Performance
The integrated real-time system provides reliable, continuous measures that allow early detection of abnormal trends. When combined with visualization tools and automated alerts, the system enhances the site's ability to respond quickly and maintain safe operating conditions.
d) Trigger Action Response Plan (TARP) Integration
Monitoring results are directly linked to TARP procedures, converting data into clear operational actions. This linkage ensures systematic escalation, timely field inspections, and prompt mitigation whenever threshold levels are approached.
e) Recommendations for Future Improvements
Further progress in IoT-based sensors, data connectivity, and predictive analytics will strengthen early-warning capability and optimize decision-making. Continued refinement of these technologies will help the Martabe operation—and similar facilities—achieve safer, more adaptive, and sustainable tailings management practices aligned with the Global Industry Standard on Tailings Management (GISTM).

REFERENCES

Smith, Geotechnical Engineering: Principles and Practices, 2nd ed. New York, NY, USA: Wiley, 2020.

Johnson and C. Lee, "Real-time monitoring of tailings storage facilities using inclinometers," Journal of Mining Science and Technology, vol. 15, no. 3, pp. 120-130, May 2023.

Brown, "Innovations in slope stability monitoring for sustainable infrastructure," in Proc. Int. Conf. Geotechnical Engineering, Jakarta, Indonesia, 2SSS025, pp. 45-52.

Knight Piesold, "Martabe Gold Mine TSF Monitoring Report," Knight Piesold Ltd., Johannesburg, South Africa, Rep. KPL/2023/001, Apr. 2023.

World Bank Group, "Guidelines for Tailings Storage Facilities," World Bank, Washington, DC, Tech. Rep. 2024, [Online]. Available: https://openknowledge.worldbank.org/bitstream/xyz

Agincourt Resources, "Tailings Facility Disclosure 2022," Agincourt Resources, Toronto, Canada, 2022. [Online]. Available: https://agincourtresources.com/2022/tailings-disclosure

N. Adamo, N. Al-Ansari, V. Sissakian, J. Laue, and S. Knutsson, "Dam Safety: Monitoring of Tailings Dams and Safety Reviews," Journal of Earth Sciences and Geotechnical Engineering, vol. 11, no. 1, pp. 249-289, 2021. [Online]. Available: https://www.scienpress.com/Upload/GEO/Vol%2011_1_7.pdf

"Slope Stability: Monitoring and Application Methods in Open Pit Mining Activities," International Journal of Scientific & Technology Research, Feb. 2021. [Online]. Available: https://www.ijstr.org/final-print/feb2021/A-Review-On-Slope-Monitoring-And-Application-Methods-In-Open-Pit-Mining-Activities.pdf

J. Smith and M. Doe, "Slope Stability Analysis Based on Real-time Displacement Measurements," 2018. [Online]. Available: https://www.researchgate.net/publication/327538004_Slope_Stability_Analysis_Based_on_Real-time_Displacement_Measurements

"Shapearray vs Digital In-place Inclinometer Systems," Measurand, 2023. [Online]. Available: https://measurand.com/blog/shapearray-vs-digital-in-place-inclinometer-systems/

RST Instruments, MEMS In-Place Inclinometer System Instruction Manual, 2019. [Online]. Available: https://rstinstruments.com/wp-content/uploads/ICM0062K-MEMS-In-Place-Inclinometer-System-Instruction-Manual.pdf

Lilmount, "Slope Stability Inclinometer Monitoring: Protecting Canada's Infrastructure and Natural Landscapes," 2024. [Online]. Available: https://lilmount.ca/blogs/slope-stability-inclinometer-monitoring-protecting-canadas-infrastructure-and-natural-landscapes

Waste Advantage Magazine, "Management of Slope Stability Risks Using Geotechnical Instrumentation at Landfills," 2023. [Online]. Available: https://wasteadvantagemag.com/management-of-slope-stability-risks-using-geotechnical-instrumentation-at-landfills/

Knight Piésold Pty Limited, Tailings Storage Facility Operations, Maintenance and Surveillance Manual – RL373 m Embankment (Rev. 0)., PT Agincourt Resources, Martabe Gold Project, Perth, Western Australia, Nov. 2024. [Online]. Available: Internal document, PT Agincourt Resources.

RST Instruments, "ShapeArray versus In-Place Inclinometer Systems – Webinar Q&A," 2024. [Online]. Available: https://rstinstruments.com/blog/shapearray-versus-in-place-inclinometer-systems-webinar-qa/

Measurand, "ShapeArray vs. Digital In-Place Inclinometer Systems," 2024. [Online]. Available: https://measurand.com/blog/shapearray-vs-digital-in-place-inclinometer-systems/

G. Swarbrick, "The Importance of Understanding Piezometer and Inclinometer Data for TSF Management," in Proceedings of the 2015 International Seminar on Design, Operation and Closure of Tailings Storage Facilities, Perth, Australia, Aug. 2015. [Online]. Available: https://papers.acg.uwa.edu.au/p/1508_10_Swarbrick/

This page is intentionally left blank

HIMPUNAN AHLI TEKNIK TANAH INDONESIA - HATTI
Indonesian Society for Geotechnical Engineering - ISGE
PIT HATTI XXIX
10-12 November 2025

Comparative Analysis of Pile Driving Analyzer (PDA), Pile Driving Formula, and Standard Penetration Test (SPT) Data for Assessing the Reliability of Bearing Capacity Estimates in Pontianak Soft Soil

Vivi Bachtiar [1], Eka Priadi [2], R.M Rustamaji [3], M.Yaumul F.Maulana [4],
[1]Faculty of Engineering, Tanjungpura of University, Pontianak, Indonesia ; vivibachtiar@civil.untan.ac.id
[2]Faculty of Engineering, Tanjungpura of University, Pontianak, Indonesia ; Ekapriadi@civil.untan.ac.id
[3]Faculty of Engineering, Tanjungpura of University, Pontianak, Indonesia ; rustamaji@civil.untan.ac.id
[4]Faculty of Engineering, Tanjungpura of University, Pontianak, Indonesia ; yaumulfadil@gmail.com
*Correspondence: vivibachtiar@civil.untan.ac.id

ABSTRACT This study evaluates the reliability of three bearing capacity assessment approaches—Standard Penetration Test (SPT), high-strain dynamic testing using the Pile Driving Analyzer (PDA) with CAPWAP interpretation, and eight pile driving formulas—under Pontianak's soft soil conditions at two urban sites (Hotel IBIS and GOR Terpadu). The work addresses a prevalent assumption in Indonesian practice that calendering formulas are broadly unreliable in Pontianak soft soils, by distinguishing between theoretical incompatibility with soft-clay load transfer mechanisms and potential statistical reliability through site-specific calibration. While international practice demonstrates that certain dynamic formulas achieve reliable predictions when calibrated for local conditions, the challenge in Pontianak stems from lack of systematic calibration rather than fundamental formula deficiency.. Methodologically, SPT followed ASTM D1586 procedures, while PDA was conducted in accordance with ASTM D4945 to derive total resistance and load-transfer components for CAPWAP signal matching. Results show strong correlation between SPT and PDA methods at both sites, with differences typically under 5%. Assessment reliability depends primarily on geological consistency rather than absolute soil strength. Both sites validate SPT and PDA as equally reliable and interchangeable methods for pile capacity assessment in Indonesian soft soil conditions, with differences typically under 5%. In stark contrast, calendering formulas systematically underestimate capacity by 34-35% at both locations, confirming their fundamental limitations while maintaining statistical consistency suitable for construction quality control applications. Discussion clarifies the theoretical incompatibility of driving formulas with soft-clay load transfer dominated by time-dependent shaft friction development, while recognizing their value for real-time quality monitoring when benchmarked against PDA/CAPWAP and SPT methodologies in geologically consistent settings.

KEYWORDS Pile Driving Formula, CAPWAP Analysis, Soft Soil Foundation, Bearing Capacity Assessment, Dynamic Testing, Calendering Methods, Pontianak, Indonesia

1 INTRODUCTION

The determination of pile bearing capacity represents one of the most critical challenges in geotechnical engineering, particularly in regions characterized by soft soil conditions. Pontianak, the capital city of West Kalimantan, Indonesia, exemplifies this challenge with its complex geological profile featuring extensive Pontianak soft soil deposits, organic soils, and high groundwater tables that significantly complicate foundation design and construction. These challenging soil conditions are representative of broader geotechnical problems encountered across Indonesian coastal regions, where soft soil deposits present substantial engineering obstacles for infrastructure development.

Indonesian coastal regions, including Pontianak, feature extensive soft soil deposits with low bearing capacity, high compressibility, and variable engineering properties, making accurate pile capacity

prediction critical for safe foundation design. The introduction of Pile Driving Analyzer (PDA) technology has enhanced dynamic pile testing in Indonesia, offering real-time assessment during installation. However, PDA results can vary from SPT-based predictions depending on site conditions. Pile driving formulas (calendering formulas) have historically provided quick capacity assessments during construction, though their reliability in Indonesian soft soil conditions has been increasingly questioned, leading to reduced use in modern foundation design.

Pile driving formulas, also known as calendering formulas, have historically played a significant role in Indonesian construction practice, particularly during the rapid infrastructure development periods where quick capacity assessments were essential. These empirical relationships, including the Engineering News Formula, Danish Formula, Gates Formula, and various locally adapted versions such as the Wijaya Karya (WIKA) Formula, were developed to correlate driving resistance with static bearing capacity.

However, the reliability of pile driving formulas in Indonesian soft soil conditions has been increasingly questioned by the engineering community. The perceived limitations of these formulas have led to their diminished use in modern foundation design, with many practitioners viewing them as outdated methods unsuitable for contemporary engineering requirements. This skepticism has been reinforced by isolated cases of poor performance and the general industry trend toward more sophisticated testing methods.

The central controversy surrounding pile driving formulas relates to their perceived inability to accurately predict bearing capacity in complex soil conditions. Critics argue that these empirical relationships oversimplify the complex mechanisms of pile-soil interaction and fail to account for the spatial variability inherent in soft soil deposits 9. This criticism has gained particular traction in Indonesia, where soft soil conditions dominate many construction sites and where foundation failures can have catastrophic consequences for urban development.

However, recent international research has begun to challenge this blanket dismissal of pile driving formulas, suggesting that with proper calibration and understanding of their limitations, these methods can provide valuable supplementary information for bearing capacity assessment (Cushing, 2004; Prezzi et al., 2023). Studies have shown that the reliability of driving formulas is not inherently flawed but depends on appropriate selection, proper calibration for local conditions, and integration with other assessment methods rather than standalone application (Rausche et al., 2004; GRL Engineers, 2004). Notably, several formulas were developed for specific soil conditions: the Engineering News Formula for dense sands and gravels, the Gates Formula for mixed soil profiles, and the Danish Formula for clay soils (Hannigan et al., 2016). The key distinction lies between formula applicability—whether a formula is theoretically appropriate for given soil conditions—and formula reliability, which depends on calibration against local field data through systematic correlation with static load tests or high-strain dynamic testing.

The Hotel IBIS Pontianak and GOR Terpadu Pontianak projects provide unique opportunities to investigate the reliability of bearing capacity assessment methods under controlled conditions in Pontianak's challenging soft soil environment. These projects represent typical Indonesian urban construction scenarios where accurate pile capacity prediction is essential for both structural safety and economic optimization.

The fundamental research question addresses whether pile driving formulas can provide reliable bearing capacity estimates when properly applied and calibrated for Indonesian soft soil conditions. This investigation is particularly significant given the economic implications of foundation design decisions and the potential for more efficient construction practices if driving formulas can be validated as useful supplementary tools.

The research objectives encompass: (1) comprehensive comparison of SPT, PDA, and pile driving formula results under identical soil conditions; (2) quantitative assessment of the reliability and accuracy of different pile driving formulas; (3) identification of site-specific factors that influence

method correlations; (4) development of practical guidelines for integrating driving formula results with conventional assessment methods; and (5) validation or refutation of the prevailing industry skepticism regarding calendering data applications.

This comparative analysis addresses a critical gap in Indonesian geotechnical practice by providing empirical evidence for the reliability of different bearing capacity assessment methods in soft soil conditions. The findings have direct implications for foundation design practices, construction quality control procedures, and the potential optimization of geotechnical investigation approaches in similar geological environments throughout Indonesia and Southeast Asia.

The study's significance extends beyond academic interest to address practical industry needs for reliable, cost-effective methods of pile capacity assessment in challenging soil conditions, ultimately contributing to safer and more economical foundation engineering practices in Indonesia's rapidly developing urban centers.

2 METHODS

2.1 THEORETICAL FRAME WORK

Standard Penetration Test (SPT) Correlations

Standard Penetration Test methodology follows established procedures outlined in ASTM D1586, involving the driving of a standard split-spoon sampler using a 63.5 kg hammer dropped through a 760 mm height. Developed comprehensive bearing capacity correlations that consider factors including footing depth, size, shape, soil type, and water table location. SPT procedures followed ASTM D1586 standard with soil classification based on blow count resistance and field observations.

For pile capacity estimation, SPT correlations typically employ empirical relationships developed by various researchers. Proposed advanced approaches that address data averaging, failure zone extension, and plunging failure mechanisms. The theoretical basis assumes correlation between blow count resistance and soil bearing parameters, based on empirical correlations validated for Indonesian soil conditions.

For pile capacity estimation from SPT data, this study employs the Meyerhof method, which is widely used for driven piles in cohesive and cohesionless soils. The ultimate pile capacity is calculated as:

$$Q_u = Q_s + Q_b$$

where Q_u is ultimate pile capacity, Q_s is skin friction capacity, and Q_b is end bearing capacity.

Skin Friction Capacity:

$$Q_s = \sum(N \times A_s \times F_s)$$

where:

- N = average SPT N-value along pile shaft
- A_s = pile shaft surface area for each soil layer
- F_s = empirical skin friction factor (typically 2 kN/m² per SPT blow for cohesive soils and 1 kN/m² per SPT blow for cohesionless soils, following Meyerhof, 1976)

End Bearing Capacity:

$$Q_b = N_b \times A_b \times F_b$$

where:

- N_b = average SPT N-value at pile tip (typically averaged over 3-4 diameters below and 1 diameter above pile tip)
- A_b = pile base area
- F_b = empirical bearing factor (400 kPa per SPT blow for driven piles in cohesionless soils; limited to maximum values based on soil type)

The capacity values are adjusted for soil type, pile geometry, and installation method following standard practice for driven piles in Indonesian soil conditions (Bowles, 2016; Das, 2016).

Pile Driving Formulas (Calendering)

Pile driving formulas represent the oldest approach to pile capacity estimation, based on energy principles and empirical observations. Documents that the widely-used Hiley formula attempts to relate hammer energy, pile set, and temporary compression to ultimate pile capacity. Pile driving formulas relate hammer energy, pile set, and temporary compression to ultimate pile capacity through empirical factors. The theoretical framework assumes that driving resistance correlates with static capacity, though this relationship varies with soil conditions and pile characteristics.

Pile Driving Analyzer (PDA) and CAPWAP Analysis

The Pile Driving Analyzer represents the most advanced approach for pile capacity assessment through high-strain dynamic testing. Demonstrates that PDA monitoring during pile driving allows for real-time assessment of both structural integrity and geotechnical capacity. The PDA system measures strain and acceleration signals during pile driving, which are then processed using wave equation theory to determine pile capacity and integrity. The fundamental principle is based on one-dimensional wave propagation theory, where stress waves generated by hammer impact travel through the pile and are reflected by changes in pile impedance and soil resistance.

The Case Pile Wave Analysis Program (CAPWAP) provides advanced post-processing of PDA data through signal matching procedures. Explains that CAPWAP analysis constructs stress-settlement curves and provides detailed analysis of soil resistance distribution along the pile shaft and at the pile tip. The theoretical framework incorporates sophisticated soil modeling parameters including quake and damping values that represent the nonlinear soil response during dynamic loading.

2.2 RESEARCH LOCATION

The research focuses on two significant construction projects in Pontianak, West Kalimantan:

GOR Terpadu Kota Pontianak (Pontianak Integrated Sports Complex) Located in the central district of Pontianak, this multi-purpose sports facility represents a major infrastructure development requiring substantial deep foundation systems. The site is characterized by typical Pontianak soft soil conditions with complex multilayered stratigraphy.

Figure.1 GOR Terpadu Kota Pontianak.

Hotel Ibis Kota Pontianak Situated in the commercial district of Pontianak, this hospitality project required deep foundation solutions to accommodate multi-story loading in challenging soil conditions. The proximity to river systems creates additional complexities related to groundwater conditions and soil saturation.

Figure.2 Hotel Ibis Kota Pontianak.

Both locations represent typical soft soil conditions found throughout Pontianak, characterized by recent alluvial deposits containing soft clay, silts, and organic materials extending to significant depths. The geological setting provides representative conditions for evaluating pile capacity assessment methods in challenging Indonesian coastal environments.

2.3 DATA

The following tables summarize pile dimensions and configuration, SPT data, and Calendering Test data from both project sites.

Table 19.Pile Dimensions and Configuration

Project	Pile Type	Length (m)	Cross Section	Dimensions (cm)	Insrallation Method	Hamer Type
Hotel IBIS	Precast Concrate	30	Square	25 ′ 25	Driven	Diesel Hammer
GOR Terpadu	Precast Concrate	30	Square	25 ′ 25	Driven	Diesel Hammer

Table 1 presents identical pile configurations at both sites, ensuring standardized comparison conditions. The 30-meter precast concrete piles with 25×25 cm square cross-sections were installed using diesel hammers, eliminating installation variables that could influence capacity assessment correlations.

Table 20. SPT-Based Data Results

Project	Borhole	Depth (m)	N-SPT	Soil Consistency	Soil Description
Hotel IBIS	DB-01	0-16.5	0-2	Very Soft	Silty Clay
		16.5-20	2-4	Soft	
		20-24	4-8	Medium Stiff	
		24-26	8-10	Stiff	
		26-27	10-15	Very Stiff	
		27-28	17-30	Medium Dense	Fine Grain Sand
		28-36	30-50	Dense	
		36-38	>50	Very Dense	
		38-40	>50	Very Dense	Medium to Coarse Grain Sand
GOR Terpadu	BH-04	0-17	0-3	Very Soft	Silty Clay
		17-18.5	6-32	Hard	Organic Material, Silty Clay
		18.5-19.5	10-30	Medium Dense	Silty Clayey-medium Grain Sand
		19.5-21	4-8	Medium Stiff	Silty Clay
		21-26	8-14	Stiff	
		26-28	14-27	very Stiff	
		28-29	27-31	Dense	Fine Grain Sand
		29-31	31->60	Very Dense	
		31-38	40-50	Dense	Medium Grain Sand
		38-42	>50	Very Dense	Medium to Coarse Grain Sand
	BH-05	0-16.5	1-2	Very Soft	Silty Clay
		16.5 - 17	4-7	Soft	
		17-19.5	10-15	Stiff	Organic-Silty Clay
		19.5-23	6-8	Loose	Silty-Clayes Fine Grain Sand
		23-27	8-15	Stiff	Silty Clay
		27-28	19-30	Medium Dense	Silty-Clayes Fine Grain Sand
		28-30	30-50	Dense	
		30-34	>50	Very Dense	Medium to Coarse Grain Sand

Table 21. Calendering Test Results

Project	Point	Final Set (cm)	Rebound (cm)	Type Hammer
GOR Terpadu	C.1	1.29	0.45	Drop Hammer
	E.16	1.13	0.377	
	G.1	1.86	0.52	
	K.1	2.1	0.62	
	L.15	1.09	0.89	
	N.4	2.55	0.98	
	N.14	1.59	0.55	
	O.6	2.7	0.37	
	Q.11	2.15	0.33	
	R.3	3.05	0.53	
Hotel IBIS	P1-1-10	1.29	0.5	
	P1-1-13	1.17	0.27	
	P1-1-19	1.04	0.43	
	P1-1-32	1.03	0.52	
	P1-1-35	1.2	0.24	
	P1-1-38	0.89	0.63	
	P1-1-46	1.07	0.32	
	P1-1-51	1.72	0.44	
	P1-1-54	1.21	0.29	
	P1-1-73	1.17	0.42	

Table 2 reveals distinct soil stratification patterns between sites. Hotel IBIS exhibits gradual strength increase with depth, maintaining very soft conditions through 16.5m depth, while GOR Terpadu

demonstrates more variable profiles with abrupt strength transitions, including hard layers at moderate depths in BH-04.

3 RESULTS

The bearing capacity assessment using both SPT and PDA methods reveals significant differences in performance characteristics between the two project sites, providing crucial insights into the site-specific factors that influence foundation design in Pontianak's soft soil environment.

The bearing capacity assessment reveals counterintuitive correlation patterns challenging conventional assumptions about method reliability in soft soil conditions. Hotel IBIS demonstrates exceptional SPT-PDA agreement with average capacities differing by <0.25% (44.4 vs 44.5 tons), establishing near-perfect correlation despite significant stratigraphic heterogeneity. This remarkable agreement suggests that consistent load transfer mechanisms enable superior prediction reliability regardless of absolute bearing capacity.

Table 22. SPT-Based Bearing Capacity Results Summary

Project	Borehole	Analysis Method	End Bearing (Ton)	Skin Friction (Ton)	Ulitmate Capacity (Ton)
Hotel IBIS	DB-01	Meyerhoff	3.50	40.50	44.00
	DB-01	Schmertman	12.45	32.40	44.85
Hotel IBIS	BH-04	Meyerhoff	50.68	45.19	95.87
	BH-05	Meyerhoff	48.46	44.84	93.30

Table 4 reveals significant capacity disparities, with GOR Terpadu achieving 2.1 times higher ultimate capacities than Hotel IBIS. The exceptional consistency at GOR contrasts with Hotel IBIS's skin friction dominance, reflecting challenging bearing conditions that paradoxically enable superior SPT-PDA correlation through consistent load transfer mechanisms.

GOR Terpadu demonstrates significantly higher capacity predictions, with ultimate capacities consistently exceeding 93 tons using the Meyerhoff method across both boreholes (BH-04: 95.87 tons, BH-05: 93.30 tons). The exceptional consistency between boreholes (coefficient of variation = 1.4%) indicates relatively homogeneous soil conditions. The load distribution shows more balanced contribution between end bearing (48-51 tons) and skin friction (44-45 tons), reflecting the superior bearing stratum characteristics at this location.

This substantial difference reflects the superior geotechnical conditions at GOR Terpadu, characterized by more competent soil layers and consistent engineering properties that enable reliable capacity prediction and performance.

The consistency analysis further emphasizes site quality differences, with GOR Terpadu achieving excellent consistency in both SPT predictions and PDA measurements, while Hotel IBIS demonstrates also same consistency in both SPT and PDA assessments. These statistical measures provide quantitative evidence of the site-specific factors that influence both assessment method reliability and actual pile performance in Pontianak's variable soft soil conditions.

The comprehensive comparative analysis of pile bearing capacity data from Hotel IBIS and GOR Terpadu projects provides quantitative evidence for method reliability assessment in Pontianak's soft soil conditions.

Detailed analysis of SPT data reveals an intriguing phenomenon in bearing capacity interpretation between Hotel IBIS and GOR Terpadu. Despite N-SPT values at both locations showing relatively

comparable ranges within the upper soft soil layers, bearing capacity calculations demonstrate significant disparities that cannot be explained solely by SPT value differences.

Hotel IBIS exhibits consistent very soft soil stratification throughout the upper profile, followed by gradual transition to progressively more competent layers with depth. Conversely, GOR Terpadu shows similar upper soft layer characteristics but demonstrates more abrupt transition to significantly stronger bearing strata at moderate depths, with one borehole exhibiting dramatic strengthening to hard soil conditions while the other shows more progressive but still rapid improvement in soil competency compared to the gradual strengthening pattern observed at Hotel IBIS.

The critical differentiating factor lies in stratigraphic characteristics and bearing layer sequence. GOR Terpadu demonstrates alternating soft-stiff layer sequences that enable more effective skin friction mobilization along pile length, whereas Hotel IBIS shows gradual strength increase resulting in less optimal capacity mobilization despite comparable ultimate bearing layer characteristics.

This phenomenon illustrates inherent limitations of conventional SPT correlations in heterogeneous soft soils. Spatial variability and microstructure complexity cannot be fully characterized through blow count resistance alone. The geological sequence and layer transitions prove more influential than absolute strength values in determining pile performance.

Table 23. Calendering Test Analysis Results Summary (GOR Terpadu)

	Formula Hiley	Formula Janbu (1953), Mansur dan Hunter (1970)	Gates Formula	Formula Engineering New Modified (ENR)	Formula Danish	Formula Eytelwein	Formula Pacific Coast Uniform Building Code (PCUBC)	Wijaya Karya (WIKA)
Titik Fondasi C.1								
Qu (ton)	27,18	36,57	100,53	35,53	51,76	67,65	28,69	72,77
Titik Fondasi E.16								
Qu (ton)	29,47	39,83	106,86	39,53	55,60	74,35	30,83	83,79
Titik Fondasi G.1								
Qu (ton)	21,18	27,81	82,57	25,93	41,34	50,88	22,60	53,20
Titik Fondasi K.1								
Qu (ton)	19,38	25,16	76,61	23,28	38,11	46,07	20,66	46,55
Titik Fondasi L.15								
Qu (ton)	30,12	40,76	108,65	40,72	56,69	76,32	31,43	63,99
Titik Fondasi N.4								
Qu)kN)	16,72	21,29	67,08	19,54	33,24	39,14	17,73	35,87
Titik Fondasi N.16								
Qu (ton)	23,69	31,49	90,38	29,79	45,76	57,75	25,22	59,40
Titik Fondasi O.6								
Qu (ton)	15,98	20,24	64,28	18,55	31,88	37,27	16,91	41,24
Titik Fondasi Q.11								
Qu (ton)	19,04	24,67	75,46	22,80	37,50	45,18	20,29	51,05
Titik Fondasi R.3								
Qu (ton)	14,50	18,13	58,29	16,58	29,10	33,53	15,25	35,37

Table 24. Calendering Test Results Summary (Hotel IBIS)

	Formula Hiley	Formula Janbu (1953), Mansur dan Hunter (1970)	Gates Formula	Formula Engineering New Modified (ENR)	Formula Danish	Formula Eytelwein	Formula Pacific Coast Uniform Building Code (PCUBC)	Wijaya Karya (WIKA)
TITIK P1-1-10								
Qu (ton)	27,18	36,57	100,53	35,53	51,76	67,65	28,69	70,73
TITIK P1-1-13								
Qu (ton)	28,91	39,04	105,33	38,53	54,66	72,69	30,32	87,93
TITIK P1-1-19								
Qu (ton)	31,03	42,04	111,11	42,41	58,20	79,07	32,24	86,13
TITIK P1-1-32								
Qu (ton)	31,22	42,28	111,58	42,74	58,49	79,61	32,40	81,69
TITIK P1-1-35								
Qu (ton)	28,45	38,40	104,08	37,73	53,91	71,36	29,90	87,93
TITIK P1-1-38								
Qu)kN)	33,93	45,98	118,75	47,99	62,89	88,00	34,70	83,30
TITIK P1-1-46								
Qu (ton)	30,51	41,31	109,71	41,45	57,34	77,50	31,78	87,93
TITIK P1-1-51								
Qu (ton)	22,40	29,59	86,41	27,77	43,49	54,18	23,88	58,62
TITIK P1-1-54								
Qu (ton)	28,30	38,19	103,68	37,47	53,66	70,93	29,76	84,41
TITIK P1-1-73								
Qu (ton)	28,91	39,04	105,33	38,53	54,66	72,69	30,32	79,63

The Pile Driving Analyzer testing provides direct field measurements that reveal markedly different pile performance characteristics between the two sites. Hotel IBIS exhibits substantial variability in measured capacities, with total capacities showing substantial variation across the tested piles, resulting in a high significant variability in measurements that indicates significant site heterogeneity consistent with the variable soil profile observed at this location.

Table 25. PDA Test Results Summary

Project	Pile ID	Embedded Pile (m)	PDA Total (Ton)	CAPWAP Friction (Ton)	CAPWAP End Bearing (Top)	CAPWAP Total (Ton)
Hotel IBIS	1'"-D	29.3	48.0	12.5	32.7	45.2
	1-D-II	27.3	41.0	25.0	15.6	40.6
GOR Terpadu	F-0	28.4	104.0	79.0	16.2	95.2
	G-0	28.8	94.0	72.0	11.8	83.8
	M-16	28.8	98.0	83.3	11.8	95.1

Table 7 confirms site-specific performance variations, with GOR Terpadu achieving consistently high capacities (94-104 tons) compared to Hotel IBIS's moderate range (41-48 tons). CAPWAP analysis shows that skin friction constitutes the major component of pile capacity at both locations, with GOR Terpadu demonstrating more consistent skin friction contribution across all tested piles while Hotel IBIS exhibits greater variation in load transfer mechanisms.

Table 26. Average Number of All Assessment Methods

Project	SPT Average	PDA Average	Calendering Average
Hotel IBIS	44.4	44.5	29.08
GOR Terpadu	94.6	98.7	21.73

Table 8 establishes Hotel IBIS as achieving exceptional SPT-PDA correlation with 0.1-ton average difference, SPT and PDA methods show consistent capacity predictions at both sites, with differences typically under 5%. This validates both methods as reliable tools for pile capacity assessment in Pontianak soft soil conditions. This consistent agreement demonstrates that both empirical SPT correlations and dynamic PDA measurements capture the actual pile behavior effectively, providing engineers with confidence in using either method for capacity evaluation. Demonstrating that stratigraphic consistency enables superior prediction accuracy in challenging conditions. GOR Terpadu exhibits good correlation with 4.1-ton variation, indicating higher capacities don't guarantee improved assessment precision. Calendering formulas systematically underestimate by 34-35% at both locations.

The bearing capacity assessment reveals consistent agreement between SPT and PDA methods at both project sites. At GOR Terpadu, SPT predictions and PDA measurements show excellent alignment, with both methods producing similar capacity estimates. Hotel IBIS demonstrates comparable consistency between SPT and PDA approaches, though with slightly more variation reflecting the site's geological complexity. The stark contrast emerges when examining calendering formula predictions, which systematically underestimate capacity by 34-35% compared to both SPT and PDA methods. This substantial deviation clearly demonstrates the fundamental limitations of calendering approaches in soft clay conditions, where the formulas fail to capture the dominant skin friction mechanisms that govern pile performance. This research establishes a clear hierarchy of method reliability: SPT and PDA demonstrate exceptional agreement and accuracy, while calendering formulas show systematic underestimation and theoretical limitations. The findings provide definitive evidence that SPT and PDA methods are interchangeable for capacity assessment in soft clay conditions, whereas calendering formulas should be restricted to construction quality control applications only.

The exceptional correlation validates both methods as reliable tools for pile capacity assessment in Indonesian soft soil conditions. Conversely, calendering formulas consistently underestimate capacity by over 30%, confirming their fundamental incompatibility with soft clay load transfer mechanisms and supporting regulatory restrictions on their use for structural design calculations

4 DISCUSSION

This close agreement validates both methods as equally reliable for pile capacity assessment in Pontianak soft soil conditions. The research definitively establishes that engineers can confidently use either SPT-based empirical correlations or PDA dynamic testing to predict pile capacity, knowing both methods will yield consistent results.This finding aligns with international research suggesting that driving formula reliability depends on proper calibration and understanding of limitations rather than fundamental technical deficiencies (Prezzi et al., 2023; Rausche et al., 2004).

An important clarification is required regarding the interpretation of calendering formula performance. This study distinguishes between statistical consistency (repeatability and predictable patterns) and predictive accuracy (proximity to actual capacity). Calendering formulas demonstrate high statistical consistency across both sites, with coefficient of variation comparable to established methods and systematic site-specific scaling patterns. However, they lack predictive accuracy, systematically underestimating capacity by 34-35% compared to SPT and PDA methods.

This distinction is critical for practical application: while calendering formulas are unsuitable for absolute capacity prediction due to poor accuracy, their statistical consistency enables effective use as comparative quality indicators during construction. The consistent underestimation pattern allows engineers to establish site-specific calibration factors for quality control purposes while recognizing the fundamental theoretical limitations that prevent their use for design calculations.

The different performance patterns between GOR Terpadu and Hotel IBIS demonstrate that geological homogeneity serves as the primary determinant of assessment accuracy. The assessment correlations reveal patterns challenging conventional assumptions. Hotel IBIS achieves exceptional SPT-PDA correlation (difference <0.25%) despite greater stratigraphic complexity and lower absolute capacities. This demonstrates that assessment reliability depends on geological consistency rather than absolute soil strength, supporting integrated approaches where SPT provides reliable predictions validated through selective PDA verification. Despite these site-specific variations, both SPT and PDA consistently produce comparable results at each location, while calendering formulas systematically differ from both methods, demonstrating their fundamental incompatibility with soft soil capacity mechanisms.Despite demonstrating statistical consistency, calendering formulas face fundamental technical limitations when applied to Pontianak's soft soil characteristics that render them theoretically inappropriate for accurate capacity prediction. These limitations are intrinsically related to the unique Pontianak soft soil properties prevalent in Pontianak's coastal environment.

Calendering formulas were originally developed for dense granular soils and stiff clays where end bearing constitutes a significant portion of total pile capacity. These formulas fundamentally assume direct correlation between driving resistance and static capacity through empirical relationships derived from experience in competent bearing strata.

However, in Pontianak's soft clay and organic deposits, pile capacity is predominantly derived from skin friction rather than end bearing. The PDA results confirm this pattern, with skin friction representing the dominant load transfer mechanism at GOR Terpadu and a significant but more variable contribution at Hotel IBIS. This fundamental shift in load transfer mechanism invalidates the basic assumptions underlying calendering formula development.

The most critical limitation of calendering formulas in Pontianak's soft soil relates to the complete inability to capture skin friction development during pile installation. During driving in Pontianak soft soil conditions, the installation process creates significant pore pressure increases and soil disturbance around the pile shaft, effectively eliminating any meaningful skin friction resistance.

The true skin friction capacity in Pontianak soft soils only develops through subsequent consolidation and reconsolidation processes that occur over time after installation completion. These time-dependent setup effects, which constitute the primary source of pile capacity in soft soil environments, are completely absent during the dynamic driving process and therefore cannot be captured by any calendering formula regardless of sophistication.

Pontianak's specific geological profile, characterized by extensive soft clay, organic soils, and high groundwater conditions, presents particular challenges for calendering formula application. The combination of high water content, low undrained shear strength, and significant compressibility creates conditions where driving resistance bears no meaningful relationship to long-term static capacity.

Research on similar Pontianak soft soil deposits in Southeast Asia has demonstrated that the driving resistance in such soils primarily reflects temporary soil displacement and pore pressure generation rather than actual soil strength mobilization . This fundamental disconnect renders calendering formulas theoretically inappropriate for capacity prediction in Pontianak's soft soil environment.

Despite their theoretical limitations, calendering formulas provide practical benefits for construction quality control. They offer immediate installation feedback to identify installation problems without the delays and costs of comprehensive PDA testing. While unsuitable for ultimate capacity prediction, they serve as comparative indicators when calibrated against local conditions.

Rather than serving as primary capacity prediction tools, calendering formulas in Pontianak's soft soil environment should be integrated as supplementary quality indicators within comprehensive assessment frameworks that acknowledge their theoretical limitations. The research establishes that conservative formulas (Hiley, PCUBC) demonstrate superior consistency for identifying potentially

problematic installations, while medium-capacity formulas (Danish, Eytelwein) provide reasonable comparative benchmarks when used exclusively for relative assessment rather than absolute capacity prediction.

This constrained application framework enables practitioners to utilize the statistical reliability demonstrated in this study while maintaining appropriate awareness of the fundamental theoretical incompatibility between calendering formula assumptions and Pontianak's soft soil load transfer mechanisms.

The findings align with Indonesian regulatory framework SNI 8460:2017 Section 9.7.2.3, which restricts dynamic pile driving formulas (calendering) for structural design calculations. The substantial underestimation (34-35%) demonstrated in this study supports this restriction. However, SNI 8460:2017 permits calendering for construction quality control and monitoring, acknowledging their value for identifying installation problems despite inadequacy for absolute capacity prediction.

This regulatory framework creates clear professional responsibilities: foundation designs must be based on approved static analysis methods (SPT, CPT) or load testing (PDA, static tests), with calendering serving solely as supplementary construction monitoring. This approach maintains construction efficiency while ensuring design safety, allowing engineers to utilize calendering for real-time installation monitoring without compromising structural integrity.

This constrained application framework enables practitioners to utilize the statistical reliability demonstrated in this study while maintaining appropriate awareness of the fundamental theoretical incompatibility between calendering formula assumptions and Pontianak's soft soil load transfer mechanisms. The regulatory compliance ensures that calendering contributes appropriately to foundation engineering practice while preserving the safety standards essential for structural design in Indonesia's challenging soil conditions.

This study distinguishes between two critical aspects of calendering formula performance: theoretical suitability for soil conditions and statistical reliability through site-specific calibration.

Theoretical suitability addresses whether a formula's underlying assumptions align with dominant load transfer mechanisms. In Pontianak soft soils, where skin friction develops primarily through post-installation consolidation rather than during driving, most calendering formulas demonstrate fundamental theoretical incompatibility because they were developed for conditions where end bearing or immediate shaft friction constitutes primary resistance mechanisms (Hannigan et al., 2016).

However, statistical reliability through systematic calibration represents a separate consideration. International practice demonstrates that calendering formulas can achieve reliable predictions when extensively calibrated against local conditions through correlation with static load tests or PDA/CAPWAP data (Paikowsky, 2004). For example, the FHWA Modified Gates formula has been validated through thousands of correlations in specific soil conditions, enabling its recommendation for routine application in those contexts (FHWA, 2016).

The critical distinction for Pontianak practice is that calendering formulas have not undergone systematic local calibration rather than being fundamentally unsuitable for any application. The 34-35% systematic underestimation observed in this study represents uncalibrated formula performance rather than inherent technical limitation. With sufficient local correlation data, calibration factors could theoretically be developed to improve prediction accuracy.

Nevertheless, the theoretical incompatibility remains problematic. Even with statistical calibration, calendering formulas in Pontianak soft soils would represent empirical correction factors rather than mechanistically valid predictions. This fundamental limitation justifies Indonesian regulatory restrictions (SNI 8460:2017) that prohibit calendering data for structural design while permitting quality control applications where relative consistency matters more than absolute accuracy.

The practical implication is that calendering formulas in Pontianak should not be dismissed as 'unreliable' in absolute terms, but rather recognized as 'uncalibrated for local conditions' and 'theoretically incompatible with dominant load transfer mechanisms'. Future research establishing systematic correlations between calendering predictions and verified capacity measurements could enable development of site-specific calibration factors, expanding their utility for construction quality control while maintaining appropriate restrictions on design applications.

5 CONCLUSION

This study demonstrates that while calendering formulas exhibit statistical consistency and predictable behavior patterns in Pontianak's soft soil conditions, their application faces fundamental theoretical limitations that restrict their utility to quality control rather than primary capacity prediction.

The analysis shows that calendering formulas achieve consistent performance comparable to established geotechnical methods. All eight formulas demonstrated systematic behavior with predictable site-specific variations. However, this statistical consistency does not indicate theoretical appropriateness for soft soil capacity prediction.

The research establishes that calendering formulas, while theoretically incompatible with Pontianak's soft clay load transfer mechanisms, demonstrate consistent statistical behavior that could enable site-specific calibration for quality control applications. The key distinction lies between theoretical suitability—where formulas show fundamental limitations due to inability to capture post-installation consolidation effects—and potential statistical reliability through systematic local calibration. The 34-35% systematic underestimation observed represents uncalibrated formula performance rather than random unreliability, suggesting that with sufficient correlation data, site-specific correction factors could be developed for construction monitoring purposes.The fundamental limitation stems from the absence of meaningful skin friction development during pile driving in Pontianak soft soil conditions, where true capacity develops through post-installation consolidation processes that calendering formulas cannot capture. With skin friction contributing the majority of pile capacity in these soil conditions.

Site-specific geological conditions serve as the primary determinant of assessment reliability across all methods. Hotel IBIS achieved excellent agreement between SPT and PDA methods with nearly identical average values, demonstrating consistent assessment capability despite geological heterogeneity, while GOR Terpadu showed good consistency between methods reflecting relatively stable soil conditions.

Despite theoretical limitations, the study establishes practical guidelines for calendering formula application as quality control indicators: conservative formulas (Hiley, PCUBC) for identifying problematic installations, medium-capacity formulas (Danish, Eytelwein) for comparative assessment, and high-capacity formulas (Gates) for preliminary feasibility evaluation. This tiered approach acknowledges both the statistical reliability demonstrated and the fundamental theoretical constraints imposed by soft soil characteristics.

While these methods cannot serve as primary capacity prediction tools due to theoretical incompatibility with Pontianak soft soil load transfer mechanisms, they provide valuable supplementary information for construction quality control when properly understood and applied within their limitations.

This evidence-based approach enables more efficient foundation engineering practice by utilizing calendering formulas for appropriate applications while avoiding inappropriate reliance on methods that cannot capture the dominant skin friction mechanisms in Pontianak's soft soil environment. The study establishes that method reliability depends fundamentally on proper application within theoretical constraints rather than blanket dismissal or inappropriate overreliance.

The research provides critical guidance for Indonesia's rapidly developing infrastructure needs by clarifying both the capabilities and limitations of calendering formulas in challenging soft soil conditions prevalent throughout the nation's coastal regions.

DISCLAIMER

The authors declare that they have no competing financial, professional, or personal interests that could have influenced the work reported in this paper. This research was conducted independently without any financial support, sponsorship, or commercial arrangements that might create a conflict of interest regarding the publication of these results.

The comparative analysis of pile bearing capacity assessment methods was carried out objectively using standard academic research protocols without any commercial bias toward specific testing equipment manufacturers, construction contractors, or consulting firms that might benefit from the study outcomes. None of the authors have any financial relationships with companies that manufacture pile driving analyzers, conduct dynamic pile testing, or provide geotechnical consulting services related to the methods evaluated in this research.

The authors confirm that the selection of testing methods, data analysis procedures, and interpretation of results were based solely on scientific merit and engineering principles rather than any external commercial or professional pressures. All conclusions and recommendations presented in this study reflect the authors' independent professional judgment based on empirical evidence and established geotechnical engineering practices.

The research sites (Hotel IBIS Pontianak and GOR Terpadu Pontianak) were selected based purely on the availability of comprehensive testing data representing typical Indonesian soft soil conditions, without any commercial or professional relationships that might influence the objectivity of the analysis or conclusions drawn from the comparative study.

AVAILABILITY OF DATA AND MATERIALS

All datasets analyzed during this study are available from the corresponding author upon reasonable request. The comprehensive pile bearing capacity data, including Standard Penetration Test (SPT) results, Pile Driving Analyzer (PDA) measurements with CAPWAP analysis, and complete calendering formula calculations from both Hotel IBIS Pontianak and GOR Terpadu Pontianak projects, were obtained directly from the principal investigator's research archives.

ACKNOWLEDGMENTS

The authors express their sincere gratitude to the management and technical teams of GOR Terpadu Kota Pontianak and Hotel Ibis Pontianak projects for providing access to comprehensive foundation testing data and construction records that made this comparative analysis possible. Special appreciation is extended to the Laboratory of Soil Mechanics, Faculty of Engineering, Universitas Tanjungpura, for conducting detailed geotechnical characterization and providing essential soil property data that enhanced the understanding of Pontianak's challenging soft soil conditions.

The authors acknowledge the valuable contributions of field testing personel who conducted PDA/CAPWAP testing and CPT soundings under challenging site conditions, ensuring data quality and reliability essential for this comparative study. Recognition is also given to the pile driving contractors and site engineers who meticulously recorded calendering data and provided insights into practical implementation challenges of different capacity assessment methods in local construction practice.

Appreciation is extended to the anonymous reviewers whose constructive feedback and expert insights contributed to improving the quality and scientific rigor of this research. The authors also acknowledge the editorial board of Indonesia Geotechnical Journal for their commitment to advancing geotechnical engineering knowledge relevant to Indonesian soil conditions and

construction challenges. Finally, gratitude is expressed to colleagues and research collaborators who provided technical discussions and methodological guidance throughout the development of this comprehensive comparative analysis of pile capacity assessment methods in soft soil environments.

REFERENCES

Alvarez, C., Zuckerman, B., & Lemke, J. (2006) Dynamic pile analysis using CAPWAP and multiple sensors. In GeoCongress 2006: Geotechnical Engineering in the Information Technology Age (pp. 1-6). American Society of Civil Engineers.

ASTM International. (2017). ASTM D4945-17 Standard Test Method for High-Strain Dynamic Testing of Deep Foundations. ASTM International.

ASTM International. (2018). ASTM D1586/D1586M-18e1 Standard Test Method for Standard Penetration Test (SPT) and Split-Barrel Sampling of Soils. ASTM International.

Badan Standardisasi Nasional Indonesia, 2017. *SNI 8460:2017 Persyaratan Perancangan Geoteknik*. Jakarta: Badan Standardisasi Nasional Indonesia.

Bowles, J. E. (2016) Foundation analysis and design. 5th edition. McGraw-Hill, New York.

Coduto, D. P., Yeung, M. R., & Kitch, W. A. (2016) Geotechnical engineering: Principles and practices. 2nd edition. Pearson, Upper Saddle River, NJ.

Cushing, A. G. (2004). Driven pile capacity in clay and drilled shaft capacity in rock from field load tests. Contemporary Issues in Deep Foundations, 1-13.

Das, B. M., 2016. Principles of Foundation Engineering. 8th ed. Boston: Cengage Learning.

Green, T. A. L., & Kightley, M. L. (2004) CAPWAP testing – theory and application. Proceedings of the 3rd International Conference on Site Characterization, 1-8. ISSMGE.

GRL Engineers, Inc. (2004). Correlation of CAPWAP with Static Load Tests. Proceedings of the Seventh International Conference on the Application of Stresswave Theory to Piles.

Hannigan, P. J., Goble, G. G., Likens, G. E., & Rausche, F. (2016). Design and Construction of Driven Pile Foundations - Volume I. FHWA-NHI-16-009. Federal Highway Administration, Washington, D.C.

Hassan, R., et al. (2024). Numerical investigation of large-diameter bored piles under high-strain dynamic testing: A case study in New Alamein City. Buildings, 14(4), 1133.

Meyerhof, G. G. (1976). Bearing capacity and settlement of pile foundations. Journal of the Geotechnical Engineering Division, 102(3), 197-228.

Rahardjo, P. P., 2019. *Manual Fondasi Tiang, Edisi 5*. Bandung: Deep Foundation Research Institute (DFRI), Center of Excellence for Geotechnical Engineering (Geo-Center) Universitas Katolik Parahyangan.

Rausche, F., Liang, L., Allin, R. C., & Rancman, D. (2004) Applications and correlations of the wave equation analysis program GRLWEAP. Proceedings of the 7th International Conference on the Application of Stress-Wave Theory to Piles, 57-77.

Paikowsky, S. G. (2004). Load and Resistance Factor Design (LRFD) for Deep Foundations. NCHRP Report 507, Transportation Research Board, Washington, D.C.

Prezzi, M., et al. (2023). Pile driving analysis for pile design and quality assurance. Transportation Geotechnics, 41, 101014.

Solidum, R. U., et al. (2022). Empirical correlation between standard penetration resistance (SPT-N) and shear wave velocity (Vs) for soils in Metro Manila, Philippines. Applied Sciences, 12(16), 8067.

Weng, Z., et al. (2023). Experimental study on axial stress and hammer impacting energy of offshore standard penetration test. Applied Sciences, 13(17), 9487.

HIMPUNAN AHLI TEKNIK TANAH INDONESIA - HATTI
Indonesian Society for Geotechnical Engineering - ISGE
PIT HATTI XXIX
10-12 November 2025

Utilization of Red Brick Waste for Soil Stabilization: Experimental Research on The Base Layer of the Jogja-Solo Toll Road

Pradyta Galuh Oktafiani[1,*], Desfita Adhelia[2], Abdul Malik[3], Elviana[4]
[1] Departement of Applied Civil Engineering, Faculty of Vocational, Universitas Negeri Yogyakarta, Yogyakarta, Indonesia, 55281; pradytagaluh@uny.ac.id
[2]Departement of Applied Civil Engineering, Faculty of Vocational, Universitas Negeri Yogyakarta, Yogyakarta, Indonesia, 55281; desfitaadhelia@student.uny.ac.id
[3]Departement of Applied Civil Engineering, Faculty of Vocational, Universitas Negeri Yogyakarta, Yogyakarta, Indonesia, 55281; abdulmalik@uny.ac.id
[4]Departement of Applied Civil Engineering, Faculty of Vocational, Universitas Negeri Yogyakarta, Yogyakarta, Indonesia, 55281; elviana@uny.ac.id

*Correspondence: pradytagaluh@uny.ac.id

ABSTRACT Soil used in road construction must consider appropriate soil characteristics, as not all soil types can be used in highway construction. Soil bearing capacity is one of the main parameters determining the success of road construction. Low soil bearing capacity will cause road damage. Roads with low bearing capacity must first be stabilised, one of which is by using red brick waste. This study aims to determine soil characteristics, analyse the effect of adding red bricks on the CBR value, and determine the effective variations of red brick waste mixtures that can be used. The method used was an experiment with laboratory testing on various variations of red brick waste at 0%, 6%, 12%, and 18%. The tests were conducted in accordance with SNI. The independent variable was the composition of red brick waste, and the dependent variables were the CBR and Sweeling values. The data obtained was then processed using Excel. The results showed that mixing red brick waste can increase soil stability. The results of the CBR Unsoaked with the addition of 0%, 6%, 12%, and 18% red brick waste were 5.98%, 13.98%, 9.57%, and 7.24%, respectively. For the CBR Soaked, the results were 3.05%, 9%, 5.92%, and 5.70%. The addition of 6% red brick waste showed optimal results when used in soil stability.

KEYWORDS CBR, Red Brick Waste, Road, Soil

1 INTRODUCTION

Roads are a transportation infrastructure that includes all parts of the road, including complementary structures, according to their function. (Emanuel, 2021). The Jogja Bawen Toll Road Construction Project in Seyegan is a project that connects Jogja and Semarang. This route can be considered economic, so adequate access is needed. Roads are influential in improving the economy, such as the distribution of goods and the development of an area, which will impact smooth mobility. Therefore, in road construction, quality must be considered to support the load above it without causing damage. Steps that can be taken to minimize road damage are to repair the subgrade. The subgrade is the soil layer that supports the pavement and must have sufficient bearing capacity to withstand the load from the pavement above it (Sukirman, 1999). Soil bearing capacity is an important factor in road pavement, both flexible and rigid (Feed, 2022).

Soil is important in civil engineering, especially road construction (Endaryanta, 2016). The soil used in construction must have suitable characteristics, as not all soil types can be used in road construction. One type of soil that is problematic in construction is organic clay soil. Soil with low bearing capacity and rugged to withstand structural loads is defined as clay (Bowles, 1994). Clay soil is difficult to handle because it has high plasticity, so it requires special handling to overcome this (Hardiyatmo, 2010). The Jogja Bawen Toll Road Project has poor soil conditions, as can be seen during the dry season when the soil cracks, but during the rainy season, the soil becomes wavy, causing obstacles during the road construction process. In addition to observing the soil conditions,

direct identification was carried out in the field. The identification was done by taking soil samples at the location. From the results of the field identification, the soil was dark brown in color and soft in texture. Dark brown clay soil has a relatively high organic content (Hakim, 2025). Clay soil has high plasticity and low bearing capacity (A. Waruwu et al., 2024). Soil bearing capacity is the ability of the soil to resist subsidence (Puspita et al., 2022).

Increasing the CBR value must stabilize low soil bearing capacity (Wibowo & Endaryanta, 2017). The California Bearing Ratio (CBR) test was chosen over other soil tests because it illustrates the soil's ability to withstand traffic loads, especially on road subgrades. CBR (California Bearing Ratio) is the ratio between the load that can be carried by the subgrade and the standard load expressed in CBR values (Wardani et al., 2023). The CBR used on freeways on subgrade soil with a recommended CBR value of at least 6% so that the base layer can support traffic loads properly (Marga, 2024).

The Godean area is famous for one of its growing industries: red brick production. This industry has become the primary source of livelihood for the residents of Godean. With an abundant supply of raw materials in the form of clay, the red brick industry in Godean continues to grow. However, despite its positive economic impact, red brick production poses several environmental challenges, particularly concerning production waste. The waste generated in a single production run can reach around 5-10% of the total production. Red brick waste can come from defective, cracked, or substandard bricks discarded without reusing. Red brick waste can become an environmental problem, such as pollution. The accumulation of this waste creates problems for the environment and poses challenges for the industry in its management. However, red brick waste can be used as a soil stabilizing material in the construction world. Red brick waste has high cohesion, making it suitable for soil stabilization mixtures (Bowles, 1994). Studies on soil stabilization using red brick waste in road projects show up to 30% cost efficiency. In addition, it was found that in road projects, red brick waste increases the bearing capacity of the subgrade soil by up to twice that of the original soil (Fuadi et al., 2020). Red brick waste is an alternative solution, a stabilizing material. By varying the composition, it is hoped that the most effective combination can increase the CBR value and improve soil conditions in the Jogja-Bawen Toll Road Project. Based on the background description, the researcher is interested in further examining the Variation in the Composition of Red Brick Waste on Soil Improvement in the Jogja-Bawen Toll Road Project.

2 METHODS

2.1 Location

The research location was at the Jogja – Bawen Toll Road Project Section I STA 57 + 450 – 57 + 600. The location is precisely in the Sleman area. The location was chosen based on the condition of the subgrade in the area, which is dominated by clay soil with low bearing capacity, potentially causing problems for toll road construction. This type of soil tends to have high plasticity, is prone to volume changes due to moisture content, and is susceptible to settlement when subjected to heavy traffic loads.

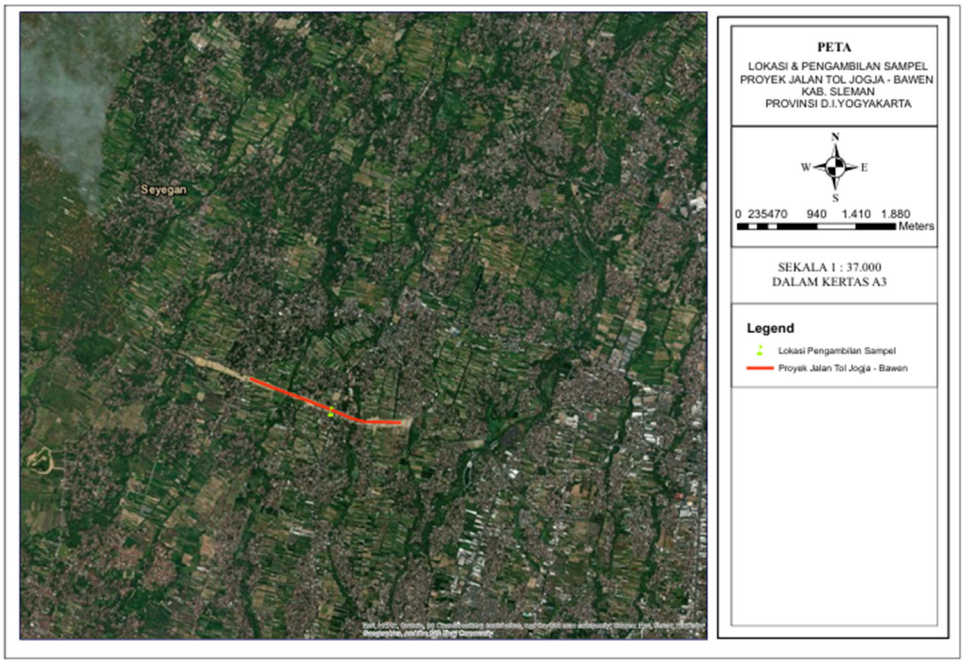

Figure 41 Reasearch Location

2.2 Variable

This test refers to SNI and previous tests. The variables used in this study are:

a) Independent Variables
Independent variables influence or cause changes in dependent variables (Arib et al., 2024). In this study, the independent variables are variations in the composition of red brick waste, namely 6%, 12%, and 18%.
b) Dependent Variables
Dependent variables are variables that are influenced by or result from independent variables. In this study, the variables are soil tested for CBR and Swelling.

2.3 Guidelines Testing

No	Testing	Unit	Guidelines	Results
1.	Moisture content	%	SNI 1965-2008	To determine the amount of water in the soil
2.	Spesific gravity	-	SNI 1964 – 2008	To determine the specific gravity of solid particles.
3	Liquid limit	%	SNI 1967-2008	To classify soil based on its cohesive properties and to determine the swelling and shrinkage properties of soil.

No	Testing	Unit	Guidelines	Results
4.	Plastic limit	%	SNI 1966-2018	To calculate the IP, which indicates the range of moisture content at which soil is plastic.
5.	Sieve Analysis	mm	SNI 3423:2008	To determine the size of soil particles.
6.	Proctor		SNI 1742:2008	To obtain the optimum moisture content (%)
7.	CBR	%	SNI 1744 – 2012	To compare the load on the soil sample and the standard load at the same penetration.

2.4 Method

Sampling was conducted on the Jogja Bawen Toll Road, and red bricks were taken from Godean Sleman. Sampling was carried out using the disturbed method. The mixture variations were based on previous research that found the lower, middle, and upper limits. The variations used were 6%, 12% and 18% and the curing time was 4 days for CBR immersion per SNI standards. The red brick mixture used was taken from the planned percentage multiplied by the weight of the soil. Samples were labelled with codes A to D. Code A was native soil without mixture, code B was soil + 6% brick, code C was soil + 12% brick, and code D was soil + 18% brick. The sample requirements used can be seen in Table 2.

Table 27 Soil Requirements

Soil Requirements				
Sample	**Code**	**Unsoaked (gr)**	**Soaked (gr)**	**Total (gr)**
A (0%)	A1	4500	4500	9000
	A2	4500	4500	9000
B (6%)	B1	4230	4230	8460
	B2	4230	4230	8460
C (12%)	C1	3960	3960	7920
	C2	3960	3960	7920
D (18%)	D1	3690	3690	7380
	D2	3690	3690	7380
Total				65520

Table 28 Red Brick Waste Requirements

Red Bricks Waste Requirements				
Sample	**Code**	**Unsoaked (gr)**	**Soaked (gr)**	**Total (gr)**
A (0%)	A1	0	0	0
	A2	0	0	0
B (6%)	B1	270	270	540
	B2	270	270	540
C (12%)	C1	540	540	1080
	C2	540	540	1080
D (18%)	D1	810	810	1620
	D2	810	810	1620
Total				6480

The testing began with preparing soil samples with the compositions in Tables 2 and 3. The soil was tested for CBR, considering the optimum moisture content obtained in the previous Proctor test with maximum density. Next, CBR testing was carried out under non-saturated and saturated conditions. In addition to the CBR value, observations were made on the swelling. Furthermore, X-Ray Fluorescence (XRF) testing was also conducted on red brick waste for its content.

3 RESULT AND DISCUSSION

3.1 CHARACTERISTICS OF RED BRICK WASTE

Utilizing red brick waste as a soil stabilizer is an alternative solution. Chemical testing is required to determine the contents of red bricks. This testing aims to identify and understand the chemical composition of red bricks that can affect soil particles.

X-Ray Fluorescence (XRF) testing is a non-destructive analysis method used to determine the chemical content of a material, whether solid or powder (Desfitri et al., 2022). The working principle of XRF is to shoot X-rays at a sample so that the atoms in it are excited and emit fluorescence with a specific wavelength according to the characteristics of their constituent elements. Each element has a unique spectrum, so the type and content of each element can be determined from the intensity and energy of the emitted fluorescence. The chemical elements contained in red brick waste can be seen in Table 3.

Table 29 Red brick test results

Chemicals Element	Content (%)
SiO_2	65.6
Al_2O_3	19.4
Fe_2O_3	10.3
CaO	2.24
K_2O	1.126
MgO	0.72
TIO_2	0.556
P_2O_5	0.06
ZnO	0.001

These chemical contents have their respective functions in soil stability. Based on the results of X-Ray Fluorescence (XRF) testing on red bricks, it is known that the main contents consist of 65.6% SiO_2, 19.4% Al_2O_3, and 10.3% Fe_2O_3, while the minor contents include CaO (2.24%), K_2O (1.126%), MgO (0.72%), and other oxides such as TiO_2, P_2O_5, and ZnO with small percentages. The high SiO_2

content fills the voids between soil particles, increasing density and reducing plasticity (Sartika et al., 2022). Al_2O_3 and Fe_2O_3 act as natural binders that strengthen the bonds between particles, while CaO and MgO support the cementation process through reactions with water, even though their relatively small levels. With this composition, red brick waste has excellent potential for use as a soil stabilizing material, especially in plastic clay soils, because it can improve the physical and mechanical properties of the soil and increase the CBR value in both saturated and unsaturated conditions.

In addition to conducting X-Ray Fluorescence (XRF) testing to determine the chemical content of red brick waste, this study also conducted specific gravity testing. The specific gravity test results were 2.32. The specific gravity test results for red brick waste were then compared with the specific gravity of the original soil. The original soil test results showed a specific gravity of 2.58 > 2.32, indicating lighter red brick particles. Nevertheless, adding red brick powder can improve soil structure because its fine particles fill the voids between soil grains, resulting in a denser structure and increased density.

Thus, combining chemical content data from XRF testing and physical data from specific gravity testing provides a more comprehensive picture of the potential of red brick waste as a soil stabilisation material. The oxide content, such as SiO_2, Al_2O_3, and Fe_2O_3, supports the binding and pore-filling processes, while the specific gravity results show the ability of this material to balance soil density. These two test results are the basis for considering red brick waste effective for improving the quality of subgrade soil in road construction projects.

3.2 SOIL CHARACTERISTICS

Soil density testing aims to determine the density of soil particles. Soil density describes the ratio of dry soil particles' weight to water's weight in the same volume, without considering the pore space between soil particles (SNI 1964, 2008). The average density test results from 50 ml and 100 ml pycnometers were 2.58. According to Hardiyatmo 2010, this soil is classified as organic clay soil. Differences in organic content in the soil affect the increase in soil strength (Oktafiani et al., 2022). Organic matter has a much lower specific gravity than soil minerals. Soil classified as organic clay can cause construction problems because it has low bearing capacity, so soil improvement is necessary.

Sieve analysis and hydrometer tests were conducted to determine the soil's particle size distribution. Hydrometer analysis was used because the soil has fine particles. The results of the tests are shown in Figure 13.

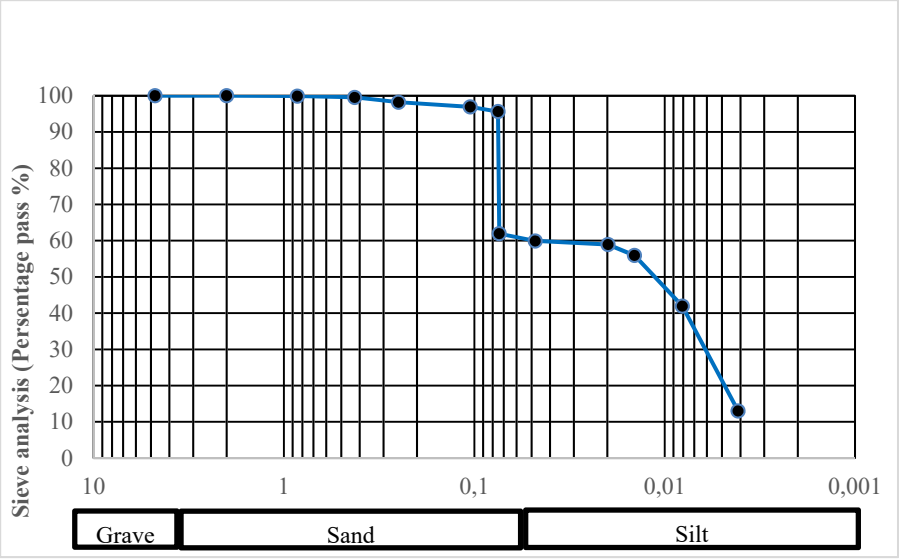

Figure 42 Sieve Analysis

AASHTO classification results show that if the No. 200 passing rate is > 35%, the soil falls into category A-7-6, with low bearing capacity. The soil particle distribution obtained is 0.00% gravel, 4.36% sand, and 95.64% silt. The calculation results show that Cu = 5 and Cc = 1.09. Based on the ASTM soil gradation classification criteria, a Cu value greater than 4 indicates that this fine-grained soil has a pretty good gradation. Meanwhile, a Cc value between 1 and 3 indicates that the particle size distribution is relatively uniform. Thus, this soil can be categorized as having good gradation. However, the sieve analysis results also show that a silt fraction of 95.64% dominates the soil. This means that even though the Cu and Cc values indicate good gradation, the dominant nature of silt still has a significant effect on the characteristics of the soil, namely, low plasticity, poor drainage, and relatively low bearing capacity. These conditions are fundamental to consider in construction planning, especially for toll road projects that require a high-strength subgrade.

The Atterberg limits were determined to determine the soil's plastic properties against changes in water content in the soil, which is the boundary between its liquid and plastic states. The results show that the soil has a liquid limit of 37.37%, a plastic limit of 19%, and a plasticity index of 18.37%. The data can be classified into two categories, AASHTO and USCS classifications. Based on the results in Table 13 of the AASHTO classification, because LL = 37.37 < 40 and IP = 18.37 > LL – 30, we get 18.37 > 7.37. Based on the soil classification results analysis according to AASHTO, the soil is classified as group A–7–6, clayey soil with high plasticity. This type of soil tends to be expansive, readily absorbs water, and undergoes significant volume changes when wet or dry, resulting in low bearing capacity. In civil engineering applications, A-7-6 soil often requires improvement or stabilization before being used as a road base layer. The classification results according to USCS obtained a plasticity index of 18.37. According to USCS, it is classified as ML soil, which is clayey soil. It is ML because the LL point = 37.37 and PI = 18.37 are located above Line A, where Line A is used as the boundary between clay and silt soils. Soil with a high PI value, such as in the sample, has a high potential for swelling and shrinkage and low shear strength when saturated. Soil is not recommended for direct use as a construction base without stabilisation.

The Proctor test was taken with a density value of 100% to achieve the maximum test results. The effect of using 100% density with the addition of stabilization material can be tested optimally (Barman & Dash, 2022). The test obtained a maximum dry density value of 1.36 g/cm³ with 700 ml of water. These results were obtained from a graph with the x-axis representing the water content and the y-axis representing the dry volume weight (g/cm³). The graph shows the maximum dry bulk density at a certain optimum moisture content. Dry bulk density increases as moisture content increases, and above the optimum moisture content, dry bulk density decreases due to pore filling by water (Ludfian & Wibowo, 2017). The test results produced a graph as shown in Figure 4.

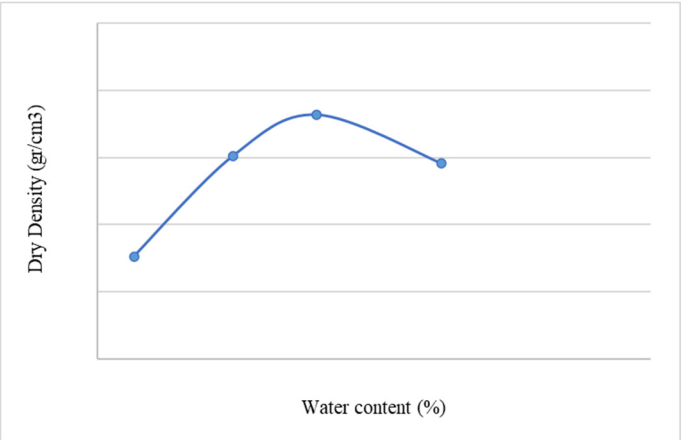

Figure 43 Proctor Results

3.3 IMPROVEMENT OF CBR IN SOAKED AND UNSOAKED CONDITION

California Bearing Ratio (CBR) testing is a commonly used method to evaluate soil's strength and bearing capacity as a base layer for road construction (Kusuma et al., 2022). This test provides an overview of the soil's ability to withstand traffic loads by comparing the pressure required for standard penetration of soil samples with standard materials. This CBR test focuses on the optimum moisture content. Based on SNI 1744 2012, each sample to be tested must be prepared in approximately 4.5 kg. Furthermore, the calculation of water addition to the sample is based on the optimum moisture content value obtained from the proctor test, which is 690 ml for each variation. Two samples were used for each variation, and the results of the two samples were averaged to obtain the results for each variation. The CBR test was conducted in two ways, namely unsoaked CBR and Soaked CBR. The results of the unsoaked CBR are shown in Figure 4.

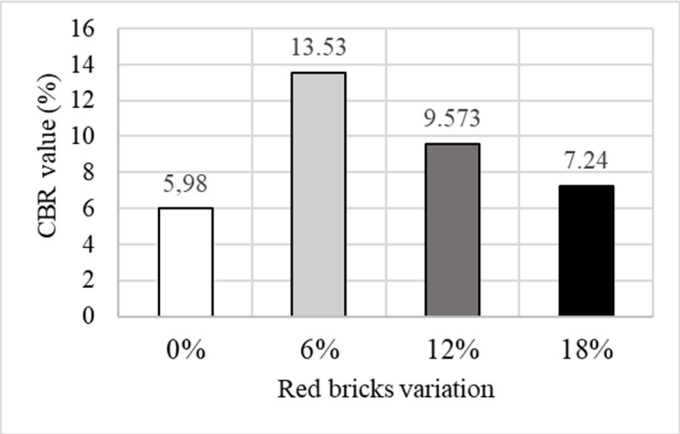

Figure 44 Results of the unsoaked CBR

Figure 5 shows that the maximum result was obtained at a variation of 6%, but at 12% and 18% variations, the results began to decline. At a content of 6%, red brick waste is an additional material that helps fill voids in the soil structure, thereby increasing density and soil bearing capacity (CBR). Soil stability with granular material aims to increase density and improve soil particle structure by filling the voids between grains, forming an interlocking grain arrangement and distributing the load more evenly (Hardiyatmo, 2010). The 12% and 18% variations experienced a decrease because brick waste caused the proportion of particles to be too coarse, making the material less dense. Adding excessive waste material can cause over-stabilization, where the particle size distribution becomes unbalanced. This causes the soil to lose its optimal density because the coarse material no longer effectively fills the voids between particles. 2. CBR Soak Test The CBR soak test was conducted by soaking the test specimen for 96 hours, followed by a CBR test. The results of the CBR soak test can be seen in Figure 5.

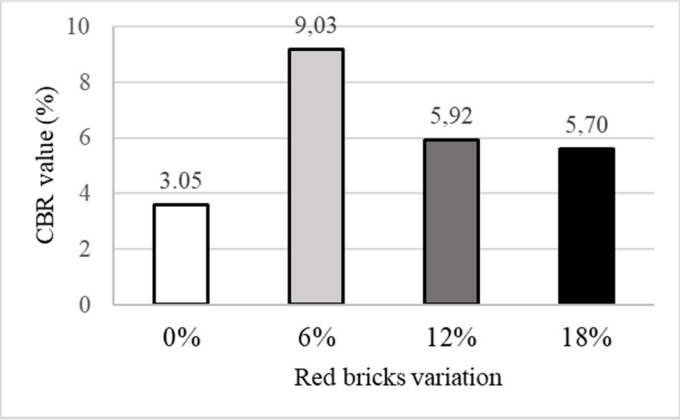

Figure 45 Results of the soaked CBR

The CBR value was only 3% without adding red brick. Soil with a CBR value of less than 5% is classified as very low, indicating that the soil is unsuitable for road base layers without improvement (DPU, 2005). At the 6% variation, there was a significant increase to 9%. This shows that the addition of brick waste improves the bearing capacity of the soil, possibly due to the coarse aggregate properties of the bricks, which help strengthen the soil structure. However, at 12% and 18% variations, the CBR value decreased to 5%. This shows that excessive waste addition is ineffective, possibly due to uneven particle distribution. Uneven distribution can cause a decline in soil quality because an inhomogeneous mixture results in uneven strength. Adding stabilization materials such as red bricks is optimal at a certain level, after which the mechanical properties can decrease due to increased porosity and disruption of the natural soil structure (Santoso et al., 2025). Porosity plays an important role in assessing the effectiveness of additives. Fine particles from red brick powder can enter and fill the soil pores, reducing the total pore volume and increasing soil density. This decrease in porosity results in a reduction in the potential for soil volume changes due to variations in moisture content and an increase in soil bearing capacity. Thus, controlling porosity through the addition of stabilizing materials not only improves the physical properties of the soil but also increases its stability and mechanical strength.

3.4 SWELLING POTENTIAL OF SOIL SAMPLE

CBR soak testing is also related to soil swelling. The swelling testing aims to determine how much soil will undergo volume changes when saturated with water (Eryunaningsih & Wulandari, 2024). This is important because soil with high swelling can cause a significant decrease in CBR values, which can cause damage to road construction. By measuring the swelling value, planners can determine the need for soil stabilization, for example, with red brick waste, so that expansion is reduced and the CBR value remains stable in the long term. The results of soil swelling that has been soaked for 4 days are shown in Figure 6.

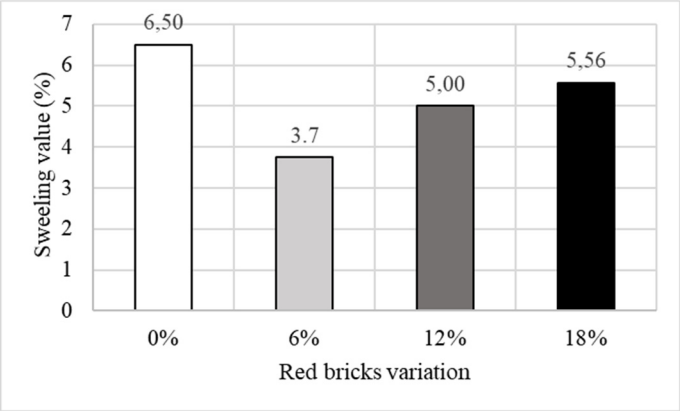

Figure 46 Results of the swelling CBR

The addition of 6% brick waste significantly reduced swelling to 3%, indicating the effectiveness of the addition in inhibiting water absorption. At 12% and 18% variations, the swelling value increased again to 5% and 5.5%. This shows that after passing the optimum point, the material's ability to inhibit water expansion becomes ineffective, possibly due to unstable material distribution and increased inter-particle voids. The addition of stabilizing materials, such as solid waste, must be optimum because excessive amounts can increase soil moisture and worsen expansive properties (Muliyah, 2020). Soil swelling occurs due to water entering the soil pores, especially in clayey soils with expansive minerals (Dewi et al., 2022). A slight swelling is caused by a low plasticity index (PI), and good soil density also plays a role in suppressing soil volume expansion. Swell can also be minimized through stabilization efforts using additional materials, including red brick waste. Red brick material is non-expansive and functions to fill the voids between soil particles, thereby reducing the pore space that water can occupy. In addition, the pozzolanic reaction of red brick waste can help bind fine soil particles, making the soil structure more compact and stable. According to Das (1993), good compaction and stabilization materials can reduce the potential for soil expansion and its

bearing capacity. A close and inverse relationship exists between swelling and the California Bearing Ratio (CBR) value. The smaller the swelling, the higher the CBR value, because the soil remains compact and able to withstand loads even when saturated with water. Conversely, if swelling is high, soil density decreases, causing the CBR value to drop significantly. Mixing clay soil with red brick waste reduces the swelling value and increases the CBR value, making the soil more suitable for use as a highway foundation layer (Irawan, 2020). This proves that controlling swelling is important in increasing soil bearing capacity. The addition of red brick waste increases the CBR value and reduces the plasticity and swelling value of the soil. This shows that red brick waste functions as a filler in the soil structure and contributes to improving the bond between soil particles. An addition of 6% with a CBR result of 9% is appropriate because the CBR of a good road subgrade must meet a CBR value of more than 5 (Afrida & Rum, 2023).

4 CONCLUSION

From the results of the research that has been conducted, it can be concluded that:

1. The results of specific gravity testing, sieve analysis, and Atterberg testing can be used to determine soil classification. The research was conducted on the Jogja Bawen Toll Road STA 57 + 450 – 57 + 600. The soil can be classified as clay with high plasticity.
2. The results of the CBR without soaking are 5.9 for 0% variation, 13.5 for 6% variation, 9.5 for 12% variation, and 7.2 for 18% variation. The CBR values with variations of 0%, 6%, 12%, and 18% are 3, 9, 5.9, and 5.7, respectively. The addition of red brick waste can increase soil bearing capacity and reduce swelling.
3. The most effective variation of red brick is 6%. The 6% variation showed the most optimal value. The 12% and 18% variations showed a decrease because the excessive addition of additives could not improve the soil structure.

DISCLAIMER

The authors declare no conflict of interest.

AVAILABILITY OF DATA AND MATERIALS

All data are available from the author.

REFERENCES

Afrida, M. F. D., & Senja Rum Harnaeni. (2023). Analisa Nilai Kepadatan Tanah Dasar (Subgrade) Dengan Pengujian Dynamic Cone Penetrometer (Dcp) Pekerjaan Akses Jalan Bandara Internasional Dhoho Kediri. *Jurnal Prosiding Universitas Muhammadiyah Surakarta*, 367–374.

Agustian Arif, M. R., Salimah, A., & Maha Agung, P. A. (2020). Pengaruh Penambahan Serbuk Bata Merah Terhadap Nilai Cbr. *PROKONS : Jurusan Teknik Sipil*, *14*(2), 47. https://doi.org/10.33795/prokons.v14i2.298

Arib, M. F., Rahayu, M. S., Sidorj, R. A., & Afgani, M. W. (2024). Experimental Research Dalam Penelitian Pendidikan. *Innovative: Journal Of Social Science Research*, *4*(1), 5497–5511.

Arifin, M., Putri, N. D., Sandrawati, A., & Harryanto, R. (2019). Pengaruh Posisi Lereng terhadap Sifat Fisika dan Kimia Tanah pada Inceptisols di Jatinangor. *SoilREns*, *16*(2), 37–44. https://doi.org/10.24198/soilrens.v16i2.20858

Asrar, dkk. (2021). Jurnal kacapuri. *Keilmuan Teknik Sipil*, *4*(1), 115–125.

Barman, D., & Dash, S. K. (2022). Stabilization of expansive soils using chemical additives: A review. *Journal of Rock Mechanics and Geotechnical Engineering*, *14*(4), 1319–1342. https://doi.org/10.1016/j.jrmge.2022.02.011

Bowles, J. E. (1989). *Sifat-sifat Fisis dan Geoteknis Tanah*. Erlangga.

Bowles, J. E. (1994). *Analisis dan Desain Pondasi.* (Jilid I Edisi empat). Erlangga.

Candra, A. I., Hanafi, M. A. A., Heru, R., Sipil, J. T., Kadiri, U., Kediri, K., Pengajar, S., Sipil, J. T., Kadiri, U., Kediri, K., Sipil, J. T., Kadiri, U., Kediri, K., Sipil, J. T., Kadiri, U., Kediri, K., Sipil, J. T., Kadiri, U., & Kediri, K. (2022). Kadiri Dengan Uji Kuat Geser Langsung. *Jurnal*

Riset Rekayasa Sipil Universitas Sebelas Maret, *6*(1), 12–20. https://jurnal.uns.ac.id/jrrs/article/view/61580

Das, B. M. (1993). *Prinsip Prinsip Rekayasa Geoteknis* (Edisi Kedu). https://www.slideshare.net/slideshow/mekanika-tanah-jilid-2-braja-m-das/53226428#2

Das, B. M. (1995). *Mekanika Tanah 1*. Erlangga.

Desfitri, E. R., Desmiarti, R., Martynis, M., & Dhani, S. R. (2022). Analisis dan Karakterisasi Potensi Pozzolan Sebagai Sumber Silika (SiO2) Untuk Meningkatkan Nilai Sumber Daya Lokal. *Jurnal Rekayasa Hijau*, *6*(2), 96–105. https://doi.org/10.26760/jrh.v6i2.96-105

Dewi, R., Idris, Y., San, I. C., Lien DYN, & Putri Tisya R. (2022). Sifat Fisis Tanah Lempung Ekspansif yang Disubstitusi dengan Serbuk Limbah Keramik. *Cantilever: Jurnal Penelitian Dan Kajian Bidang Teknik Sipil*, *11*(2), 73–80. https://doi.org/10.35139/cantilever.v11i2.118

DPU. (2005). *Kontruksi Indonesia*.

Ellitan. (2009). *Pemanfaatan Abu Terbang Batubara (Fly Ash) Sebagai Bahan Batako Yang Ramah Lingkungan*. *19*(19), 19.

Emanuel, V. (2021). Wewenang Penyelenggara Jalan Oleh Pemerintah Kabupaten Berdasarkan Undang-Undang Republik Indonesia Nomor 38 Tahun 2004 Tentang Jalan (Studi Di Wilayah Kabupaten Sintang). *Perahu (Penerangan Hukum) : Jurnal Ilmu Hukum*, *9*(1). https://doi.org/10.51826/perahu.v9i1.491

Endaryanta. (2010). 10543-25616-1-SM. *INERSIA*, 149–157.

Endaryanta, D. E. W. &. (2016). Upaya Meningkatkan Kuat Geser Tanah Lempung Dengan Memanfaatkan Limbah Plastik. *INERSIA Lnformasi Dan Ekspose Hasil Riset Teknik Sipil Dan Arsitektur*, *12*(1), 1–12. https://doi.org/10.21831/inersia.v12i1.10341

Eryunaningsih, R. T., & Wulandari, S. (2024). Pengaruh Penambahan Serbuk Bata Merah dan Limbah Polyethylene Terephtalate pada Tanah Lempung. *Jurnal Teknik Sipil*, *20*(1), 111–125. https://doi.org/10.28932/jts.v20i1.6644

Feed, A. R. (2022). Jurnal Sains dan Teknologi Peternakan. *Jurnal Sains Dan Teknologi*, *2*(1), 23–28. https://media.neliti.com/media/publications/439086-none-c93b042b.pdf

Fuadi, D. A., Gazali, A., & Purnamasari, E. (2020). *Pengaruh Campuran Serbuk Batu Bata Merah Terhadap Nilai Daya Dukung Pada Tanah Lempung Di Kabupaten Barito Kuala*.

Hakim, N. (2025). *Dasar Dasar Ilmu Tanah* (Edisi Kedua).

Hardiyatmo. (2015). *Pemeliharaan jalan raya*. Gadjah Mada University Press. https://library.bpk.go.id/koleksi/detil/jkpkbpkpp-p201614114

Hardiyatmo, H. . (2010). *Mekanika Tanah 1*. Gadjah Mada Univesity Press.

Hardiyatmo, H. C. (2011). *Analisis dan Perancangan Fondasi I* (Edisi Kedua). Gadjah Mada University Press.

Herman, M. A. (2022). Pemanfaatan Limbah Batu Bata Merah dalam Meningkatkan Daya Dukung Tanah Lempung. *Http://Jurnal.Ensiklopediaku.Org*, *4*(2). http://jurnal.ensiklopediaku.org

Irawan, D. (2020). 2020, Pengaruh pemanfaatan limbah bata merah sebagai bahan campuran terhadap sifat mekanik batako. *Skripsi). Universitas Muhammadiyah Mataram*, *1*, 1–55.

Kusuma Indra, M. E. & F. (2022). *Pemanfaatan Limbah Serbuk Batu Bata Merah Sebagai Bahan Stabilisasi Tanah Lempung*. *19*(2). http://ejournal2.pnp.ac.id/index.php/jirs/TerakreditasiSINTAPeringkat5

Leweherilla, J. A. &, & Maria, K. (2022). Analisis Perencanaan Tebal Perkerasan Lentur Dengan Menggunakan Motode Manual Desain Perkerasan (MDP) 2018 Pada Ruas Jalan Desa Lauran Kecamatan Tanimabr Selatan Kabupaten Kepulauan Tanimbar. *Jurnal Manumata*, *8*(1), 1–52. https://doi.org/10.21608/pshj.2022.250026

Ludfian, M., & Wibowo, D. E. (2017). Pemadatan Laboratorium. *INERSIA*, *XIII*(1), 66–75.

Marga DJB. (2024). Manual Desain Perkerasan Jalan 2024. *Kementrian PUPR*, 31–52.

Oktafiani, P. G., Putra, H., & Sutoyo, S. (2022). Pengaruh Dissolved Organic Carbon (DOC) pada Efektivitas Perbaikan Tanah Gambut dengan Metode Calcite Precipitation. *Jurnal Aplikasi Teknik Sipil*, *20*(1), 109. https://doi.org/10.12962/j2579-891x.v20i1.9637

Patrick Alexander Ho, A. T. M. & A. N. S. (2021). Analisis Pengaruh Campuran Garam Dan Belerang Pada Tanah Pasir Terhadap Kuat Geser. *Tekno*, *19*(April), 1–5. https://ejournal.unsrat.ac.id/index.php/tekno/article/view/32707%0Ahttps://ejournal.unsrat.ac.id/index.php/tekno/article/download/32707/30913

Pipit Muliyah, D. (2020). Korosi Dan Perlindungan Material. In *Journal GEEJ* (Vol. 7, Issue 2).

Prayuda Hakas, S. E. A. dan, & Fadillawaty, S. (2018). Analisis Sifat Fisik Dan Mekanik Batu Bata Merah Di Yogyakarta. *Jurnal Riset Rekayasa Sipil*, *1*(2), 94–104.

PUPR. (2017). *Manual Perkerasan Jalan*. *11*(1), 92–105.

Purwandhito, P. A., & Nugroho, S. (2015). Analisis Penyebab Kegagalan Produksi Batu Bata Hasil Mesin Extruder dengan Menggunakan Metode FTA (Fault Tree Analysis) (Studi kasus di Perajin Batu Bata Ngunut, Kabupaten Klaten). *Industrial Engineering Online Journal*, *4*(3), 1–12.

Puspita, S. A., Sophian, R. I., & Haryanto, I. (2022). Daya Dukung Pondasi Dalam Pada Tanah Lapukan Formasi Citalang Berdasarkan N-Spt. *Padjadjaran Geoscience Journal*, *6*(2), 780–785.

Ridwan, F. S., & Nadia. (2017). Analisis Pengaruh Pemanfaatan Abu Sekam Sebagai Filler Pada Campuran Aspal Beton. *Jurnal Konstruksia*, *8*(2), 1–8.

Safitri, S. I., Yudono, A., & Firdausiyah, N. (2024). *Pengaruh Jalan Tol Terhadap Pertumbuhan Ekonomi Kota/Kabupaten Yang Dilalui Jalan Tol Surabaya-Malang*. *13*(0341), 183–193.

Santoso, H., Wijayanti, A. P., Agia, Z. A., & ... (2025). Teknologi Peningkatan Sifat Mekanis Tanah Lempung dengan Metode Campuran Bahan Limbah: Reviu Artikel. *... Teknik Sipil UMS*, 362–373.

SNI. (1994). *SNI 03 -3439 - 1994*.

SNI 03-1966-1990. (2005). *Batas plastis dan indeks plastisitas tanah*.

SNI 03-1968-1990. (1990). Metode Pengujian Tentang Analisis Saringan Agregat Halus dan Kasar. *Sni 03-1968-1990*, 1–5. https://binamarga.pu.go.id/index.php/nspk/detail/sni-1970-2016-cara-uji-berat-jenis-dan-penyerapan-air-agregat-halus

SNI 03-3423-1994. (2018). Cara uji analisis ukuran butir tanah. *Badan Standardisasi Nasional*, *20*(2).

SNI 1744. (2012). Metode uji CBR laboratorium Badan Standardisasi Nasional. *Badan Standardisasi Nasional*, 1–28. www.bsn.go.id

SNI 1964. (2008). SNI 1964:2008 Uji Berat Jenis Tanah. *Badan Standardisasi Nasional*, *SNI*, 1–24.

SNI 1965: (2008). Cara Uji Penentuan Kadar Air untuk Tanah dan Batuan di Laboratorium. *Sni 1965:2008*, 1–16.

SNI1742. (2008). Cara Uji Kepadatan Ringan Untuk Tanah. *Standar Nasional Indonesia*, 1–20.

SNI1967. (2008). Cara uji penentuan batas cair tanah. *Badan Standardisasi Nasional*, *SNI*, 25.

Sudus, misbah dan wikal. (2021). Pemanfaatan Limbah Batu Bata Merah Dalam Stabilisasi Tanah Lempung. *Http://Jurnal.Ensiklopediaku.Org*, *3*. http://jurnal.ensiklopediaku.org

Sukirman. (1999). *Dasar-dasar perencanaan geometrik jalan* (Edisi keti).

Sunarno, Y., Tumpu, M., Kandou, C., Kabo, D. R. G., Tumengkol, H., & Rangan, P. R. (2025). Strength and Sustainability in Concrete: The Dual Role of Fly Ash and Accelerators in Reducing Environmental Impacts. *Engineering, Technology and Applied Science Research*, *15*(3), 23260–23267. https://doi.org/10.48084/etasr.10451

Tri Sartika, Ulfi Sepani, Putri, S. A., & Yayuk Apriyanti. (2022). Stabilisasi Tanah Gambut Menggunakan Campuran Serbuk Cangkang Kerang dan Fly Ash Ditinjau dari Nilai CBR Tanah dan Tingkat Keasaman Tanah. *Potensi: Jurnal Sipil Politeknik*, *24*(1), 15–22. https://doi.org/10.35313/potensi.v24i1.3613

Wardani, O., Cahyono, A. D., Aisyah, F. W. M., Putri, Y. M. A., Mahendra, D., Anam, A. K., & Risnanda, A. (2023). Pengaruh Tanah Lanau Berpasir Pada Nilai CBR Tanah Subgrade Jalan. *Cived*, *10*(2), 528–536. https://doi.org/10.24036/cived.v10i2.409

Waruwu, A., Celline, F., Sinaga, R., & Gandawijaya, D. G. (2024). Kajian Daya Dukung Tanah Lempung Distabilisasi dengan Abu Marmer. *Jurnal Saintis*, *24*(01), 11–20. https://doi.org/10.25299/saintis.2024.vol24(01).12710

Waruwu, M., Pu`at, S. N., Utami, P. R., Yanti, E., & Rusydiana, M. (2025). Metode Penelitian Kuantitatif: Konsep, Jenis, Tahapan dan Kelebihan. *Jurnal Ilmiah Profesi Pendidikan*, *10*(1), 917–932. https://doi.org/10.29303/jipp.v10i1.3057

Wibowo, D. E., & Endaryanta, E. (2017). Pemanfaatan Limbah Karbit Dan Pasir Sebagai Usaha Perbaikan Tanah Lempung Menggunakan Uji Cbr Dan Konsolidasi Dengan Pemadatan Laboratorium. *INERSIA Lnformasi Dan Ekspose Hasil Riset Teknik Sipil Dan Arsitektur*, *13*(2),

178–188. https://doi.org/10.21831/inersia.v13i2.17181

Yang L, J. Z. & Z. Y. (2015). *Effects of nano-TiO2 on strength, shrinkage and microstructure of alkali activated slag pastes*. Cement and Concrete Composites.

Yi, Y., Liska, M., Unluer, C., & Al-Tabbaa, A. (2013). Carbonating magnesia for soil stabilization. *Canadian Geotechnical Journal*, *50*(8), 899–905. https://doi.org/10.1139/cgj-2012-0364

Yong, L. L., Perera, S. V. A. D. N. J., Syamsir, A., Emmanuel, E., Paul, S. C., & Anggraini, V. (2019). Stabilization of a residual soil using calcium and magnesium hydroxide nanoparticles: A quick precipitation method. *Applied Sciences (Switzerland)*, *9*(20), 1–15. https://doi.org/10.3390/app9204325

This page is left blank intentionally

Stabilization Behavior of Sepaku Clay Shale Using Bacillus Subtilis

Yuswal Subhy[1], Achmad Bakri Muhiddin[2], Ardy Arsyad[3]
[1]Doctoral Student in Civil Engineering Program, Hasanuddin University, Makassar, Indonesia
[2]Lecturer at the Departement of Civil Engineering, Hasanuddin University, Makassar, Indonesia
[3]Lecturer at the Departement of Civil Engineering, Hasanuddin University, Makassar, Indonesia

*Correspondence: yuswalsubhy1971@gmail.com

ABSTRACT Clay Shale memiliki kandungan mineral terdiri dari lempung seperti Kaolinit, Illit dan Montmorillonit serta campuran kuarsa, feldspar, karbonat dan bahan organik. Kondisi slaking berulang, Clay Shale dapat mengalami pelapukan mekanis dan kimia yang mengubah kekuatan dan stabilitasnya. Soil Test dilakukan dengan Boring Test guna memperoleh data stratigrafi dan parameter geoteknik (SNI 8460:2017, SNI 03-1990, SNI 03-2835-2002) serta sampel DS batuan, kemudian dilaksanakan pengujian Slake Durability Test (ASTM D4644) bertujuan mengevaluasi ketahanan batuan sedimen, khususnya batuan lunak Clay Shale, terhadap pelapukan slaking. Potensi disintegrasi atau pelapukan pada batuan pada kondisi lingkungan nyata, khususnya geoteknik dapat dinilai. Kemudian pengujian XRD dan SEM bertujuan untuk menentukan jenis mineralogi Clay Shale, mengukur proporsi mineral kristalin, mendeteksi potensi ekspansif, mengevaluasi tingkat pelapukan dan memberikan data dasar untuk stabilisasi tanah. Pengambilan sampel Clay Shale yang telah mengalami pelapukan, guna pengujian Triaxial Test, Direct Shear Test, Konsolidasi, Water Content, Atterberg Limits, Specific Gravity dan Permeabilitas (ASTM D1587, ASTM D4767). Setelah metode pengujian Geologi maupun Geoteknik dilaksanakan dan dianalisis, didapatkan propertis dan karakteristik Clay Shale, sifat Geoteknik Clay Shale, permasalahan Clay Shale dan mineral umum dalam Clay Shale. Dalam hal tersebut penanganan perilaku stabilisasi Clay Shale kondisi slaking menggunakan Bacillus Subtilis metode biocementation kadar 4%, 6% dan 8% serta masa biocementation umur kultur 7 hari, 14 hari dan 28 hari apakah dapat meningkatkan parameter sifat Geoteknik Clay Shale (Kohesi, Sudut Geser Dalam, Swelling dan Konsolidasi), serta dari hasil pengujian tersebut apakah mempengaruhi perilaku stabilisasi Clay Shale Sepaku.
KEYWORDS Clay-Shale, XRD, SEM, Bacillus-Subtilis.

1. PENDAHULUAN

Penelitian ini diharapkan dapat memberikan kontribusi dan jalan keluar dalam meningkatkan standar penggunaan material tanah timbunan pada industri jasa konstruksi pada wilayah Sepaku yang dipilih menjadi Ibu Kota Negara. Sejumlah daerah di kawasan IKN Kalimantan Timur merupakan tanah Clay Shale dengan daya dukung sangat rendah. Tanah jenis ini, meskipun memiliki potensi untuk dimanfaatkan dalam berbagai aspek pembangunan, juga membawa tantangan besar yang harus diatasi dengan hati-hati. Kepala Otorita IKN Basuki Hadimuljono menjelaskan bahwa tanah Clay Shale yang ditemukan di IKN memerlukan penanganan khusus agar menjadi lebih kuat dan stabil untuk mendukung berbagai infrastruktur yang akan dibangun di kawasan tersebut. Lokasi test Boring SPT dan pengambilan sampel Clay Shale di Jl. Negara, Sukaraja, Sepaku, Penajam Paser Utara, Kalimantan Timur. Pekerjaan tanah timbunan melalui proses stabilisasi Clay Shale menggunakan campuran Bacillus Subtilis dengan proses biocementation dalam waktu terjadwal guna mendapatkan daya dukung tanah yang stabil, meskipun ada sebagian yang akan tergradasi akibat air hujan dan panas matahari. Dengan menggabungkan analisis mendalam tentang Clay Shale yang di stabilisasi dengan menggunakan Bacillus Subtilis metode biocementation kadar 4%, 6% dan 8% serta masa biocementation umur kultur 7 hari, 14 hari dan 28 hari, kemudian melaksanakan pengujian secara mekanis, tinjauan literatur yang komprehensif dan wawasan praktis dari proyek-proyek konstruksi nyata. Penelitian ini bertujuan untuk memberikan jalan keluar praktis bagi industri jasa konstruksi, khususnya pekerjaan tanah timbunan dalam upaya meningkatkan daya dukung Clay Shale dilapangan dan memastikan keberlanjutan proyek konstruksi di masa depan yang ramah lingkungan.

2. LANDASAN TEORI

Definisi Clay Shale menurut para ahli dan literatur; “Clay Shale adalah batuan sedimen berbutir sangat halus yang terbentuk dari akumulasi partikel lempung, bersifat mudah hancur ketika mengalami siklus basah-kering, dan memiliki struktur berlapis (laminasi).” Franklin, J.A., & Chandra, R. (1972). The Slake-Durability Test. “Clay Shale adalah batuan lempung yang telah mengalami litifikasi, biasanya menunjukan struktur laminasi halus, kekuatan rendah hingga sedang, dan bersifat sangat sensitif terhadap pelapukan fisik (khususnya pembasahan dan pengeringan).” Bell, F.G. (2007). Engineering Geology. 2nd Edition. “Shale

(termasuk clay shale) adalah batuan sedimen yang terbentuk dari dominasi partikel lempung dan lanau, memiliki kecendurangan belah mengikuti bidang laminasi dan sangat rentan terhadap pelemahan akibat pembasahan." Hoek, E. & Bray, J. (1981). Rock Slope Engineering. "Clay Shale merupakan batuan sedimen halus yang terdiri dari mineral lempung yang mengalami kompaksi dan sedikit sementasi, sering kali rapuh, dan memiliki daya tahan rendah terhadap perubahan kelembaban lingkungan." ISRM (International Society for Rock Mechanics, 1981). ISRM Suggested Methods.

Tabel 1. Ciri-ciri Umum Clay Shale (dari Literatur Teknik Geologi)

Karakteristik	Penjelasan
Komposisi	Didominasi mineral lempung seperti Illite, Kaolinit, Montmorillonite
Struktur	Laminasi halus (berlapis-lapis), sering menunjukan rekahan paralel
Perilaku Mekanik	Kekuatan rendah, sangat dipengaruhi oleh kelembaban
Durabilitas	Rendah terhadap siklus basah-kering (mudah lapuk)
Pengaruh Pelapukan	Sangat mudah berubah sifat akibat pelapukan kimia dan fisik
Kegunaan	Perlu distabilisasi bila digunakan sebagai material timbunan atau pondasi

Tabel 2. Klasifikasi Durabilitas (Gamble, 1971)

Kelas Ketahanan	% Retensi setelah 1 Siklus (10 menit, Berat Kering)	% Retensi setelah 2 Siklus (10 menit masing-masing)
Very High	> 99	> 98
High	98 – 99	95 – 98
Medium High	95 – 98	85 – 95
Medium	85 – 95	60 – 85
Low	60 – 85	30 – 60
Very Low	< 60	< 30

Gambar 1. Pola XRD sampel shale/tanah liat
(Minia University, M.A. Tantawy, January 2004)

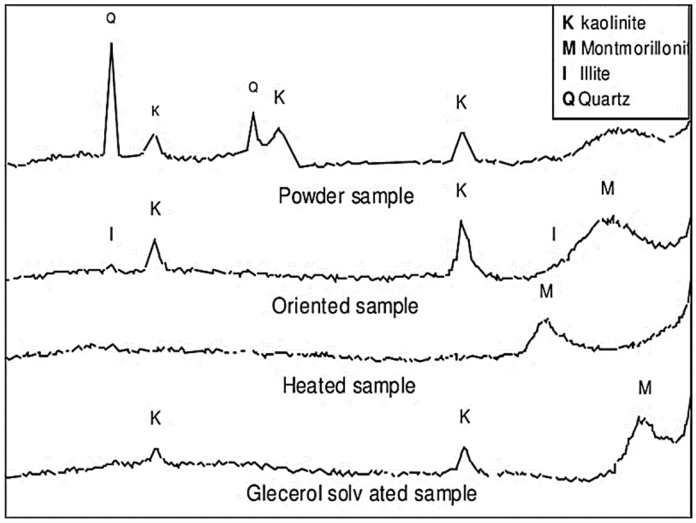

Keterangan: Pola XRD Clay Shale, menunjukan puncak difraksi utama seperti kuarsa, dengan sinyal mineral lempung.

Gambar 2. Hasil pola difraksi sinar-X (XRD) dari clay shale
(Jilin University, Hanzhi Yang, November 2022)

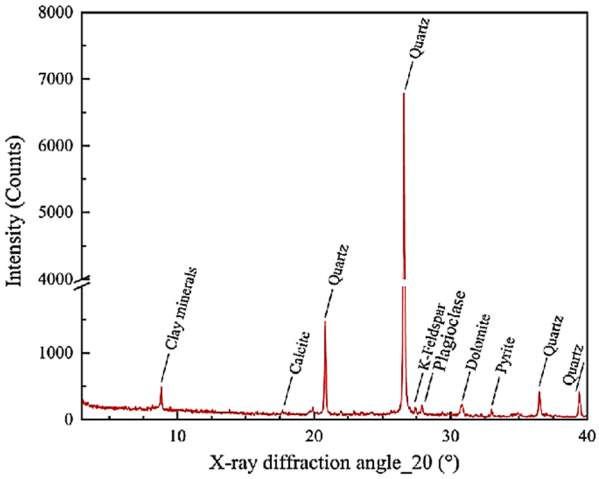

Keterangan: Pola Clay Shale, beberapa sampel dengan intensitas puncak berbeda, memperlihatkan adanya variasi mineral penyusun.

Gambar 3. Pola XRD dari shale utuh dan materi organik pada sampel 3 dan sampel 9.
(C = Mineral liat. Q = Kuarsa. Py = Pirit. F = Feldspar.)
(Southwest Petroleum University, Hui Han, February 2019)

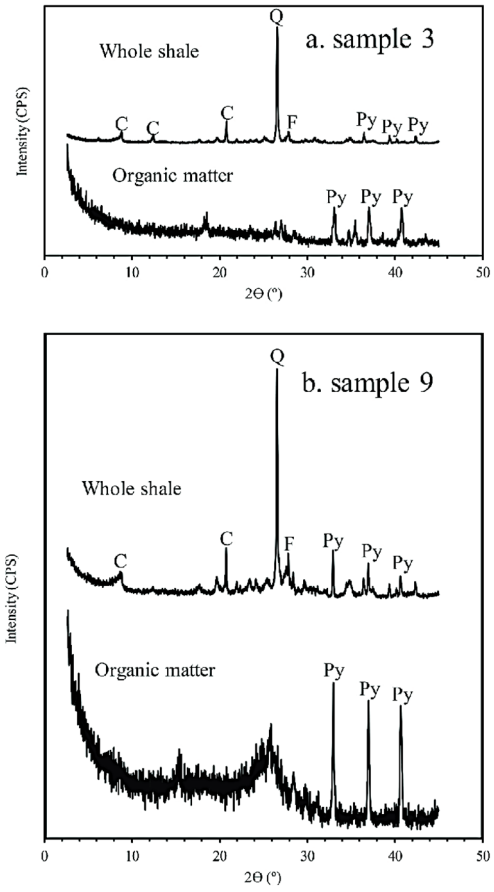

Keterangan: XRD dari whole shale dan dari bagian materi organik, identifikasi kuarsa, pirit, mineral lempung, feldspar.

Gambar 4. Pola difraksi sinar-X batuan lempung: a-clay shale, b-argillite, c-lempung
(Tbilisi State University, Marina, A.A, December 2023)

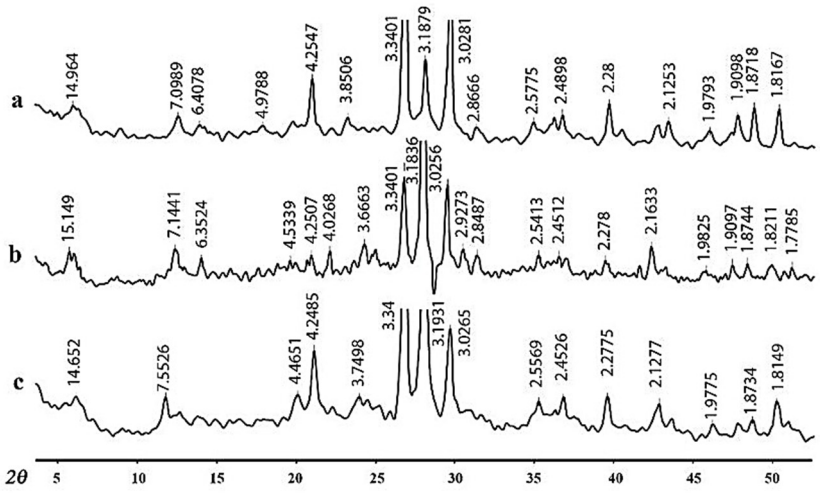

Keterangan: Perbandingan pola XRD dari shale, argillite, dan clay; menunjukkan perbedaan puncak khas tiap jenis material.

Gambar 5. Hasil Uji SEM (Scanning Electron Microscopy) dari clay shale / shale yang struktur mikro nya mirip – memperlihatkan pori, retakan mikro, orientasi mineral lempung, dan organik.
(The University of Manchester, Lin Ma, June 2021)

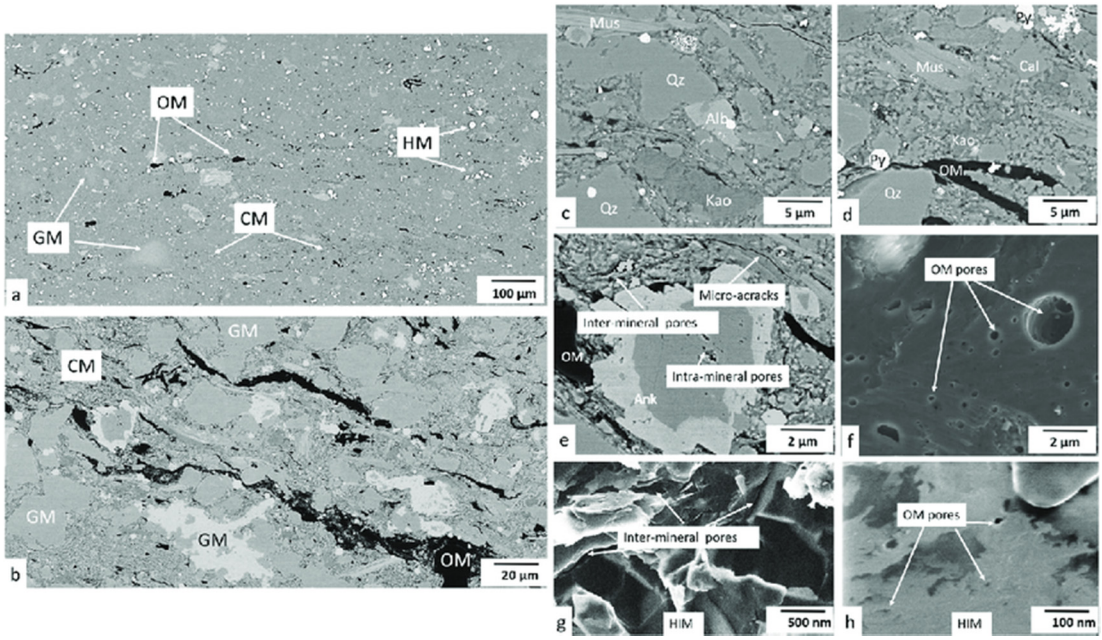

Keterangan: Gambar SEM dari formasi Bowland. (a) Gambaran umum struktur mikro sampel; (b) gambaran umum struktur mikro sampel dengan resolusi lebih tinggi; identifikasi (c) mineral granular dan mineral liat; (d) mineral berat dan partikel materi organik; (e) pori-pori mineral dan retakan mikro; (f) pori-pori materi organik; (g) pori-pori antar-mineral (diambil dengan HIM); (h) pori-pori materi organik (diambil dengan HIM). GM - mineral granular, CM - mineral liat, OM - materi organik, HM - mineral berat. Qz - kuarsa, Alb - albite, Cal - kalsit, Ank - ankerit, Py - pirit, Mus - muskovit, Kao - kaolinit. HIM - mikroskopi ion Helion.

Gambar 6. Hasil Uji SEM permukaan sampel shale yang telah dipoles
(Los Alamos National Laboratory, Kane C, Bennet, January 2015)

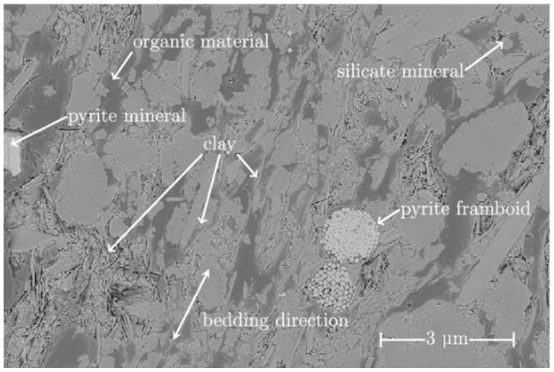

Keterangan: Permukaan shale yang dipoles, menampilkan retakan mikro dan permukaan kasar sebagai hasil fragmen partikel lempung.

Gambar 7. Hasil Uji SEM dari sampel batuan serpih laut utara yang khas
(SINTEF, Trondheim, Norway, Dr. Mohammad H.B, March 2020)

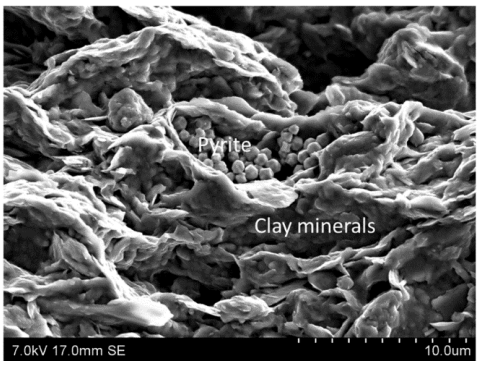

Keterangan: Gambar shale Laut Utara, menunjukkan hubungan antar partikel lempung, retakan kecil, dan pori antar mineral.

Gambar 8. Hasil Uji SEM Microstructure of the Longmaxi
(Chendu University of Technology, Qiaomu Qi, November 2020)

a) **b)**

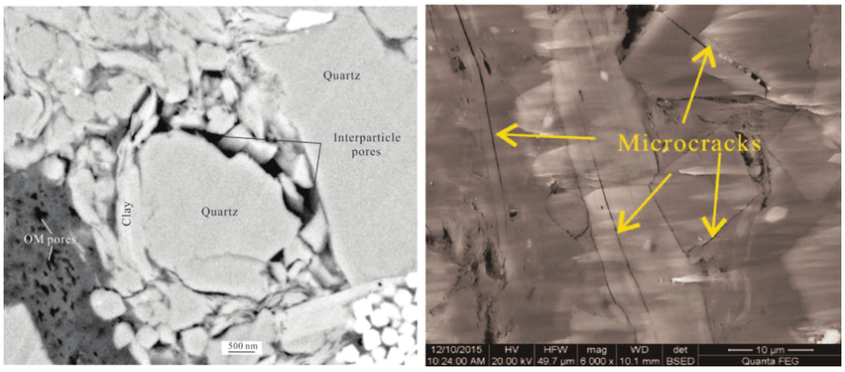

Keterangan: Gambar detail pori intra partikel dan antar partikel pada shale yang kaya organik, menunjukkan rongga halus di dalam partikel organik dan di antara mineral lempung dan kuarsa.

Menurut para ahli dan literaur, Bacillus Subtilis bukanlah istilah geologi, melainkan mikroorganisme (bakteri) yang kini digunakan dalam bidang geoteknik dan geologi Teknik untuk keperluan rekayasa tanah dan perkuatan struktur bawah tanah. Meskipun berasal dari mikrobiologi, para ahli geologi teknik dan geoteknik telah memulai banyak meniliti penggunaannya, khususnya dalam bioteknik tanah *(biogeotechnical engineering)*. Pengertian Bacillus Subtilis dalam konteks Geologi Teknik menurut pada ahli: “Bacillus Subtilis adalah bakteri gram positif yang mampu menghasilkan enzim urease, yang berperan dalam proses microbially induced calcite precipitation (MICP). Dalam konteks geoteknik, Bacillus Subtilis digunakan untuk

meningkatkan kekuatan tanah dan mengurangi permeabilitas melalui presipitasi kalsit di antara pori-pori tanah." DeJong et al. (2006, 2010). Pioneer in Bio-mediated Soil Improvement. "Bacillus Subtilis dapat dimanfaatkan untuk menghasilkan senyawa karbonat (seperti kalsit) melalui metabolisme mikrobiologis yang mengikat partikel tanah, memperbaiki kekuatan geser tanah dan meningkatkan stabilitas struktur geoteknik." Ivanov, V., & Chu, J. (2008). Applications of Microorganisms to Geotechnical Engineering. "Bacillus Subtilis memiliki kemampuan biomineralisasi, yaitu mengendapkan mineral (terutama $CaCO_3$) di dalam pori-pori tanah atau batuan, menjadikannya agen biologis yang efisien dalam stabilisasi tanah atau perbaikan struktur batuan lunak seperti clay shale atau siltstone." Achal, V., & Pan, X. (2011). Improvement of Concrete Durability with Microbial Calcite Precipitation. "Bacillus Subtilis digunakan sebagai agen biostabilisasi pada tanah lempung dan batuan lunak di Indonesia, seperti clay shale, untuk meningkatkan daya tahan terhadap pelapukan dan kekuatan tekan bebas melalui metode MICP." Putra, H., dkk. (2022). Penggunaan Bacillus Subtilis dalam stabilisasi tanah lempung lunak, Prosiding Geoteknik Nasional. Kesimpulannya, dalam geologi Teknik dan geoteknik, Bacillus Subtilis dipahami sebagai Bakteri ramah lingkungan yang dimanfaatkan dalam Teknik perbaikan tanah melalui proses biokimia (biocementation/ biomineralisasi) untuk:

a. Mingkatan kekuatan geser tanah (terutama lempung dan clay shale),
b. Mengurangi permeabilitas dan resapan air,
c. Memperbaiki durabilitas material tanah terhadap pelapukan,
d. Digunakan dalam proyek perbaikan pondasi, lereng, dinding penahan, dan reklamasi.

Gambar 9. Hasil Uji SEM terkait Bacillus Subtilis
(Chendu University of Technology, Qiaomu Qi, November 2020)

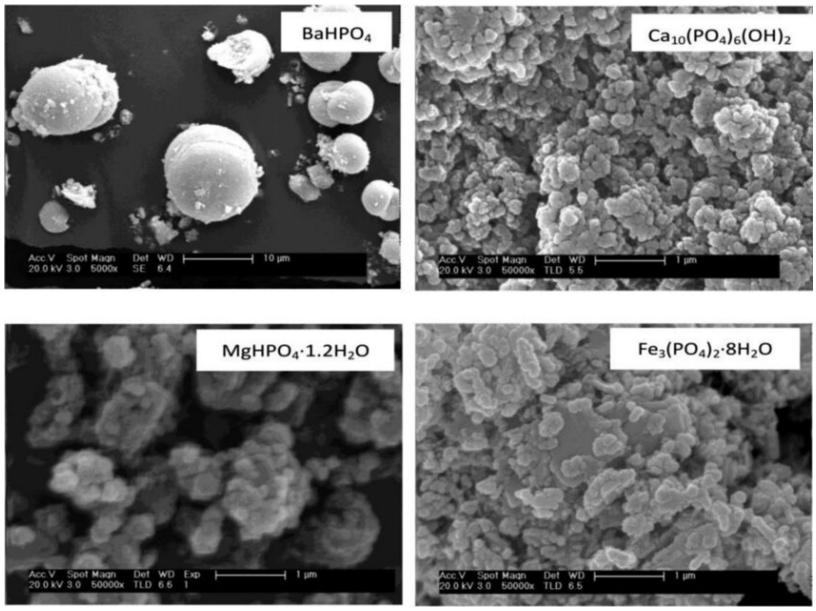

Keterangan: Gambar endapan fosfat yang diinduksi oleh *Bacillus Subtilis* – partikel mineral terbentuk, melekat pada substrat dan antar sel.

Dikutip dari buku Fundamentas of Soil Behavior, edisi ketiga, oleh (James K. Mitchell dan Kenichi Soga, 2005). Metode analisa guna menentukan komposisi kandungan mineral dari tanah lempung dan bukan tanah lempung, dijelaskan pada table berikut:

Table 3. Difraksi Sinar-X untuk Mineral Lempung dan Mineral Non-Lempung Umum

d (*A*)	Mineral[a]	*d* (*A*)	Mineral[a]
14	Mont. (VS) Chl. Verm. (VS)[b]	2.93 – 3.00	Felds.
12	Sepiolite, heated corrensite	2.89 – 2.90	Carb.
10	Illite, Mica (S), Halloysite	2.86	Felds.
9.23	Heated Verm.	2.84	Carb. Chl.
7	Kaol. (S), Chl	2.84 – 2.87	Chl.
6.90	Chl.	2.73	Carb.
6.44	Attapulgite	2.61	Attapulgite

6.39	Felds.		2.60	Verm., Sepiol.
4.90 – 5.00	Illite, Mica, Halloysite		2.56	Illite (VS), Kaol.
4.70 – 4.79	Chlor. (S)		2.53 – 2.56	Chlor., Felds., Mont.
4.60	Verm. (S)		2.49	Kaol. (VS)
4.45 – 4.50	Illite (VS), Sepiolite		2.46	Quartz, heated Verm.
4.46	Kaol.		2.43 – 2.46	Chlorite
4.36	Kaol		2.39	Verm., Illite
4.26	Quartz (S)		2.38	Kaol.
4.18	Kaol.		2.34	Kaol. (VS)
4.02 – 4.04	Felds. (S)		2.29	Kaol. (VS)
3.85 – 3.90	Felds.		2.28	Quartz, Sepiol.
3.82	Sepiol.		2.23	Illite, Chl.
3.78	Felds.		2.13	Quartz, Mica
3.67	Felds.		2.05 – 2.06	Kaol. (WK)
3.58	Carbonate, Chl.		1.99 – 2.00	Mica, Illite (S), Kaol. Chl.
3.57	Kaol. (VS), Chl.		1.90	Kaol.
3.54 – 3.56	Verm.		1.83	Carb.
3.50	Felds., Chlor.		1.82	Quartz
3.40	Carb.		1.79	Kaol.
3.34	Quartz (VS)		1.68	Quartz
3.32 – 3.35	Illite (VS)		1.66	Kaolin
3.30	Carb.		1.62	Kaolin
3.23	Attapulgite		1.54B	Verm. (S), Quartz
3.21	Felds.		1.55	Quartz
3.20	Mica		1.58	Chl.
3.19	Felds. (VS)		1.53	Verm., Illite
3.05	Mont.		1.50	Illite (S), Kaol.
3.04	Carb. (VS)		1.48 – 1.50	Kaol. (VS), Mont.
3.02	Felds.		1.45B	Kaol.
3.00	Heated Verm.		1.38	Quartz, Chl.
2.98	Mica (S)		1.31, 1.34, 1.36	Kaol. (B)

3. ANALISIS DAN PERANCANGAN SISTEM/ METODE PENELITIAN

Tujuan Penelitian, guna mengembangkan metode stabilisasi clay shale Sepaku menggunakan Bacillus Subtilis melalui proses Microbial Induced Calcite Precipitation (MICP). Penelitian akan diawali dengan studi literatur komprehensif, diikuti dengan karakteristik mendalam terhadap clay shale Sepaku, optimasi kultur Bacillus Subtilis dan formulasi larutan injeksi, serta perancangan dan pelaksanaan percobaan stabilisasi multi-parameter. Tahapan selanjutnya meliputi pengujian sifat geoteknik dan mekanika tanah yang distabilkan, analisis mikrostruktural untuk memahami mekanisme stabilisasi, evaluasi kinerja dengan analisis statistic, dan diakhiri dengan pembahasan temuan serta implikasi praktis. Metodologi ini dirancang berdasarkan praktik terbaik dan inovasi terbaru yang ditemukan dalam jurnal-jurnal internasional terkini untuk memastikan validitas dan relevansi ilmiah.

3.1. Studi Literatur Komprehensif dan Terkini

Studi ini akan diawali dengan tinjauan literatur ilmiah internasional terbaru, focus pada publikasi dalam 5-10 tahun terakhir, untuk mengidentifikasi dan menganalisis informasi krusial terkait:

a. Karakteristik Clay Shale Sepaku: Meliputi tinjauan sifat geologi, geoteknik (misalnya, plastisitas tinggi, permeabilitas terbatas, potensi mengembang-menyusut), dan komposisi mineralogi (kaolinit, illit, smektit, kuarsa, feldspar). Penting untuk memahami degradasi saat terpapar lingkungan, yang dapat mengubahnya dari batuan keras menjadi lempung lunak, serta dampaknya terhadap stabilitas lereng dan infrastrukur. (Sagitaningrum et al., 2023), dan (Rahardjo, 2023).

b. Mekanisme Stabilisasi Tanah Menggunakan Bacillus Subtilis (MICP): Mempelajari prinsip-prinsip dasar MICP, dimana Bacillus Subtilis menginduksi presipitasi kalsium karbonat melalui aktivitas urease. Penelitian akan mencakup optimalisasi genetik Bacillus Subtilis untuk meningkatkan aktivitas ureolitiknya, serta peran enzim Carbonic Anhydrase (CA) dalam proses ini. (Wright et al., 2020), (Gilmour, et al., 2024)., dan (Hoffmann et al., 2024).

c. Studi Kasus dan Inovasi Terbaru dalam Stabilisasi Tanah Lempung Ekspansif: Mengidentifikasi penelitian yang menggunakan Bacillus Subtilis untuk stabilisasi tanah lempung, termasuk studi yang mengevaluasi peningkatan kuat tekan bebas (UCS), California Bearing Ratio (CBR), dan modulus reaksi tanah. Tinjauan juga akan mencakup studi yang mengeksplorasi penggunaan polimer sebagai agen stabilisasi tambahan dan metode injeksi yang relevan. (Hasriana, et al., 2018), dan (Almajed, et al., 2022).

Tinjauan ini akan berfungsi untuk mengidentifikasi kesenjangan penelitian dan metodologi yang relevan untuk penelitian disertasi ini.

3.2. Karakterisasi Awal Clay Shale Sepaku Secara Mendalam

Langkah ini berfokus pada karakterisasi sampel *clay shale* Sepaku yang belum distabilkan. Jika data spesifik *clay shale* Sepaku tidak tersedia, karakteristik *clay shale* dari wilayah lain dengan kesamaan geoteknik dan geologi akan menjadi referensi. Pengujian yang akan dilakukan meliputi:

a. Pengujian Geoteknik: Penentuan batas Atterberg (batas cair >50%), distribusi ukuran partikel, berat jenis, uji konsolidasi, permeabilitas, dan kuat geser tanah. Sifat-sifat ini krusial untuk memahami perilaku dasar clay shale dan potensi pengembangannya. (Ilori et al., 2025), dan (Nazir et al., 2024).
b. Pengujian Kimia: Analisis pH dan kandungan organik untuk memberikan gambaran lingkungan kimia sampel tanah.
c. Analisis Mineralogi: Menggunakan X-Ray Diffraction (XRD) untuk mengidentifikasi komposisi mineral lempung (misalnya, kaolinit, ilit, smektit) dan X-Ray Energy Dispersive Spectroscopy (SEM-EDX) untuk menganalisis morfologi permukaan dan komposisi unsur. Ini penting untuk mengidentifikasi potensi pengembangan (swelling potential) dan reaktivitas mineral lempung. (Ru Jia et al., 2023), dan (Ardebili et al., 2025).

Data dari karakterisasi awal ini akan menjadi dasar perbandingan untuk mengevaluasi efektivitas stabilisasi.

3.3. Pengembangan dan Optimasi Kultur Bacillus Subtilis serta Larutan Injeksi

Bagian ini akan mengembangkan protokol untuk memastikan efektivitas MICP:

a. Preparasi Kultur Bacillus Subtilis: Mengidentifikasi strain Bacillus Subtilis yang paling efisien untuk induksi presipitasi kalsit dari literatur. Protokol akan mencakup pemilihan media nutrisi optimal, kondisi pertumbuhan (suhu 30°C optimal untuk aktivitas enzim CA), waktu inkubasi, dan konsentrasi bakteri yang efektif untuk memaksimalkan produksi urease dan presipitasi kalsit. (Gilmour et al., 2024), dan (Hoffmann et al., 2021).
b. Formulasi Larutan Sementasi: Mendesain formulasi larutan berbasis urea dan kalsium klorida yang optimal. Optimasi akan mempertimbangkan rasio urea terhadap kalsium klorida, konsentrasi, dan pengaruhnya terhadap keseragaman pengendapan karbonat. Tujuan adalah untuk mencapai pengendapan kalsit yang efisien dan seragam dalam matriks clay shale. (Fronczyk et al., 2023), (Konstantinou et al., 2021)., dan (Zheng et al., 2022).

3.4. Desain dan Pelaksanaan Percobaan Stabilisasi Multi-Parameter

Percobaan stabilisasi akan dirancang untuk menguji pengaruh berbagai parameter terhadap efektivitas MICP pada clay shale Sepaku:

a. Variasi Parameter Kunci: Meliputi konsentrasi Bacillus Subtilis, konsentrasi larutan sementasi, metode injeksi (misalnya, perendaman atau injeksi berulang), frekuensi injeksi, dan durasi curing.
b. Metode Injeksi: Menggunakan metode yang direkomendasikan dalam literatur, yang mungkin melibatkan injeksi larutan bio-sementasi ke dalam sampel tanah. Beberapa penelitian juga menunjukkan relevansi penggunaan polimer dalam stabilisasi tanah melalui injeksi, yang dapat menjadi referensi untuk desain metode injeksi. (Almajed et al., 2022), (Wang et al., 2024)., dan (Pratter et al., 2022).
c. Desain Percobaan: Menggunakan desain faktorial atau pendekatan statistik lainnya untuk mengidentifikasi interaksi antar parameter dan mengoptimalkan kondisi stabilisasi.

3.5. Pengujian Sifat Geoteknik dan Mekanik Tanah yang Distabilkan

Setelah stabilisasi dan periode curing yang ditentukan, sampel clay shale yang telah distabilkan akan diuji untuk mengevaluasi peningkatan sifat-sifatnya:

a. Uji Kuat Tekan Bebas (UCS): Untuk mengukur peningkatan kekuatan tekan tanah. Beberapa studi menunjukkan peningkatan kekuatan tekan tanah setelah stabilisasi dengan Bacillus Subtilis. (Ibrahim et al., 2025), dan (Rokhman et al., 2024).
b. Uji Kuat Geser Langsung/Triaksial: Untuk mengevaluasi peningkatan kuat geser tanah.
c. Uji Konsolidasi dan Permeabilitas: Untuk menilai perubahan kompresibilitas dan aliran air melalui tanah.
d. Uji Durabilitas: Jika memungkinkan, uji siklus basah-kering akan dilakukan untuk mengevaluasi ketahanan tanah yang distabilkan terhadap perubahan kondisi lingkungan, merefleksikan degradasi yang sering terjadi pada clay shale di lapangan. (Sagitaningrum et al., 2023).

3.6. Analisis Mikrostruktural dan Mekanisme Stabilisasi Lanjutan

Teknik karakterisasi mikroskopis akan digunakan untuk memahami mekanisme di balik stabilisasi:

a. Scanning Electron Microscopy (SEM): Untuk memvisualisasikan morfologi permukaan sampel yang distabilkan dan mengidentifikasi distribusi kristal kalsit yang terbentuk.
b. Energy-Dispersive X-ray Spectroscopy (EDX): Untuk analisis unsur dan konfirmasi pembentukan kalsit (calcium carbonate).
c. X-ray Diffraction (XRD): Untuk mengidentifikasi fasa mineral baru yang terbentuk (terutama kalsit) dan perubahan dalam komposisi mineral lempung.
d. Fourier Transform Infrared Spectroscopy (FTIR): Untuk menganalisis ikatan kimia dan interaksi molekuler antara mikroorganisme, kalsit, dan partikel tanah.

Hasil analisis ini akan membantu mengkonfirmasi pembentukan kalsit dan menjelaskan bagaimana MICP memodifikasi struktur mikro *clay shale*, berkontribusi pada peningkatan sifat mekaniknya.

3.7. Evaluasi Kinerja, Pemodelan, dan Analisis Data Statistik

Data yang terkumpul dari pengujian akan dianalisis secara statistik:

a. Perbandingan Kinerja: Membandingkan hasil pengujian sifat geoteknik dan mekanik antara sampel yang distabilkan dengan Bacillus Subtilis dan sampel kontrol (tanpa stabilisasi), serta antar variasi perlakuan.
b. Analisis Statistik: Menggunakan metode statistik seperti ANOVA (Analysis of Variance) atau uji-t untuk menilai signifikansi perbedaan antara kelompok perlakuan.
c. Pemodelan: Jika data memungkinkan, model empiris atau numerik dapat dikembangkan untuk memprediksi perilaku stabilisasi clay shale Sepaku berdasarkan parameter yang divariasikan, mengacu pada model yang digunakan dalam penelitian serupa.

3.8. Pembahasan Temuan, Inovasi, dan Implikasi Praktis

Tahap akhir ini melibatkan interpretasi dan diskusi mendalam terhadap seluruh temuan:

a. Diskusi Komprehensif: Mengaitkan hasil penelitian dengan literatur terbaru, mengidentifikasi kontribusi ilmiah baru dalam pemahaman stabilisasi clay shale Sepaku menggunakan MICP.
b. Kelebihan dan Keterbatasan: Mengevaluasi efektivitas, kelebihan, dan keterbatasan metode Bacillus Subtilis untuk stabilisasi clay shale Sepaku dalam konteks teknis dan lingkungan.
c. Implikasi Praktis: Menguraikan potensi aplikasi praktis dari temuan ini di lapangan, misalnya dalam perbaikan lereng, fondasi, atau konstruksi jalan di daerah dengan clay shale serupa.
d. Arah Penelitian Masa Depan: Mengidentifikasi area penelitian lebih lanjut yang dapat dikembangkan dari disertasi ini, termasuk potensi optimasi lebih lanjut atau penerapan pada jenis tanah lain.

Gambar 10. Peta Provinsi Kalimantan Timur
(Google Maps. 30 Juni 2025)

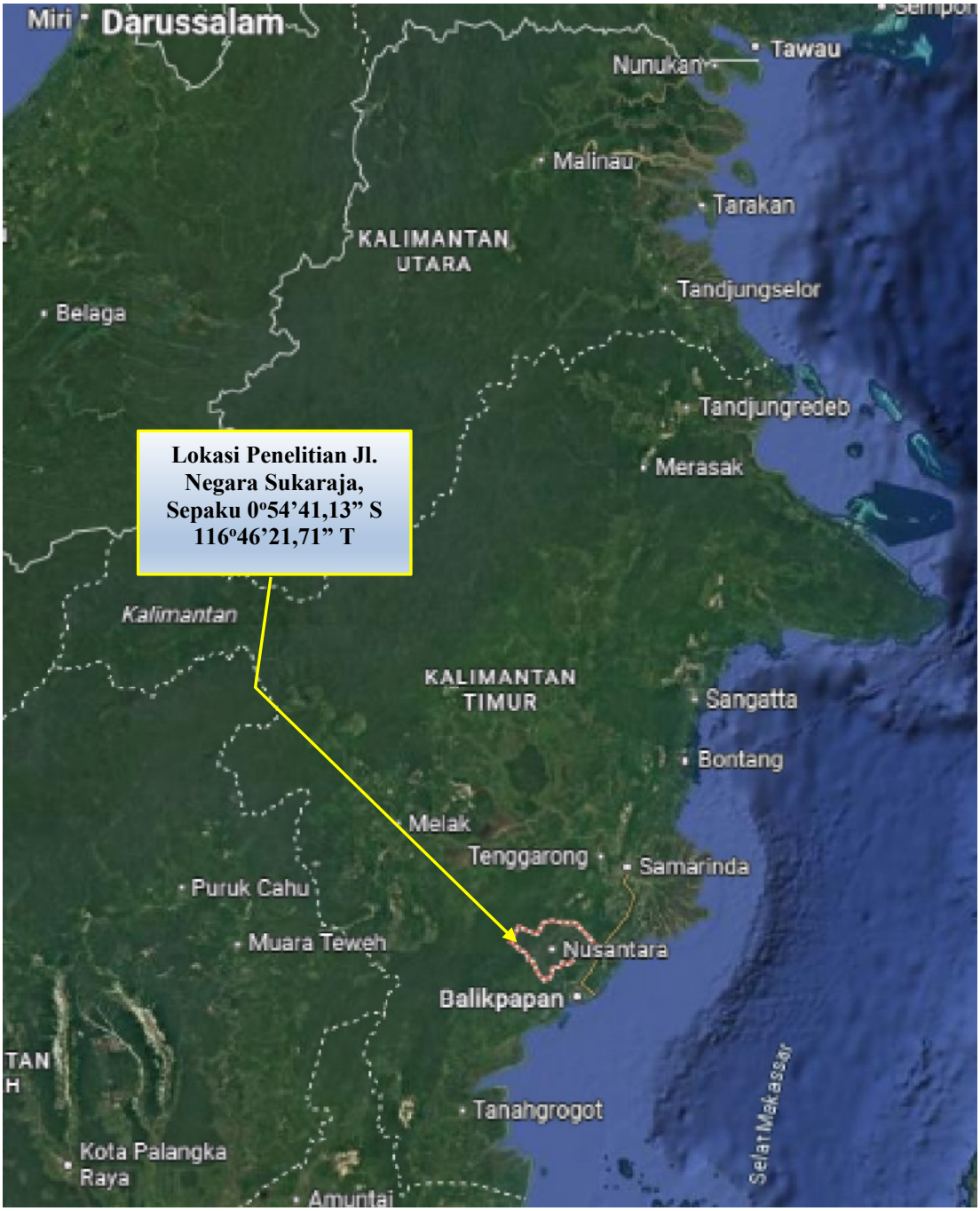

Gambar 11. Peta Kecamatan Sepaku
(Google Maps. 30 Juni 2025)

4. HASIL DAN PEMBAHASAN

Ruang Lingkup pengujian meliputi:

a. Pengujian Test Boring 2 (dua) titik.
b. Pengujian Test SPT pada titik boring setiap interval 2 m atau sesuai kondisi lapangan.
c. Pengambilan contoh tanah terganggu (DS) sebanyak 6 (enam) buah sampel setiap boring, sebagai bahan pengujian di Laboratorium.
d. Pengujian Laboratorium meliputi, engineering properties yaitu: Slake Durability.

Gambar 12. Bor Log Exploration titik BH. 01 & 02
(SNI 4153:2008)

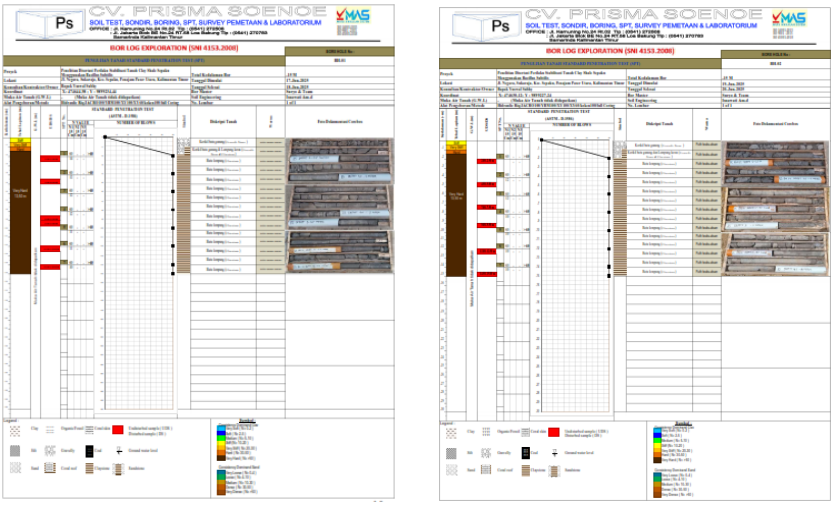

Gambar 13. Pelaksanaan test SPT
dengan Boring Mesin

Pengamatan dan pengambilan hasil pengujian lapangan dengan boring mesin berupa sampel corebox dengan masing-masing titik, BH.1 dan BH.2, secara visual didapatkan hasil sebagai berikut:

Table 4. Visual Description BH.1 & BH.2

No.	Jenis Tanah vs Nilai N (Blosw/Feet)	BH.1
1.	Kerikil batu gunung warna putih keabu-abuan Ketebalan Stiff (meter) Nilai "N"	-0,0 sd -0,5 0,5 10 sd 20
2.	Kerikil batu gunung warna putih keabu-abuan Ketebalan Very Stiff (meter) Nilai "N"	-0,5 sd -1,0 0,5 20 sd 30
3.	Kerikil batu gunung & lempung keras warna putih keabu-abuan Ketebalan Hard (meter) Nilai "N"	-0,0 sd -0,5 0,5 10 sd 30
4.	Batu lempung padat warna putih keabu-abuan Ketebalan Very Hard (meter) Nilai "N"	-1,5 sd -15 13,5 >50

No.	Jenis Tanah vs Nilai N (Blosw/Feet)	BH.2
1.	Kerikil batu gunung warna putih keabu-abuan Ketebalan Stiff (meter) Nilai "N"	-0,0 sd -0,5 0,5 10 sd 20
2.	Kerikil batu gunung warna putih keabu-abuan Ketebalan Very Stiff (meter) Nilai "N"	-0,5 sd -1,0 0,5 20 sd 30
3.	Kerikil batu gunung & lempung keras warna putih keabu-abuan Ketebalan Hard (meter) Nilai "N"	-1 sd -1,5 0,5 10 sd 30
4.	Batu lempung padat warna putih keabu-abuan Ketebalan Very Hard (meter) Nilai "N"	-1,5 sd -15 13,5 >50

Hasil sampel disturb (corebox) dari titik BH.1 dan BH.2, berdasarkan hasil pengujian memiliki nilai N SPT dan pengamatan visual yang sama, maka peneliti mengambil kesimpulan untuk pengujian dengan alat Slake Durability Test hanya pada corebox titik BH.1, litologi Clay Stone kedalaman 2,5 meter. Berikut hasil pengujian slake durability (ASTM D-4644-08) dan (SNI 3406-2011).

Table 5. Slake Durability Test

No.	Sample Code	BH.2		
1.	Deskripsi	Clay Stone		
2.	Berat Sampel (gram)	577,9		
3.	Berat Kering Sampel (gram)	509,6		
4.	Kadar Air, ω(%)	13,40		
5.	Siklus	1	2	3
6.	Berat Kering Sample Setelah Rotasi 10 menit	342,1	89,9	39,1
7.	Indeks Slake Durability, Id (%)	67,13	17,64	7,67
8.	Klasifikasi	Very Low Durability		

Gambar 14. Awal dan Siklus 1

Gambar 15. Siklus 2 dan Siklus 3

Gambar 7. Siklus 2 dan Siklus 3 Menurut (Gamble, 1971), klasifikasi slake durability (ketahanan lapuk/ketahanan hancur batuan saat siklus basah-kering) dibagi berdasarkan Slake Durability Index (Id_2), yaitu nilai ketahanan sampel setelah siklus kedua pengujian. Berikut tabel klasifikasinya:

Table 6. Slake Durability Test

Slake Durability Index (Id_2, %)	Klasifikasi Durability	Deskripsi
< 25 %	Very Low Durability	Sangat mudah hancur, rapuh terhadap air & siklus kering-basah
25 – 50 %	Low Durability	Mudah hancur, ketahanan rendah terhadap pelapukan
50 – 75 %	Medium Durability	Ketahanan sedang, Sebagian hancur saat diuji
75 – 90 %	High Durability	Ketahanan tinggi, hanya sedikit hancur
> 90 %	Very High Durability	Sangat tahan, hampir tidak ada kerusakan setelah pengujian

Semakin tinggi nilai Id_2, semakin tahan batuan terhadap proses pelapukan basah-kering. Rumus Slake Durability Index:
$W_{initial}$ = berat awal sampel kering (dimasukan ke drum uji)
W_{final} = berat sampel sisa setelah pengujian (ditimbang kering udara)
Dihitung setelah siklus ke-2, hasilnya = Id_2

$$Id2 = \frac{W_{final}}{W_{initial}} x100\% \quad (1)$$

Gambar 16. Alat Slake Durability

Sampel tanah terganggu (DS) hasil boring test dilakukan dengan pengujian kuat tekan bebas (unconfined compressive strength) dengan menggunakan alat uji Universal Testing Machine (UTM). Hasil perhitungan kuat tekan bebas (UCS) claystone sebagai berikut:

- Diameter sampel D = 5,55 cm
- Tinggi sampel h = 14,52 cm
- Beban maksimum P_u = 6,18 kN
- Regangan aksial pada patah = 1%

Luas awal:

$$A_0 = \frac{\pi D^2}{4} = 0{,}002419\ m^2 \quad (2)$$

- Luas terkoreksi (SNI 3638:2012, koreksi area):

$$A_c = \frac{A_0}{1-\epsilon} = \frac{0{,}002419}{1-0{,}01} \approx 0{,}002444\ m^2 \quad (3)$$

- Kuat tekan bebas:

$$q_u = \frac{P_u}{A_c} = \frac{6{,}18}{0{,}002444} \approx 2529\ kN/m^2 = 2{,}53MPa$$

- Kuat geser tak terdrain (undrained shear strength):

$$s_u \approx \frac{P_u}{2} \approx 1{,}26\ Mpa \quad (4)$$

Hasil pengujian XRD yang berupa grafik yang menampilkan pola difraksi sampel (warna merah) yang dibandingkan dengan database mineral standar (warna biru, pink, hijau, dan ungu) untuk identifikasi mineral. Fase dominan tampak adalah kuarsa (quartz) refleksi kuat di sekitar 2θ ≈ 26° (d ≈ 3.34–3.40 Å) menunjukkan mineral kristalin silika dominan. Ada kontribusi fasa lempung/ mineral lempung (clay minerals) sebagai fase sekunder, terlihat dari beberapa puncak pada 2θ rendah–sedang (mis. 2θ ≈ 20° → d ≈ 4.35 Å, serta puncak-puncak kecil lain) dan banyak puncak kecil lebar yang tipikal sampel argilik/shale. Fasa minor kemungkinan termasuk muscovite/illite atau kaolinit dan kemungkinan sedikit feldspar/klorit, ini bersifat hipotesis berdasarkan d-spacing yang tercatat; konfirmasi butuh perbandingan ke database/difraksi perlakuan (glycolation / heating).

Gambar 17. Grafik X-Ray Diffraction

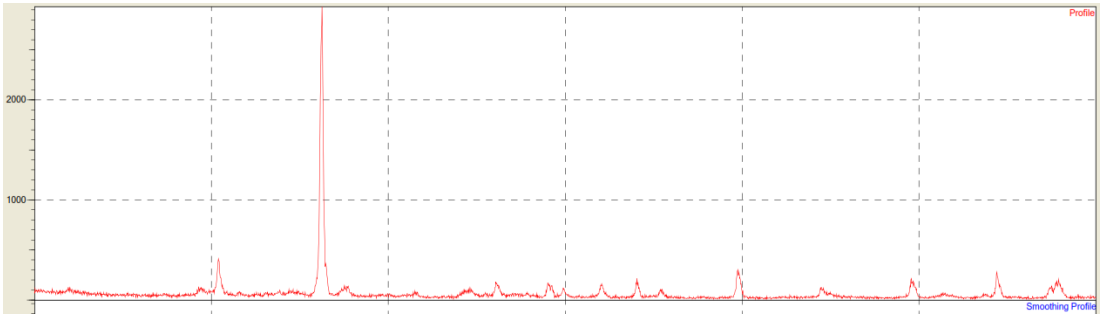

Gambar 17. Grafik X-Ray Diffraction

Interpretasi Citra SEM (x5000, WD = 8.4 mm) pada pembesaran tinggi ini terlihat partikel-partikel berbentuk lempeng (lamelar) dengan ukuran bervariasi antara 2–10 µm, saling bertumpukan membentuk agregat rapat. Morfologi tersebut merupakan ciri khas dari mineral lempung tipe kaolinit dan illit, yang umumnya berbentuk lembaran-lembaran pipih dengan permukaan halus dan saling menempel akibat gaya Van der Waals antar partikel. Di beberapa area tampak adanya lembaran yang terlipat dan menggulung sebagian, memperlihatkan plastisitas material yang tinggi, sifat yang juga diperkuat oleh hasil XRD yang mengindikasikan kehadiran montmorillonit sebagai mineral ekspansif minor. Selain itu, di antara lapisan-lapisan halus tersebut terlihat beberapa partikel berukuran lebih besar dengan bentuk lebih padat dan permukaan agak kasar, kemungkinan merupakan butiran kuarsa halus atau feldspar yang terdispersi di antara matriks lempung. Keberadaan butiran ini memperkuat hasil XRD yang menunjukkan puncak intensitas kuat pada 2θ sekitar 26,2° (kuarsa) dan 27–29° (feldspar). Secara umum, tekstur mikro pada citra ini memperlihatkan struktur komposit antara matriks lempung halus dan butiran keras silikat, yang memberikan kombinasi sifat mekanik plastis namun cukup padat dan kohesif. Citra SEM ini, dengan demikian memperkuat hasil analisis XRD bahwa sampel memiliki dominasi mineral kaolinit, illit, dan kuarsa, dengan kontribusi minor dari montmorillonit dan feldspar. Pola mikrostruktur berlapis menunjukkan potensi kemampuan menahan air dan ekspansi sedang, tipikal material clay shale atau mudstone yang telah mengalami proses diagenesis sebagian. (e.g., Mitchell, J.K. and Soga, K. ,2005). *Fundamentals of Soil Behavior (3rd Ed). Wiley.*

Gambar 18. Citra SEM (Serbuk) Gambar 19. Citra SEM (Batu)

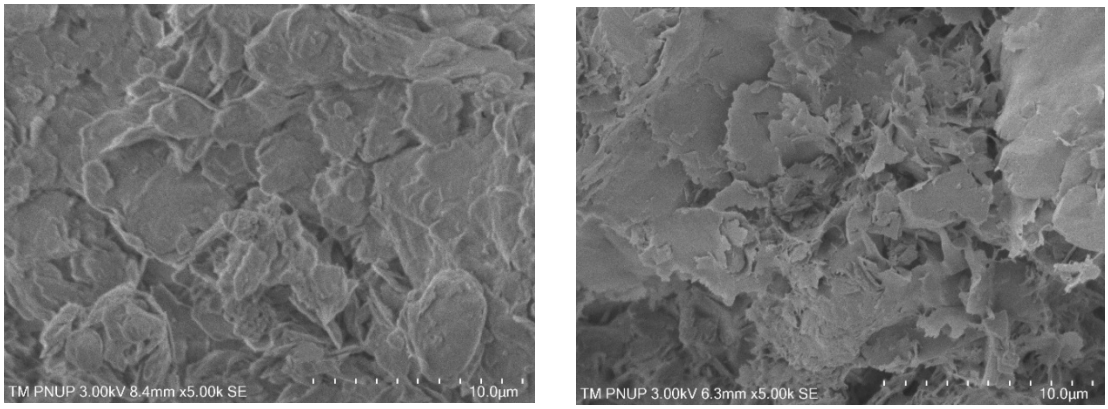

Gambar 20. Sampel DS (Disturbed Soil Sample)
(Hasil Pengujian Lapangan)

5. KESIMPULAN

Test Boring – SPT
Hasil pengujian tanah ini disimpulkan sebagai berikut:

1. Pada titik boring 1 (BH.1), kepadatan tanah Sangat/Very Hard dengan nilai N > 60 didapat pada kedalaman -2,0 m. Pada lokasi tersebut, kedalaman 0,0 m sd -0,5 m adalah termasuk jenis tanah kerikil batu gunung (putih keabu-abuan), termasuk jenis tanah dengan kepadatan kaku/Stiff. Kedalaman -0,5 m sd -1,0 m adalah termasuk jenis kerikil batu gunung (putih keabu-abuan), termasuk jenis tanah dengan kepadatan sangat kaku/Very Stiff. Kedalaman -1,0 m sd 1,5 m termasuk jenis tanah kerikil batu gunung dan lempung keras (putih keabu-abuan) termasuk jenias tanah dengan kepadatan keras/Hard. Kedalaman -1,5 m sd -15 m termasuk jenis batu lempung padat (putih keabu-abuan), termasuk jenis tanah dengan kepadatan sangat keras/Very Hard.
2. Pada titik boring 2 (BH.2), kepadatan tanah sangat keras/Very Hard dengan nilai N > 60 didapat pada kedalaman -2,0 m. Pada lokasi tersebut, kedalaman 0,0 m sd -0,5 m adalah termasuk jenis tanah kerikil batu gunung (putih keabu-abuan), termasuk jenis tanah dengan kepadatan kaku/Stiff. Kedalaman -0,5 m sd -1,0 m adalah termasuk jenis kerikil batu gunung (putih keabu-abuan), termasuk jenis tanah dengan kepadatan sangat kaku/Very Stiff. Kedalaman -1,0 m sd -1,5 m termasuk jenis tanah kerikil batu gunung dan lempung keras (putih keabu-abuan) termasuk jenis tanah dengan kepadatan keras/Hard. Kedalaman -1,5 m sd 15 m termasuk jenis tanah dengan kepadatan sangat keras/Very Hard.

Test Laboratorium

Hasil pengujian pada Laboratorium Tanah, sifat-sifat mekanis (engineering properties) Slake Durability Test Siklus 2, Indeks Slake Durability Id = 17,64%, dengan klasifikasi Very Low Durability.

Dari hasil pengujian Laboratorium MIPA Unhas (XRD/ X-Ray Diffraction) berupa grafik, puncak dominan pada 26.6^{o} (kuarsa) sebesar 79% yang memperlihatkan sifat pasir silika tinggi, sangat umum pada material sedimen kuarsa atau tanah residu. Puncak sekunder pada 20.8^{o} (kaolinit) sebesar 10% yang mengindikasikan komponen clay (lempung aluminium silikat). Puncak minor (36^{o}-50^{o}) sebesar 2% dengan kahadiran feldspar, illit, klorit, dan mika menandakan material berasal dari pelapukan felspatik atau batuan beku. Kombinasi ini menunjukan tanah lempung-pasir, dengan plastisitas rendah-sedang dan kandungan silika tinggi.

Dan hasil pengujian Laboratorium Politeknik Ujung Pandang (SEM/ Scanning Electron Microscope). Citra yang ditampilkan dengan pembesaran 5.000x dan skala 10 µm. Citra SEM (batu) menunjukkan tekstur lempung halus dan berlapis, mendukung hasil XRD yang menegaskan adanya kaolinit dan illit. Adanya kuarsa dan feldspar memperlihatkan sisa mineral asal batuan induk. Kombinasi ini menandakan material merupakan tanah lempung pelapukan feldspatik, dengan plastisitas sedang tinggi dan permeabilitas rendah.

REFERENCES

Abdullah Almajed, Kehinde Lemboye., & Arif Ali Baig Moghal (2022). *A Critical Review on the Feasibility of Synthetic Polymers Inclusion in Enhancing the Geotechnical Behavior of Soils*. National Library of Medicine. https://pmc.ncbi.nlm.nih.gov/articles/PMC9694698/

Abidemi Olujide Ilori, Anthony Michael George., Ini Christopher Umoh., Ediomo O. Eyakndue., & Ubong Udoette Ukpekpe (2025). Springer Nature Link. https://link.springer.com/article/10.1007/s44288-025-00114-9

Alexandra Clara Saracho., Stuart K. Haigh., Toshiro Hata., Kenichi Soga., Ning-Jun Jiang & Koji Yamamoto (2025). *Experimental Observation of the Effect of MICP on the Deformation Mechanism of a Layered Formation during Sand Production.* ASCE Library, Journal of Geotechnical and Geoenvironmental Engineering. https://doi.org/10.1061/JGGEFK.GTENG-12819

Albert Johan., Andy Sugianto., & Paulus P. Rahardjo (2023). *Replacement of Weathered Clay Shale Using Soil Cement for Bridge Approach Embankment in Purwakarta – Indonesia.* Indonesian Geotechnical Journal, December 2023, Vol 2 (3). Page 123 – 138 DOI: https://doi.org/10.56144/igj.v2i3.58
E-ISSN:2829-7520

A.G.R. Kennedy., Y.S. Jhuo., & L. Ge A (2023). *Laboratory Investigation of Using Enzyme Induced Calcite Precipitation for Soil Strength Improvement.* Smart Geotechnics for Smart Societies – Zhussupbekov, Sarsembayeva & Kaliakin (Eds) © 2023 The Author(s), ISBN 978-1-003-29912-7 Open Access: www.taylorfrancis.com, CC BY-NC-ND 4.0 license

Bo Liu., Chao-Sheng Tang., Xiao-Hua Pan., Jin-Jian Xu and Xi-Ying Zhang (2024). *Suppressing Drought – Induced Soil Desiccation Cracking Using MICP: Field Demonstration and Insights.* ASCE Library, Journal of Geotechnical and Geoenvironmental Engineering. https://doi.org/10.1061/JGGEFK.GTENG-12011

Bell, F.G. (2007). Engineering Geology (2nd Ed.). *Buku ini membahas berbagai jenis batuan, termasuk batuan lunak seperti shale dan mudstone, dalam konteks teknik sipil dan geoteknik.* Penekanan diberikan pada sifat fisik dan mekanik serta pengaruh pelapukan. https://geomuseu.ist.utl.pt/SEMINAR2012/Livros/EngenhariaGeologica.pdf?utm_source=chatgpt.com

Charalampos Konstantinou, Yuze Wang., Giovanna Biscontin., & Kenichi Soga (2021). *The Role of Bacterial Urease Activity on the Uniformity of Carbonate Precipitation Profiles of Bio-Treated Coarse Sand Specimens*. National Library Medicine. https://pmc.ncbi.nlm.nih.gov/articles/PMC7969948/

Chao Lv., Chao-Sheng Tang., Jun-Zheng Zhang., Hao Liu and Xiao-Hua Pan (2024). *Regulating the Process of Microbially Induced Calcium Carbonate Precipitation through Apllied Electric Fields: Evidence and Insights Using Microfluidics.* ASCE Library, Journal of Geotechnical and Geoenvironmental Engineering. https://doi.org/10.1061/JGGEFK.GTENG-12532

Dejan Kurlov., & Tej Marcovic (2023). *Experimental Study of Improving the Physical Properties of Peat Soil Using Sand and Bio-Grouting Techniques with the Assistance of Bacillus Subtilis Bacteria.* Journal of Geoscience, Engineering, Environment, and Technology (JGEET) P-ISSN: 2503-216X E-ISSN: 2541-5794. http://journal.uir.ac.id/index.php/JGEET

Fathiyah Hakim Sagitaningrum, Samira Albati Kamaruddin., Budi Susilo Soepandji., & Idrus Muhammad Alatas (2023). *Review of Clay Shale Soil its Future Research*. Journal of AIP Conference Proceedings. https://scholar.ui.ac.id/en/publications/review-of-clay-shale-soil-and-its-future-research

Hasriana, Lawalenna Samang., M. Natsir Djide., & Tri Harianto (2018). *A Study on Clay Soil Improvement with Bacillus Subtilis Bacteria as the Road Subbase Layer*. International Journal of Geomate. https://www.academia.edu/56149364/A_Study_on_Clay_Soil_Improvement_with_Bacillus_Subtilis_Bacteria_as_the_Road_Subbase_Layer

Hai Lin, Yi Dong., Joon Soo Park., & Brina M. Montoya (2023). *Cementation Stress Characteristic Curve for Sands Treated by Microbially Induced Carbonate Precipitation.* ASCE Library, Journal of Geotechnical and Geoenvironmental Engineering. https://doi.org/10.1061/JGGEFK.GTENG-11403

Joanna Fronczyk, Nadella Marchelina., Adam Puzik., & Malgorzata Franus (2023*). Assessment of the Composition Effect of a Bio-Cementation Solution on the Efficiency of Microbially Induced Calcite Precipitation Processes in Loose Sandy Soil*. National Library of Medicine. https://pmc.ncbi.nlm.nih.gov/articles/PMC10488806/

Jennifer Wright, Polly Moreland., Anil Wipat., Meng Zhang., & Martyn Dade-Robertson (2020). Engineered ureolytic Bacillus Subtilis and its future in Microbial Induced Calcium Carbonate Precipitation (MICCP). Microbiology Society. https://www.microbiologyresearch.org/content/journal/acmi/10.1099/acmi.ac2020.po0143

Jun-Zheng Zhang, Chao-Sheng Tang., Chao Lv., Qi-You Zhaou and Bin Shi (2023). *Monitoring and Characterizing the Whole Process of Microbially Induced Calcium Carbonate Precipitation Using Electrical Resistivity Tomography.* ASCE Library, Journal of Geotechnical and Geoenvironmental Engineering. https://doi.org/10.1061/JGGEFK.GTENG-11782

Katie A. Gilmour, Prakriti Sharma Ghimire., Jennifer Wright., Jamie Haystead., Martyn Dade-Robertson., Meng Zhang., & Paul James (2024). *Microbially induced calcium carbonate precipitation through CO_2 sequestration via an engineered Bacillus subtilis*. BMC Part of Springer Nature. https://microbialcellfactories.biomedcentral.com/articles/10.1186/s12934-024-02437-7

Kimberly K. Martin., Hamed Khodadadi Tirkolaei and Edward Kavazanjian (2024). *Field-Scale EICP Biocemented Columns for Ground Improvement.* ASCE Library, Journal of Geotechnical and Geoenvironmental Engineering. https://doi.org/10.1061/JGGEFK.GTENG-11635

Kewei Gao., Pierre Bick., Muhannad T. Suleimen., Xiwei Li., Jeffrey Helm., Derick G. Brown and Nabil Zouari (2023). *Wind Erosion Mitigation Using Microbial-Induced Carbonate Precipitation.* ASCE Library, Journal of Geotechnical and Geoenvironmental Engineering. https://doi.org/10.1061/JGGEFK.GTENG-11140

Lina Wang, Xiaodong Yang., Yueliang Diao., & Chengchao Guo (2024). *Study on Bonding Characteristics of Polymer Grouted Concrete-Soil Interface*. MDPI, Advancing Open Science. https://www.mdpi.com/2073-4360/16/15/2207

Lutfian R Daryono., Tomohiko Abe., Masanao Kano., Kazunori Nakashima., & Satoru Kawasaki (2024). *Fiber-Reinforcement MICP for Durability Improvements.* Indonesian Geotechnical Journal, August 2024, Vol 3 (2). Page 1-16 DOI: https://doi.org/10.56144/igj.v3i1.79 EISSN: 2829-7520 https://indonesian-geotechnical-journal.org/index.php/JGI/issue/archive

Muhammad, AAS., Tommy, T., Rety, W., Revia, O., Windhu, N., Lucia, LR., & Henny, M. (2025). *Analisis Pengaruh Number of Cycles terhadap Pengujian Durability Slake Batulempung pada Formasi Balikpapan dan Formasi Kampung Baru Kabupaten Kutai Kertanegara Provinsi Kalimantan Timur.* Globe: Publikasi Ilmu Teknik, Teknologi Kebumian, Ilmu Perkapalan. Volume 3, Nomor 3, Agustus 2025. https://journal.aritekin.or.id/index.php/Globe

Osama Ahmed Ibrahim, Ahmed Ibrahim Hassanin Mohamed., Wael Ibrahim., Raghda Osama Abd-Al Ftah., Shimaa R. Hamed., & Sherif Fakhry M. Abd-Elnaby. The Influence of Adding B. Subtilis Bacteria on The Mechanical and Chemical Properties of Cement Mortar. Springer Open. https://bjbas.springeropen.com/articles/10.1186/s43088-024-00591-w

Paul Pratter, Conrad Boley., & Yashar Forouzandeh (2022). *Innovative Ground Improvement with Chemical Grouts: Potential and Limits of Partial Saturation with Polymers*. Springer Nature Link. https://link.springer.com/article/10.1007/s10706-022-02301-8

Pooya Naghizadeh Ardebili, Golnaz Jozanikohan., & Ali Moradzadeh (2025). *The Characterization of Clay Mierals in The Kashafrud Formation in a Gas Field in Northeast Iran*. Scientific Reports. https://www.nature.com/articles/s41598-025-93930-5

Paulus Rahardjo (2023). *Replacement of Weathered Clay Shale Using Soil Cement for Bridge Approach Embankment in Purwakarta – Indonesia*. Indonesian Geotechnical Journal. https://www.academia.edu/124906913/Replacement_of_Weathered_Clay_Shale_Using_Soil_Cement_for_Bridge_Approach_Embankment_in_Purwakarta_Indonesia

Pinar Gunyol., Mohammad Khosravi., Adrienne Phillips., Kathryn Plymesser and Albert Parker (2024). *Effect of Fines Content on Calcium Carbonate Precipitation and Thermal Properties of Biocemented Sand.* ASCE Library, Journal of Geotechnical and Geoenvironmental Engineering. https://doi.org/10.1061/JGGEFK.GTENG-11925

Pegah Ghasemi and Brina M. Montoya (2022). *Field Implementation of Microbially Induced Calcium Carbonate Precipitation for Surface Erosion Rdeuction of a Coastal Plain Sandy Slope.* ASCE Library, Journal of Geotechnical and Geoenvironmental Engineering. https://doi.org/10.1061/(ASCE)GT.1943-5606.0002836

Qiaomu Qi., Li-Yun Fu., Jixin Deng., & Junxin Cao (2021). *Attenuation Methods for Quantifying Gas Saturation in Organic-Rich Shale and Tight Gas Formations.* GEOPHYSICS, Journal Article. https://doi.org/10.1190/geo2020-0291.1

Ramli Nazir, Paulus P. Rahardjo., & Amir Hamzah Mustapha (2024). *Construction Challenges in Tropical Clay Shale Environments*. Springer Nature Link. https://link.springer.com/chapter/10.1007/978-981-97-9364-8_10

Rokhman, Achmad Muhiddin., Ardy Arsyad., & Tri Harianto (2024). *Characteristics of Soft Soil Stabilization with Bacillus subtilis Bacteria on Unconfined Compression Strength and Shear Stress of Soils*. Scopus Indexed. Impact Factor. https://www.researchgate.net/publication/379683467_Characteristics_of_Soft_Soil_Stabilization_with_Bacillus_subtilis_Bacteria_on_Unconfined_Compression_Strength_and_Shear_Stress_of_Soils

Ru Jia, Xiaofei Fu., Yejun Jin., Tong Wu., Sheng Wang., & Huijie Cheng (2023). *Mechanical Properties of Mudstone Caprock and Influencing Factors: Implications for Evaluation of Caprock Integrity*. Frontiers in Earth Science. https://www.frontiersin.org/journals/earth-science/articles/10.3389/feart.2023.1229851/full

Ray Harran., Dimitrios Terzis and Lyesse Laloui (2022). *Characterizing the Deformation Evolution with Stress and Time of Biocemented Sands.* ASCE Library, Journal of Geotechnical and Geoenvironmental Engineering. https://doi.org/10.1061/(ASCE)GT.1943-5606.0002871

Seung-Hun Baek., Tae-Hyuk Kwon and Jason T. DeJong (2024). *Reduction in Hydraulic Conductivity of Sands Caused by Microbially Induced Calcium Carbonate Precipitation.* ASCE Library, Journal of Geotechnical and Geoenvironmental Engineering. https://doi.org/10.1061/JGGEFK.GTENG-11570

Soo-Min Ham., Alejandro Martinez., Gyeol Han and Tae-Hyuk Kwon (2022). *Grain-Scale Tensile and Shear Strengths of Glass Beads Cemented by MICP.* ASCE Library, Journal of Geotechnical and Geoenvironmental Engineering. https://doi.org/10.1061/(ASCE)GT.1943-5606.0002863

Timothy D. Hoffmann, Kevin Paine., & Susanne Gebhard (2021). *Genetic Optimisation of Bacteria-Induced Calcite Precipitation in Bacillus Subtilis*. BMC Part of Springer Nature. https://microbialcellfactories.biomedcentral.com/articles/10.1186/s12934-021-01704-1

Tianzheng Fu and Stuart Kenneth Haigh (2024). *Biocementation of a Well-Graded Gravelly Soil and Macromechanical Characterization.* ASCE Library, Journal of Geotechnical and Geoenvironmental Engineering. https://doi.org/10.1061/JGGEFK.GTENG-12091

Vishnu Diyaljee (2022). *Discussion of "Effects of Enzyme and Microbially Induced Carbonate Precipitation Treatments on The Response of Axially Loaded Pervious Concrete Piles"* by Hai Lin, Sean T. O'Donnell, Muhannad T. Suleiman, Edward Kavazanjian Jr., and Derick G. Brown. ASCE Library, Journal of Geotechnical and Geoenvironmental Engineering. https://doi.org/10.1061/(ASCE)GT.1943-5606.0002858

Xuegui Zheng, Xinyu Lu., Min Zhou., Wei Huang., Zhitao Zhong., Xuheng Wu., & Baoyun Zhao (2022). *Experimental Study on Mechanical Properties of Root–Soil Composite Reinforced by MICP*. National Library Medicine. https://pmc.ncbi.nlm.nih.gov/articles/PMC9147924/

Xiaohao Sun., Linchang Miao., Runfa Chen., Hengxing Wang and Linyu Wu (2023). *A Revised Porous Media Model of Microbially Induced Carbonate Precipitation for Loess Solidification.* ASCE Library, Journal of Geotechnical and Geoenvironmental Engineering. https://doi.org/10.1061/JGGEFK.GTENG-10309

Xiaohao Sun., Linchang Miao., Hengxing Wang., Linyu Wu., Guangcai Fan and Jinxin Xia (2022). *Sand Foreshore Slope Stability and Erosion Mitigation Based on Microbiota and Enzyme Mix-Induced Carbonate Precipitation.* ASCE Library, Journal of Geotechnical and Geoenvironmental Engineering. https://doi.org/10.1061/(ASCE)GT.1943-5606.0002839

Yao Xiao., Huafeng Deng., Wenxi Zhu., Eleyas Assefa., Lei Cheng., Yu Xiong and C.F. Lee (2025). *Durability Evolution Mechanism of MICP-Treated Calcareous Sand Exposed to Seawater Dry-Wet Cycles.* ASCE Library, Journal of Geotechnical and Geoenvironmental Engineering. https://doi.org/10.1061/JGGEFK.GTENG-13301

Yi-Jie Wang., Weh-Bo Chen., Jian-Hua Yin., Xiao-Li Han., Yu Zhang., Yan-Jun Du and Ning-Jun Jiang (2023). *Role of Biochar in Drained Shear Strength Enhancement and Ammonimum Removal of Biostimulated MICP-Treated Calcareous Sand.* ASCE Library, Journal of Geotechnical and Geoenvironmental Engineering. https://doi.org/10.1061/JGGEFK.GTENG-11809

Yuze Wang., Yong Wang and Charalampos Konstantinou (2023). *Strength Behavior of Temperature-Dependent MICP-Treated Soil.* ASCE Library, Journal of Geotechnical and Geoenvironmental Engineering. https://doi.org/10.1061/JGGEFK.GTENG-11526

Yang Xiao., Xiang He., Armin W. Stuedlein., Jian Chu., T. Matthew Evans and Leon A. van Paassen (2022). *Crystal Growth of MICP through Microfluidic Chip Test.* ASCE Library, Journal of Geotechnical and Geoenvironmental Engineering. https://doi.org/10.1061/(ASCE)GT.1943-5606.0002756

Zahra Faeli., Brina M. Montoya and Mohammad A. Gabr (2023). *Various Bacterial Attachment Functions and Modeling od Biomass Distribution in MICP Implementations.* ASCE Library, Journal of Geotechnical and Geoenvironmental Engineering. https://doi.org/10.1061/JGGEFK.GTENG-10812

HIMPUNAN AHLI TEKNIK TANAH INDONESIA - HATTI
Indonesian Society for Geotechnical Engineering - ISGE
PIT HATTI XXIX
10-12 November 2025

Comparative Site Classification Using Conventional Penetration Testing (SPT) and Microtremor Array Measurement (MAM): Case Study of Three Industrial Estates in Karawang, Indonesia

Ayu Wijayanti Kurnia Dewi[1] , Ryan Rahmat Setiaji[1,2,*], Baiq Melly Ciptayuni Asmarani[2]
[1]PT Nusantara Geo Science, North Jakarta, Indonesia, 14450;
[2]PT Artha Geo Integritas, North Jakarta, Indonesia, 14450;
*Correspondence: ryan.setiaji@gmail.com

ABSTRACT Site classification is a fundamental component of geotechnical engineering and seismic hazard assessment, providing essential parameters for structural design and risk mitigation. This study integrates Standard Penetration Test (SPT) data with shear wave velocity (Vs) profiles obtained from Microtremor Array Measurement (MAM) to classify sites within three major industrial estates in Karawang, Indonesia. According to the NEHRP framework, both methods consistently categorize the study areas as Site Class D (stiff soil) - Site Class E (soft soil). Vs30 values derived from MAM (266–320 m/s) exhibit strong correlation with depth-dependent increases in SPT blow counts, underscoring the complementary reliability of the two approaches. While SPT provides localized subsurface information, MAM constitutes a more advanced technique due to its capacity for spatially continuous site classification, enhancing the resolution of large-scale assessments. These results demonstrate the effectiveness of advanced seismic sensing, particularly MAM, in geotechnical site characterization and in improving the understanding of subsurface conditions in critical industrial zones.

KEYWORDS Shear wave velocity (Vs); Standard Penetration Test (SPT); NEHRP Site Classification

1 INTRODUCTION

Site characterization is a critical process in geotechnical and earthquake engineering. In Indonesia, the Standard Penetration Test (SPT) remains the most widely applied conventional method for subsurface investigation; however, it is intrusive, time-consuming, and spatially constrained. By contrast, advanced seismic sensing techniques such as Microtremor Array Measurement (MAM) enable the non-intrusive and rapid derivation of shear wave velocity (Vs) profiles. The integration of these approaches provides a robust framework for reliable and efficient subsurface characterization.

This paper investigates the combined application of conventional geotechnical testing, represented by SPT, and advanced seismic sensing using MAM for site classification across diverse site conditions. The study was conducted in three major industrial estates in Karawang, West Java: Karawang International Industrial City (KIIC), Greenland International Industrial Center (GIIC), and Surya Cipta. Key objectives include establishing local correlations between SPT N-values and Vs, calculating Vs30, determining site classes under the NEHRP framework, and demonstrating the benefits of integrating penetration testing with seismic sensing in geotechnical site characterization.

2 GEOLOGICAL & REGIONAL SEISMIC CONDITIONS

2.1 Geological Setting

Karawang Regency, located in the northern part of West Java, is one of the most important industrial corridors in Indonesia. The region hosts several large-scale industrial estates, including Karawang International Industrial City (KIIC), Greenland International Industrial Center (GIIC), and Surya Cipta City of Industry (Surya Cipta), which together accommodate hundreds of manufacturing and logistics facilities. Due to their economic significance, the seismic and geotechnical conditions of these estates are of great concern for disaster mitigation and infrastructure resilience.

The research location is in a complex series of Tertiary to Quaternary deposits which greatly influences its geotechnical and seismic characteristics. From a geological perspective, these three estates are situated on different lithological units, reflecting the complexity of the North West Java Basin (Figure 1).

a) KIIC is primarily underlain by the Subang Formation (Tms), consisting of claystone, marl, and intercalations of sandstone with tuffaceous materials. This formation is generally of Pliocene age and represents relatively soft sedimentary deposits, with moderate strength but potentially compressible characteristics. Studies by Sadisun, Shimada & Matsui (2000) show that claystone in the Subang Formation undergoes strength degradation due to weathering, affecting its engineering properties.
b) GIIC lies within the Cihoe Formation (Tpc), a unit dominated by volcanic tuffaceous sandstones and breccias. The Cihoe Formation offers relatively lower bearing capacity, and some weathering zones may exhibit reduced stiffness.
c) Surya Cipta Industrial Estate is located on Quaternary alluvial deposits (Qaf), which consist of unconsolidated clay, silt, and sand from riverine and floodplain processes. These young sediments are typically soft and saturated, making them susceptible to settlement, liquefaction, and strong seismic amplification.

The variation in geological settings across KIIC, GIIC, and Surya Cipta demonstrates that even within the same industrial corridor, site conditions can differ significantly. This highlights the importance of site-specific geotechnical and geophysical investigations, such as Standard Penetration Tests (SPT) and microtremor-based shear wave velocity (Vs) profiling, to accurately characterize local soil conditions. Understanding these geological contrasts not only improves seismic microzonation but also supports the development of earthquake-resilient industrial infrastructures in Karawang.

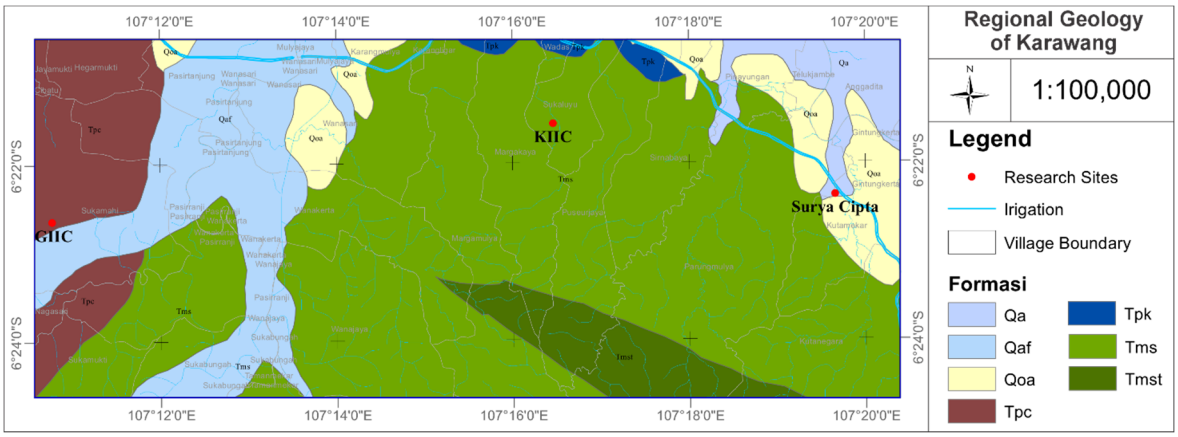

Figure 1. Regional Geology Map of Karawang.

2.2 Regional Seismic Conditions

The research location is relatively close to the Java megathrust subduction zone to the south and is surrounded by several active local faults. Although it is not situated directly above a known major fault trace, the seismic potential in the region is significant. For example, the shallow Mw ~5.0 earthquake that occurred in West Java in September 2024 was strongly felt in Bandung and Karawang (BMKG, 2024; USGS, 2024). Probabilistic seismic hazard analyses for West Java indicate moderate to high seismic hazard levels for the Karawang area. Damanik et al. (2023) report that mean peak ground acceleration (PGA) for Jakarta-bedrock sites lies roughly in the range 0.2–0.4 g for a 10% probability of exceedance in 50 years, increasing to the order of 0.3–0.5 g (or higher at some locations) for a 2% probability of exceedance — values that imply the possibility of strong ground shaking during major events in nearby parts of West Java.

The seismic intensity in Karawang can also be expressed in terms of Modified Mercalli Intensity (MMI), which relates ground motion parameters to perceived shaking and structural impact. Empirical correlations derived from BMKG data show that MMI can be estimated using ground velocity (PGV) or acceleration (PGA), expressed as IMM = 3.56 log (PGV) + 2.88 or IMM = 3.69 log (PGA) – 1.12. These relationships provide a practical framework to evaluate the expected shaking levels and their potential effects on structures. Overall, the seismic conditions across the three sites highlight the necessity of detailed geotechnical site characterization, integrating both SPT and Vs data to assess local amplification effects and to establish site classification.

3 STANDARD PENETRATION TEST (SPT)

The Standard Penetration Test (SPT) in this study was carried out in accordance with ASTM D1586 and the Indonesian standard SNI 4153:2008. In the study location, the test was performed inside boreholes drilled using the rotary wash boring method, with a diameter of 73 mm. At specific depth intervals, every 1.5 – 2 meters, the SPT was conducted alongside soil sampling. In this study, a total of 21 Standard Penetration Test (SPT) boreholes were carried out across three major industrial estates in Karawang. At KIIC (Karawang International Industrial City), seven SPT soundings were conducted; at GIIC (Greenland International Industrial Center), eight SPT soundings were performed; and at Surya Cipta City of Industry, six SPT soundings were obtained. The boreholes were drilled to varying depths depending on site conditions, with SPT measurements conducted at regular intervals of approximately 1.5 – 2 meters.

a) The SPT dataset at KIIC (Figure 2a) exhibits a consistent increase of blow counts with depth: near-surface intervals (0–5 m) commonly show N values in the 2–15 range, mid-depth zones (5–15 m) present moderate resistance (N ≈ 10–30), while deeper intervals (>15–20 m) reach very high blow counts (N ≈ 30–50 or refusal). This vertical trend is compatible with the regional Subang Formation lithology — weathered, fine-grained surficial material overlying progressively compacted tuffaceous/sandstone units. The SPT results therefore confirm that KIIC predominantly comprises stiff to very dense subsurface strata at engineering depths, with localized pockets of softer material near the surface. From a seismic and geotechnical standpoint, these conditions imply moderate site amplification potential confined to the shallow layer, low susceptibility to liquefaction at depth, and generally favourable bearing conditions for foundations, subject to local ground improvement where shallow soft layers are present.
b) The SPT profiles at GIIC (Figure 2b) demonstrate a highly variable subsurface condition. Near-surface layers (0–5 m) exhibit very low blow counts (N < 10), reflecting weathered soils and soft clayey deposits, while intermediate depths (5–15 m) show moderate resistance (N ≈ 10–25). At greater depths (>20 m), several boreholes reach high blow counts (N = 30–50), suggesting the presence of dense tuffaceous sandstone layers typical of the Cihoe Formation. However, the irregular distribution of N values across boreholes indicates lateral heterogeneity caused by differential weathering and interbedded lithologies. Geotechnically, the site provides competent bearing layers at depth, although shallow soft strata may require ground improvement for foundation support.

c) The SPT dataset from Surya Cipta (Figure 2c) displays pronounced lateral and vertical variability consistent with Quaternary alluvial deposition. Near-surface layers commonly record very low blow counts (N < 10), while deeper intervals show intermittent dense lenses (N > 30) interbedded within soft deposits. This stochastic N-profile is characteristic of floodplain/alluvial facies and implies localized but significant site amplification potential, heterogeneous bearing conditions, and notable liquefaction susceptibility where loose sandy layers are saturated. Consequently, foundation design and seismic microzonation at Surya Cipta require dense infill investigation (CPT/SCPT and pore-water measurement) and site-specific mitigation measures in areas with persistent low N values.

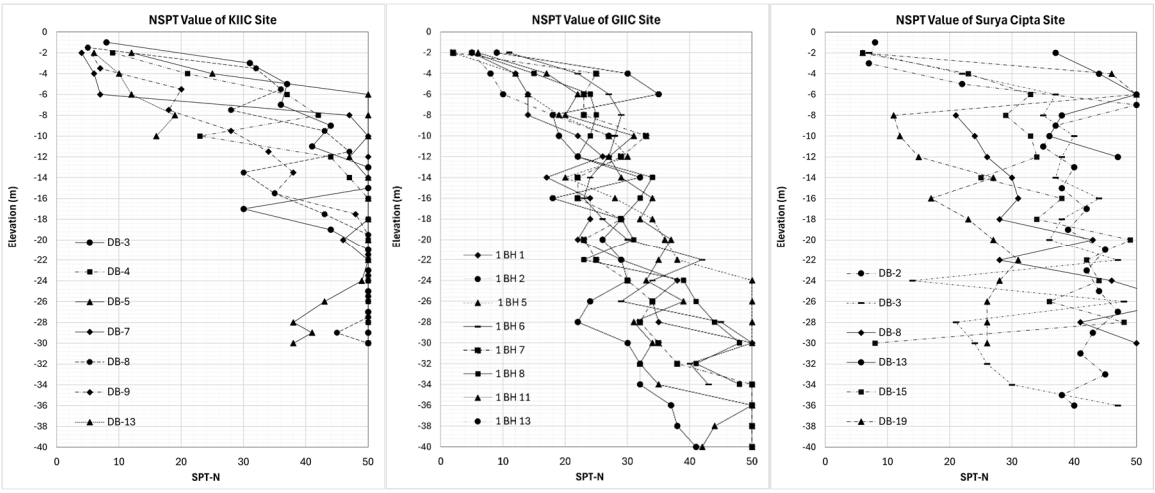

(a) (b) (c)

Figure 2. (a) NSPT Value of KIIC Site, (b) NSPT Value of GIIC Site, (c) NSPT Value of Surya Cipta Site

Standard Penetration Test (SPT) data serve as a practical proxy for evaluating subsurface stiffness when shear wave velocity (Vs) measurements are limited or unavailable. The National Earthquake Hazards Reduction Program (NEHRP) provisions permit the use of average N-values within the upper 30 m as an alternative to Vs_{30} for preliminary site classification (FEMA 222/222A; FEMA 450; FEMA P-2082-1). As outlined in Table 1, the SPT N-value ranges observed at KIIC, GIIC, and Surya Cipta can be systematically correlated with NEHRP thresholds, enabling consistent site class determination. This integrated approach reinforces the connection between conventional geotechnical testing and seismic site characterization, ensuring that local site response and foundation performance are appropriately accounted for in seismic design. The outcomes of this classification are presented in Table 2.

Table 1. NEHRP Classification Based on N value

Site Class	Vs30 (m/s)	N-SPT	Su (kPa)	Description
A	> 1500	–	–	Hard Rock
B	760 – 1500	–	–	Rock
C	360 – 760	> 50	> 100	Very Dense Soil and Soft Rock
D	180 – 360	15 – 50	50 – 100	Stiff Soil
E	< 180	< 15	< 50	Soft Soil

Table 2. Preliminary NEHRP Site Classification Based on SPT Profiles

Site / Estate	Dominant SPT Characteristics (0–30 m)	Remarks	NEHRP Site Class
KIIC	N = 2–15 near surface; N = 10–30 at 5–15 m; N = 30–50 (dense/ refusal) below 15 m	Predominantly stiff to very dense strata; localized soft pockets at shallow depth, low liquefaction potential.	D (Stiff soil)
GIIC	N < 10 at 0–5 m; N = 10–25 at 5–15 m; N = 30–50 at depth	Softer surface deposits than KIIC; lateral heterogeneity increases amplification potential.	D (Stiff soil)
Surya Cipta	N < 10 dominant near surface; interbedded dense lenses (N > 30) at depth	Alluvial deposits with significant amplification potential; higher liquefaction susceptibility in loose sands.	E (Soft soil)

4 MICROTREMOR ARRAY MEASUREMENT (MAM)

Microtremor Array Measurement (MAM) has been gaining popularity over conventional geophysical methods in the last decade, as this technique is non-invasive, rapid, and inexpensive. The method is particularly suitable for application in areas with complex geological features and unconsolidated soil conditions. In addition, MAM provides reliable estimates of surface wave velocity, which reflects localized soil variations and is highly advantageous for engineering design and seismic hazard assessment. Unlike conventional seismic surveys that rely on active sources, MAM depends entirely on ambient noise or microtremor vibrations generated by natural and anthropogenic activities such as winds, ocean waves, traffic, industrial machinery, and household appliances.

Several studies have demonstrated the effectiveness of MAM in characterizing subsurface conditions in Indonesia. For example, Setiawan et al. (2020) applied ambient noise analysis to derive dynamic soil parameters in Aceh, highlighting its practicality for rapid site characterization. Prabowo, Ferdiyan & Amalia (2021) successfully utilized microtremor measurements to estimate soft layer thickness and identify landslide potential in Central Java, proving its capability in detecting weak subsurface zones. Similarly, Ridwan et al. (2014) conducted microtremor array surveys in Jakarta and established shear wave velocity profiles that were crucial for subsurface modeling in urban environments.

(a) (b)

Figure 3. (a) MAM instruments, (b) Set up site of MAM instruments.

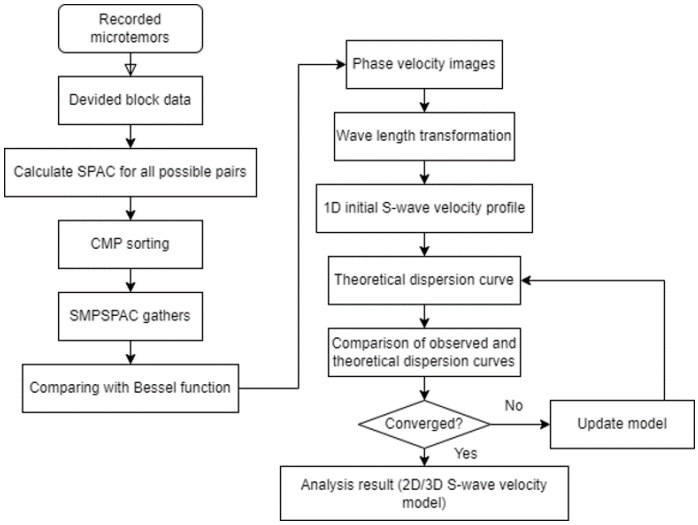

Figure 4. Processing Flow of SMPSPAC Analysis.

These applications confirm that MAM is not only a cost-effective tool but also a robust complement to conventional geotechnical testing, particularly in regions underlain by young alluvial deposits or volcanic sediments. In this study, data acquisition was conducted using the ATOM passive seismic system (Figure 3a), in which each autonomous unit integrates an A/D converter, internal memory, battery, and GPS clock to facilitate cable-free and time-synchronized recording across the array. Vertical 2 Hz geophones were employed, with soil coupling achieved through spike geophones and concrete coupling through tripod mounts. The arrays were deployed in a linear configuration with an inter-station spacing of 3 m, accommodating up to 30 ATOM units depending on site conditions and potential obstructions (Figure 3b). The recorded data were processed using the Common-Midpoint Spatial Autocorrelation (CMP-SPAC) workflow (Figure 4), which is similar to CMP stacking in reflection seismics but applied to the vertical component of ambient noise.

Continuous recordings were divided into overlapping time windows for pre-processing. For each time segment and receiver pair, complex coherency functions were computed in the frequency domain by normalizing the cross-spectral density with the auto-spectra. These coherencies were averaged over all time blocks to improve the signal-to-noise ratio. The averaged coherencies were then grouped into CMP-SPAC gathers to enhance lateral resolution and simulate a larger array aperture. Observed SPAC functions were compared with theoretical Bessel functions to obtain dispersion curves at each CMP location.

Initial 1D shear-wave velocity (Vs) models were estimated using a wavelength-to-depth ratio of one-third, where wavelength equals phase velocity divided by frequency. These models served as the starting point for non-linear least-squares inversion, constrained by horizontal smoothing, to produce pseudo-2D and 3D Vs sections. The CMP-SPAC approach effectively generated stable phase-velocity dispersion curves even in noisy urban settings, with investigation depth extended by increasing array aperture. Consistent application of windowing, coherency averaging, Bessel-function fitting, and inversion ensured coherent Vs models across all arrays. Three microtremor survey lines were deployed at each site to capture lateral variations in the shear-wave velocity structure.

4.1 Karawang International Industrial City (KIIC)

Shear wave velocity profiles at KIIC were obtained from microtremor measurements with a total length of 1.020 meters. Subsurface interpretations are supported by SI logs, which identify clay and cemented silt layers with SPT-N values up to 50. Across all three profiles (Figure 5), a consistent stratigraphic pattern is evident. Medium-stiff soils ($200 \leq Vs < 300$ m/s, SPT-N 10–40) dominate the lateral margins, while the central corridor is characterized by very stiff to hard soils ($Vs \geq 300$ m/s, SPT-N ≥ 50). Localized pockets of very soft soils ($Vs < 200$ m/s, SPT-N < 10) occur near the surface,

and deeper zones (>25–30 m) commonly show velocities exceeding 500 m/s, indicative of very hard soil (Figure 6).

Line A, a thick medium-stiff layer extends from 0–180 m, locally underlain by very soft soil at the surface (0–40 m). Beyond 180 m, the near-surface transitions into very stiff to hard soils, with a distinct high-velocity zone (>500 m/s) at 25–50 m depth. Localized low-density anomalies are also present within the stiff matrix.

Line C, both ends of the profile show thick medium stiff soils extending to ~45 m depth, interspersed with shallow soft-soil zones. The central section is underlain by very stiff to hard soil, including a pronounced high-velocity zone (>500 m/s) between 140–300 m survey distance. Localized density anomalies are mapped at depth.

Line E, Vs generally increases with depth, from medium stiff soils near the surface to very stiff/hard soils below ~20 m. A soft zone (Vs < 200 m/s) is noted between 210–330 m, likely reflecting high clay content. A deeper high-velocity zone (>500 m/s) is observed at 30–50 m depth between 20–120 m distance, similar to Line C. Localized density anomalies are again present at depth.

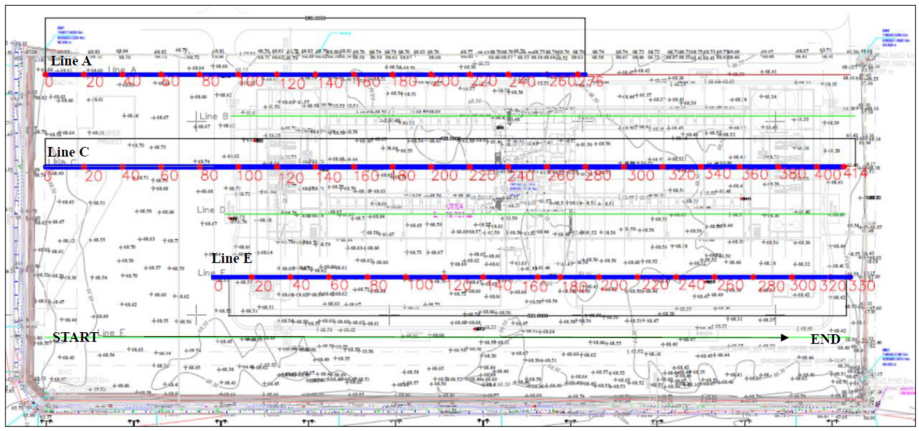

Figure 5. Layout Plan – KIIC Site.

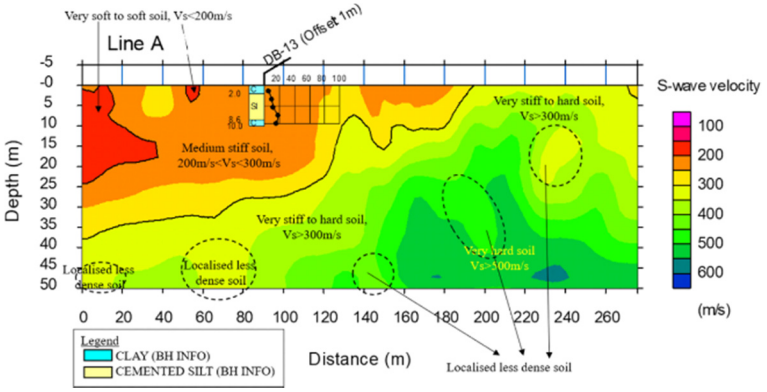

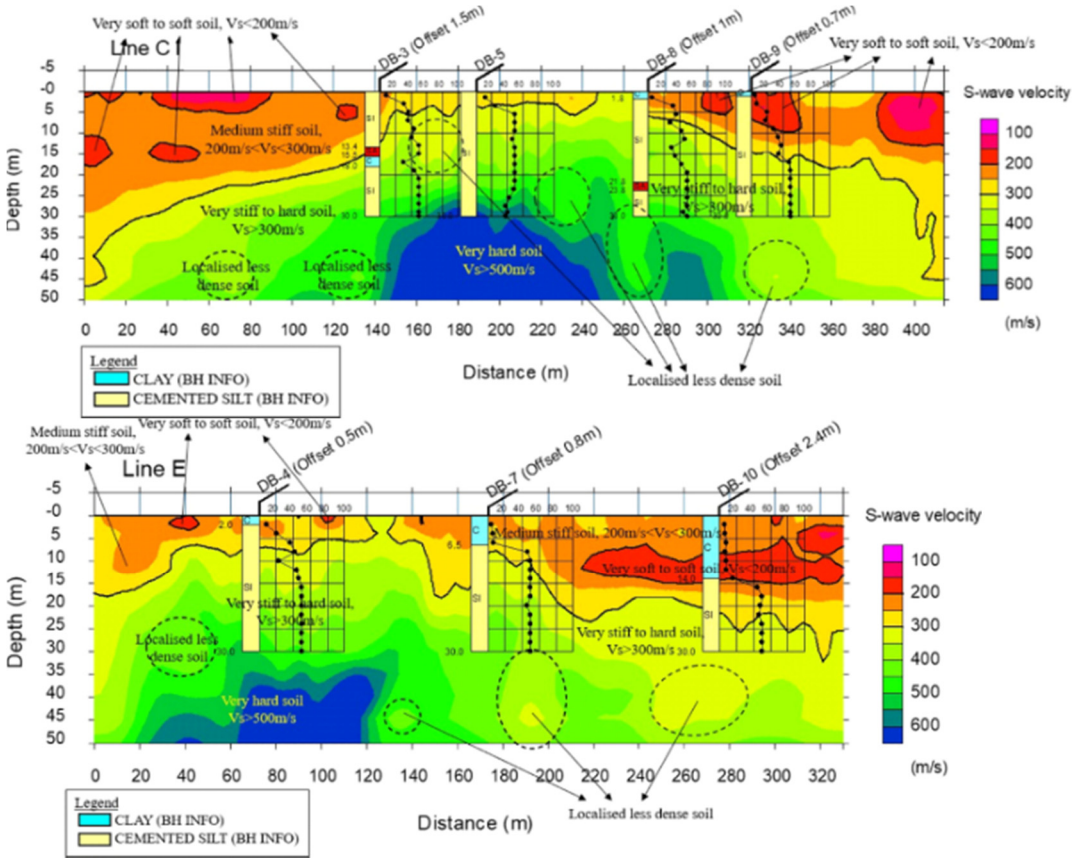

Figure 6. S-wave Velocity Cross Section Lines – KIIC Site.

Overall, the KIIC subsurface is typified by alternating medium-stiff and very stiff/hard soils, with soft near-surface pockets and deeper very hard zones. These features align with the Subang Formation as a soil dominated by stiffness to rock-like material.

4.2 Greenland International Industrial Center (GIIC)

Shear wave velocity profiles of GIIC sites (Figure 7) obtained from microtremor measurements with a total length of 909 meters show a generally consistent subsurface stratigraphy throughout the survey area with slight variations in depth and alignment. These interpretations are supported by geotechnical borehole logs, which indicate a predominance of clay and silt layers with varying stiffness, corroborated by Standard Penetration Test (SPT-N) values commonly exceeding 50 at depth.

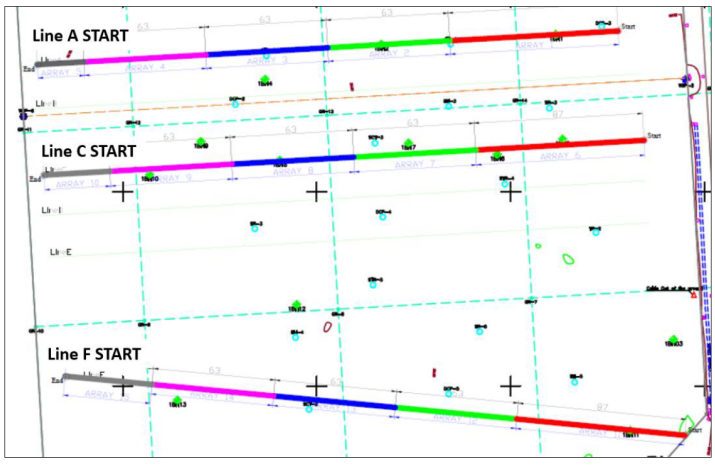

Figure 7. Layout Plan – GIIC Site.

Line A exhibits a near-surface soft to firm layer extending to approximately 5–15 meters, underlain by medium stiff soils that gradually transition to very stiff to hard soils at depth (Figure 8). A localized zone of stiff soil is also observed near the surface between 160 and 240 meters. The stiff-to-hard layer becomes shallower toward the latter half of the line compared to its deeper occurrence at the beginning. Zones of relatively lower density materials are identified at depths of 20–40 meters (90–110 m distance) and 30–45 meters (210–230 m distance).

Line C shows a similar overall stratigraphic pattern to Line A. In addition to the near-surface soft to firm layer, two localized stiff soil zones occur near the surface between distances of 80–150 meters and 200–260 meters. Three distinct zones of relatively less dense material are observed between 40 and 160 meters at depths of 15–48 meters, separated by a central zone of very stiff to hard soil.

Line F, which is the longest, also displays a general increase in Vs with depth. The near-surface profile consists of very soft to firm soils extending to about 12 meters, particularly between 20 and 80 meters, and gradually stiffens toward the end of the line. The very stiff to hard layer appears shallower toward the latter half of the line compared to its initial section. Two localized zones of relatively low-density materials are identified around 60 meters and 120 meters, extending from 15 to 45 meters depth (Figure 8).

Overall, the stratigraphy across the three lines follows a similar trend. The near-surface zone, typically within the upper 5–15 meters, consists of very soft to firm soils ($Vs < 200$ m/s, SPT-N < 10) transitioning into medium stiff soils (200–300 m/s, SPT-N 10–40). At greater depths, the soil profile develops into very stiff to hard soils ($Vs \geq 300$ m/s, SPT-N ≥ 40). In addition, several localized zones of relatively lower-density materials are identified between depths of 20–45 meters along specific portions of the profiles.

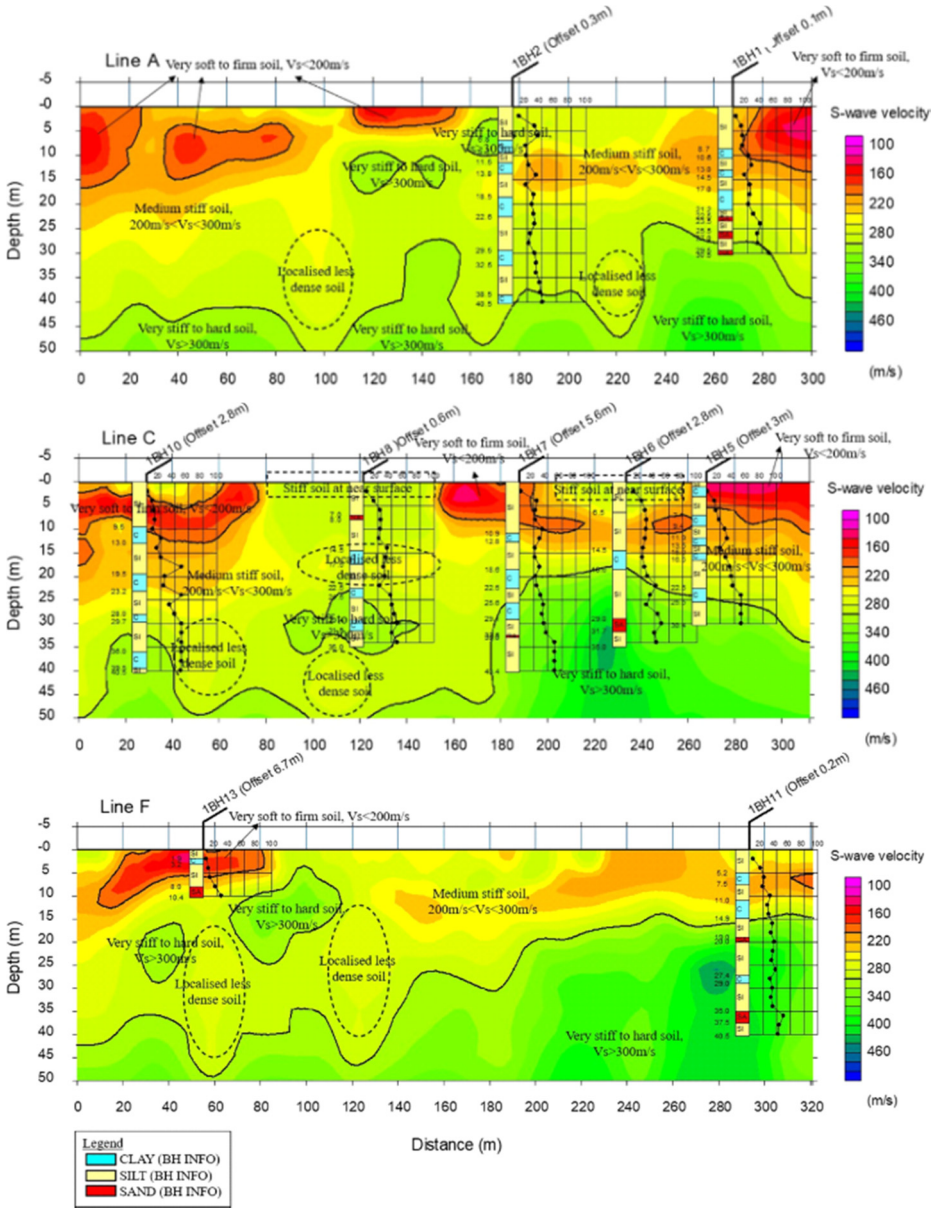

Figure 8. S-wave Velocity Cross Section Lines – GIIC Site.

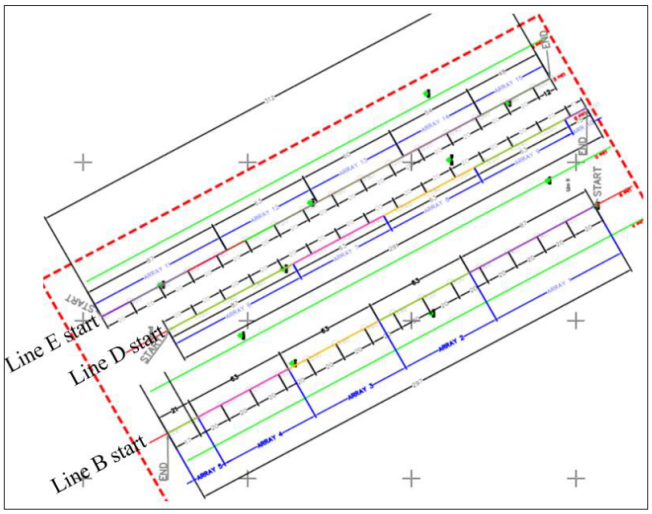

Figure 9. Layout Plan – Surya Cipta Site.

4.3 Surya Cipta City of Industry

Microtremor measurements were conducted at the Surya Cipta research site over a total length of 904 meters. Along these three lines, the soil profile is dominated by stiff to dense materials, with shear wave velocities (Vs) generally exceeding 300 m/s (Figure 9). For classification, soils are categorized as follows: very soft to firm (Vs < 200 m/s), medium stiff (200–300 m/s), very stiff to hard (Vs ≥ 300 m/s), and very hard (Vs > 500 m/s).

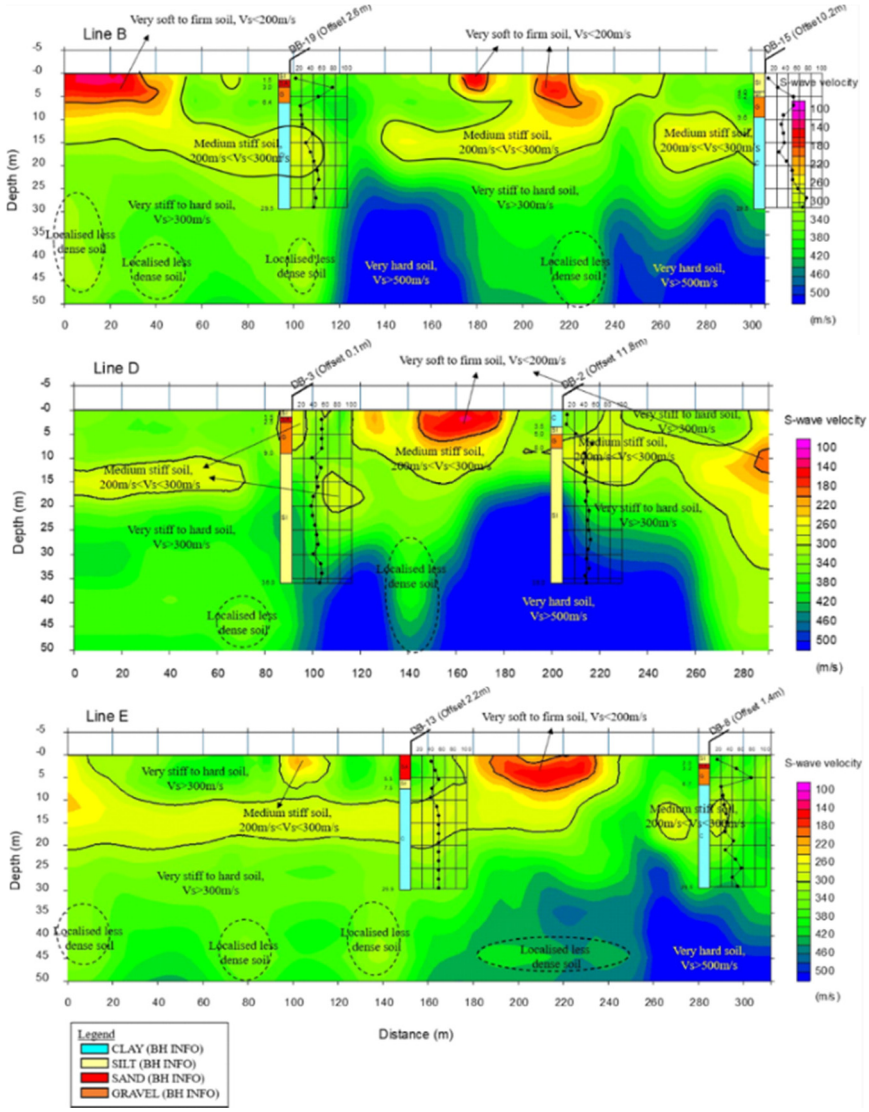

Figure 10. S-wave Velocity Cross Section Lines – Surya Cipta Site.

Line B reveals a near-surface zone of very soft to firm soil extending to depths of 5–7 meters at specific intervals: 0–40 m, 170–185 m, and 210–225 m. These weaker zones are surrounded by medium-stiff soils, typically extending to about 20 m depth. A discontinuous horizontal band of medium-stiff soil is observed along much of the profile between 10 and 20 m depth. At greater depths, the profile is dominated by very stiff to very hard soils. Localized zones of relatively lower density soil were identified at the following intervals: (a) 0–20 m, depth 25–47 m; (b) 30–50 m, depth 40–50 m; (c) 100–110 m, depth 35–47 m; and (d) 210–240 m, depth 35–50 m (Figure 10).

Line D exhibits a similar overall stratigraphy to Line B. The near-surface soft to firm soils are surrounded by medium stiff soils, which are more pronounced in the initial section (0–80 m) between 12 and 18 m depth. Towards the latter part of the profile, the medium stiff layer thickens to depths of about 33 m. Beneath these layers, very stiff to very hard soils dominate. Two zones of relatively less dense soils were identified: (a) 60–80 m, depth 40–50 m, and (b) 130–150 m, depth 30–50 m.

Line E, the longest survey line, shows near-surface very soft to firm soils around 180–240 m distance. A horizontal layer of medium-stiff soil is present between 10 and 20 m depth, extending across much of the line. At greater depths, very stiff to very hard soils dominate, with localized low-density materials identified at: (a) 0–20 m, depth 30–45 m; (b) 70–85 m, depth 30–50 m; and (c) 200–240 m, depth 30–50 m (Figure 10).

5 INTEGRATION FRAMEWORK

5.1 Vs – NSPT Correlations

The correlation between shear wave velocity (Vs) and Standard Penetration Test (SPT-N) values has long been recognized as an essential approach for evaluating subsurface stiffness and soil behavior. In this study, the available Vs and SPT datasets from the three investigated sites (KIIC, GIIC, and Surya Cipta) were systematically compared against widely established empirical correlations (Figure 11c), such as those proposed by Imai and Yoshimura (1970), Ohba and Toriumi (1970), and other studies, as shown in Table 3. In this study, correlations were established between the N-SPT values obtained from borehole data at the research sites and the shear wave velocities (Vs, m/s) derived from microtremor measurements (Figure 11 a). A simple regression analysis (Figure 11 b) was applied to these data sets, for all soil the proposed relation between Vs (m/s) and N values is as follows.

$$Vs = 67.264N^{0.4158}$$

This relation has a correlation coefficient $R^2 = 0.7941$, which is a reasonably good value.

Table 3. Existing correlations between Vs and SPT-N (Modified from Daag et al. (2022))

Authors(s)	Vs (m/s)		
	All Soil	Sands	Clays
Imai and Yoshimura (1970)	$V_s = 76N^{0.33}$	-	-
Ohba and Toriumi (1970)	$V_s = 84N^{0.31}$	-	-
Fujiwara (1972)	$V_s = 92.1N^{0.337}$	-	-
Ohsaki and Iwasaki (1973)	$V_s = 81.4N^{0.39}$	-	-
Ohta and Got0 (1978)	$V_s = 85.35N^{0.348}$	$V_s = 88.0N^{0.340}$	-
Seed and Idriss (1981)	$V_s = 61N^{0.500}$	-	-
Tonouchi et al. (1983)	$V_s = 97N^{0.314}$	-	-
Athanasopoulos (1995)	$V_s = 107.6N^{0.360}$	-	-
Jafari et al. (2002)	$V_s = 121.0N^{0.270}$	$V_s = 80.0N^{0.330}$	$V_s = 100.0N^{0.330}$
Hasancebi and Ulusay (2007)	$V_s = 90N^{0.309}$	$V_s = 90.8N^{0.319}$	$V_s = 97.9N^{0.269}$
Hanumantharao and Ramana (2008)	$V_s = 82.6N^{0.430}$	$V_s = 79.0N^{0.434}$	-
Uma Maheswari et al. (2010)	$V_s = 95.64N^{0.301}$	$V_s = 100.53N^{0.265}$	$V_s = 89.3N^{0.358}$
Fauzi (2014)	$V_s = 105.03N^{0.286}$	-	-

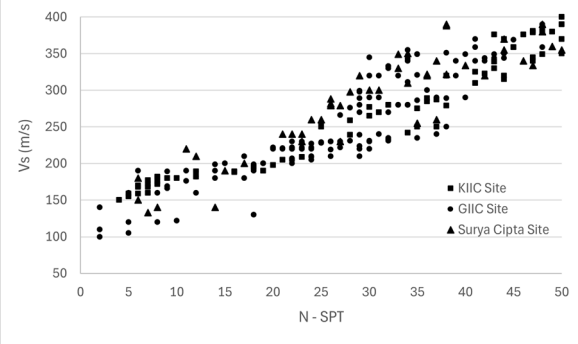

(a)

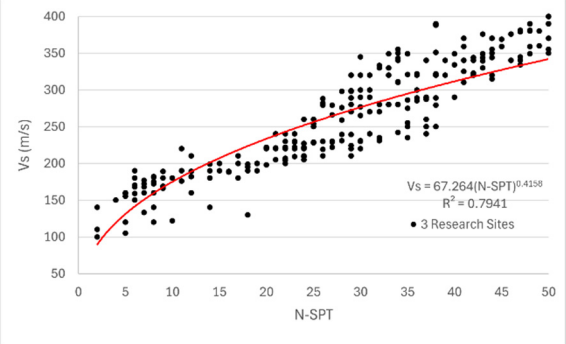

(b)

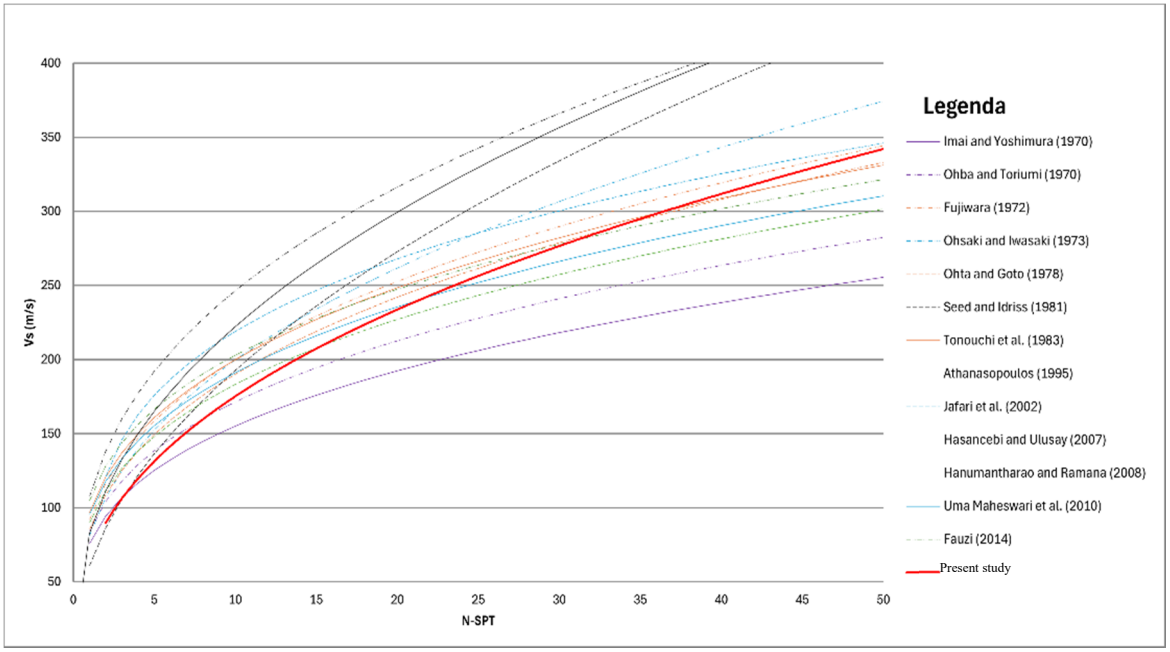

(c)

Figure 11. (a) Plotting N values and Vs (m/s), (b) Correlation N values and Vs (m/s), (c) Correlation between Vs and N for all soils.

5.2 Vs30 and Site Classification

The parameter Vs30 refers to the time-averaged shear wave velocity of the upper 30 meters of the subsurface. It is a widely accepted metric used in geotechnical and earthquake engineering to characterize site conditions and evaluate the dynamic response of soil layers to seismic loading. Vs30 is calculated as the harmonic mean of shear wave velocities measured across soil and rock strata within the upper 30 m depth. According to the National Earthquake Hazards Reduction Program (NEHRP) site classification system, Vs30 is the principal parameter used to categorize sites into different soil classes. This classification is essential in seismic design, as it directly governs the ground motion amplification factors applied in structural analysis. Determining Vs30 and assigning the appropriate NEHRP site class ensures that local soil conditions are properly incorporated into seismic hazard assessments and earthquake-resistant design. The NEHRP site classification based on Vs30 is summarized in Table 4.

Table 4. NEHRP Classification Based on Vs30

Vs30 Range (m/s)	General Description
> 1500	Hard Rock
760 – 1500	Rock
360 – 760	Very Dense Soil and Soft Rock
180 – 360	Stiff Soil
< 180	Soft Soil
_	Special soils (e.g., liquefiable soils, sensitive clays, organic soils) requiring site-specific evaluation

Table 5. NEHRP Classification Result

Site Location	Profile / Array	Vs30 (m/s)	NEHRP Site Class	Description
KIIC	Profile A	294	D	Stiff Soil
	Profile C	345	D	Stiff Soil
	Profile E	320	D	Stiff Soil
GIIC	Profile A	305	D	Stiff Soil
	Profile C	265	D	Stiff Soil
	Profile F	310	D	Stiff Soil
Surya Cipta	Profile A	304	D	Stiff Soil
	Profile D	248	D	Stiff Soil
	Profile E	247	D	Stiff Soil

In this study, the time-averaged shear wave velocity of the upper 30 meters (Vs30) was evaluated to characterize the seismic site conditions in the KIIC, GIIC, and Surya Cipta industrial areas. Vs30 is a fundamental parameter in geotechnical earthquake engineering, providing a standardized measure of near-surface soil stiffness and serving as the primary basis for site classification in seismic hazard assessments (BSSC, 2003). The values of Vs30 were calculated using the harmonic mean of shear wave velocity (Vs) data derived from microtremor measurements conducted at each site. The calculated Vs30 values were subsequently classified according to the National Earthquake Hazards Reduction Program (NEHRP) site classification system, which links soil stiffness to expected levels of seismic ground motion amplification. The classification results for each location are presented in Table 5.

The calculated Vs30 values across the three study areas indicate that all sites fall under the NEHRP Site Class D (Stiff Soil) category. At the KIIC site, Vs30 ranges from 294 to 345 m/s with an average value of 320 m/s, while the GIIC site yields values between 265 and 310 m/s with an average of 293 m/s. Meanwhile, the Surya Cipta site shows slightly lower velocities, ranging from 247 to 304 m/s with an average of 266 m/s. Although variations are observed among individual profiles, the overall classification remains consistent across all study locations. This indicates that the subsurface conditions are predominantly composed of stiff soil layers, which may moderately amplify seismic ground motions compared to rock or very dense soil sites.

6 CONCLUSION

The results of this study demonstrate the effectiveness of integrating conventional penetration testing with advanced seismic sensing in geotechnical site characterization. Specifically, the findings confirm that the Microtremor Array Measurement (MAM) technique provides a scientifically robust and spatially extensive means of evaluating subsurface stiffness, thereby complementing and extending the applicability of SPT data in areas where borehole information is limited.

a. The integration of SPT and MAM has proven effective for geotechnical site characterization in the Karawang industrial estates. This result shows that combining both methods provides more reliable subsurface information than using either technique alone. It also supports previous findings that integrating geotechnical and geophysical data improves the accuracy of site classification.
b. Microtremor Array Measurement (MAM) provides reliable and spatially extensive shear wave velocity (Vs) data, complementing limited borehole SPT data. This finding suggests that MAM can effectively fill data gaps in areas with sparse borehole coverage, enhancing the overall accuracy of subsurface characterization.
c. A strong correlation was observed between Vs and SPT-N values at the study sites, consistent with previous global empirical correlations. The proposed correlation for all soil types is $Vs = 67.264\ N^{0.4158}$, with a correlation coefficient of R2 = 7941. This result confirms that the proposed correlation is reliable for representing local soil conditions and can be applied for preliminary site characterization when direct data are unavailable.

d. NEHRP site classifications derived from both Vs_{30} and SPT-N values show consistent results, with KIIC and GIIC identified as Site Class D (stiff soil) and Surya Cipta as Site Class E (soft soil). This consistency indicates that both parameters provide comparable reliability for site classification and confirm the suitability of the integrated approach for seismic hazard assessment in the study area.
e. The consistency between Vs-based and SPT-based classifications confirms the robustness of the Vs–SPT correlation in the study area. This indicates that both approaches can be used interchangeably for preliminary site classification.
f. Geotechnically, Site Class E conditions at Surya Cipta imply higher seismic amplification potential and may require soil improvement for safe foundation design. This finding highlights the importance of integrating geophysical and geotechnical data in identifying zones that demand special engineering consideration.

This integrated approach demonstrates the practical advantages of combining conventional penetration testing with advanced seismic sensing for earthquake-resistant planning in industrial regions.

DISCLAIMER

The authors declare no conflict of interest.

AVAILABILITY OF DATA AND MATERIALS

All data are available from the author.

REFERENCES

ASTM International, 2011. *ASTM D1586-11: Standard Test Method for Standard Penetration Test (SPT) and Split-Barrel Sampling of Soils*. West Conshohocken, PA: ASTM International.

Athanasopoulos, G. A., 1995. Empirical correlations Vs–N for soil deposits in Greece. *Soils and Foundations*, 35(4), pp. 197–203.

Badan Standardisasi Nasional (BSN), 2008. *SNI 4153:2008 – Cara uji penetrasi standar (SPT)*. Jakarta: BSN.

BMKG, 2024. *Earthquake report: West Java Mw 5.0 event*. Badan Meteorologi, Klimatologi, dan Geofisika (BMKG). [Online] Available at: https://www.bmkg.go.id [Accessed 2024].

Building Seismic Safety Council (BSSC), 2003. *NEHRP recommended provisions for seismic regulations for new buildings and other structures (FEMA 450)*. Washington, DC: Federal Emergency Management Agency (FEMA).

Daag, A. S., et al., 2022. Empirical correlation between standard penetration resistance (SPT-N) and shear wave velocity (Vs) for soils in Metro Manila, Philippines. *Applied Sciences*, 12(16), 8067. https://doi.org/10.3390/app12168067.

Damanik, R., et al., 2023. New assessment of the probabilistic seismic hazard analysis for the greater Jakarta area, Indonesia. *Geomatics, Natural Hazards & Risk*, 14(1), Article 2202805. https://doi.org/10.1080/19475705.2023.2202805.

Fauzi, U., 2014. Correlation of shear wave velocity and SPT-N value for Padang soils, West Sumatra. *International Journal of GEOMATE*, 6(2), pp. 891–897.

Federal Emergency Management Agency (FEMA), 1994. *FEMA 222/222A: NEHRP Recommended Provisions for the Development of Seismic Regulations for New Buildings*. Washington, DC: FEMA.

Federal Emergency Management Agency (FEMA), 2003. *FEMA 450: NEHRP Recommended Provisions for Seismic Regulations for New Buildings and Other Structures*. Washington, DC: FEMA.

Federal Emergency Management Agency (FEMA), 2020. *FEMA P-2082-1: NEHRP Recommended Seismic Provisions for New Buildings and Other Structures — Part 1, Provisions*. Washington, DC: FEMA.

Fujiwara, T., 1972. Technical note on the relation between soil properties and shear wave velocity. *Railway Technical Research Institute*. Japan.

Hanumantharao, C. & Ramana, G. V., 2008. Dynamic soil properties for microzonation of Delhi, India. *Journal of Earth System Science*, 117(S2), pp. 719–730.

Hasançebi, N. & Ulusay, R., 2007. Empirical correlations between shear wave velocity and penetration resistance for ground shaking assessments. *Engineering Geology*, 97(3–4), pp. 149–170.

Imai, T. & Yoshimura, Y., 1970. The relation of mechanical properties of soils to P- and S-wave velocities for ground in Japan. *Urana Research Institute Report*. Tokyo: OYO Corporation.

Jafari, M. K., Shafiee, A. & Razmkhah, A., 2002. Shear wave velocity–SPT correlations in Tehran soils. *Soil Dynamics and Earthquake Engineering*, 22(9–12), pp. 851–856.

Ohba, S. & Toriumi, I., 1970. Dynamic response characteristics of ground in Tokyo area. *OYO Technical Report*. Tokyo.

Ohsaki, Y. & Iwasaki, R., 1973. On dynamic shear moduli and Poisson's ratio of soil deposits. *Soils and Foundations*, 13(4), pp. 61–73.

Ohta, Y. & Goto, N., 1978. Empirical shear wave velocity equations in terms of characteristic soil indexes. *Earthquake Engineering & Structural Dynamics*, 6(2), pp. 167–187.

Prabowo, U. N., Ferdiyan, A. & Amalia, A. F., 2021. The soft layer thickness estimation using microtremor measurement to identify landslide potential in Watukumpul, Central Java, Indonesia. *Journal of Geoscience/Proceedings*. (Available in institutional repository).

Ridwan, M., et al., 2014. Estimation of S-wave velocity structures by using microtremor array measurements for subsurface modeling in Jakarta. *Geological Society of London Special Publication*, 2016 (related publication).

Sadisun, I. A., Shimada, H., & Matsui, K., 2000. *Characterization of weathered claystone and their engineering significance*. *Proceedings of the Indonesian Scientific Meeting 2000*.

Seed, H. B. & Idriss, I. M., 1981. Evaluation of liquefaction potential of sand deposits based on SPT results. *Journal of Soil Mechanics and Foundations, ASCE*, 97(8), pp. 123–147.

Setiawan, B., et al., 2020. Ambient noise analysis for characterizing sub-surface dynamic parameters. *IOP Conference Series: Materials Science and Engineering*, 712, 012012. https://doi.org/10.1088/1757-899X/712/1/012012.

Tonouchi, K., Ohta, Y. & Goto, N., 1983. Empirical shear wave velocity equations in terms of soil index properties. *Journal of Japan Society of Civil Engineers*, 328, pp. 83–90.

Uma Maheswari, R., Boominathan, A. & Dodagoudar, G. R., 2010. Use of surface waves in statistical correlations of shear wave velocity and penetration resistance of Chennai soils. *Geotechnical and Geological Engineering*, 28(2), pp. 119–137.

USGS, 2024. *M 5.0 – West Java, Indonesia*. U.S. Geological Survey. [Online] Available at: https://earthquake.usgs.gov [Accessed 2024].

HIMPUNAN AHLI TEKNIK TANAH INDONESIA - HATTI
Indonesian Society for Geotechnical Engineering - ISGE
PIT HATTI XXIX
10-12 November 2025

Stability Assessment of Homogeneous Embankment Dam under Variable Drawdown Rates Using Unsaturated Soil Parameters

Muhammad Adi Ibrahim[1], Azwar Anas[2]
[1]Infrastructure 1 Division, PT Wijaya Karya (Persero) Tbk, Jakarta, Indonesia, 13340; muhammadadiibrahim@gmail.com
[2]Infrastructure 1 Division, PT Wijaya Karya (Persero) Tbk, Jakarta, Indonesia, 13340; kanganas1992@gmail.com
*Correspondence: muhammadadiibrahim@gmail.com

ABSTRACT Embankment dams are critical for sustainable water resources management, providing irrigation, hydropower, flood control, and water supply. One of the critical threats to their stability is rapid drawdown, when reservoir levels fall faster than pore pressures dissipate in the upstream slope. This condition reduces shear strength and can trigger failure. One of the commonly used methods for rapid drawdown assessment is the three-stage approach developed in the early 1990s, which provides a practical framework by combining drained and undrained soil strength. However, these methods do not explicitly consider the influence of drawdown rate, which can strongly affect stability. This study evaluates the effect of drawdown rate on the stability of an embankment dam using an unsaturated soil mechanics framework and compares the results with those from the three-stage method. Numerical analyses were carried out using coupled seepage and slope stability modelling. The soil-water characteristic curve of the clay core was estimated from index properties. Three drawdown variations were examined: half a meter per day, one meter per day, and two meters per day. The result showed that the three-stage method produced higher factors of safety, and the unsaturated framework showed decreasing stability at faster drawdown rates due to pore-pressure dissipation, highlighting that the three-stage method may overestimate stability during rapid drawdown. Incorporating unsaturated soil mechanics provides a more realistic assessment and offers insights for improving dam safety, particularly under conditions where faster drawdown may occur.

KEYWORDS Rapid drawdown; Embankment dam stability; Unsaturated soil mechanics; Drawdown rate; Three-stage method

This paper will be published in the future issues of Indonesian Geotechnical Journal

This page is intentionally left blank

HIMPUNAN AHLI TEKNIK TANAH INDONESIA - HATTI
Indonesian Society for Geotechnical Engineering - ISGE
PIT HATTI XXIX
10-12 November 2025

Mitigating Reclamation-Induced Settlement Using Rigid Inclusions: A Ground Improvement Case from Ahmad Yani Airport, Indonesia

Ryan Rahmat Setiaji[1,*], Ayu Wijayanti Kurnia Dewi[1], Baiq Melly Ciptayuni Asmarani[1]
[1]PT Artha Geo Integritas, North Jakarta, Indonesia, 14450
*Correspondence: ryan.setiaji@gmail.com

ABSTRACT This study examines the application of rigid inclusions (RI) as a remedial ground improvement technique to control severe settlement and pavement distress along the access road to Ahmad Yani Airport in Semarang. The road, originally constructed over reclaimed swamp land with an embankment height of about 5 m, is underlain by more than 14 m of soft marine clay that had not undergone prior ground treatment. This condition resulted in extensive pavement damage and pronounced differential settlement between the suspended-slab and the adjoining road sections. Subsurface investigations, including SPT, CPT, and laboratory tests, indicated highly compressible clay with predicted settlements exceeding 1.4 m, necessitating immediate ground improvement measures. Several ground improvement options were evaluated, and rigid inclusions were selected for their high efficiency, low environmental impact, and suitability for active infrastructure. The study outlines the RI design, construction, and performance assessment. Analytical results show that the proposed RI system can limit post-construction settlement to within 100 mm, confirming its potential as a reliable and sustainable solution for soft-soil road embankments.

KEYWORDS Rigid Inclusion; Ground Improvement; Settlement; Soft Soil

1 INTRODUCTION

Ahmad Yani Airport is located in Semarang, Central Java, an area widely recognized for its soft soil deposits and reclaimed land (Setiaji & Dewi, 2025). As part of the airport's expansion project, a new terminal, parking area, and access road were constructed to support increasing passenger and operational demands. The access road to the pick-up zone, however, has experienced considerable settlement. This zone was originally a swamp area that had been reclaimed around eight years earlier, with an estimated fill thickness of 4 to 5 meters. While the terminal building and elevated slab were supported by piled foundations, the access road was left untreated. As a result, noticeable differential settlement developed between the piled structures and the road surface, creating both structural concerns and discomfort for the public.

The settlement was primarily attributed to the self-weight of the embankment fill and the additional pavement and traffic load acting on the underlying soft marine clay. In the absence of prior ground treatment, the soil underwent substantial consolidation. The lack of soil improvement during the reclamation phase, which began in February 2015, significantly worsened the problem, with settlements reportedly ranging from 300 mm to 600 mm along the access road by 2023. Over time, the continued deformation caused extensive pavement damage and deterioration of surrounding infrastructure, emphasizing the urgent need for ground improvement and remediation measures.

By early 2024, the airport authority initiated the reconstruction of the access road to seek a permanent solution to address the recurring subsidence problem. Ground improvement was deemed essential to ensure the long-term performance and safety of the infrastructure. Accordingly, this study investigates the settlement issues observed at Ahmad Yani Airport and analyzes the available

geotechnical and construction records. Based on the evaluation of several potential ground improvement alternatives, the study identifies and justifies the implementation of rigid inclusions as the most appropriate and sustainable solution to mitigate the recurring settlement problem.

The objective is to present the effectiveness of RI in mitigating settlement within reclaimed soft-soil environments and to share practical insights that can guide future infrastructure development in coastal and soft-ground regions.

2 LITERATURE REVIEW

Rigid inclusion is a ground improvement technique that installs high-stiffness columns through compressible soils to transfer loads to deeper, stronger layers. Arranged in a regular grid with defined spacing and diameter, RI systems reduce total and differential settlement by combining the stiffness of the inclusions with the surrounding soft soil. Most of the load is carried by the rigid columns, while the remaining portion is transferred through a compacted granular Load Transfer Platform (LTP) that mobilizes arching effects and redistributes stresses between the inclusions and the soil. Shear mechanisms within the LTP and along the column shafts are activated by differential settlement between the stiff inclusions and the soft ground, allowing part of the load transfer to occur above the inclusion heads (ASIRI, 2012).

This interaction produces specific planes of equal settlement within the LTP, along the column length, and below the tip, where soil and inclusions deform compatibly as in Figure 1. Such behavior defines the unique load-sharing mechanism of the RI system and distinguishes it from other ground improvement methods (ASIRI,2012; Simon, 2012).

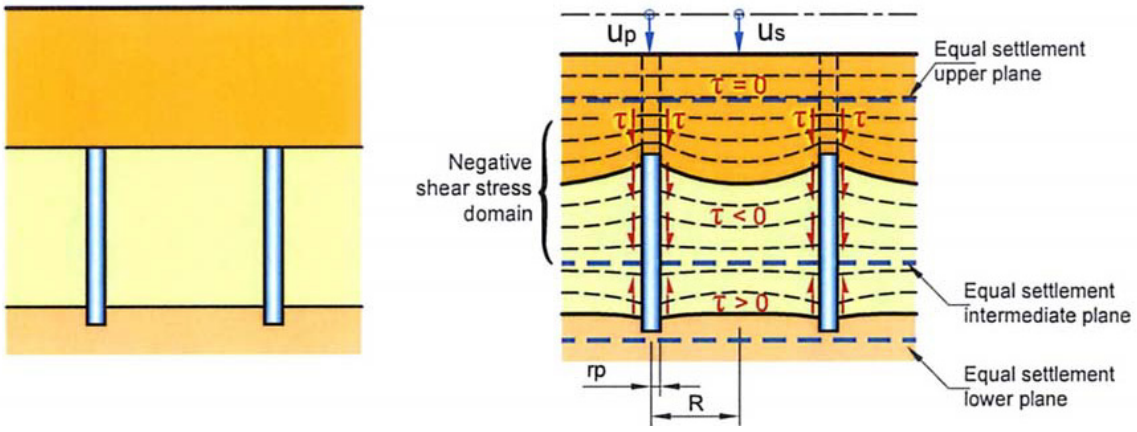

Figure 1. Equal settlement planes that develop in a rigid inclusions under an embankment (Simon, 2012).

The concept was first formalized by Combarieu (1988), who introduced the principle of load sharing and deformation compatibility between rigid inclusions and surrounding soil, establishing the theoretical foundation for modern RI design. Building on this, the ASIRI project (2012) developed comprehensive guidelines that standardized RI design and construction practices. Since then, rigid inclusions have been successfully applied in various infrastructure projects.

In Indonesia, rigid inclusion (RI) method has been successfully implemented in several major infrastructure projects, demonstrating its effectiveness in improving soft ground performance. At Soekarno–Hatta International Airport, RI was installed beneath the runway, taxiway, and apron to control settlement and enhance bearing capacity (Yee et al., 2012; Aulia, 2015). The technique was also applied in Central Java toll roads to stabilize embankments founded on soft alluvial and marine clays (Setiaji et al., 2018; Ahmad & Yee, 2018), and in the Mandalika MotoGP Circuit to reduce settlement and mitigate potential liquefaction hazards (Syofyan et al, 2023; Fitriyana et al, 2025). Several other unpublished projects, including airport, industrial facilities, storage tanks and

transportation infrastructure developments, have also adopted RI technology, underscoring its growing utilization and proven reliability in Indonesian geotechnical engineering practice.

3 REVIEW ON GEOTECHNICAL DATA

3.1 Soil Investigation Data

Subsurface investigations for the access road at Ahmad Yani Airport, Semarang, were conducted in two phases: 2020 and 2024 (Figure 2). The first phase, conducted in 2020 along the road edge to prevent pavement damage, included drilling two boreholes (BH1 and BH2), four CPTs (S01–S04), and two CPTu tests (CPTu-01 and CPTu-02). The second phase in 2024 focused directly on the pavement section and included two additional boreholes (BH-1 and BH-2) and one CPT test (CPT-01). The Microtremor Array Method (MAM) has also been applied to verify subsurface conditions and confirm the thickness of the soft soil layer (Setiaji & Dewi, 2025). The purpose of this second investigation was to collect supplementary data and validate the previous soil data.

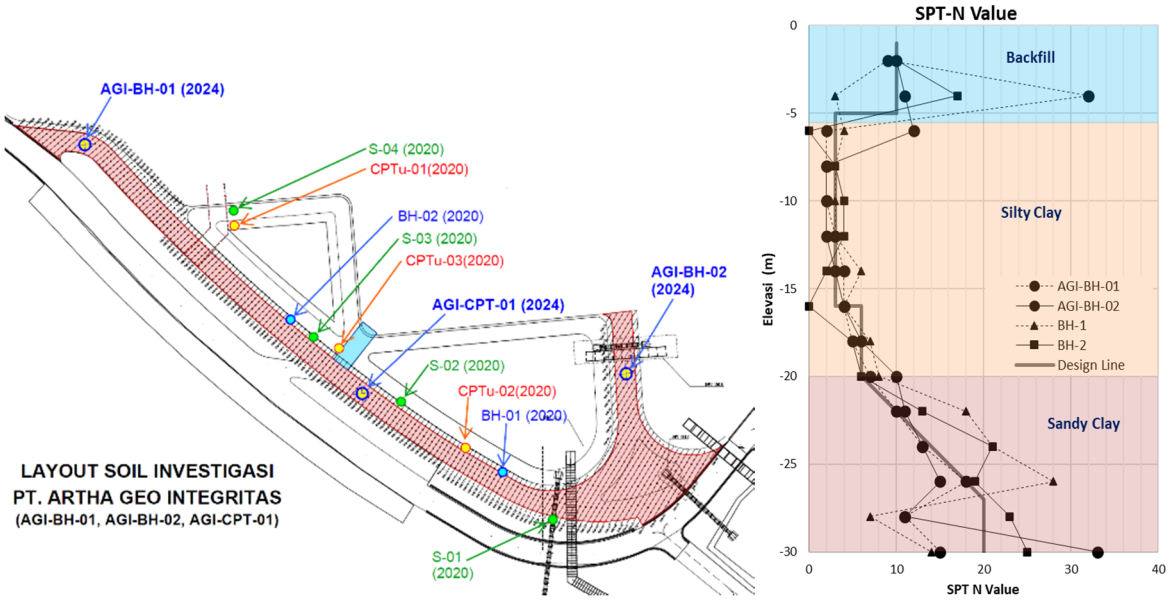

Figure 2. Soil Investigation points, and N-SPT Chart.

Borehole log data from the 2020 geotechnical investigation indicate that the fill layer extends to a depth of about 3–5 meters. This layer is characterized by relatively high N-SPT values and a sandy clay composition, typical of backfill material. Below the fill, a soft clay layer with N-SPT values less than 6 was encountered, with a thickness of approximately 13–14 meters from the base of the fill. This is underlain by a silty sand layer with N-SPT values ranging from 6 to 20, representing a transition to stiff to very stiff sandy clay layer.

The 2024 borehole data showed a stratigraphy similar to the 2020 results, though with a slightly thicker fill layer of about 5–6 meters. Beneath the fill, a soft clay layer with N-SPT values below 6 was again found, extending about 13–14 meters. This was followed by a sandy clay or clayey sand layer with N-SPT values of 10–20, indicating stiff soil conditions. Taken together, the four borehole records suggest that the soft clay layer consistently extends to an elevation of approximately 20 meters below the ground surface (Figure 2).

Similarly, CPTu data obtained in 2020 (Figure 3 left) indicated that the soft clay beneath the Ahmad Yani Airport access road extended to elevations of approximately 18 to–20 m. A fill layer characterized by relatively high cone tip resistance (qc) values was identified to a depth of about 4 m. Below this layer, qc values gradually increased, suggesting a transition to granular soils such as silty sand. Subsequent CPT results from 2024 (Figure 3 right), conducted directly on the access road,

revealed a stiffer 5 m-thick fill layer that was too dense for cone penetration and required pre-boring. Beneath this fill, a soft clay deposit about 15 m thick was observed, extending to roughly 20 m. Below that depth, qc values increased sharply, confirming the presence of silty sand until cone refusal, where penetration ceased due to very stiff soil conditions.

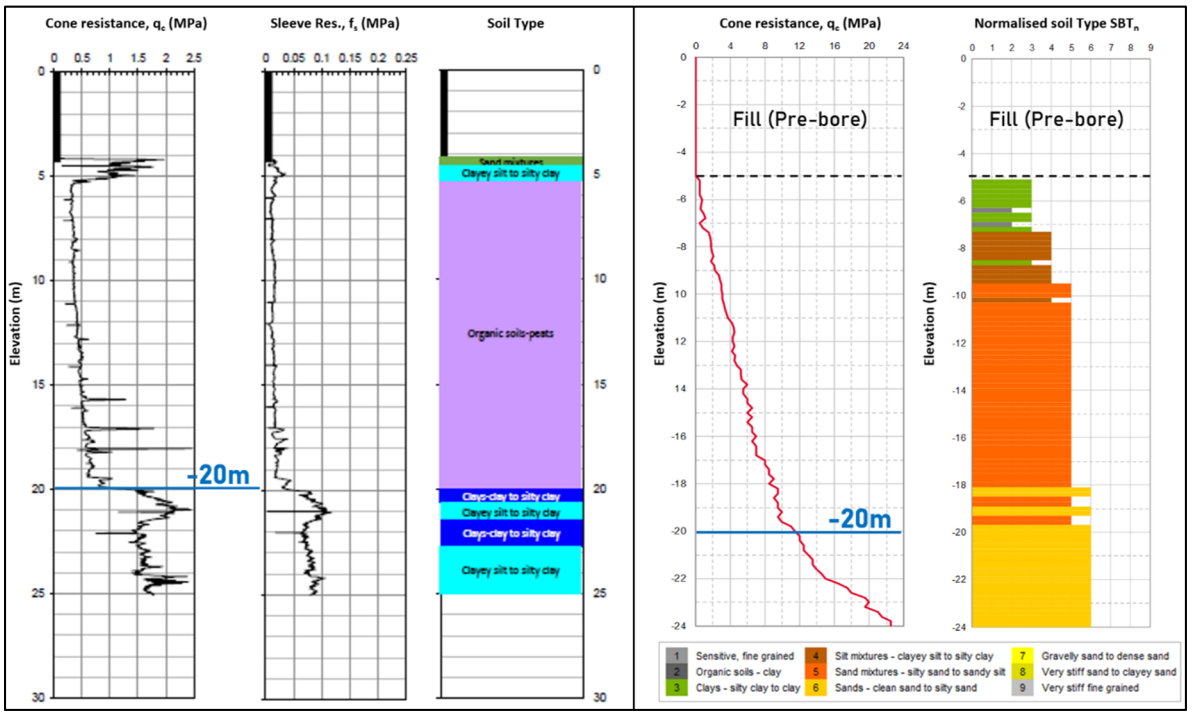

Figure 3. Typical CPT data (CPTu-02: 2020 left & AGI-CPT-01:2024 right).

Based on the subsurface investigation data, a representative soil stratigraphy model was developed. This interpretation combined BH and CPT data to define design soil layers that reflect the general subsurface conditions beneath the access road. For each layer, representative soil parameters were selected from laboratory results, applying conservative assumptions appropriate for design. These values were assigned to the interpreted soil layers and are summarized in the following Table 1. The table provides the basis for subsequent settlement analyses, stability evaluations, and the planning of ground improvement measures for the project.

Table 1. Soil Parameter

Soil / Material	Depth (m)	SPT N	Modulus (MPa)			γ (kN/m^3)	eo	Cc	Shear strength			k (m/s)
			E	E_{oed}	E_{UR}				Cu (kPa)	c' (kPa)	Phi'	
FILL	0 - 5	10	10	8	40	17	-	-	25	5	28	1.0E-08
Upper Clay	5 - 15	3	2	1.6	8	15.5	1.8	0.55	7	1	22	1.0E-09
Lower Clay	15 - 20	6	4.8	3.8	19.2	16	1.5	0.5	12	2	23	1.0E-09
Stiff Clay	20 - 27	6-20	6	4.8	24	17	-	-	20	5	25	1.0E-09
Sandy Clay	> 27	20	18	14.4	72	18	-	-	30	5	28	1.0E-08
Ground Improvement properties :												
Sand - LTP	4 - 5	-	20	16	60	18	-	-	1	1	35	1.0E-06
Rigid Inclusion	-	-	5000			24						

3.2 Reclamation history

The soil improvement project along the access road to Ahmad Yani Airport in Semarang was initiated following reports of ground settlement ranging from 30 to 60 cm by the project owner and consultants. Since consolidation settlement is a function of both load and time, reconstructing the construction chronology was essential to support the back-analysis of the observed subsidence. However, no official records were available regarding the construction timeline. Therefore, the historical timeline from satellite imagery from Google Earth was utilized to trace the sequence of reclamation and road development (Figure 4). Although the timeline derived from imagery is only approximate, it provides a valuable reference for evaluating the settlement behavior.

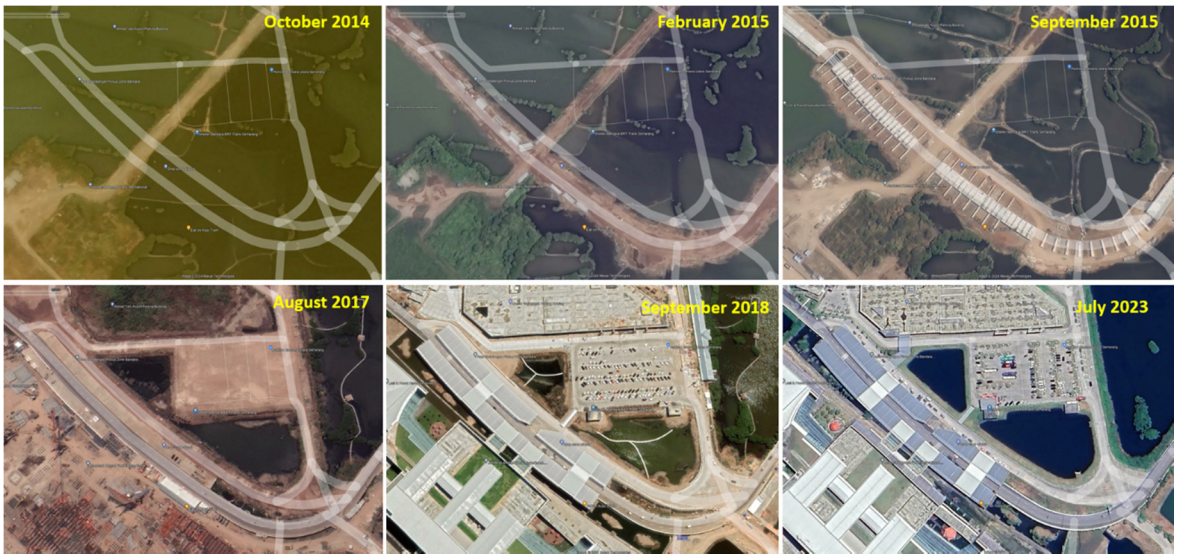

Figure 4. Major construction timeline.

Satellite imagery indicates that reclamation of the access road area began in February 2015 and was likely completed by September of the same year, forming the reclaimed platform leading to the terminal zone. The road remained largely unchanged until 2017, when reclamation activities shifted toward terminal development. By September 2018, construction of both the terminal and access road commenced concurrently. From the initial reclamation to the planned ground improvement in early 2024, the access road has been in service for approximately 8.5 years (Table 2). The timeline of major construction activities is summarized in the following table.

Table 2. Reclamation Timeline (Estimate).

ESTIMATED DATE	ACTIVITY	DURATION
Oct 2014	No reclamation yet	-
Feb 2015	Reclamation process of Access Road	-
Sep 2015	Access Road reclamation completed	Duration: 7 months (t = 0)
Aug 2017	Access road remains the same. Terminal reclamation process	Access road embankment has existed for ~2 years (t ≈ 2 years)
Sep 2018	Construction of access road and terminal + operational access	Access Road (t ≈ 3 years)
Mar 2024	Current condition	Access Road (t ≈ 8 years 6 months)

3.3 Settlement calculation

To evaluate settlement behavior, a consolidation analysis was performed using the Finite Element Method (FEM) with Plaxis 2D software. Prior to the analysis, a detailed construction sequence was established to reflect the timeline of reclamation and the application of loads on the access road, including fill placement, pavement layers, and vehicular traffic. This step was essential to estimate

the degree of consolidation that had already occurred and to calculate the remaining or future consolidation based on residual excess pore pressure. An axisymmetric analysis was then carried out following the construction sequence outlined below:

Step 1 Initial Condition
Step 2 Reclamation : 120 days
Step 3 Consolidation : 720 days (2 year)
Step 4 Road + Traffic : 365 days (1 year)
Step 5 Consolidation to date : 2008 days (5.5yr)
Step 6 Future Consolidation : minimum pore pressure

The FEM results indicated that by 2024, just before the planned ground improvement works, the site had experienced a settlement of approximately 595.1 mm (see the chart at Figure 5). However, the clay layer was still undergoing consolidation, as the excess pore pressure within the soft clay had not fully dissipated. The model predicts that settlement will continue over time, reaching a total of about 1,264 mm (Plaxis output at Figure 5). These findings can be compared with actual field measurements to validate the model and provide justification for ground improvement at the site, where observed settlement currently ranges from 300 to 600 mm.

The findings confirm that progressive ground subsidence is ongoing and underscore the urgent need for remedial measures to permanently mitigate ground settlement and associated structural damage.

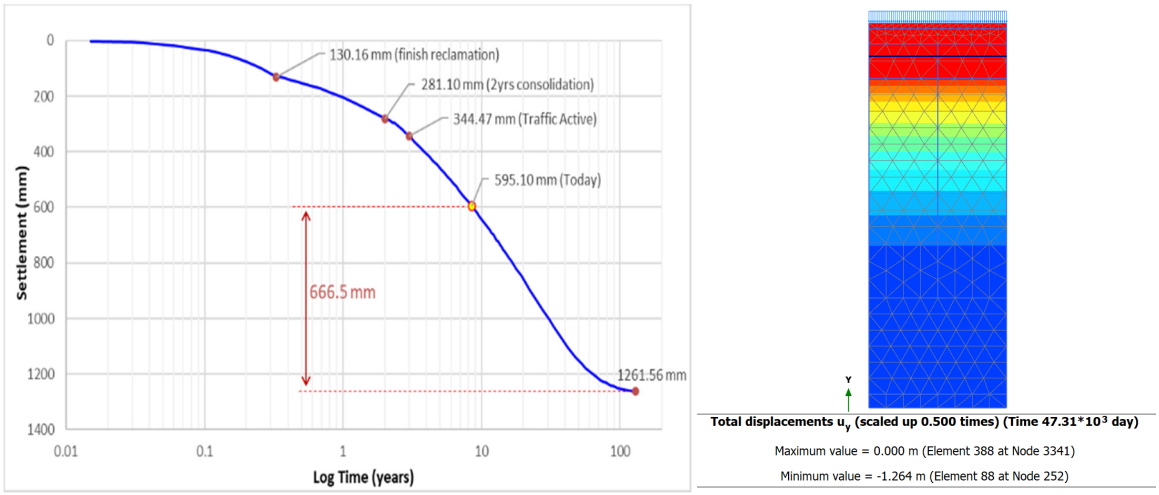

Figure 5. Ground Settlement Curve in Logarithmic Time.

4 ASSESMENT FOR GROUND IMPROVEMENT OPTIONS

There are several ground improvement methods commonly recommended in the Indonesian Geotechnical Standard (SNI Geoteknik 8460, 2017). In the case of Ahmad Yani Airport, the access road is located immediately adjacent to the passenger pick-up point of the terminal building. Since the airport operates continuously, any ground improvement work must be carried out without interrupting airport activities or compromising the safety of nearby structures. With this constraint, the consultants conducted a comparative study to evaluate the feasibility of different ground improvement methods, as summarized in Table 2. The options included prefabricated vertical drains (PVD) with preloading or vacuum preloading, deep soil mixing (DSM), rigid inclusions (RI), and stone columns.

Rigid inclusion was ultimately chosen as the most suitable ground improvement method for the project. It offers several advantages: high installation productivity (up to 1,000 linear meters per rig per shift), consistent treatment quality across large areas, minimal environmental disturbance due to vibration-free and low-noise installation, and flexibility that allows parallel construction activities to proceed without disruption. These benefits make it highly compatible with the operational

constraints of the airport environment. A detailed comparison of the features of each method is provided in Table 3, and the scoring evaluation is presented in Table 4. The scoring system ranged from 1 (least suitable) to 5 (most suitable). Rigid inclusions achieved the highest score, with a total of 38 points, confirming its suitability under the project's technical, operational, and environmental requirements.

Table 3. Comparison of Ground Improvement Techniques.

Description	PVD/ Vacuum Preloading	Deep Soil Mixing (DSM)	Rigid Inclusion (RI)	Stone Column (SC)
Soil suitability	Soft Clay SPT N < 12	Clay – Sand SPT N<18	Clay – Sand SPT N<25	Clay – Sand SPT N<18
Methode/ technique	Accelerate consolidation process	Creating a column of soil and cement mixing	Strengthening by piling	Strengthening by Stone pile/ column
Material	PVD and soil surcharge	Cement-water paste	Mortar fc'15-25MPa	gravel 30 – 50mm
Productivity	Very slow. (it requires waiting time around >6 months)	Slow to medium. Productivity: 160 – 200 m per rig per day	High. Productivity: ~1000m' per rig per shift	Slow to medium. Productivity: 160 – 200 m per rig per day
Homogeinity of treatment result	High. The improved soil is homogenic with similar preloading height	Medium. The diameter of column may varies depending on soil layer. Amount of cement shall be adjusted periodically.	Very high, material is homogenic from concrete batching plant	Medium. The diameter of column may varies depending on soil layer.
Impact to environment	PVD causes excessive settlement, it may give impact to surrounding properties. It may cause lateral soil movement. Suitable mainly for new development. May not be performed along with other construction.	It requires big working area for cement silo and mixing plant It causes dirty working environment. It may require cleaning and spoil transport.	Installation is fast and not causing any vibration and noice. The work can be done in parallel to other construction.	Installation process may cause vibration and noise. It causes dirty working environment. It requires material transport.

Table 4. Scoring of Ground Improvement Techniques.

Description	PVD/ Vacuum Preloading	Deep Soil Mixing (DSM)	Rigid Inclusion (RI)	Stone Column (SC)
Ability to improve soft soil condition	5	5	5	5
High productivity	1	2	5	2
Easy to obtain material	5	4	4	3
Clean working environment/ not causing soil polution	1	2	5	2
Able to reduce vibration or noise	5	3	5	2
Homogeinity of technique	4	2	5	3
Can be performed in parallel with other work	1	3	5	3
Easy to find local vendor in Indonesia	5	3	4	3
TOTAL	27	24	38	23

The project owner specified strict selection criteria: the method must avoid adverse impacts on surrounding facilities, minimize disturbance to daily operations, and comply with the airport's safety and aesthetic requirements. Methods based on preloading, such as PVD and vacuum preloading, were deemed unsuitable. This is because the long consolidation process could generate large ground movements, creating differential settlement and endangering the nearby terminal foundation. Furthermore, preloading requires the placement of large soil embankments, which would negatively affect the airport's appearance and cleanliness, making it incompatible with an active international terminal environment.

Stone columns and DSM were also considered impractical. Both techniques rely on heavy machinery and generate significant vibration and noise during installation. These disturbances are unacceptable in a sensitive operational zone, where passenger safety and comfort are critical. Similarly, reinforced concrete (RC) pile driving was excluded for the same reasons, as it would introduce disruptive vibrations and noise and potentially compromise nearby airport operations. The elimination of these alternatives effectively narrowed the viable solution to rigid inclusions.

5 RIGID INCLUSION DESIGN

The design of the ground improvement system using rigid inclusion was carried out in accordance with the ASIRI (2012), which provides established guidelines for rigid inclusion applications in soft soil. The analysis and design were performed using the Finite Element Method (FEM) with both axisymmetric and plane-strain models to evaluate settlement reduction, stress distribution, and overall system stability.

5.1 Axissymmetrical Modelling

The RI columns were designed to penetrate the entire soft clay layer and terminate at the refusal layer, approximately 20 m deep, to ensure efficient load transfer to the stiff underlying stratum. Several spacing configurations were analyzed to obtain an optimal design. An axissymmetry analysis is performed using a construction sequence as follows:

Step 1	Initial Condition	
Step 2	Reclamation	: 120 days
Step 3	Consolidation	: 720 days (2 year)
Step 4	Road + Traffic	: 365 days (1 year)
Step 5	Consolidation to date	: 2,008 days (5.5yr)
Step 6	Hack pavement	: 60 days
Step 7	Rigid inclusion	: 30 days
Step 8	LTP + Pavement	: 60 days
Step 9	Future Consolidation	: minimum pore pressure

Based on axisymmetric FEM model, the final RI configuration adopted 0.42 m diameter columns with a 2.2 m spacing arranged in a rectangular grid. The simulation indicated that, after the installation of RI, the long-term settlement was approximately 714.5 mm (Step 9), while the settlement during construction stage was about 631.9 mm (from Step 1 to Step 7), yielding a post-construction settlement of 82.6 mm (Figure 6). In contrast, the condition without ground improvement predicted an additional settlement of 666.5 mm (Figure 5), demonstrating that the RI system reduced total settlement by 87%. The settlement progression from the initial reclamation stage to the present condition and the projected consolidation phase is illustrated in Figure 7.

Subsequently, the stress acting on the RI columns reached 2,263 kN/m², which represents a critical parameter in determining the required material strength. This ensures that the RI columns can safely withstand the vertical loads imposed by the embankment and traffic. Based on this design, concrete with a compressive strength of 15,000 kPa (15 MPa) was adopted for the RI columns, providing a substantial safety margin well above the calculated stress level.

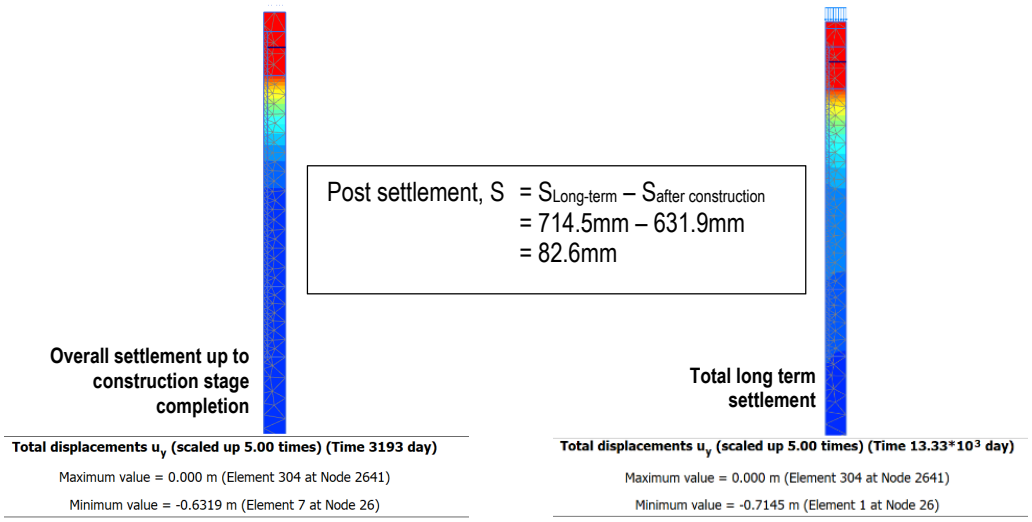

Figure 6. Settlement (with rigid Inclusion).

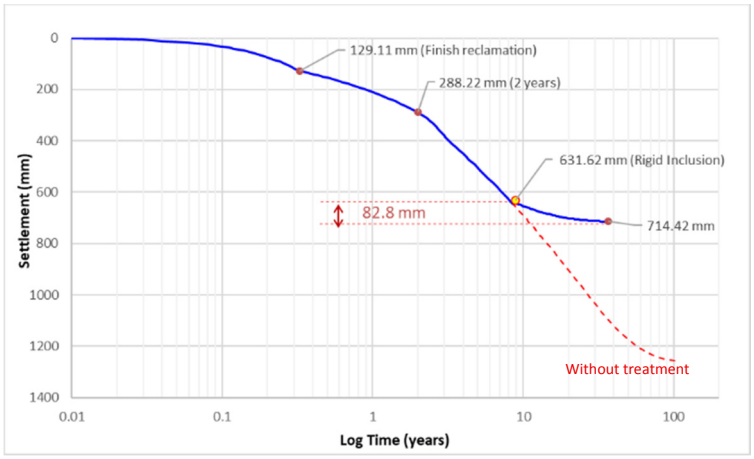

Figure 7. Settlement Curve in Logarithmic Time.

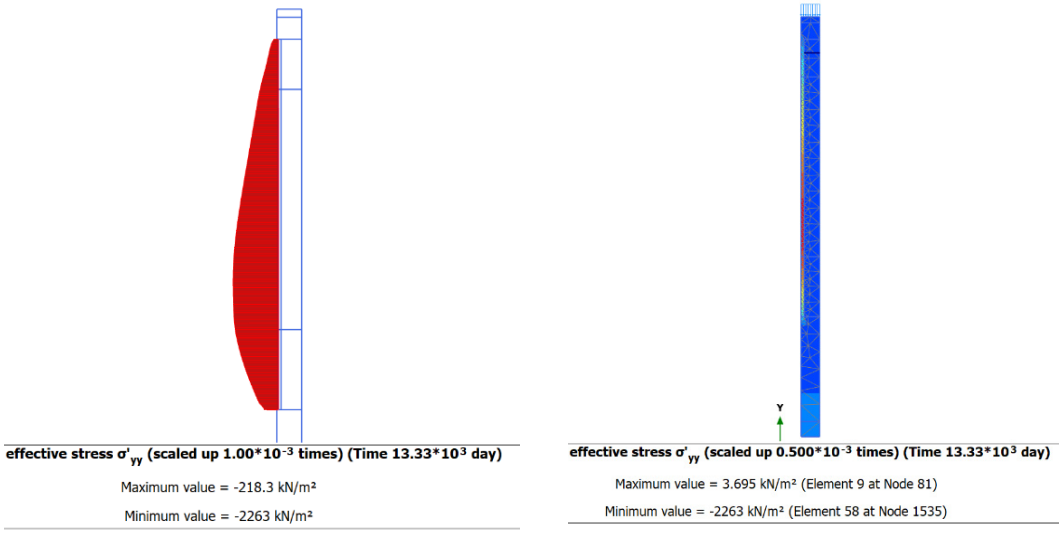

Figure 8. Stresses on rigid Inclusion columns.

An important aspect of the design is the Load Transfer Platform (LTP), which distributes embankment loads between the RI columns and the surrounding soft soil. The LTP also develops the arching effect, allowing lateral load redistribution through the granular fill and reducing direct stress on the clay layer. Based on numerical analysis and the adopted RI configuration, the minimum required LTP thickness was estimated at about 1.2 m, considered adequate for effective load transfer. This value may be refined depending on granular material properties, surface traffic loads, and FEM results.

5.2 Plane Strain Modelling

In addition to the axisymmetric analysis, a plane strain model was also employed using Plaxis to perform validation of the predicted settlements and to assess the overall stability of the ground improvement system. The plane strain model allows a better representation of continuous embankment loading and pavement behavior, as well as improved visualization of stress and lateral deformation patterns across the improved area.

The results from the plane strain analysis indicated that in the absence of ground improvement, the maximum total settlement could reach up to 1,436 mm (Figure 9 left). This value is slightly higher than that obtained from the axisymmetric analysis, likely due to additional lateral deformation occurring near the slope area. Nevertheless, the application of rigid inclusions was able to reduce the total ground settlement to only 88.94 mm (Figure 9 right). This reduction further confirms the effectiveness of the RI system in controlling vertical deformation and enhancing the stability of the embankment, reducing the risk of excessive settlement or potential shear failure.

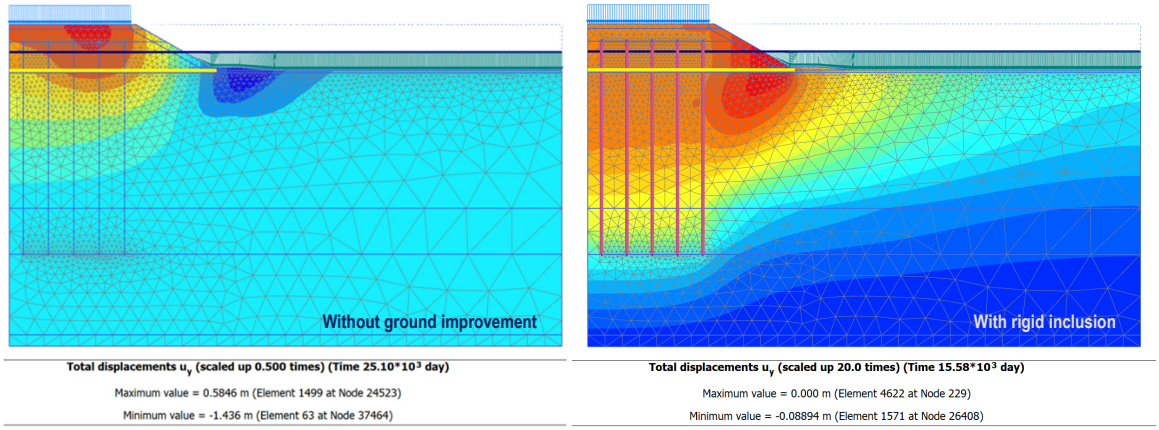

Figure 9. Settlement without and with ground improvement

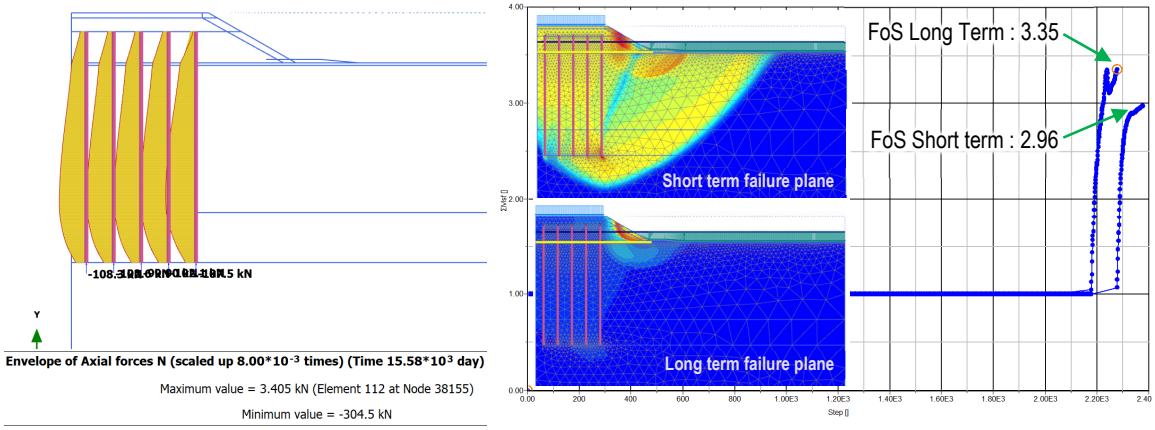

Figure 10. Axial force on RI Column and overal Factor of safety.

A structural check was conducted to verify that the rigid inclusion columns could also safely resist the vertical loads transferred from the embankment and traffic. Based on the plane-strain analysis, the maximum axial force acting on the columns was 304.5 kN/m (Figure 10). With a column spacing of 2.2 m, this corresponds to a total vertical load of 669.9 kN per column. For a column diameter of 0.42 m (sectional area ≈ 0.1385 m²), the resulting vertical stress is 4,835 kPa. This stress level is well below the maximum allowable limit of 7 MPa specified by the ASIRI guidelines and remains safely within the concrete compressive strength of 15 MPa adopted for construction. These results confirm that the RI columns are structurally adequate and well within safe limits under the expected vertical loading conditions.

As part of the stability assessment, the factor of safety (FoS) of the embankment and ground improvement system was analyzed using this plane-strain model in PLAXIS. Two critical conditions were evaluated: the short-term stage, representing the period immediately after construction and before full consolidation, and the long-term stage, after excess pore pressure had dissipated. The results showed FoS values of 2.96 and 3.35 for the short-term and long-term conditions, respectively, indicating excellent stability improvement as consolidation progressed. Both values exceed the typical design requirement of FoS ≥ 1.5 for embankments, confirming that the implemented rigid inclusion system provides a safe and effective solution. Corresponding FoS diagrams are presented in Figure 10 to illustrate these results.

5.3 Reinforcement Check

Following the structural assessment, the RI columns were further evaluated in accordance with ASIRI (2012) and Eurocode BS EN 1992-1-1 (2004) to determine the necessity of reinforcement. The procedure involved summarizing the axial load and bending moment obtained from the plane-strain analysis. The eccentricity was then calculated by dividing the moment by the axial load, allowing the determination of the load offset from the column centerline. Using this eccentricity, the effective compression area of the column was derived as illustrated in Figure 11, and the allowable compressive capacity was computed for the portion of the section resisting the load (indicated in green at Figure 11). when the calculated compressive capacity exceeded the applied axial load, reinforcement was deemed unnecessary; otherwise, rebar design would be required to resist the induced moment.

Based on the structural check, reinforcement was found to be not required, as the column capacity exceeded the applied load. However, due to contractual requirements, reinforcement was still required by the owner. To optimize the design, the rebar length was reduced from 7 m to 6 m compared with the original tender specification. For construction consistency and practicality, the same number of longitudinal bars and stirrups links was retained, with only the rebar length adjusted as part of the optimization.

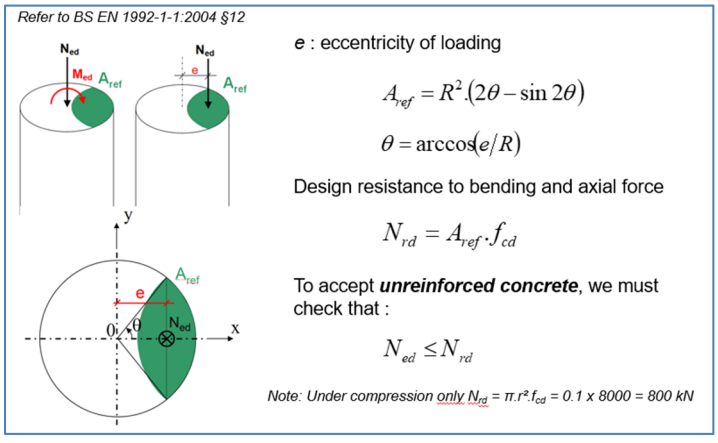

Figure 11. Rebar requirement checking procedure.

6 QUALITY CONTROL AND MONITORING

6.1 Concrete material Test

As part of the quality control process for ground improvement using rigid inclusions, material testing is carried out on the grout used to form the columns. A standard procedure is the compressive strength test. For every 4,000–5,000 m³ of cement grout placed, six samples are taken for laboratory testing: three are tested at 7 days (f_7), and three are tested at 28 days (f_{28}). The required grout strength for RI is 15 MPa. The primary objective of this testing is to ensure that the grout achieves sufficient compressive strength so that the RI columns can safely transfer and support the loads from the embankment and traffic above. In addition, the test results provide verification that the material quality complies with design specifications, serving as a critical element in guaranteeing the long-term performance of the ground improvement system.

6.2 Working Load Test

Another important quality control step in rigid inclusion construction is the working load test. This test measures how much an RI column settles when gradually loaded, confirming that the ground improvement system works as designed. The number of tested column shall be based on ASIRI (2012) guideline. During the test, the load is applied step by step, starting from 5% and increasing up to 120–150% of the design load. Settlement is measured at each stage to see how the column deforms under design load as in Figure 12. The results show how the RI column behaves under real working conditions and confirm whether the settlement control meets the design expectations. This test also helps verify that field performance is consistent with the predicted numerical analysis.

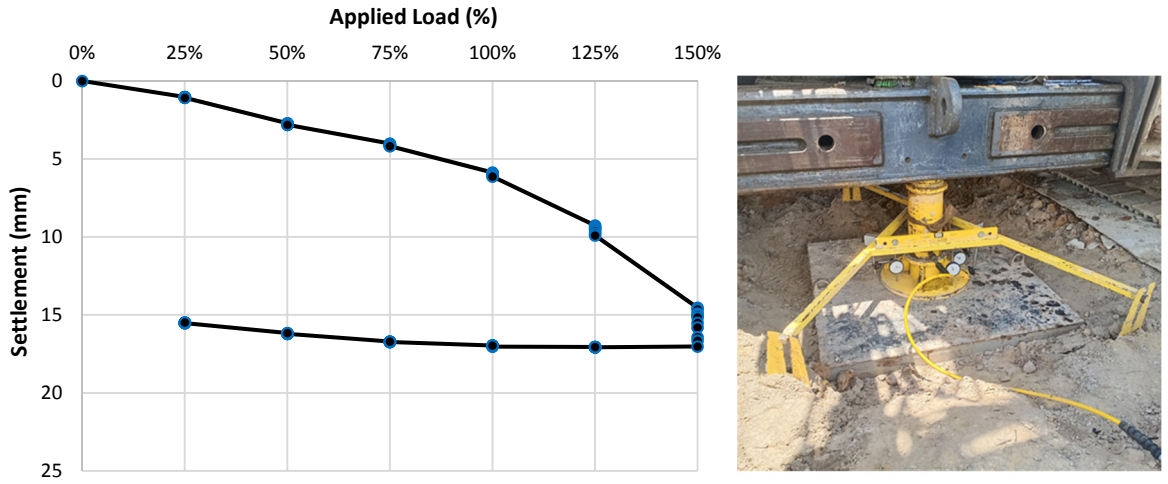

Figure 12. Working Load Test result (Typical).

6.3 Instruments and monitoring

For quality control and long-term monitoring of ground improvement using rigid inclusions, settlement instruments are proposed, consisting of settlement plates and surface settlement markers installed during. Settlement plates are positioned either directly above RI columns head to measure deformation at the inclusion head. They are embedded and connected to the surface through access pipes, enabling continuous measurement of vertical ground movement. Their primary function is to monitor post-installation settlement and evaluate the effectiveness of the RI system in reducing ground deformation.

In addition, settlement markers are installed on the pavement surface to measure the total settlement of the roadway, which must be maintained below 100 mm throughout the service life (Figure 13). The difference between readings from the settlement markers and settlement plates also provides an indication of deformation within the Load Transfer Platform (LTP). Together, these instruments

supply valuable data for verifying long-term ground performance and confirming that settlements remain within design limits.

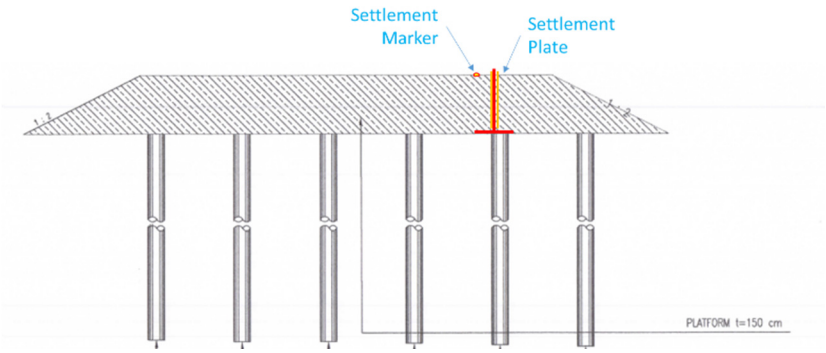

Figure 13. Long-term monitoring of RI.

The instrumentation will continue to be monitored throughout the service life of the access road, with data collection and interpretation carried out by the project owner or an appointed representative. The project was completed in December 2024, and as of this writing, monitoring is still being performed regularly. The results from the instrumentation and any related back-analysis based on field data are not included in the scope of this paper and will be addressed in future studies.

7 DISCUSSION AND CONCLUSION

This study demonstrated the effectiveness of rigid inclusions as a ground improvement technique for mitigating long-term settlement in reclaimed soft clay deposits at Ahmad Yani Airport, Semarang, Indonesia. Through soil investigations, laboratory testing, numerical modeling, and field considerations, several key conclusions and insights can be drawn:

a) Effectiveness in Reducing Settlement

Numerical analyses confirmed that without ground improvement, settlements could reach 1.2 – 1.4 meters, severely compromising the serviceability of the access road. With RI, long-term post-construction settlement was reduced to 82.6–88.9 mm, achieving an 87–94% reduction. This outcome aligns with international experiences on RI in soft soils and validates its applicability in tropical, high-plasticity marine clay environments.

b) Enhanced Stability and Safety

Both axisymmetric and plane strain models showed that RI not only reduced vertical deformation but also significantly improved global stability. Factors of Safety exceeded 2.9 in the short term and 3.3 in the long term, far above the typical design threshold of 1.5 for embankments. This margin of safety provides high confidence in the method's reliability under both immediate and consolidated conditions.

c) Operational and Environmental Compatibility

In active airport environments, construction methods must avoid excessive vibration, noise, or aesthetic disruption. Conventional options such as PVD with preloading, DSM, stone columns, and RC piles were excluded due to these limitations. RI was proven to be the only viable method, combining fast installation, minimal disturbance, and the ability to proceed in parallel with other airport operations. This underscores RI's unique suitability in sensitive operational zones such as airports, ports, and urban transport hubs.

d) Structural Adequacy and Design Optimization

Stress analysis indicated that the maximum load on the RI columns remained well below international design limits (ASIRI guidelines). Structural checks confirmed that reinforcement was not required, enabling an optimized design with reduced rebar lengths while retaining practical construction measures. This highlights the potential of RI not only as a safe solution but also as an economically optimized method, reducing unnecessary material use without compromising safety.

The Ahmad Yani case reinforces the role of RI as a sustainable and transferable solution for soft soil environments in Indonesia and Southeast Asia. It addresses gaps where traditional ground improvement methods are impractical due to operational or environmental constraints. The findings also contribute to the body of knowledge by providing empirical and numerical evidence on RI behavior in highly compressible tropical clays, which remain under-documented compared to European or North American case histories.

REFERENCES

ASIRI, 2012, *Recommendation for the Design, Construction and Control of Rigid Inclusion Ground Improvements*. Paris, IREX

Aulia Ghifari, 2015, *Evaluasi Penggunaan Controlled Modulus Columns di Bandara Soekarno-Hatta*, Yogyakarta: Tugas Akhir. Department of Civil and Environmental Engineering. Universitas Gadjah Mada.

Combarieu, O., 1988 , *Amélioration des sols par inclusions rigides verticales*. Application à l'édification des remblais sur sols médiocres. French Geotechnical Review (Revue Française de Géotechnique), No. 44, pp. 57–79.

Fitriyana L., Pratikso, Karlinasari R., Susanto T.A., Saputra Z.A.E., 2025, *Evaluation of the Use of Rigid Inclusion for Liquefaction Mitigation in Mandalika Circuit with Numerical Method*, The 1st International Conference Urban Planning 2025 (U-Plan 2025)

Rizal M., Yee K., 2018, *Bridge Approach Embankments on Rigid Inclusions*, International Conference on Geotechnics, 24-26 July, 2018 Yogyakarta, Indonesia

Setiaji R.R., Utomo P., KM Abuhuroyroh, 2018, *A New Breakthrough – Application of Control Modulus Column for Settlement and Stability Control under Soft Soil and High Embankment Load at Pemalang-Batang Toll Road*, Proceeding 20th Southeast Asian Geotechnical Conference - 3rd AGSSEA Conference 2018, and 22th annual Indonesian National Conference on Geotechnical Engineering – Jakarta Indonesia, November 2018.

Setiaji R.R and Ayu W.K. Dewi, 2025, *Determining Soft Soil Thickness for Ground Improvement Using Microtremor Array Method: Case Studies from Ahmad Yani and Juwata Airports*, The 9th International Conference on Eco Engineering Development 2025

Simon Bruno, 2012, *General report S5 Rigid Inclusions and Stone Columns*, ISSMGE - TC 211 International Symposium on Ground Improvement IS-GI Brussels May 31st & June 1st 2012

SNI Geoteknik 8460: 2017, *Persyaratan Perancangan Geoteknik*, Badan Standarisasi Nasional (Jakarta: BSN).

Syofyan M.F., Triyatmojo A., Karlinasari R., *Soil Improvement due to Liquefaction in Earthquake Prone Locations for the Mandalika Circuit*, ResearchGate, DOI:10.13140/RG.2.2.34937.85601, September 2023

Yee Kenny, Setiawan R.A., Bechet O., 2012, *Controlled Modulus Columns (CMC): A New Trend in Ground Improvement and Potential Applications to Indonesian Soils*, ISSMGE - TC 211 International Symposium on Ground Improvement IS-GI Brussels 31 May & 1 June 2012

Settlement Fitting of Soil Improvement on Toll Road Project in Northern Jakarta

Muhammad Amhar W Yanreginata[1,*], Budiwan A Tirta[2]
[1]Geotechnical Engineer, PT Witteveen Bos Indonesia
[2]Senior Geotechnical Engineer, PT Witteveen Bos Indonesia
*Correspondence: amhar.yanreginata@witteveenbos.com

ABSTRACT A big differential settlement at transition area between embankment and piled-structure is a common problem observed in most current toll road projects built on very soft clays. The problem relates to ride comfort when crossings bridges and culverts or even safety due to damage of the pavements at the transition. Moreover, it causes a high maintenance period, traffic disruption and overrun on the operational cost. The aim of this paper is to suggest an approach on how to evaluate performance of a soil improvement method, supported by monitoring programs and together with a back analysis that can help to control and accurately predict the on-going settlement. Therefore, it can be used as a guidance for design decisions. The paper will cover evaluation performance of vacuum consolidation (VC) of soil embankment followed by an additional surcharge pre-loading. A simple one-dimensional settlement model equipped with the most advance constitutive settlement formula for soft clay is used to carry out the best fitting analysis and to predict the long term settlements with the available field monitoring data from piezometers and settlement plates. The back analysis procedure adjusts not only the consolidation parameters but also the applied pressures and pore water pressure, all together to match the monitored field data. Data quality issues including loss in vacuum pressures and errors in manual surveys are acknowledged. Result shows that during the vacuum consolidation (VC), pore pressures drop by about seventy two (72) kilopascals at the depths of five and ten meters with the corresponding pressure of 89% efficiency. Settlement readings trace the continuous movement not only during the vacuum consolidation (VC) period, but also when bouncing back when pump was off and the additional surcharge phase. The result of the fitting follows the trends of the observation data, though exact values vary. Across the phases, the fitted consolidation parameters stay largely within the range of the geotechnical parameters, with some data not fitting perfectly due to the errors. It can be observed that without the additional surcharge, the long term settlement could exceed ten centimeters in ten years which was not satisfy the requirement. In general, with a temporary PVD surcharge, the final settlement can be reduced to roughly forty percent (40%), staying below ten centimeters in ten years operational of the toll road. In conclusion, a careful monitoring program and evaluation of a complex soil improvement (for such a combined use of VC and surcharge pre loading) that was implemented in different sequence of phases, offer a practical way to manage residual settlement during the operational time. Future work should cover the details of adjusted consolidation parameters for the back-fitting analysis with improved data collection until actual secondary settlement achieved.
KEYWORDS Consolidation Settlements; Soft soil; Soil Improvement; Monitoring; Back Analysis

1 BACKGROUND

Embankment-type design for toll roads usually beneficial in matter of costs and methods. However, crossing such as rivers, existing traffic lanes, and drainage structures require permanent solutions with deep foundations, culverts, and traffic boxes. The transition between the embankment and these structures are usually bringing out some problems, one of them is the differential settlement. Differential settlement occurs when there is excessive residual settlement on the embankment while the structure barely settle. This problem can reduce ride comfort, traffic accident, and result in substantial long-term maintenance (Bahumdain, 2022).

An approach slab can help to smoothen the transition between them. Zhou (2017) studied that a transition without approach slab can cause bumpy road as the response of the pavement under impact

load of the vehicle is larger than the static load. Nevertheless, soil beneath the approach slab has to be settled enough in short and long period to ensure the slope of the approach slab remain on the threshold. The most common factors that contribute to the existence of the vertical deformation at the approach slab is the settlement of the natural soils (Seyed et al, 2016; Saride et al, 2009; Laguros et al, 1990).

The natural soils play much role in the settlement of the embankment. A very soft clay material can have a significant long-term settlement, hence a soil improvement needed to treat the natural soil before taking load from the embankment. Several methods applicated for the soil improvement are the PVD vacuum consolidation and the PVD surcharge pre-loading. Those two methods are widely used for the soil improvement on very soft clay materials, studies also widely conducted (Bergado et al, 1998; Khrishnapriya 2015; Nguyen, 2021; Song Ding Bao, 2024;).

2 INTRODUCTION

Toll roads built in the northern part of Jakarta has a significant potential of differential settlement between the embankment and the settled structure. In this particular project, the condition of the natural soil is a very soft clay material (NSPT 0 - 2) with average thickness of 8 meters to 10 meters.

Through that basis, soil improvement needed to reinforce the natural soils against the excessive settlement. Moreover, the implementation of settlement monitoring system would be necessary to obtain successful result of the project.

The main objective of this paper is to show the approaches taken into account prior, during and after the monitoring campaign. This paper focuses on the monitoring and back-analysis framework but gives limited detail on the adjusted parameters used in the back-fitting process. While consolidation parameters such as Compression Ratio (CR); Recompression Ratio (RR); Coefficient of Consolidation (Cv); and Secondary Compression ($C\alpha$), were tuned to match the observed data. The paper does not specify initial values, parameter ranges, or the parameter-fitting method.

it is important to set an approach to accurately estimate residual settlement and set criteria to prevent excessive residual settlement to be avoided during operational of the toll road. The criteria of maximum residual settlement that considered for the soil embankment in toll road is 10 cm including creep within the first 10 years operational period after the handover time. This is more lenient than the requirement for polder area which is 30 cm in 50 years. Even more, this is slightly lenient than the 15 cm in 10,000 days as used in toll roads in the Netherlands (Bina Marga, 2013; CROW, 2004)

The schematic illustration of settlement phases can be seen in Figure 1. The primary and secondary consolidation that occur in the operational time need to be acknowledged before the handover time period.

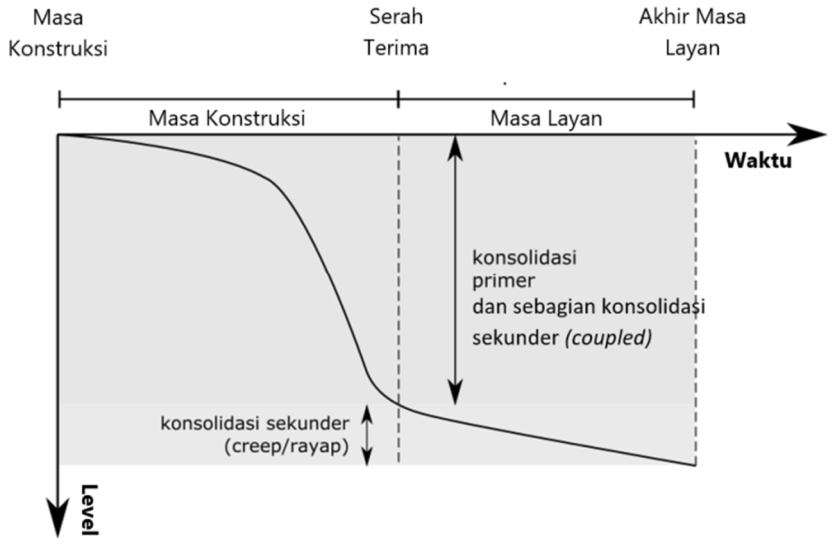

Figure 1. Schematic illustration of settlement phases.

The first work of this project began with the initial back fill for the construction platform back in 2013 to 2015. After the first platform was set, a second sand platform with thickness of 0.25 m for the Vacuum Consolidation (VC) work was built at around 2018-2019. The VC program ran simultaneously with monitoring campaign in the late 2018-2019.

Following VC completion, fill works to designated elevation began to initiate. In this phase, back-analysis to review the VC works was conducted. The result of the VC works determined the necessity of the additional surcharge pre-loading. The back-analysis of the VC showed that the residual settlement still exceed the settlement requirement. Hence, additional surcharge pre-loading was implemented with 2.5 - 3.5 meter height of embankment.

The soil improvement works (VC and Surcharge preloading) and the back-analysis were carried out across 13 zones along 7 km stretch. However, this paper presents result from a single representative zone illustrating the VC implementation and the additional surcharge preloading.

Table 1 shows the overview milestone of the phases in this project.

Table 1. Milestone of the Phases in the Project

No	Phase	Year	Remarks
1	Initial Back fill for platform	2013 - 2015	Between 2 to 3 m fill for each zone.
2	Platform for VC	2018 - 2019	0.25 m sand fill
3	Vacuum Consolidation (VC)	2019 - 2020	Between 200 to 250 days
4	Fill to design level	2023	Ranging from 2 to 4 m
5	Fill to pre-loading platform	2023	Ranging from 2.5 m to 3.5 m
6	Surcharge pre-loading	2023 - 2024	Between 30 to 120 days
7	Surcharge removal	2024	-
8	Pavement	2024 - 2025	additional 12.5 kPa/m

3 METHOD

3.1 Model

Models were generated using the D-SETTLEMENT software to predict a long-term soil settlement analysis with different increment loading. 1D model for each zone is made to represent the soil profile and the material characteristics. Example of the model which developed for the analysis is shown in Figure 2.

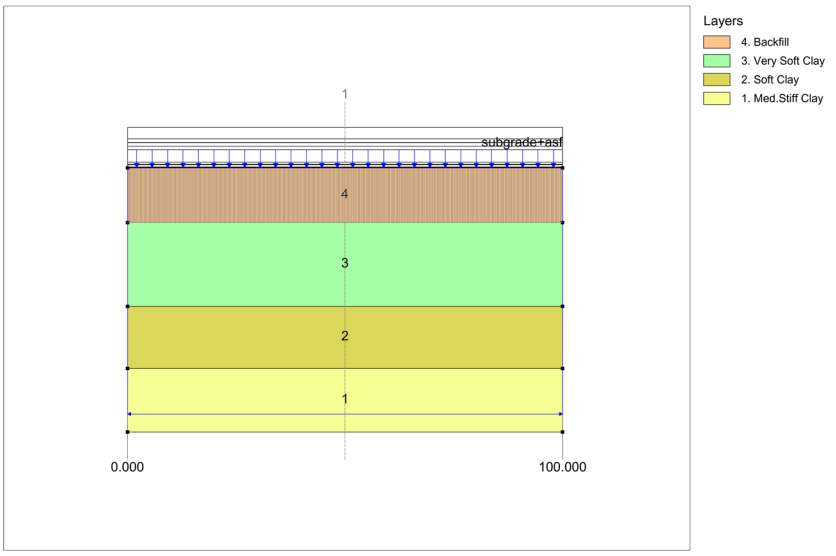

Figure 2. Example of settlement model

The main approach in choosing settlement model considered the following aspects:

1. To include also the creep in determining settlement (total and residual).
2. To consider advance settlement model, is therefore, should be used to consider coupled between the primary and secondary (creep) settlement.

The analysis was using the NEN-Bjerrum strain model which assumes that the creep rate will reduce with the increasing of over-consolidation and that over-consolidation will grow by unloading and by ageing. Different from the classic models, for instance Terzaghi, which separate the primary and secondary contribution to the settlement, NEN-Bjerrum model assumes that the total strain (ε^C) consists of direct elastic contribution (primary) [ε_s^C] and transient viscous (secondary) [ε_d^C] contribution, Equation (1) shows the strain decomposition of NEN-Bjerrum model. The principle of this model is the same with the a/b/c/ isotache model, which stated that all inelastic compression results from visco-plastic creep. However, the NEN-Bjerrum model supports the common linear strain parameters such as CR, RR, C_v, and C_α (Bjerrum, 1972 and Deltares, 2021).

$$\varepsilon^C = \varepsilon_s^C + \varepsilon_d^C \tag{1}$$

Other consideration for the settlement models such as ground water level is controlled constant within certain level for all zones. Moreover, the Pre-febricated Vertical Drain (PVD) were installed within all zones. The PVD extends until N_{SPT} >15 for each zone.

3.2 Monitoring Data Acquisition

The monitoring program was set on two different phase which is the PVD Vacuum Consolidation (VC) phase and Surcharge Pre-loading phase. In the PVD VC phase, piezometer coupled with settlement plate were applied to monitor the pore water pressure and settlement at the ground surface. For the Surcharge Preloading phase, only settlement plate was implemented.

3.2.1 PVD Vacuum Consolidation (VC)

The PVD Vacuum Consolidation method for soil improvement was conducted in the first stage of the soil improvement campaign. The PVD VC was running simultaneously with the monitoring of the settlement and piezometer. After the platform was set and the drain strip injected, geomembrane installed above the ground surface and additional water load (1.50 meter water height) was implemented.

Figure 3. Installation of vertical and horizontal drain

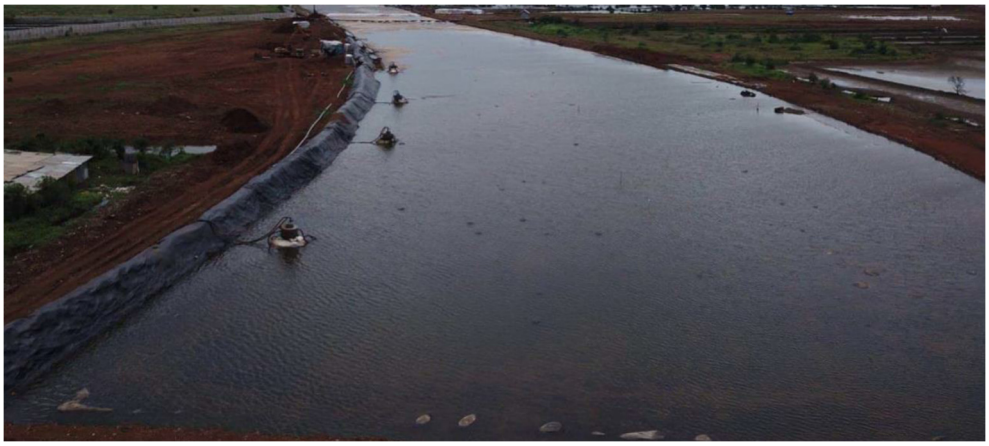

Figure 4. Water load for 1.5 meter height

During the vacuum consolidation phase, combination of piezometer and settlement plate were used to give the pore pressure and the difference of settlement data during the works.

Figure 5. Installation of piezometer and settlement plate for VC phase

Several issues during the implementation and the monitoring of the PVD-Vacuum were experienced such as membrane break which resulting in a non-constant vacuum pressure, pumping stopped due to operational causes and problem with natural soils such as sand layer.

3.2.2 PVD Surcharge Preloading Consolidation

Considering the result of the VC which not satisfy the residual settlement's requirement, an additional surcharge pre-loading was implemented. The surcharge pre-loading was set to be 2.5 - 3.5 m high (considering the stability of the slope) wtth a duration of 30-120 days depending on each zone. After the removal of the pre-loading material, pavement works also monitored, the estimation of the load induced by the pavement layers are 12.5 kPa/m.

During the surcharge pre-loading phase, a simple method by monitoring the settlement plate was carried out. Figure 4 and Figure 5 shows the temporary embankment and the Settlement Plate used during the monitoring progress respectively.

Figure 6. Temporary surcharge embankment

Figure 7. Schematic Illustration of Settlement Plate and Survey Reading

In reality, not all data can be captured perfectly. Several issues during the implementation of PVD-Surcharge such as the limitation of pre-loading's height due to the stability of the interface to the structures and due to human error during the monitoring survey.

3.3 Settlement Fitting (Back-Analysis)

Fitting of the settlement parameters was conducted to obtain the best fit with the monitoring data (Piezometer and settlement plate). Several main parameters that were controlled are the CC, CR, C_v and C_α. The unit weight of the natural soil remains constant as it shows a consistent result in the laboratory test.

The fitting was conducted continuously from the Vacuum Consolidation works until the Surcharge pre-loading works. Parametric study between the parameters were conducted to obtain the best fitting result, although the errors from the data might still occur.

The monitoring data was not always be as good as the settlement prediction analysis. However, in several conditions we might calibrate the monitoring data into the settlement curve. In case in the middle of the monitoring there was an error or a non-collectible data, we still continue the monitoring and re-calibrate the site survey.

4 RESULT

4.1 Back Analysis of Vacuum Consolidation

4.1.1 Pore Water Pressure

An extensive evaluation of pore water pressure during the vacuum consolidation works has been performed by monitoring the piezometer. The pore pressure sensor was placed at 5 m and 10 m depth. A pore pressure prediction using the settlement model also compared to verified the result of the piezometer. Moreover, the vacuum gauge and water load pressure also monitored to verify the consistency of pressure during the VC.

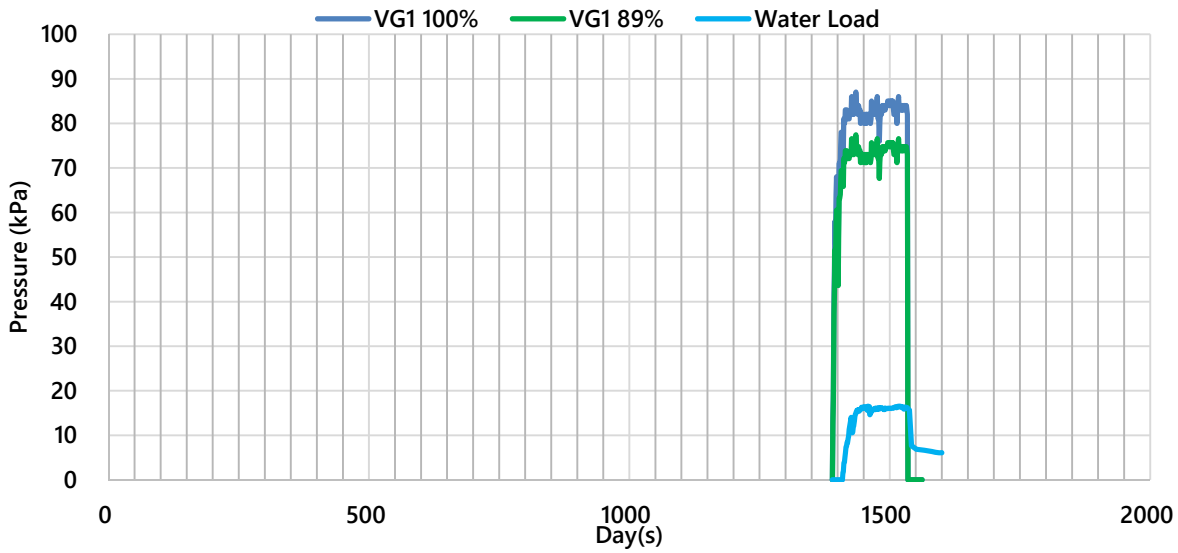

Figure 8. Vacuum Gauge and Water Load Pressures

The pressure of the vacuum gauge in reality only effective for 89% of the desired pressure (80 kPa). While the water pressure remains constant for the entire VC works at around 15 kPa (1.5 m water height). The graph in figure 8 and figure 9 shows the vacuum & water pressures and pore water pressure from the piezometer respectively. Which the initial day (day 0) is the day after backfill platform was set (around 2015) and VC started at approximately day 1400 (around 2019). The VC pressure was released after approximately 180 to 200 days at around day 1580-1600.

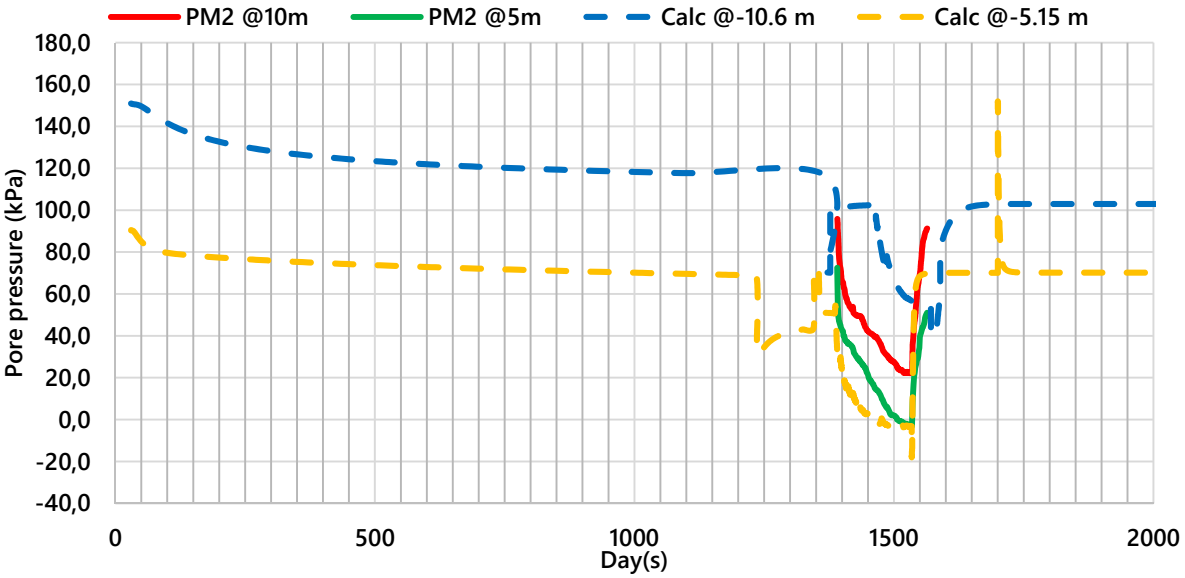

Figure 9. Pore Pressure from Piezometers and Calculation

The reading of Piezometer showed that the pore water pressure during the VC were reduced approximately to 72 kPa at depths of 5 m and 10 m. Then, the pore pressure bounced-back after the vacuum pressure was released (day 1580-1600). Although the predicted model of pore pressure did not precisely match the measured values by numbers, but it indicated the consistency of trend between the model (dashed line) and the actual monitored data (solid line).

4.1.2 Settlement in VC phase

Apart from the piezometer, the settlement was monitored during the entire VC program using Settlement Plate and it was compared with the prediction from the settlement model. The fitting result between the actual and predicted settlement can be seen in Figure 10.

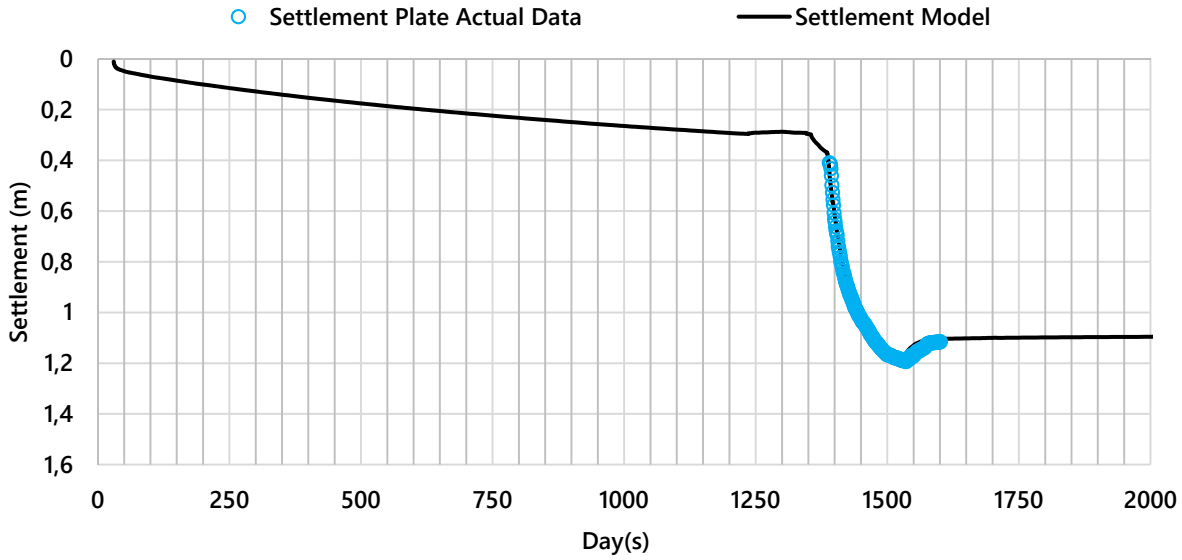

Figure 10. Result of Settlement Fitting in VC Phase

The fitting between predicted and actual settlement data shows a good fit between each other which shown by the actual monitoring data (blue dots) following the trend of the settlement model line (black line). The initial settlement plate data (around day 1400) where VC was initially started were calibrated with the initial settlement point from the model. During fitting, several soil parameters were adjusted, with consolidation parameters identified as the primary controlling factors. Graph in the Figure 10 shows the initial day (day 0) is the day after backfill platform was set (around 2015) and VC started at approximately day 1400 (around 2019). The VC works done after approximately 180 to 200 days in around day 1580.

4.2 Determination of Additional Preloading Surcharge

Following the completion of back-analysis for VC result, the residual settlement after handover time is still potentially exceed 10 cm in 10 years. Due to that matter, an additional surcharge pre-loading using temporary embankment was proposed. Initial analysis showed that the pre-loading needs a temporary embankment with 2.5 meter - 3.5 meter height and duration between 2-6 months depending on the subsurface conditions.

In Figure 11, shows the analysis, which comparing the embankment with and without the additional surcharge pre-loading (temporary embankment). On the same figure, day 2750 to day 3140 indicates that the embankment to reach the designated level at 5.00 mPP*. After that, surcharge preload with 3.0 meter height was introduced for 60 days (day 3140-3200). Handover time was set 90 days after the surcharge time at day 3290.

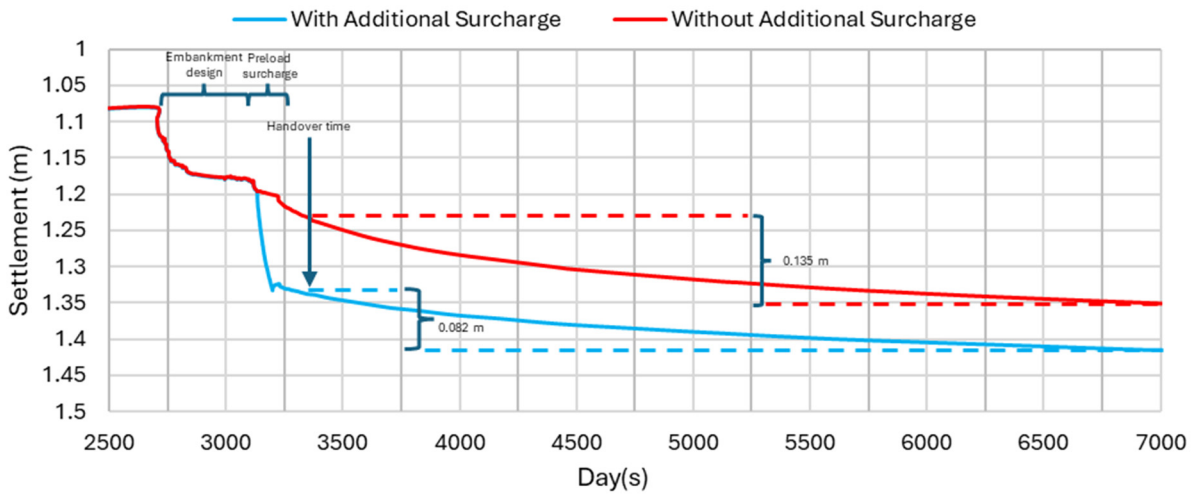

Figure 11. Comparison of Embankment With and Without Additional Surcharge Pre-Loading

Without additional temporary surcharge, long -term settlement was expected to exceed 10 cm in 10 years post-handover time. The surcharge preload could reduce the long-term settlement to about 40%, yielding a maximum long term settlement of less than 10 cm in 10 years.

Table 2. Results of Settlement With and Without Additional Surcharge Pre-Loading

No	Conditions	Temporary Surcharge		Settlement in 10 Years After Handover Time (m)
		Height (m)	Duration (days)	
1	Without Additional Surcharge	-	-	0.135
2	With Additional Surcharge	2.50	65	0.082

4.3 Back Analysis of Surcharge Pre Loading

The back-analysis continued to the surcharge pre-loading phase by fitting the settlement during the surcharge loading. Figure 10 shows the ground level by the working days, the ground level data was obtained by field survey and was input to the settlement model. Surcharge load was introduced on day 3140 and released after day 3200.

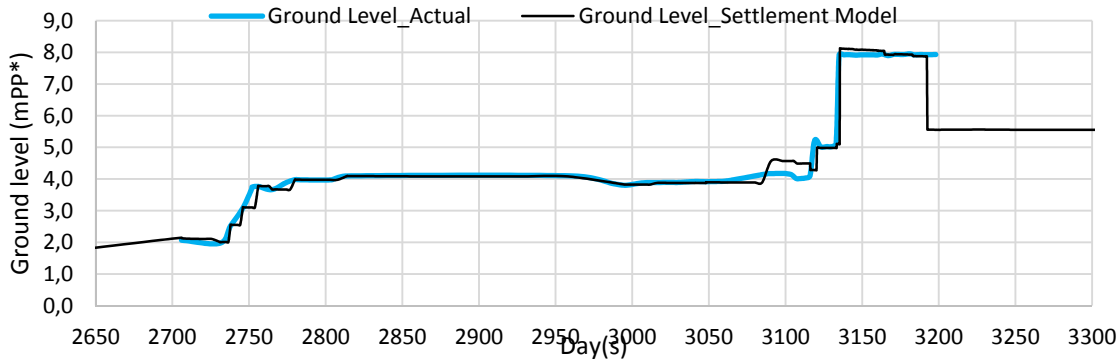

Figure 10. Actual Ground Level vs Ground Level in Settlement Model

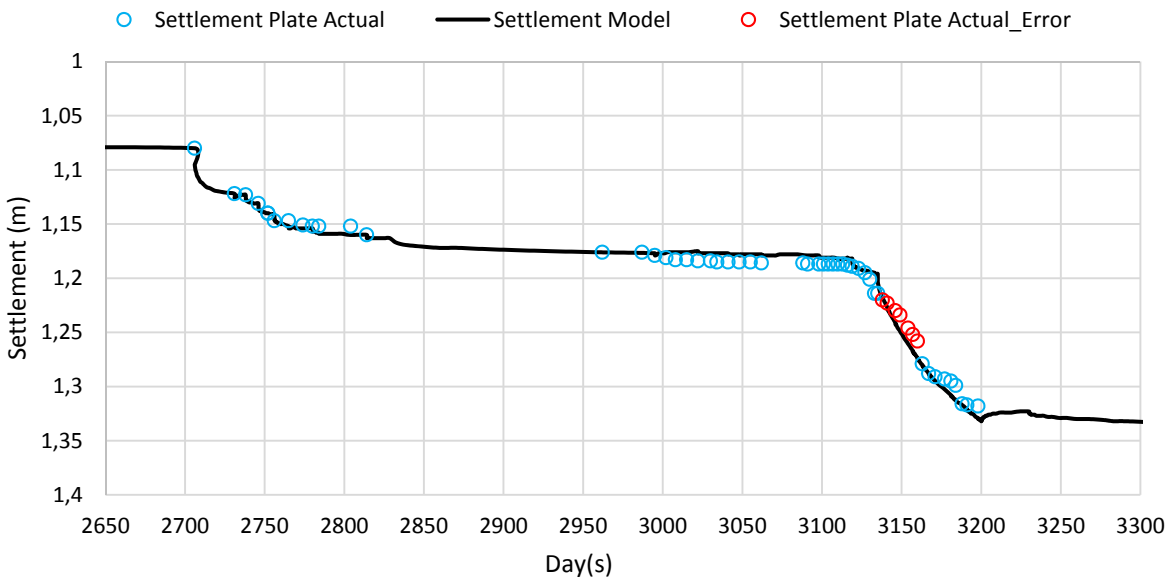

Figure 11. Result of Settlement Fitting in Additional PVD Surcharge Pre-Loading Phase

Settlement fitting during the surcharge pre-loading phase showed good performance shown by the actual monitored data (blue dots) aligned with the settlement model (black line). Although some data errors occurred (red dots), the fit captured the overall trend of settlement from the pre-loading stage. Moreover, the fitting results from two different phases (VC and pre-loading surcharge) was using a relatively constant settlement parameters which indicates that the behavior of the soil has been captured successfully.

In several zones, achieving a perfect fit between actual observations and model predictions was challenging. For VC, discrepancies can arise from factors such as drain efficiency, loss of vacuum pressure and broken geomembranes. For surcharge pre-loading, monitoring was relied on manual surveys which can introduce measurement errors.

Nevertheless, a robust assessment of fit focuses on the trend of the settlement curve and the final settlement value, which were satisfactorily reproduced in most zones.

5 CONCLUSION

The study was conducted on a toll road project with soil improvement using PVD Vacuum Consolidation (VC) and PVD surcharge pre-loading. It spans along the main road with 13 zones along a 7 km strecth, though only one zone is presented detail in this paper. it showed that the Vacuum Consolidation (VC) followed by surcharge pre-loading which supported by monitoring and back-analysis fitting can effectively manage the long-term settlement of embankment in soft clays. Piezometer readings showed the actual pore pressures were aligned with the best predicted calculations. Settlement plates were used to obtain settlement value during the VC, post pumping off and surcharge pre-loading. Back-analysis were conducted with adjusted consolidation parameters (CR, RR, C_v, C_α) to match the monitored data, achieving a generally good fit even though some data did not fit perfectly in numbers. The VC combined with surcharge pre-loading reduced long term settlement risk in soft clay by 40% comparing to only VC applied. The long term settlement is predicted way below the criteria of 10 cm in 10 years. Future work should cover the details of adjusted consolidation parameters for the back-fitting analysis with improved data collection until secondary settlement achieved. It is also planned that long term settlement measurement will be continued to validate the prediction, although the model's result has already shown consistency in different phases of the construction.

DISCLAIMER

The authors declare that there are no conflict of interest that could have appeared to influence the work reported in this paper.

REFERENCES

Bahumdain, A., Tabatabai, H. and Titi, H. (2022) 'Analysis of Soil Settlement Behind Bridge Abutment', Transportation Geotechnics.

Bergado, D.T., Chai, J.C., Miura, N. and Balasubramaniam, A.S. (1998) 'PVD improvement of soft Bangkok clay with combined vacuum and reduced sand embankment preloading', Geotechnical Engineering Journal, 29(1), 95–121.

Bjerrum, L. (1967) 'Engineering geology of Norwegian normally consolidated marine clays as related to the settlements of buildings', Géotechnique, 17, 83–118.

CROW (2004) Betrouwbaarheid van zettingsprognoses. November 2004. CROW Report 204.

Direktorat Jenderal Bina Marga (2013) Manual Desain Perkerasan Jalan Nomor 02/M/BM/2013.

D-Settlement (2021) Embankment design and soil settlement prediction: User Manual. Deltares.

Krishnapriya, P.B., Sandeep, M.N. and Antony Jency (2015) 'Efficiency of Vacuum Preloading on Consolidation Behavior of Cochin Marine Clay', in International Conference on Emerging Trends in Engineering, Science, and Technology, 2015.

Laguros, J.G., Zaman, M.M. and Mahmood, I.U. (1990) 'Evaluation of Causes of Excessive Settlements of Pavements Behind Bridge Abutments and their Remedies: Phase II', Rep. No. FHWA/OK 89(07), Oklahoma Department of Transportation.

Nguyen, T.N., Bergado, D.T., Kikumoto, M., Dang, P.H., Chaiyaput, S. and Nguyen, P. (2021) 'A simple solution for prefabricated vertical drain with surcharge preloading combined with vacuum consolidation', Geotextiles and Geomembranes, 49, 304–322.

Saride, S., Puppala, A. and Archeewa, E. (2009) 'Bridge Approach Settlements—an Issue due to Design or Construction Practices?', Indian Geotechnical Society, Geotide. (Note: verify exact publication venue/title if you have the official record, as this item contains some unclear elements.)

Song, D., Pan, Y., Chen, W., Yin, Z., Feng, Q. and Yin, J. (2024) 'Experimental and numerical modelling on vacuum consolidation behavior of staged-filled slurry with prefabricated horizontal drain and flocculant', Journal of Rock Mechanics and Geotechnical Engineering, 16, 5231–5248.

Yasrobi, S.Y., Ng, K.W., Edgar, T.V. and Menghini, M. (2016) 'Investigation of Approach Slab Settlement for Toll road Infrastructure', Transportation Geotechnics.

Zhou, J., Zheng, M., Wang, C., Jing, W., Meng, J. and Chen, J. (2017) 'Dynamic Response Analysis of Road–Bridge Transition Section without Slab', International Journal of Pavement Research and Technology, 10, 526–535.

HIMPUNAN AHLI TEKNIK TANAH INDONESIA - HATTI
Indonesian Society for Geotechnical Engineering - ISGE
PIT HATTI XXIX
10-12 November 2025

Performance Evaluation of Freestanding Soldier Pile System for a 9-m Excavation in Clayshale Formation at IKN Using the Hardening Soil Model

Muhammad Risyad Alditio[1,*], Muhammad Siddiq Rezawan[2]
[1]PT. Wijaya Karya (Persero) Tbk, DKI Jakarta, Indonesia; alditio01@gmail.com
[2]PT. Wijaya Karya (Persero) Tbk, DKI Jakarta, Indonesia; siddiq@wikamail.id
*Correspondence: alditio01@gmail.com

ABSTRACT A 9-meter deep excavation was required for the construction of the reservoir in the Interconnection Water Treatment Plant (IPA) Sepaku Project at the Nusantara Capital City (IKN). Subsurface investigations at the site indicate that the soil is dominated by clayshale, which is a problematic geomaterial that is prone to rapid degradation when exposed to atmospheric conditions. Therefore, a freestanding soldier pile system was selected as the excavation support. This study evaluates the performance of this system using the hardening soil (HS) constitutive model in Plaxis 2D. The primary soil parameters, including c', φ', E_{50}, and E_{ur}, were determined based on laboratory test data and analyzed in accordance with the recommendations of the hardening soil model literature. The results show that the maximum lateral wall deformation was less than 0.9% of the excavation depth. This value is still acceptable considering that the structure functions as a temporary excavation support system, and deformation monitoring was performed periodically during construction. In addition, the maximum bending moment developed in the soldier pile system reached 666.4 kNm, while the safety factor remained within the required design criteria. This study provides a performance evaluation of freestanding soldier pile systems in clayshale conditions using the Hardening Soil Model, and the findings may serve as a reference for similar deep excavation cases in IKN and other regions with claystone formations that are highly susceptible to rapid weathering.

KEYWORDS Soldier Pile; Hardening Soil Model; Deep Excavation; Clayshale.

1 INTRODUCTION

1.1 Introduction

The Nusantara Capital City (IKN) development in East Kalimantan has initiated the construction of multiple strategic infrastructures, including the Interconnection Water Treatment Plant (IPA) Sepaku. One of the critical components of this facility is a 9-meter deep excavation required for the reservoir construction. Previous studies indicate that clayshale in this region is a problematic geomaterial due to its susceptibility to rapid degradation once exposed to atmospheric conditions (Zarkasi et al., 2018). Recent geological investigations further confirm that the subsurface in IKN is dominated by stiff residual soils and weathered sedimentary formations, including claystone and clay shale units with high variability in strength and weathering degree (Herman et al., 2021; Badan Geologi, 2022). Such characteristics significantly increase geotechnical risks during deep excavations and therefore require special engineering consideration.

Numerical modelling is widely used to evaluate the behavior of deep excavations. The hardening soil (HS) constitutive model has been demonstrated to be more capable in representing non-linear stress–strain behavior of soils compared to the mohr–coulomb (MC) model, particularly in cases involving high-stress levels and unloading–reloading phases (Schanz & Vermeer, 1996). Previous studies have applied HS model for tunnelling and slope problems in shale formations (Bobet & Einstein, 2008), however, studies that specifically address the performance of freestanding soldier pile systems in tropical clayshale conditions, particularly within the context of IKN, remain limited.

Based on this gap, this study aims to evaluate the performance of a freestanding soldier pile system for a 9-meter deep excavation in clayshale formation at the IPA Sepaku site using the hardening soil

model in Plaxis 2D. This work contributes by providing numerical evidence and engineering interpretation of deformation and bending moment behavior of soldier piles in tropical clayshale formations, and the findings are expected to serve as a technical reference for similar deep excavations in IKN and other regions with rapidly weathered clayshale.

2 MATERIAL AND METHODOLOGY

2.1 Data Collection

Geotechnical data were obtained through a combination of field investigations and laboratory testing. The field investigation included Standard Penetration Tests (SPT) as shown in Table 30. BH Reservoir Outlet, which were used to identify the soil stratigraphy at the site. Laboratory testing consisted of physical and mechanical tests to determine the effective shear strength parameters and stiffness parameters required for numerical modeling as shown in . These data then served as the basis for interpreting soil parameters and selecting input parameters for the Hardening Soil (HS) constitutive model.

Table 30. BH Reservoir Outlet

Elevation	NSPT	Description
0	-	Clay, brown, medium plasticity, very stiff
-2	9	Clay with rock inclusion, brown, medium plasticity, very stiff
-4	12	Clay with rock inclusion, gray, medium plasticity, very stiff
-6	58	Clay with rock inclusion, grayish-brown, medium plasticity, very hard
-8 to -16	60	Clay stone, brownish-gray, very hard

Table 31. Data Uji Laboratorium

Sample (Depth 1.5-2.0 m)		Units	
Index Properties	Water Content	%	32.68
	Specific Gravity (Gs)		2.647
	Bulk Density (γt)	g/cm^3	2.036
	Grain Size Distribution Analysis		
	Passing No. 4 Sieve	%	100
	Passing No. 200 Sieve	%	86.4
	Hydrometer Analysis		
	Silt Fraction (0.06–0.002 mm)	%	81.958
	Clay Fraction (<0.002 mm)	%	40.460
	Grain Size		
	Gravel	%	0
	Sand	%	13.6
	Silt	%	45.94
	Clay	%	40.46
	Atterberg Limits		
	Liquid Limit (LL)	%	48.90
	Plastic Limit (PL)	%	22.15
	Plasticity Index (PI)	%	26.75
	Activity Value (PI / %Clay Fraction)		0.33
	AASHTO Soil Classification		A-7-5
	USCS Classification System		CL
	Permeability (k)	cm/d	0.00000205
Engineering Properties (Triaxial UU)	Friction Angle	°	19.009
	Cohesion (c)	kg/cm^2	0.421

2.2 Hardening Soil & Soil Parameter Interpretation

The main HS parameters are generally similar to the MC model, namely Poisson's ratio (ν), internal friction angle (ϕ), cohesion (c), and dilatancy (ψ). Meanwhile, it has 3 types of stiffness, namely

secant stiffness (E50), tangent stiffness for primary oedometer loading (Eoed), and unloading reloading stiffness (Eur). The Plaxis use of superscript notation "ref" that refers to the normalized pressure (Pref) is 100 kPa. The last HS parameter is dependent on stress (m). Referring to Padfield (1983), as presented in Equation (1), Equation (2), and Equation (3).

$$E_u = (150 - 200)\, C_u \quad (1)$$

$$E_{50} = 0{,}67 - 0{,}75\, E_u \quad (2)$$

$$E_{ur} = 3\, E_{50} \quad (3)$$

The effective shear strength parameters were determined by referring to the approach proposed by Gartung (1986) in evaluating the degree of weathering. Gartung classified clay shale into several weathering zones, ranging from unweathered clayshale to highly weathered clayshale. A residual friction angle of φ_r' = 8.60 was used as a conservative value for analysis, since using peak strength parameters may lead to unsafe evaluations. For design purposes, Gartung recommended the use of φ' = 20° and c' = 20 kPa.

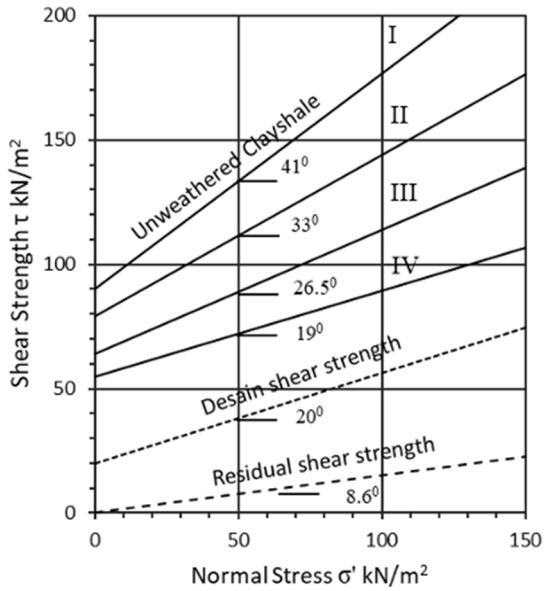

Figure 47. Effective shear strength parameters use the suggestion from Gartung (1986) (op cit. Irsyam et al., 2007)

Table 32. Soil parameter for hardening soil model

Elevasi	c'	ϕ'	ψ'	E_u^{ref}	E_{50}^{ref}	E_{ur}^{ref}	Rf	v_{ur}
0 – 3	8	12,80	0	18900	14175	42525	0.75	0.3
3 – 5	11	13,40	0	25200	18900	56700	0.75	0.3
5 – 7	87	21,88	0	121800	91350	274050	0.75	0.3
7 - 30	90	22,00	0	126000	94500	283500	0.75	0.3

2.3 Parameter of Soldier Pile

The soldier pile system was designed using reinforced concrete bored piles installed as freestanding elements to support the 9-meter deep excavation. The pile configuration consists of uniform pile diameter, pile length, and center-to-center spacing which were selected to achieve adequate flexural

stiffness and lateral resistance under excavation-induced loading. In this study, the structural stiffness properties of the soldier pile were represented by the elastic modulus and unit weight of reinforced concrete, while the geometric properties (diameter and embedment depth) were specified according to the final design configuration at the project location. The detailed properties of the soldier pile used as numerical input parameters in the Plaxis 2D model are summarized in Table 33.

Table 33. Plate parameter for soldier pile

Parameter		Unit	Value
Normal Stiffness	(EA)	kN/m	7.38 E+06
Flexural Rigidity	(EI)	kN/m^2/m	2.95 E+05
Weight	(w)	kN/m/m	12.06
Poisson Ratio	(v)	-	0.2

3 RESULTS AND DISCUSSION

3.1 Cross Section Analysis Using Plaxis

The cross-section analysis was performed on the most critical section with a 9-meter excavation depth to evaluate the local lateral response of the soldier pile system under clayshale conditions. The soldier pile was modeled as a bored pile with a diameter of 0.8 m, a total length of 21 m, and a center-to-center spacing of 1.6 m. In the model, deep foundation elements located on both the left and right sides of the excavation—representing the foundations of the existing buildings—were also included to assess their interaction with the overall excavation stability.

The analysis results indicate that the maximum lateral deformation reached 4.806 cm, corresponding to approximately 0.5% of the total excavation depth (H). This magnitude remains within the acceptable limits for temporary excavation support systems. The bending moment distribution profile shows that the maximum bending moment occurred around the -9 m elevation, with a value of 476.4 kNm. This value is still below the design capacity of the soldier pile section, indicating that the structural configuration can be considered safe under these conditions.

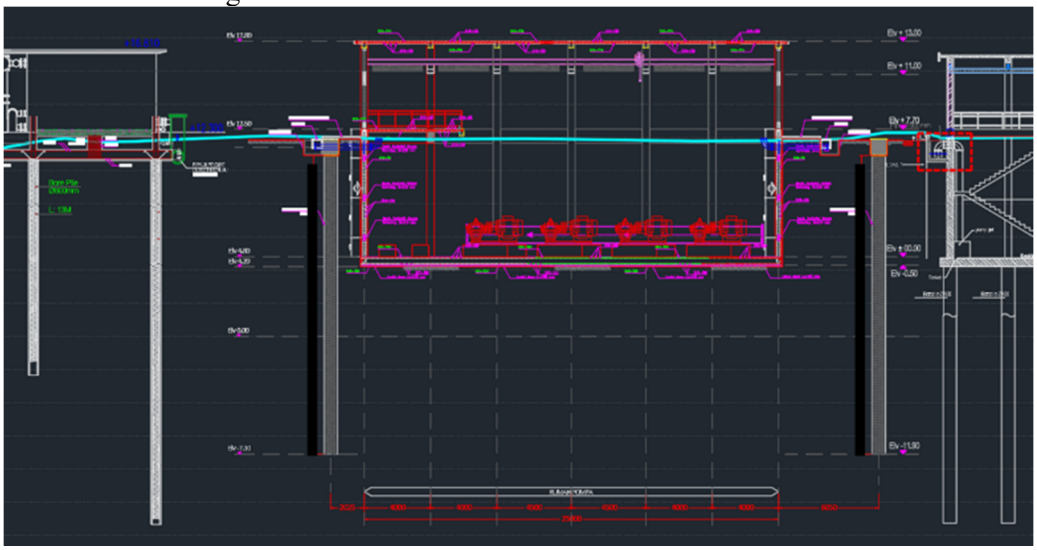

Figure 48. Geometry of Cross Section with Soldier Pile

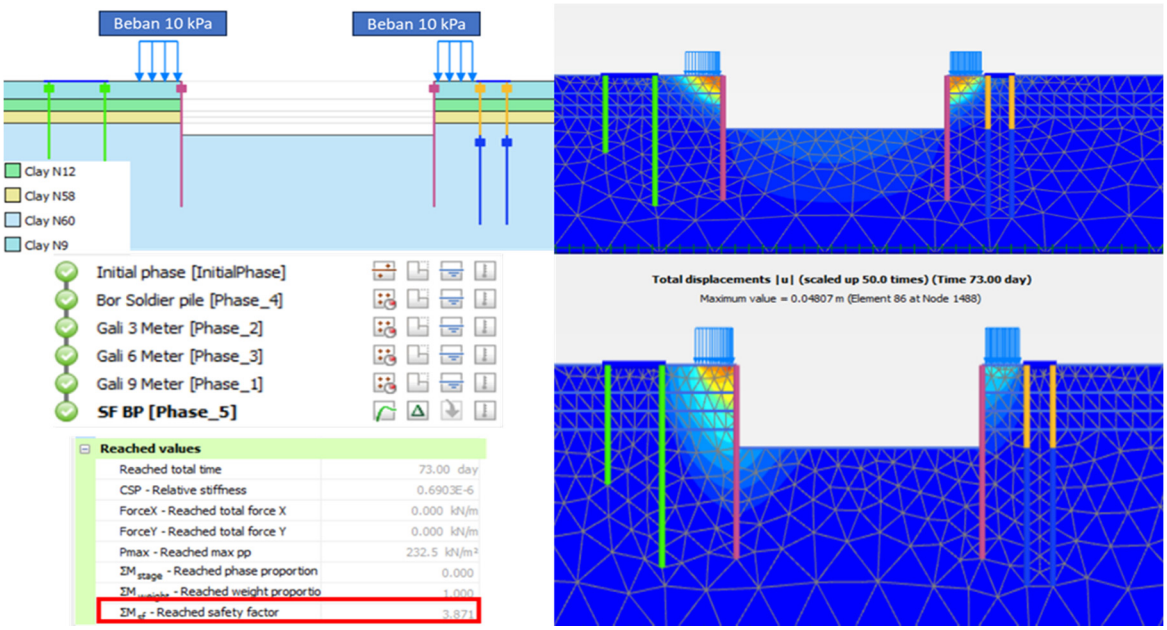

Figure 49. Safety Factor of Cross Section with Soldier Pile

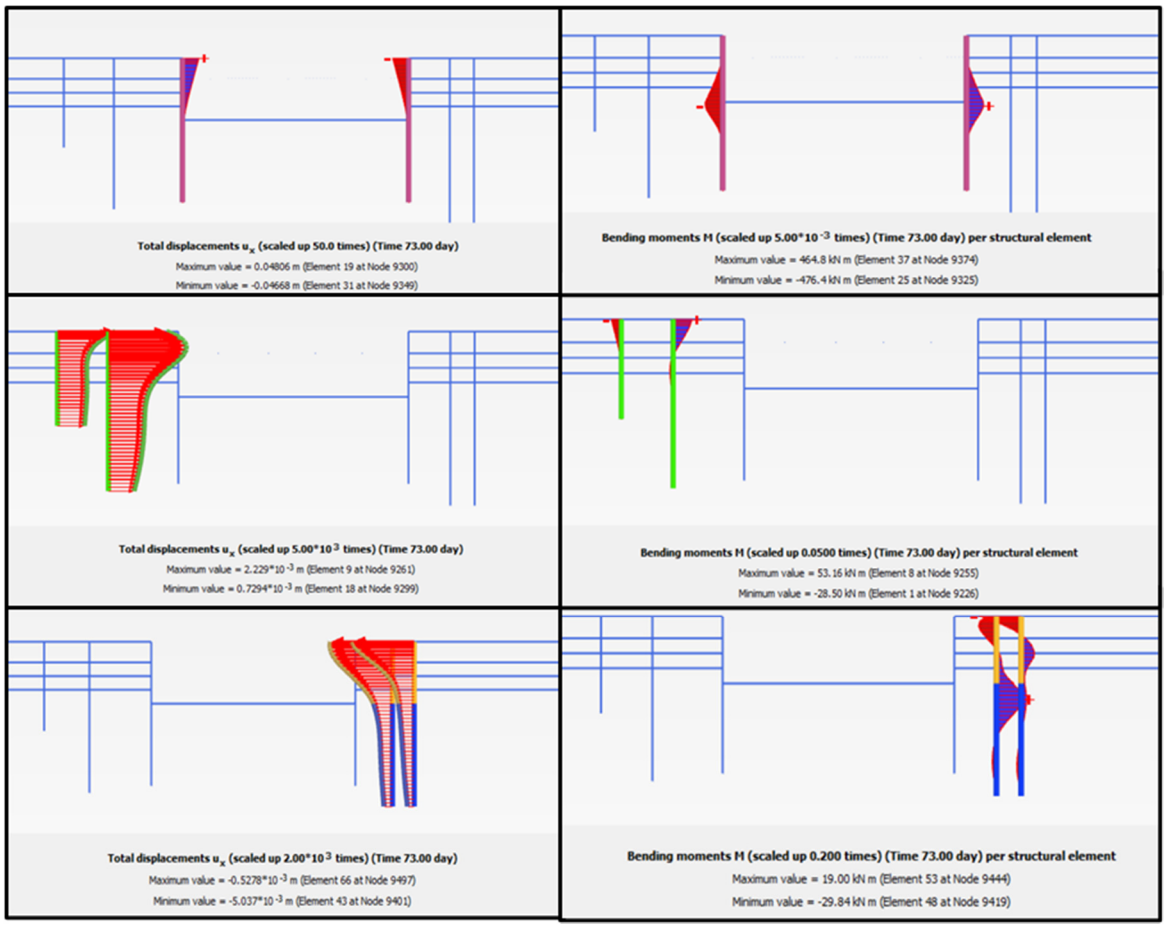

Figure 50. Modeling Output and Internal Forces in Piles

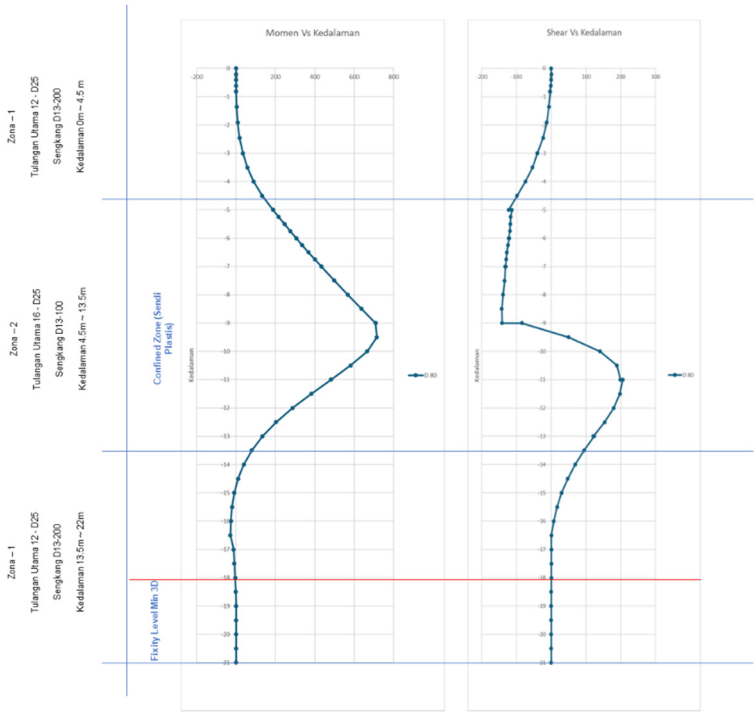

Figure 51. Fixity Point Results in Cross-Section Analysis

The results indicate that the slope stability factor remains above the minimum design criteria, the pile deformation of the soldier pile is within the allowable deformation limits, and the impact on the existing deep foundations is relatively minor.

The analysis also confirms that the fixity point was achieved as the lateral response and bending moment resistance were accurately represented. At this depth below the ground surface, the soldier pile is sufficiently embedded to resist bending moments, such that rotational movement at the fixity point can be considered negligible (approaching zero). Below this point, the pile is assumed to be rigid against lateral rotation induced by external loads.

3.2 Long Section Analysis Using Plaxis

The longitudinal section analysis was carried out to evaluate the variation of excavation system response, particularly with respect to changes in topographic condition and the elevation of the existing ground surface. The analysis results indicate variations in deformation and bending moment values along the longitudinal direction; however, the peak values still occur at the section with the maximum excavation depth (9 meters). The longitudinal section was modeled in 2D to represent the excavation area adjacent to a high slope with residential loading. The soldier pile was modeled as a bored pile with a diameter of 0.8 m, a total length of 21 m, and a center-to-center spacing of 1.6 m.

The maximum lateral deformation and maximum bending moment along the longitudinal section were obtained at 8.394 cm and 666.4 kNm, respectively. The lateral deformation corresponds to approximately 0.9% of the freestanding excavation height. This value is relatively high, as it approaches the commonly referenced limit of 1% H. However, considering that this system is used only for temporary excavation support, this deformation is considered acceptable, provided that periodic deformation monitoring is implemented during construction. The Strength Reduction Factor (SRF) obtained from the longitudinal section analysis also remains above the minimum threshold required for temporary structures, indicating that the freestanding soldier pile system in this condition can be categorized as globally stable.

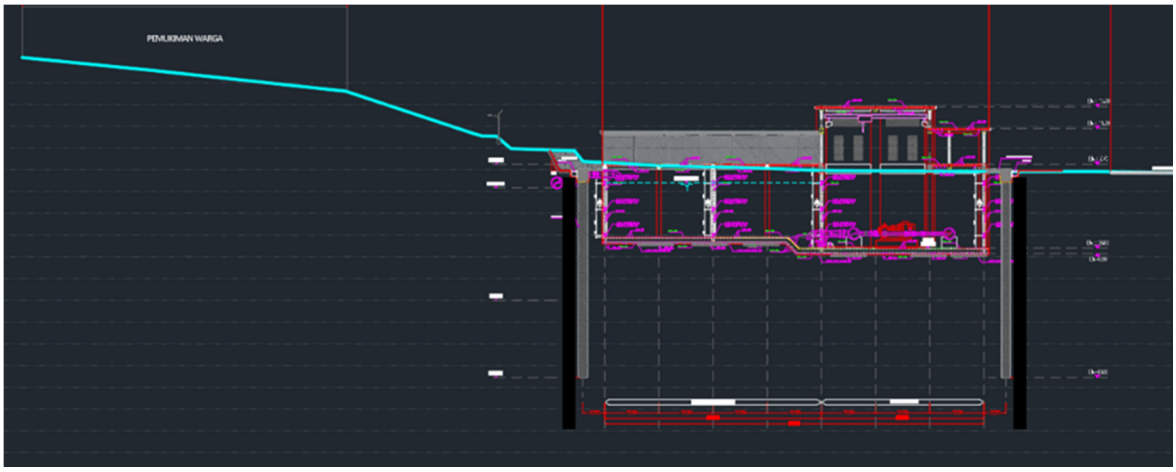

Figure 52. Geometry of Longitudinal Section with Soldier Pile

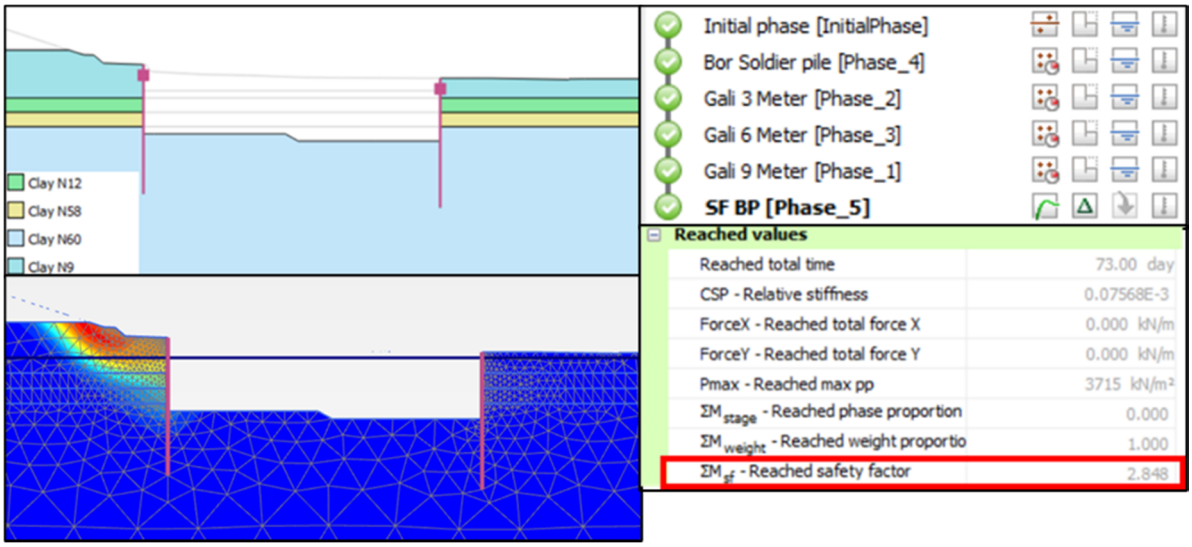

Figure 53. Slip Surface Longitudinal Section with Soldier Pile

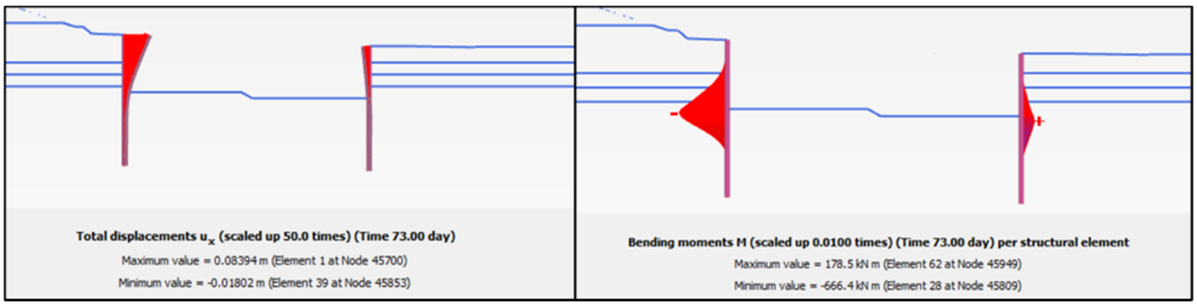

Figure 54. Internal Forces Output in Soldier Pile (Longitudinal Section)

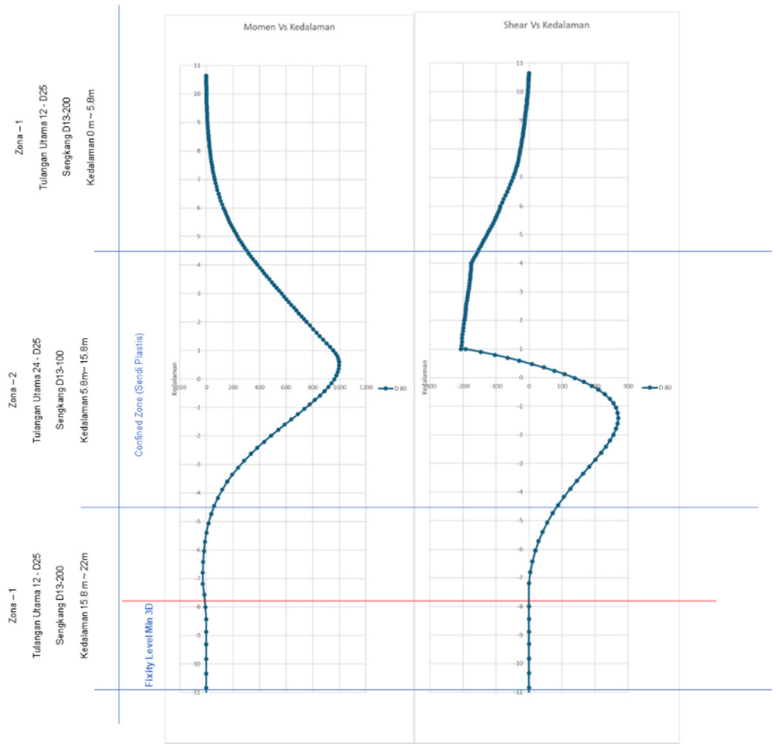

Figure 55. Fixity Point in Longitudinal Section Modeling

The results demonstrate that the slope stability factor remains above the minimum design requirement, the pile deformation of the soldier pile is within allowable design limits, and the impact on existing deep foundations located on both sides of the planned reservoir structure is relatively minor.

As in the cross-section model, the analysis satisfies the fixity point criteria, ensuring accurate representation of lateral response and bending moment resistance. The soldier pile was sufficiently embedded to restrain bending moments, making the rotational movement at the fixity point negligible. Below this depth, the pile behaves as a rigid element against lateral rotation due to external loading.

Overall, the results from both cross-section and longitudinal analyses demonstrate consistent structural behavior of the freestanding soldier pile system, where the governing response is driven by the deepest excavation section. While the longitudinal section exhibits larger deformation due to the combined influence of ground elevation variation and external surcharge from residential loading, both analyses confirm that the system remains within acceptable service limits for temporary excavation support. Therefore, the Hardening Soil model successfully captures the deformation mechanism and bending response of the soldier pile in clayshale conditions at the IPA Sepaku site, and the adopted configuration may be considered feasible for similar deep excavation applications within the IKN region.

3.3 Field Deformation Monitoring Result

As part of the verification process of the excavation support performance in the field, lateral deformation monitoring was carried out during the excavation stage when the cut reached the elevation of -9 m. The summary of maximum lateral deformations recorded from three instrument points is presented in

Table 34. Summary of lateral deformation monitoring results at the -9 m excavation stage

Instrument Code	Allowable Maximum Deflection	Maximum Lateral Deformation Measured	
		Longitudinal Axis	Transverse Axis
IN-01	46,48 mm	9,42 mm	2,71 mm
IN-02	83,94 mm	14,68 mm	4,15 mm
IN-03	48,06 mm	6,95 mm	4,11 mm

Overall, the monitoring results indicate that the maximum recorded deformations along both the longitudinal and transverse axes remain significantly below their respective allowable limits. This confirms that the freestanding soldier pile system operated within acceptable performance boundaries during the critical excavation stage, and validates that the predicted numerical behavior is consistent with actual field conditions.

4 CONCLUSIONS

This study evaluated the performance of a freestanding soldier pile system for a 9-meter excavation in clayshale formation at the IPA Sepaku Project using the Hardening Soil model. Numerical results from the critical cross-section indicated a maximum lateral deformation of 4.806 cm (≈0.5% H) with a maximum bending moment of 476.4 kNm, while the longitudinal section resulted in a higher deformation of 8.394 cm (≈0.9% H) and a maximum bending moment of 666.4 kNm. Field monitoring during the -9 m excavation stage confirmed that the maximum recorded lateral deformation remained below the allowable limits, with measured values ranging between 6.95 mm–14.68 mm in the longitudinal axis, and 2.71 mm–4.15 mm in the transverse axis. These results validate that the numerical predictions were representative of the actual field behavior. Based on both numerical and field observations, the freestanding soldier pile configuration can be considered feasible and stable for temporary excavation support in highly weatherable clayshale conditions at IKN, provided that deformation monitoring continues throughout construction. This outcome may serve as a technical reference for similar deep excavation works within the clayshale-dominated regions of the IKN area.

DISCLAIMER

The authors declare no conflict of interest.

AVAILABILITY OF DATA AND MATERIALS

All data are available from the author.

REFERENCES

Badan Standardisasi Nasional (2017) *SNI 8460:2017 – Persyaratan Perancangan Geoteknik*. Jakarta: BSN.

Bobet, A. & Einstein, H.H. (2008) 'Tunnel design in swelling rock', *Rock Mechanics and Rock Engineering*, 41(1), pp. 1–27.

Bonini, M., et al. (2009) 'Engineering behavior of clay shales', *Engineering Geology*, 108(1–2), pp. 34–46.

Brinkgreve, R.B.J., Engin, E. & Swolfs, W.M. (2012) *PLAXIS 2D: Material Models Manual*. Delft: Plaxis bv.
Clough, G.W. & O'Rourke, T.D. (1990) 'Construction induced movements of in-situ walls', in *Design and Performance of Earth Retaining Structures*. ASCE Geotechnical Special Publication 25, Ithaca, NY, pp. 439–470.
Das, B.M. and Sobhan, K. (2018) *Principles of Geotechnical Engineering*. 9th edn. Boston, MA: Cengage Learning.
Gartung, E. (1986) 'Stability of slopes in weathered claystones', in *Proceedings of the Fifth International Symposium on Landslides*. Lausanne, pp. 1505–1510.
Padfield, C.D. (1983) *The Behaviour of Clays Under Repeated Loading*. Cambridge: Cambridge University Press.
Schanz, T. & Vermeer, P.A. (1996) 'Angles of friction and dilatancy of sand', in *Geotechnical Engineering for Hard Soils–Soft Rocks*, Rotterdam: Balkema.
Schofield, A.N. & Wroth, C.P. (1968) *Critical State Soil Mechanics*. New York: McGraw-Hill.
SNI 8460:2017 (2017) *Persyaratan Perancangan Geoteknik*. Jakarta: Badan Standardisasi Nasional.
Zarkasi, A., et al. (2018) 'Behavior and characterization of clay shale in West Java', *Journal of Engineering Geology*, 10(2).

HIMPUNAN AHLI TEKNIK TANAH INDONESIA - HATTI
Indonesian Society for Geotechnical Engineering - ISGE
PIT HATTI XXIX
10-12 November 2025

Underwater Subsurface Imaging of the North Java Sea using Marine Resistivity Tomography

Bagus Endar B. Nurhandoko[1*], Syukri Fitriadi[2], Kaswandhi Triyoso[3], Satryo Agung Wibowo[3], Insan Rizal Komara[3], Wisnu Guntara[3], Diah Asmawati[3], Gogot Panca Parijogo[2], Ratih Pratiwi[1], Maria Cindrawati[1], Harry Mahardika[1], Alvina Kusumadewi Kuncoro[1], Eko B. Supriyanto[3]

[1]Earth Physics and Complex System Research Division, Faculty of Mathematics and Natural Sciences, Institut Teknologi Bandung, Bandung, Indonesia, 40132
[2]Taka Hydrocore Indonesia, Bandung, Indonesia, 40295
[3]Lembaga Pengembangan Inovasi dan Kewirausahaan ITB, Bandung, Indonesia, 40132
*Correspondence: bagus@itb.ac.id

ABSTRACT Covering approximately 62% of its territory, Indonesia's marine deposits have a lot of unrevealed underwater resources potential. Since water is characterized by high conductivity, resistivity tomography was offered as a method to produce valid marine environment imaging. Marine Resistivity Tomography (MRT) is still challenging to be implemented due to the vulnerability of electric measurement equipment and acquisition uncertainty coming from interfered conductivity of saline water. In this paper, an improved measurement system of MRT was applied to characterize subsurface lithology along the offshore area of Cirebon in the North Java Sea, two heavy-effected land subsidence coastal areas. As current was injected to the water by two electrodes, electrical potential was then acquired by 22 electrodes connected by 300 m cable with spacing of 15 m between adjacent electrodes. Eventually, the resistivity representing conductivity of the marine could be obtained based on Ohm Law. All of the electrodes were floated and towed behind a 700 HP vessel at 3-4 km/h speed. Dynamic measurement had been carried out during vessel movement using reciprocal Schlumberger configuration intended to optimize signal response in saline environments with water depths between 5-30 m. Data processing and inversion were conducted to generate 2D resistivity tomograms, which were then interpreted in terms of lithological variations and seabed layering. The lithological distribution particularly sand and clay as indicators of sediment layer variability were interpreted from this inversion. Resistivity anomalies that may indicate hydrocarbon seepage or paleo-shoreline deposits were assessed. In addition, the variations in resistivity corresponding to both soft and hard seabed layers give evidence of a consolidated high-resistivity unit underlying unconsolidated sediments. The interpreted data established baseline insights to guide coastal hazard management and to design offshore infrastructure in northern West Java, and also identified natural resources provided by underwater subsurfaces.

KEYWORDS Underwater Imaging, Marine Resistivity Tomography, Subsurface Seabed, Coastal Infrastructure, North Java Sea

1 INTRODUCTION

The northern coast of West Java has damaging issues of erosion, accretion, pollution, inundation, and land subsidence (Solihuddin, et al., 2021a). Figure 1 shows Cirebon, one of areas included in Pantai Utara Jawa (Pantura) route, has for twenty years (1994-2014) experienced a significant shift in the coastline, according to research by Harahap, et al. (2019). There has been an average shift of the coastline of approximately 986 meters, almost all of which caused by accretion. This discovery was agreed by (Solihuddin, et al., 2021b) stating that Cirebon bears accretion and sedimentation through active rivers that drain off into the Java Sea. These phenomena are urgent to be solved considering their impacts on Cirebon high population density and rapid urban maneuver. Some

efforts performed by local residents including mangrove planting and revetment building. Nevertheless, the abrasion rate outpaces these accomplishments.

Figure 1. The survey area, in Cirebon Bay West Java with inset Indonesia map.

An initial attempt to manage the coastal hazard is figuring out its water environment. A common method conducted is satellite imagery. A long-term monitoring of coastal events can be visualized with some captured sequence of figures. However, the particular limitation of this method is its confinement to image lateral area, lack of depth imaging capability. The high resolution capturing is also a significant concern that requires improvement.

The underwater ecosystem and its activity gives unignored impacts to the land, as the whole water circulates back and forth between sea and land. Besides physical change which has been described earlier, any pollution experienced by the sea water proposed noticeable disadvantages to the land life. An increment of seawater inducing freshwaters threatens the quality of available consumable water. Moreover, the fault movement detection. Along with the destruction, underwater formation generates natural wealth including potential oil and gas accommodated in hydrocarbon seepage, indicated by gas intrusion to the water column (Logan et al., 2008). The presence of mentioned phenomena lead us to consider the critical of coastal and offshore detailed monitoring for both scientific and practical reasons.

Resistivity tomography offers a well-established method that was commonly used in near surface geophysics and lately has been developed for deep various geological surveys in onshore territories (Balasco et al., 2022; Nurhandoko et al., 2025). Nurhandoko et al. (2022) conducted near-surface resistivity imaging using resistivity tomography in North Lombok Island following the 2018 earthquake of magnitude 6.9. In a different context, resistivity tomography has been employed to characterize complex subsurface conditions dominated by older strata, clay-rich layers, and intensive thrust faulting. This approach has also proven effective in delineating an overhang structure of a thrust fault with a strike fault segment as well as identifying an oblique thrust fault system (Nurhandoko et al., 2020, 2025).

In seaside settings, marine resistivity tomography (MRT), with the same basic concept as that of the land one, can be applied as well for numerous subsea interpretations. MRT exists as a non-invasive and non-explosive geophysical technique widely applied in shallow marine environments. Unlike conventional seismic or acoustic methods, MRT provides direct electrical imaging of subsurface resistivity variations, which are strongly influenced by lithology, porosity, salinity, and fluid content (Constable, 2010; Loke et al., 2013). This makes MRT particularly suitable for resolving near-surface heterogeneities, detecting fluid pathways, and imaging stratigraphic features in coastal and offshore settings.

Over the past two decades, MRT has been successfully applied in multiple domains. Applications include hydrocarbon seepage detection (Constable, 2010), exploring shallow methane hydrate beneath the seafloor (Chiang et al., 2012), mapping groundwater–seawater interactions in coastal aquifers (Folorunso, 2021; Niculescu and Andrei, 2021; Moulds et al., 2023; Oyeyemi et al., 2023; Ren et al., 2025), identifying submerged archaeological remains (Passaro, 2010; Papadopoulos et al., 2022; Chabrol et al., 2023; Beltrame et al., 2025), investigating seafloor massive material deposits (Ishizu et al., 2019), and mitigating risks at shallow depth beneath the seafloor in maritime project developments (D'Eu et al., 2025). These studies demonstrate the versatility of MRT as a tool for subsurface characterizations across geological, environmental, and engineering contexts. In contrast to its diverse applications in other countries, the application of resistivity tomography in marine environments remains relatively novel in Indonesia, an archipelagic country encompassing vast marine territories. Existing research scopes have primarily focused on identifying seawater intrusion in groundwater zones and characterizing subsurface layers in coastal areas (Rahmaniah et al., 2021; Muzambiq et al., 2025; Minarto et al., 2025).

The saline water gives a challenge in MRT surveys regarding its high conductivity that may impact the true subsurface conductivity distribution. The presented research proposes an effective method to produce good interpretation in saline water vicinity under MRT Schlumberger configuration in Cirebon beach. Furthermore, the interpreted data established baseline insights to guide the offshore infrastructure design in northern West Java.

2 DATA AND METHODS

Marine resistivity tomography (MRT) surveys were conducted along the northern coast of West Java, particularly near Cirebon. The acquisition used a floating electrode array towed behind a 700 HP vessel at very low speed of 3–4 km/h. A 300 m cable with 24 electrodes (15 m spacing) was deployed, consisting of 22 potential electrodes and 2 current electrodes. The acquisition system utilized one of the TomoResIP series, as shown in Figure 2.

Figure 2. One of the series of TomoResIP was used for the marine resistivity tomography data acquisition.

Measurements were made using a reciprocal-Schlumberger configuration to optimize signal response in saline environments with water depths between 5-30 m. Figure 2 illustrates the electrode configuration used in the survey, where 'C' and 'P' denote the current and potential electrodes,

respectively. Additionally, the spacing between electrodes is represented by ‘a’, while the layer index is indicated by ‘n’.

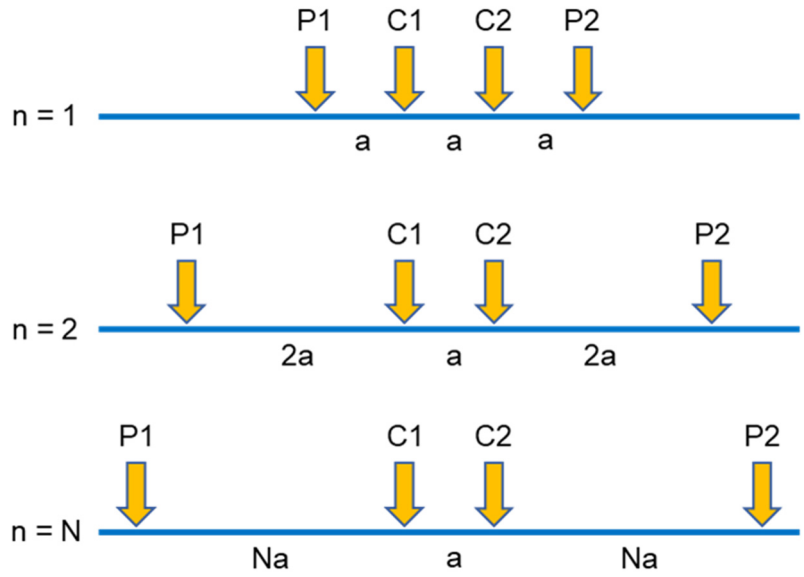

Figure 3. Reciprocal Schlumberger configuration.

The survey employed a dynamic measurement approach where the measurement was performed during vessel movement using a reciprocal Schlumberger setup. Voltage and current data were initially acquired through field measurements. These datasets were then processed to compute the apparent resistivity distribution. To obtain a realistic two-dimensional subsurface resistivity tomograms, inversion technique was also conducted, which were then interpreted in terms of lithological variations and seabed layering. Figure 4 illustrates the marine resistivity tomography measurement applying a floated electrode array.

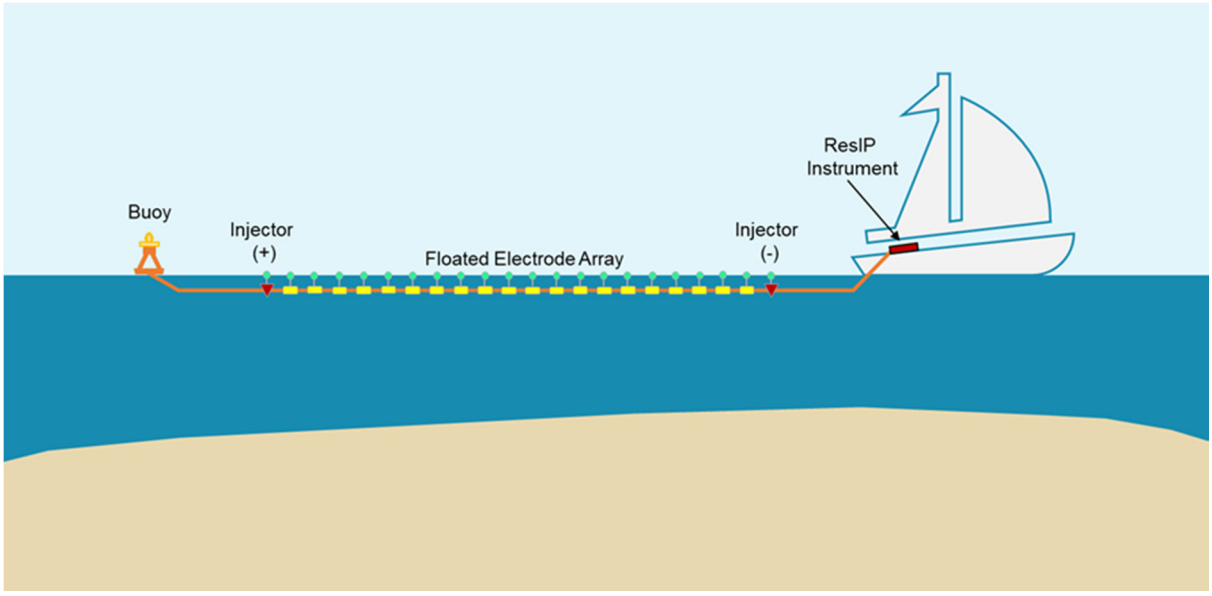

Figure 4. Illustration of Marine Resistivity Tomography data acquisition using floated electrode array.

Figure 5. Marine tomography resistivity acquisition for subsurface imaging in Cirebon Bay.

Figure 5 illustrates the resistivity data acquisition setup deployed aboard the survey vessel. The figure highlights the configuration of the electrode array, which was arranged and floated on the seawater surface to ensure consistent contact and signal transmission. This layout corresponds to the floated electrode arrangement previously described in Figure 4, providing visual continuity between the schematic and the actual field implementation.

Figure 6. Detailed subsurface imaging location in Cirebon Bay.

The marine resistivity survey was conducted along a 2.73 km transect, oriented from the Southeast to the Northwest. This survey line is illustrated by the yellow arrow trace in Figure 6, representing the deployment path of the floated electrode array previously introduced in Figures 4 and 5.

3 RESULTS AND DISCUSSION

The resistivity sections reveal distinct subsurface features beneath the surveyed coastal areas. Low resistivity zones (0.1–0.2 Ωm) correspond to unconsolidated sediments such as clay and silt, whereas higher resistivity values (>0.5 Ωm) indicate the presence of a more consolidated layer with more sandstones dominated or compacted seabed layers. The observed resistivity value of approximately

0.5 Ωm may also indicate a tidal sand bar within a tide-dominated delta environment, where the presence of saline pore water contributes to low overall resistivity. Nevertheless, a notable higher-resistivity horizon was observed beneath the Cirebon coast, suggesting a relatively hard seabed unit which provides important information for infrastructures.

These results are consistent with previous coastal geophysical studies that link resistivity contrasts to variations in lithology, salinity, and pore fluid saturation (Constable, 2010; Loke *et al.*, 2013). Furthermore, the presence of resistive horizons may indicate paleo-shoreline deposits related to Quaternary marine transgressions, which have shaped much of the modern North Java coastline.

The ability of MRT to resolve near-surface structures makes it suitable for applications in coastal erosion studies, hydrocarbon seepage detection, and groundwater-seawater interaction monitoring. When correlated with borehole and seismic data, MRT could enhance the reliability of subsurface models for the North Java Sea.

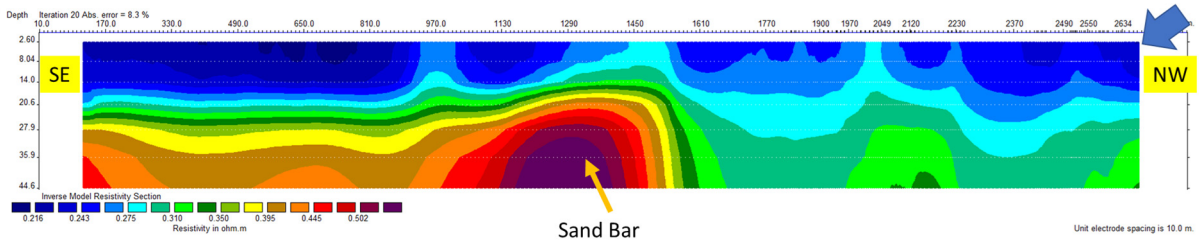

Figure 7. Inversion result showing the resistivity tomography result along the 2.73 km line, showing the ability of the Marine Resistivity Tomography equipment to image the sand bar beneath the sea surface.

4 CONCLUSIONS

Marine resistivity tomography has produced subsurface lithology imaging of the offshore area of Cirebon, North Java Sea. The measurements constructed by reciprocal Schlumberger configuration reveal the coastal environment imaging including soft sedimentary deposits and hard consolidated seabed layers. In relation to the attempt of hazard mitigation, the layers and deposits can be guidance for infrastructure design planning around coastal areas. In relation to monitoring development, the resistivity tomography imaging shows the presence of resistive horizons which may indicate paleo-shoreline deposits related to Quaternary marine transgressions. These deposits have shaped much of the modern North Java coastline. In addition, the resistivity interpretation shows the potential tidal sandbar dominating delta environment, indicating seawater-freshwater interaction. The performed data acquisition and proposed method demonstrate the prospect of MRT for: (1) supporting coastal management by mapping abrasion-prone zones, (2) detecting hydrocarbon seepage pathways, and (3) providing baseline data for the design of underwater infrastructure. Future work should focus on integrating MRT with seismic surveys, borehole logging, and rock physics analysis for a more comprehensive subsurface characterization.

REFERENCES

Balasco, M., Lapenna, V., Rizzo, E. and Telesca, L. (2022) "Deep Electrical Resistivity Tomography for Geophysical Investigations: The State of the Art and Future Directions," *Geosciences (Switzerland)*, 12(12). Available at: https://doi.org/10.3390/geosciences12120438.

Beltrame, C., Costa, E., Mozzi, P., Carrera, A. and Boaga, J. (2025) "Geophysical Prospecting for the Detection of Buried and Shallow Submerged Archaeological Sites of Roman Period in the Lagoon of Venice (Italy)," *Archaeological Prospection*, n/a(n/a). Available at: https://doi.org/https://doi.org/10.1002/arp.70004.

Chabrol, A., Beuzen-Waller, T., Virmoux, C., Chavand, D., Fouache, E. and Orgeolet, R. (2023) "Geoarchaeological investigation of a prehistoric tell in a coastal environment: the lowest levels at

Kirrha (Plain of Delphi, Phocis, Greece),” *Journal of Archaeological Science: Reports*, 51, p. 104151. Available at: https://doi.org/https://doi.org/10.1016/j.jasrep.2023.104151.

Chiang, C.W., Goto, T.N., Mikada, H., Chen, C.C. and Hsu, S.K. (2012) “Sensitivity of deep-towed marine electrical resistivity imaging using two-dimensional inversion: A case study on methane hydrate,” *Terrestrial, Atmospheric and Oceanic Sciences*, 23(6), pp. 725–732. Available at: https://doi.org/10.3319/TAO.2012.06.19.01(T).

Constable, S. (2010) “Ten years of marine CSEM for hydrocarbon exploration,” *GEOPHYSICS*, 75(5), pp. 75A67-75A81. Available at: https://doi.org/10.1190/1.3483451.

D’Eu, J.-F., Maisonneuve, A., Colin, F. and Weller, A. (2025) “Mitigating Shallow Subsurface Risk with Marine Electrical Resistivity Tomography (MERT),” in *OCEANS 2025 Brest*, pp. 1–4. Available at: https://doi.org/10.1109/OCEANS58557.2025.11104763.

Folorunso, A.F. (2021) “Mapping a spatial salinity flow from seawater to groundwater using electrical resistivity topography techniques,” *Scientific African*, 13, p. e00957. Available at: https://doi.org/10.1016/j.sciaf.2021.e00957.

Harahap, S.A., Purba, N.P. and Syamsuddin, M.L. (2019) “Trend of Coastline Change for Twenty Years (1994-2014) in Cirebon, Indonesia.”*World Scientific News*, 138(2) pp. 79-92.

Ishizu, K., Goto, T., Ohta, Y., Kasaya, T., Iwamoto, H., Vachiratienchai, C., Siripunvaraporn, W., Tsuji, T., Kumagai, H. and Koike, K. (2019) “Internal Structure of a Seafloor Massive Sulfide Deposit by Electrical Resistivity Tomography, Okinawa Trough,” *Geophysical Research Letters*, 46(20), pp. 11025–11034. Available at: https://doi.org/10.1029/2019GL083749.

Logan, G.A. (2008) *Review of Australian offshore natural hydrocarbon seepage studies*. Canberra: Geoscience Australia.

Loke, M.H., Chambers, J.E., Rucker, D.F., Kuras, O. and Wilkinson, P.B. (2013) “Recent developments in the direct-current geoelectrical imaging method,” *Journal of Applied Geophysics*, 95, pp. 135–156. Available at: https://doi.org/https://doi.org/10.1016/j.jappgeo.2013.02.017.

Moulds, M., Gould, I., Wright, I., Webster, D. and Magnone, D. (2023) “Use of electrical resistivity tomography to reveal the shallow freshwater–saline interface in The Fens coastal groundwater, eastern England (UK),” *Hydrogeology Journal*, 31(2), pp. 335–349. Available at: https://doi.org/10.1007/s10040-022-02586-2.

Muzambiq, S., Husin, A., Herlina, N. and Gultom, T.M. (2025) “Identification of the Distribution of Seawater Intrusion Using the Resistivity 2D Method in the Belawan Area, North Sumatra Province,” *Jurnal Ilmu Lingkungan*, 23(1), pp. 85–93. Available at: https://doi.org/10.14710/jil.23.1.85-93.

Niculescu, B.M. and Andrei, G. (2021) “Application of electrical resistivity tomography for imaging seawater intrusion in a coastal aquifer,” *Acta Geophysica*, 69(2), pp. 613–630. Available at: https://doi.org/10.1007/s11600-020-00529-7.

Nur, S.H. and Hilmi, E. (2021) “The correlation between mangrove ecosystem with shoreline change in Indramayu coast,” *IOP Conference Series: Earth and Environmental Science*, 819(1). Available at: https://doi.org/10.1088/1755-1315/819/1/012015.

Nurhandoko, B.E., Triyoso, K., Hadi, M.R.A., Rizal, I., Widarto, D.S. and Nurhasan, N. (2020) “Karakterisasi Akuifer Berumur Miosen di Daerah Geologi Kompleks Thrust Fault Zona Kendeng dengan Rock Physics dan Tomografi Resistivitas,” *Jurnal Geofisika*, 18(2), p. 53. Available at: https://doi.org/10.36435/jgf.v18i2.433.

Nurhandoko, B.E.B., Sukrisna, B., Widowati, S., Asmarahadi, M.R., Yasin, S., Kurniawidi, D.W., Martha, R., Triyoso, K., Asmawati, D., Fatiah, E., Hariman, Y., Susilowati, Supriyanto, E.B., Guntara, W.A., Bakti, I.R., Wibowo, S.A. and Sukmana, I. (2022) "Near-surface resistivity imaging using resistivity Tomography in some most impacted areas due to the 2018 Earthquake in North Lombok Island," *Journal of Physics: Conference Series*, 2243(1). Available at: https://doi.org/10.1088/1742-6596/2243/1/012033.

Nurhandoko, B.E.B., Triyoso, K., Wibowo, S.A., Komara, I.R., Guntara, W., Asmawati, D., Martha, R.K., Widowati, S., Supriyanto, E.B., Suryolaksana, A., Nefrizal, N., Nurani, A., Endartyanto, A. and Nurhasan, N. (2025) "Subsurface Characterization and Revealing Geometry of the Baribis Fault in the Eastern Part of West Java Using Long-Offset Resistivity Tomography," *Journal of Earthquake and Tsunami*, 19(2). Available at: https://doi.org/10.1142/S1793431124500313.

Oyeyemi, K.D., Abuka-Joshua, J., Rotimi, O.J., Dieppois, B., Gomo, M., Olaojo, A.A., Falae, P.O. and Metwaly, M. (2023) "Geoelectrical Characterization of Coastal Aquifers in Agbado-Ijaye, Lagos, Southwestern Nigeria; Implications for Groundwater Resources Sustainability," *Sustainability (Switzerland)*, 15(4), pp. 1–22. Available at: https://doi.org/10.3390/su15043538.

Papadopoulos, N., Oikonomou, D., Simyrdanis, K. and Heng, L.M. (2022) "Practical considerations for shallow submerged archaeological prospection with 3-D electrical resistivity tomography," *Archaeological Prospection*, 29(1), pp. 103–123. Available at: https://doi.org/https://doi.org/10.1002/arp.1841.

Passaro, S. (2010) "Marine electrical resistivity tomography for shipwreck detection in very shallow water: a case study from Agropoli (Salerno, southern Italy)," *Journal of Archaeological Science*, 37(8), pp. 1989–1998. Available at: https://doi.org/https://doi.org/10.1016/j.jas.2010.03.004.

Rahmaniah, Wahyuni, A., Massinai, M.F.I., Mun'im, A. and Massinai, M.A. (2021) "Resistivity Method for Characterising Subsurface Layers of Coastal Areas In South Sulawesi, Indonesia," *Journal of Geoscience, Engineering, Environment, and Technology*, 6(4), pp. 217–225. Available at: https://doi.org/10.25299/jgeet.2021.6.4.6242.

Ren, Y., Glazunov, V. V, Efimova, N.N. and Shevnin, V.A. (2025) "Specific features of electrical resistivity tomography in coastal areas of sea waters," *Marine Geophysical Research*, 46(3), p. 19. Available at: https://doi.org/10.1007/s11001-025-09581-8.

Sodikin, S., Ardiansyah, A.N., Arif, M., Syaripulloh, S., Ilyas, Y. and Astriyandi, A.A. (2024) "Analisis Kerusakan Pantai dan Prioritas Penanganannya di Wilayah Pesisir Kecamatan Sukra Kabupaten Indramayu Provinsi Jawa Barat," *Journal of Marine Research*, 13(4), pp. 671–680. Available at: https://doi.org/10.14710/jmr.v13i4.43276.

Solihuddin, T., Husrin, S., Mustikasari, E., Heriati, A., Kepel, T.L., Salim, H.L., Risandi, J. and Dwiyanti, D. (2021a) "Coastal Inundation and Land Subsidence in North Coast of West Java: A New Hazard?," *IOP Conference Series: Earth and Environmental Science*, 925(1). Available at: https://doi.org/10.1088/1755-1315/925/1/012015.

Solihuddin, T., Husrin, S., Salim, H.L., et al. (2021b) "Coastal erosion on the north coast of Java: adaptation strategies and coastal management," IOP Conference Series: Earth and Environmental Science, 777(1), p. 012035. Available at: https://doi.org/10.1088/1755-1315/777/1/012035.

HIMPUNAN AHLI TEKNIK TANAH INDONESIA - HATTI
Indonesian Society for Geotechnical Engineering - ISGE
PIT HATTI XXIX
10-12 November 2025

Adhesion Factor (α) of Drilled Piles in Clay Shale with Static and Dynamic Load

Eddy Triyanto Sudjatmiko[1,*], The Cin Hok[2]
[1] Department of Civil Engineering, President University, Bekasi, Indonesia, 17550; triyanto_eddy@icloud.com
[2] Department of Civil Engineering, Parahyangan Catholic University, Bandung, Indonesia, 40141; thecinhokl@gmail.com
*Correspondence: triyanto_eddy@icloud.com

ABSTRACT The adhesion factor (α) is one of the significant factors in the calculation of the bearing capacity of pile foundations, both for driven piles and drilled piles in clay soils. In practice, the α value only been estimated based on the available empirical correlations. This correlation becomes a question remark for drill pile construction on expansive soil and clay shale. Clay shale is known as one of the problematic soils, due to its physical properties that rapidly soften once exposed to water/moisture and lose of pressure. This physical sensitivity becomes crucial in drilled/bored pile constructions. Especially in drilling and casting process when the soil is exposed to water as well as loss of horizontal pressure causing reduction in soil shear strength. This study investigates the load transfer behavior of a bore pile in clay shale formation axially loaded through dynamic and static load tests up to 700 tons equipped with load cells, vibrating wire strain gauges and telltale. These instruments provide accurate strain measurement of each segment of the pile relating to stress induces. Through pile load-settlement, *t-z* and *q-z* curves the load transfer mechanism and the interaction of drilled pile and the clay shale soil can be analyzed. By performing back analysis, the actual skin friction (*fs*), and adhesion factor (*α*), of drilled piles in clay shale can be determined. The study results show that in expansive clay which is clay shale that have experienced slaking (with 30 < NSPT < 70) the adhesion factor (*α*) = 0.12 ~ 0.18. While for fresh clay shale (NSPT > 70), the adhesion factor (*α*) = 0.32 ~ 0,35. These values is significantly lower than α = 0.55 which is usually applied in practice as well as some previous studies, including the value recommended by Reese and Wright (1979).

KEYWORDS clay shale, bored pile, drilled pile, adhesion factor, skin friction

This paper will be published in the future issues of Indonesian Geotechnical Journal

This page is intentionally left blank

HIMPUNAN AHLI TEKNIK TANAH INDONESIA - HATTI
Indonesian Society for Geotechnical Engineering - ISGE
PIT HATTI XXIX
10-12 November 2025

Evaluasi Performa Penurunan Konsolidasi Jangka Panjang Dengan Metode CMC Pada Konstruksi *Runway* Studi Kasus Bandara Rendani

Azliny Azreen[1,*], Kiagus Muhammad Abuhuroyroch[2]
[1]Teknik Sipil, Teknik, Universitas Muhammadiyah Surakarta, Sukoharjo, 57162; azrnazlny@gmail.com
[2]Geotechnical Engineering, BUT Menard Geosystems Indonesia, Jakarta Selatan, DKI Jakarta, 12430; Roy@menard-asia.com
*Correspondence: azrnazlny@gmail.com

ABSTRAK Bandara Rendani di Kabupaten Manokwari, Provinsi Papua Barat, direncanakan akan memperpanjang landas pacunya sepanjang 300 meter, dari 2.000 menjadi 2.300 meter sehingga pesawat berbadan lebar yang membutuhkan landasan pacu lebih panjang dapat mendarat dengan aman. Penyelidikan tanah menunjukkan bahwa lokasi didominasi oleh tanah lunak, terutama lempung dan lanau, yang memiliki daya dukung rendah dan rentan mengalami penurunan besar jika tidak dilakukan perkuatan. Untuk mengatasi permasalahan ini, dilakukan perkuatan tanah menggunakan *Controlled Modulus Column* (CMC) karena dapat diaplikasikan pada berbagai jenis tanah lunak, mampu mengurangi penurunan tanah serta dapat meningkatkan daya dukung tanah. Penelitian ini mengevaluasi penurunan akibat konsolidasi jangka panjang dengan dan tanpa metode CMC menggunakan *drained analysis* parameter efektif dengan model material Mohr-Coulomb pada Plaxis 2D (model *Axisymmetry*). Parameter tanah dalam penelitian ini diperoleh melalui korelasi antara jenis tanah dan nilai N-design, dengan rentang nilai parameter mengacu pada literatur. N-Design merupakan nilai yang didapatkan berdasarkan kombinasi nilai N-SPT yang diambil berdasarkan data paling buruk pada tiap elevasinya. Pemodelan dilakukan menggunakan Plaxis 2D untuk meninjau penurunan tanah sebelum dan sesudah perkuatan dan tegangan efektif vertikal sesudah perkuatan. Hasil menunjukkan bahwa tanpa perkuatan, tanah mengalami penurunan sebesar 568,70 mm. Dengan perkuatan CMC, penurunan berkurang menjadi 92,68 mm, dan tegangan efektif vertikal meningkat menjadi 2333 kN/m². Hal ini menunjukkan bahwa penggunaan CMC mampu mengurangi penurunan hingga 83,70%, sehingga terbukti efektif untuk diterapkan pada kondisi tanah lunak. Penurunan menggunakan perkuatan dengan CMC juga memenuhi kriteria desainnya yaitu maksimal penurunan jangka panjang sebesar 100 mm selama 10 tahun pasca perbaikan tanah dilakukan.

KATA KUNCI *Controlled Modulus Column*; penurunan; perkuatan tanah; Plaxis 2D; tanah lunak

1 PENDAHULUAN

Saat ini, terdapat lebih dari 500 bandara di Indonesia yang tercatat pada Direktorat Jenderal Perhubungan Udara baik penggunaan domestik maupun penggunaan internasional. Salah satu dari 500 bandara yang terdapat di Indonesia adalah Bandara Rendani yang terletak di Kabupaten Manokwari, Provinsi Papua Barat. Dalam rangka mendukung pertumbuhan ekonomi di daerah Papua, Kementerian Perhubungan memutuskan untuk melakukan perpanjangan *runway* yang berdampak pada hadirnya maskapai penerbangan lain di Papua, sehingga pesawat berbadan lebar yang membutuhkan landasan pacu lebih panjang dapat mendarat dengan aman. *Runway* diperpanjang sepanjang 300 meter, dari sebelumnya 2.000 meter menjadi 2.300 meter.

Pada perpanjangan *runway* Bandara Rendani dilakukan penyelidikan tanah dengan *Standard Penetration Test* (SPT) pada empat titik bor, yang hasil pengujiannya menunjukkan bahwa tanah di lokasi didominasi oleh tanah lunak, khususnya tanah lempung dan tanah lanau. Tanah lunak memiliki daya dukung yang rendah, apabila tidak dilakukan perbaikan atau perkuatan pada tanah dasarnya akan timbul permasalahan seperti penurunan yang besar. Untuk memperbaiki tanah lunak, terdapat beberapa metode yang dapat dilakukan seperti stone column, PVD, kolom semen dan salah

satunya *Controlled Modulus Columns* (CMC), CMC dipilih dalam perbaikan tanah pada proyek ini karena dapat diaplikasikan pada berbagai jenis tanah lunak, mampu mengurangi penurunan tanah serta dapat meningkatkan daya dukung tanah.

Penelitian yang dilakukan Adhi (2022) berjudul "Evaluasi Perkuatan Tanah Dasar Menggunakan *Controlled Modulus Columns* (CMC) pada Pekerjaan Pembangunan Sirkuit Mandalika dengan Pemodelan Plaxis 8.6". Penelitian ini bertujuan untuk mengetahui jenis tanah dasar, mengetahui pengaruh CMC untuk lintasan sirkuit, dan mengetahui nilai *settlement* pada tanah. Nilai penurunan dan konsolidasi dianalisis selama 1 tahun, 3 tahun dan 10 tahun. Berdasarkan hasil dalam penelitian ini didapatkan bahwa penggunaan teknik CMC dapat menurunkan nilai *displacement* pada lokasi penelitian dan efektif dalam menurunkan nilai *pore water pressure* yang awalnya sebesar $-61{,}60\times10^{-15}$ kPa menjadi $-23{,}06\times10^{-12}$ setelah penggunaan CMC.

Penelitian Qoidunnas (2020) berjudul "Evaluasi Perkuatan Tanah Dasar Menggunakan *Controlled Modulus Columns* (CMC) pada Proyek Perpanjangan *Runway* Bandara Internasional Banyuwangi". Penelitian ini memiliki tujuan untuk mengetahui pemodelan perhitungan perkuatan tanah dengan CMC dan tanpa metode CMC dengan menggunakan *software* Plaxis 2D dan untuk mengetahui apakah CMC dapat diaplikasikan untuk meningkatkan daya dukung tanah dan mengurangi *settlement* di *runway*. Pada penelitian ini, pemodelan tanpa menggunakan CMC mendapatkan hasil penurunan konsolidasi sebesar 239 mm. Sedangkan pemodelan dengan CMC tiang tunggal dilakukan dua macam pemodelan, tanpa *prescribed* sebesar 8,125 mm dan dengan *prescribed* sebesar 5,322 mm. Pemodelan dengan CMC menggunakan *prescribed* menunjukkan nilai penurunan lebih rendah apabila dibandingkan dengan CMC tanpa *prescribed*, sehingga CMC *prescribed* dapat diaplikasikan untuk memperkecil penurunan.

Penelitian Aulia (2015) berjudul "Evaluasi Penggunaan *Controlled Modulus Columns* (CMC) di Bandara Soekarno-Hatta". Penelitian ini bertujuan untuk menganalis pengaruh teknik CMC dan mengevaluasi teknik CMC dengan data geoteknik yang telah didapat. Berdasarkan hasil dalam penelitian ini didapatkan bahwa pengaruh teknik CMC terdapat pada besarnya penurunan nilai defleksi tanpa CMC dan dengan CMC sebesar 48,90 mm. Pada penelitian ini, pemodelan tanpa CMC dan dengan CMC menunjukkan bahwa perbaikan tanah dengan CMC tidak mempercepat waktu konsolidasi. Pada pemodelan dalam penelitian ini juga terdapat perbedaan pada metode analisis dengan pihak sub-kontraktor sehingga menghasilkan hasil akhir yang berbeda

Tujuan dari penelitian ini adalah untuk mengevaluasi penurunan akibat konsolidasi jangka panjang tanpa metode CMC dan dengan metode CMC menggunakan *drained analysis* parameter efektif dengan material model Mohr-Coulomb pada software Plaxis 2D model *Axisymmetry*. Berdasarkan penelitian-penelitian terdahulu, belum terdapat pembahasan mengenai konsolidasi jangka panjang dengan menggunakan *drained analysis* parameter efektif.

2 METODOLOGI

Penelitian ini dilakukan di perpanjangan proyek *runway* Bandara Rendani yang terletak di Kelurahan Sowi, Kecamatan Manokwari Selatan, Kabupaten Manokwari, Provinsi Papua Barat.

Gambar 1. Lokasi perpanjangan *runway* Bandara Rendani

2.1 Konsep dan Mekanisme Kerja CMC

CMC merupakan salah satu jenis perkuatan tanah dengan menggunakan metode *rigid inclusions*. *Rigid inclusions* merupakan sebuah metode perbaikan tanah yang melibatkan penanaman elemen struktural yang kuat dan kaku ke dalam tanah lunak. Menurut Larisch (2014), *rigid Inclusions* merupakan salah satu perbaikan tanah yang dikembangkan di Prancis pada tahun 1990-an. Instalasi *rigid inclusions* biasanya dilakukan dengan alat pemancang. Tetapi, *rigid inclusions* berbeda dengan fondasi tiang karena perilaku penyebaran bebannya berbeda. Pada *rigid inclusions* beban didistribusikan antara kolom dan tanah sekitarnya, sedangkan fondasi tiang umumnya mentransfer beban hampir seluruhnya ke tanah keras melalui ujung atau gesekan samping.

CMC merupakan sistem perkuatan tanah dengan cara memasukkan auger berongga ke dalam tanah lunak, kemudian memompa grout melalui bagian tengah auger tersebut. Auger dikendalikan oleh alat berat dengan kapasitas torsi tinggi dan gaya tekan ke bawah yang besar, sehingga mendorong tanah ke samping dan tanpa sisa galian. Hal ini membuat kepadatan tanah di sekitar kolom meningkat sehingga daya dukung tanah juga meningkat. Ketika pengeboran telah mencapai kedalamannya, grout dipompa melalui tengah auger berongga seiring dengan proses penarikan auger ke atas sehingga membentuk kolom (Plomteux, dkk., 2004).

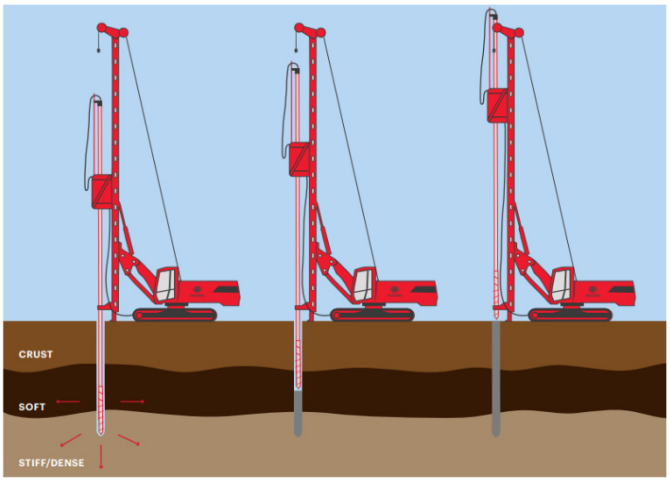

Gambar 2. Pemasangan CMC

Prinsip kerja metode CMC melibatkan penciptaan massa komposit antara tanah asli dan kolom grout yang memungkinkan peningkatan kekuatan atau daya dukung tanah dan pengurangan penurunan tanah. Massa komposit dalam metode CMC dihasilkan dari interaksi antara kolom grout dan tanah lunak. Daya dukung CMC berasal dari tahanan ujung pada kolom CMC yang memasuki lapisan tanah keras dan berasal dari gaya gesek (*side friction*) antara kolom dengan tanah yang berada di sekelilingnya. CMC menggunakan timbunan sebagai *Load Transfer Platform* (LTP) yang berfungsi untuk menyebarkan beban ke tiang kolom CMC dan beban kepada tanah dibawah timbunan.

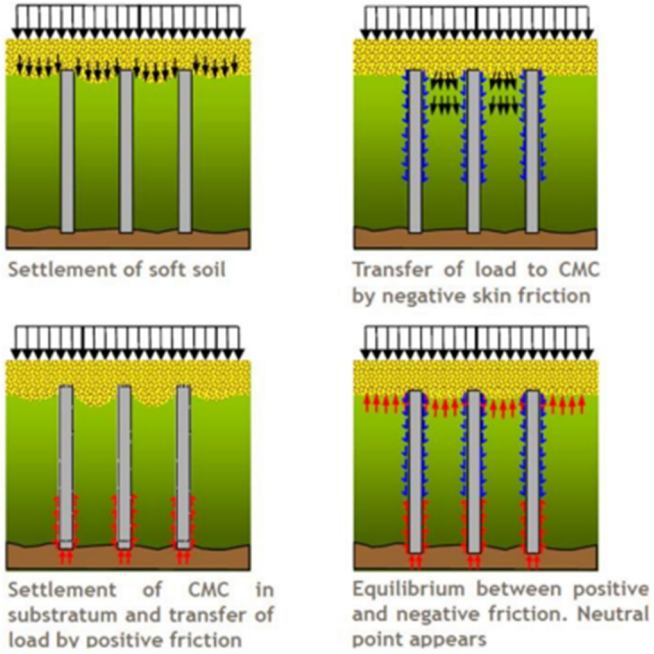

Gambar 3. Prinsip kerja CMC menurut Menard

2.2 Kriteria Desain Struktur *Runway*

Pada penelitian ini, terdapat kriteria desain yang menjadi acuan keberhasilan dari pemodelan yang akan dilakukan. Kriteria desain ini ditetapkan dengan mengacu pada Rencana Kerja dan Syarat (RKS) yang memuat persyaratan teknis dan standar pelaksanaan konstruksi. Kriteria desain tersebut diantaranya sebagai berikut:

a) Maksimal penurunan jangka panjang sebesar 100 mm selama 10 tahun pasca perbaikan tanah dilakukan.
b) *Differential settlement* pada *runway* baru maksimal 30 mm pada jarak 45 m.

Pada penelitian ini, hanya akan membahas maksimal penurunan sedangkan *differential settlement* tidak dibahas.

2.3 Analisis Data Tanah

Pada proyek perpanjangan runway Bandara Rendani, digunakan empat titik bor yaitu ADBH-01, ADBH-02, ADBH-03 dan ADBH-04.

2.3.1 Pembuatan stratigrafi

Pada perpanjangan *runway* Bandara Rendani, elevasi desain pada *runway* baru harus mengikuti elevasi dari *runway* eksisting. Kondisi natural pada area pekerjaan menunjukkan perbedaan elevasi, dimana elevasi dasar permukaan eksisting berada di bawah permukaan elevasi *runway* eksisting.

Kondisi ini mengharuskan adanya penimbunan di sekitar area rencana *runway* baru guna menyamakan elevasi dengan *runway* eksisting. Berdasarkan data tanah yang diterima, area dengan timbunan akan menimbulkan suatu masalah penurunan mengingat kondisi tanah di area tersebut didominasi oleh tanah lunak.

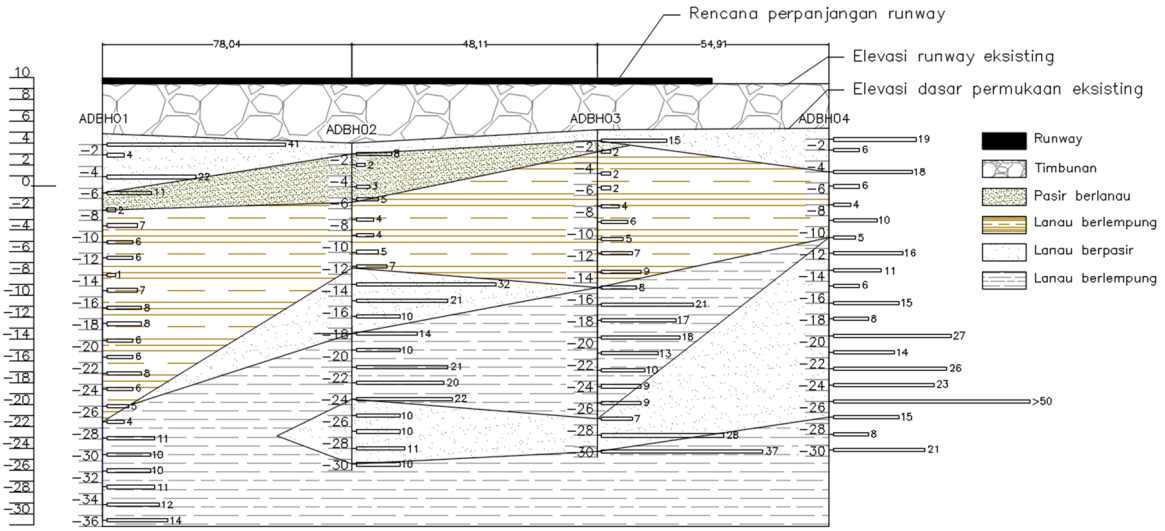

Gambar 4. Stratigrafi tanah

Berdasarkan Gambar 4, skema konstruksi akan melakukan penimbunan pada area rencana *runway* baru hingga menemui elevasi rencana pada desain. Elevasi permukaan tanah eksisting berada pada elevasi +3 m hingga +4 m dan elevasi desain akhir akan berada di elevasi +9,4 m. Sehingga, timbunan akan dilakukan hingga mencapai elevasi desain akhir dengan ketebalan sekitar 5 m.

2.3.2 Penentuan nilai N-*Design*

Berdasarkan data N-SPT dan elevasi yang ditunjukkan Gambar 4, dapat dibuat grafik yang menunjukkan nilai N-SPT pada elevasi yang sama pada setiap titik bornya.

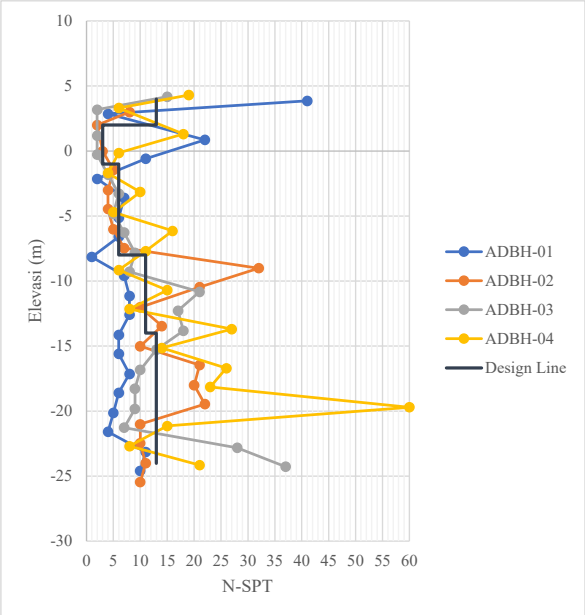

Gambar 5. Grafik hubungan N-SPT dengan elevasi.

Garis hitam pada grafik merupakan garis N-Design yang akan digunakan sebagai dasar untuk menentukan parameter tanah. Garis N-Design diperoleh berdasarkan data paling buruk pada tiap elevasinya, data yang buruk menunjukkan bahwa tanah pada elevasi tersebut memiliki N-SPT yang rendah. Menurut Hardiyatmo (2014), N-SPT di bawah delapan dalam jenis tanah lempung termasuk tanah dengan konsistensi lunak, sehingga dapat dikatakan tanah tersebut bermasalah dan dibutuhkan perbaikan atau perkuatan pada tanah dasarnya agar tidak terjadi penurunan yang tinggi di kemudian

hari. Berdasarkan Gambar 5, kedalaman elevasi dan lapisan tanah dapat disesuaikan dengan nilai N-SPT seperti pada Tabel 9 berikut:

Tabel 1. Nilai N-Design pada tiap lapisan tanah berdasarkan elevasi

No	Lapisan Tanah	Elevasi (m)		Ketebalan lapisan (m)	N-Design
		Atas	Bawah		
1	Lanau berpasir (kepadatan sedang)	4	2	2	13
2	Pasir berlanau (sangat lepas)	2	-1	1	3
3	Lanau berlempung (kekakuan sedang)	-1	-8	7	6
4	Lanau berlempung (kaku)	-8	-14	6	11
5	Lanau berpasir (kepadatan sedang)	-14	-24	10	13

2.4 Korelasi Parameter Tanah

Pada penelitian ini, pemodelan dilakukan untuk menganalisis konsolidasi jangka panjang, sehingga pemodelan menggunakan *drained analysis* dengan parameter efektif. Parameter efektif merupakan parameter yang telah terdrainase, dalam penelitian ini digunakan parameter kuat geser efektif (c' dan ϕ'). Parameter lain yang digunakan dalam pemodelan meliputi berat volume tanah, modulus young (E), *Poisson's ratio* (v') dan permeabilitas (k). Parameter tanah dalam penelitian ini diperoleh melalui korelasi antara jenis tanah dan nilai N-Design, dengan rentang nilai parameter mengacu pada literatur.

2.4.1 Berat volume tanah

Berat volume tanah adalah perbandingan antara berat tanah dengan volume totalnya, termasuk ruang kosong (*void*) yang berada di dalam tanah. Mengacu pada parameter berat volume tanah yang disarankan oleh John Wiley & Sons (2000) (dalam Dicky, 2016), hasil korelasi terhadap lapisan tanah yang dapat dilihat pada tabel berikut:

Tabel 2. Parameter berat volume tanah

No	Lapisan Tanah	γsat (kN/m^3)	γdry (kN/m^3)
1	Lanau berpasir	19	16
2	Pasir berlanau	17	15
3	Lanau berlempung	16	14
4	Lanau berlempung	18	16
5	Lanau berpasir	19	16

2.4.2 Kohesi efektif (c') dan sudut geser dalam efektif (ϕ')

Karena pemodelan pada penelitian ini untuk analisis konsolidasi jangka panjang, maka pemodelan menggunakan *drained analysis* yang menggunakan parameter efektif. Parameter efektif merupakan parameter yang telah terdrainase, dalam penelitian ini digunakan parameter kuat geser efektif (c' dan ϕ'). Kohesi efektif dan sudut geser dalam efektif merupakan dua parameter dalam analisis kekuatan geser tanah yang dapat mempengaruhi stabilitas dan daya dukung tanah. *Australian Standards for retaining walls* (AS 4678) mengusulkan kedua parameter tersebut berdasarkan kelompok tanah.

Tabel 3. Parameter kuat geser kohesi efektif dan sudut geser dalam efektif

No	Lapisan Tanah	c' (kPa)	ϕ' (°)
1	Lanau berpasir	1	30
2	Pasir berlanau	1	23
3	Lanau berlempung	5	25
4	Lanau berlempung	5	25
5	Lanau berpasir	1	30

2.4.3 Modulus Young (E) dan *Poisson's Ratio* (v')

Modulus young merupakan nilai elastisitas suatu lapisan tanah yang hasilnya merupakan nilai perbandingan antara tegangan yang terjadi terhadap regangan. Menurut Bowles (1996), nilai modulus elastisitas dapat diperoleh dengan menggunakan data N-SPT berdasarkan jenis tanahnya. Selain dengan data N-SPT, menurut Bowles (1995) nilai modulus young dan *Poisson's ratio* juga dapat diperoleh berdasarkan dengan jenis lapisan tanah di tempat penyelidikan, untuk nilainya dapat dilihat pada Tabel 4 berikut:

Tabel 4. Parameter modulus young dan *Poisson's ratio*

No	Lapisan Tanah	N-Design	v' (kPa)	Ey (kPa)
1	Lanau berpasir	13	0,35	5.700
2	Pasir berlanau	3	0,40	2.700
3	Lanau berlempung	6	0,30	3.600
4	Lanau berlempung	11	0,30	5.100
5	Lanau berpasir	13	0,35	5.700

2.4.4 Permeabilitas (k)

Menurut Darwis (2018), permeabilitas merupakan kemampuan yang dimiliki tanah untuk meloloskan aliran air melalui pori-pori tanah tersebut. Pasir memiliki permeabilitas yang tinggi, hal ini berakibat kepada laju aliran air yang tinggi. Sementara itu, jenis tanah lempung termasuk ke dalam tanah halus yang memiliki ukuran butir yang lebih kecil, sehingga ruang kosong yang tercipta di antara partikel-partikel tanah menjadi terbatas dan air sulit untuk mengalir.

Nilai korelasi parameter permeabilitas dengan jenis tanah dapat dilihat pada Tabel 5 berdasarkan penelitian yang dilakukan oleh Verruijt pada tahun 2001 mengenai koefisien permeabilitas pada berbagai jenis tanah yang sudah dikonversi dalam satuan meter per hari.

Tabel 5. Parameter permeabilitas

No	Lapisan Tanah	k (m/hari)
1	Lanau berpasir	0,00864
2	Pasir berlanau	0,0864
3	Lanau berlempung	0,000864
4	Lanau berlempung	0,000864
5	Lanau berpasir	0,00864

Material model dalam pemodelan ini menggunakan Mohr-Coloumb. Rekapitulasi hasil dari korelasi parameter tanah dapat dilihat pada Tabel 6 berikut:

Tabel 6. Hasil korelasi parameter tanah

No	Lapisan Tanah	N-Design	γsat (kN/m^3)	γdry (kN/m^3)	ν' (kPa)	c' (kPa)	ϕ' (deg)	Ey (kPa)	k (*m/day*)
1	Lanau berpasir	13	19	16	0,35	1	30	5.700	0,00864
2	Pasir berlanau	3	17	15	0,40	1	23	2.700	0,0864
3	Lanau berlempung	6	16	14	0,30	5	25	3.600	0,000864
4	Lanau berlempung	11	18	16	0,30	5	25	5.100	0,000864
5	Lanau berpasir	13	19	16	0,35	1	30	5.700	0,00864

2.5 Perencanaan Pembebanan

Karena penelitian ini menggunakan pemodelan *Axisymmetry*, maka terdapat beberapa lapisan yang tidak masuk ke dalam pemodelan. Oleh sebab itu, dilakukan asumsi beban yang bekerja di atas *runway* yang dapat dilihat pada Tabel 7 berikut:

Tabel 7. Beban yang bekerja pada *runway* (Menard, 2021)

Material	Berat (kN/m^3)	Tebal (m)	Beban (kPa)
Aircraft load	-	-	15,00
Ashpalt	23	0,10	2,30
Base layer	20	0,20	4,00
Base course	23	0,30	6,90
Total			28,20

Pada material *aircraft load,* asumsi beban didapat berdasarkan pada Rencana Kerja dan Syarat (RKS). *Aircraft load* adalah beban pesawat yang akan melintasi *runway*.

2.6 Perhitungan Tebal LTP (*Load Transfer Platform*)

CMC menggunakan timbunan sebagai *Load Transfer Platform* (LTP) yang berfungsi untuk menyebarkan beban ke tiang kolom CMC dan beban kepada tanah dibawah timbunan. Dalam Tabel 8, Menard menyarankan perhitungan tebal minimal LTP berdasarkan dengan estimasi penurunan tanah tanpa perkuatan CMC. Nilai penurunan tanah yang telah diperoleh kemudian diklasifikasikan ke dalam rentang perkiraan penurunan untuk menentukan rumus yang digunakan dalam perhitungan tebal LTP.

Tabel 8. Tebal minimum LTP (Menard, 2021)

Perkiraan Penurunan Tanah Termasuk *Creep Settlement* Tanpa Perkuatan Tanah	Rekomendasi Menard
W < 5 cm (2 inci)	Tidak ada rekomendasi
5 cm (2 inci) ≤ w ≤ 12,5 cm (5 inci)	$H_{crit} = 0{,}7\ (s - a)$ $s \leq a + H/0\,{,}7$
12,5 cm (5 inci) ≤ w ≤ 25 cm (10 inci)	$H_{crit} = 1{,}0\ (s - a)$ $s \leq a + H$
25 cm (10 inci) ≤ w ≤ 50 cm (20 inci)	$H_{crit} = 1{,}5\ (s - a)$ $s \leq a + H/1{,}5$
w > 50 cm (20 inci)	$H_{crit} = 1{,}8\ (s - a)$ $s \leq a + H/1{,}8$

dengan:

w = perkiraan penurunan tanah tanpa perkuatan

H_{crit} = ketebalan LTP yang akan digunakan

H = ketebalan LTP yang digunakan

s = spasi antar kolom

a = diameter kolom

Nilai tebal LTP awal diasumsikan untuk memperoleh perkiraan nilai penurunan dan pada pemodelan awal tebal LTP diasumsikan 1,70 m. Dengan tebal LTP 1,70 m, diperoleh penurunan sebesar 59,65 cm. Berdasarkan hasil penurunan dari simulasi awal tersebut, digunakan rumus rekomendasi Menard untuk menghitung tebal LTP yang direkomendasikan. Dari hasil perhitungan tersebut diperoleh nilai tebal LTP yang akan digunakan pada pemodelan selanjutnya sebesar 2 m.

Tabel 9. Elevasi timbunan dan LTP

No	Lapisan Tanah	Elevasi (m)		Ketebalan lapisan (m)
		Atas	Bawah	
1	Timbunan	9,40	6,00	3,40
2	LTP	6,00	4,00	2,00

Selain itu, dalam pemodelan juga dibutuhkan parameter untuk timbunan dan LTP yang dapat dilihat pada Tabel 10 berikut:

Tabel 10. Parameter timbunan dan LTP

No	Lapisan Tanah	γsat (kN/m^3)	γdry (kN/m^3)	ν' (kPa)	c' (kPa)	ϕ' (deg)	Ey (kPa)	k (*m/day*)
1	Timbunan	20	18	0,30	1	20	25.000	86,40
2	LTP	20	18	0,35	1	32	40.000	86,40

2.7 Pemodelan dengan Plaxis 2D Model *Axisymmetry*

Pemodelan pada penelitian ini menggunakan model *Axisymmetry*, model ini digunakan pada struktur yang berbentuk melingkar dengan beban atau tekanan yang berada di sekelilingnya dianggap sama pada seluruh bagian benda tersebut. Pada model ini, lingkup geometri yang dapat dimodelkan hanya satu buah CMC, sehingga diameter yang digunakan untuk pemodelan adalah setengah dari diameter aslinya.

Pemodelan dilakukan menggunakan model *Axisymmetry* untuk merepresentasikan perilaku lokal di sekitar satu kolom CMC yang bekerja di bawah beban merata. Meskipun kondisi asli pada konstruksi *runway* bersifat *plane strain* tetapi pendekatan *Axisymmetry* masih dianggap representatif. Hal ini dikarenakan jarak antar kolom CMC yang seragam serta distribusi beban di atas permukaan tanah yang relatif merata, sehingga setiap kolom mengalami kondisi pembebanan yang hampir identik.

Karena pada penelitian ini pemodelan yang digunakan merupakan model *Axisymmetry*, maka posisi permukaan air tanah pada keempat titik bor akan ditentukan dengan rata-rata. Nilai *Groundwater Level* (GWL) atau posisi permukaan air tanah masing-masing titik bor berdasarkan data *Bore log* apabila dihitung rata-ratanya berada di elevasi +2,53 m.

Pemodelan pada penelitian ini menggunakan *calculation type Plastic*, karena analisis dilakukan dengan parameter efektif (*drained analysis*). Pemilihan kondisi *drained* dilakukan karena penelitian berfokus pada evaluasi penurunan jangka panjang (*long-term settlement*) setelah proses konsolidasi selesai, di mana tekanan air pori berlebih telah terdisipasi dan tanah berperilaku dalam kondisi *drained*. Maka dari itu *calculation type Consolidation* juga tidak digunakan.

Pada proyek perpanjangan runway Bandara Rendani, CMC dipasang dalam pola grid persegi dengan spasi antar tiang 1,50 m, diameter sebesar 420 mm, dan panjang 24 m. CMC dipasang menggunakan pola grid persegi dan dengan material mortar dengan fc 15 MPa.

Karena CMC dipasang menggunakan pola grid persegi tetapi dalam model *Axisymmetry* hanya dapat memodelkan dalam bentuk lingkaran, menurut IREX (2012), bentuk persegi dari satu kolom grid diubah menjadi lingkaran yang luasnya sama dengan luas grid sebenarnya. Oleh karena itu, dibutuhkan nilai jari-jari ekuivalen dari lingkaran yang akan digunakan sebagai batas geometri sumbu x. Konfigurasi tiang juga dapat memengaruhi dimensi pada model, khususnya pada pemodelan *Axisymmetry*. Hal ini karena untuk menentukan dimensi model dibutuhkan data pola dan jarak antar tiang CMC guna memperoleh nilai jari-jari ekuivalen yang digunakan dalam pemodelan. Untuk mencari jari-jari ekuivalen tersebut dapat menggunakan perhitungan sebagai berikut:

$$R = \sqrt{\frac{spasi \times spasi}{\pi}} \quad (1)$$

$$R = \sqrt{\frac{1{,}5 \times 1{,}5}{\pi}}$$

$$R = 0{,}846\ m$$

Berdasarkan pada perhitungan di atas, batas geometri untuk sumbu x maksimal yang digunakan pada penelitian ini adalah 0,846 m.

2.7.1 Pemodelan tanah timbunan tanpa perkuatan

Pemodelan yang pertama dilakukan pada penelitian ini adalah memodelkan tanah timbunan tanpa perkuatan. Model yang diaktifkan hanya timbunan, LTP, lapisan tanah dan beban merata sebesar 28,20 kPa di atas *runway*.

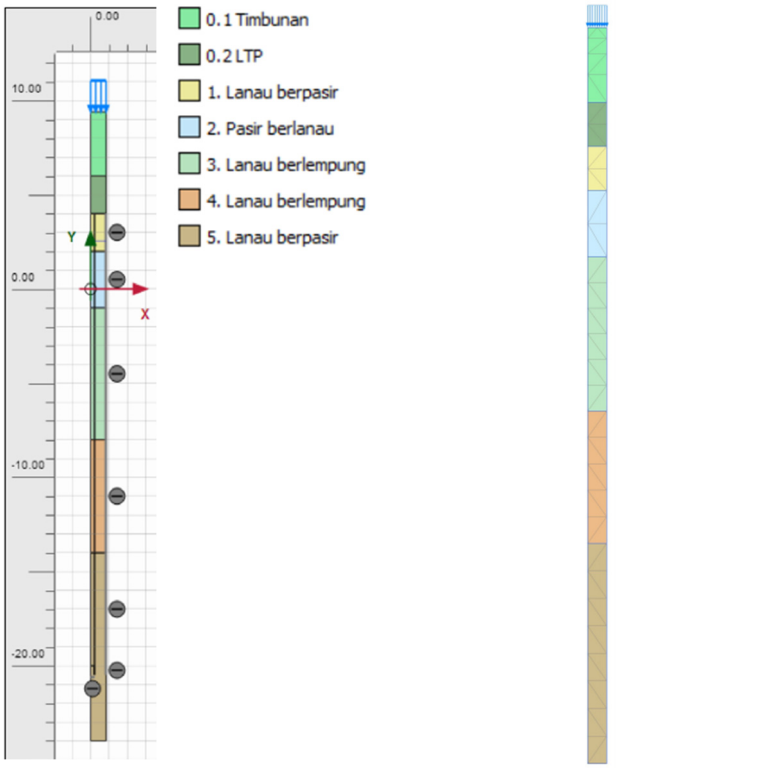

a) Pemodelan geometri tanpa perkuatan **b) M*esh model* tanpa perkuatan**

Gambar 6. Pemodelan tanpa perkuatan

Didapatkan besarnya penurunan tanah tanpa perkuatan sebesar 0,57 m dapat dilihat pada Gambar 7 berikut:

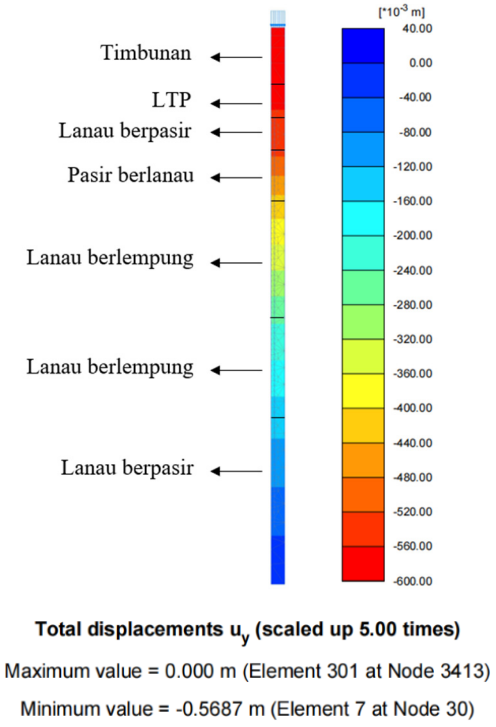

Gambar 7. Hasil pemodelan tanpa perkuatan

2.7.2 Pemodelan tanah timbunan dengan perkuatan CMC

Selanjutnya, pemodelan dilakukan dengan perkuatan CMC. Untuk model yang diaktifkan sama seperti sebelumnya namun ditambah dengan model CMC dan *interface*. *Interface* berfungsi sebagai elemen pemodelan yang mempresentasikan kondisi kontak antara tanah dan struktur, seperti pada perkuatan CMC. Nilai kekuatan relatif pada elemen tersebut dinyatakan dengan Rinter, Rinter merupakan faktor reduksi yang digunakan untuk merepresentasikan kekuatan geser relatif pada antarmuka struktur tanah terhadap kekuatan geser tanah asli. Berdasarkan Brinkgreve & Shen dalam Gouw (2014), rentang nilai Rinter untuk interaksi pasir dengan beton adalah 0,8 – 1,0 dan untuk lempung dengan beton adalah 0,7 – 1,0. Oleh karena itu, dipilih nilai tengah yang merepresentasikan kedua sifat tanah tersebut, yaitu 0,9.

Pemodelan CMC akan digunakan setengah dari diameter sebenarnya yaitu sebesar 0,21 m. CMC juga membutuhkan parameter yang akan diinput untuk pemodelan pada Plaxis. Menurut IREX (2012), modulus elastisitas untuk mortar yang digunakan pada CMC dapat menggunakan persamaan di bawah ini.

$$E = 2.700\, f_{ck}^{\frac{1}{3}} \qquad (2)$$

dengan:

f_{ck} = kuat tekan mortar pada umur 28 hari (MPa)

Apabila menggunakan perhitungan dalam persamaan (2) maka nilai modulus elastisitas CMC diperoleh sebesar 6658772,601 dalam satuan kPa. Sehingga, dapat direkapitulasi input parameter CMC pada Tabel 11 di bawah ini:

Tabel 11. Input parameter CMC

Tipe	*Material model*	*Drainage tupe*	E' (kPa)	ν' (kPa)
CMC	*Linear elastic*	*Drained*	6658772,601	0,200

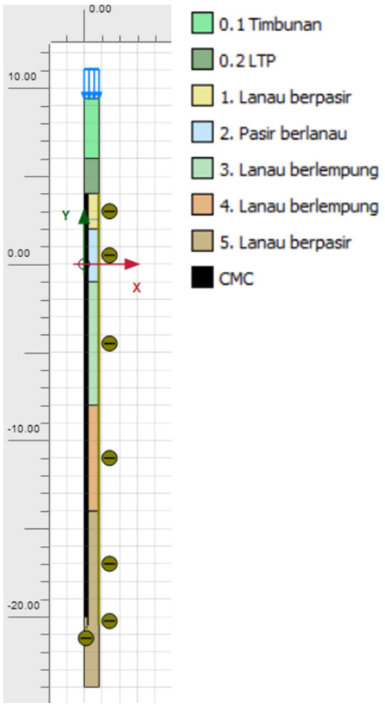

a) Pemodelan geometri dengan perkuatan CMC **b) *Mesh model* dengan perkuatan CMC**

Gambar 8. Pemodelan dengan perkuatan CMC

Didapatkan besarnya penurunan tanah dengan perkuatan CMC sebesar 0,093 m dan tegangan efektif sebesar 2333 kN/m^2 dapat dilihat pada Gambar 9 berikut:

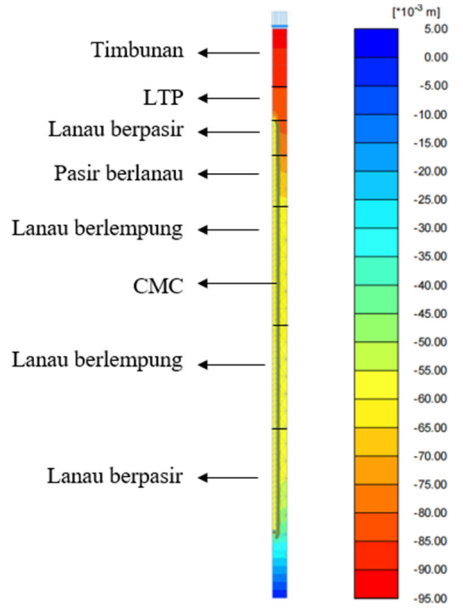

Total displacements u_y (scaled up 10.0 times)

Maximum value = 0.000 m (Element 301 at Node 3413)

Minimum value = -0.09268 m (Element 7 at Node 7)

a) Total penurunan dengan CMC

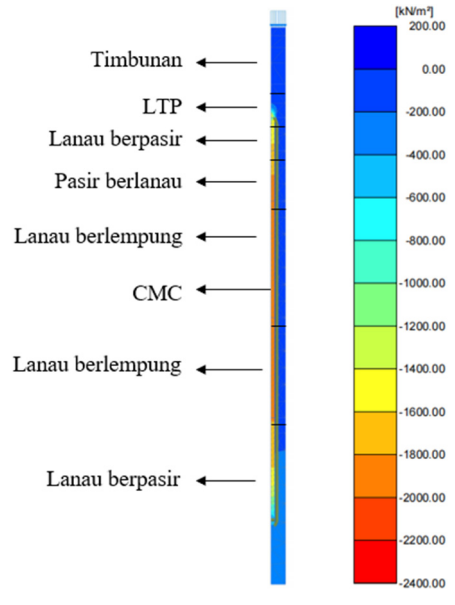

Cartesian effective stress σ'_{yy} (scaled up 0.500*10^{-3} times)

Maximum value = -2.343 kN/m² (Element 41 at Node 254)

Minimum value = -2333 kN/m² (Element 27 at Node 248)

b) Tegangan efektif dengan CMC

Gambar 9. Hasil pemodelan dengan perkuatan CMC

Tabel 12. Pengecekan tegangan pada kolom CMC

Diameter CMC (m)	Area CMC (m^2)	σ'yy (MPa)	*Allowable stress* (MPa)	Keterangan
0,42	0,14	2,33	7	σ'yy < σ *allowable* = OK

Berdasarkan hasil di atas, penurunan jangka panjang yang terjadi adalah sebesar 92,68 mm dimana nilai ini di bawah dari penurunan izin yaitu sebesar 100 mm selama 10 tahun. Sementara itu, tegangan yang terjadi pada kolom CMC pada beban maksimum sebesar 2,33 MPa yang mana menurut IREX (2012), nilai ini di bawah tegangan izinnya sebesar 7 MPa. Dalam kondisi ini, CMC tidak dalam kondisi *overstress*.

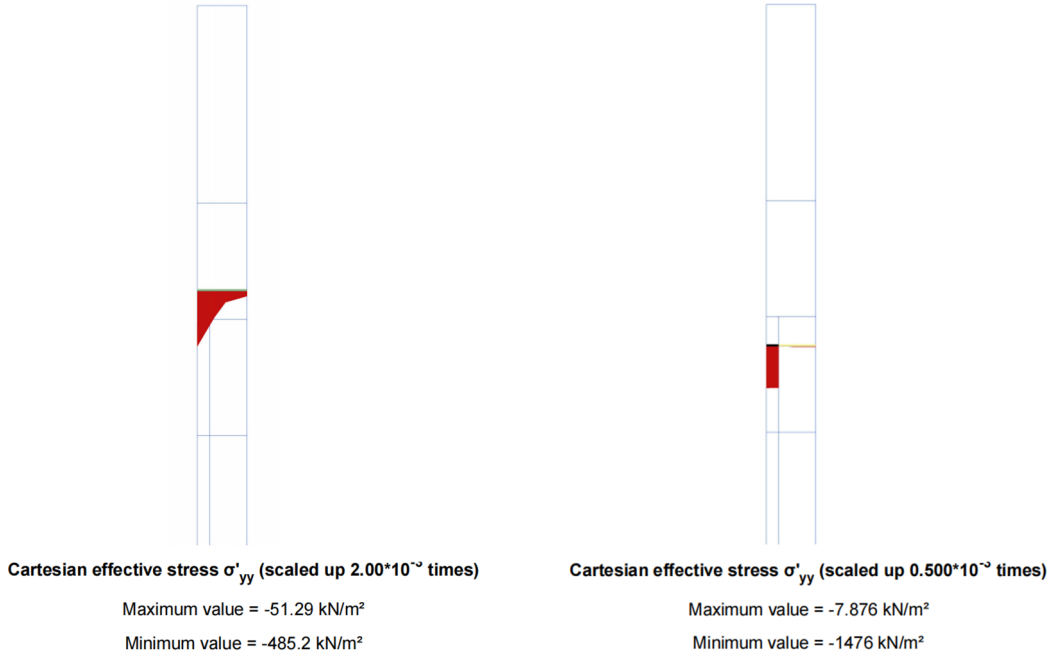

a) Tegangan efektif pada tanah b) Tegangan efektif pada CMC

Gambar 10. Tegangan efektif pada tanah dan CMC

Berdasarkan gambar 10, hasil menunjukkan bahwa tegangan efektif vertikal pada CMC lebih besar dibanding tanah di sekitarnya. Hal ini menandakan bahwa beban dari permukaan lebih mendominasi diteruskan melalui CMC karena kekakuannya yang lebih tinggi, kemudian sebagian beban ditransfer ke tanah melalui gesekan di sepanjang sisi kolom dan pada ujung kolom. Dengan demikian, transfer beban terjadi secara kombinasi antara CMC dan tanah, membentuk sistem kerja komposit.

3 HASIL DAN PEMBAHASAN

Dari hasil analisis pada penelitian ini, didapatkan hasil penurunan tanah serta tegangan efektif tanah tanpa perkuatan dan dengan perkuatan CMC. Hasil rangkuman dapat dilihat pada Tabel 13 berikut:

Tabel 13 Hasil pemodelan dengan Plaxis 2D

Pemodelan	Total penurunan (mm)	Tegangan efektif vertikal (MPa)
0,42	0,14	2,33

Berdasarkan hasil pemodelan di atas, perkuatan tanah dengan menggunakan CMC mampu mengurangi penurunan tanah hingga 83,70% dibandingkan dengan kondisi tanah tanpa perkuatan. Metode ini dapat dikatakan sangat efektif untuk diterapkan pada kondisi tanah lunak seperti di lokasi penelitian untuk mengurangi penurunan tanah pada konsolidasi jangka panjang. Penurunan dengan menggunakan CMC juga termasuk memenuhi syarat kriteria desain yaitu berada di bawah 100 mm selama 10 tahun.

Tegangan efektif pada kondisi menggunakan perkuatan tanah dengan CMC menunjukan distribusi beban tidak hanya tersalurkan ke tanah lunak, tetapi juga disalurkan ke elemen CMC yang lebih kaku. Perbedaan kekakuan ini menyebabkan pembagian beban tidak merata, di mana beban terfokus pada kolom dengan luas penampang yang relatif kecil, sehingga menghasilkan nilai tegangan yang lebih besar.

4 KESIMPULAN

4.1 Kesimpulan

Berdasarkan hasil pemodelan studi kasus yang dilakukan pada perpanjangan *runway* Bandara Rendani, dapat disimpulkan bahwa:

a) Berdasarkan hasil analisis, diperoleh jenis tanah beserta elevasi dan nilai N-Design untuk perencanaan:
   Elevasi +4 m s.d. +2 m : Lanau berpasir (N-design = 13)
   Elevasi +2 m s.d. -1 m : Pasir berlanau (N-design = 3)
   Elevasi -1 m s.d. -8 m : Lanau berlempung (N-design = 6)
   Elevasi -8 m s.d. -14 m : Lanau berlempung (N-design = 11)
   Elevasi -14 m s.d. -24 m : Lanau berpasir (N-design = 13)
b) Dari perhitungan yang dilakukan pada pemodelan tanah tanpa perkuatan, didapat penurunan tanah sebesar 568,70 mm. Sedangkan, pada pemodelan tanah dengan perkuatan, didapat penurunan tanah sebesar 92,68 mm dan tegangan efektif vertikal sebesar 2333 kN/m^2.
c) Perkuatan tanah menggunakan metode CMC mampu mengurangi 83,70% dibandingkan dengan kondisi tanah tanpa perkuatan. Hal ini dapat menunjukkan bahwa metode perkuatan tanah dengan CMC sangat efektif untuk mengurangi penurunan tanah akibat konsolidasi jangka panjang.
d) Penurunan pada pemodelan ini sudah sesuai dengan kriteria izin yaitu di bawah 100 mm.
e) Untuk menghindari estimasi penurunan dengan menggunakan *undrained A*, dapat menggunakan *drained analysis* untuk menentukan potensi penurunan jangka panjang tanpa ada pengaruh *excess pore pressure*.

4.2 Saran

Dengan mempertimbangkan batasan dan metode pada penelitian ini, disampaikan beberapa saran untuk mendukung pengembangan penelitian selanjutnya sebagai berikut:

a) Dalam pemodelan menggunakan Plaxis 2D, dapat menggunakan material model tanah yang lebih representatif terhadap kondisi nyata seperti *Hardening Soil* dan *Soft Soil*.
b) Pemodelan ini menggunakan *drained analysis* sehingga tidak menggunakan *staged construction*, pada pemodelan selanjutnya dapat menggunakan *Undrained A analysis* dengan *staged construction* sehingga dapat dilakukan pengecekan penurunan pada tiap tahapan konstruksi.
c) Untuk memperoleh *differential settlement* dapat dilakukan pemodelan dengan menggunakan masing-masing *bore log* dengan jarak 45 m pada tiap lokasinya.
d) Pemodelan dalam penelitian ini menggunakan model *Axisymmetry*, dengan asumsi beban operasional tersebar seragam sepanjang kedalaman. Karena pendekatan ini cenderung konservatif, perlu dilakukan analisa *Plane Strain* untuk melihat penurunan akibat beban yang tersebar secara lebih nyata.

DAFTAR PUSTAKA

Adhi, H. E. M. A., 2022. *Evaluasi Perkuatan Tanah Dasar Menggunakan Controlled Modulus Columns (CMC) pada Pekerjaan Pembangunan Sirkuit Mandalika dengan Pemodelan Plaxis 8.6*, Yogyakarta: Bachelor Thesis Report. Department of Civil and Environmental Engineering. Universitas Gadjah Mada.

Aulia, G., 2015. *Evaluasi Penggunaan Controlled Modulus Columns (CMC) di Bandara Soekarno-Hatta*, Yogyakarta: Bachelor Thesis Report. Department of Civil and Environmental Engineering. Universitas Gadjah Mada.

Bowles, J. E., 1996. *Foundation Analysis and Design*. Singapore: The Mc-Graw-Hill Companies.

Darwis, 2018. *Dasar-dasar Mekanika Tanah*. Yogyakarta: Pena Idris.

Das, B. M., 1995. *Mekanika Tanah (Prinsip-prinsip Rekayasa Geoteknis)*. Jakarta: Penerbit Erlangga.

Dinard, T. & Hubaut, A., 2022. *Application of CMC for treatment of steel fuel tank foundations in Kwinana, Western Australia*. Australia, International Conference on Soil Mechanics and Geotechnical Engineering.

Gouw. T.-L., 2014. Common Mistakes on the Application of Plaxis 2D in Analyzing Excavation Problems. *International Journal of Applied Engineering Research 9*, pp. 8291–8311.

Gusnadi, Z., Handiman, I. & Fitriana, S., 2023. Analisa Perbaikan Tanah Lunak Menggunakan Controlled Modulus Columns (CMC) pada Konstruksi Timbunan Jalan. *Jurnal Ilmiah Teknik Sipil 4*, pp. 11–16.

Hardiyatmo, H. C., 2014. *Analisis dan Perancangan Fondasi I*. Yogyakarta: Gadjah Mada University Press.

IREX, 2012. *ASIRI National Project: Recommendations for the design, construction and control of rigid inclusion ground improvements*, Paris.

Larisch, M., 2014. *Behaviour of stiff, fine-grained soil during the instalation of screw auger displacement*, Queensland: Doctoral Dissertation. Geotechnical Engineering Centre. The University of Queensland.

Plomteux, C., Porbaha, A. & Spaulding, C., 2004. CMC Foundation System for Embankment Support - A Case History. *GeoSupport 2004: Drilled Shafts, Micropiling, Deep Mixing, Remedial Methods, and Specialty Foundation Systems*, pp. 980–992.

Qoidunnas, A., 2020. *Evaluasi Perkuatan Tanah Dasar Menggunakan Controlled Modulus Columns (CMC) pada Proyek Perpanjangan Runway Bandara Internasional Banyuwangi*, Surabaya: Bachelor Thesis Report. Departemen Teknik Infrastruktur Sipil. Institut Teknologi Sepuluh November.

Veeruijt, A., 2001. *Soil Mechanics*. Delft: Delft University of Technology.

This page is intentionally left blank

HIMPUNAN AHLI TEKNIK TANAH INDONESIA - HATTI
Indonesian Society for Geotechnical Engineering - ISGE
PIT HATTI XXIX
10-12 November 2025

Development Distributed Acoustic Wave Sensing with Fiber Optics for Vibration and Structural Monitoring

Bagus Endar B. Nurhandoko[1*], Fadhil Muddasir[1], Insan Rizal Komara[2,3], Wisnu Adi Guntara[2,3], Indriani Sukmana[2,3], Wildan Fauzi Akbar[2,3], Yoga Hariman[2,3], Harry Mahardika[1], Alvina K. Kuncoro[1], Alfi Nur Albab[2], Ratih Pratiwi[2,3]

[1]Earth Physics and Complex System Research Division, Faculty of Mathematics and Natural Sciences, Institut Teknologi Bandung, Indonesia, 40132
[2]Wave Inversion and Subsurface Imaging Research Lab, Faculty of Mathematics and Natural Sciences, Institut Teknologi Bandung, Indonesia, 40132
[3]Rock Fluid Imaging Lab., Bandung, Indonesia, 40124
*Correspondence: bagus@itb.ac.id

ABSTRACT Fiber optic cables can provide distributed strain and wave sensing. When laser light is emitted from one end of the optical fiber and it propagates toward the opposite end, a small portion of this light is scattered by minor defects and changes in material properties. Then it reflects along the length of the fiber optic cables. The anomaly of fiber optic material produces backscattering phenomena that can propagate in the direction back toward the laser source. The characteristics of the scattered light can be put into the three primary categories: Rayleigh, Brillouin, and Raman scattering. In the Distributed Acoustic Sensing (DAS) fiber optic wave sensing, we consider Rayleigh's scattering as the primary source of backscattering wave energy. The DAS systems based on Rayleigh scattering provide distributed strain and wave sensing by performing some interference processing through optical and numerical processing. This optical-acoustics wave measurement technology is relatively new in Indonesia. In this paper, we show laboratory test of fiber optics wave sensing. The pressure wave through backscattering laser light were detected using a high-speed Analog to Digital Converter (ADC). It indicated the position of acoustic wave in a fiber optic cable with hundreds over thousands of meters in length. Under conditions of "vibration on", the test results demonstrate the feasibility of fiber optics as distributed acoustic wave sensing.

KEYWORDS: Fiber Optic Sensing; Distributed Acoustic Wave Sensing; Rayleigh Scattering

1 INTRODUCTION

Given their wide frequency range, acoustic waves are both feasible and essential to be monitored. The detection of acoustic waves serves as a valuable indicator across diverse fields, including but not limited to structural health monitoring (Dang et al., 2020), information security (Liu et al., 2021), pipeline leakage monitoring (Hull et al., 2020), characterization of fracture geometry and propagation in hydraulic fracturing (Zhang et al., 2020), and earthquake detection (Hernandez et al., 2022). Traditionally, the detection of acoustic waves has been acquired by applying piezoelectric crystals that have stretch-ability and integrate-ability for diverse applications (Sezer and Koc, 2021). However, piezoelectric sensing capability is restricted to dynamic measurements, as an electrical charge is only generated if there is pressure or strain variation. Thus, it is not suitable for detecting static forces. In contrast, for example in seismic cases, fault slip as a significant deformation can occur even under relatively constant stress levels (Zoback, 2007).

More recently, fiber optics has been developed to cover the drawback of piezoelectric as an acoustic wave sensor. In spite of the higher cost of individual optical fiber sensor and acoustic laser interferometry than that of piezoelectric transducers, the single acoustic laser interferometry can monitor many sensors simultaneously, often reducing the overall cost of an acoustic wave measurement system (Soman et al., 2021). In addition, fiber optic cables can maintain the wave amplitude or energy in order to transmit the wave signal to a longer distance, owing to their inherently low transmission loss (Bao and Wang, 2021).

This study aims to examine the sensing of distributed strain and acoustic waves using fiber optics in laboratory scale under DAS measurement. Among three primary categories of scattered light, we consider Rayleigh's backscattering (RBS) as the primary source of backscattering wave energy which provides distributed strain and acoustic waves. We applied a high-speed ADC with significantly higher sample rate than the wave highest frequency intended for detecting a rapid change in wave pressure through the backscattering of the laser light to capture the waveform accurately.

2 METHODS

The DAS is set up as configuration shown by Figure 1. The setup system of DAS consists of fiber optic cables as a transducer, laser interferometry system as light source generator and converter hardware, and a PC as the main processor of the measured waveform.

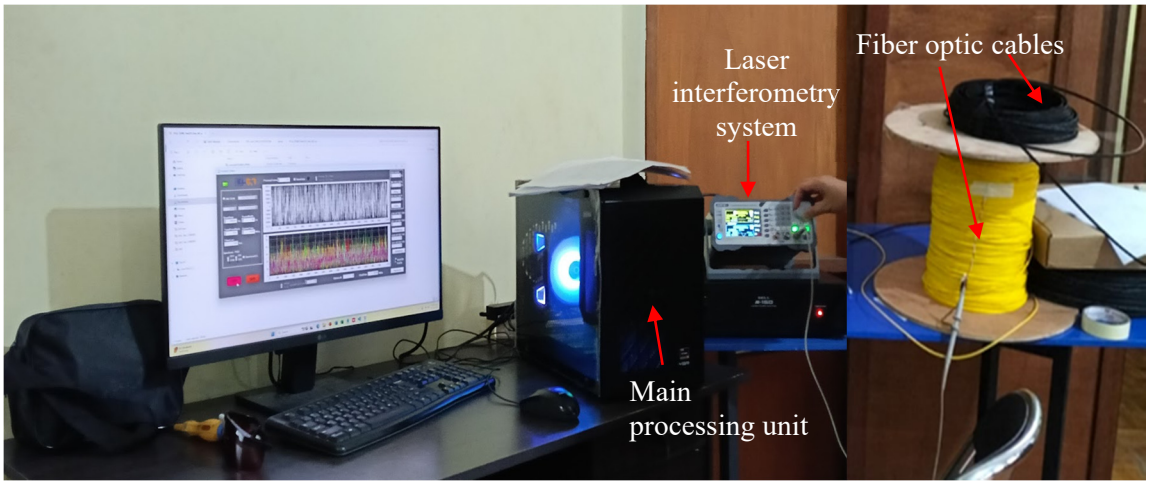

Figure 1. Laboratory setup of the DAS.

The working principle of the system is based on Optical Time Domain Reflectometry (OTDR), as shown in Figure 2. From a Narrow Linewidth Laser (NLL) inside an acoustic laser interferometry, a coherent laser light ($\approx$ 1550 nm) was shot to activate the DAS system. Optical Coupler 1(OC1) is used to direct light from one input (a laser light) to two light emissions with a delay fiber to separate them temporarily. The first light emission passed Acousto-Optic Modulators 1 (AOM1) and was then sent to OC2, while the second light propagated through AOM2 and was subsequently transmitted through the delay fiber for frequency shifting. As the second signal -functioned as the "reference arm of the interferometer"- arrived at OC2, it was combined with the first one to create a single signal. This signal was then amplified by Erbium-doped Fiber Amplifier (EDFA), then injected to the fiber cables through a circulator. The three-port circulator transferred the backscattered Rayleigh signal carrying vibration information from the fiber toward another EDFA. The amplified optical signal was passed through an optical filter to suppress amplified spontaneous emission noise, after which it was detected by a Balanced Photodiode (BPD) to generate a beat signal. Beat signal then was sampled by Data Acquisition Card (DAQ) to split its in-phase (I) and quadrature (Q) part of the signal.

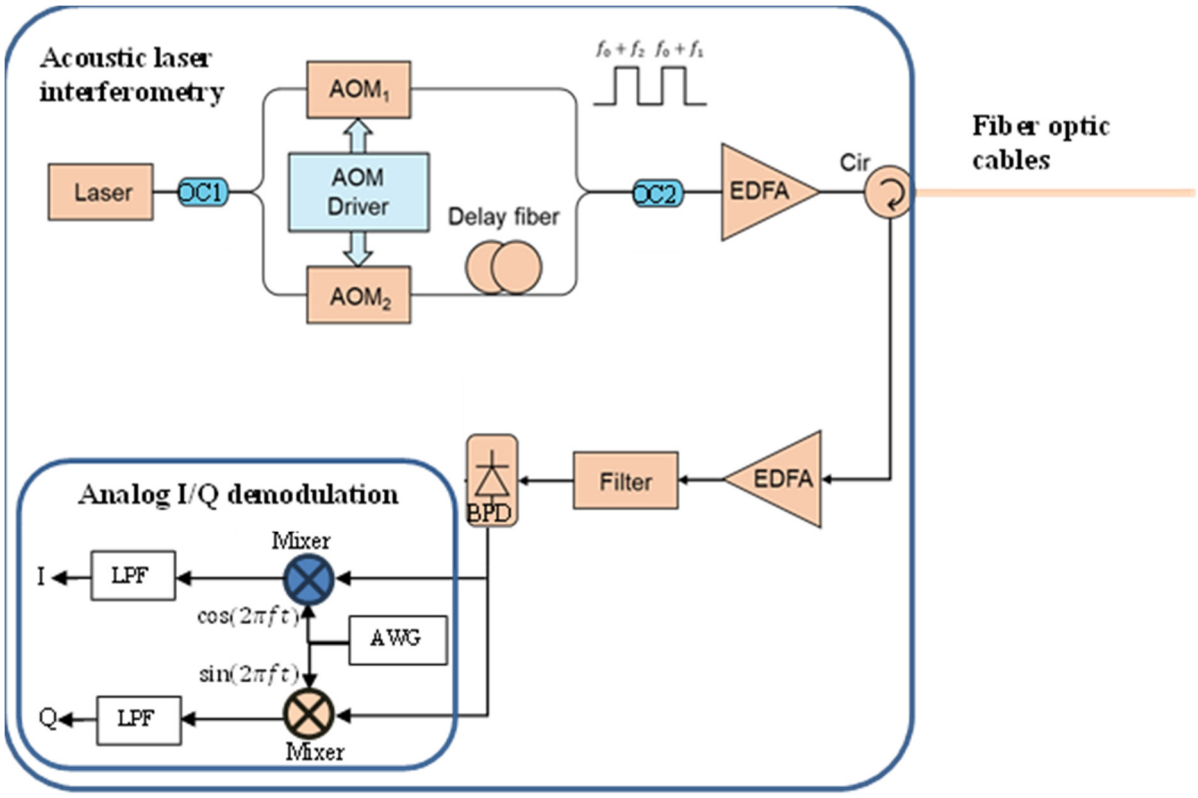

Figure 2. The DAS optical processing diagram (He et al., 2017)

As the laser signal is distributed along the fiber cables, a tiny stochastic RBS light occurs naturally (Rosello, 2020; Ismail et al., 2021). When an acoustic wave exerts pressure to fiber optic cables, the transmitted optical signal undergoes attenuation and a phase shift between the Rayleigh backscattering (RBS) from the leading and trailing edges of the optical pulse. Physically, the wave pressure also elongates the fiber cables and eventually creates strain. The phase-shifted optical backscattered signal travels to the acoustic laser interferometry and undergoes interference with the laser pulse along the fiber optic (see Figure 3). The acoustic laser interferometry then can be inferred to behave as a coherent ϕ-OTDR, since it detects the phase shift arising from the interference between the backscattered light and the coherent laser pulse it generates.

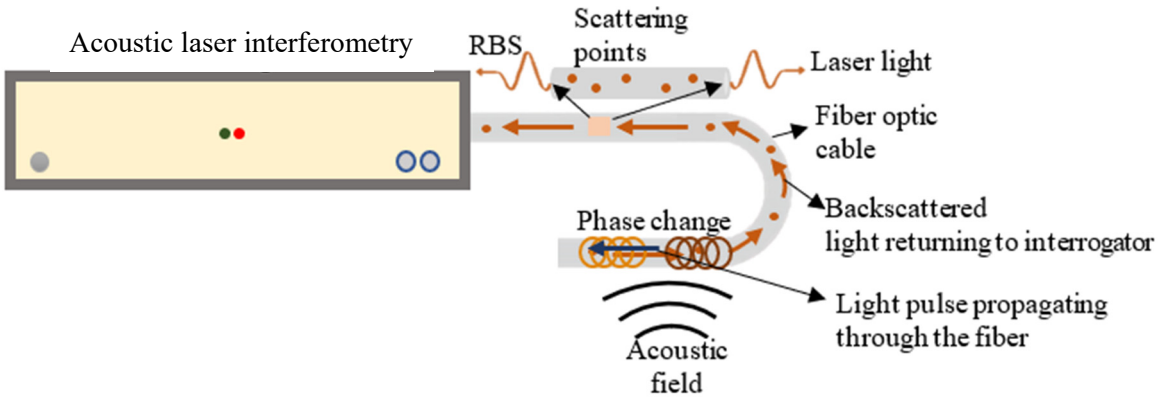

Figure 3. Operation principle of DAS (modified from Shatalin et al., 2022).

The robust perturbation detection in any point of the cables is enabled by waveguide function inside a single-mode fiber cable. A typical single-mode optical fiber consists of a glass core surrounded by cladding glass (see Figure 4) and is further protected by additional layers, such as a coating and an outer jacket. The core and cladding are pre-fabricated with distinct refractive indices to enable

waveguide function. This coaxial-structured optical fiber cables maintains the full amplitude of the light wave energy across a propagation distance of several hundred meters.

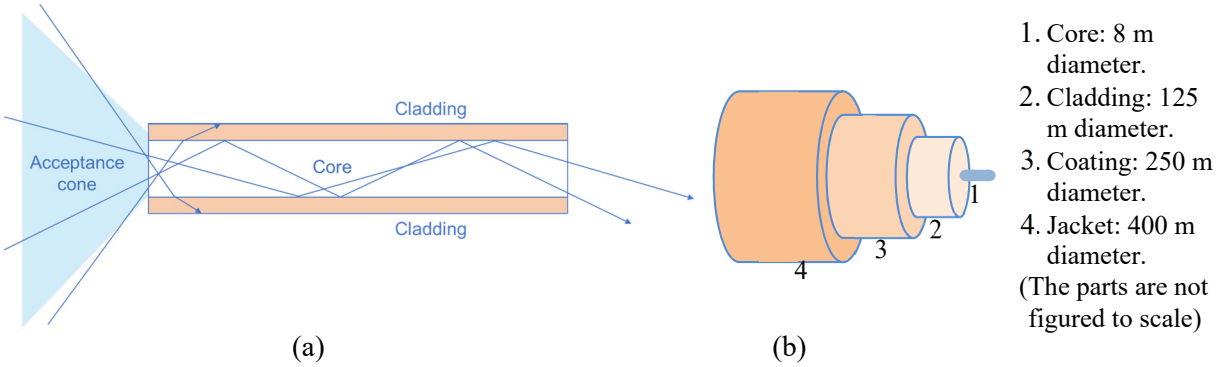

Figure 4. Inside a fiber optic cable (a) Total reflection of fiber optic. The propagation of light through a fiber optic (Modified after Lamelot, M., 2007 in Merzougui et al. 2020). (b) A cable structure of typical single mode fiber optics.

The acquisition procedure of our experiment is described as follow: Over 208-meter fiber optic cable, A 100 ns-width laser pulse was injected with a sampling rate of 500 Hz (1 ms). The data was sampled at precisely 512 points, corresponding to a 4 ns interval. All used modules are given in Figure 5. The BPD photodetector within the ϕ-OTDR detected interference signals (phase modulation of acoustic and Rayleigh backscattered lightwaves), producing a modulated electrical beat signal. The I/Q components were directly acquired using an analog demodulation data acquisition (DAQ) module. The split signal from BPD mixed with Local Oscillator (LO) having orthogonally paired each other. Therefore, there will be two independent signals which were mentioned earlier as I and Q, as shown by Figure 2. The LO was served by Arbitrary Wave Generator (AWG).

Subsequently, an ADC converted the separated I/Q components at a high sampling rate. By splitting the signal through multiplication with a cosine function for the I component and a sine function for the Q component, followed by low-pass filtering (LPF), the amplitude and phase of the acoustic signal can subsequently be extracted in-phase demodulation stage.

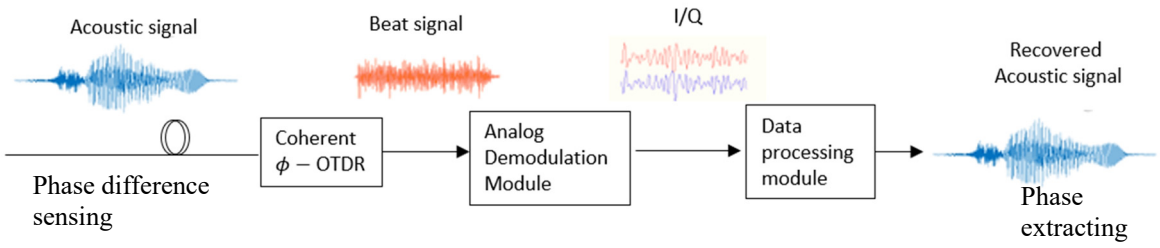

Figure 5. Block diagram of interconnection of all DAS system components (modified from Fei Jiang et al., 2019).

After being digitized, the I/Q components were processed by the data processing unit through two main stages, i.e., phase unwrapping and Fast Fourier Transform (FFT). The initial curve of time-dependent amplitude spreads between $-\infty$ to ∞. Moreover, the phase unwrapping process constrains the range from $-\pi$ rad to π rad, facilitating smoother plot and sinusoidal graph representation. Finally, the FFT process transforms the smoothed time domain signal into frequency domain and allows physical interpretation.

We examined our DAS sensing system capability under vibration coming from hand drilling machine. To extract the demodulated frequency and amplitude of RBS lightwave, we obtained optical (analog) I/Q demodulation using Hilbert transformation process. Then, we have phase

information along fiber optics by calculating arc tan (I/Q). The phase difference is equal to strain wave which is analog to the acoustic which beats the fiber optic cable. The phase difference is proportional directly to the beat signal.

3 RESULT AND DISCUSSION

After the low-pass filter was applied to the beat signal, the I/Q signals were produced. Figure 6 shows the In-phase amplitude signal over time. Noise dominating sinusoidal waves was observed. The DAS acquisition system is inferred to be capable of detecting vibrations exerted in its surrounding area. As the cable roll was laid (see Figure 1) in an undamped indoor environment, arbitrary, unpredictable vibrations could affect the cables. Under these conditions, our DAS system detected accountable vibrations.

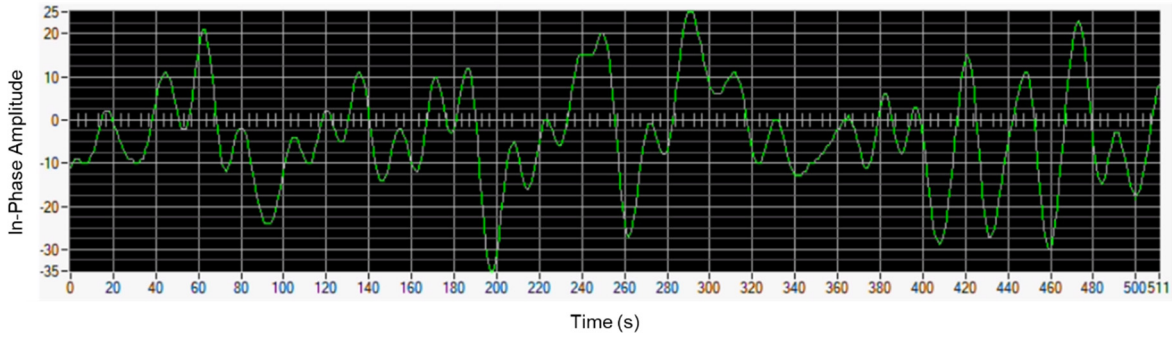

Figure 6. The examination results of in-phase graph for condition with vibration.

The accounted vibration was generated using an impact drill at specific points under the fiber cable. Since the vibration possessed sufficient power and speed, the initial in-phase wave increased significantly. Acoustic laser interferometry inherently introduces high-frequency noise (Lin et al., 2025); the light source also introduces phase noise, and the electrical system introduces thermal noise and shot noise (Lu et al., 2010). Together, they may generate random signals even in quiet observation areas. We used a fiber cable with a maximum lateral sensing range of 52.4288 km. At such distances, various disturbances can affect fiber-optic sensing. Therefore, some signal pre-processing (e.g., noise reduction and gain modulation) is required before further analysis, including the use of a whitening filter.

Figure 7 shows the 300 Hz sound signal data detected using DAS fiber-optic sensing. The signal seems clearly detected.

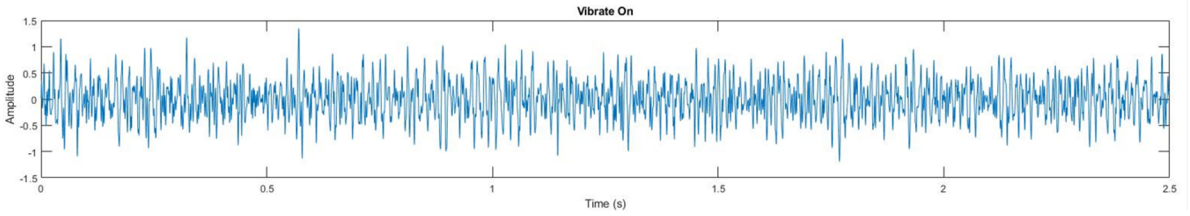

4 CONCLUSIONS

In this paper, we show that fiber-optic cable can be used for acoustic sensing. The acoustic signal, which was beaten by the fiber optics, produced phase differences. These phase differences are equal to the fiber-optic cable's strain length. The DAS fiber optics cable can detect the acoustic signal clearly through the demodulation signal of the acoustic phase, which modulates the light wave signal.

DISCLAIMER

The authors declare no conflict of interest.

REFERENCES

Bao, X. and Wang, Y. (2021) "Recent Advancements in Rayleigh Scattering-Based Distributed Fiber Sensors," *Advanced Devices & Instrumentation*, 2021, p. 2021/8696571. Available at: https://doi.org/10.34133/2021/8696571.

Dang, N., Huynh, T., Pham, Q., Lee, S., and Kim, J. (2020) "Damage-sensitive impedance sensor placement on multi-strand anchorage based on local stress variation analysis" *Structural Control and Health Monitoring*, 27(7). Available at: https://doi.org/10.1002/stc.2547.

He, X., Yi, D., Liu, F., and Zhang, M. (2017) "Distributed acoustic sensing technique and its field trial in SAGD well," in L. Wei et al. (eds.) *AOPC 2017: Fiber Optic Sensing and Optical Communications*. *Optical Information and Network (Optical Fiber Sensors)*, Beijing, China: SPIE, p. 2810. Available at: https://doi.org/10.1117/12.2285742.

Hernandez, P. D., Ramírez, J. A., and Soto, M. A. (2022) "Deep-Learning-Based Earthquake Detection for Fiber-Optic Distributed Acoustic Sensing" *Journal of Lightwave Technology*, 40(8), pp. 2639–2650. Available at: https://doi.org/10.1109/JLT.2021.3138724.

Hull, R., Woerpel, C., Trujillo, K., and Bohn, R. (2020). Hydraulic fracture characterization using fiber optic DAS and DTS data. 500-504. 10.1190/segam2020-3425789.1.

Ismail, A., Sulaiman, A. H. B., and Abdullah, F. (2021) "Characterization of DWT as Denoising Method for φ-OTDR Signal." *J. of Nanoelectr. and Optoelect.* 14. 333-340

Jiang, F., Lu, Z., Cai, F., Li, H., Zhang, Z., Zhang, Y., and Zhang, X. (2019) "Low Computational Cost Distributed Acoustic Sensing Using Analog I/Q Demodulation" *Sensors*, 19. Available at: https://doi.org/10.3390/s19173753.

Lin, C. R., Specht, S., Ma, K., Ohrnberger, M., and Cotton, F. (2025) "Analysis of saturation effects of distributed acoustic sensing and detection on signal clipping for strong motions," *Geophysical Journal International*, 241(2), pp. 971–985. Available at: https://doi.org/10.1093/gji/ggaf089.

Liu, W. B., Fan, P. Z., Wang, M. H., Li, Y. K., and Ding, J. F. (2021) "Optical, Acoustic and Electromagnetic Vulnerability Detection for Information Security" *Journal of Physics: Conference Series*, 1775(1), p. 012001. Available at: https://doi.org/10.1088/1742-6596/1775/1/012001.

Lu, Y., Zhu, T., Chen, L., and Bao, X. (2010) "Distributed Vibration Sensor Based on Coherent Detection of Phase-OTDR" *Journal Lightware Technology*, 28, pp. 3243-3249. Available at: https://doi.org/10.1109/JLT.2010.2078798

Merzougui, S. M., Belkacem, A., and Borsali, A. R. (2020) "Transmission Simultanée Fixe FTTH et Mobile 5G sur Fibre Optique basée sur les Modulations à Double Polarisation" Thesis. Available at: https://10.13140/RG.2.2.32392.65286

Rosello (2020) "Contribution to The Development of Distributed Fiber Optic Sensors Based on The Brillouin and Rayleigh Scattering Effects" Dissertation. Universidad P´ublica de Navarra Electric and Electronical Engineering Department.

Sezer, N. and Koc, M. (2021) "A Comprehensive Review on The State-Of-The-Art of Piezoelectric Energy Harvesting" *Nano Energy,* 80.

Shatalin, S., Parker, T., and Farhadiroushan, M. (2022) "High Definition Seismic and Microseismic Data Acquisition Using Distributed and Engineered Fiber Optic Acoustic Sensors" in *Distributed Acoustic Sensing in Geophysics: Methods and Applications, Geophysical Monograph 268,* 1st ed., edited by Yingping Li, Martin Karrenbach, and Jonathan B. Ajo-Franklin. (John Wiley & Sons, Inc.). Available at: https://10.1002/9781119521808.ch01.

Soman, R., Wee, J., and Peters, K. (2021) "Optical Fiber Sensors for Ultrasonic Structural Health Monitoring: A Review" *Sensors*, 21(21), p. 7345. Available at: https://doi.org/10.3390/s21217345.

Zhang, Z., Houc, L., Yuana, M., Fuc, M., Qiana, X., Duanmud, W., and Lia, Y. (2020). “Optimization monitoring distribution method for gas pipeline leakage detection in underground spaces”. *Tunnelling and Underground Space Technology*. 104. 103545. Available at: https://doi.org/10.1016/j.tust.2020.103545.

Zoback, M.D. (2007) *Reservoir geomechanics*. Cambridge: Cambridge university press.

This page is intentionally left blank

HIMPUNAN AHLI TEKNIK TANAH INDONESIA - HATTI
Indonesian Society for Geotechnical Engineering - ISGE
PIT HATTI XXIX
10-12 November 2025

The Effect of Fly Ash Addition on Clay Stabilization Using Clean Set Cement

Efan Tifani[1,*]
[1]Department of Civil Engineering, Politeknik Negeri Bengkalis, Bengkalis, Indonesia, 28711; polbeng@polbeng.ac.id
*Correspondence: efantifani@polbeng.ac.id

ABSTRACT Fly Ash (FA) and Clean Set Cement (CSC) are very light materials and have strong adhesive bonds. FA comes from combustion waste found in coal processing plants, where this waste can be categorized as non-B3 (Hazardous and Toxic Materials). The abundant availability of FA and easily obtained CSC will be tried to be utilized as a reinforcement of the subgrade layer for road pavement by mixing it with clay, as an effort to stabilize the soil to obtain a CBR value in accordance with the requirements (min CBR of subgrade = 6% - 7%). CBR testing in the laboratory using ASTM and SNI methods to determine the properties and effects of stabilized clay. The type of clay soil is obtained through sieve analysis (93.87% passing #200), Atterberg limits (LL = 46.12%, PI = 19.77%) with high plasticity clay (A-7-6) based on the AASHTO classification. The results specific gravity = 2.64 with MDD Modified Proctor test for the SO type (100% clay) = 1.361 gr/cm^3, OMC = 20.17%. The highest MDD value for the SFC-3 type (10% clay + 75% FA + 15% Clean Set Cement) = 2.426 gr/cm^3, OMC = 25.81% with modified compaction. The lowest unsoaked laboratory CBR with results for SO (100% clay) = 2.83%, for the highest MDD value for the SFC-3 type (10% clay + 75% FA + 15% Clean Set Cement) against the unsoaked CBR with results = 21.43%. The test results concluded that the higher the percentage of FA mixed with clay + Clean Set Cement, the higher the CBR value of the soil mixture. This is because FA and Clean Set Cement contain high pozzolanic properties, which can significantly increase the cohesion of clay soil, resulting in an increase in density and CBR value.

KEYWORDS Fly Ash; Clean Set Cement; Clay Soil; CBR Laboratory

1 INTRODUCTION

The quality of the road will be good if it is supported by good subgrade conditions (Tifani, 2023), because the vehicle load received by the top layer of road pavement will be distributed to the layer below it, so that the bottom layer/subgrade (subgrade) can withstand repeated (cyclic) load repetitions from the vehicle, strong materials are needed. Apart from material strength, there are other requirements that can affect the quality of road pavement, namely the lack of contact interaction between the subgrade layer and water, which requires materials that have water-resistant properties. In this research, materials were determined that have water-resistant characteristics, one of which is Fly Ash material, Fly Ash is a residual material from processing coal in refining. Fly Ash can be used as a pozzolan material so that it is possible to be used as a soil stabilization material and also its absorption in reuse becomes greater. The availability of Fly Ash is abundant and this material also has good waterproof and cohesion properties, so that the bond between Fly Ash and soil becomes stronger and can become denser. For Clean Set Cement (CSC) is a type of chemical developed by Sugiarto dan Hariyono. This material is in the form of a grayish powder that functions to improve, for example, clay sediment mud. When CSC is mixed with soil, it will reduce the soil's air content, causing CSC to be able to bind air molecules in a soil compound. CSC is also able to increase or enhance soil strength (Soepartoko and Agustinus, 2005). The type of CS series 60 (CS-60) used in this study is because it has a high binding capacity for clay soil with high swelling and shrinkage and mud sedimentation (PT. Indo Clean Set Cement). In order for the binding capacity to be high, a large water content is needed to increase and enhance soil strength. Fly ash are waste products from combustion found in coal processing factories, where this waste can be categorized as non-B3

(Hazardous and Toxic Materials). Where the use of fly ash material will replace some of the original clay material available through soil stabilization efforts to determine the bearing capacity of the subgrade through the CBR value parameter. For this reason, subgrade stabilization needs to be carried out to ensure the quality of the subgrade to support flexible and rigid pavement types on roads. This research aims to determine the influence and how big the CBR value of clay soil obtained is on clay soil by mixing fly ash and CS-60 material.

CBR (California Bearing Ratio) or the bearing capacity ratio of subgrade based on the material standards of the City of California, United States is an important parameter of pavement road where the higher the CBR value of the soil, the better the bearing capacity of the soil. The high CBR value of subgrade serves to increase the strength of soil which provides bearing capacity to road layer above it, and also serves to reduce the amount of unwanted soil settlement (Mahardika AG and Pratama, MF 2020). In soil compaction, optimum moisture content (OMC) to achieve the maximum dry density ($\gamma_{d\,max}$) the proctor test, it parameters be reference for determining CBR Laboratory value.

2 RESEARCH METHODS

In this study, the clay soil of Sungai Alam Village, Bengkalis Regency, Riau Province was used, it take samples of clay soil, dig the original clay soil to a depth of ± 50 cm. Most of the soil sample is then dried by drying it in the sun for 5 days and a small part by placing it in the oven for 24 hours with temperature 105 ± 5^{o}c, so that the soil water content is close to zero. testing the water content of soil that is dried in the sun and oven to obtain the difference in water content values while the FA (Fly Ash) material came from various Coal Mills Factory in Dumai City and its surroundings, Riau Province. FA sampling is carried out by filtering with a sieve size close to sieve no. 40 (0.425 mm) to sieve no. 200 (0.075 mm).

Fly ash resembles a fine powder and can be produced with a 10–20% success rate, with a density of 1,600 kg/m³. Fly ash is a pozzolanic material. It consists primarily of oxides of silica (SiO_2), aluminum (Al_2O_3), iron (Fe_2O_3), and calcium (CaO), along with small amounts of potassium, sodium, titanium, and sulfur (Antoni & Nugraha, 2007 in Ansari & Prianto, 2021). Fly ash is divided into two classes: Class F coal fly ash, produced from the combustion of anthracite or bituminous coal. It has pozzolanic properties and requires the addition of quick lime, hydrated lime, or cement to achieve cementitious properties. Class F fly ash has a low lime content (CaO < 10%), while Class C fly ash is produced from the combustion of lignite or sub-bituminous coal. It not only has pozzolanic properties but also exhibits self-cementing properties (the ability to harden and increase strength when reacted with water), which occurs without the addition of lime. It typically contains >20% lime (CaO) (Wardani, 2008 in Ansari & Prianto, 2021). FA is mostly mixed with residual coal deposits in the form of lumps, so filtering is required to separate the material. To process and prepare the FA material to be used as a test sample after collection, the FA sample is dried in an oven for 24 hours. The physical properties of FA are tested based on standard clay soils, taking into account the characteristics of FA that behave similarly to clay (having a fine grain size and cohesion).

CS-60 is a type of chemical in the form of a cement stain cleaner developed by Sugiarto and Hariyono which was ordered by the author at PT Hume Concrete Indonesia, Cikarang-Bekasi, West Java. The chemical composition of CS-60 consists of silica (SiO_2) = 15,09%, aluminum (Al_2O_3) = 4,26%, iron (Fe_2O_3) = 4,26%, and calcium (CaO) = 65,9%, MgO = 1,77% and SO_3 = 1,52%. Samples were taken by screening with a material size that passed through a sieve number 200 (0.075 mm), then dried in an oven for 24 hours with temperature 105 ± 5^{o}c. This material has a very fine grain gradation so it is hoped that with the presence of CS-60, the soil sample can be more watertight and increase cohesion between soil particles. In addition to the CS-60 being sieved through a sieve number 200, the CS-60 material was also tested for specific gravity to determine its density. As for FA and CS-60 materials, There are no standards for specific test procedures in ASTM and SNI. Meanwhile, CBR testing is carried out in conditions not submerged in water (CBR Unsoaked type).

The flow chart study is shown in Figure 1, the research method in the laboratory based on ASTM and SNI which includes testing the clay and FA properties and the effect of clay on CS-60. Determination of type clay based the AASHTO soil classification. The flow chart, type, method of testing carried out and samples number used can be seen in Figure 1 and Tables 1, 2 follows:

Table 1. Types of soil properties testing methods and soil effects with FA and CS-60

No	Test Type	Testing Method
1	Sieve analysis test	ASTM D-422
2	Atterberg limit test	ASTM D-4318-00
3	Specific gravity	ASTM D-854
4	Standard Proctor Test	ASTM D-698-12
5	Modified Proctor Test	ASTM D-1557
6	CBR Unsoaked Laboratory Testing	ASTM D 1183-16

Table 2. Combination the number of soil samples and the effect with FA (Fly Ash) and CS-60 (Clean Set Cement type 60)

Sample Code	Composition (%)			Number Samples and Water content		
	Clay	FA	CS-60	N *Proctor*	Moisture Content (%)	N CBR Lab
SO (Soil Original as Control)	100	0	0	5 (Standart = Std & Modification=Mod)	10, 13, 16, 19, 22	2 (Mod)
SFC-1 (Soil + Fly Ash + Clean Set Cement type 60)-1	30	55	15	5 (Standart = Std & Modification=Mod)	20, 23, 26, 29, 32	2 (Mod)
SFC-2 (Soil + Fly Ash + Clean Set Cement type 60)-2	20	65	15	5 (Standart = Std & Modification=Mod)	18, 21, 24, 27, 30	2 (Mod)
SFC-3 (Soil + Fly Ash + Clean Set Cement type 60)-3	10	75	15	5 (Standart = Std & Modification=Mod)	16, 19, 22, 25, 28	2 (Mod)

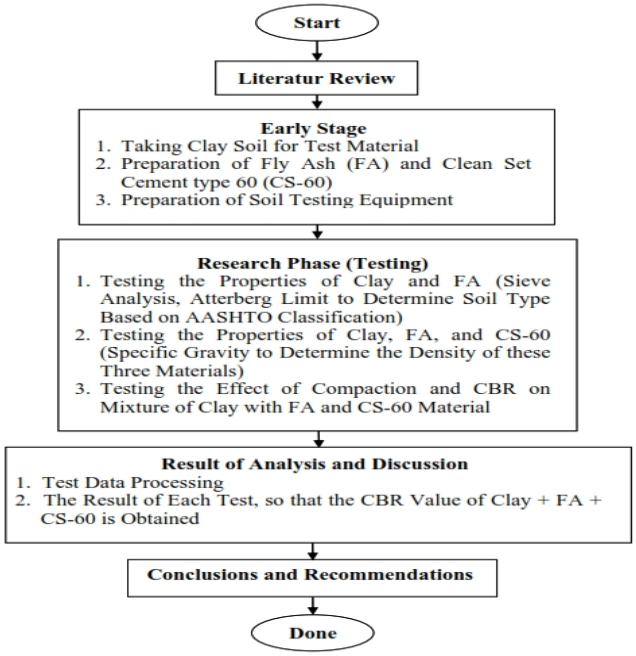

Figure 1. Research Flowchart.

3 RESULT AND DISCUSSION

3.1 Determination of Soil Classification Results

Determination of AASHTO soil classification is based on sieve analysis and Atterberg limit tests for fine-grained soils (FGS) the type of soil, fly ash (FA) and Clean Set Cement type 60 (CS-60) characteristics tested (Table 3):

Table 3. Test results on physical properties of clay, FA and CS-60 samples

No	Test Type	Test result	AASHTO Terms
1	Sieve analysis test	93.87% pass #200	>35% pass #200
2	Atterberg limit test (Clay)	LL=46.12%, PI=19.77%	LL = >40%, PI = >10%
3	Specific gravity (Clay)	2.64	-
4	Specific gravity (FA)	2,39	-
5	Specific gravity (CS-60)	3,08	-

From the graph of results (Figure 2) the sieve analysis above, it can be seen that the the percentage of clay that passes sieve number 200 (0.075 mm) is 93.87% > 35% (at least 36%) according to the AASHTO soil classification is A-7-6, it is stated that the soil is classified as a fine-grained soil type. (mud/silt and clay).

For the fine-grained soil/clay, the Atterberg limit test was carried out, so that the results obtained were the liquid limit value = LL, which was 46.12% > 40% (at least 41%) and the plasticity index = PI, which was 19.77%. > 10% (minimum 11%) according to AASHTO soil classification. For FA the liquid limit value = LL, which was 68.03% and the plasticity index = PI, which was 6.64%.

This value indicates that high water content is required for the FA sample to become slightly plastic. Low water content causes the FA sample to be unable to bind the grains perfectly, so the FA sample only forms a slightly wet and non-sticky clump (pozzolan). These pozzolan-like characteristics will affect changes in the properties of the clay mixed with the FA material. With a low plasticity index value, high water content is required to reach the plastic limit value. If the FA material has reached its plastic limit value, the FA material's properties become difficult for water to penetrate (watertight).

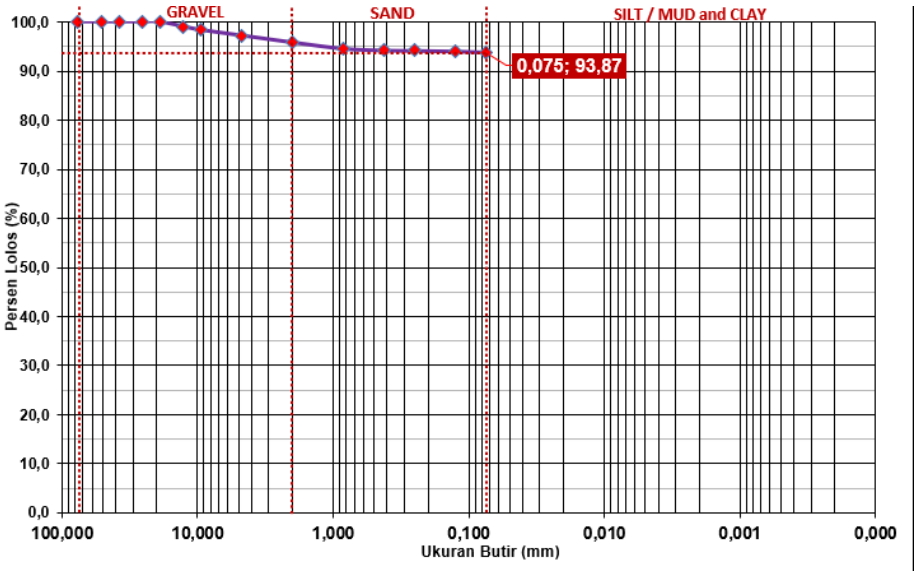

Figure 2. Graph of Soil Sieve Analysis Results According to AASHTO Classification

Table 4. Determination of soil types according to the AASHTO classification based on the results of sieve analysis and Atterberg Limit tests (Hardiyatmo, 2010)

General Classification	Silt - cCay Soil (More than 35% of all soil samples pass the No.200 sieve			
Group Classification	A-4	A-5	A-6	A-7 A-7-5* A-7-6+
Sieve Analysis (% lolos) No. 10 No. 40 No. 200	Min 36	Min 36	Min 36	Min 36
Properties of the fraction that passes Sieve No. 40 Liquid limit (LL) Plasticity index	Max 40 Max 10	Max 41 Max 10	Mx 40 Max 11	Min 41 Min 11
Most dominant material type	Silty soil		Clayey soil	
Assessment as subgrade material	Fair to poor			
*For A-7-5, $PI \leq LL - 30$ +For A-7-6, $PI > LL - 30$				

Based on table 4, it can be seen that the determination of the clay type shows that the soil is categorized as clay with the soil symbol A-7.

To determine whether the tested clay soil (A-7) contains silt grains (A-5) resulting in A-7-5 (silty clay) or pure clay (A-7) + (A-6) = A-7-6 (pure clay), then it is determined through the relationship between the plasticity index = PI, liquid limit = LL to the plastic limit value = PL = 30, in accordance with the provisions of the AASHTO classification (Das, 1995):

If the value of PI□ ≤ LL – 30, then the soil is categorized as A-7-5 (silty clay)
If the PI value > LL – 30, then the soil is categorized as A-7-6 (pure clay)
From the data from the LL and PL test results, it can then be determined that the clay is categorized as A-7-6 with the following calculations:

PI (19.77%) > LL (46.12%) – PL (30)
Value 19.77% > 16.12% soil is categorized: A-7-6.

Another way to determine the soil category is A-7-6 is to use a graph of the relationship between PI and LL values (Figure 3) according to the AASHTO classification.

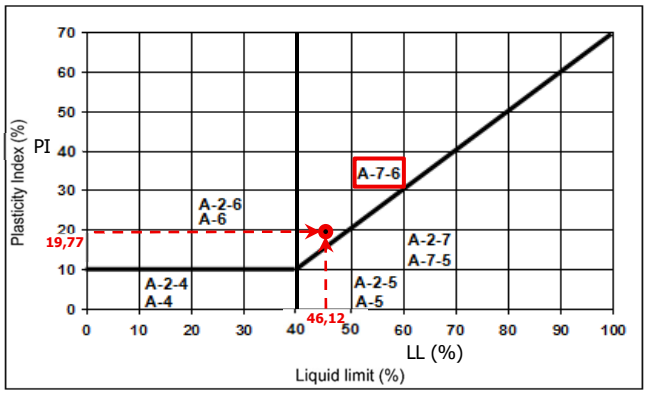

Figure 3. Graph of PI with LL based on AASHTO classification.

3.2 Determination of the Result of Soil Compaction

A. The results of the standard compaction test (Std) are based on Method B in ASTM D-698-00a (Soedarmo and Purnomo, 1993) for 100% clay content (SO = original soil) + 0% FA + 0% CS-60 for 5 samples, with experimental water content-trial (w_{trial}) = 19% obtained the value of wet soil density (□γ_b) = 1.595 gr/cm^3 with the water content after testing (w) = 21.13%, whereas for modification compaction test (Mod) with experimental water content-trial (w_{trial}) = 19% obtained the value of wet soil density (□γ_b) = 1.635 gr/cm^3 with the water content after testing (w) = 20.17% so that from the following analysis the maximum dry density value (□$\gamma_{d\,max}$) (Hardiyatmo, 2010) by:

$$\gamma_{dmax} = \frac{\gamma_b}{1+w} = \frac{1{,}635 gr/cm^3}{1+0{,}2017} = 1{,}361 gr/cm^3$$

Based on the parameter values generated from the Proctor test for the SO sample (from table 5), make a graph of the relationship between the water content value after the test (w) and dry density (γ_d) of the 5 samples is drawn (figure 4).

Table 5. Proctor test results for SO samples code

Sampel Code (*SO*)	w_{trial} (%)	γ_b (gr/cm^3)	w (%)	γ_d (gr/cm^3)
Std-1	13	1,342	14,22	1,175
Mod-1	13	1,398	12,83	1,239
Std-2	16	1,515	18,91	1,274
Mod-2	16	1,546	18,82	1,301
Std-3	19	1,595	21,13	1,317
Mod-3	19	1,635	20,17	1,361
Std-4	22	1,502	24,83	1,203
Mod-4	22	1,584	23,06	1,287
Std-5	25	1,455	27,36	1,142
Mod-5	25	1,538	25,11	1,229

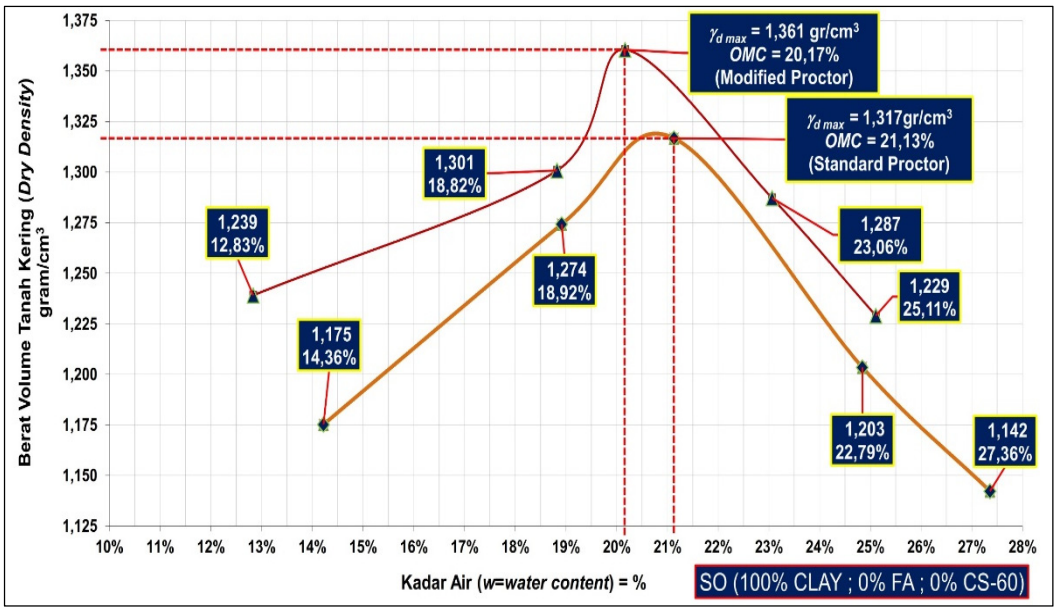

Figure 4. Graph Proctor test for SO Sample Code.

From the graph in Figure 4, it can be seen that the highest dry density (γ_d) is 1.361 gr/cm^3 ($\gamma_{d\ max}$) with the water content value to achieve the maximum compaction of the among 20.17% (OMC=optimum moisture content) on modification compaction. The water content value after testing for each modified compaction sample decreased compared to standard compaction, this is because the modified compaction energy is greater, causing more water to be compressed and the soil to become denser (the $\gamma_{d\ max}$ value is higher).

B. The Results of standard and modified compaction tests for 5 samples of original clay (SO) with the composition:

- SO (Soil Original as Control) = 100 % Clay + FA = 0 % + CS-60 = 0 %
- SFC-1 (Soil + Fly Ash + Clean Set Cement)-1 = 30 % Clay + FA = 55 % + CS-60 = 15 %
- SFC-2 (Soil + Fly Ash + Clean Set Cement)-1 = 20 % Clay + FA = 65 % + CS-60 = 15 %
- SFC-3 (Soil + Fly Ash + Clean Set Cement)-1 = 10 % Clay + FA = 75 % + CS-60 = 15 %

For the trial water content values of samples SFC-1 to SFC-3 cannot be made the same as the trial water content values (w_{trial}) of SO samples, this is due to the difference in the amount of water absorbed in clay soil when mixed with FA + CS-60. The clay soil mixed with FA + CS-60 becomes difficult to compact due to a lack of water compared to clay alone (SO) which can be compacted at the same water content, so the optimum water content (OMC) of the three SFC sample variations may not be ever achieved, even with the same CS-60 percentage for the 3 sample variations. From this, so that the SFC sample can be compacted, a water content value that is greater than the water content of the SO sample is needed by trial and error until the SFC-1 to SFC-3 samples can be compacted. From table 6, standard and modified compaction test data are presented at the highest value conditions ($\gamma_{d\ max}$ and OMC) for original clay soil and the three variations in sample composition.

Table 6. Proctor test results for samples SO, SFC-1 to SFC-3 based on conditions γ_d max and OMC

Sampel Code	w_{trial} (%)	γ_b (gr/cm^3)	w (%)	γ_d (gr/cm^3)
SO (Std)	19	1,595	21,13	1,317
SO (Mod)	19	1,635	20,17	1,361
SFC-1 (Std)	26	2,482	31,11	1,893
SFC-1 (Mod)	26	2,593	30,12	1,993
SFC-2 (Std)	24	2,782	27,89	2,175
SFC-2 (Mod)	24	2,809	27,32	2,207
SFC-3 (Std)	22	3.008	26,09	2,386
SFC-3 (Mod)	22	3,053	25,81	2,426

Based on the parameter values resulting from the Proctor test for SO and SFC-1 to SFC-3 samples, a graph of the relationship between the water content value after testing (w) and the dry soil volume weight (γ_d) of the 5 (five) samples was created (figure 5).

From the graph in Figure 5 it can be seen that the highest maximum dry soil volume weight value is modified compaction for variations in SFC-3 composition (10% clay + 75% FA content + 15% CS-60 content) with a value of $\gamma_{d\ max}$ = 2.426 gr/ cm^3 and OMC = 25.81%, this shows that the higher the percentage of addition of Fly Ash (FA) even with the same CS-60 percentage, the higher the dry density / maximum dry density ($\gamma_{d\ max}$) and the greater The optimum water content (OMC) value of the three variations in sample composition (SFC-1 to SFC-3) is low compared to the original clay soil, so that the sample weight becomes larger and denser, so that the sample weight becomes greater.

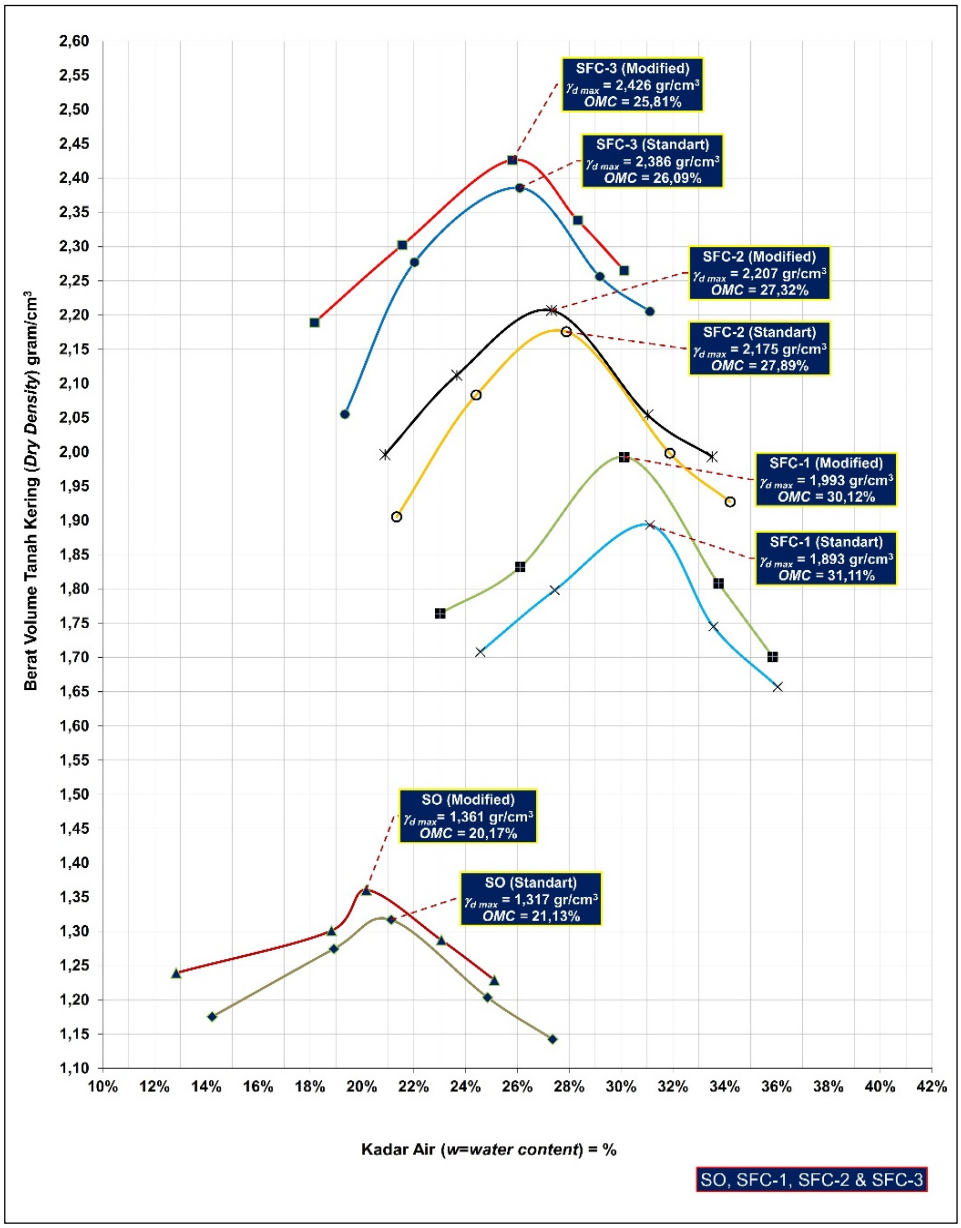

Figure 5. Graph Proctor test for samples SO, SFC-1 ~ SFC-3 based on conditions $\gamma_{d\ max}$ and OMC

This is because Fly Ash (FA) material has high cohesion and good water resistance so that it can increase the value of dry soil volume weight. The role of CS-60 mixed with clay soil material with a constant percentage of 15 percent can also increase soil density by increasing the bond of air molecules in the soil compound of the soil mixture, where there is a tendency to increase the value of soil cohesion due to fly ash and the presence of CS-60 can increase soil density, so that this factor can affect the increase in the value of dry soil volume weight for 3 variations of soil sample mixtures compared to the original soil.

Based on the graph in Figure 5, it is stated that if original clay soil is added with Fly Ash (FA) and Clean Set Cement type 60 (CS-60), then more (higher) water content is needed to achieve optimum moisture content (OMC) conditions for the soil original clay, so that this can increase the maximum dry density value for SFC-1 to SFC-3.

3.3 Determination Determination of CBR Laboratory Value Results

A. The results of the CBR Laboratory test to determine the penetration test (P_t) with 100% clay content (SO = original soil) + 0% SFC in made 2 samples based on the optimum moisture content (OMC) = 20.17% with maximum dry density ($\gamma_{d\,max}$) = 1.361 gr/cm^3 from the modification compaction. So that from the following analysis the value of the CBR compression test for clay soils (Hardiyatmo, 2010) is determined with the penetration test (P_t) and penetration standard (P_s) (table 7) with penetration of 2.54 mm and 5.08 mm highest value of the 2 samples as follows:

Table 7. Standard load values (*Ps*) for CBR experiments (Soedarmo and Purnomo, 1993)

No	Penetration (mm)	Penetration of Standar (kg)	Penetration of Standar (kN)
1	2,54	1370	13,50
2	5,08	2055	20,00
3	7,50	2630	25,50
4	10,00	3180	31,00
5	12,50	3600	35,00

$$CBR_{2,54} = \frac{P_t}{P_s} \times 100\% = \frac{0{,}41\ kN}{13{,}5\ kN} \times 100\% = 3{,}07\%$$

$$CBR_{5,08} = \frac{P_t}{P_s} \times 100\% = \frac{0{,}61\ kN}{20{,}0\ kN} \times 100\% = 3{,}06\%$$

Based on the provisions of ASTM D-1883-73 (Soedarmo and Purnomo, 1993) if the CBR Laboratory value with penetration of 5.08 mm is greater than the penetration of 2.54 mm, then the penetration of 5.08 mm is taken as the design CBR value.

From this statement, it can be determined that the CBR Laboratory value with 100% clay content (SO = original soil) + 0% SFC is 3.07%. The value of the penetration test (P_t) is shown in Figure 7.

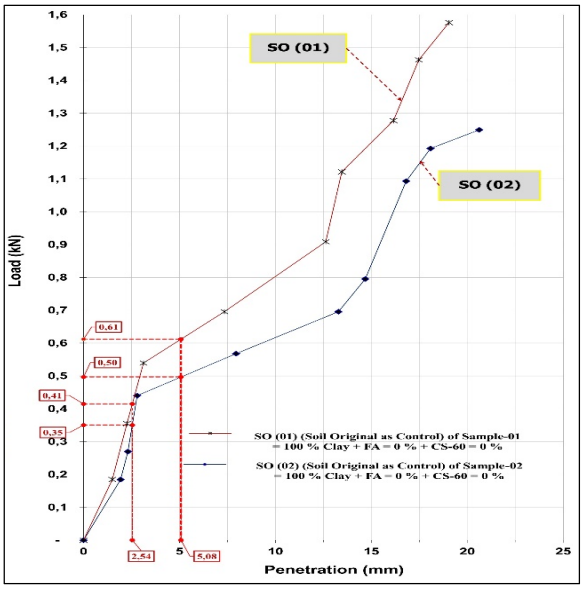

Figure 7. Penetration test (P_t) value of CBR Laboratory compression test on SO Samples 01 and 02

For table 8, the CBR values obtained for 2 test samples at penetrations of 2.54 mm and 5.08 mm are as follows:

Table 8. Laboratory CBR value results for SO samples 01 and 02.

SO Samples (Modification Proctor)	CBR Test Numbers	Penetration	Load (kN)		CBR Value
		Standard (mm)	Standard (P_s)	Test (P_t)	(%)
Sample-01	1	**2,54**	13,50	0,41	**3,07**
	2	**5,08**	20,00	0,61	**3,06**
Sample-02	1	**2,54**	13,50	0,35	**2,60**
	2	**5,08**	20,00	0,50	**2,48**

For table 9, the average CBR value obtained from 2 test samples at a penetration of 2.54 mm is as follows:

Table 9. CBR value for SO samples (P_s) = 2.54 mm

SO Samples (Modification Proctor)	CBR Test Numbers	Penetration	P_s = 13,50 kN		CBR Value
		Standard (mm)	Test (P_t)	Average of P_t	Average (%)
Sample-01	1	**2,54**	0,41	0,38	**2,83**
Sample-02	1	**2,54**	0,35		

B. The results of the CBR Laboratory test to determine the penetration test (P_t) for sample SO=*soil original* and sample of SFC (Soil + Fly Ash + CS-60) in made 2 samples for 4 various according to table 6 based on the maximum dry density value ($\gamma_{d\,max}$) and optimum moisture content (OMC) to modification compaction from the Proctor test. From figure 8, the penetration test is obtained from the corrected graph for a total of 8 test samples.

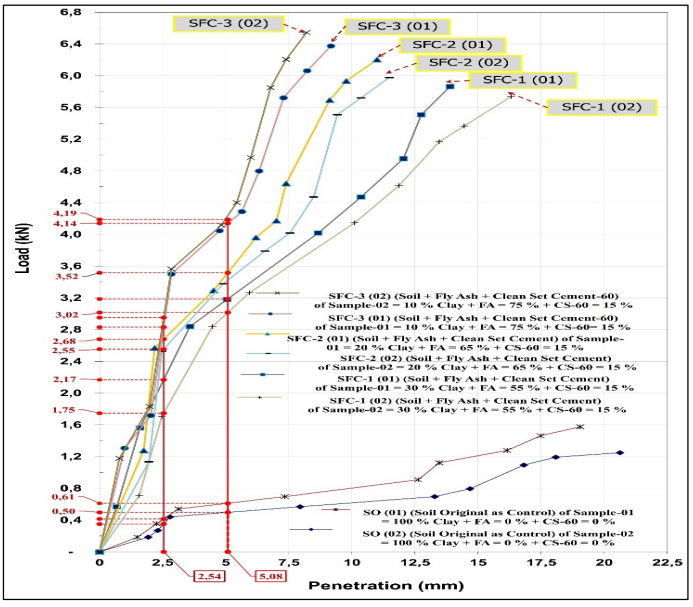

Figure 8. Penetration test (P_t) value of CBR Laboratory compression test on SO, SFC-1,

SFC-2 and SFC-3 samples.
From this statement, the highest Laboratory CBR value was determined, namely for the SFC-3 sample (Soil + Fly Ash + CS-60)-3 = 10% Clay + FA = 75% + CS-60 = 15%, amounting to 21.42%. For table 10, the CBR values obtained for 8 test samples at penetrations of 2.54 mm and 5.08 mm are as follows:

Table 10. Laboratory CBR value results for SO, SFC-1, SFC-2 and SFC-3 samples

SO Samples (Modification Proctor)	CBR Test Numbers	Penetration	Load (kN)		CBR Value
		Standard (mm)	Standard (P_s)	Test (P_t)	(%)
SO Sample-01	1	**2,54**	13,50	0,41	**3,07**
	2	**5,08**	20,00	0,61	**3,06**
SO Sample-02	1	**2,54**	13,50	0,35	**2,60**
	2	**5,08**	20,00	0,50	**2,48**
SFC-01 Sample-01	1	**2,54**	13,50	2,17	**16,06**
	2	**5,08**	20,00	3,19	**15,93**
SFC-01 Sample-02	1	**2,54**	13,50	1,75	**12,94**
	2	**5,08**	20,00	3,02	**15,08**
SFC-02 Sample-01	1	**2,54**	13,50	2,68	**19,85**
	2	**5,08**	20,00	3,52	**17,58**
SFC-02 Sample-02	1	**2,54**	13,50	2,55	**18,92**
	2	**5,08**	20,00	3,42	**17,12**
SFC-03 Sample-01	1	**2,54**	13,50	2,83	**20,97**
	2	**5,08**	20,00	4,14	**20,70**
SFC-03 Sample-02	1	**2,54**	13,50	2,95	**21,87**
	2	**5,08**	20,00	4,19	**20,94**

The laboratory CBR pressure test value was obtained on the SFC-3 (Soil + Fly Ash + CS-60)-3 sample 01 for penetration of 2.54 mm and 5.08 mm with the equation:

$$CBR_{2,54} = \frac{P_t}{P_s} \times 100\% = \frac{2,95\ kN}{13,5\ kN} \times 100\% = 21,87\%$$

$$CBR_{5,08} = \frac{P_t}{P_s} \times 100\% = \frac{4,19\ kN}{20,0\ kN} \times 100\% = 20,94\%$$

For table 11, The average CBR values obtained from 8 test samples at the highest penetration load values for penetrations of 2.54 mm for SO, SFC-1 S-1, SFC-2, SFC-3 and 5.08 mm for SFC-1 S-02 are as follows:

Table 11. Laboratory CBR value results for SO, SFC-1, SFC-2 and SFC-3 samples at Ps = 2.54 mm

SO Samples (Modification Proctor)	CBR Test Numbers	Penetration	Load (kN)			CBR Value
		Standard (mm)	Standard (P_s)	Test (P_t)	Average of P_t	Average (%)
SO Sampel-01	1	**2,54**	13,50	0,41	0,38	**2,83**
SO Sampel-02	1	**2,54**	13,50	0,35		
SFC-1 S-01	1	**2,54**	13,50	2,17	2,60	**15,57**
SFC-1 S-02	1	**5,08**	13,50	3,02		
SFC-2 S-01	1	**2,54**	13,50	2,68	2,62	**19,38**
SFC-2 S-02	1	**2,54**	20,00	2,55		

SFC-3 S-01	1	**2,54**	13,50	2,83	2,89	**21,42**
SFC-3 S-02	1	**2,54**	13,50	2,95		

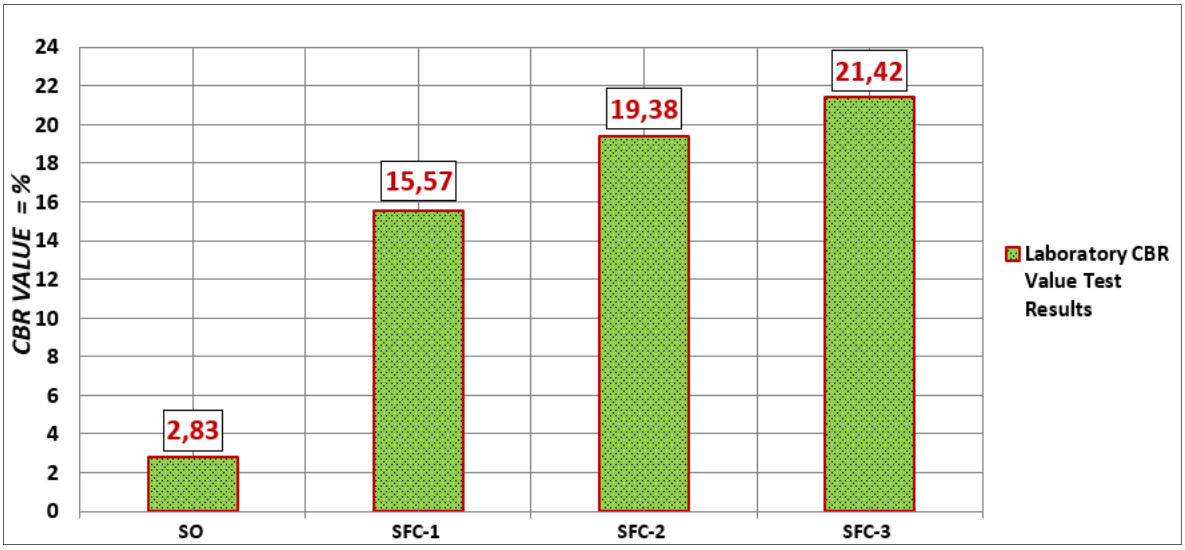

Figure 9. Laboratory CBR value results at P_s = 2.54 mm (for SO, SFC-1 S-1, SFC-2, SFC-3) and 5.08 mm (for SFC-1 S-2)

From the results of the table 11 and figure 9 it can be stated that the higher the percentage of addition of Fly Ash (FA) and Clean Set Cement type 60 (CS-60), the higher value of the soil bearing capacity ratio (CBR=%). It was also stated that the greater percentage of FA while percentage of CS-60 remains the same added, the lower the water absorption that occurs to reach optimum water content (OMC) conditions, so that it can increase the maximum dry density value at SFC-1 to SFC-3.

The increase in the CBR value tends to be caused by the Fly Ash (FA) material having high cohesion and good water resistance so that it can increase the value of dry soil volume weight. The role of CS-60 mixed with clay soil material with a constant percentage of 15 percent can also increase soil density by increasing the bond of air molecules in the soil compound of the soil mixture, where there is a tendency to increase the value of soil cohesion due to fly ash and the presence of CS-60 can increase soil density, so that this factor can affect the increase in the value of dry soil volume weight for 3 variations of soil sample mixtures compared to the original soil.

3.4 Relationship Between Compaction Values and Laboratory CBR Values

The combined CBR Laboratory test results at P_s = 2.54 mm (for SO, SFC-1 S-1, SFC-2, SFC-3) and 5.08 mm (for SFC-1 S-2) for 4 sample variations recapitulated the water content value after testing (w) and the dry soil volume weight value based on maximum conditions ($\gamma_{d\,max}$) can be seen in table 12 as follows:

Table 12. Results of laboratory CBR values for SO, SFC-1, SFC-2 and SFC-3 samples from $\gamma_{d\,max}$ and OMC conditions

Sampel Code	Composition (%)			$\gamma_{d\,max}$ (gr/cm^3)	*CBR* (%)
	Clay	Fly Ash	CS-60		
SO	100	0	0	1,339	2,83
SFC-1	30	55	15	1,943	15,57
SFC-2	20	65	15	2,191	19,38
SFC-3	10	75	15	2,406	21,42

Based on the resulting parameter values, there is a linear relationship between the dry soil volume weight value ($\gamma_{d\ max}$) and the soil CBR value, where the greater the value ($\gamma_{d\ max}$), the greater the soil CBR value, along with the increasing the greater percentage of FA while percentage of CS-60 remains the same added. This is because FA and Clean Set Cement contain high pozzolanic properties, which can significantly increase the cohesion of clay soil, resulting in an increase in density and CBR value.

4. CONCLUSIONS AND RECOMMENDATIONS

From the overall test results involving the increasing influence of the addition of Flys Ash (FA) and Clean Set Cement type 60 (CS-60) materials to clay soil, it can cause the following:

1. Increased dry density value / maximum dry soil volume weight ($\gamma_{d\ max}$),
2. Increasing the value of the soil bearing capacity ratio (CBR),
3. There is a linear relationship between the dry soil volume weight value ($\gamma_{d\ max}$) and the soil CBR value, where the higher the value ($\gamma_{d\ max}$), the greater the soil CBR value.

Suggestions for further research are:

1. Not only using clay soil, fly ash and clean set cements materials in carrying out soil stabilization efforts, but also using other materials, such as Limestone Ash, Coconut Ash, Uyung Sago, etc. which are mixed with clay soil fly ash and clean set cements materials, so that there is the possibility can increase the soil CBR value to be higher than this research,
2. Conduct research similar to the author, but made in the form of a 1:1 full scale experiment (full scale test), this is done to ensure that the results obtained are closer to real conditions in the field,
3. It is necessary to conduct laboratory CBR testing with the condition of adding and increasing the percentage of CS-60 in several sample variations to see the effect of changes in the behavior and strength of the CBR value of the soil.
4. For every test carried out using any type of stabilization material, it is recommended to carry out a soaked (soaked) CBR test, this is because the CBR value of the soil always changes depending on weather conditions for fine-grained soil types, such as silt and clay. By carrying out the immersion CBR test, you will get the minimum CBR value for the worst conditions.

ACKNOWLEDGEMENTS

The highest appreciation is given to PT. Dumai Hijau Abadi as a supplier and provider of Fly Ash (FA) materials from Palm Oil Mills (PKS) and Coal Processing in the Dumai City area and its surroundings, Riau Province and PT Hume Concrete Indonesia as a supplier Clean Set Cement type 60 (CS-60) Cikarang-Bekasi, West Java used by the author in this study.

REFERENCES

Ansari V dan Prianto, E., 2021, *Ciptakan Rumah Ramah Lingkungan dengan Material Dinding Limbah Fly Ash dan Bottom Ash (FABA), 11th SNST Proceedings*; 2021, ISBN 978-602-52386-5-9, pp. 01–06: Fakultas Teknik Universitas Wahid Hasyim Semarang.

ASTM D-4318-00, 2000, *Liquid Limit, Plastic Limit, and Plasticity Index of Soils,* ASTM, 100 Barr Harbor Drive, West Conshohocken, PA 19428-2959, United States.

ASTM D-4318-00, 2000, *Laboratory Compaction Characteristics of Soil Using Standard Effort,* ASTM, 100 Barr Harbor Drive, West Conshohocken, PA 19428-2959, United States.

ASTM D-4318-00, 2016, *California Bearing Ratio (CBR) of Laboratory-Compacted Soils,* ASTM, 100 Barr Harbor Drive, West Conshohocken, PA 19428-2959, United States.

Badan Standarisasi Nasional. (2012), *Metode Uji CBR Laboratorium,* SNI 1744:2012, Jakarta.

Das, BM, 1995, *Mekanika Tanah* (*Prinsip-prinsip Rekayasa Geoteknik*) Jilid 1*,* Erlangga, Surabaya.

Direktorat Jenderal Bina Marga., 2017, *Manual Perkerasan Jalan* (*Revisi Juni 2017*), Kementerian Pekerjaan Umum dan Perumahan Rakyat, Jakarta.

Hardiyatmo, HC, 2010, *Mekanika Tanah 1,* Gadjah Mada University Press Yogyakarta.

Hendry, A, et al., 2021, *Stabilisasi Tanah Lempung dengan Campuran Fly Ash* (*FA*) *dan Expanded Polystrene* (*EPS*) *Sebagai Alternatif Timbunan Ringan Pada Lapisan Subgrade,* Jurnal Ilmu Pengetahuan dan Teknologi, Teknologi Sipil; April 2021, vol 23 (1), hlm. 41–50: Jurusan Teknik Sipil, Politeknik Negeri Bandung, Bandung.

Mahardika AG dan Pratama, MF., 2020, *Pengujian Pemadatan Tanah Metode Standard Proctor dengan Alat Uji Pemadat Standard,* ISU Teknologi; Desember 2020, vol 15 (2), pp. 64–68: Sekolah Tinggi Teknologi Mandala, Bandung.

Soedarmo, D & Purnomo, E., 1997, *Mekanika Tanah 1,* Kanisius Yogyakarta.

Sumarno, A, et al., 2021, *Pemanfaatan Limbah Spent Bleaching Earth pada Stabilisasi Tanah Lempung dengan Clean Set Cement,* Jurnal Teknologi Lingkungan; Januari 2021, vol 22 (1), pp. 104–110: Pusat Penelitian Biomaterial Lembaga Ilmu Pengetahuan Indonesia, Bogor.

Tifani, E, 2023, *Pengaruh Penambahan Fly Ash Bottom Ash pada Stabilisasi Tanah Lempung terhadap Nilai CBR, 27th Annual National Conference on Geotechnical Engineering*; November 2023, ISSN No. 2964-1802 vol 27, pp. 176–185: Himpunan Ahli Teknik Tanah Indonesia (HATTI) Jakarta.

Tifani, E, 2024, *The Effect of Adding Bottom Ash and Spent Bleaching Earth on Clay Stablizatio to CBR Value, 28th Annual National Conference on Geotechnical Engineering*; November 2024, ISSN No. 2964-1802 vol 28, pp. 931–944: Himpunan Ahli Teknik Tanah Indonesia (HATTI) Jakarta.

Ground Improvement of High-Organic Clay Using Sand Columns: Settlement and Stability Analysis

Luthfi Amri Wicaksono[1,*], Paksitya Purnama Putra[2], Indra Nurtjahjaningtyas[3], Sely Rohmah[4]

[1]Civil Engineering Department, Faculty of Engineering, Universitas Jember, Jember, Indonesia, 68121 1; luthfiamri.teknik@unej.ac.id
[2]Civil Engineering Department, Faculty of Engineering, Universitas Jember, Jember, Indonesia, 68121 1; paksitya.putra@unej.ac.id
[3]Civil Engineering Department, Faculty of Engineering, Universitas Jember, Jember, Indonesia, 68121 1; indran.teknik@unej.ac.id
4Civil Engineering Department, Faculty of Engineering, Universitas Jember, Jember, Indonesia, 68121 1; e-mail@e-mail.com
*Correspondence: luthfiamri.teknik@unej.ac.id

ABSTRACT Construction on soft, highly organic soils presents significant geotechnical challenges due to low bearing capacity and high compressibility, hindering infrastructure development in tropical regions like Indonesia. Research on practical ground improvement techniques for these specific soil types is limited. This study aims to evaluate the performance of sand columns in improving the stability and settlement characteristics of high-organic clay. The primary objectives were to assess soil stability, analyze the amount of settlement under construction loads, and investigate the overall effectiveness of sand columns as a practical improvement method. This investigation utilized a numerical experimental approach, employing Plaxis 2D finite element software to model an embankment on a problematic soil profile. The analysis compared the site's performance before and after the installation of 6-meter deep sand columns, with results cross-referenced against manual calculations. The findings revealed that the unreinforced soil was fundamentally unstable, showing a catastrophic failure with a safety factor below unity and a total displacement of 1.19 meters. Following reinforcement, the soil's performance improved dramatically, achieving a stable safety factor of 1.267 and reducing the total displacement to a serviceable level of 0.0187 meters. Furthermore, the time required for 90 percent primary consolidation was reduced from 15.283 years to 9.921 years. In conclusion, sand columns are a highly effective engineering solution, successfully transforming an unstable subgrade into a competent foundation by significantly enhancing stability and controlling settlement, thereby confirming their suitability as a practical and economically viable technique for developing infrastructure on challenging organic soils.

KEYWORDS Sand Column; Organic Soils; Ground Improvement; Soil Stability

1 INTRODUCTION

Organic soils, such as clay and peat, are found throughout the world, particularly in tropical and subtropical regions. Many researchers and construction experts consider these soils problematic due to their poor characteristics, including low bearing capacity (Agaiby et al., 2022), high shrinkage and expansion (Brandl, 2019), and significant long-term settlement (Kamao, 2019). These characteristics undoubtedly make infrastructure development, such as roads, ports, and industrial buildings, unsafe (Mohaman et al., 2016). Several countries worldwide, such as Malaysia (Ling et al., 2014), the Netherlands (Limsiri, 2008), and Canada (Phokarel et al., 2021), also experience similar problems. Therefore, to address this issue, soil improvement techniques are needed to ensure stable and sustainable development.

In Indonesia, soils with high organic content are often found in coastal areas, swamps, and areas with high humidity(Sukarman et al., 2024). This type of soil is found predominantly on the islands of Sumatra, Kalimantan, and Papua(Hikmatullah & Sukarman, 2015). Many important infrastructure

projects, such as transportation networks, energy facilities, and industrial areas, are being built in these locations(Manudianto & Endah, 2025). However, the presence of clay soil with a high organic content can significantly impact the performance of these projects(Mukhlisin et al., 2021). If soil improvement is not carried out properly, access roads to the project and post-construction infrastructure will experience obstacles or even failure(Oktopani et al., 2024). Therefore, studies are needed on appropriate soil improvement, especially for soils with a high organic content, to support Indonesia's rapid infrastructure development(Oktopani et al., 2024).

Soil improvement methods have been widely studied, including chemical, physical, and mechanical methods(Ningsih et al., 2018). Chemical soil stabilization with lime, cement, or other materials has proven effective for some types of soft soils (Martinón-Torres, 2022) (Okonkwo and Kennedy, 2023), but is less effective for soils with a high organic content due to inadequate chemical interactions (Harris et al., 2009) and high costs (Pandey et al., 2024). Other common methods include preloading and vertical drains(Naseer, 2021). However, this method also requires a long time to achieve the desired results (Bhattacharya et al., 2011). On the other hand, mechanical methods such as stone columns and sand columns have also proven effective in strengthening soil, accelerating consolidation, and reducing settlement(Ningsih et al., 2018).

International and local researchers have found the effectiveness of using sand columns in soft soils(Naseer, 2021)The use of sand columns can increase the bearing capacity of marine clay soil by 12% for single sand columns and 18% for grouped sand columns (Prasad & Satyanarayana, 2021). The use of sand columns can also accelerate consolidation and significantly reduce settlement, both in plain sand columns and lime-stabilized sand columns (Al-Saoudi et al., 2014) (Prakash & Krishnamoorthy, 2022). The effect of using grouped sand columns in other studies also shows that shorter sand column spacing can increase efficiency, but larger spacing can result in reduced axial bearing capacity (Sohaib et al., 2020). Different sand column widths can also significantly increase the shear strength and unconfined compressive strength in soft clay soils (Hernina et al., 2023). Foundations using sand columns also show significant increases in bearing capacity and can be a practical and economical option for soft soil locations (Fahira et al., 2020). Indonesian researchers also explain that sand columns can be easily used in Indonesia due to the abundant availability of sand (Guswantoro et al., 2022). Although the use of sand columns has been extensively researched and applied to soft soils, their performance on high-organic clay soils remains incompletely understood(Jasim & Ahmed, 2024). Characteristics of high-organic clay soils, such as high water and fiber content, and long secondary consolidation, can affect the load transfer mechanisms and interactions between the sand columns and the surrounding soil (Naseer, 2021). Given this gap, further research to provide insight into the use and effectiveness of sand columns in improving high-organic clay soils, especially in tropical regions like Indonesia, is crucial.

This study generally aims to determine the performance of sand columns on high-organic clay soils. In detail, there are three main objectives: to evaluate soil stability before and after the installation of sand columns, to determine the level of settlement due to construction loads, and to determine the effectiveness of sand columns as an economical and beneficial soil improvement method for application on high-organic clay soils. The results of this study are expected to assist Indonesia in developing sustainable soil stabilization techniques and provide useful information for global research on improving organic soil characteristics.

2 METHODS

This study was conducted using a numerical experimental approach, with Plaxis 2D software serving as the analytical tool. The numerical method was selected because it has been proven to model the behavior of soft soil more realistically, particularly concerning embankment deformation and stability, as reported by Brinkgreve et al. (2016). Reinforcement with Sand Columns was considered because this technique is known to be effective in improving bearing capacity and accelerating the consolidation of soft soil (Bergado et al., 1996; Nayak et al., 2021).

The research was located at the Akatara Gas Plant Facility Project in Jambi, Indonesia, focusing on a specific road section within the area. Data for the study were obtained from field investigations and the project's technical documents. Soil data were collected from N-SPT and laboratory soil mechanics tests. Additional data included Detail Engineering Design (DED) drawings, embankment plans, and projected traffic loads. All data were subsequently analyzed to determine the parameters required for the model.

The analysis was performed in several stages. First, the collected soil data were processed and analyzed to develop a soil stratigraphy diagram. This diagram was created to illustrate the stratification and thickness of the soil layers for use in modeling and calculations. Unknown parameters were derived by correlating N-SPT and laboratory data using the correlations proposed by Bowles (1997). Slope stability analysis was carried out using the PLAXIS 2D software with the Mohr–Coulomb constitutive model, which represents soil behavior through five main parameters: cohesion (c), internal friction angle (ϕ), elastic modulus (E), Poisson's ratio (ν), and unit weight (γ). The main outputs of the analysis were the safety factor (SF) and total soil deformation. For comparison, manual calculations of soil settlement were also performed, applying elasticity theory for immediate settlement, primary consolidation theory, and secondary settlement calculations based on the secondary consolidation coefficient (Terzaghi et al., 1996).

In this research, the Sand Columns were first designed to analyze their impact. The Sand Column design involved determining the diameter, spacing, area replacement ratio, and installation pattern based on the theory presented by Bergado et al. (1996) determine in eq. 1.

$$D = S\sqrt{\frac{a_s}{c_1}} \qquad (1)$$

Where $c_1 = \pi/4$ for square pattern and $c_1 = \pi/2\sqrt{3}$. In this study, a column depth of 6 meters was adopted, which falls within the typical range of 6–12 meters reported in previous research (Bergado et al., 1996; Nayak et al., 2021). In this study, a column depth of 6 meters was adopted on a trial basis to observe its influence on settlement behavior in soft clay. The selected depth serves as an initial reference to evaluate the improvement efficiency compared to untreated ground conditions. The settlement behavior of the original subsoil was analyzed to evaluate its deformation characteristics under embankment loading. Settlement analysis considered three main components immediate, primary, and secondary settlements, expressed as :

$$S_{total} = S_i + S_c + S_s \qquad (2)$$

Immediate settlement was estimated using elastic theory from Boussinesq (1885) :

$$S_i = \frac{q_n . B}{E} I_p \qquad (3)$$

while primary consolidation settlement followed Terzaghi's equation :

$Sc = \frac{C_C . H}{1+e_0} \log\left(\frac{p'o + \Delta p}{p'o}\right)$ (4); $Sc = \frac{C_s . H}{1+e_0} \log\left(\frac{p'o + \Delta p}{p'o}\right)$ (5); $Sc = \frac{C_s . H}{1+e_0} \log\frac{pc}{po} + \frac{C_s . H}{1+e_0} \log\left(\frac{p'o + \Delta p}{p'o}\right)$ (6)

Eq. 4 is if the type of consolidation is normal or OCR = 1, with eq. 5 and eq. 6 for over consolidation, with $po' + \Delta p < pc'$ for equation 5 and $po' + \Delta p > pc'$ for eq. 6.

Secondary compression settlement was determined by :

$$S_S = C_\alpha H log(t_2/t_1) \qquad (7)$$

Following this, the settlement of the reinforced soil was calculated by applying a reduction factor to the total settlement of the unreinforced soil (Panguriseng and Makassar, 2018), equation determine on eq. 8.

$$S_c = \frac{1}{n} \times S_t \qquad (8)$$

Sc is the settlement of soil reinforced with sand columns, and St is the settlement of the soil before reinforced, while n is the settlement factor derived from the deformation modulus.

In numerical modeling with PLAXIS 2D, the actual cylindrical column is represented as an equivalent wall using the area equivalence method (Tan et al., 2008) to maintain the same area replacement ratio between 3D and 2D conditions. The equivalent column width is calculated as :

$$b_c = B\left(\frac{r_c^2}{R}\right) \qquad (9)$$

With $B = s/2$ and $R = 1.13B$ for square grid spacing. This method provides more accurate settlement and deformation behavior compared to the simplified approach where $bc = rc$ or the radius in 2D is the same as the radius in 3D. Therefore, this conversion approach was adopted in this study to ensure realistic representation of sand column performance in PLAXIS 2D simulations. Through the combination of numerical analysis with Plaxis 2D and manual calculations, this study will provide a comprehensive overview of the effectiveness of Sand Column reinforcement for improving the soft soil at the research location.

3 RESULTS

3.1 Soil Stratigraphy

The soil stratigraphy between boreholes BH-01 and BH-02 is shown in Figure 1. The laboratory test results indicate that the soil at BH-01 contained 28.66% organic material and was classified as organic clay, while BH-02 contained 96.98% organic material and was classified as peat.

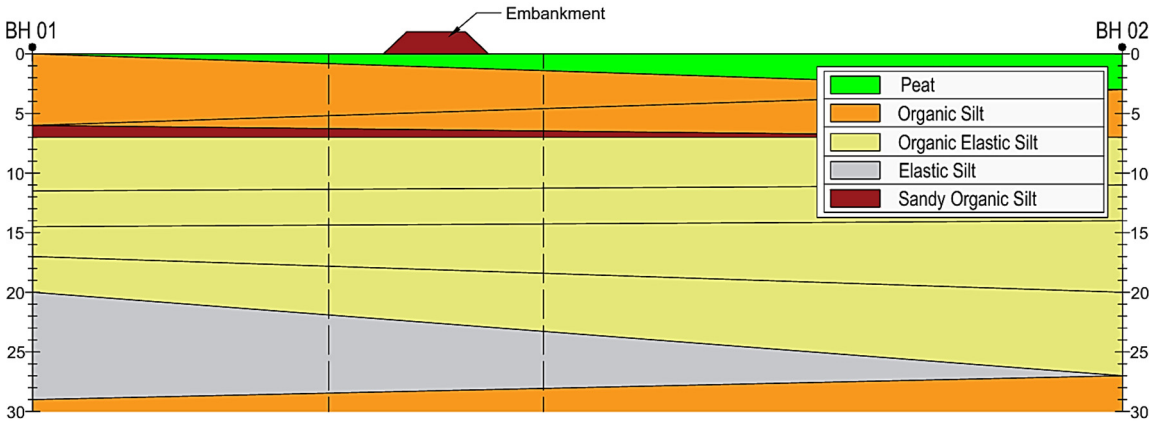

Figure 1. Soil stratigraphy diagram

3.2 Consolidation Analysis

Figure 2. shows the relationship between the degree of consolidation and soil depth, calculated using Eq. 4, Eq. 5, and Eq. 6. The results indicate that consolidation increases in the upper layers and stabilizes at a 14.5m depth . The depth where the curve becomes constant is defined as the limit of the compressible soil layer, which still undergoes compression under load.

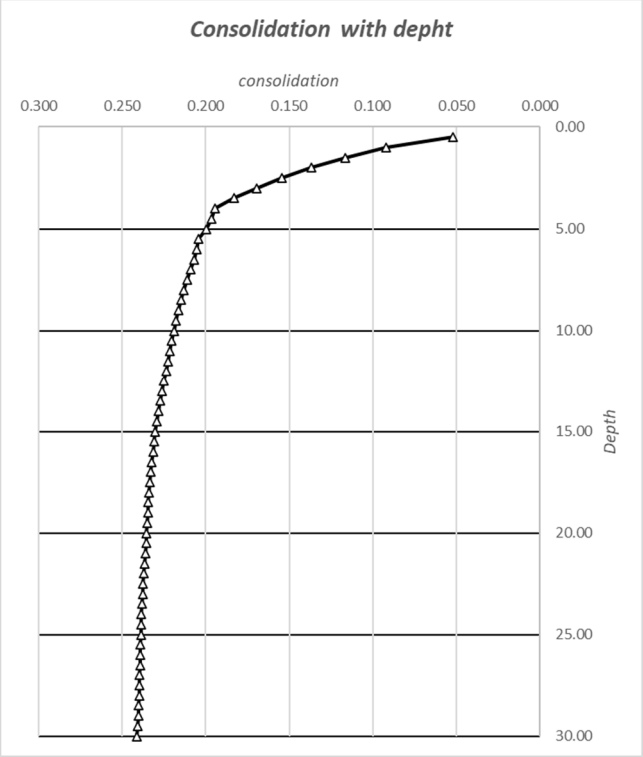

Figure 2. Consolidation relation with depth

3.3 Stability Analysis of Existing Soil

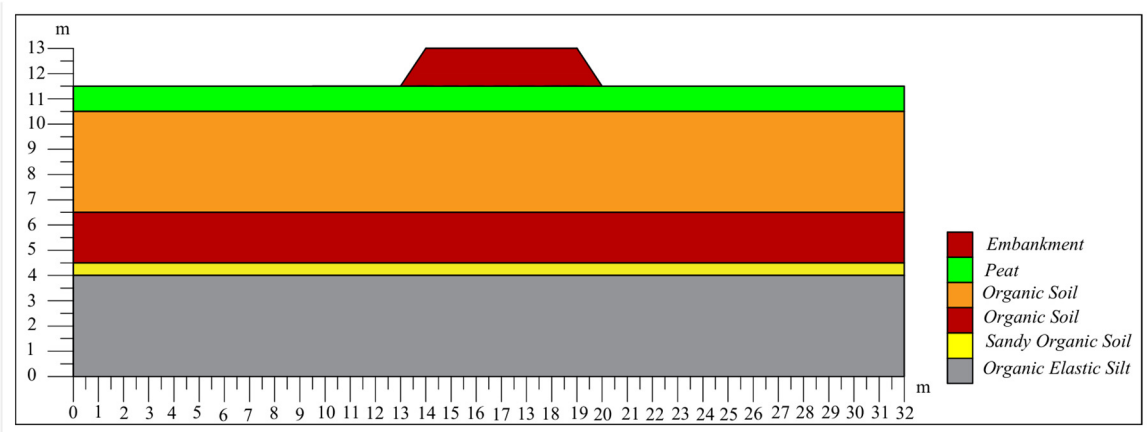

Figure 3. Embankment modeling in Plaxis 2D

The embankment model with a height of 1.5 m and traffic load of 15.00 kN/m² is shown in Figure 2. The numerical analysis using PLAXIS software begins with the modeling of the embankment geometry and soil layer configuration, representing the actual field conditions. The subsequent stage involves inputting the soil parameters, including the physical and mechanical properties of the materials, which serve as the basis for calculating deformation responses and slope stability. The *meshing* process is then carried out to discretize the model domain into finite elements, ensuring accurate and convergent analysis results. Finally, the calculation is performed through several phases, namely the *initial phase*, *plastic phase* for embankment construction, and *consolidation phase.* The total displacement of 0.2165 m occurred at the node shown in Figure 4. The deformed mesh is presented in Figure 5.

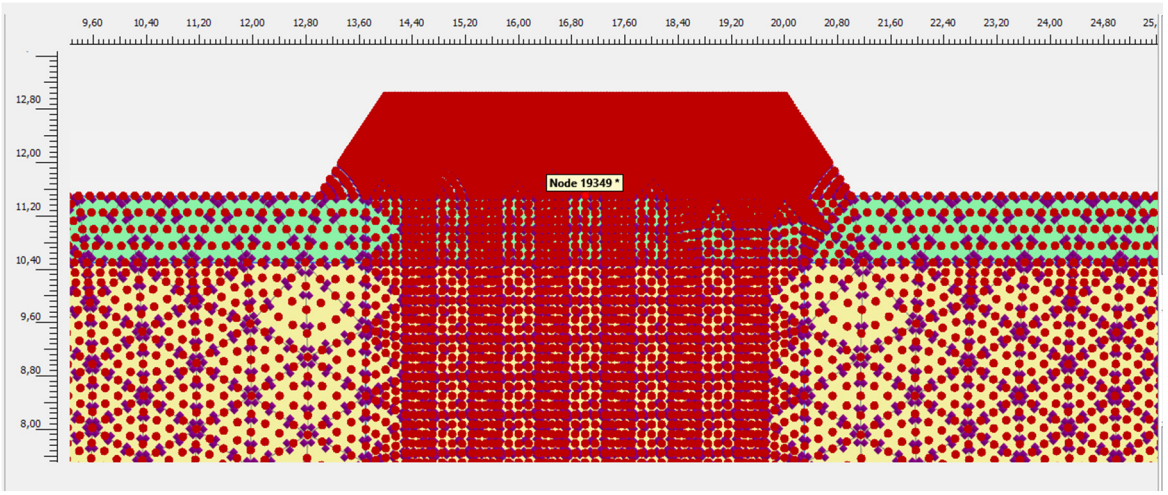

Figure 4. Calculation node

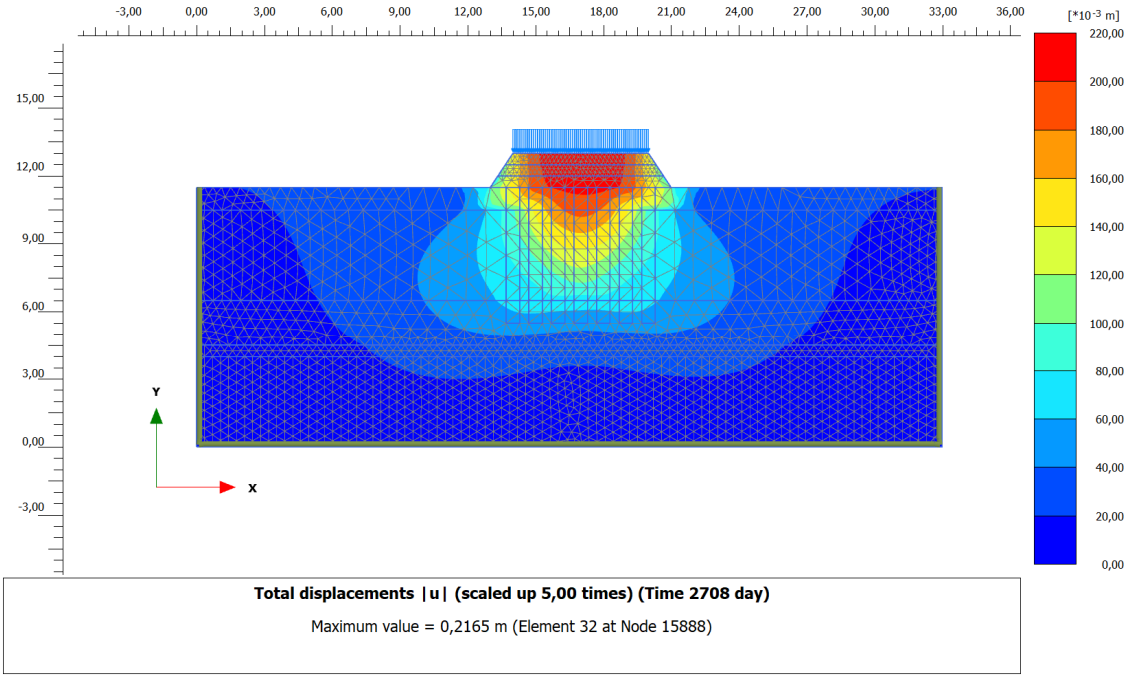

Figure 5. Deformed mesh of existing condition

3.4 Settlement Calculation of Existing Soil

The design load for this research was 75.895 kN/m², consisting of embankment and traffic load. The immediate, primary consolidation, and secondary consolidation settlement values after calculation use eq. 2 shown in Table 1.

The total settlement before Sand Column installation for 14,5 m soil layers was calculated as 0.36992 m. The estimated consolidation time for each soil layer is presented in Table 2, showing that 90% consolidation required 15.283 years in total.

Table 1. Immediate settlement, primary consolidation and secondary consolidation settlement of soil layers

Depth	Soil Type	H (m)	Si (m)	Ss (m)	Ss (m)	St (m)
0–1	Peat	1	0.00401	0.092	0.00001	0.09586
1–4	Organic Soil	4	0.03250	0.103	0.00014	0.13538
4–6	Organic Soil	2	0.01079	0.011	0.02605	0.04788
6–6,5	Sandy Organic Soil	0.5	0.00290	0.001	0.00389	0.00796
6,5–11,5	Organic Elastic Silt	4	0.01981	0.016	0.00469	0.04007
11,5–14,5	Organic Elastic Silt	3	0.01596	0.007	0.01968	0.04277
Total						0.36992

Table 2. Consolidation time of soil layers

Soil Layer	Time (years)
Peat	0,038
Organic Soil	5,14
Sandy Organic Soil	0,015
Organic Elastic Silt	7,42

3.5 Sand Column Design Parameters

From the Eq. 1 the Sand Column was calculated as diameter of 0.6 m by, spacing of 1 m, and a triangular installation pattern. The equivalent diameter (De) was designed 1.05 m from Bergado approach , and the replacement area ratio as 025% . The Sand Column was tested with a design depth of 6 m to evaluate its performance. The ultimate bearing capacity of the Sand Column group was calculated as 120.461 kN/m². This value exceeded the applied load of 75.895 kN/m², confirming adequacy of the design.

3.6 Plaxis 2D Modeling of Sand Column

The soil layers and Sand Column parameters used in Plaxis 2D modeling are summarized in Table 3. The Plaxis 2D model of the Sand Column with a depth of 6 m is shown in Figure 4. In PLAXIS 2D, the circular stone column in three-dimensional (axisymmetric) conditions was represented by an equivalent wall under plane strain conditions with b_c = 0,28 m. Total settlement was 0,1069 m. The deformation and total settlement are shown in Figure 7 and Figure 8, respectively.

Table 3. Input parameters for Plaxis 2D modeling

Layer Number/Soil Type	Material Parameters									
	Type	γ_{unsat} (kN/m^3)	γ_{sat} - (kN/m^3)	K_x (m/day)	K_y (m/day)	E_{ref} (kN/m^2)	υ	C (kN/m^2)	Φ (°)	Ψ (°)
1-Peat	Undrained A	7,93	8,747	0,002	0,001	1172	0,4	5,67	0	0
2- Organic Soil	Undrained A	14,82	29,31	0,002	0,001	1254	0,4	9,59	0	0
3-Organic Soil	Undrained A	15,52	34,02	0,002	0,001	1258	0,4	5	0	0
4-Sandy Organic Soil	Undrained A	9,77	14,45	0,1	0,1	1890	0,4	5	0	0
5-Organic Elastic Silt	Undrained A	12,37	14,96	0,1	0,1	2056	0,4	5	0	0
Sand Column	*Drained*	12	20	1,2	1,2	50000	0,3	0,01	38	8
Embankment	*Drained*	16	19	1	1	3000	0,3	10	30	0

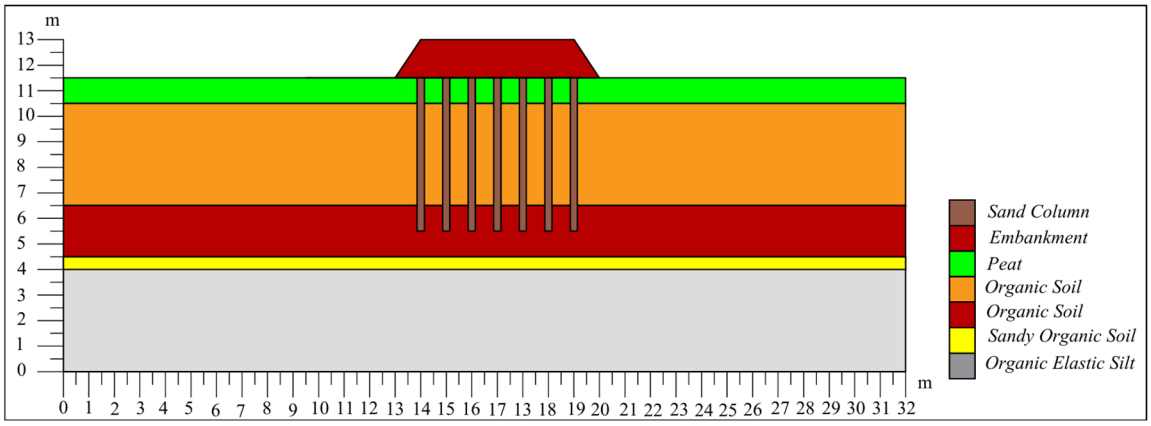

Figure 6. Plaxis 2D model of Sand Column (depth 6 m)

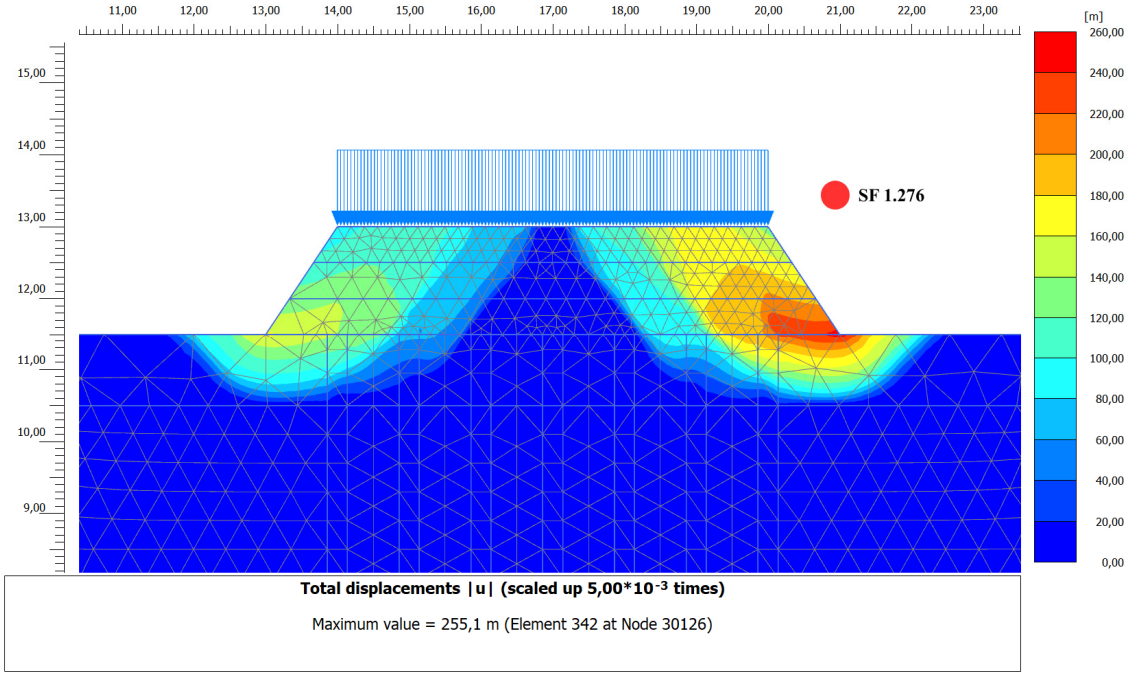

Figure 7.Total deformation of Sand Column model

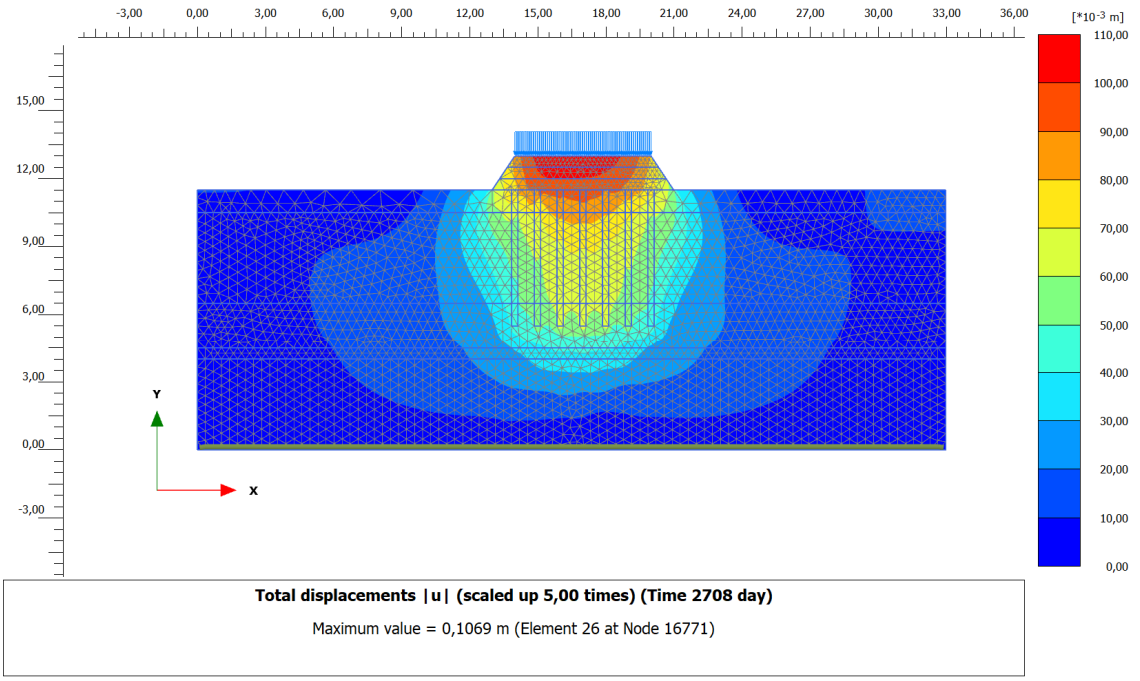

Figure 8. Total settlement of embankment

3.7 Settlement with Sand Column

Based on manual calculations using Eq.8. comparison between the settlement values before and after soil improvement is presented in Figure 8. Without improvement, the total settlement at a depth of 14.5 m reached 0.37 m, whereas after the installation of a 6 m sand column, the settlement decreased to 0.0967 m. This indicates that the sand column installation effectively reduced 73.8% from the total settlement. Meanwhile, the FEM method showed a reduction in settlement from 0.22 m to 0.1069 m (figure 8).

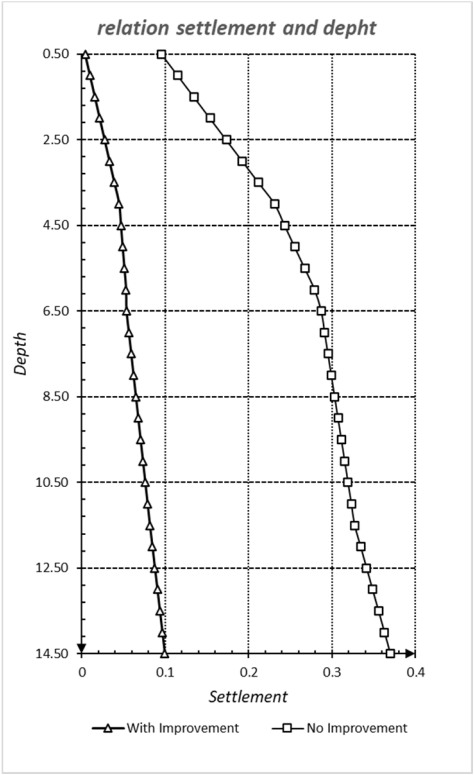

Figure 8 Relation settlement and depth

The settlement–depth relationship shows that the curve with improvement exhibits a gentler slope than that without improvement. This demonstrates that the use of sand columns effectively enhances soil bearing capacity, accelerates the consolidation process, and reduces vertical deformation within the compressible soil layer.

DISCUSSION

Based on the results, Sand Column is highly effective, transforming a problematic subgrade into a stable foundation engineered to support the anticipated structural loads. The initial geotechnical modelling revealed that the unimproved ground was inadequate, exhibiting a bearing capacity SF = 1.138. The implementation of a 6-meter deep Sand Column reinforcement resulted in a significant improvement in embankment stability. The Plaxis 2D simulation for this reinforced condition produced a safety factor of 1.276, validating the design's effectiveness. This outcome confirms that the columns successfully improve bearing capacity by enhancing the composite shear strength of the soil mass.

The analysis also calculated amount of ground settlement. In the FEM method, the consolidation settlement decreased from 0.22 m to 0.11 m, indicating an efficiency improvement of 50%. Meanwhile, in the numerical method, the deformation decreased from 0.37 m to 0.10 m, equivalent to a 72.97% reduction. Both methodologies confirm that the Sand Columns are exceptionally effective in mitigating settlement. This is achieved through stress redistribution to the stiffer column elements and the acceleration of consolidation via enhanced drainage.

The analysis indicates a significant reduction in the time required to achieve 90% primary consolidation (t90) was reduced by 35.1%, from 15.283 years to 9.921 years. This accelerated settlement time is highly beneficial for the project, improving the feasibility of meeting its schedule and budget. And because the plan just uses standard building methods and common materials like sand, it's a really practical and affordable fix for these tricky organic soils. Therefore, the findings not only present a validated design solution for the project site but also contribute pertinent data to the broader practice of geotechnical engineering.

4 CONCLUSION

This study was conducted to evaluate the effectiveness of sand columns in improving the stability and settlement characteristics of high-organic clay, addressing a notable gap in the existing literature. The major findings confirm that this ground improvement technique is highly effective. Initially, the unimproved soil was fundamentally unstable, exhibiting bearing capacity failure (SF = 1.138) and predicting total settlement of 0.22 m from numerical model and 0.37 m from analytic calculation. Following the installation of 6-meter deep sand columns, the site's geotechnical performance was radically improved, achieving a stable safety factor of 1.276 and reducing the total displacement to a serviceable level of 0.1069 m in the numerical model and 0.10 m in analytic. Furthermore, the time required to achieve 90% primary consolidation was reduced by approximately 35.1%, from 15.283 years to 9.921 years, confirming the technique's ability to accelerate settlement significantly. This research contributes valuable, quantitative data on the successful application of sand columns in problematic organic soils, providing a practical engineering solution for similar conditions prevalent in Indonesia and other tropical regions. A key limitation of this study is its reliance on numerical modelling and analytical calculations; therefore, future research should aim to validate these findings through large-scale physical model tests or in-situ monitoring of a field trial. Further investigation into the long-term secondary consolidation behaviour of sand column-reinforced organic soils is also recommended to enhance the understanding of their performance over the project lifecycle.

DISCLAIMER

The authors declare no conflict of interest.

AVAILABILITY OF DATA AND MATERIALS

All data are available from the author.

REFERENCES

Agaiby, S.S., Hassan, A.K., Dakhli, A. & Elhakim, A.F., 2022. Sawdust effect on compressibility and shear strength characteristics of highly organic clay. *Engineering Research Journal*, 45, pp.379–387. doi:10.21608/erjm.2022.127027.1151.

Al-Saoudi, N.K.S., Joni, H.H. & Al-Gharbawi, A.S.A., 2014. Single Sand Column stabilized by lime embedded in soft soil. *Engineering and Technology Journal*, 32(4), pp.1028–1037. doi:10.30684/etj.32.4A.16.

Bhattacharya, A.K. & Basack, S., 2011. A review of the use of the pre-loading technique and vertical drains for soil consolidation. In: *Proceedings of the Indian Geotechnical Conference*, Kochi, 15–17 December 2011.

Brandl, H., 2019. Long-term settlement (creeping) of soft soils, and ground improvement. In: H. Brandl, ed. *Proceedings of GeoMEast 2019 – Sustainable Civil Infrastructures*. Cham: Springer, pp.125–144. doi:10.1007/978-3-030-34184-8_9.

Guswantoro, T., Suppa, R., Azahra, St. & Sulaiman, L., 2022. The study of sand qualities from flash flood impact in North Luwu Regency to be used as a fine aggregate. In: *Proceedings of EAI International Conference on Disaster Mitigation*. doi:10.4108/eai.17-11-2021.2318671.

Harris, J.P., Harvey, O.R., Puppala, A.J., Sebesta, S., Chikyala, S.R. & Saride, S., 2009. *Mitigating the effects of organics in stabilized soils: Technical report*. College Station, TX: Texas Transportation Institute. Available at: https://d2dtl5nnlpfr0r.cloudfront.net/tti.tamu.edu/documents/0-5540-1.pdf [Accessed 24 September 2025].

Hernina, N.H., Handayani, N.P. & Saputra, N.A., 2023. Pengaruh perkuatan kolom pasir terhadap kekuatan tanah lempung. *Jurnal Komposit*, 7(2). doi:10.32832/komposit.v7i2.9127.

Kamao, S., 2019. A prediction method for long-term settlement of highly organic soft soil. *International Journal of Geomate*, 17, pp.162–169. doi:10.21660/2019.60.8169.

Limsiri, C., 2008. *Very soft organic clay applied for road embankment: Modelling and optimisation approach*. Delft: UNESCO-IHE PhD Thesis. CRC Press.

Ling, F.N.L., Kassim, K.A., Karim, A.T.A., Tan, C.K. & Tiong, K.P.C., 2014. Geotechnical properties of Malaysian organic soils: Case study in Batu Pahat, Johor. *International Journal of Integrated Engineering*, 6(1), pp.1–8.

Martinón-Torres, M., 2022. Stabilization of expansive soils using chemical additives: A review. *Journal of Rock Mechanics and Geotechnical Engineering*, 14(6), pp.1319–1342. doi:10.1016/j.jrmge.2022.02.011.

Mohamad, N.O., Razali, C.E., Hadi, A.A.A., Som, P.P., Eng, B.C., Rusli, M.B. & Mohamad, F.R., 2016. Challenges in construction over soft soil: Case studies in Malaysia. *IOP Conference Series: Materials Science and Engineering*, 136, p.012002. doi:10.1088/1757-899X/136/1/012002.

Okonkwo, U.N. & Kennedy, C., 2023. The effectiveness of cement and lime as stabilizers for subgrade soils with high plasticity and swelling potential. *Saudi Journal of Civil Engineering*, 7(3), pp.40–60. doi:10.36348/sjce.2023.v07i03.001.

Pandey, V.K., Dhiman, S. & Bharti, K., 2024. A review on the use of lime in soil stabilization. In: S. Singh & S. Kaur, eds. *Latest Trends in Engineering and Technology*. Boca Raton: CRC Press, pp.414–421. doi:10.1201/9781032665443-59.

Pokharel, B. & Siddiqua, S., 2021. Effect of calcium bentonite clay and fly ash on the stabilization of organic soil from Alberta, Canada. *Engineering Geology*, 293, p.106291. doi:10.1016/j.enggeo.2021.106291.

Prakash, K. & Krishnamoorthy, A., 2022. Stability of embankment constructed on soft soil treated with soil–cement columns. *Transportation Infrastructure Geotechnology*, 10, pp.595–615. doi:10.1007/s40515-022-00237-3.

Prasad, S.S.G. & Satyanarayana, P.V.V., 2021. Stabilization of soft soils using single and group of Sand Columns. In: S. Biswas, S. Metya, S. Kumar & P. Samui, eds. *Advances in Sustainable Construction Materials*. Lecture Notes in Civil Engineering, vol.124. Singapore: Springer, pp.407–415. doi:10.1007/978-981-33-4590-4_35.

Sohaib, N., SarfrazFaiz, M. & Sami, M.F., 2020. Experimental study on improvement of soft clay using Sand Columns. *Journal of Civil Engineering and Architecture*, 14(7), pp.329–338. doi:10.17265/1934-7359/2020.07.006.

Interpretasi Bidang Gelincir Lereng Menggunakan Kombinasi Uji Geoteknik dan Geofisika

Metta Devi Hartadi[1,*], Muhammad Ihsan Rezqa[2], Nurindahsih Setionegoro[3]
[1]Senior Geotechnical Engineer, PT Tarumanegara Bumiyasa, Jakarta, Indonesia, 11540; mettadevi92@gmail.com
[2]Geophysicist, PT Tarumanegara Bumiyasa, Jakarta, Indonesia, 11540; ihsanrezzqa@gmail.com
[3]Senior Geotechnical Advisor, PT Tarumanegara Bumiyasa, Jakarta, Indonesia, 11540; heynurindahsih@gmail.com
*Correspondence: mettadevi92@gmail.com

ABSTRAK Proses analisis stabilitas lereng memerlukan data geoteknik yang komprehensif mengenai kondisi lokasi setempat. Namun sering kali terdapat keterbatasan data yang diperoleh dari pengujian geoteknik pada umumnya seperti uji pengeboran, *Standard Penetration Test*, maupun *Cone Penetration Test*. Penelitian ini membahas penerapan metode geofisika, yaitu uji geolistrik dua dimensi, untuk mendapatkan gambaran lebih baik terkait kondisi bawah permukaan pada studi kasus di Bali. Hasil uji geolistrik menunjukkan gambaran bidang gelincir yang lebih detail dibandingkan dengan hanya menggunakan metode pada umumnya. Profil yang dihasilkan kemudian dimodelkan menggunakan metode elemen hingga pada program PLAXIS 2D untuk mengevaluasi faktor keamanan dari lereng tersebut. Dari penelitian ini, dapat disimpulkan bahwa pengaplikasian metode geolistrik dapat memberikan gambaran lebih detail terhadap kondisi bawah permukaan sehingga analisis stabilitas lereng dapat dilakukan lebih akurat. Namun terdapat batasan dimana pengaruh pengujian geolistrik belum tentu menghasilkan efek yang signifikan terhadap desain dikarenakan ketergantungan terhadap kondisi bawah permukaan proyek terkait.

KEYWORDS Stabilitas Lereng, Geofisika, Geolistrik, Bidang Gelincir

1 PENDAHULUAN

Tanah merupakan material yang unik karena memiliki kemungkinan lapisan yang tak tentu, berbeda dengan material-material lain seperti beton dan baja yang dapat terukur dengan pasti besaran kekuatannya. Maka untuk melakukan analisa yang berhubungan dengan tanah, diperlukan serangkaian pengujian, mulai dari uji lapangan hingga uji laboratorium.

Uji lapangan (*site investigation*) yang umumnya dilakukan dapat berupa sondir dan pengeboran tanah yang dilengkapi dengan pengujian SPT (*Standard Penetration Test*). Pengujian ini dapat memberikan gambaran langsung mengenai kondisi tanah di area proyek (yang akan dianalisa). Untuk mendapatkan gambaran lebih detail tentu dibutuhkan jumlah uji yang banyak agar dapat memperkirakan *profiling* lapisan tanah. Namun keterbatasan biaya dan waktu seringkali menjadi hambatan utama. Minimnya uji lapangan yang dilakukan ini membuat perencanaan/analisa geoteknik menjadi lebih sulit karena kurangnya gambaran mengenai profil lapisan tanah.

Untuk mengatasi kesulitan ini, dapat digunakan kombinasi antara pengujian geoteknik konvensional dengan pengujian geofisika secara lebih khusus pengujian geolistrik 2 dimensi atau *Electrical Resistivity Tomography (ERT)*. Pengujian geofisika ini dapat memberikan gambaran secara 2 dimensi terkait kondisi bawah permukaan jika dibandingkan dengan investigasi geoteknik yang umumnya hanya 1 dimensi. Namun, di samping dari kepraktisannya, pengujian geofisika juga memiliki beberapa keterbatasan. Salah satunya adalah *Non-Uniqueness*, yaitu satu data dapat menghasilkan beberapa model berbeda (A. Roy, 1962). Untuk mengatasi keterbatasan inilah dibutuhkan data pembanding seperti data pengeboran tanah dan data geologi setempat. Selain itu kedalaman investigasi juga dipengaruhi oleh panjang lintasan (1:3 s.d. 1:5 panjang lintasan)(U.S. Environmental Protection Agency).

2 STUDI KASUS (VILLA BALI)

Lokasi penelitian berada di Bali, yang direncanakan akan dibangun bangunan villa 2 lantai dengan 1 lapis basement yang terletak di area perbukitan. Karena lahan berkontur, maka akan dilakukan cut & fill untuk mencapai elevasi rencana. Stabilitas lereng terkait cut & fill ini akan dilakukan menggunakan program PLAXIS 2D berbasis metode elemen hingga.

Untuk keperluan analisa, dilakukan *soil investigation* berupa (4) titik sondir dan (2) titik pengeboran tanah. Denah *soil investigation* yang dilakukan dapat dilihat selengkapnya pada Gambar. 1.

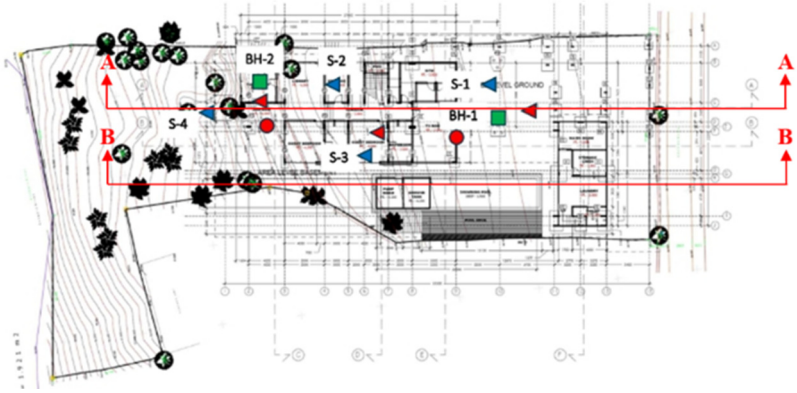

Gambar 1. Denah Penyelidikan Tanah

Selain pengujian geoteknik berupa sondir dan pengeboran tanah, pengujian geofisika juga dilakukan. Pengujian geofisika yang dilakukan berupa pengujian geolistrik yang memanfaatkan perambatan arus listrik pada tanah. Dimana hasil yang didapatkan dari pengujian geolistrik ini berupa resistivitas tanah dalam satuan Ohm.m. Pengujian geolistrik ini sudah terbukti dapat memberikan gambaran yang baik terkait bidang gelincir terutama untuk keperluan Analisa stabilitas lereng (Hazreek, 2018; Santie, 2024; Sianturi, 2023).

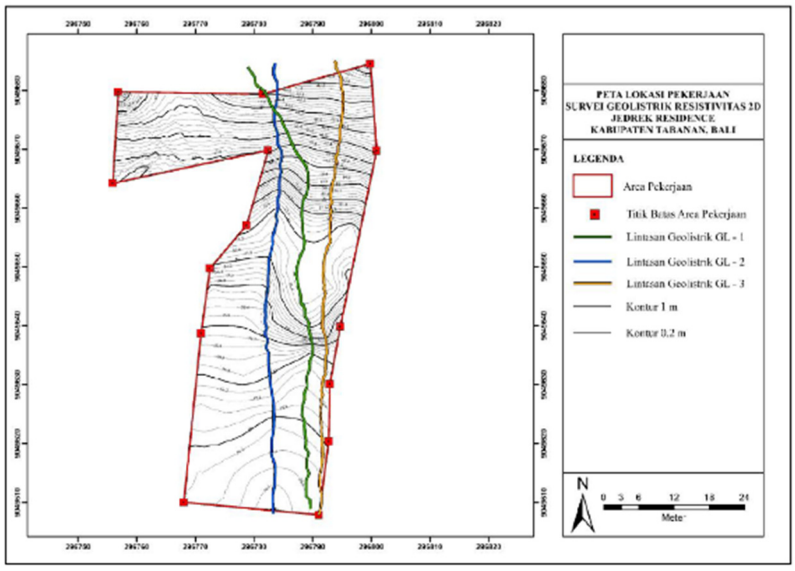

Gambar 2. Denah Pekerjaan Geolistrik

Dari hasil pengeboran tanah, 2.00 s.d. 4.00 teratas berupa lapisan lanau kelempungan dan lempung kelanauan dengan konsistensi lunak hingga kekakuan sedang. Lapisan selanjutnya berupa lanau kepasiran dan lanau kelempungan dengan konsistensi sangat kaku hingga keras yang dilanjutkan dengan lapisan pasir dan pasir kelanauan yang sangat padat.

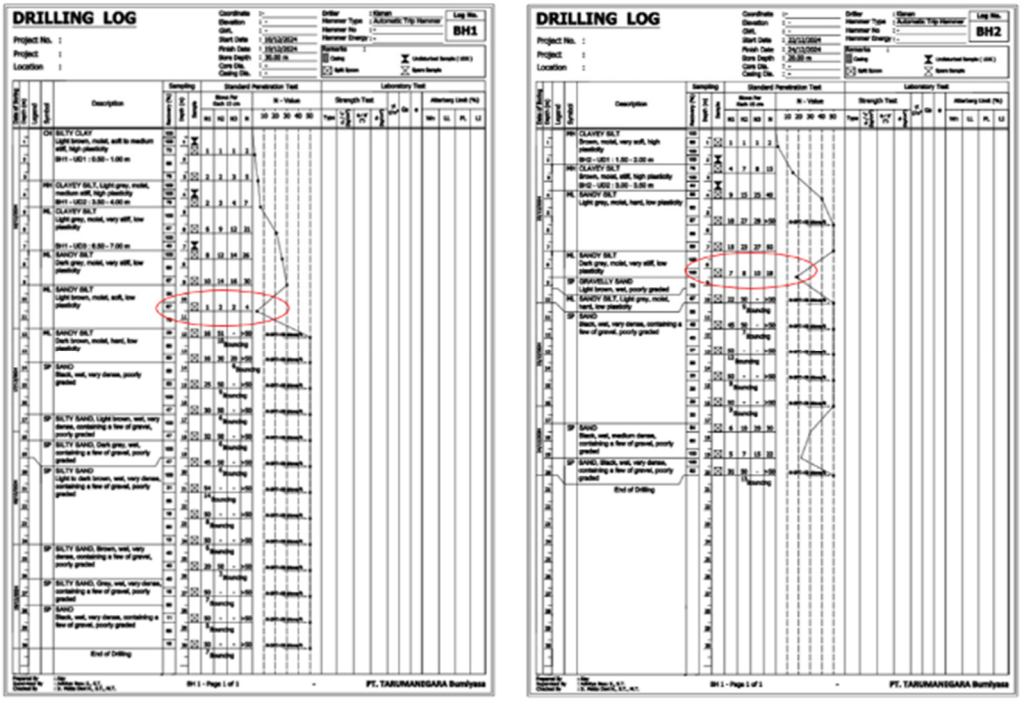

Gambar 3. *Drilling Log* proyek Villa Bali

Namun di sekitar kedalaman 7.00 s.d 8.50 meter (area BH2) dan 9.00 s.d. 11.50 meter (area BH1), terdapat "pelunakan" yang ditandai dengan NSPT yang mengecil pada kedalaman tersebut. *Drilling Log* selengkapnya dapat dilihat pada Gambar 3.

Kemudian dari hasil pengujian geolistrik, diduga bahwa di sekitar kedalaman tersebut terdapat rembesan air. Hal ini juga terkonfirmasi dengan pengamatan visual di lapangan dimana terdapat air yang keluar di sekitar BH2 (Gambar 4.).

Hasil pengujian geolistrik (lintasan GL-3) dapat dilihat selengkapnya pada Gambar 5. Hasil pengujian geolistrik (lintasan GL-3) ini dikorelasikan dengan data bor dan sondir yang dapat dilihat selengkapnya pada Gambar 6. Terlihat dari korelasi tersebut, terdapat dugaan aliran air yang menjadi bidang gelincir dari lereng. Selanjutnya, potensi bidang gelincir ini juga ikut dimodelkan dalam analisa stabilitas lereng menggunakan program PLAXIS 2D.

Gambar 4. Dugaan Rembesan Air dari Hasil Pengamatan Visual Lapangan

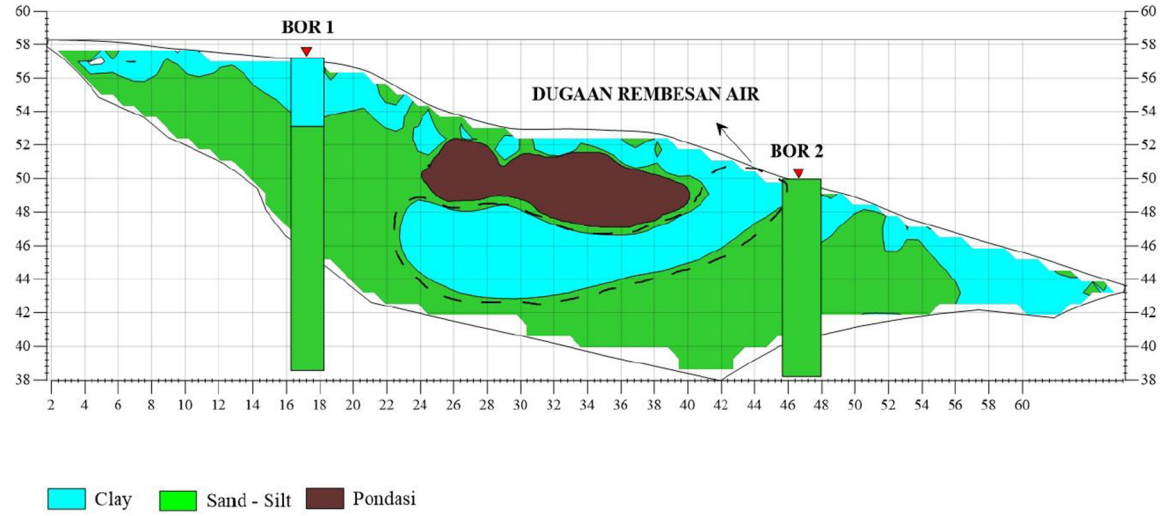

Gambar 5. Hasil Pengujian Geolistrik (Lintasan GL-03)

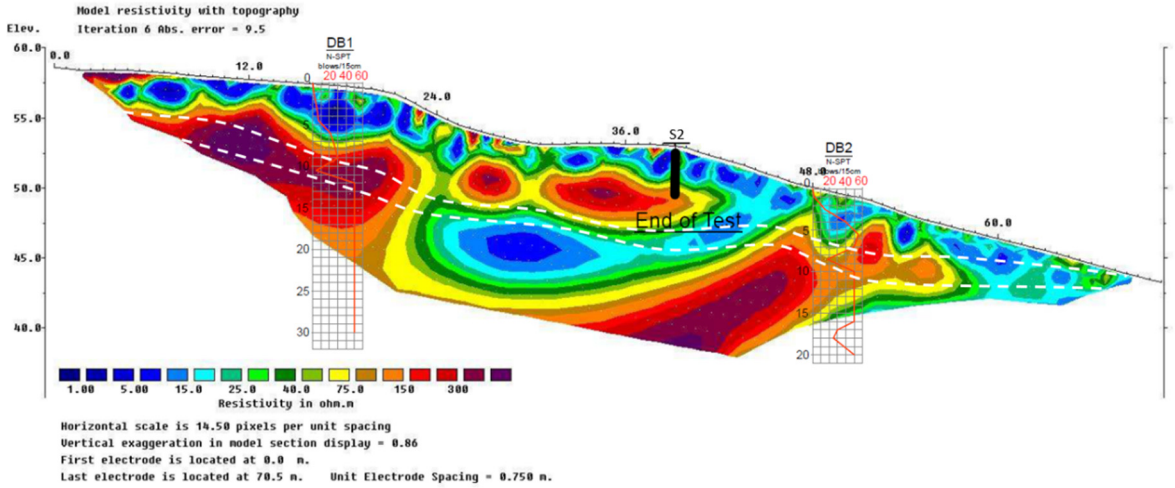

Gambar 6. Korelasi Hasil Pengujian Geolistrik (Lintasan GL-03) dengan Data Bor & Sondir

3 HASIL PENELITIAN

Dari data-data uji lapangan dan uji laboratorium, dilakukan analisa stabilitas lereng menggunakan program PLAXIS 2D berbasis metode elemen hingga. Dari hasil uji geolistrik, diketahui potensi bidang gelincir pada lereng yang juga merupakan lapisan dengan kandungan air yang cukup besar. Maka pada pemodelan lereng untuk analisa stabilitas, dimodelkan pula bidang gelincir tersebut. Dimana bidang gelincir tersebut dimodelkan menggunakan *interface* pada PLAXIS 2D. Sebagai perbandingan, dilakukan juga pemodelan berdasarkan data geoteknik saja tanpa memasukkan bidang gelincir.

Karena lereng ini diperuntukkan untuk kondisi permanen, maka faktor keamanan minimum yang harus dicapai sesuai dengan persyaratan SNI adalah 1.5. Namun pada penelitian ini, analisis hanya dilakukan sebatas *review* terhadap desain yang sudah dilakukan di lapangan dan tidak sampai tahap perkuatan untuk memperoleh faktor keamanan minimum

Tabel 1. Nilai Minimum Faktor Keamanan Lereng Galian berdasarkan SNI Geoteknik

Kondisi Lingkungan dan Risiko	Keandalan Parameter Tanah			
	Kurang		Cukup	
Sifat Galian	Sementara	Tetap	Sementara	Tetap
Tidak ada Hunian Manusia atau Bangunan Sekitar	1.30	1.50	1.25	1.30
Banyak Bangunan Sekitar	1.50	2.00	1.30	**1.50**

Tabel 2. Nilai Minimum Faktor Keamanan Lereng berdasarkan NAVFAC DM-7

Faktor Keamanan	Keterangan
≥1.5	Untuk kondisi pembebanan tetap atau berkelanjutan
≥2	Untuk fondasi struktur
1.25-1.3	Untuk pembebanan sementara atau jika nilai stabilitas mencapai minimum saat proses konstruksi
≥1.5	Untuk pembebanan sesaat seperti saat gempa

Analisa stabilitas lereng dilakukan terhadap 2 potongan, yaitu *Section* A-A dan *Section* B-B.

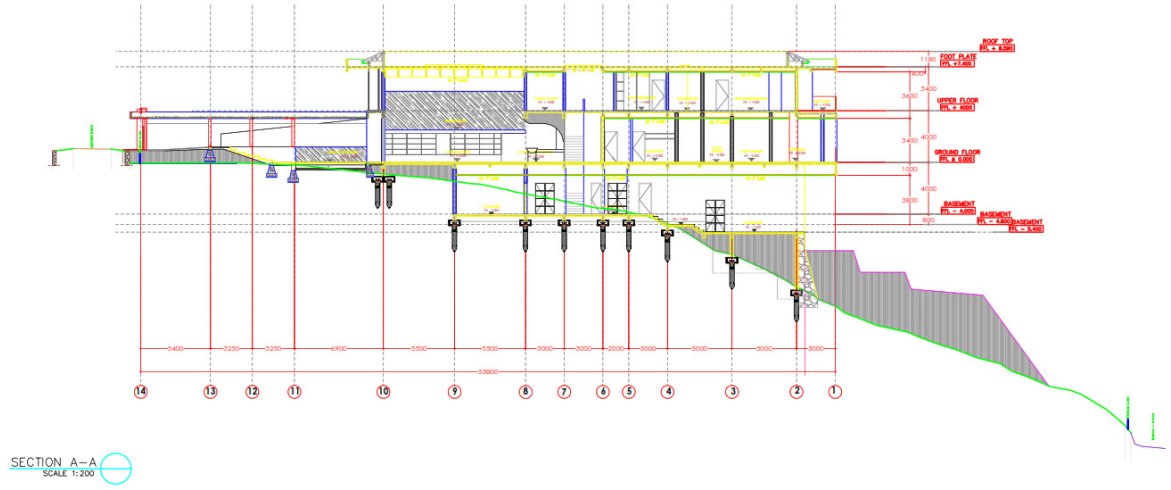

Gambar. 7. Lereng *Section* A-A

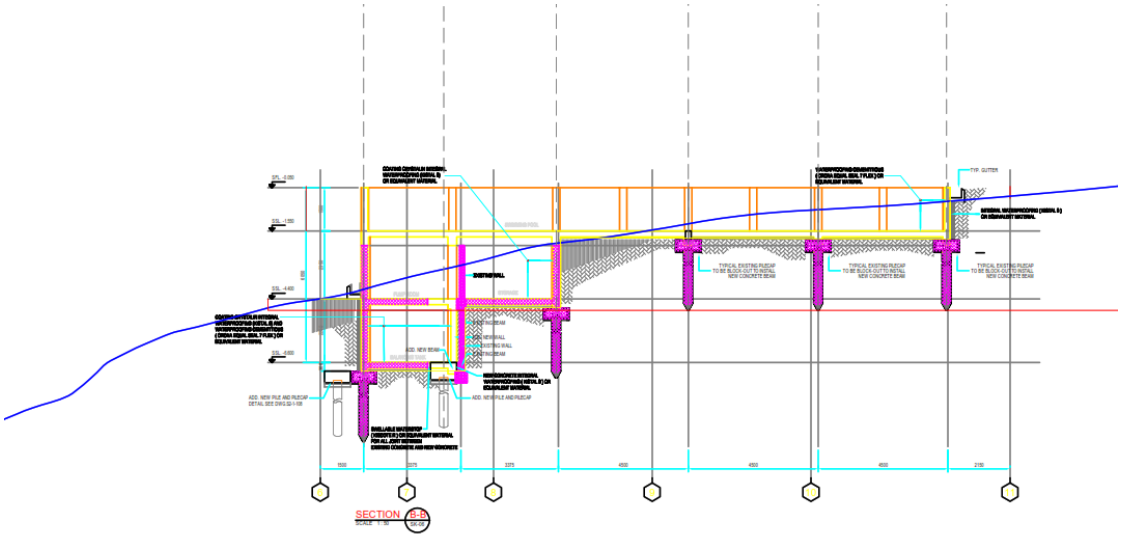

Gambar 8. Lereng *Section* B-B

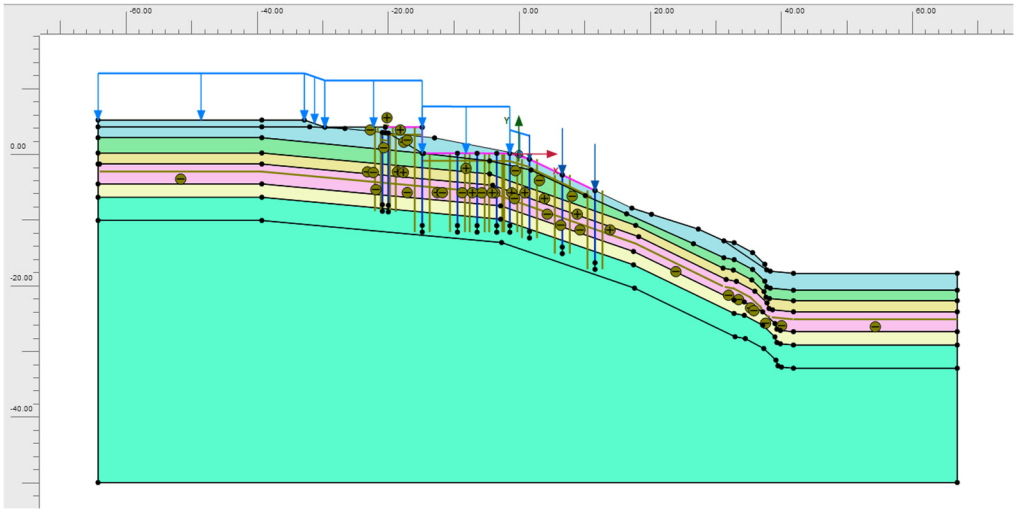

Gambar 9. Pemodelan *Section* A-A

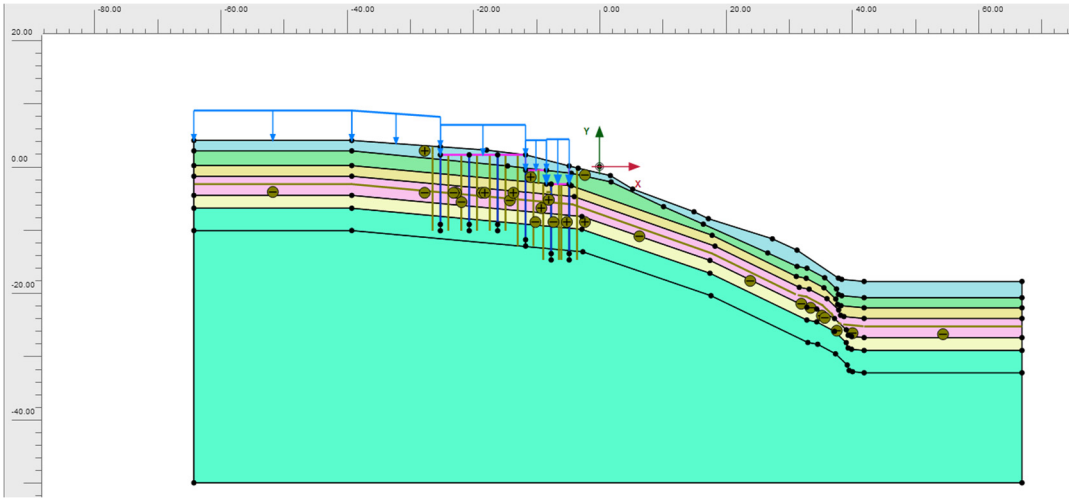

Gambar 10. Pemodelan *Section* B-B

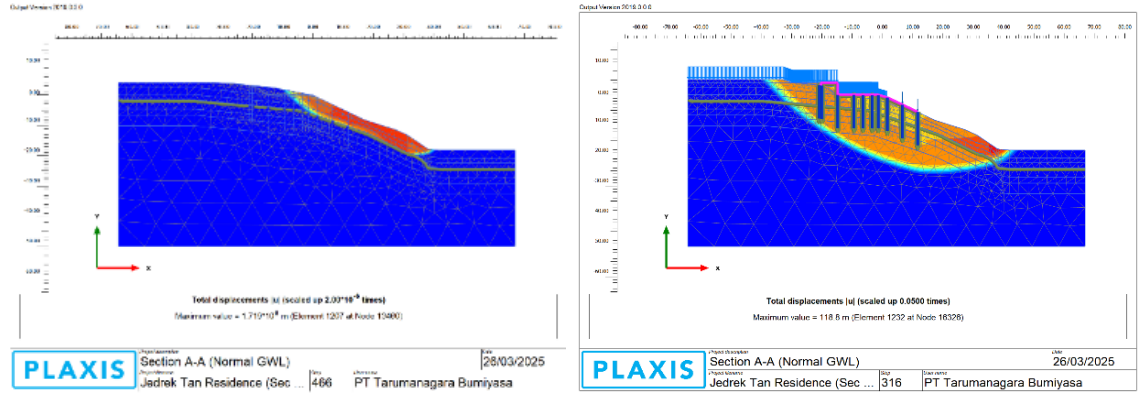

Gambar 11. Hasil Pemodelan pada Plaxis 2D Section A-A dengan slip-surface untuk kondisi awal (kiri) dan kondisi akhir (kanan)

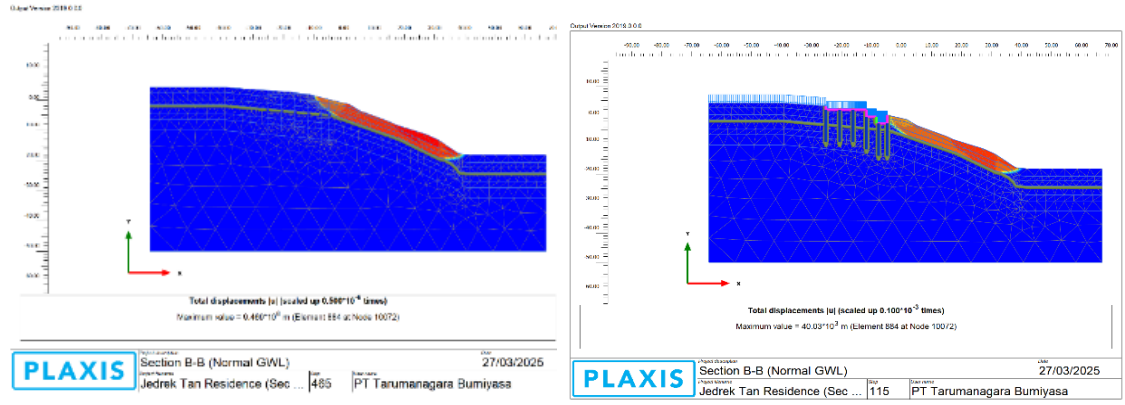

Gambar 12. Hasil Pemodelan pada Plaxis 2D *Section* B-B dengan slip-surface untuk kondisi awal (kiri) dan kondisi akhir (kanan)

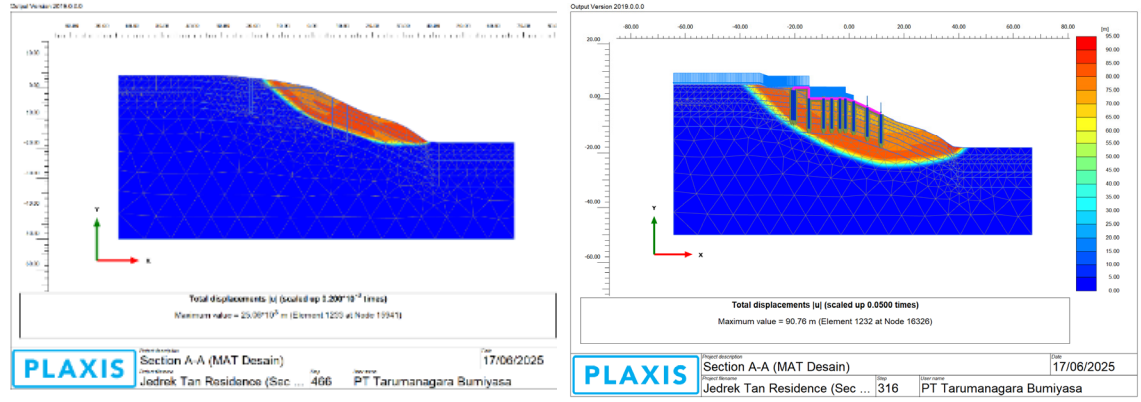

Gambar 13. Hasil Pemodelan pada Plaxis 2D *Section* A-A tanpa slip-surface untuk kondisi awal (kiri) dan kondisi akhir (kanan)

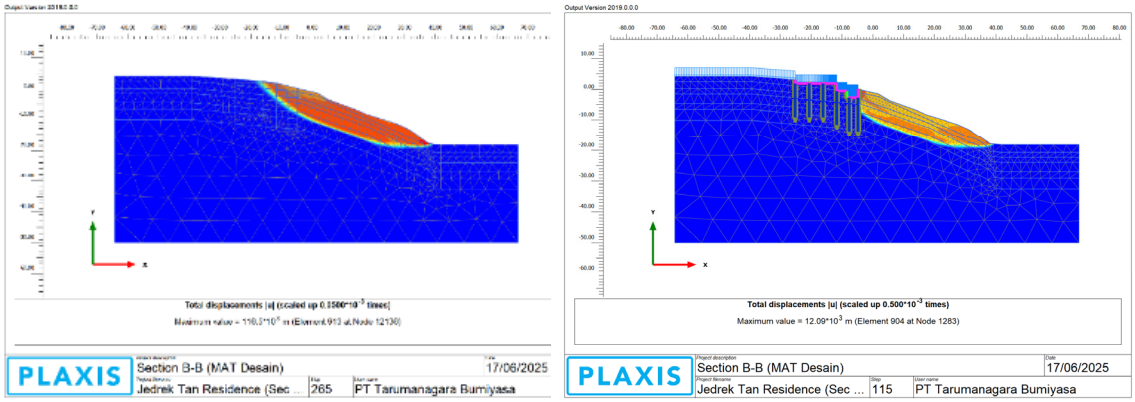

Gambar 14. Hasil Pemodelan pada Plaxis 2D *Section* A-A tanpa slip-surface untuk kondisi awal (kiri) dan kondisi akhir (kanan)

Dari hasil analisa, dapat dilihat pada Gambar 11 dan 12, kedalaman dari Lokasi potensi bidang gelincir lebih dangkal dibandingkan dengan lokasi bidang gelincir yang dihasilkan dari analisa tanpa berdasarkan data geolistrik Gambar 13 dan 14. Hal ini akan menyebabkan desain akan menjadi lebih boros (tidak efisien).

Tabel 3. Nilai Faktor Keamanan Hasil Analisa

Section	Faktor Keamanan			
	Dengan Geolistrik		Tanpa Geolistrik	
	Kondisi Awal	Kondisi Akhir	Kondisi Awal	Kondisi Akhir
Section A-A	1.249	1.318	1.266	1.325
Section B-B	1.250	1.256	1.299	1.341

Dari hasil analisa faktor keamanan, dapat dilihat bahwa dengan dilakukannya pengujian geofisika, nilai faktor keamanan menjadi lebih kecil jika dibandingkan dengan analisa tanpa pengujian tambahan. Hal ini menunjukkan bahwa tambahan data yang dapat memberikan gambaran lebih baik terkait kondisi bawah permukaan dapat memberikan tambahan pertimbangan yang berpengaruh terhadap analisa desain nantinya. Namun terlihat perbedaan antara hasil analisa dengan geolistrik dan tanpa geolistrik tidak signifikan. Hal ini menjadi batasan dikarenakan hasil dari pengujian geolistrik tetap tergantung terhadap kondisi bawah permukaan di Lokasi yang hendak ditinjau sehingga belum tentu pengujian geolistrik dapat memberikan pengaruh yang besar terhadap proses analisa selanjutnya.

4 KESIMPULAN

Tanah memiliki karakteristik unik dan kompleks yang memerlukan pengujian menyeluruh dari lapangan hingga laboratorium untuk analisa geoteknik yang akurat. Pengujian pada uumunya seperti sondir dan pengeboran dengan SPT memberikan gambaran satu dimensi kondisi tanah, namun keterbatasan biaya dan waktu sering membatasi jumlah pengujian sehingga profil tanah kurang lengkap.

Pengujian geofisika, khususnya geolistrik, dapat melengkapi data dengan memberikan gambaran dua dimensi bawah permukaan, seperti mendeteksi keberadaan air dan bidang gelincir yang tidak mudah terlihat dari pengujian pada umumnya. Studi kasus di lokasi pembangunan villa di Bali menunjukkan

potensi rembesan air dan bidang gelincir pada kedalaman tertentu yang terkonfirmasi lewat gabungan data geolistrik dan pengeboran.

Analisa stabilitas lereng menggunakan program PLAXIS 2D menunjukkan bahwa pemodelan yang memasukkan data geolistrik menghasilkan faktor keamanan lereng sedikit lebih rendah, yang berarti desain akan cenderung lebih konservatif namun lebih realistis. Meski begitu, perbedaan faktor keamanan antara analisa dengan dan tanpa data geolistrik tidak signifikan, menandakan pengaruh tambahan data geofisika masih tergantung pada kondisi spesifik lapangan. Secara keseluruhan, penggunaan kombinasi pengujian geoteknik dan geofisika dapat meningkatkan keakuratan evaluasi kondisi tanah dan stabilitas lereng dalam perencanaan teknik.

5 REFERENCES

Badan Standardisasi Nasional (BSN) (2017) SNI 8460:2017 Persyaratan Perancangan Geoteknik. Jakarta: Badan Standardisasi Nasional.

Geotechnical Engineering Center (2015) Manual Kestabilan Lereng dan Penanganan Longsoran, 3rd edn. Unpar.

Hazreek, Z.A.M., Nizam, Z.M., Aziman, M., Md Dan, M.F., Shaylinda, M.Z.N., Faizal, T.B.M., Aishah, M.A.N., Ambak, K., Rosli, S., Rais, Y., Ashraf, M.I.M. and Alel, M.N.A. (2018) 'Mapping on slope seepage problem using electrical resistivity imaging (ERI)', Journal of Physics: Conference Series, 995(1), p. 012091. doi: 10.1088/1742-6596/995/1/012091.

NAVFAC (1986) Design Manual DM7 - Soil Mechanics, Foundations, and Earth Structures. U.S. Naval Facilities Engineering Command.

Pasaribu, F.H., Sonntag, W., Johannes, M. and Sianturi, R. (2023) 'Analysis of landslide using resistivity method in the avalanche area of Tolnaku, Kupang Regency, East Nusa Tenggara, Indonesia', International Journal of Safety and Security Engineering, 13(5), pp. 481–492. doi: 10.18280/ijsse.130516.

PLAXIS b.v. (2007) PLAXIS 2D - Ver. 8 Indonesia. Delft: PLAXIS b.v.

Roy, A. (1962) 'Ambiguity in geophysical interpretation', Geophysics, 27(1), pp. 90–99.

Santie, P.A.W., Wilopo, W. and Faris, F. (2024) 'Slope stability analysis using electrical resistivity tomography and limit equilibrium method: A case study from Girimulyo, Kulon Progo', Journal of Applied Geology, 9(1), pp. 37–50. doi: 10.22146/jag.97467.

Telford, W.M., Geldart, L.P. and Sheriff, R.E. (1990) Applied Geophysics. Cambridge: Cambridge University Press.

United States Environmental Protection Agency (EPA) (no date) *Electrical resistivity*. Available at: https://www.epa.gov/environmental-geophysics/electrical-resistivity (Accessed: 2 September 2025).

This page is intentionally left blank

HIMPUNAN AHLI TEKNIK TANAH INDONESIA - HATTI
Indonesian Society for Geotechnical Engineering - ISGE
PIT HATTI XXIX
10-12 November 2025

Performance of Ground Improvement with Preloading and PVD on the Serang–Panimbang Toll Road: Analytical and Numerical Verification

Ilham Hadiid Akbar[1], Agus Himawan[2,*], Masyhur Irsyam[3]
[1]Bachelor's Student of Department of Civil Engineering, Faculty of Civil & Environmental Engineering, Bandung Institute of Technology, Bandung, Indonesia 40132; ilhamhda11@gmail.com
[2]Department of Civil Engineering, Faculty of Engineering and Design, Institut Teknologi Sains Bandung, Kota Deltamas Cikarang Pusat, Jawa Barat, Indonesia 17530; agus.himawan@itsb.ac.id
[3]Department of Cilvil Engineering, Faculty of Civil & Environmental Engineering, Bandung Institute of Technology, Bandung, Indonesia, 40132; masyhur.irsyam@yahoo.co.id
*Correspondence: agus.himawan@itsb.ac.id

ABSTRACT Constructing infrastructure on soft soil deposits presents significant challenges related to settlement and stability. This study investigates a section of the Serang-Panimbang Toll Road, built on soft ground improved with preloading and prefabricated vertical drains (PVDs). The primary objective was to verify and refine laboratory-derived geotechnical parameters by calibrating analytical and numerical models against field performance data from two monitoring locations. The back-analysis employed an analytical model (combining Terzaghi's and Hansbo's theories) and numerical Finite Element Method (FEM) models using both the Soft Soil (SSM) and Hardening Soil (HSM) constitutive models. Initial analyses using direct laboratory parameters confirmed a significant discrepancy with field data, with models substantially overestimating settlement. A systematic calibration was performed, and a primary finding was that the laboratory-derived compressibility indices (C_c and C_s) required a substantial reduction, ranging from 60% to 90%, to match the measured field settlement. This discrepancy is attributed to known factors such as sample disturbance and scale effects. Furthermore, calibrated permeability (k) and smear zone ratios (k_h/k_s) varied significantly between the two locations, confirming soil heterogeneity. A comparative analysis with the calibrated models revealed that the numerical methods predicted a greater increase in undrained shear strength (strength gain) and a more realistic Factor of Safety (SF) during construction. The Soft Soil Model demonstrated superior performance, proving more representative for this application than the HSM. This research validates a replicable back-analysis methodology and underscores that this process is essential for producing reliable, site-specific design parameters and avoiding erroneous designs based on uncalibrated laboratory data.

KEYWORDS Analytical and numerical verification; Soft soil; Soil Improvement; Prefabricated Vertical Drain; Back Analysis

1 INTRODUCTION

The construction of the Serang-Panimbang Toll Road in Banten, Indonesia, serves as a key case study for addressing complex geotechnical issues. A significant portion of the project's alignment traverses areas with soft, compressible soils, which are characterized by low shear strength and high compressibility. These soil conditions pose substantial risks of excessive long-term settlement and potential bearing capacity failure. To mitigate these risks, the project employed a widely accepted ground improvement technique: the combination of Preloading with Prefabricated Vertical Drains (PVD). This method is designed to accelerate the natural consolidation process by installing a dense grid of PVDs, which shorten the drainage paths for pore water and allow for much faster dissipation of excess pore pressure under the applied surcharge load.

A fundamental and well-documented issue in geotechnical practice is the discrepancy between soil parameters determined from laboratory tests and the actual in-situ behavior of the soil mass. Factors such as sample disturbance, stress relief, and scale effects mean that laboratory samples often exhibit higher compressibility than the soil mass in the field (Terzaghi, Peck & Mesri, 1996). This finding is strongly supported by Lim et al. (2018), who demonstrated that sampling disturbance from common techniques (e.g., Shelby tubes) yields "misleading" soil properties compared to high-quality block samples. They showed this disturbance "strongly affected" settlement predictions by altering key compressibility parameters, including the yield stress (σ'_{yield}) and compression index (C_c). This confirms that parameters from disturbed samples require significant calibration against field data to avoid erroneous designs. Consequently, predictive models that rely solely on these laboratory parameters consistently overestimate the magnitude of settlement. This phenomenon was clearly observed in the Serang-Panimbang project and has been documented in similar ground improvement works, where initial numerical models required significant correction to align with field data (Sari, et al., 2025).

To ensure an accurate and efficient design for the toll road, it was therefore essential to perform a back-analysis by calibrating the design models against field performance data from settlement plates. This verification process has been proven to be a reliable method for refining both analytical and numerical models until their predictions closely match the observed settlement behavior (Lam, et al., 2015). The calibration focuses on systematically adjusting the key parameters that govern the consolidation process. The magnitude of settlement is primarily controlled by the compressibility indices (C_c and C_s), while the rate of settlement is governed by flow parameters. Among these, the permeability ratio between the undisturbed soil and the disturbed "smear zone" around the PVD (k_h /k_s) is recognized as a dominant factor, and back-analysis is crucial for determining its representative value for the site (Voottipruex, et al., 2014).

This study verifies both analytical and numerical models using actual settlement data from field monitoring. Through back-analysis, we adjust the soil parameters until the models accurately replicate the actual settlement. The primary goal is to establish a validated set of design parameters. Beyond that, the analysis also compares how each model predicts the increase in shear strength (gain strength) and the resulting Factor of Safety (SF). This provides a critical look at the performance of each approach, which helps improve the accuracy and reliability of designs for similar projects.

2 METHODS

2.1 Site Descriptions

The Serang-Panimbang toll road provides a critical 83.67 km transportation link between Serang and two key destinations: the Tanjung Lesung Special Economic Zone for Tourism and the Ujung Kulon National Park. A significant geotechnical challenge during the construction of this three-section route was the presence of soft soil deposits along the alignment. These conditions necessitated extensive ground improvement, for which a combination of preloading and Prefabricated Vertical Drains (PVD) was employed. This paper presents a case study from a treated area within Section 3 of the project. An overview of the site location, along with photographic documentation of the PVD installation process, is shown in Figure 1.

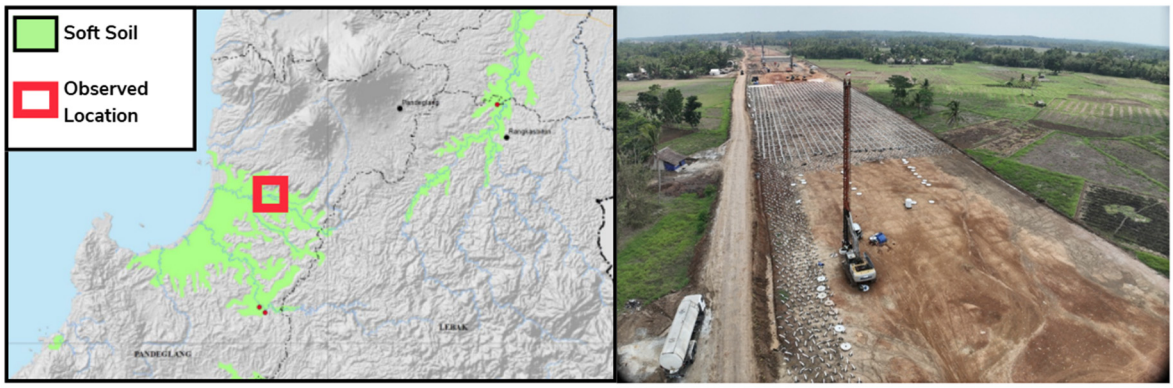

Figure 56 Case Study location (modified from Wardoyo et al., 2019) and documentation of PVD installation process

The study area covers two cross-sections, BH-16 and BH-17, located in Zone F of the Serang-Panimbang toll road (Section 3), as depicted in Figure 2. The ground improvement consisted of Prefabricated Vertical Drains (PVDs) installed in a triangular pattern to depths of 10 m (BH-16) and 22 m (BH-17). Following the installation, an impermeable membrane was placed over the treated area. To track the performance of the ground improvement, settlement plates were installed to record the vertical deformation. This settlement data is fundamental for the back-analysis of both the analytical and numerical models used in this study.

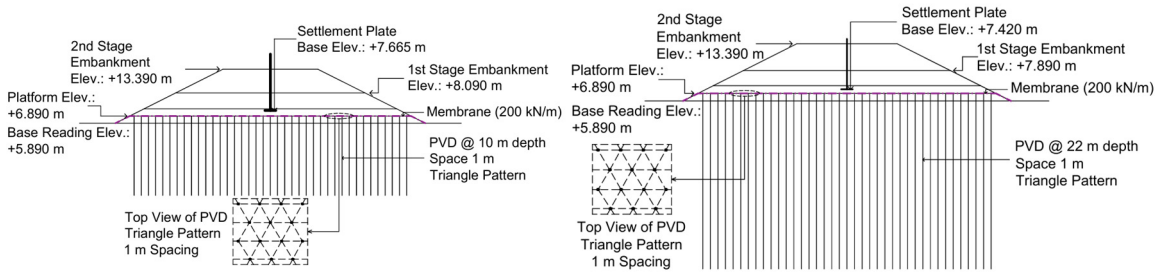

Figure 57 Preloading & PVD soil improvement and field instrumentation of Serang-Panimbang Toll Road BH-16 (left) & BH-17 (right)

2.2 Soil Conditions and Parameters

A soil investigation, including Standard Penetration Tests (SPT), was conducted in Zone F, Section 3 of the Serang-Panimbang Toll Road (Figure 3), confirming the presence of significant soft, compressible soil layers. At borehole BH-16, a 10-meter thick, soft layer was identified, with a ground water level (GWL) measured at 1.6 m below the ground surface. Conditions at the BH-17 location were found to be more critical, revealing a 14-meter thick layer of very soft to soft clay with a GWL at 3.94 m. The SPT N-values within this stratum were exceptionally low (N=0–4), indicating poor shear strength and high compressibility. To address these challenging conditions, Prefabricated Vertical Drains (PVDs) were installed to a depth of 22 meters at the BH-17 location to accelerate consolidation. This design ensures the drains pass completely through the soft clay and reach the firmer, medium stiff clay layer underneath. This creates a good drainage path, which helps to speed up the ground settlement process. The soil at BH-18 had only a thin, 1-meter soft layer. Therefore, this location was not considered important for the ground improvement analysis and was excluded.

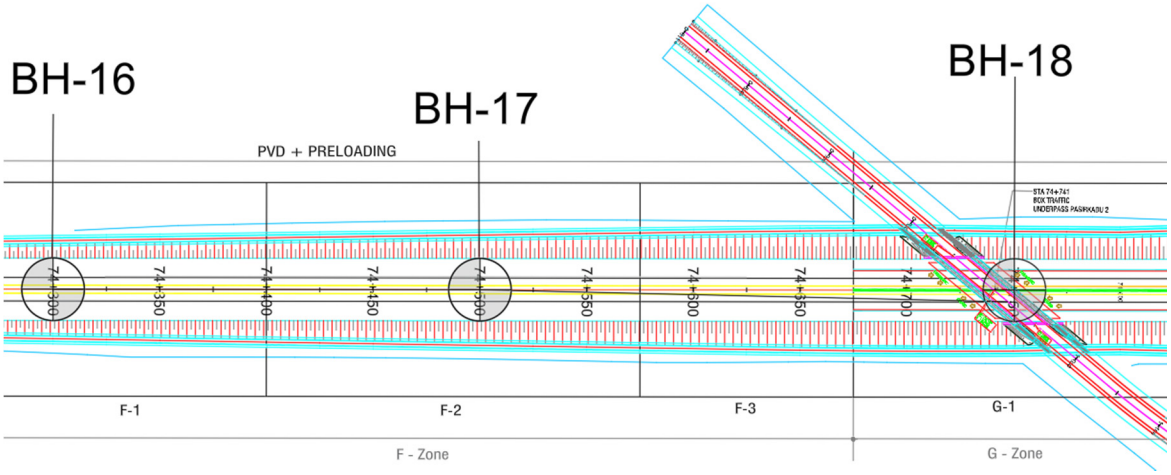

Figure 58 Location of Soil Investigation (BH-16; BH-17; BH-18)

The site investigation revealed a compressible layer of very soft to soft silty clay, indicating significant settlement potential and low bearing capacity. As delineated from NSPT data (Figure 4), this layer extends to a depth of approximately 10 m at location BH-16 and 14 m at BH-17. At BH-16, this layer is characterized by high initial void ratios (e_0) ranging from 1.6 to 2.0, a high compression index (C_c) between 0.65 and 0.85, and low undrained shear strength (S_u) from 4.9 to 12.8 kPa; it is also lightly overconsolidated, with an Overconsolidation Ratio (OCR) between 1.1 and 2.9. In contrast, the clay at BH-17 is comparatively stiffer and less compressible, exhibiting lower void ratios (e_0) of 1.1 to 1.2, a reduced compression index (C_c) of 0.53 to 0.56, and higher shear strength (S_u) of 20 to 22 kPa. These parameters were established from a geotechnical laboratory investigation that was more comprehensive for BH-16; consequently, where laboratory data was unavailable for BH-17, parameters were estimated using empirical correlations. The sand fill, used for both the platform and the embankment layers, was modeled using the Hardening Soil (HS) model based on the parameters specified in Table 1.

The soil parameters adopted for the numerical model are summarized in Table 35. These values were derived from a synthesized approach, integrating direct laboratory test results with established empirical correlations and typical values from geotechnical literature. Specifically, the effective cohesion (c') was assumed as 10% of the undrained shear strength (Su), and the drained friction angle (φ') was correlated to the plasticity index, both following Sorensen & Okkels (2013). The moist unit weight (γ) was determined from laboratory data and typical values (Bowles, 1984), with the saturated unit weight (γ_{sat}) taken as γ + 1 kN/m³. For compressibility, the compression index (C_c) was based on laboratory tests and benchmarked against values from Azzouz et al. (1978), while the swelling index (C_s) was estimated as $0.15C_c$ (Das, 2010). The primary stiffness parameter, the reference secant stiffness (E_{50}^{ref}), was derived from an empirical equation dependent on soil description (Phien-wej & Humza, 2012). The remaining stiffness moduli for the Hardening Soil model were not derived independently; they were automatically calculated using the standard PLAXIS software defaults based on this input, namely an unloading/reloading stiffness $E_{ur}^{ref} = 3 \times E_{50}^{ref}$ and an oedometer stiffness $E_{ur}^{ref} = E_{50}^{ref}$. Finally, the modified compression (λ*) and swelling (κ*) indices were calculated from their theoretical relationship with C_c, C_s, and the initial void ratio (e_0) as shown in Equation (1) to (2).

$$\lambda^* = \frac{C_c}{2.3(1+e_0)} \quad (1)$$

$$k^* = \frac{2C_s}{2.3(1+e_0)} \quad (2)$$

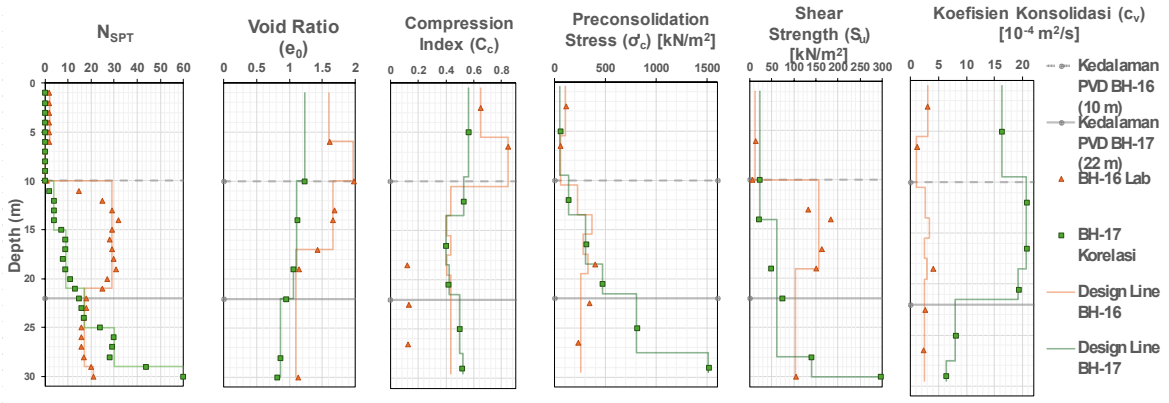

Figure 59 Geotechnical properties derived from in-situ investigations and laboratory analysis

Table 35 Soil parameters used for BH-16 (top), BH-17 (middle), and embankment (bottom)

Depth (m)	Consistency	N SPT	γ_{sat} (kN/m^3)	c' (kN/m^2)	ϕ'(°)	C_c	C_s	λ*	κ*	E_{50} (kN/m^2)	Soil Model
0-6	Soft	2	16.50	1.28	22	0.65	0.13	0.11	0.04	-	SS/HS
6-10	Very Soft	0	15.72	0.49	22	0.85	0.17	0.12	0.05	-	SS/HS
10-13	Very Stiff	23	18.66	13.11	26	0.43	0.09	-	-	15400	HS
13-14	Hard	32	19.50	18.24	25	0.41	0.08	-	-	21000	HS
14-17	Very Stiff	29	18.66	16.34	25	0.43	0.09	-	-	18900	HS
17-19	Hard	31	19.50	14.92	25	0.41	0.08	-	-	20300	HS
19-30	Very Stiff	19	18.66	10.38	25	0.43	0.09	-	-	12600	HS
Depth (m)	Consistency	N SPT	γ_{sat} (kN/m^3)	c' (kN/m^2)	ϕ'(°)	C_c	C_s	λ*	κ*	E_{50} (kN/m^2)	Soil Model
0-10	Very Soft	0	16.75	2.26	26	0.56	0.11	0.11	0.04	-	SS/HS
10-14	Soft	4	17.52	2.00	27	0.53	0.11	0.11	0.04	-	SS/HS
14-19	Medium Stiff	8	17.98	4.79	27	0.40	0.08	0.08	0.03	-	SS/HS
19-22	Stiff	13	18.74	7.41	27	0.42	0.08	0.09	0.04	-	SS/HS
22-28	Very Stiff	24	19.06	13.91	26	0.50	0.10	-	-	16000	HS
28-30	Hard	52	20.65	29.64	26	0.52	0.10	-	-	34500	HS
Depth (m)	Soil Type	N SPT	γ_{sat} (kN/m^3)	c' (kN/m^2)	ϕ'(°)	C_c	C_s	λ*	κ*	E_{50} (kN/m^2)	Soil Model
-	Sand	-	19.00	2.5	38	-	-	-		20000	HS

For the analytical modeling, a supplementary set of parameters was required, as summarized in Table 36. These parameters include coefficient of consolidation (c_v) and coefficient of permeability (k). The coefficient of consolidation (c_v) was also sourced from laboratory data where available; otherwise, it was estimated from the Liquid Limit (LL) using the empirical correlation chart from the U.S. Navy (1982). Furthermore, the coefficient of permeability (k) was calculated using the relationship proposed by Carrier III & Beckman (1984), which is a function of the void ratio (e), Plastic Limit (PL), and Plasticity Index (PI).

Table 36 Additional parameters used for BH-16 (top) and BH-17 (bottom)

Depth (m)	Consistency	k_h (m/day)	k_v (m/day)	c_h (cm^2/s)	c_v (cm^2/s)
0-6	Soft	1.4E-05	5.6E-06	1.6E-03	6.2E-04
6-10	Very Soft	2.8E-05	1.1E-05	2.7E-04	1.1E-04
10-13	Very Stiff	1.7E-04	6.8E-05	1.9E-03	7.5E-04
13-14	Hard	6.5E-05	2.6E-05	1.3E-03	5.1E-04

14-17	Very Stiff	3.0E-05	1.2E-05	1.1E-03	4.4E-04
17-19	Hard	1.7E-05	6.9E-06	7.7E-04	3.1E-04
19-30	Very Stiff	1.9E-05	7.5E-06	5.9E-04	2.4E-04
Depth (m)	Consistency	k_h (m/day)	k_v (m/day)	c_h (cm^2/s)	c_v (cm^2/s)
0-10	Very Soft	5.6E-05	2.2E-05	6.6E-03	2.6E-03
10-14	Soft	3.1E-05	1.3E-05	8.7E-03	3.5E-03
14-19	Medium Stiff	2.1E-05	8.2E-06	8.7E-03	3.5E-03
19-22	Stiff	8.1E-06	3.2E-06	8.3E-03	3.3E-03
22-28	Very Stiff	2.1E-11	8.3E-12	2.0E-03	8.0E-04
28-30	Hard	2.9E-10	1.2E-10	1.6E-03	6.3E-04

2.3 Analytical and Nummerical Verification Models

Verification of both the numerical and analytical models was achieved through a systematic back-analysis. An initial simulation using the baseline parameters from laboratory tests confirmed that both models significantly overestimated the actual settlement recorded by the field settlement plates. Consequently, a systematic calibration was necessary to match the observed performance. This process focused first on adjusting the parameters that control settlement magnitude; specifically, the compressibility indices (C_c and C_s) were reduced to align with the measured data. Following this, the parameters that determine the rate of consolidation, which include the soil's coefficient of permeability (k) and the smear zone permeability ratio (k_h/k_s), were adjusted to match the curvature of the time-settlement plot. To ensure this process was structured and traceable, these adjustments were not arbitrary but were conducted by applying scaling factors (e.g., $C_{c,calibrated} = 0.6 \times C_{c,lab}$) to the initial parameter set. This methodical approach provided a robust and systematic verification for both models.

To enhance analytical precision, the soil profile at each borehole was first discretized into one-meter-thick sub-layers, facilitating a detailed evaluation of stress and parameter variations with depth. The analytical procedure commenced with the calculation of total settlement, which comprises both immediate (elastic) and primary consolidation components. The increase in vertical effective stress ($\Delta\sigma_v'$) from the superimposed embankment load was computed for each sub-layer using Boussinesq's theory (Das, 1994) as shown in Equation (3), while elastic settlement was estimated using methodologies for shallow foundations (Das, 2010) as shown in Equation (4).

$$\Delta\sigma_v' = 2 \times I \times q \tag{3}$$

$$S_i = \Delta\sigma B \left(\frac{1-\mu_s^2}{E_s}\right) I_s I_f \tag{4}$$

Where, I = boussinesq's influence factor (dimensionless), q = effective vertical stress (kPa), B = embankment width (m), μ_s = poisson's ratio (dimensionlesss), E_s = soil elastic modulus (Mpa), I_s = shape factor (dimensionless), and I_f = depth factor (dimensionless).

The governing equation for primary consolidation (S_c) was subsequently selected based on each sub-layer's Overconsolidation Ratio (OCR) and the value of total vertical effective stress ($\sigma_o' + \Delta\sigma_v'$) as shown in Equation (5) to (7).

For Normally Consolidated Soil (NC-Soil)

$$S_c = \frac{C_c H}{1+e_0} \log\left(\frac{\sigma'_0+\Delta\sigma}{\sigma'_0}\right) \tag{5}$$

For Over Consolidated Soil (OC-Soil)

If $(\sigma'_0 + \Delta\sigma) \leq \sigma'_c$

$$S_c = \frac{C_s H}{1+e_0} \log\left(\frac{\sigma'_0+\Delta\sigma}{\sigma'_0}\right) \quad (6)$$

If $(\sigma'_0 + \Delta\sigma) > \sigma'_c$

$$S_c = \frac{C_s H}{1+e_0} \log\left(\frac{\sigma'_c}{\sigma'_0}\right) + \frac{C_c H}{1+e_0} \log\left(\frac{\sigma'_0+\Delta\sigma}{\sigma'_0}\right) \quad (7)$$

Where, C_c = compression index (dimensionless), C_s = swelling index (dimensionless), e_0 = void ratio (dimensionless), H = thickness of consolidating layer (m), σ'_0 = overburden stress (kPa), and σ'_c = preconsolidation stress (kPa).

The time-rate of settlement was then analyzed by modeling combined vertical and radial consolidation. A conservative coefficient of consolidation (C_v) was adopted, with vertical consolidation (U_v) modeled by Terzaghi's (1943) theory and radial drainage toward the Prefabricated Vertical Drains (PVDs) modeled by Hansbo's (1981) solution as shown in Equation (8) to (9). The combined degree of consolidation (U_{vr}) was determined using the relationship proposed by Carrillo (1942) as shown in Equation (10).

$$U_v = \sqrt{\frac{4T_v}{\pi}} \quad (8)$$

$$U_r = 1 - \exp\left[-\frac{8}{F_m} T_r\right] \quad (9)$$

$$U_{vr} = 1 - (1 - U_v)(1 - U_r) \quad (10)$$

Where, T_v = vertical time factor (dimensionless), T_r = radial time factor (dimensionless), and F_m = PVD factor (dimensionless).

The time-dependent analysis was conducted iteratively to simulate the staged construction schedule shown in Figure 5 A 7-day time step (Δt) was used, following the principles for staged loading outlined by Olson (1997). The cumulative total settlement at any given time, $S_{total}(t)$, was computed by summing the full immediate (elastic) settlement (S_e) with the time-dependent consolidation settlement, which was calculated as the product of the total primary consolidation settlement ($S_{c\,total}$) and the combined degree of consolidation ($U_{vr}(t)$) as shown in Equation (11).

$$S_{total}(t) = S_e + U_{vr}(t) \times S_{c\,total} \quad (11)$$

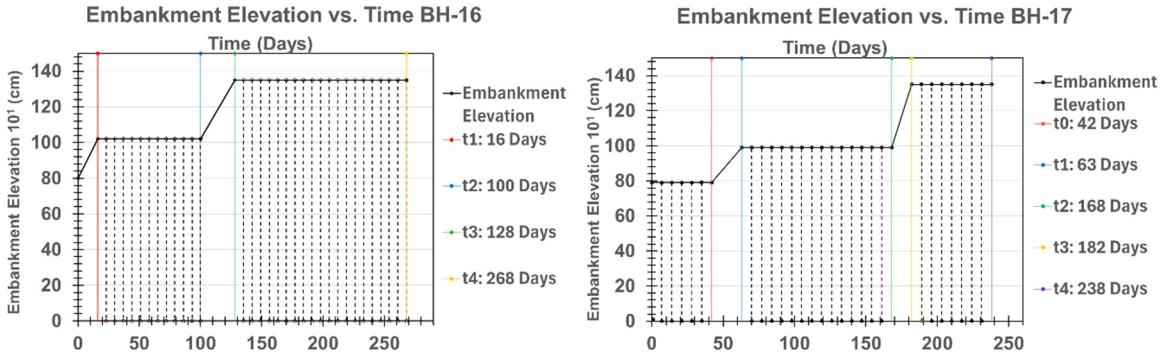

Figure 60 Embankment Construction Phasing and Timeline

A numerical analysis was performed using the finite element software PLAXIS 2D, in which the subsurface profiles were modeled with seven layers for BH-16 and six for BH-17. The platform and embankment were represented as soil clusters, and two primary constitutive modeling scenarios were investigated: the first utilized the Soft Soil (SS) model for the soft clay and the Hardening Soil (HS) model for stiffer strata, while the second applied the HS model to all native soil layers. In both cases,

the Prefabricated Vertical Drains (PVDs) were represented by drain elements at a 1-meter spacing, and the embankment material was assigned to the HS model. To accurately simulate the performance of the PVDs within the 2D plane strain framework, a permeability equivalence procedure was required. This procedure transforms the three-dimensional (3D) axisymmetric flow around a single drain into an equivalent 2D system by modifying the soil's hydraulic conductivity parameters, thereby ensuring the model replicates the accelerated rate of consolidation. The calculation of the equivalent horizontal ($k_{h,eq}$) and vertical ($k_{v,eq}$) permeabilities was performed using the relationships presented in Equations (12) to (14). The calculated equivalent permeability values from each method are shown in Table 3.

$$\frac{k_{h,eq}}{kh} = \frac{2}{\left[ln\left(\frac{de}{ds}\right)+\left(\frac{kh}{ks}\right)ln\left(\frac{de}{dc}\right)-\frac{3}{4}\right]} \tag{12}$$

$$\mu = \ln\left(\frac{N_D}{N_S}\right) + \frac{kh}{ks}\ln(N_s) - \frac{3}{4} + \frac{\pi 2 H_{dr}^2 k_h}{2 q_w} \tag{13}$$

$$k_{v,eq} = \left(1 + \frac{2.5 H_{dr}^2}{\mu d_e^2}\frac{kh}{kv}\right) k_v \tag{14}$$

Where, k_v = vertical permeability (m/day), k_h = horizontal permeability (m/day), k_s = smear zone permeability (m/day), and d_e = equivalent diameter of PVD (m), d_c = drainage diameter of PVD (m), $N_D = d_e/d_c$ ratio (dimensionless), $N_s = d_s/d_c$ ratio (dimensionless), H_{dr} = drainage path length (m), q_w = discharge capacity of PVD (m^3/day), and μ = resistance factor of PVD (dimensionless).

The numerical simulation modeled the prescribed staged construction sequence for both the BH-16 and BH-17 profiles, using the previously determined equivalent permeability values. For the BH-16 profile, the First Stage embankment (2.2 m) was constructed over 23 days, followed by a 70-day consolidation period. Subsequently, the Second Stage embankment, consisting of an additional 3.3 m of fill, was constructed over 21 days and followed by a final consolidation period of 154 days. The analysis for the BH-17 profile involved constructing a 2.0 m First Stage embankment over 63 days with a 70-day consolidation phase; this was followed by the Second Stage construction of a 3.5 m embankment over 35 days with a subsequent 70-day consolidation period. The specific model geometries utilized for the BH-16 and BH-17 analyses are illustrated in Figures 6 and 7, respectively.

Table 37 Equivalent permeability for BH-16 and BH-17

Boring Location	Depth (m)	Consistency	d_e (m)	d_c (mm)	d_s (mm)	d_e/d_c Ratio (N_D)	d_s/d_c Ratio (N_S)	$k_{h,eq}$ (m/day)	$k_{v,eq}$ (m/day)
BH-16	0-6	Soft	1.05	59.59	148.97	17.62	2.5	3.9E-06	2.4E-04
	6-10	Very Soft						7.9E-06	2.2E-04
BH-17	0-10	Very Soft						1.57E-05	9.6E-04
	10-14	Soft						8.85E-06	2.5E-04
	14-19	Medium Stiff						5.78E-06	2.5E-04
	19-22	Stiff						2.27E-06	3.7E-05

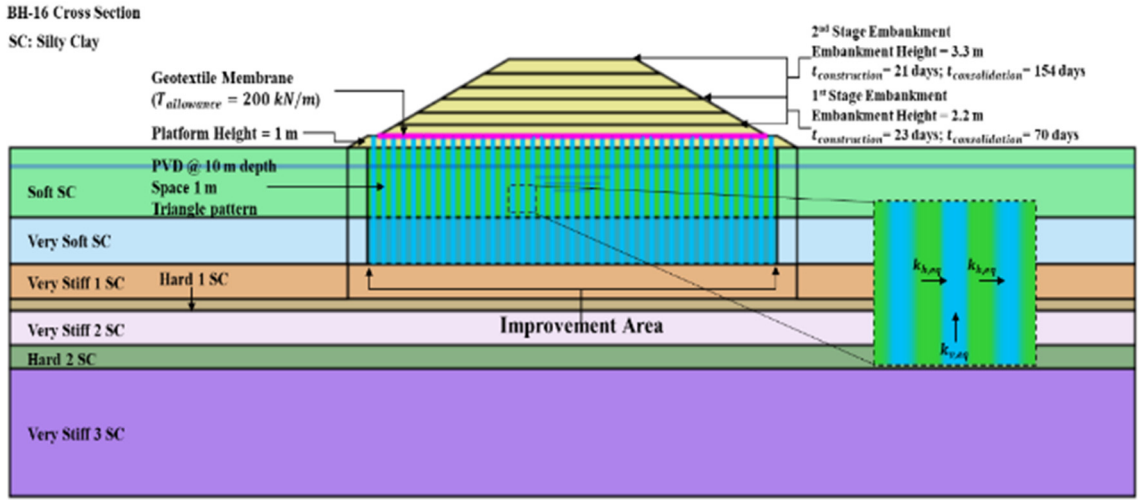

(a)

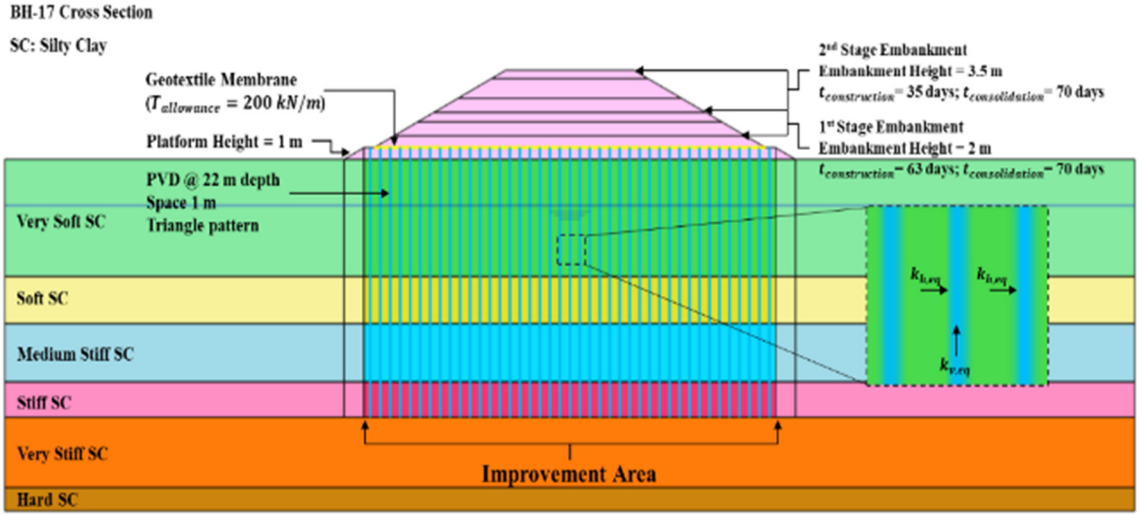

(b)

Figure 61 Numerical Model Geometry: (a) BH-16 & (b) BH-17

2.4 Methodology for Strength Gain and Factor of Safety Analysis

The application of the staged embankment load induces pore water pressure dissipation, a process accelerated by the PVDs, which leads to a progressive increase in the soil's undrained shear strength (S_u). To quantify this strength gain, the value of S_u was evaluated at the end of each construction and consolidation phase. Distinct methodologies were employed for the analytical and numerical models to perform this analysis. For the analytical model, the increase in undrained shear strength was calculated using the simplified empirical approach proposed by Ladd (1991), as presented in Equation (15).

$$\Delta S_u(t) = 0.25 \times U_{vr}(t) \times \Delta\sigma_{stage-n} \quad (15)$$

Where, $\Delta S_u(t)$ = strength gain (kPa), $U_{vr}(t)$ = combined degree of consolidation (dimensionless), and $\Delta\sigma_{stage-n}$ = increase in vertical stress due to the embankment (kPa).

For the numerical models, the strength gain was evaluated using the "Soil Test" feature within PLAXIS 2D. This powerful feature simulates an undrained triaxial test on a soil element at its specific in-situ stress state at the end of any given construction stage. The

primary inputs for the Soil Test include the Cartesian effective stresses (σ_{xx}' & σ_{yy}') extracted from the model output at a representative location (the midpoint of the upper soft clay layer) and the soil's vertical preconsolidation pressure. The simulation generates a stress path diagram (p'-q), from which the shear stress at failure ($q_{failure}$) is obtained. The undrained shear strength is then determined using the fundamental relationship $Su = q_{failure}/2$, where $q_{failure}$ geometrically represents the diameter of the Mohr circle at failure. This procedure was repeated for the end of each loading stage for both the Soft Soil and Hardening Soil model analyses.

The Factor of Safety (FS) was evaluated using distinct methodologies appropriate to each modeling approach: a limit equilibrium method for the analytical model and a strength reduction method for the numerical model. For the analytical approach, a conventional Limit Equilibrium Method (LEM) was employed, as represented by the formulation in Equation (16). This calculation, often based on principles from methods like Bishop's Modified Method for circular failure surfaces, was performed for each construction stage. The analysis utilized the updated undrained shear strength at that stage, which is the sum of the initial strength and the calculated strength gain.

$$FS = \frac{N_c \times S_u(t)}{\gamma_{embankment} \times H_{embankment}(t)} \quad (16)$$

Where, N_c = bearing capacity factor (dimensionless), $S_u(t)$ = total shear strength at time [t] (kPa), $\gamma_{embankment}$ = unit weight of embankment (kN/m^3), and $H_{embankment}$ = total embankment height at time [t] (m).

In contrast, the numerical analysis determined the Factor of Safety using the Shear Strength Reduction (SSR) method, a standard feature in PLAXIS 2D. This is a robust finite element technique where the soil's shear strength parameters (cohesion, c, and friction angle, ϕ) are progressively and automatically reduced by a common factor until the model fails to achieve convergence, indicating the onset of global instability. The resulting Factor of Safety is this critical strength reduction factor. A significant advantage of the SSR method is its ability to identify the location of the most critical failure surface without prior assumptions about its shape, which is revealed by zones of concentrated shear strain. This approach is a well-established and widely accepted standard in computational geotechnics.

3 RESULTS AND DISCUSSION

The verification process started with an initial simulation using the parameters from Tables (1) – (3). This simulation was the first step in a systematic back-analysis to calibrate the models against the field settlement plate data. The calibration was performed in two main steps. First, the compressibility indices (C_c and C_s) were adjusted to match the total amount of settlement. Second, the parameters that control the consolidation rate, such as the smear zone permeability ratio (k_h/k_s) and the coefficient of permeability (k), were adjusted to match the shape of the time-settlement curve.

The initial simulation showed that the compressibility indices from the laboratory were too high for both sites, causing the models to predict much larger settlements than what was measured (as seen in Figures 7a, 7c, 8a, and 8c). Therefore, a calibration was performed to better match the field data, with the results shown in Figures 7b, 7d, 8b, and 8d. For the analytical model at BH-16, the compressibility indices were reduced to 60% of their initial values and the smear ratio (k_h/k_s) was set to 2. For the BH-17 analytical model, these values

were adjusted to 70% and 6, respectively. The numerical model (Soft Soil) for BH-16 required reducing the indices to 70%, a smear ratio of 2, and increasing permeability to 175%. Finally, the BH-17 numerical model was calibrated by reducing the indices to 90%, setting the smear ratio to 6, and reducing permeability to 60% of its initial value.

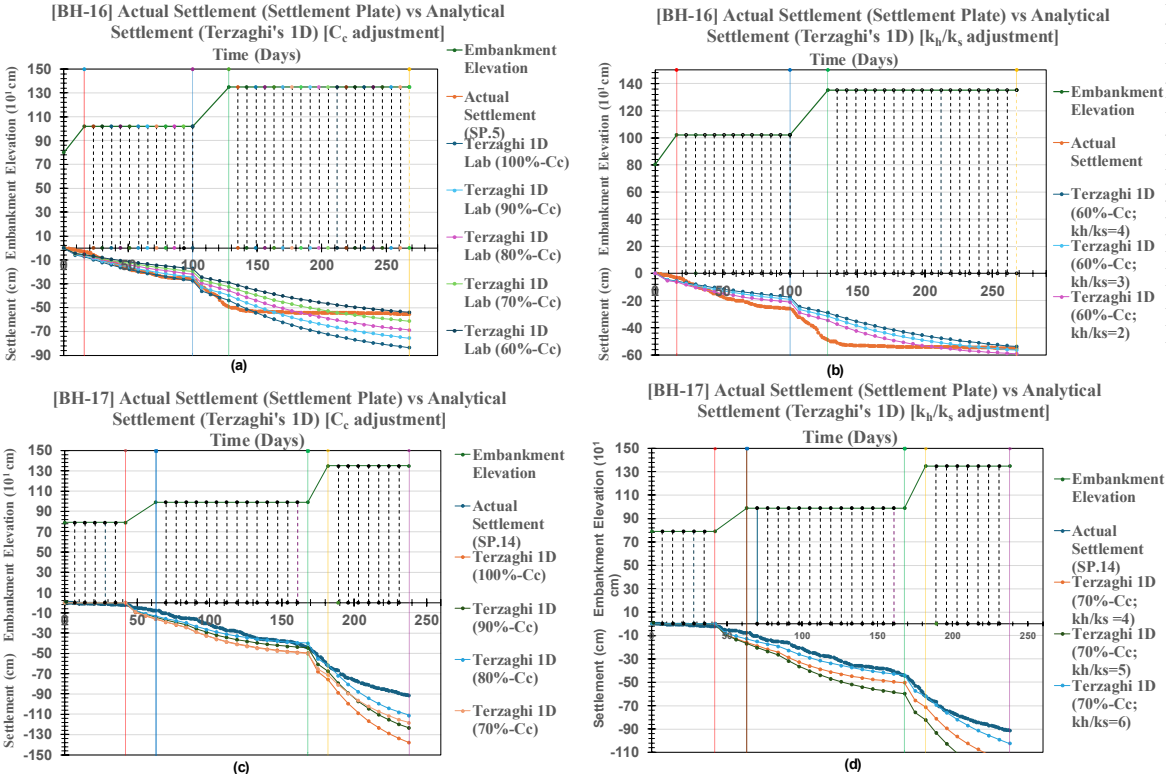

Figure 62 Analytical model verification: (a) C_c adjustment BH-16; (b) k_h/k_s adjustment BH-16; (c) C_c adjustment BH-17; (d) k_h/k_s adjustment BH-17

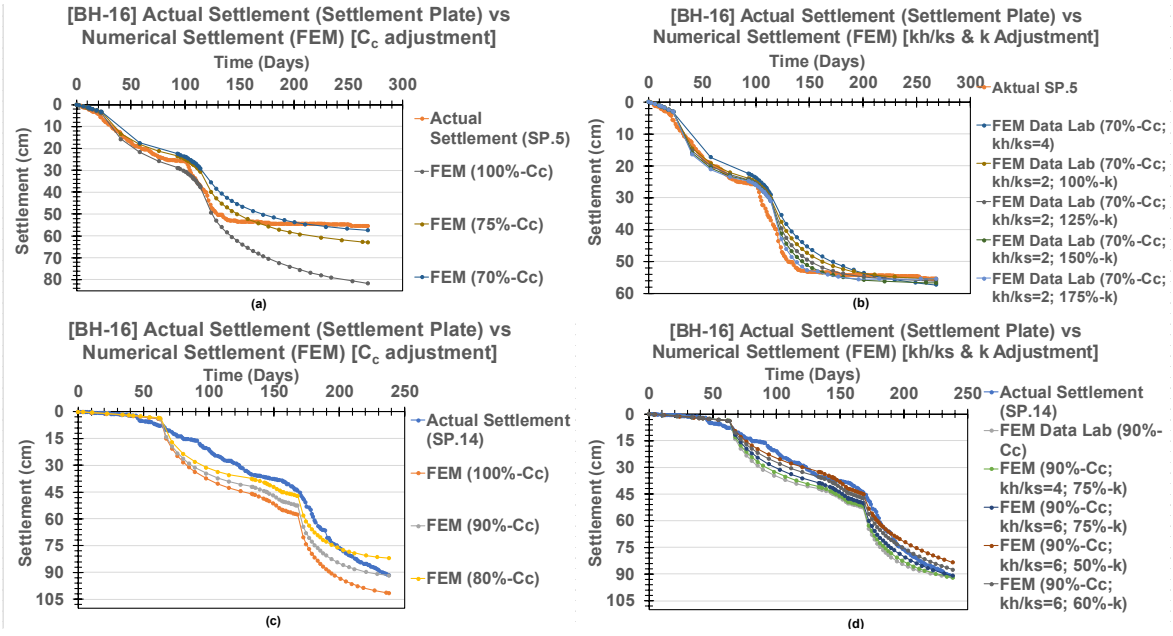

Figure 63 Numerical model verification: (a) C_c adjustment BH-16; (b) k_h/k_s & k adjustment BH-16; (c) C_c adjustment BH-17; (d) k_h/k_s & k adjustment BH-17

In addition, a verification was performed for the Hardening Soil (HS) model at both borehole locations. This process began by using the final calibrated parameters from the Soft Soil (SS) model as a starting point for the HS model. An initial simulation showed that the HS model still predicted slightly larger settlements than the field data, as seen in Figure 9, so further adjustments were required to achieve a closer match. The final calibrated parameters for the Hardening Soil model were determined as follows: for the BH-16 model, the compressibility indices (C_c and C_s) were reduced to 60% of their initial values, the smear zone permeability ratio (k_h/k_s) was set to 2, and the coefficient of permeability (k) was increased to 175%. For the BH-17 model, the compressibility indices were reduced to 80%, the smear ratio was set to 6, and the coefficient of permeability (k_h/k_s) was reduced to 60% of its initial value.

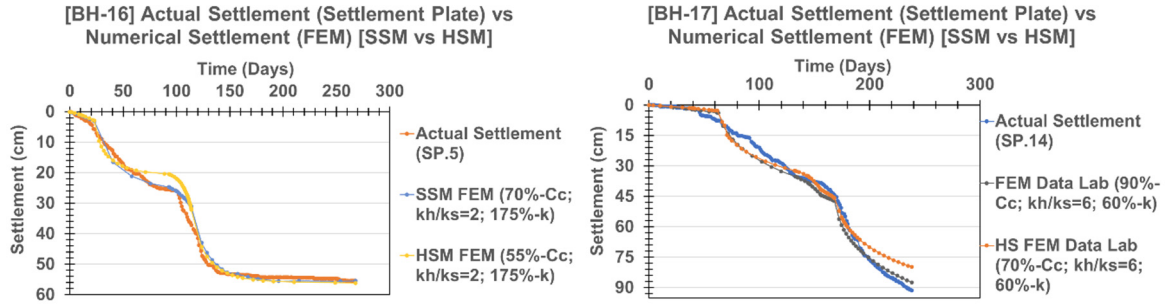

Figure 64 Numerical model verification: (a) Soft Soil Model vs Hardening Soil Model for BH-16; (b) Soft Soil Model vs Hardening Soil Model for BH-17

The predicted increase in undrained shear strength (S_u) over time for the analytical and numerical models is compared in Figures 11a and 11b. For the BH-16 analysis, the analytical model generally predicted a lower strength gain than the numerical models, except during the final consolidation stage where it surpassed them. Within the numerical results for BH-16, the Hardening Soil Model (HSM) consistently yielded a slightly higher shear strength than the Soft Soil Model (SSM). Conversely, for the BH-17 analysis, the analytical model predicted the lowest strength gain only during the initial construction stage, after which it consistently yielded the highest strength values. In contrast to the BH-16 results, the SSM predicted a significantly higher strength gain than the HSM for BH-17 throughout most of the timeline.

Using the calibrated numerical models, a stability analysis was performed with Plaxis 2D to determine the Factor of Safety (FS). This analysis also utilizes the incremental deviatoric strain output to visualize failure mechanisms. This output illustrates how strain changes due to loading, with concentrated zones indicating the intensity of shear deformation and potential failure planes. A clear example is seen in the Soft Soil Model analysis for the construction stage: the BH-16 model showed a significantly higher maximum deviatoric strain (0.1026) than the BH-17 model (0.01554). This finding directly correlates with the calculated stability, as BH-16 also had a lower Factor of Safety (FS = 1.34) compared to BH-17 (FS = 1.40). This comparison, illustrating the localized failure mechanism, is presented in Figure 10. The overall calculated FS values for all construction and consolidation stages are then plotted against time in Figures 11c and 11d. At the BH-16 location, the analytical model produced a lower Factor of Safety compared to both numerical models for nearly all stages, except for the final consolidation phase. The numerical results consistently showed the SSM producing a higher FS than the HSM. For the BH-17 location, the analytical model yielded a lower FS during the active construction stages but ultimately predicted the highest final Factor of Safety. Similar to the BH-16 results, the SSM analysis resulted in a slightly higher Factor of Safety than the HSM across all stages.

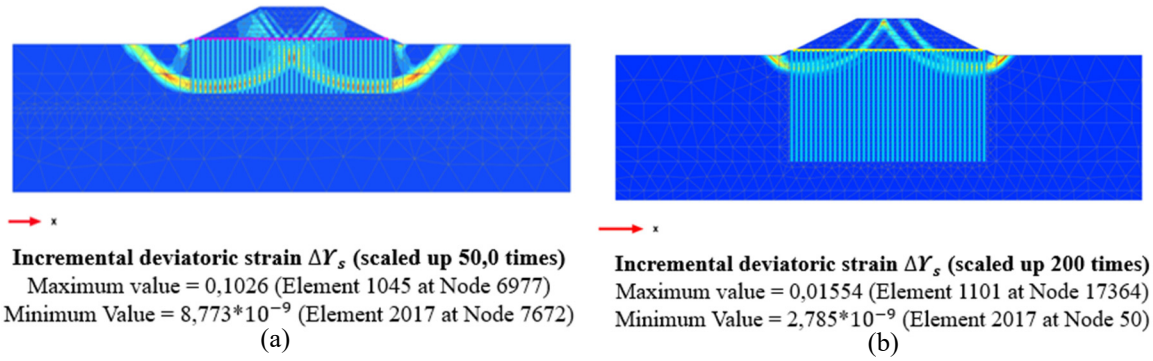

Incremental deviatoric strain $\Delta\gamma_s$ (scaled up 50,0 times)
Maximum value = 0,1026 (Element 1045 at Node 6977)
Minimum Value = $8{,}773*10^{-9}$ (Element 2017 at Node 7672)
(a)

Incremental deviatoric strain $\Delta\gamma_s$ (scaled up 200 times)
Maximum value = 0,01554 (Element 1101 at Node 17364)
Minimum Value = $2{,}785*10^{-9}$ (Element 2017 at Node 50)
(b)

Figure 65 Example of safety analysis results during construction (with SSM): (a) BH-16, FS = 1.34; (b) BH-17, FS = 1.4

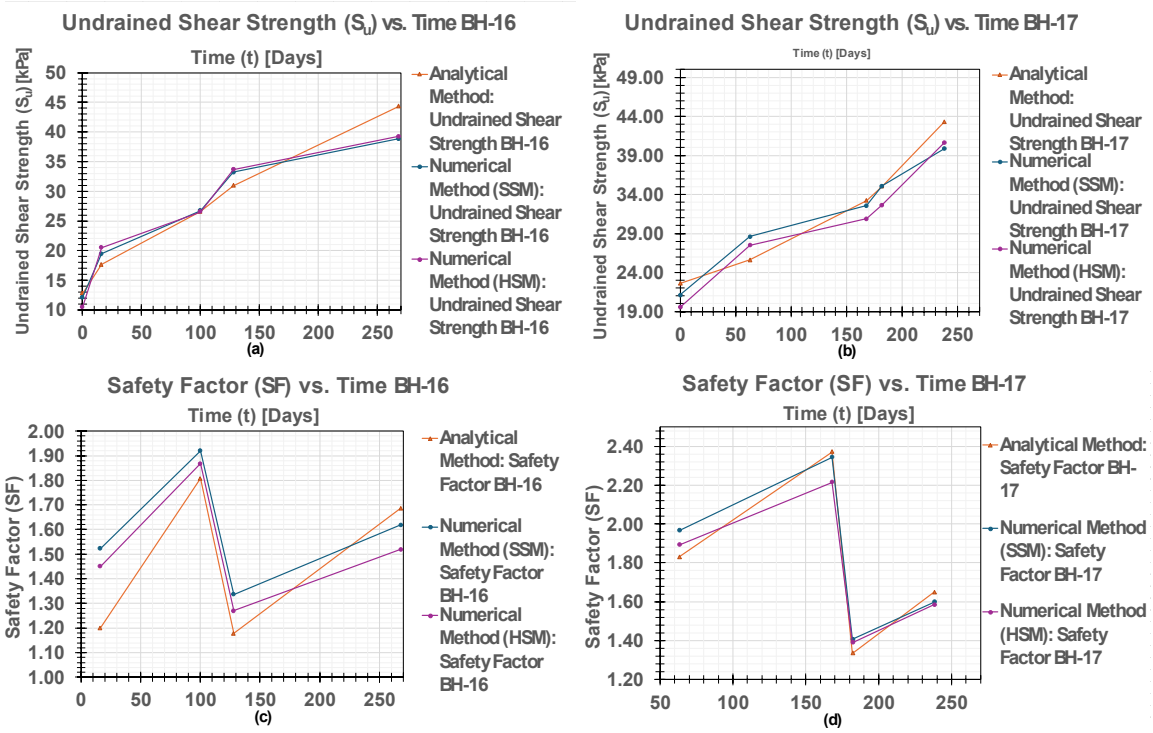

Figure 66 Undrained shear strength (S_u) vs. time: (a) BH-16 & (b) BH-17; Safety factor (SF) vs. time: (c) BH-16 & (d) BH-17

The back-analysis revealed a significant gap between the soil parameters derived from laboratory tests and the actual in-situ soil behavior. A key finding was that the laboratory-derived compressibility indices (C_c and C_s) required a significant reduction, ranging from 60% to 90%, to match the measured field settlement. This discrepancy is attributed to known factors such as sample disturbance and scale effects. Furthermore, the calibrated values for permeability (k) and the smear zone ratio (k_h/k_s) varied significantly between the two borehole locations, confirming the high degree of soil heterogeneity and the variable impact of PVD installation. While the resulting calibrated parameters are strictly site-specific, the primary contribution of this study is the validation of the back-analysis methodology itself, which can be reliably replicated on future projects where field monitoring data is available.

A comparison of modeling approaches demonstrated the superiority of numerical methods for this analysis. The Finite Element Models (FEM) consistently predicted higher strength gain (S_u) and a greater Factor of Safety (FS) than the simplified analytical method. This is because numerical analysis can capture complex, multi-dimensional processes like stress redistribution, which

analytical theories cannot. Within the numerical framework, the Soft Soil Model (SSM) proved more representative than the Hardening Soil Model (HSM), requiring less parameter adjustment to align with field data, as its formulation is specifically designed for the compressive behavior of soft clays.

The results from this verification process have direct applications for engineering design on soft soils. Firstly, the study confirms that back-analysis against field monitoring data is an essential step to avoid significant design errors, particularly the overestimation of settlement from uncalibrated laboratory parameters. Secondly, while analytical methods are useful for preliminary studies, numerical modeling is strongly recommended for final design due to its realistic simulation of complex soil behavior. Finally, the choice of an appropriate constitutive model is crucial, with specialized models like the SSM providing more reliable predictions with less calibration effort for soft clay consolidation.

4 CONCLUSION

This study confirms that uncalibrated soil parameters from laboratory tests lead to a significant overestimation of settlement, highlighting the critical need for calibration against field data to avoid inefficient designs. A comparison of modeling approaches revealed that numerical methods (FEM) are superior to simplified analytical techniques, consistently predicting higher strength gain and a greater Factor of Safety by capturing complex, multi-dimensional soil behavior. Within the numerical framework, the Soft Soil Model (SSM) proved more representative for this case, requiring less parameter adjustment than the Hardening Soil Model (HSM). Ultimately, this research unequivocally demonstrates that a back-analysis procedure, using field monitoring data to calibrate predictive models, is an essential step to ensure the accuracy of settlement predictions and prevent flawed design decisions.

DISCLAIMER

The authors declare no conflict of interest.

AVAILABILITY OF DATA AND MATERIALS

All data are available from the author.

REFERENCES

Ameratunga, J., Sivakugan, N. and Das, B.M., 2016. Correlations of Soil and Rock Properties in Geotechnical Engineering. Australia: Springer. Available at: http://www.springer.com/series/13410.

Bowles, J. E., 1984. Physical and Geotechnical Properties of Soils. The McGraw-Hill Companies, Inc.

Das, B. M., 2010. Principles of Geotechnical Engineering (7th ed.). Cengage Learning.

Han, J., 2015. Principles and Practices of Ground Improvement. New jersey: John Wiley & Sons.

Hansbo, S., 1979. Consolidation of Clay with Special Reference to Influence of Vertical Drains. Proceedings of the International Conference on Soil Mechanics and Foundation Engineering, 3, pp. 677-682.

Indraratna, B., Chu, J., & Rujikiatkamjorn, C., 2016. Ground Improvement Case Histories: Embankments with Special Reference to Consolidation and Other Physical Methods. Butterworth-Heinemann.

Lam, L. G., Bergado, D. T., & Hino, T., 2015. PVD improvement of soft Bangkok clay with and without vacuum preloading using analytical and numerical analyses. Geotextiles and Geomembranes, 43(6), pp. 547–557. https://doi.org/10.1016/j.geotexmem.2015.07.013.

Lim, G. T., Pineda, J., et al., 2018. Effects of sampling disturbance in geotechnical design. *Proceedings of the 2018 Australian Geomechanics Society (AGS) Symposium*. https://doi.org/10.1139/cgj-2018-0016

Maleki, M., Alielahi, H., & Rahmani, I., 2022. Effect of Smear Zone Characteristics on PVD-Improved Soft Soils Using Field Data and Numerical Simulations. Indian Geotechnical Journal, 52, pp. 1025–1045. https://doi.org/10.1007/s40098-022-00645-9.

Pusat Litbang Jalan dan Jembatan., 2001. Panduan Geoteknik 1: Proses Pembentukan dan Sifat-Sifat Dasar Tanah Lunak. Kementerian Pekerjaan Umum dan Perumahan Rakyat, Direktorat Jenderal Bina Marga.

Pusat Litbang Jalan dan Jembatan., 2001. Panduan Geoteknik 4: Desain dan Konstruksi. Kementerian Pekerjaan Umum dan Perumahan Rakyat, Direktorat Jenderal Bina Marga.

Sari, U. C., Wardani, S. P. R., Muntohar, A. S., & Partono, W., 2025. Evaluation of the consolidation parameters obtained from laboratory tests for numerical modeling of improved soft soil using PVD at Semarang - Demak Toll Road, Indonesia. Journal of Engineering and Technological Sciences, 57(2), pp. 196–213. https://doi.org/10.5614/j.eng.technol.sci.2025.57.2.5.

Schaefer, V. R., & Berg, R. R., 2012. Geotechnical Solutions for Soil Improvement, Rapid Embankment Construction, and Stabilization of the Pavement Working Platform. Strategic Highway Research Program (SHRP) II R02, National Academy of Sciences.

Sorensen, & Okkels., 2013. Correlation Between Drained Shear Strength and Plasticity Index of Undisturbed Overconsolidated Clays. Proceedings of the 18th International Conference on Soil Mechanics and Geotechnical Engineering, pp. 423-428. Paris: Presses des Ponts.

Voottipruex, P., Bergado, D. T., Lam, L. G., & Hino, T., 2014. Back-analyses of flow parameters of PVD improved soft Bangkok clay with and without vacuum preloading from settlement data and numerical simulations. Geotextiles and Geomembranes, 42(5), pp. 457–467. https://doi.org/10.1016/j.geotexmem.2014.07.004.

Wardoyo, Sarwondo, Destiasari, F., Wahyudin, Wiyono, Hasibuan, G., & Sollu, W. P., 2019. Atlas Sebaran Tanah Lunak Indonesia (Andiani, Sugalang, D. Murdohardono, & Kardiyanto (eds.)). Badan Geologi Kementerian Energi dan Sumber Daya Mineral.

This page is intentionally left blank

Characterization and Shear Strength Evaluation of Sensitive Volcanic Residual Soils in West Java

Mirna Dwi[1*], Hendra Jitno[2,3], Irma Fudji[1], Nisrina Aulia[1], Antania Hanjani[1]
[1] Geotechnical Engineer, PT Solusi Geotek Optima, Bandung, Indonesia
[2]Director, PT Solusi Geotek Optima, Bandung, Indonesia
[3]Adjunct Associate Professor, Dept. of Civil Engineering, Nasional Institute of Technology, Bandung, Indonesia
*Correspondence: mirna.dwi@ptsgo.id

ABSTRACT Volcanic residual soils in tropical regions exhibit unique engineering behavior that differs significantly from sedimentary soils. These soils often contain amorphous clay minerals such as allophane and halloysite, which contribute to their sensitivity and unusual strength characteristics. Field observations in West Java revealed near-vertical, free-standing cuts up to 12 meters high, indicating apparent cohesion supported by natural cementation and unsaturated conditions. A geotechnical investigation was carried out using Standard Penetration Tests (SPT), Cone Penetration Tests with pore pressure measurement (CPTu), and laboratory tests including Atterberg limits, index properties, and unconsolidated-undrained triaxial tests. Results show that Su values obtained from CPTu are more consistent with laboratory triaxial data, while SPT correlations tend to underestimate strength due to sample disturbance. Furthermore, particle size analyses confirm the gap-graded nature of volcanic residual soils, reflecting differential weathering processes. This study aims to establish representative undrained shear strength parameters of sensitive volcanic residual soils in West Java by integrating field and laboratory investigations. The findings highlight the importance of careful sample handling, the use of less-disturbing in-situ tests, and the selection of appropriate testing methods to obtain reliable soil parameters for engineering design. These findings provide practical implications for the characterization and modeling of sensitive volcanic residual soils in engineering applications.

KEYWORDS residual soil, volcanic soil, undrained shear strength, soil investigation, sample disturbance

This paper will be published in the future issues of Indonesian Geotechnical Journal

This page is intentionally left blank

Rasio Kecepatan Longsor Berdasarkan Data *Gradient Modulus Young* Dan *Strain* Pada Uji *Ucs* Untuk *Setting* Alarm Pada *Slope Stability Radar*

Ivan Bahder[1], Alam Tronics[2]

[1]Departement Geology, Geotechnical Section PT. Kaltim Prima Coal, Kalimantan Timur, Indonesia [2]Departement Geology, Geotechnical Section PT. Kaltim Prima Coal, Kalimantan Timur, Indonesia

Email: Ivan.Bahder@kpc.co.id, Alam.Tronic@kpc.co.id

ABSTRAK: keselamatan operasional tambang terbuka sangat bergantung pada efektivitas sistem peringatan dini terhadap potensi longsor namun terbatas pada penentuan nilai alarm yang biasanya didapat dari riset data *backanalysis* longsor. Penelitian ini adalah pendekatan baru dalam penelitian internal perusahaan yaitu korelasi antara rasio kecepatan longsor dari data slope stability radar (ssr) dengan gradient modulus young dan pembacaan data *time vs strain* uji uniaxial compressive strength (ucs) laboratorium batuan geoteknik kpc. Penelitian ini bertujuan untuk mengembangkan model prediksi deformasi kritis yang dapat digunakan sebagai dasar penetapan threshold alarm pada sistem radar deformasi. Metodologi dilakukan dengan pengujian ucs terhadap sampel batuan dari berbagai zona geoteknik di lereng tambang, diikuti dengan perhitungan modulus elastisitas (e) dan estimasi gradient perubahan e terhadap strain. Selanjutnya, data radar ssr dari area yang sama dikaji untuk memperoleh kecepatan deformasi aktual dalam kurun waktu tertentu. Hasil penelitian menunjukkan bahwa rasio kecepatan progressif sebesar 4 sampai dengan 7 kali lipat kecepatan linear dan keruntuhan terjadi pada 8 sampai dengan 10 kali kecepatan linear. Korelasi ini memberikan pendekatan kuantitatif untuk setting alarm radar berbasis properti mekanik lokal, tanpa memerlukan backanalysis dari sebuah longsor aktual. Kesimpulan dari studi ini menegaskan bahwa integrasi data ucs dan deformasi radar memungkinkan pengaturan ambang batas alarm yang lebih adaptif, responsif, dan berbasis geoteknik terutama pada area-area dengan design optimalisasi.

Kata Kunci: *Sistem Peringatan Dini Longsor, Slope Stability Radar (SSR), uniaxial compression stress (UCS), model prediksi deformasi kritis*

ABSTRACT: Operational safety in open-pit mining heavily relies on the effectiveness of early warning systems for potential landslides, which are often limited to determining alarm thresholds based on back-analysis of past landslide data. This study introduces a novel approach, explored only in internal research, which investigates the correlation between landslide velocity ratios from Slope Stability Radar (SSR) data and the gradient of Young's modulus derived from strain-time records of Uniaxial Compressive Strength (UCS) tests on geotechnical rock samples from KPC. The objective is to develop a predictive model for critical deformation that can serve as a basis for setting alarm thresholds in radar-based deformation monitoring systems. The methodology involves UCS testing of rock samples from various geotechnical zones of the mine slope, followed by calculations of elastic modulus (E) and estimation of its gradient change with respect to strain. Subsequently, SSR radar data from the same areas are analyzed to obtain actual deformation velocities over a specific time period. he research results show that the Progressive velocity ratio is 4 to 7 times the linear velocity, and failure occurs at 8 to 10 times the linear velocity. This correlation provides a quantitative approach for setting radar alarms based on local mechanical properties, without requiring back-analysis of actual landslides. The study concludes that integrating UCS and radar deformation data

enables more adaptive, responsive, and geotechnically grounded alarm threshold settings, especially in areas with optimized slope designs.

Keywords: Landslide Early Warning System, Slope Stability Radar (SSR), Uniaxial Compressive Strength (UCS), Critical Deformation Prediction Model

1. PENDAHULUAN

Sistem pemantauan lereng berbasis radar (Slope Stability Radar/SSR, Ground Base Radar-SAR) merupakan salah satu teknologi utama dalam mitigasi risiko longsor pada tambang terbuka. Tantangan besar dalam implementasi sistem ini adalah penentuan ambang alarm (threshold alarm) yang tepat. Selama ini, ambang alarm biasanya ditetapkan berdasarkan back-analysis dari peristiwa longsor yang sudah terjadi. Dengan kata lain, dibutuhkan histori longsor di lokasi yang sama agar bisa mengkalibrasi kecepatan dan akselerasi kritis. Hal ini menjadi kendala serius pada lokasi baru atau litologi berbeda, karena tidak tersedia data longsor terdahulu.

Sebagai solusi, pendekatan berbasis sifat mekanik material dapat digunakan. Uji kuat tekan uniaxial (Uniaxial Compressive Strength, UCS) dengan menambahkan pengukuran waktu pada setiap divisi perubahan Regangan menyediakan data fundamental berupa kurva tegangan–regangan batuan vs Time. Dari data ini dapat diturunkan parameter kekakuan (modulus Young) baik pada fase ucs titik linear maupun saat material melemah (fase progresif/softening). Rasio antara Gradien Regresi UCS saat modulus elastik dan modulus progresif dapat digunakan untuk memetakan fase stabil–transisi–akseleratif tanpa perlu menunggu longsor aktual

2. METODOLOGI PENELITIAN

Alur penelitian ini sesuai dengan Gambar 1, sebagai berikut:

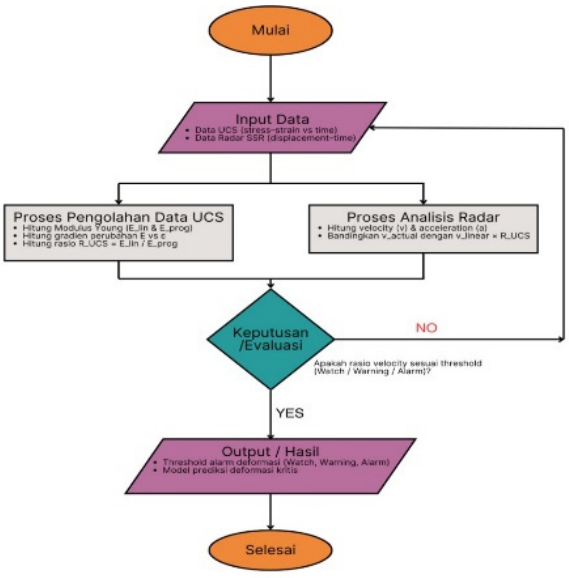

Gambar 1. Diagram alir penelitian

2.1 Dasar Teori

Dari perspektif teori mekanika dasar, hubungan deformasi batuan dapat dianalogikan dengan teori pegas Hooke:

$$\sigma = E \cdot \varepsilon$$

di mana tegangan (σ) berbanding lurus dengan regangan (ε) melalui modulus elastisitas (E). Menurut **Beer dkk (2020)** pada fase elastik, batuan berperilaku layaknya pegas ideal—deformasi masih dapat kembali (*reversibel*). Namun ketika terjadi penurunan E (akibat mikro-retakan), sistem berpindah menuju fase plastis, dan masuk ke fase linier. Dalam kerangka ini, percepatan deformasi yang terekam pada radar dapat dikonversi sebagai persamaan sistem pegas yang kehilangan kekakuannya: semakin kecil nilai E, semakin besar kecepatan serta akselerasi deformasi meskipun gaya penggerak relatif konstan.

Menurut Callister dkk (2020) dalam konteks deformasi tanah atau batuan, hukum ini digunakan untuk memodelkan respons awal material terhadap gaya eksternal seperti gaya geser dan gaya normal.

Menurut Gere (2012) jika Modulus Tangen dan Softening terbentuk ketika material melemah, modulus Young tangen E(ε) menurun terhadap ε. Laju perubahan modulus ditunjukkan dengan:

$$\frac{dE}{d\varepsilon} = \frac{d^2\sigma}{d\varepsilon^2}$$

Jika modulus berubah dan Nilai negatif menandakan softening, turunan tegangan terhadap waktu adalah:

$$\frac{d\sigma}{dt} = \left(E - \frac{\varepsilon . dE}{d\varepsilon}\right) . \frac{d\varepsilon}{dt}$$

Sedangkan ini turunan tegangan terhadap waktu disebut kekakuan efektif, maka bisa dituliskan sbb:

$$E_{eff} = E - \varepsilon \left|\frac{dE}{d\varepsilon}\right|$$

3. HASIL DAN PEMBAHASAN

3.1. Data Histori Radar PT Kaltim Prima Coal

Berdasarkan data aktual longsor pada beberapa area penambangan PT Kaltim Prima Coal (KPC), sistem Slope Stability Radar (SSR) telah merekam pola deformasi yang berujung pada kejadian runtuhan. Data historis pada area *Highwall* pada Gambar 2 – 7 serta *Lowwall* di Gambar 8-11 ini menunjukkan bahwa sebelum terjadinya longsor, kecepatan deformasi lereng meningkat secara progresif dari fase linear yang relatif stabil menuju fase akseleratif dengan range *Rasio Velocity* saat keruntuhan berkisar antara 7 sampai dengan 12 kali lipat fase linear sesuai data di Tabel 1. Menurut **Munthaha dkk (2022)** dikatakan ada tiga pola umum yang teridentifikasi dari data radar meliputi:

- **Fase Linear:** pergerakan lambat (*background velocity*) yang konsisten dalam jangka waktu panjang.
- **Fase Transisi/Progressif:** peningkatan kecepatan secara gradual, menandakan menurunnya kekakuan massa batuan.

- **Fase Akseleratif:** percepatan deformasi signifikan menjelang keruntuhan, sering kali mencapai kelipatan beberapa kali dari *baseline velocity*.

Data historis dari SSR di Tabel 2 ini menjadi landasan empiris untuk menguji validitas model berbasis UCS. Dengan mengaitkan rasio velocity dari radar aktual dengan rasio modulus Young (linear–progresif) dari UCS laboratorium, maka model prediksi deformasi kritis dapat dikalibrasi sesuai Gambar 16 dan diverifikasi terhadap kondisi lapangan nyata di KPC.

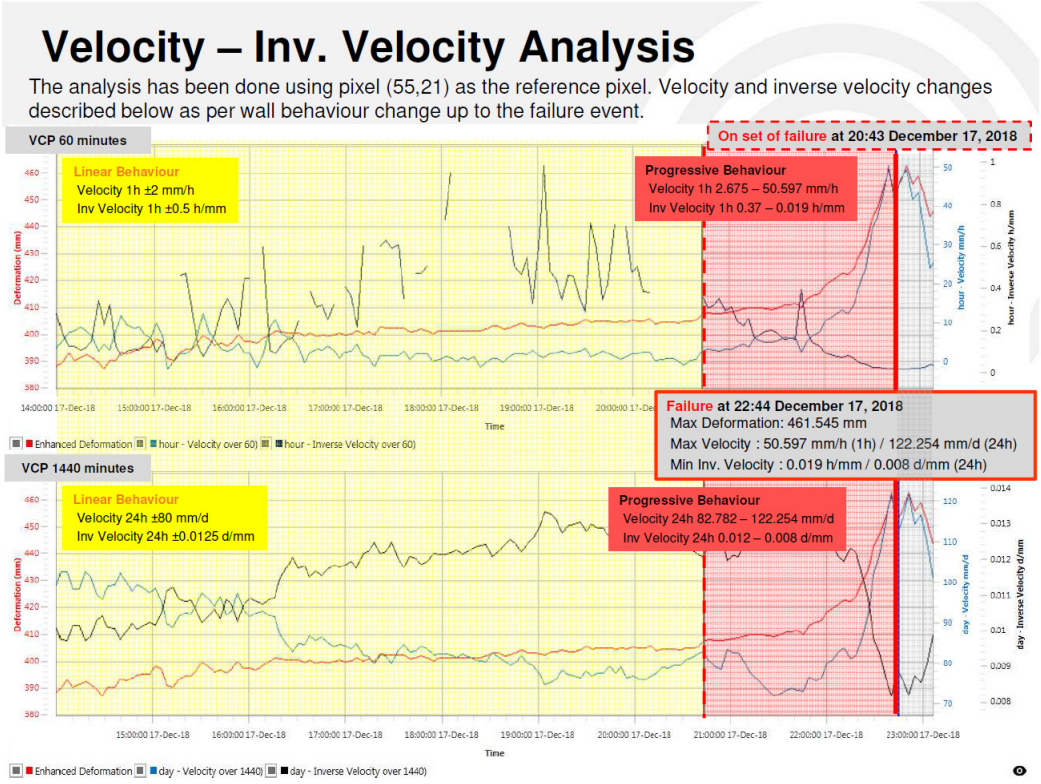

Gambar 2 – Highwall Data 1

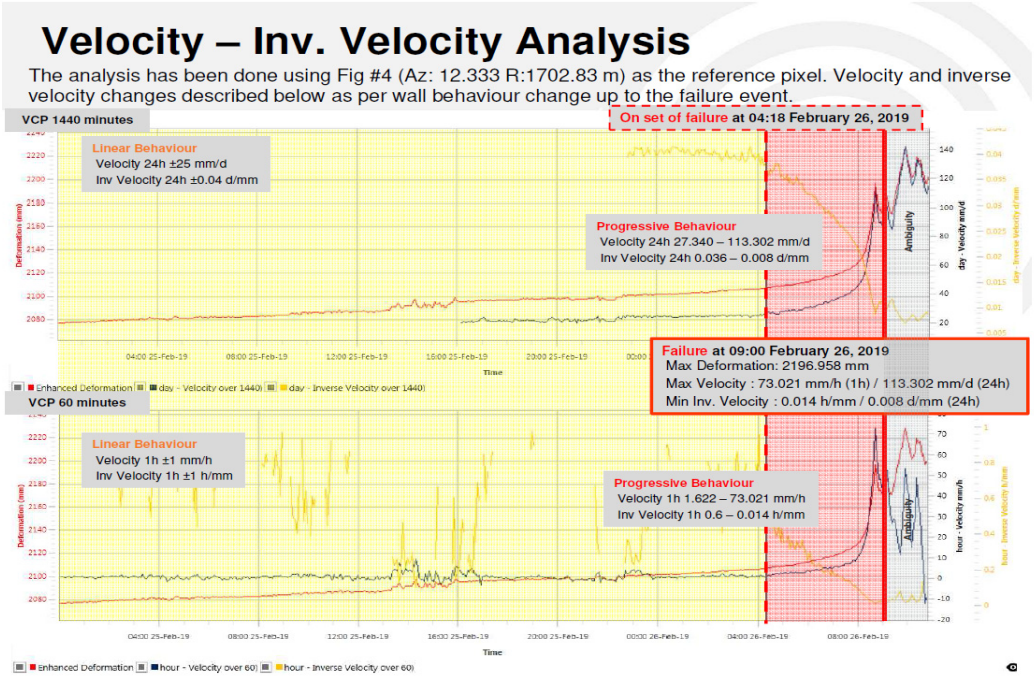

Gambar 3 – Highwall Data 2

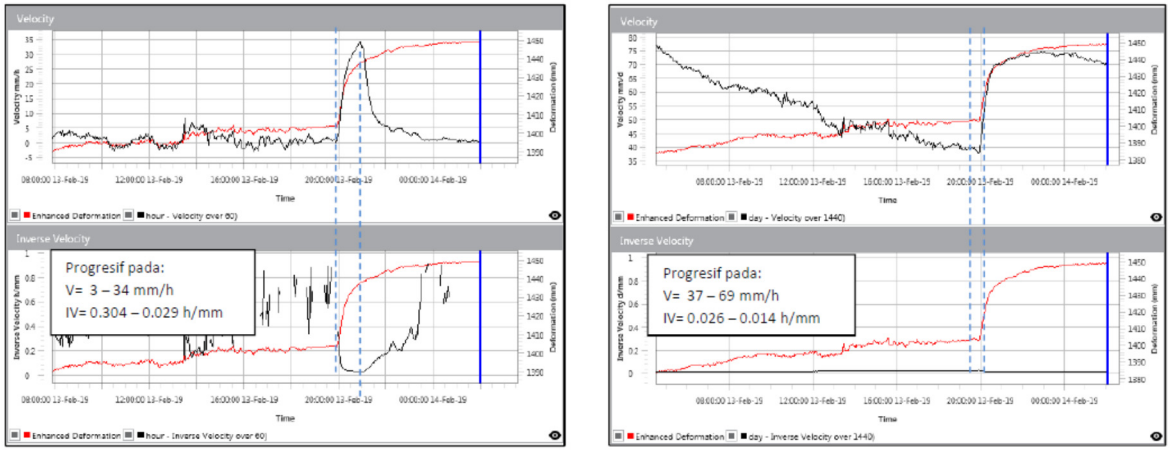

Gambar 4 – Highwall Data 3

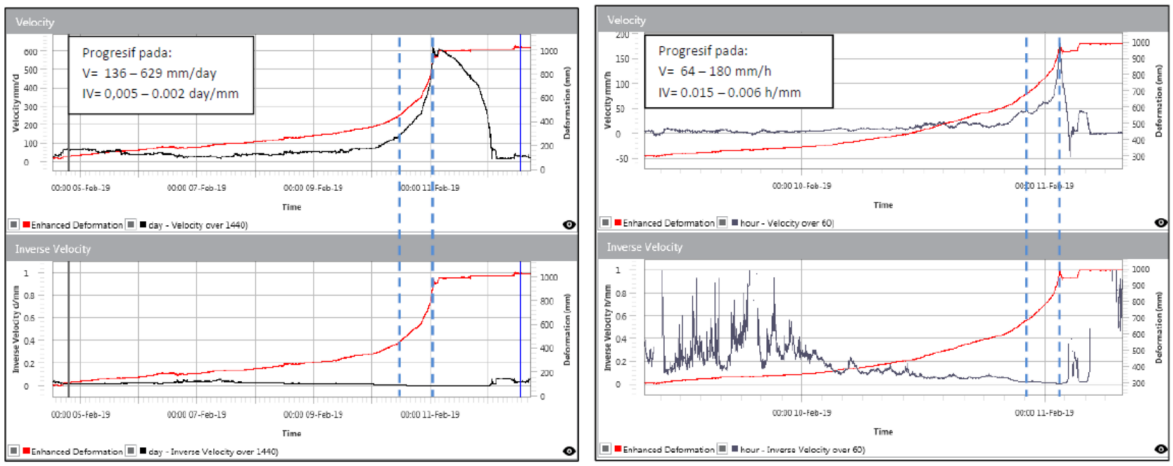

Gambar 5 – Highwall Data 4

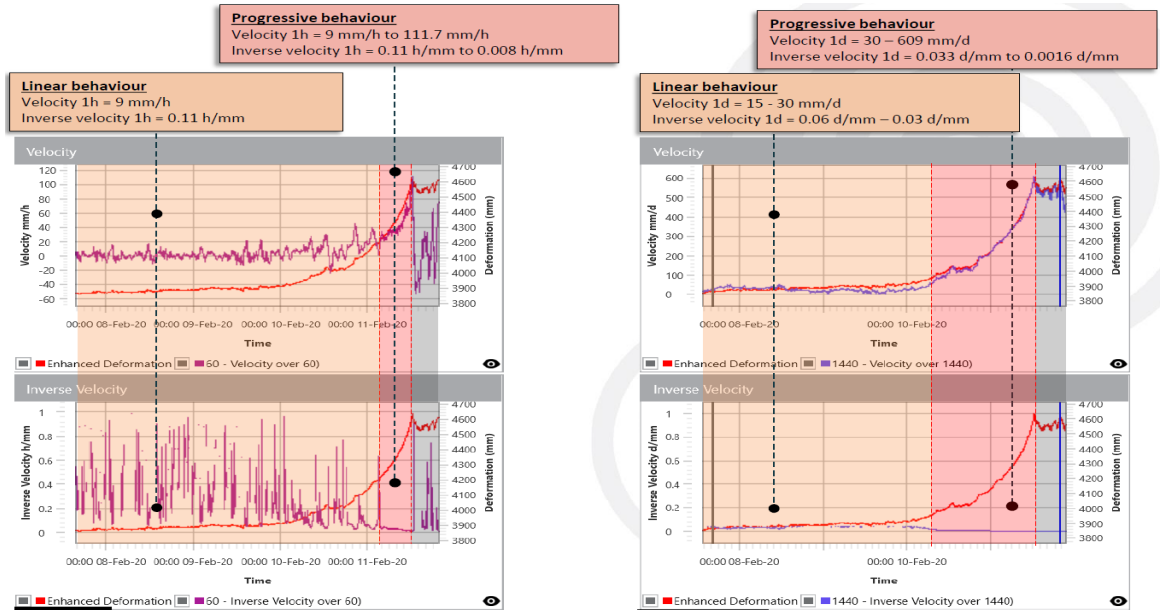

Gambar 6 – Highwall Data 5

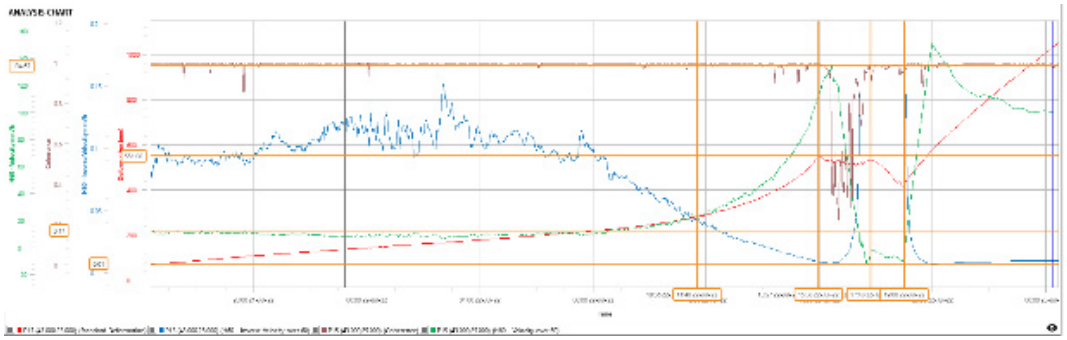

Gambar 7 – Highwall Data 6

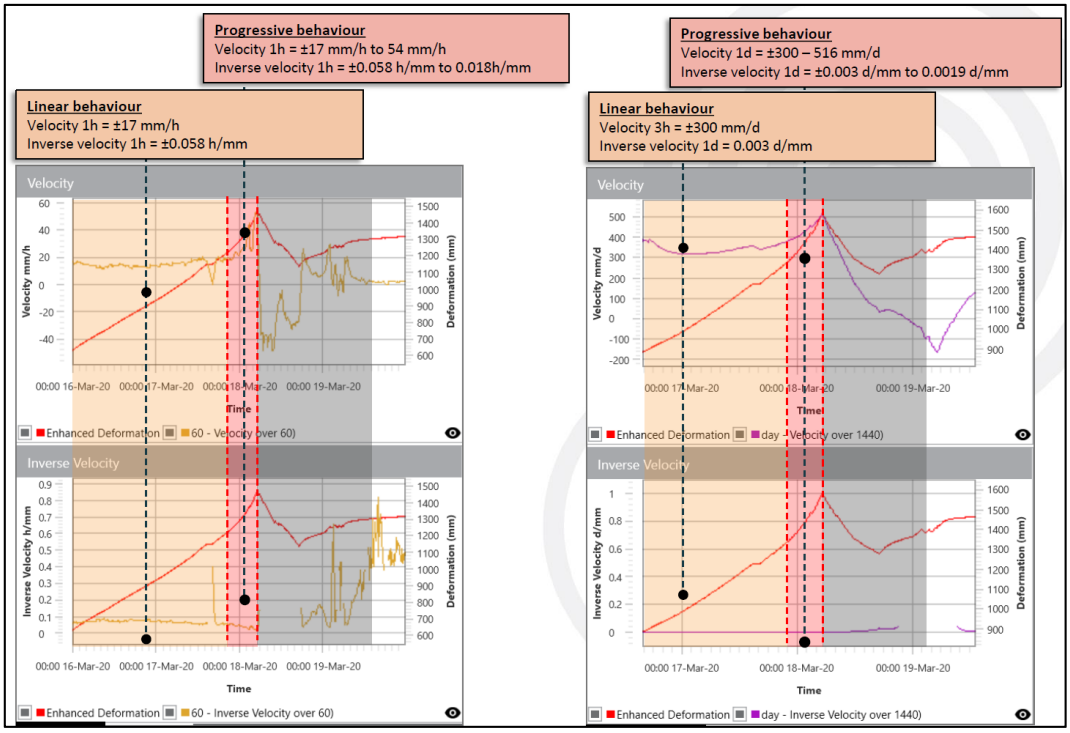

Gambar 8 – Lowwall Data 1

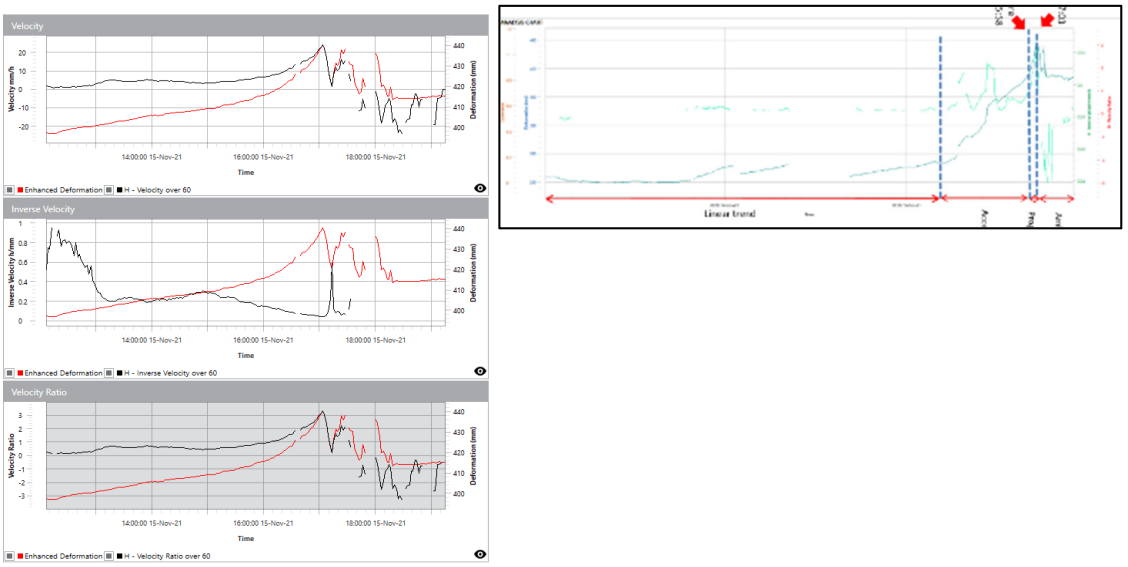

Gambar 9 – Lowwall Data 2

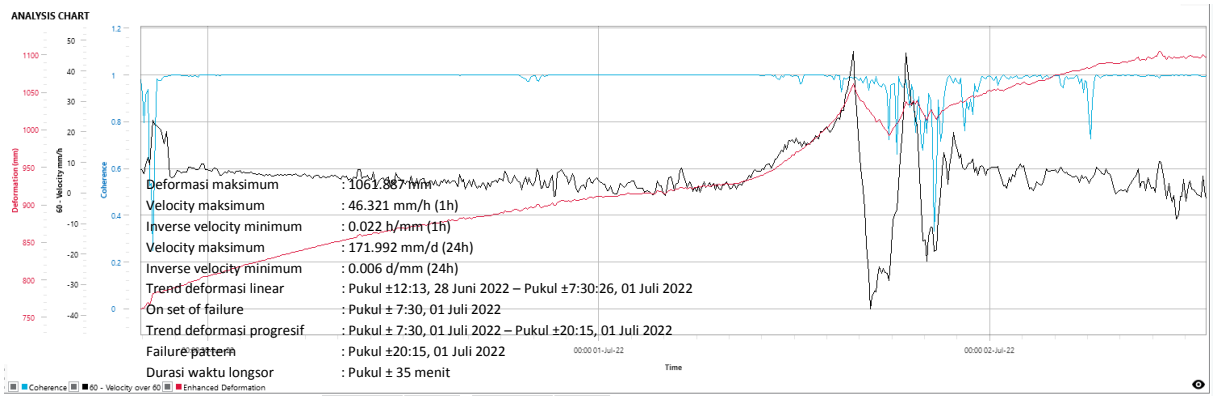

Gambar 10 – Lowwall Data 3

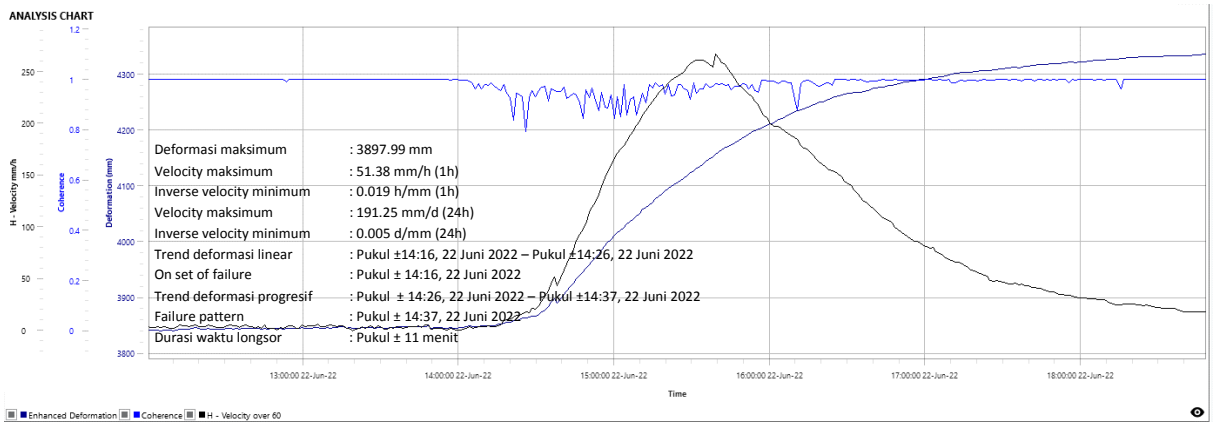

Gambar 11 – Lowwall Data 4

Tabel 1 – Inventory Kecepatan Longsor lainnya

No	SSR	Pixel		Onset Of Failure	Time of Failure	Warning Time	Linear velocity	Max. Velocity		Min. Inv. Velocity	
		x	y				60 (mm/h)	60 (mm/h)	1440 (mm/d)	60 (h/mm)	1440 (d/mm)
1	553XT	59	48	23/03/2022 23:47	24/03/2022 2:24	02:37:00	2.4	11.9	32.2	0.410	0.031
2	553XT	211	34	28/03/2022 9:30	30/03/2022 10:29	48:59:00	5.1	21.8	129.8	0.046	0.008
3	553XT	75	45	5/04/2022 11:46	5/04/2022 13:49	02:03:00	3.2	19.0	62.7	0.053	0.016
4	476XT	151	14	27/03/2022 20:26	27/03/2022 21:21	00:55:00	6.2	29.0	39.2	0.035	0.026
5	472FX	Az: -17.455	R: 2834.32	21/03/2022 22:12	22/03/2022 6:18	08:06:00	15.9	87.4	293.9	0.011	0.003
6	472FX	Az: -41.140	R: 2501.59	22/03/2022 8:15	22/03/2022 16:48	08:33:00	24.2	103.9	388.2	0.009	0.003
7	153XT	123	23	22/03/2022 3:34	22/03/2022 5:57	02:23:00	14.3	54.3	155.7	0.023	0.007
8	112XT	54	22	19/03/2022 10:16	19/03/2022 15:14	04:58:00	3.8	25.2	107.6	0.040	0.009

Tabel 2 – Rekomendasi Alarm berdasarkan Sejarah Pergerakan Lereng

No	SSR	Pixel		Onset Of Failure	Time of Failure	Warning Time	Linear Velocity	Max. Velocity		Min. Inv. Velocity	
		x	y				60 (mm/h)	60 (mm/h)	1440 (mm/d)	60 (h/mm)	1440 (d/mm)
1	746XT	62	6	4/05/2023 21:30	5/05/2023 3:21	05:51:00	12.65	73.36	224.67	0.014	0.004
2	476XT	121	19	6/02/2023 9:25	6/02/2023 15:55	06:30:00	9.43	63.2	220	0.016	0.005
3	476XT	178	12	8/06/2023 13:09	9/06/2023 8:12	19:03:00	15.75	83.5	540	0.013	0.002
4	476XT	191	12	16/06/2023 20:29	17/06/2023 17:22	20:29:00	14.77	70.89	386.38	0.02	0.003
5	476XT	298	6	22/06/2023 21:31	23/06/2023 6:39	09:08:00	13.50	81	627.88	0.012	0.002
6	476XT	55	24	11/11/2023 4:12	12/11/2023 16:18		8.28	45.23	229.067	0.022	0.004
7	476XT	63	25	1/12/2023 18:28	1/12/2023 19:14	01:02:00	2.50	15.83	25.328	0.063	-

TIME OF COLLAPSE	ALARM TYPE	GENERIC/TEST TRESHOLD	OTHER PARAMETERS	GENERIC TRIGGER	NOTIFICATION PERIOD	TRIGGER SEQUENCE
24/03/2022 2:24	Deformation	7 mm	6 pixels, 2 scans, movement both, over period since time 6h, tight mask	24/03/2022 0:09	2:14:08	1
	Velocity	4 mm/h	3 pixels, 2 scans, movement both, VCP60, tight mask	24/03/2022 0:25	1:58:57	2

TIME OF COLLAPSE	ALARM TYPE	GENERIC/TEST TRESHOLD	OTHER PARAMETERS	GENERIC TRIGGER	NOTIFICATION PERIOD	TRIGGER SEQUENCE
30/03/2022 10:29	Deformation	10 mm	3 pixels, 2 scans, movement both, over period since time 6h, tight mask	28/03/2022 2:37	55:51:00	1
	Deformation	20 mm	3 pixels, 2 scans, movement both, over period since time 6h, tight mask	29/03/2022 2:27	32:01:34	3
	Velocity	50 mm/d	3 pixels, 2 scans, movement both, VCP1440, tight mask	28/03/2022 14:54	43:34:18	2
	Inverse Velocity	0.3 d/mm	3 pixels, 2 scans, movement both, VCP1440, tight mask	29/03/2022 6:37	27:51:38	4

TIME OF COLLAPSE	ALARM TYPE	GENERIC/TEST TRESHOLD	OTHER PARAMETERS	GENERIC TRIGGER	NOTIFICATION PERIOD	TRIGGER SEQUENCE
27/03/2022 21:21	Deformation	5 mm	4 pixels, 2 scans, movement both, over period since time 6h, tight mask	27/03/2022 18:21	2:59:10	1
	Velocity	3 mm/h	4 pixels, 2 scans, movement both, VCP60, tight mask	27/03/2022 20:06	1:14:31	2
	Velocity Ratio	1	2 pixels, 2 scans, VCP180, tight mask, noise threshold 1 mm/h, ref time 27/03/22 18:31 - 20:26	27/03/2022 20:51	0:29:42	3
	Inverse Velocity	0.4 h/mm	3 pixels, 2 scans, movement both, VCP360, tight mask	27/03/2022 20:56	0:24:43	4

TIME OF COLLAPSE	ALARM TYPE	GENERIC/TEST TRESHOLD	OTHER PARAMETERS	GENERIC TRIGGER	NOTIFICATION PERIOD	TRIGGER SEQUENCE
22/03/2022 5:57	Deformation	10 mm	1 pixel, 2 scans, movement both, over period since time 1h, tight mask	22/03/2022 2:47	3:09:52	2
	Velocity	5 mm/h	1 pixel, 2 scans, movement both, VCP360, tight mask	22/03/2022 2:27	3:29:35	1
	Velocity Ratio	2	1 pixels, 2 scans, VCP180, tight mask, noise threshold 1 mm/h, ref time 21/03/22 18:02 - 00:29	22/03/2022 3:39	2:17:15	3
	Inverse Velocity	0.2 h/mm	1 pixel, 2 scans, movement both, VCP720, tight mask	22/03/2022 4:12	1:44:20	4
	Coherence	0.8	1 pixel, 2 scans, tight mask	22/03/2022 5:18	0:38:35	5

TIME OF COLLAPSE	ALARM TYPE	GENERIC/TEST TRESHOLD	OTHER PARAMETERS	GENERIC TRIGGER	NOTIFICATION PERIOD	TRIGGER SEQUENCE
19/03/2022 15:14	Deformation	10 mm	2 pixels, 2 scans, movement both, over period since time 3h, tight mask	19/03/2022 12:06	3:07:22	1
	Velocity	2 mm/h	2 pixels, 2 scans, movement both, VCP720, tight mask	19/03/2022 12:58	2:15:04	2
	Inverse Velocity	0.2 h/mm	2 pixels, 2 scans, movement both, VCP360, tight mask	19/03/2022 13:47	1:26:26	3
	Coherence	0.8	2 pixels, 2 scans, tight mask	19/03/2022 14:56	0:17:14	4

TIME OF COLLAPSE	ALARM TYPE	GENERIC/TEST TRESHOLD	OTHER PARAMETERS	GENERIC TRIGGER	NOTIFICATION PERIOD	TRIGGER SEQUENCE
22/03/2022 6:18	Deformation	20 mm	5 AP (2 Azimuth, 5 Range), 2 scans, movement both, over period since time 3h, tight mask	21/03/2022 22:36	7:41:59	1
	Velocity	6 mm/h	5 AP (2 Azimuth, 5 Range), 2 scans, movement both, VCP360, tight mask	22/03/2022 0:56	5:21:08	2
	Velocity Ratio	1.5	5 AP (2 Azimuth, 5 Range), 2 scans, VCP360, noise threshold 1 mm/h, tight mask, ref time 21/02/22 17:01 - 23:42	22/03/2022 1:24	4:53:09	3
	Inverse Velocity	0.1	4 AP (2 Azimuth, 5 Range), 2 scans, movement both, VCP180, tight mask	22/03/2022 2:12	4:05:08	4
	Coherence	0.8	4 pixels, 2 scans, tight mask	22/03/2022 5:40	0:37:07	5

3.2. Pendekatan Laboratorium – Rasio UCS (Basis Waktu dan Modulus Young Linear – Progresif)

Menurut **Yudono dkk (2021)** regresi linear adalah garis lurus yang ditarik untuk mewakili hubungan rata-rata antara dua variabel, misalnya y = a + bx. Garis ini memberikan nilai prediksi ŷ untuk setiap x. Setelah garis regresi (nilai ŷ) ditemukan, selanjutnya bisa hitung residual = y_aktual – ŷ. Residual ini menunjukkan berapa jauh titik data dari garis rata-ratanya. Jika dihitung rata-rata dan simpangan baku residual maka nilai ini dapat diubah jadi menjadi nilai vaildasi Z-score:

- Z_residual = (y − ŷ) / SD_residual

Z-score adalah ukuran seberapa jauh suatu data dari rata-rata, dinyatakan dalam satuan simpangan baku

- (SD): Z = (x - μ) / σ
  x: nilai aktual

  μ: rata-rata

  σ: simpangan baku

Z-score bukan hanya bilang data besar atau kecil, tapi juga seberapa ekstrem relatif terhadap sebaran datanya. Dengan kata lain, Z-score ini akan memberikan informasi apakah sebuah titik data terlalu jauh dari garis regresi (misalnya anomali/perubahan fase).

- Pada data UCS, titik stress–strain yang jauh dari garis regresi elastik mengindikasi kan adanya transisi ke fase plastis.
- Pada Radar, titik *velocity–time* yang Z-score-nya besar → mengindikasikan adanya akselerasi (Watch/Warning/Alarm).

Jadi, regresi linear memberi baseline, sedangkan Z-score mengukur deviasi dari baseline itu. Gabungan keduanya = alat kuantitatif untuk deteksi perubahan fase atau sinyal alarm.
Penelitian ini menggunakan hubungan strain (x) dengan stress (y) dengan Modulus linear awal digunakan sebagai acuan dan Modulus fase progresif dan dihitung pada regangan tertentu sesuai dengan perubahan waktu ke waktu dapat dilihat pada Gambar 12 -14. Rasio dari gradien regeresi UCS vs Time didefinisikan:

$$R_{UCS(t)} = \frac{(UCS)_{progressive(t)}}{(UCS)_{linier(t)}}$$

atau

$$\varphi(t) = 1 - \frac{(UCS)_{linier(t)}}{(UCS)_{progressive(t)}}$$

Interpretasi:
- $R_{UCS} \sim 1$ ($\psi \sim 0$) → fase elastik stabil.
- R_{UCS} meningkat → softening.
- R_{UCS} tinggi (ψ besar) + SE > 1 → akseleratif.

Threshold alarm dapat didasarkan pada kombinasi Rasio Gradien Linearitas saat Linear dan Progresif.

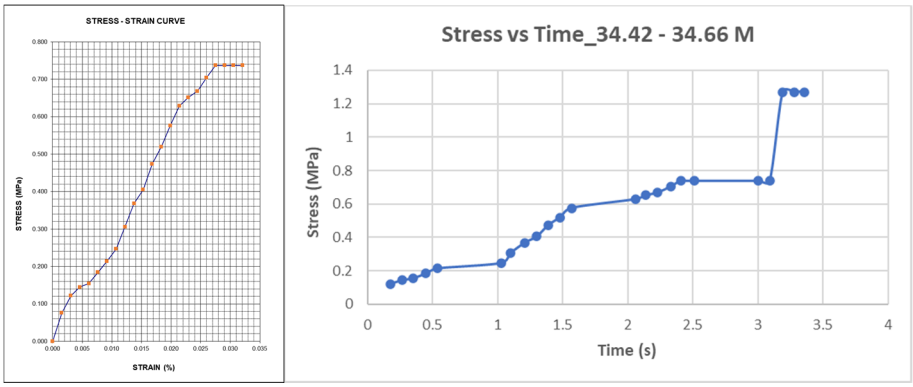

5

Gambar 12 – Data Laboratorium UCS (*Depth*: 34.42-34.66) vs Time

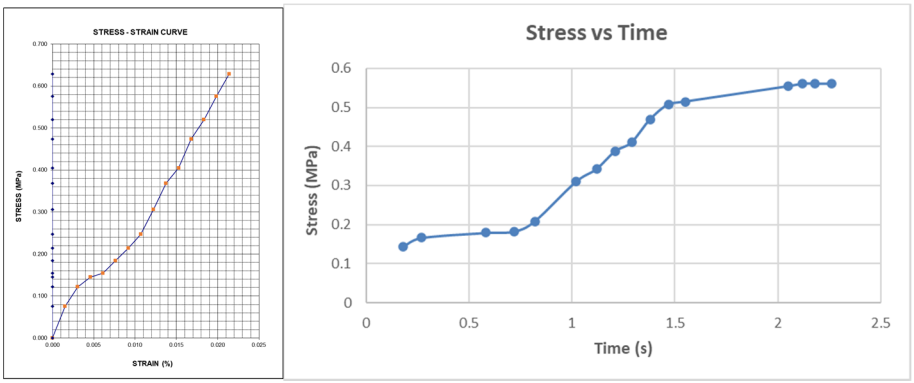

Gambar 13 – Data Laboratorium UCS(*Depth*: 41.38-41.46 vs Time

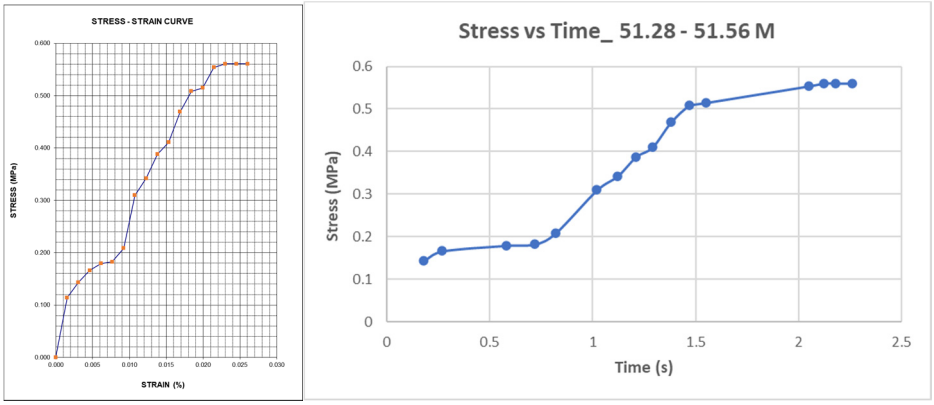

Gambar 14 – Data Laboratorium UCS (*Depth*: 51.28-51.56) vs Time

3.3. **UCS Time Series**

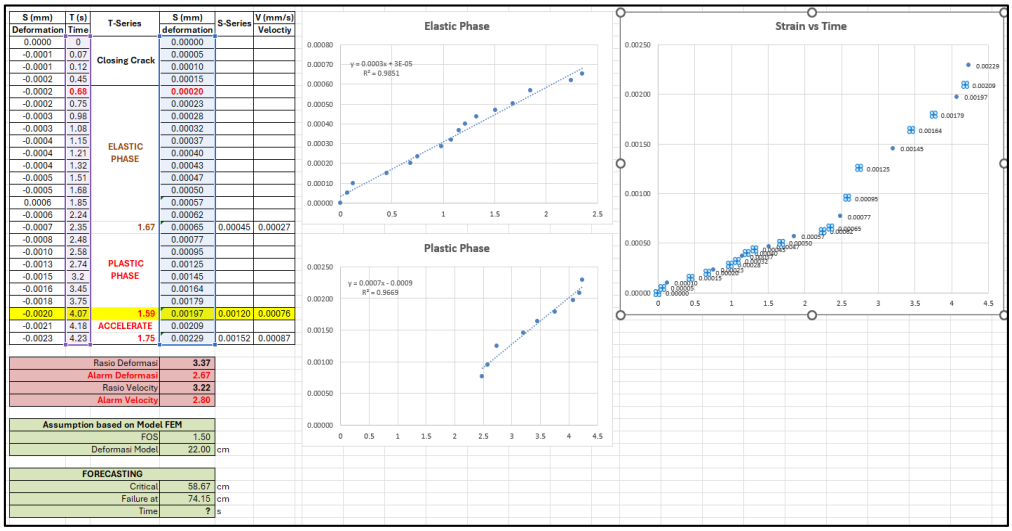

S (mm) Deformation	T (s) Time	T-Series	S (mm) deformation	S-Series	V (mm/s) Velocity
0.0000	0		0.00000		
-0.0001	0.07	Closing Crack	0.00005		
-0.0001	0.12		0.00010		
-0.0002	0.45		0.00015		
-0.0002	0.68		0.00020		
-0.0002	0.75		0.00023		
-0.0003	0.98		0.00028		
-0.0003	1.08		0.00032		
-0.0004	1.15	ELASTIC PHASE	0.00037		
-0.0004	1.21		0.00040		
-0.0004	1.32		0.00043		
-0.0005	1.51		0.00047		
-0.0005	1.68		0.00050		
0.0006	1.85		0.00057		
-0.0006	2.24		0.00062		
-0.0007	2.35	1.67	0.00065	0.00045	0.00027
-0.0008	2.48		0.00077		
-0.0010	2.58		0.00095		
-0.0013	2.74	PLASTIC PHASE	0.00125		
-0.0015	3.2		0.00145		
-0.0016	3.45		0.00164		
-0.0018	3.75		0.00179		
-0.0020	4.07	1.59	0.00197	0.00120	0.00076
-0.0021	4.18	ACCELERATE	0.00209		
-0.0023	4.23	1.75	0.00229	0.00152	0.00087

Rasio Deformasi	3.37
Alarm Deformasi	2.67
Rasio Velocity	3.22
Alarm Velocity	2.80

Assumption based on Model FEM		
FOS	1.50	
Deformasi Model	22.00	cm

FORECASTING		
Critical	58.67	cm
Failure at	74.15	cm
Time	?	s

Gambar 15 – UCS time Series

Gambar UCS Time Series ini menunjukkan secara visual bagaimana regresi linear membagi fase elastik dan plastis. Deviasi dari garis regresi (residual) bisa diproyeksikan sebagai Z-score. Nilai rasio deformasi/velocity yang sudah dihitung di tabel bisa dikorelasikan dengan ambang Z-score untuk menentukan *Watch, Warning, Alarm*.

3.4. **Kalibrasi Model FEM (Maximum Shear Strain)**

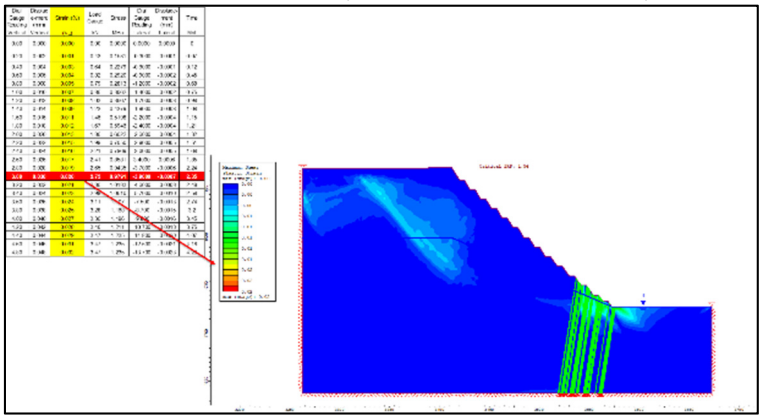

Gambar 16 – Kalibrasi model *Finite Elemen Method* (FEM)

Kalibrasi dengan FEM memastikan bahwa angka-angka rasio deformasi/velocity yang diperoleh dari UCS tidak hanya berlaku di laboratorium, tetapi juga tervalidasi dalam model geoteknik skala tambang. Dengan begitu, ketika radar mendeteksi percepatan deformasi, sistem alarm yang berbasis UCS + FEM + Z-score akan lebih akurat, adaptif, dan berbasis mekanisme fisik.

4. **KESIMPULAN**

Data *Uniaxial Compressive Strength* (UCS) batuan merupakan aset fundamental dalam pemetaan risiko keselamatan lereng tambang dan optimalisasi desain penambangan. Melalui kurva tegangan–regangan hasil uji UCS, diperoleh parameter utama seperti Modulus Young (E), rasio deformasi elastik–plastik, serta indikator penurunan kekakuan (*stiffness degradation*). Parameter-parameter ini memungkinkan pemetaan fase deformasi batuan secara kuantitatif, mulai dari kondisi stabil, transisi, hingga fase akseleratif yang berpotensi berujung pada keruntuhan.

Berdasarkan penelitian laboratorium data UCS pada lokasi pengukuran deformasi Radar PT. KPC, kriteria longsor berdasarkan Rasio Gradien Regresi UCS:

- Linear : 2 sampai dengan 3 kali lipat dari kecepatan regressif (stabil)
- Progressif : 4 sampai dengan 7 kali lipat dari kecepatan pergerakan saat linear.
- Longsor : 8 sampai dengan 10 kali lipat dari kecepatan pergerakan saat linear.

Ini berarti, baik alarm velocity, akselerasi ataupun Rasio kecepatan dapat ditentukan berdasarkan Rasio dari Gradien Regresi UCS.

Penentuan ambang kritis berbasis indikator Gradien Regresi UCS berdasarkan waktu strain menjadikan UCS sebagai dasar ilmiah dalam menetapkan threshold alarm deformasi pada sistem radar (SSR). Dengan demikian, sistem peringatan dini tidak lagi hanya mengandalkan *back-analysis* longsor aktual, melainkan langsung ditopang oleh sifat mekanik material aktual yang merepresentasikan kondisi lapangan. Hal ini meningkatkan sensitivitas, responsivitas, serta keandalan sistem pemantauan deformasi.

Dengan demikian, data UCS bukan hanya hasil uji laboratorium, melainkan fondasi ilmiah dan praktis untuk memperkuat sistem peringatan dini, meningkatkan keselamatan, sekaligus mendukung efisiensi dan keberlanjutan operasi penambangan.

6 UCAPAN TERIMA KASIH

Penulis mengucapkan terima kasih kepada PT. Kaltim Prima Coal terutama kepada Departement Geologi atas kesempatannya untuk melakukan penelitian ini.

7 DAFTAR PUSTAKA

Beer, F. P., Johnston, E. R., Dewolf, J. T., & Mazurek, D. F., 2020. *Mechanics of Materials* (8th edition.). New York: McGraw-Hill Company.

Callister, W. D., & Rethwisch, D. G., 2020. *Materials Science and Engineering: An Introduction* (10th edition). New Jersey: Jhon Wiley & Sons.

Gere, J. M., & Goodno, B. J., 2012. *Mechanics of Materials* (8th edition). Singapore: Cengage Learning.

Munthaha, D. I., Fajar, F., Tappang, G., & Irsyad, A., 2022. Pemantauan Deformasi Lereng Tambang Terbuka Paska Peledakan dengan Slope Stability Radar. *IMPJ : Indonesian Mining Professionals Journal*, 3(2), 71-82.

Yudono, A. S. dkk, 2021. *Back-Analysis of Vector Loss Effect to Line-of-Sight (LOS) pada Slope Stability Radar.* Prosiding TPT-XXX Perhapi.

HIMPUNAN AHLI TEKNIK TANAH INDONESIA - HATTI
Indonesian Society for Geotechnical Engineering - ISGE
PIT HATTI XXIX
10-12 November 2025

Recommendation of Ground Surface Design-Spectra Through Site-Specific Response Analysis (SSRA) Considering Effect of Various Depth of Bedrock, Case Study of Jakarta

Det Komerdevi[1] and I Wayan Sengara[2]

[1]*PT. WSP Engineering (det.komerdevi@wsp-engineering.com, det.komerdevi@mercubuana.ac.id)*
[2]*Bandung Institute of Technology (wayansengara@si.itb.ac.id)*

Abstract. Method of site-specific response analysis (SSRA) is considered more accurate to determine response spectra at ground surface. This method includes soil characteristics, such as dynamic modulus, damping, weight volume, and bedrock depth. The bedrock depth determination is often debated because majority it is not measured directly in the field, but estimated based on geological data or other secondary data survey. Furthermore, most of geotechnical soil investigation is limited to 30 m depth, which does not reach the bedrock layer.

Currently, for the Jakarta area, there are several references for bedrock depth. First, based on data from the Geological Research Center in 1997, the bedrock depth around the Blok M area is about 300−350 m. Second, based on previous study conducted by Ridwan et al. 2016, mentioned that the bedrock depth in Jakarta varies between 500 - 760 m. Third, based on recent investigation conducted by Rexa et al, 2023, it concluded that the bedrock layer in Jakarta is shallower between 250 - 500 meters. Given the differences of bedrock references, the author wanted to validate their impact into recommendation surface response spectra through SSRA. The SSRA was performed by the 1-Dimensional wave propagation conducted by NERA (Non-linear earthquake Analysis, Bardet & Tobita, 2001) which validate the soil profile from bedrock to the surface. The analysis results shows that the recommended surface spectrum has a significant amplification for variations of deep and shallow soil deposits. A fairly deep bedrock layer (650 m) based on Ridwan et al., 2016 produces a smaller surface response spectrum (below 80% of the SNI recommendation) compared to a shallower bedrock layer (325 m) based on Rexa et al. 2023. The bedrock depth estimated about 250 – 500 m at Jakarta seems to be more appropriate based on the waves propagation result.

Keywords: Bedrock depth, 1-D waves propagation, Response spectra, SSRA

1 INTRODUCTION

Local site effects must be considered in earthquake-resistant design and must be calculated on a case-by-case basis. There are two methods commonly used to determine ground surface response. The first is very simple procedure by multiplying the amplification factors Fa and Fv for Ss and S1, respectively. However, this method is not fully representing the response of local conditions, which have varying soil layers even within the same site class.

The second is through wave propagation using the site-specific response analysis (SSRA). The SSRA method uses one-dimensional wave propagation procedure that requires additional effort to develop one or more design ground motions that reflect the amplitude level, frequency content, and duration of specific strong motions that must be considered in the design of structures or facilities at a particular location. In addition, the shear wave velocity V_s=750 m/s must also be determined as a reference for the bedrock layer. Therefore, the site-specific response (SSRA) procedure is considered more accurate and appropriate for local geological conditions than general earthquake design standards for structural planning and earthquake risk mitigation.

The general procedure in site-specific response analysis is:

- Create a soil stratification model at the research site, including important parameters such as shear wave velocity, soil density, and soil damping.
- Determine significant earthquake sources and obtain bedrock acceleration from the selected earthquake sources.
- Performing one-dimensional ground response analysis using non-linear methods to simulate the seismic response spectrum from the bedrock to the ground surface.
- Generating output in the form of peak surface acceleration and recommended response spectrum.

The bedrock depth often is not measured directly in the field, but estimated based on geological data or other secondary data survey. Furthermore, geotechnical soil investigation data is generally collected to 30 m depth, which does not reach the bedrock layer.

To determine the bedrock layer far below the ground surface, a geophysical survey such as microtremor can be conducted, which utilizes natural ground vibrations with small amplitudes. Surface waves generated from microtremor testing can be analyzed to determine the subsurface structure without the need for excavation or drilling. This method is relatively simple, fast, inexpensive, and is effective for describing subsurface geological conditions to depths of tens to hundreds of meters.

2 SOIL PROFILE AND BEDROCK LEVEL IN JAKARTA

2.1 Soil profile of the Jakarta Site

Geologically, the Jakarta area is known to have very deep soil deposits. Based on several project data from drilling around Blok M (South of Jakarta), the drilling depth reached 200 m as shown in **Figure 1**, however no bedrock layer was found at the end of the drilling, and it is estimated that the bedrock layer is still several tens of meters below. The average N-SPT value for the top 30 m layer was correlated to obtain the shear wave velocity value, resulting in V_{s30} = 221 m/s with a site class of SD (medium soil) according to SNI 1726-2019.

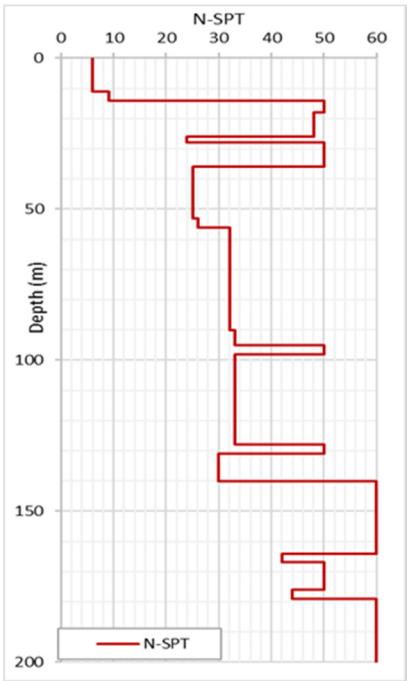

Figure 67 *Borlog at Jakarta around Blok M (south Jakarta)*

2.2 Bedrock level at the Jakarta Site

Geophysical survey and geotechnical investigation data was collected to identify the subsurface conditions of Jakarta. The results of the geophysical survey show significant differences of bedrock depth.

2.2.1 Geological Research and Development Center, 1997

Based on Geological Research and Development Center, 1997 data, the geological stratigraphic interpretation of the Blok-M area suggests that there were sinking phases by sea level twice. First phase can be interpreted with the existence of drag-stage in seismic data so that it can be predicted that if there were two sinking phases occurred then there would be two drag stages exist. Based on this interpretation, it is concluded that in Blok-M area, base rock layer was estimated at depth of approximately 300 m with ± 50 m tolerance. Similar interpretation suggests that the depth of base-rock at Jakarta Bay area is estimated about 300 - 350m. Considering the major structure of southern Jakarta and the aforementioned interpretation, it can be concluded that the depth of base-rock in southern area is shallower than that of the northern area. Whereas in eastern area is deeper than that of the western area. In addition, core drilling in Cengkareng confirms that the depth of base-rock is greater than 185 m. Geotechnical South-North profiles were generated from this limited subsurface indicating depth of base-rock is presented in **Figure 2**.

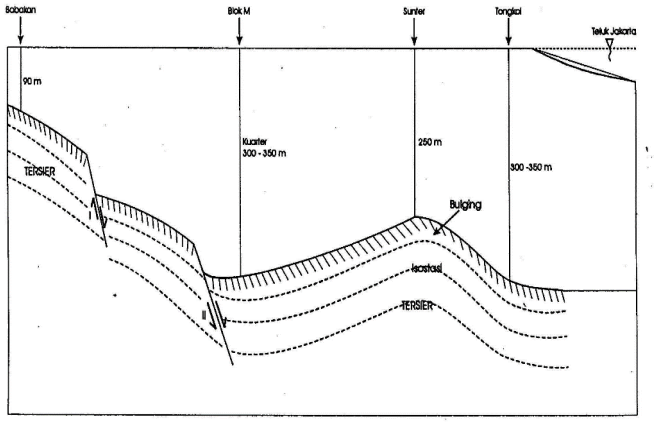

Figure 68 Base rock South-North profile for Jakarta (Source: Geological Research and Development Center, 1997)

2.2.2 Ridwan et al. (2016)

Ridwan et al, (2016) develop an engineering bedrock map beneath Jakarta based on microtremor array measurements. The microtremor data analysis was carried out using the spatial autocorrelation (SPAC) method whereas the S-wave velocity profile was estimated by inversion using a genetic algorithm. The survey has been conducted at 55 sites that covered the whole of Jakarta. The result of one-dimensional (1D) S-wave velocity profile indicates that the engineering bedrock depth (V_s = 750 m/s) throughout the Jakarta area is presented in **Figure 69**.

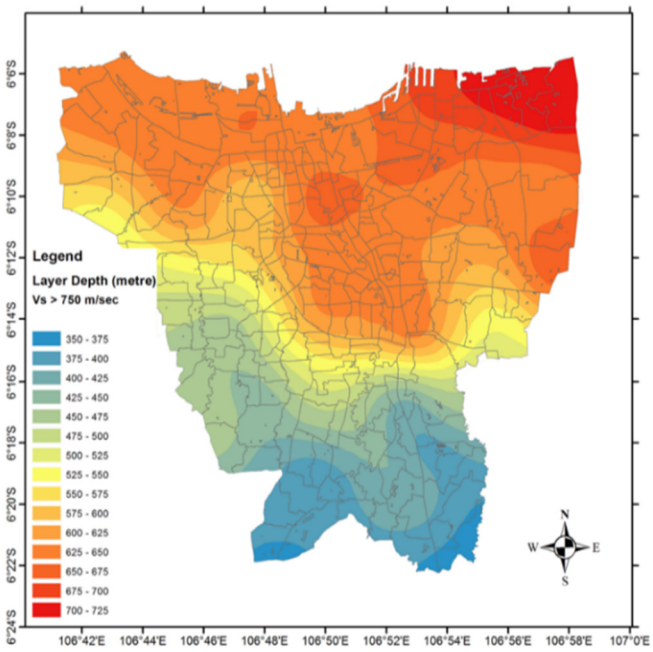

Figure 69 Map of bedrock layer depth for V_s > 750 m/s (Ridwan et al, 2016)

This result in **Figure 69** shows that the depth of engineering bedrock in northern Jakarta reaches 725 m, while in southern Jakarta it is at a depth of about 350 m. The morphology of engineering bedrock gradually increases northwards

2.2.3 Rexa et al. (2023)

Rexa et al. (2023) develop 3-D shallow shear velocity structure of the Jakarta Basin from transdimensional ambient noise tomography. The new temporary seismic network was deployed to extend the spatial coverage beyond that of a previous deployment in 2013, and sampled 143 locations through sequential deployments of 30 broad-band sensors covering Jakarta and its adjacent areas. The 2-stage transdimensional Bayesian inversion of Rayleigh wave phase velocity dispersion curves derived from seismic noise are also conducted. The tomography and 2-D phase velocity maps are constructed for periods 1–5 s. Then, at each point in a regular grid defined on these maps and invert each dispersion curve into 1-D depth profiles of V_s. The result of developed a 3-D shear-wave velocity model of the Jakarta Basin covering Jakarta and its adjacent areas of Greater Jakarta is presented in **Figure 70**. It shows the cross-section B designated as layers ‘Basin Fill I and ‘Basin Fill II. In the Southernmost part of the basin, it divides the basin into a shallow (depth < 300 m) layer with V_s in the interval 250–500 m/s, and deeper layer (200–750 m depth range) having V_s in the interval 500–800 m/s.

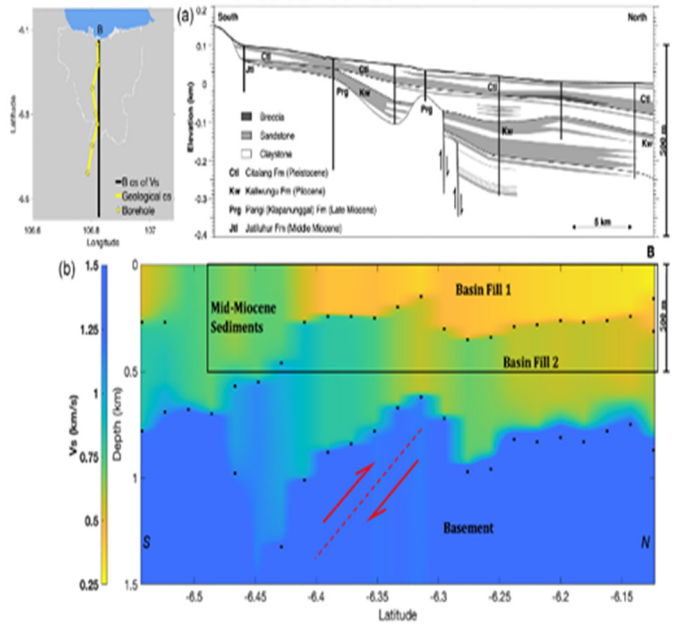

Figure 70 Cross-section Jakarta Basin Map from South to North (Rexa et al, 2023)

3 MTHODOLOGY

3.1 Bedrock Spectra at Jakarta Site

The seismic hazard analyses adopt the probabilistic (Probabilistic Seismic Hazard Analysis/PSHA) to determine spectral acceleration at bedrock with a certain level of earthquake return period. This analysis has considered the seismic design criteria based on all earthquake sources in Jakarta includes including shallow earthquake, subduction (megathtust), and shallow/deep background earthquake sources, parameters of maximum magnitude and slip rate also evaluated. Response spectra at bedrock for maximum considered Earthquake (MCER) at Jakarta is presented in **Figure 71**.

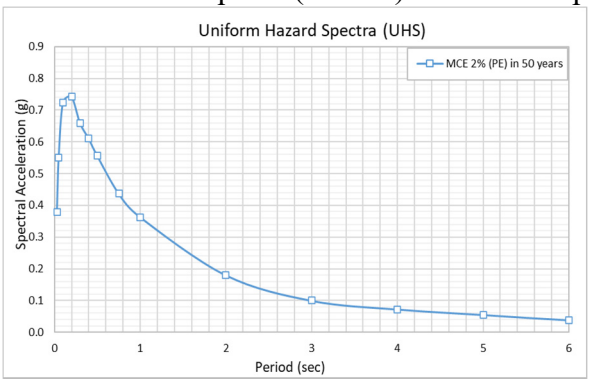

Figure 71 Bedrock Spectra for Jakarta (2% probability of exceedance in 50 years)

3.2 Ground Motion Selection & Modification

The open sources of the ground-motion catalog include databases that could be downloaded from the Pacific Earthquake Engineering Research (PEER) Center Strong Motion Database website (https://ngawest2.berkeley.edu) for shallow crustal sources, and for subduction sources could be downloaded from NGA-Sub (https://www.risksciences.ucla.edu/nhr3/nga-sub-database).

The selected ground motion has considered the source mechanism, magnitude, soil condition, usable frequency of the ground motion, period/frequency sampling, and site-to-source distance that are close/similar to the de-aggregation result. Scaling factor limits allowable of approximately 0.25 to 4.

On the other hand, the ground motion selection also considered the spectral shape because the response spectrum has to correlate with the structural response of the building.

Based on ASCE 7-16 and SNI 1726-2019, a minimum of 5 single ground motions must be determined. In this case, 11 single ground motions are selected for the building structure associated with the de-aggregation as a result of PSHA, distribution of earthquakes representative based on their contribution to the hazard curve of the Jakarta site. The selection consisted of 2 (two) ground motions from Shallow Crustal sources with a contribution 12.3%, six (6) ground motions from subduction Megathrust sources with a contribution 62.7%, and three (3) from subduction Benioff source (deep background) with the contribution 20%. It is difficult to find appropriate spectral shapes in the ground motion catalog, particularly for a high period of interest, thus, the range of magnitudes, distances, and site conditions can be relaxed so that a sufficient number of ground motions are available. The selected ground motion is tabulated in **Table 38**.

Table 38 Selected Ground Motion of MCER Level for Jakarta

No	Title	RSN	Event	Date	Mw	Station	dRup (km)	Mechanism
1	TCU065N	2618	Chi-Chi, Taiwan	Sep/20/1999	6.2	TCU065	26.05	Shallow Crustal
2	H-CAK270	322	Coalinga-01	May/02/1983	6.36	Cantua Creek	24.02	
3	ATYCN00E	3001954	Michoacan, Mexi	Sep/19/1985	7.99	ATOYAC, Igles	126.4	Megathrust
4	MT05HNE	6002253	Coastal.Chile	Sep/16/2015	8.31	MT05	169.62	
5	D5C-EW	4032480	Hokkaido.East. off	Apr/10/1994	8.28	47420	130.01	
6	IBUH01EW2	4022853	Tokachi-oki	Sep/25/2003	8.29	OIWAKE	137.85	
7	AKTH17W2	4000322	Tohoku	Nov/03/2011	9.12	NAKASEN	143.18	
8	PB02HLE	6001376	Iquique	Jan/04/2014	8.15	PB02	122.59	
9	TAP022--N	7004830	2944860	Mar/31/2002	7.12	TAP022	112.51	Benioff
10	D62-EW	4032463	Kushiro-oki	Jan/15/1993	7.59	47426	149.79	
11	YMT001-EW	4028405	SouthSanriku	May/26/2003	7.03	SAKATA	167.69	

3.3 1-D Waves Propagation

The waves propagation procedures is conducted use NERA. Nera is a computer program that utilizes FORTRAN 90 and Excel Visual Basic programming. NERA uses a finite difference formulation to solve wave propagation equations in the time domain. **Figure 6** is a schematic which shows the notation used in the NERA model to identify the various soil layers at whose boundary's nodes are placed and acceleration, velocity, and displacement are computed.

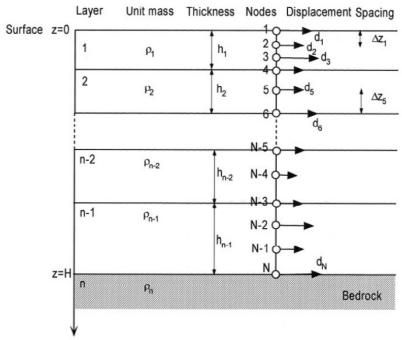

Figure 72 Schematic of a layered soil profile used in the NERA algorithm (Bardet and Tobita, 2001)

4 RESULT AND DISCUSSION

4.1 Dynamic Soil Properties

The shear waves velocity profile is applied for two different bedrock depth that is 325 m and 650 m as presented in **Figure 73**.

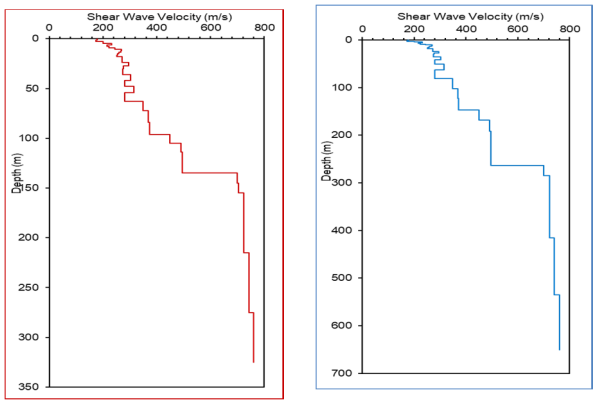

Figure 73 V_s profile for a) 325 m depth and b) 650 m depth

Shear wave velocity profiles determined based on correlation of N-SPT and combined with microtremor survey. Shear wave velocity data is applied from ground surface to the end of borehole approximated by correlation of N-SPT data, while soil deeper than 50 m is using the microtremor data.

4.2 Recommended Spectra at Ground Surface

A. Bedrock level at 325 m depth

One-dimensional waves propagation has been conducted for 11 (eleven) ground motion through 325 m depth of soil layers and provide recommendation response spectrum at ground surface is presented in

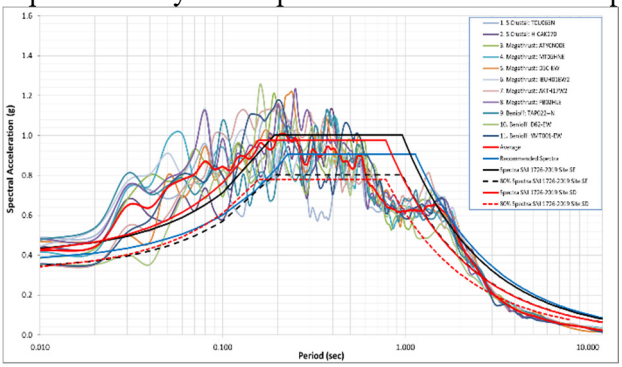

Figure 74**.** This figure shows the recommended spectrum (blue line) is slightly below code reference SNI 1726 2019 for T=PGA and T=0.2 sec, while for long period T=1.0 sec the spectra is slightly higher. In general, the recommendation spectrum is fulfilling the requirement of ASCE 7-16 and SNI 1726-2019 that is not less than minimum 80% of site interest.

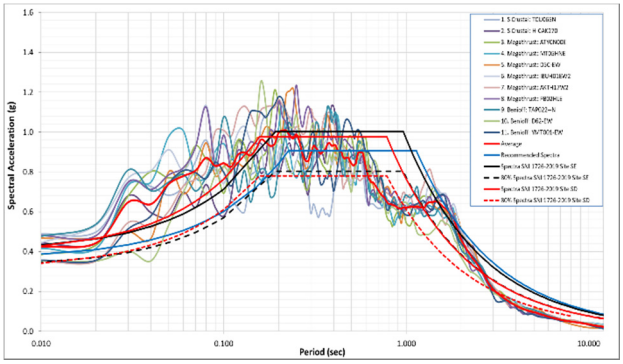

Figure 74 Recommended spectra for bedrock depth 325 m

B. Bedrock level at 650 m depth

Result of one-dimensional waves propagation for 650 m soil layers depth is presented in **Figure 75**.

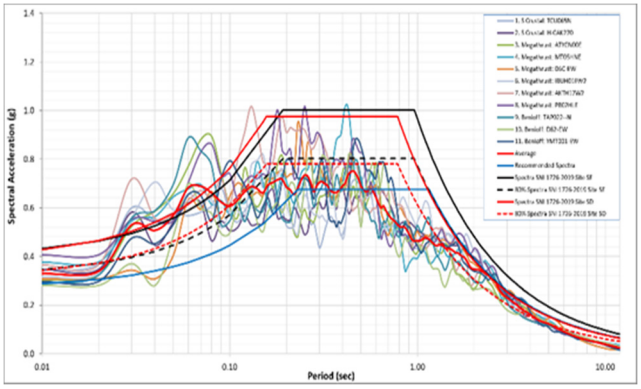

Figure 75 Recommended spectra for bedrock depth 650 m

Due to very deep soil deposit, recommendation response spectrum is far below the 80% site class SD for period T=PGA, and T=0.2 sec, that is not fulfil the requirement.

The recommendation response spectrum should be modified and adjusted with the 80% of site class SD to fulfil the ASCE 7-16 and SNI 1726-2019, as presented in **Figure 76.**

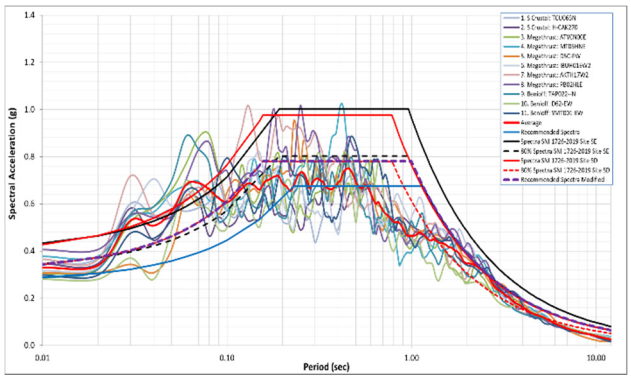

Figure 76 Modify of recommended spectra for bedrock depth 650 m

4.3 Comparison of surface response spectra.

The comparison spectra between bedrock depth 325 m and 650 m is presented in **Figure 77**.

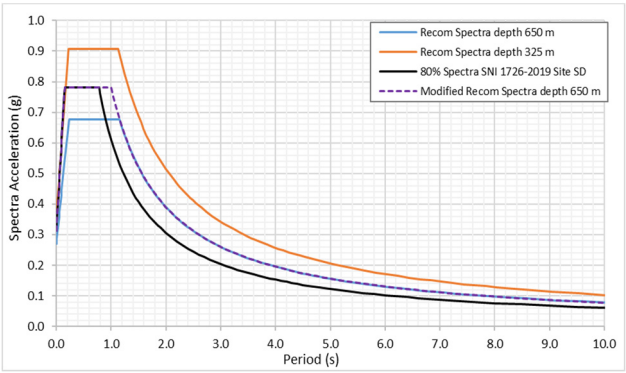

Figure 77 Comparison response spectra for bedrock depth of 325 m and 650 m

Based on the comparison it is conclude that the amplification factor of deeper bedrock layer a2 650 m will be lower about 13.9% as tabulated in **Table 39**.

Table 39 Comparison of surface spectra for bedrock layer depth 325 m and 650 m

Period (s)	Spectra Acceleration (g)		Deviation (%)
	Bedrock 325 m	Bedrock 650 m	
PGA	0.363	0.312	13.9
Ss (0.2 sec)	0.906	0.781	13.9
S1 (1.0 sec)	0.906	0.781	13.9

The bedrock depth is often debated because different depth reference of bedrock layers will affect to waves propagation result and recommended response spectra at ground surface. The deeper bedrock layer tends to produce lower response spectra even to the point below the SNI 1726-2019 criteria. The phenomenon is influenced by the site characteristic and parameters and ground motion selection that can shake the site location.

In addition, further analysis regarding to damping effect of soil layers into the wave's propagation should be study in advance to add the explanation of this phenomenon.

5 CONCLUDING REMARKS

1. Based on reference of geophysical survey at Jakarta site, there are two different of bedrock layer depth. Firstly, based on geological research center, 1997 and Rexa et al, 2023 estimated the depth of bedrock layers in Jakarta around 250 – 500 m. Secondly, based on Ridwan et al. (2016) bedrock depth is about 500 m – 760 m.
2. A single target spectrum has been applied for the Jakarta site, adopting risk-targeted maximum considered earthquake (MCER).
3. The selection of ground motions has considered de-aggregation analysis, based on the contribution of each earthquake source. The selection consisted of 2 (two) ground motions from Shallow Crustal sources with a contribution 12.3%, 7 (seven) ground motions from subduction Megathrust sources with a contribution 62.7%, and 3 (three) from subduction Benioff source (deep background) with the contribution 20%.
4. One-dimensional waves propagation using NERA has been conducted for both bedrock layers and conclude that the deeper bedrock layers 650 m will be de-amplified the response spectra at ground surface below 80% of the site class interest.
5. The recommendation response spectra at ground surface for 650 m bedrock depth is about 13.9% lower compared to and 650 m.
6. The bedrock depth estimated about 250 – 500 m at Jakarta seems to be more appropriate based on the waves propagation result.

REFERENCES

American Society of Civil Engineers Standards, ASCE SEI-7-10, Minimum Design Loads for Buildings and Other Structures, Structural Engineering Institute ASCE, Virginia, USA, (2010).

American Society of Civil Engineers Standards, ASCE SEI-7-16, Minimum Design Loads for Buildings and Other Structures, Structural Engineering Institute ASCE, Virginia, USA, (2016).

Bardet J.P., Tobita T., "NERA, A Computer Program for Nonlinear Earthquake Site Response Analyses of layered Soil Deposits", University of Southern California, (2001).

Walker Martin et. al, "From recording to Time History Analysis: A Primer on Maximum Direction Ground Motion". SEAOC 2010 Convention Proceedings, 2010.

NEHRP Recommended Seismic Provisions for New Buildings and Other Structures Volume I: Part 1 Provisions, Part 2 Commentary FEMA P-1050-1/2015 Edition, Building Seismic Safety Council, Washington D.C.

Pacific Earthquake Engineering Research Center. Tall Building Initiative Guidelines for Performance Based Seismic Design of Tall Buildings. Report N0. 2010/5. (2010).

Ridwan M, Irsyam M, Widiantor S, Afnimar, and Yamanaka H, "Development of an engineering bedrock map beneath Jakarta based on microtremor array measurements" Earth Science for Disaster Risk Reduction. (2016)

Risk Engineering, "EZ-FRISK (Software for in-depth Seismic Hazard Analysis) User's Manual", Risk Engineering Inc., Golden, Colorado, USA. (2011).

Rexha V.Ry, Phil R. C, Babak H, and Sri Widiantoro, "3D shallow shear velocity structure of the Jakarta Basin from transdimensional ambient noise tomography". Geophysical Journal International (2023).

Sengara & Komerdevi, "Site-Specific Response Analysis (SSRA) and pairs of ground motions time-history generation of a site in Jakarta". 4th International Conference on Earthquake Engineering and Disaster Mitigation (4thICEEDM), 2019 (2020)

Sengara, IW., Irsyam M., Sidi, I.D., Mulia, A., Asrurifak, M. Hutabarat, D., and Partono, W., "New 2019 Risk-Targeted Ground Motions for Spectral Design Criteria in Indonesian Seismic Building Code", 4th International Conference on Earthquake Engineering and Disaster Mitigation (4thICEEDM), 2019.

Sengara, IW., "Development of Earthquake Scenario for Three Different Sites within City of Jakarta", Earthquake Geotechnical Engineering Satellite Conference XVIIth International Conference on Soil Mechanics & Geotechnical Engineering, Alexandria, Egypt, (2009).

Sengara, IW., and Jayasaputra, U., Study of Empirical Correlations to Estimate Shear Wave Velocity based on MASW, Seismic Downhole, and Soil Investigation Data, Research Report, Geotechnical Engineering Laboratory, Inter-University Center for Engineering Science, Institut Teknologi Bandung. (2010).

Sengara, IW., Sumiartha, P., Handayani, G., and Yulman, M.A., "Report on Probabilistic Seismic Hazard and Site-Specifiv Response Analysis to Derive Seismic Design Criteria for Signature Tower – Jakarta, a Report submitted to PT. Grahamas Adisentosa, PT Georeka Indonesia. (2012).

Stewart, J.P., Archuleta, R.J., and Power, M.S., Earthquake Spectra, The Professional Journal of the Earthquake Engineering Research Institute, Special Issue on the Next Generation Attenuation Project, Volume 24, Number 1, (2008).

SNI-1726-2019, "Tata cara perencanaan ketahanan gempa untuk struktur bangunan Gedung dan nongedung", Badan Standarisasi Nasional, 2019

SNI-8899-2020, "Tata cara pemilihan dan modifikasi gerak tanah permukaan untuk perencanaan Gedung tahan gempa" Badan Standarisasi Nasional, 2020

Youngs, R. R., Chiou, S. J., Silva, W. J., Humphrey, J. R., "Strong Ground Motion Attenuation Relationship for Subduction Zone Earthquake", Bulletin of Seismological Society of America Vol. 68, No. 1. (1997).

Zhao, John X., Jian Zhang, Akihiro Asano, Yuki Ohno, Taishi Oouchi, Toshimasa Takahashi, Hiroshi Ogawa, Koijiro Irikura, Hong K. Thio, Paul G. Sommerville, Yasuhiro Fukushima, and Yoshimitsu Fukushima. Attenuation Relations of Strong ground Motion in Japan Using Site Classification Based on Predominant Period. Bulletin of the Seismological Society of America 96: 3, 898-913. (2006).

Penggunaan GI-Tube Berbahan Non Woven Dua Lapis Produksi Dalam Negeri untuk Tanggul Laut Studi Kasus Proyek Jalan Tol Semarang–Demak, Jawa Tengah

Puji Kristianingsih[1], Yashinta N.A[2], Dandung Sri Harninto[3], Abdul Aziz Avicenna[4], Ardyan Badriza[5], Muhammad Rahmat Tijani[6], Bagas Septyan Fauzi[7]

[1]Geoforce Indonesia, Jl. Penjernihan 1/12B, Tanah Abang, Jakarta Pusat 10210; tia@geoforce-indonesia.com
[2]Geoforce Indonesia, Jl. Penjernihan 1/12B, Tanah Abang, Jakarta Pusat 10210; yashinta@geoforce-indonesia.com
[3]Geoforce Indonesia, Jl. Penjernihan 1/12B, Tanah Abang, Jakarta Pusat 10210; dandung@geoforce-indonesia.com
[4]Geoforce Indonesia, Jl. Penjernihan 1/12B, Tanah Abang, Jakarta Pusat 10210; abdul.aziz@geoforce-indonesia.com
[5]Geoforce Indonesia, Jl. Penjernihan 1/12B, Tanah Abang, Jakarta Pusat 10210; ardyan@geoforce-indonesia.com
[6]Geoforce Indonesia, Jl. Penjernihan 1/12B, Tanah Abang, Jakarta Pusat 10210; rahmat@geoforce-indonesia.com
[7]Geoforce Indonesia, Jl. Penjernihan 1/12B, Tanah Abang, Jakarta Pusat 10210; bagassf63@gmail.com

ABSTRAK Pembangunan Jalan Tol Semarang–Demak merupakan salah satu Proyek Strategis Nasional (PSN) di Provinsi Jawa Tengah yang diharapkan dapat meningkatkan konektivitas serta menghubungkan kawasan industri dan pelabuhan di wilayah Demak. Salah satu komponen penting dalam proyek ini adalah pembangunan tanggul laut setinggi 12 meter, lebar 140 meter, dan panjang 6,3 km. Dalam beberapa tahun terakhir, material konvensional untuk bangunan pantai semakin sulit diperoleh dan harganya relatif mahal. Oleh karena itu, terjadi pergeseran ke penggunaan material alternatif yang lebih efisien dan mudah diperoleh seperti material geosintetik. Salah satu inovasi geosintetik yang kian populer adalah *Geotextile Tube* (GI-Tube), yaitu tabung berbahan geotekstil non-woven dua lapis yang diisi dengan pasir, kerikil, atau mortar. Makalah ini menyajikan proses produksi dari bahan baku lembaran geotekstil non-woven menjadi karung geotekstil memanjang atau disebut juga GI-Tube. Selain itu makalah ini menyajikan perbandingan antara hasil aktual melalui uji laboratorium geosintetik dengan parameter desain yang telah direncanakan sebagai tanggul sementara dalam pembangunan Jalan Tol Semarang–Demak. Material non-woven dua lapis memiliki peran penting, dengan masing-masing lapisan memiliki fungsi spesifik yang sesuai dengan kondisi lapangan. Metode ini telah terbukti menjadi solusi yang andal dan efektif dalam menjaga tanggul pasir selama pembangunan tanggul laut, memastikan tanggul terlindungi dari hantaman gelombang. Selain itu, pemilihan jenis pasir isian menjadi faktor krusial dalam menjaga kinerja GI-Tube terhadap arus laut dan badai yang sering terjadi. Hasil monitoring menunjukkan bahwa GI-Tube produksi lokal memberikan performa yang baik dan dapat direkomendasikan sebagai inovasi yang solutif. Efektivitasnya terlihat jelas dari perubahan signifikan pada area konstruksi sebelum dan sesudah pemasangan GI-Tube.

KATA KUNCI : Geotekstil non-woven dua lapis: tanggul laut GI-Tube: pasir isian: produk lokal

1 PENDAHULUAN

Jalan Pantai Utara (Pantura) merupakan jalan nasional sepanjang 1.316 km yang melintasi lima provinsi, yaitu Banten, DKI Jakarta, Jawa Barat, Jawa Tengah, dan Jawa Timur. Pertumbuhan lalu lintas di koridor Semarang–Demak semakin meningkat, diperparah dengan seringnya kejadian banjir rob yang menyebabkan kemacetan parah.

Selain itu, kondisi tanah berbutir halus yang mengalami konsolidasi alami serta kenaikan muka air laut akibat pemanasan global turut berkontribusi terhadap permasalahan banjir. Permukiman,

kawasan industri, dan infrastruktur penting, termasuk jalan raya, mengalami kerusakan serius akibat banjir rob yang terjadi hampir sepanjang tahun.

Sebagai solusi, pemerintah membangun Jalan Tol Semarang–Demak yang juga berfungsi sebagai tanggul laut. Salah satu komponen penting dalam proyek ini adalah penggunaan GI-Tube, yaitu material geotekstil non-woven dua lapis produksi dalam negeri sebagai bagian dari sistem perlindungan pantai.

Makalah ini bertujuan untuk menyampaikan hasil monitoring lapangan terhadap kinerja GI-Tube dua lapis non-woven produksi lokal, serta efektivitasnya dalam membentuk tanggul sementara di area reklamasi. Penelitian ini juga diharapkan dapat memberikan alternatif teknologi perlindungan pantai yang inovatif dan berbasis produk dalam negeri yang sudah memiliki sertifikat TKDN.

2 PERTIMBANGAN MATERIAL

Pemilihan material geotekstil dan jenis pasir isian merupakan aspek penting dalam menjamin keberhasilan GI-Tube sebagai tanggul laut.

2.1 Geotekstil Non-Woven

Material geotekstil yang digunakan terdiri atas dua lapisan non-woven, dengan warna hijau pada lapisan luar dan putih pada lapisan dalam. Lapisan dalam berfungsi sebagai **f**ilter untuk menahan partikel pasir halus, sedangkan lapisan luar bertugas melindungi struktur terhadap abrasi, gelombang, dan arus laut karena memiliki kekuatan tarik dan ketahanan abrasi yang tinggi.

Keunggulan geotekstil dua lapis ini adalah ukuran bukaan (AOS) yang lebih kecil dibandingkan geotekstil woven. AOS geotekstil woven umumnya sebesar 0,325 mm, sedangkan geotekstil dua lapis non-woven yang digunakan memiliki AOS sebesar 0,06 mm. Hal ini meningkatkan efektivitas dalam menahan pasir isian.

Tabel 1. Spesifikasi teknis geotekstil non-woven dua lapis

Parameter	Metode	Satuan	Rata-rata
Kuat Tarik MD	ASTM D 4595	kN/m	> 70
Kuat Tarik CD	ASTM D 4595	kN/m	> 80
Elongation MD	ASTM D 4595	%	< 120
Elongation CD	ASTM D 4595	%	< 120
Kuat Tusuk - CBR	ASTM D 6241	kN	> 14
Permitivity	ASTM D 4491	s^1	> 0,5
Ketebalan dibawah 2 kPa	ASTM D 5199	mm	> 7
Berat	ASTM D 5261	g/m^2	> 1200

Kementerian Perindustrian
REPUBLIK INDONESIA

TANDA SAH CAPAIAN TINGKAT KOMPONEN DALAM NEGERI

Sesuai dengan Peraturan Menteri Perindustrian No. 16/M-IND/PER/2/2011 tentang Ketentuan dan Tata Cara Penghitungan Tingkat Komponen Dalam Negeri, hasil verifikasi atas capaian Tingkat Komponen Dalam Negeri (TKDN) adalah sebagai berikut:

Jenis Produk	:	Karung Geotekstil Memanjang
Tipe	:	Non Woven Polypropylene
Spesifikasi	:	1300 gr/ m2, Double Layer, Panjang 11,2 m s/d 22,3 m, lebar 2,55 m (keliling 5 m), Panjang 11,2 m s/d 22,3 m, lebar 1,3 m (keliling 2,5 m)
Kode HS	:	59119090
Merk	:	-
Nilai TKDN	:	59.97%
Terbilang	:	Lima puluh sembilan koma sembilan tujuh persen
Standard Produk	:	-
Sertifikat Produk	:	-
No. Laporan	:	TKDN - 1611 - 2401686

yang telah ditandasahkan oleh Kementerian Perindustrian dan berlaku 3 tahun terhitung sejak tanggal tanda sah,
diberikan kepada:

Nama Perusahaan	:	PT Fokus Engineering Indonesia
Alamat	:	KAWASAN INDUSTRI TERBOYO, JL.INDUSTRI BARAT V BLOK H-1C, TRIMULYO, GENUK, Kota Semarang, Jawa Tengah, 50118
NPWP	:	74.045.764.3-518.000
Jenis Industri	:	Industri Barang Plastik Lainnya Ytdl (KBLI: 22299)
No. Tanda Sah	:	3295/SJ-IND.8/E-TKDN/6/2024

Jakarta, 6 Juni 2024
Plh. Kepala Pusat Peningkatan Produk Dalam Negeri

Mohammad Ari Kurnia Taufik

Gambar 1. Nilai TKDN geotekstil non woven dua lapis

2.2 Spesifikasi Pasir Isian

Pasir yang digunakan telah diuji melalui analisis saringan, dengan hasil bahwa hanya 5,25% partikel yang berukuran < 0,05 mm (ukuran lanau). Ini berarti 94,75% partikel pasir akan tertahan oleh geotekstil, sesuai dengan standar Koerner (2005) yang menyarankan ukuran AOS < 0,6 mm untuk tanah dengan ≤ 50% lolos saringan No. 200.

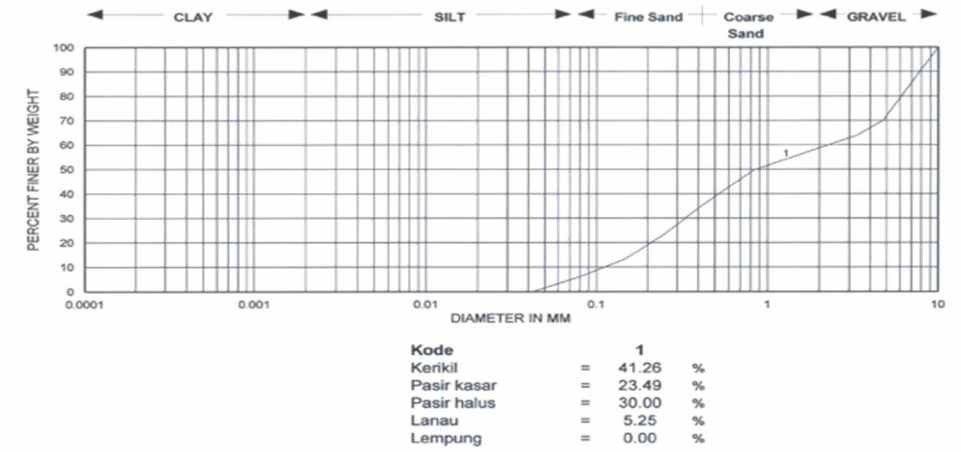

Kode		1	
Kerikil	=	41.26	%
Pasir kasar	=	23.49	%
Pasir halus	=	30.00	%
Lanau	=	5.25	%
Lempung	=	0.00	%

Gambar 2. Analisis saringan pengisian pasir

2.3 Proses Produksi GI-Tube

GI-Tube dua lapis ini diproduksi menggunakan teknologi dalam negeri

Proses produksi meliputi :

Gambar 3. Foto proses kontrol kualitas bahan baku GI-Tube

Gambar 4. Foto proses penjahitan

Gambar 5. Foto proses label material Gi-Tube

Gambar 6. Foto material Gi-Tube siap kirim

2.4 Kondisi Lapangan Setelah GI-Tube Terpasang

Setelah pemasangan, area konstruksi yang sebelumnya tergenang atau tidak stabil berubah menjadi zona yang siap ditimbun dan digunakan untuk pembangunan jalan tol.

Gambar 7. Kondisi Lapangan Sesudah Pemasangan GI-Tube (Sumber foto Proyek Semarang Demak)

3 METODE MONITORING GI-TUBE

Ada beberapa metode monitoring GI-Tube dan memiliki tujuan hasil yang sesuai kebutuhan di lapangan. Dari makalah ini akan lebih membahas metode yang dilaksanakan di proyek Semarang-Demak.

3.1 Monitoring Visual lapangan (Visual Inspection)

Tujuan : Menilai kondisi fisik GI-Tube secara langsung.

Kegiatan:

a) Pemeriksaan fisik permukaan GI-Tube (sobek, abrasi, robek, deformasi, dll.)
b) Pemeriksaan pergeseran posisi (apakah GI-Tube masih berada di lokasi semula)
c) Dokumentasi foto berkala dari sudut yang sama untuk melihat perubahan
d) Identifikasi tanda-tanda kerusakan dini, seperti pasir keluar dari sambungan

Frekuensi:

a) Harian/mingguan selama tahap awal

b) Bulanan setelah struktur stabil

3.2 Monitoring Geometrik (Survey Topografi)

Tujuan : Mengetahui apakah GI-Tube bergeser, tenggelam, atau mengalami deformasi

Metode :

a) Total Station atau GPS Geodetik digunakan untuk mengukur :
- Elevasi puncak GI-Tube
- Koordinat posisi GI-Tube

b) Membandingkan hasil pengukuran berkala dengan data awal (baseline)

Indikator :

a) Penurunan (settlement) lebih dari ambang batas menunjukkan masalah pada daya dukung dasar.
b) Pergerakan lateral menunjukkan adanya pengaruh gelombang atau arus kuat.

3.3 Monitoring Material (Pengujian Ulang Sifat Geotekstil, Opsional)

Tujuan : Memastikan geotekstil tetap memenuhi spesifikasi teknis setelah terpapar lingkungan laut.

Kegiatan :

a) Sampel uji tarik dari potongan sisa material yang terpasang (jika tersedia)
b) Uji ketahanan abrasi, porositas, dan permeabilitas
c) Perbandingan dengan data pabrik untuk melihat degradasi performa

Catatan : Biasanya dilakukan untuk riset atau pengawasan proyek besar.

4 HASIL DAN DISKUSI

Bagian bab ini membahas hasil monitoring material melalui pengujian berkala yang sampelnya diambil di setiap produksi material geotekstil dua lapis untuk penggunaan Geotube sebagai elemen utama dalam proyek. Seluruh pengujian terhadap material GI-Tube dilaksanakan di laboratorium yang memiliki fasilitas dan sertifikasi resmi, sehingga hasil uji dapat dipertanggungjawabkan secara ilmiah. Pembahasan juga mencakup perbandingan antara hasil aktual melalui uji laboratorium geosintetik dengan parameter desain yang telah direncanakan.

Tabel 2. Hasil perbandingan pengujian laboratorium disetiap produksi dengan parameter nilai desain

Parameter	Metode	Satuan	Spek Desain	Kode Uji		
				00544	01002	03372
Kuat Tarik MD	ASTM D 4595	kN/m	55	104,20	87,60	85,20
Kuat Tarik CD	ASTM D 4595	kN/m	70	80,00	86,30	128,50
Elongation MD	ASTM D 4595	%	< 120	82,60	89,80	111,80
Elongation CD	ASTM D 4595	%	< 120	116,90	108,60	109,90
Kuat Tusuk - CBR	ASTM D 6241	N	> 2.000	13.107	17.667	18.516,20
Permitivity	ASTM D 4491	s^1	> 0,2	0,56	0,54	0,52
Bukaan pori	EN ISO 12956	µm	< 60	54	53	56

Ketebalan dibawah 2 kPa	ASTM D 5199	mm	> 6	7,53	7,74	8,58
Berat	ASTM D 5261	g/m^2	> 1.200	1.266,60	1.259,50	1.514,8

5 KESIMPULAN

Penggunaan GI-Tube berbahan geotekstil non-woven dua lapis produksi lokal terbukti menjadi solusi efektif dan efisien sebagai tanggul sementara dalam proyek pembangunan Jalan Tol Semarang–Demak. Kesimpulan yang dapat diambil dari penelitian ini antara lain:

a) Efisiensi konstruksi **:** GI-Tube mudah dipasang dan hanya memerlukan alat serta tenaga kerja minimal.
b) Daya tahan tinggi **:** Kombinasi geotekstil dua lapis dan pasir isian memberikan ketahanan terhadap gelombang dan arus laut.
c) Adaptif terhadap kondisi lapangan **:** Desain modular GI-Tube memungkinkan fleksibilitas tinggi dalam pemasangan.
d) Penguatan produk dalam negeri **:** Hasil pengujian berkala terhadap material GI-Tube disetiap produksi memiliki performa yang baik

Sebanyak 281 unit GI-Tube telah dipasang sejak 2022, dan hingga saat ini berfungsi dengan baik tanpa kerusakan signifikan. Pemanfaatan material lokal ini menjadi contoh penerapan inovasi dalam negeri pada infrastruktur strategis nasional.

SANGGAHAN

Dengan ini saya menyatakan bahwa saya tidak memiliki konflik kepentingan.

KETERSEDIAAN DATA DAN MATERI

Semua data tersedia dari penulis.

UCAPAN TERIMA KASIH

Penulis studi kasus ini ingin mengucapkan terima kasih kepada seluruh tim PT. Geoforce Indonesia, Hilon, PT. Bina Marga, PT. PP (Persero) Tbk, PT. China Road and Bridge Corporation (CRBC), PT. WIKA (Persero) Tbk, dan seluruh tim terkait.

DAFTAR PUSTAKA

Koerner, R.M. (2005). *Designing with Geosynthetics* (5th ed.). Upper Saddle River, NJ: Pearson Education.

Lee, S.C., Hashim, R., & Mo, K.H. (2018). The Evaluation of Geotube Behaviors on Muddy Beach: Field Monitoring and Numerical Analysis. *KSCE Journal of Civil Engineering, 22*(2), 531–540. https://doi.org/10.1007/s12205-017-1336-9

Shin, E.C., Ahn, K.S., Oh, Y.I., & Das, B.M. (2002). Construction and Monitoring of Geotubes. *Geosynthetics International*, 9(5), 471–482.
U.S. Army Corps of Engineers. (2006). *Coastal Engineering Manual (CEM)*. Engineer Manual EM 1110-2-1100. Washington, D.C.

This page is intentionally left blank

HIMPUNAN AHLI TEKNIK TANAH INDONESIA - HATTI
Indonesian Society for Geotechnical Engineering - ISGE
PIT HATTI XXIX
10-12 November 2025

Implementation of Sludge-Filled Geotextile Tubes as a Sustainable Coastal Protection Measure in Muddy Coastline

Nastiti Tiasundari[1,*], Dandung Sri Harninto[2], Rizal A. Ady[3], Dede M. Sulaiman[4]
[1]PT. Geoforce Indonesia, Jakarta, Indonesia, 10210; nastiti.tiasundari@gmail.com
[2] PT. Geoforce Indonesia, Jakarta, Indonesia, 10210; dandung@geoforce-indonesia.com
[3] PT. Geoforce Indonesia, Jakarta, Indonesia, 10210; rizalansariady@gmail.com
[4]Former Researcher in Coastal Engineering, Jakarta, Indonesia, 10210; dedems@ymail.com

*Correspondence: nastiti.tiasundari@gmail.com

ABSTRACT Coastal erosion is one of the major challenges faced along the northern shoreline of Java Island. This phenomenon has led to dynamic and ongoing degradation of the coastline, threatening not only the local ecosystems but also the livelihoods of coastal communities. The soft, muddy coastal characteristics of this region make conventional hard-engineering structures less effective and unsustainable, prompting the need for alternate solutions. This study aims to evaluate the effectiveness of sludge-filled geotextile tubes (GI-Tubes) as an erosion control measure in muddy coastal areas. On December 2022, a small-scale field experiment was conducted using three GI-Tube units, each measuring 1.3 meters in height and 20 meters in length, installed parallel to the shoreline. The GI-Tubes were made from double-layered needle-punched staple fiber polypropylene non-woven geotextile and filled with locally sourced sludge mixed with flocculants to promote effective sediment floc formation within the tubes. The small opening size of the non-woven geotextile facilitated efficient dewatering while retaining the sludge inside, resulting in a faster settling process. The outer layer of the GI-Tube provided high UV resistance and enhanced sediment-trapping capability, offering additional protection and extended durability. The double-layered design of the geotextile tubes enhances their overall structural integrity, enabling them to withstand hydrodynamic forces such as wave and coastal currents. Upon installation, the GI-Tubes reached a final height of 1.3 meters. After five months, a height reduction of approximately 0.4 meters was observed, likely due to settlement of the sludge filling. Monitoring conducted in August 2024 indicated that the sludge fill remained solid and well-consolidated, confirming a good long-term performance of the structure. Results demonstrated shoreline accretion and a significant increase in mangrove growth—up to 30 meters beyond the initial vegetation line. These findings suggest that sludge-filled GI-Tubes can be an effective, low-cost, and sustainable solution for mitigating coastal erosion in soft-soil coastal environments.

KEYWORDS geotextile tube, sludge dewatering, flocculant, GI-Tube, sludge filled geotextile tube, coastal erosion

This paper will be published in the future issues of Indonesian Geotechnical Journal

GH 上海港湾集团 GEOHARBOUR

• China • Indonesia • Singapore • Malaysia • Vietnam • Philippines • Myanmar • Malaysia • Middle East • Australia • New Zealand • South America •

GEOTEKINDO

GROUND IMPROVEMENT SPECIALIST

ADVANCED & INNOVATIVE GEOTECHNICAL CONTRACTOR

"We're a professional entity specializing in geotechnical **investigation, design, research, construction** and **consultancy**."

BUSINESS OVERVIEW

PT. Geotekindo is a professional entity specializing in geotechnical investigation, design, research, construction and consultancy. Our parent company, Geoharbour Group (www.geoharbour.com), is a chief editor of China Standard of Reclamation Soil Treatment and a director member of Technical Committee of China Soft Soil Treatment. So far we have developed into a complex entity with business of dredging, road and bridge construction, foundation engineering and jetty construction.

500++
Large Scale Project
Over the past **13 years**

Over
15,000Ha
Soil Treatment
Involving various types of field work in the process

Over
1,500Ha
Ground Improvement
in Indonesia

Over
30 Cases
Patented Technology
Which are classified as
Green Technology

Some of Our Works

Singapore

VACUUM PRELOADING & PVD INSTALLATION WORKS CHANGI INTERNATIONAL AIRPORT

Location: Terminal 5 Changi International Airport, Singapore
Method: Vacuum Preloading

Dubai, UEA

THE WORLD ISLANDS (THE HEART OF EUROPE)

Location: Dubai, UEA
Method: Vibro-compaction, Sheet Pilling

Indonesia

KALIBARU PORT 1B

Location : North Jakarta, Indonesia
Method : Deep Cement Mixing

Vietnam

FORMOSA HA TINH STEEL MILL

Location : Ky Anh Ha Tinh, Vietnam
Method : Various Method

Indonesia

IGNITE DATA CENTER

Location : Cikarang, West Java, Indonesia
Method : Bored Pile & Spun Pile

Indonesia

GOLF ISLAND

Location : North Jakarta, Indonesia
Method : Dynamic Compaction and Vibroflotation

Gold Coast Office Liberty Tower 26th floor
Pantai Indah Kapuk, North jakarta 14470
+62 21 502 098 66
+62 21 502 085 66

click our website:

WWW.GEOTEKINDO.COM

Go. Grow. Gather.

ORIENTAL CASTLE GROUP

At Oriental Castle Group (OCG), we believe in the quiet strength of collaboration and the pride of local presence. Our group comprises dedicated teams across diverse specialties.
Since 1998, we have grown steadily, guided by a commitment to quality, integrity, and community. Oriental Castle Group (OCG) is more than a collection of companies—it is a community of professionals who care deeply about their work and the people they serve. Our strength lies in our diversity and our unity, with each entity contributing its unique expertise while sharing a common purpose.

We are now fully present in Indonesia, with full-time teams committed to building responsibly and respectfully. Over the years, we have expanded our reach and refined our capabilities to meet the evolving needs of our partners and clients. We continuously invest in innovation, technology, and human capital to ensure sustainable growth and long-term success.

Our people are at the heart of everything we do, driven by passion and a shared vision of excellence. Together, we aim to create lasting value for the communities we serve, nurture meaningful partnerships, and contribute positively to the industries and regions in which we operate.

ORIENTAL SHEET PILING | ArcelorMittal

ORIENTAL HEAVY GAUGE COLD FORMING

ORIENTAL STEEL PIPE

ORIENTAL SHORING SOLUTIONS

DPM ENGINEERING

ORIENTAL HOUSETOP

TIMURAN ENGINEERING

Website

promisco
sinergi indonesia

Pembangunan Kawasan
Bank Indonesia Karawang

Terminal Kalibaru Tahap 1B
Pelabuhan Tanjung Priok

PT Promisco Sinergi Indonesia

menyediakan konsultasi geoteknik berbasis data dan analisis mendalam serta menyediakan solusi desain yang inovatif dan sesuai standar. Selain itu PT Promisco Sinergi Indonesia juga menyediakan layanan penyelidikan tanah serta layanan pengujian laboratorium.

Berpengalaman di Seluruh Indonesia

Kompleks Perkantoran Bank Indonesia
(KOPERBI) IKN

Penyelidikan Tanah
PT. OKI Pulp & Paper Mills

Pembangunan Terminal
Kijing Pontianak

RDMP Pertamina RU V
Balikpapan

Penyelidikan Tanah CPTu
VALE

Pematang Lahan dan Apron
Ngurah Rai International Airport

www.promisco.com @promisco.id (022) 2536666 office@promisco.com Jl. Cigadung Raya Timur No.144 Bandung 40191 Indonesia

ABOUT Oriental Castle Group (OCG)

Founded in 1998 and headquartered in Kuala Lumpur, Malaysia. Oriental Castle Group (OCG) unites five specialized companies, such as:

- Oriental Sheet Piling | ArcelorMittal (OSP | AM)
- Oriental Heavy Gauge Cold Forming (OHGCF)
- Oriental Steel Pipe (OSPipe)
- DPM Engineering (DPME)
- Oriental Shoring Solutions (OSS)

Delivering integrated foundation and infrastructure solutions across Asia.
Driven by collaboration, innovation, and integrity, OCG continues to build responsibly and sustainably for the future.

#BAUERPOWER

OUR CHALLENGES AND OPPORTUNITIES

INFRASTRUCTURE

URBANIZATION

ENVIRONMENT

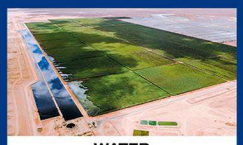
WATER

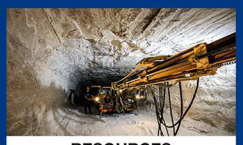
RESOURCES

CLIMATE CHANGE

OUR VISION

OUR CULTURE
- Family business
- Worldwide network
- Local presence
- The world is our market
- Standing as one
- Safety starts with me

Building foundations for the world

CONSTRUCTION
We are the world´s leading specialist foundation engineering company.

EQUIPMENT
We make specialist foundation an easy task.

RESOURCES
We are an internationally leading service provider for water, mining and environmental business.

OUR VALUES
- Responsibility
- Openness
- Appreciation
- Innovation
- Down to earth

OUR FOCUS TOPICS

Sustainability	Company synergies	Digitalization	Lean Management	Innovative products and technologies
▪ Digital construction site ▪ Bauer construction process	▪ Regional markets and major projects ▪ Sustainability in construction	▪ Expansion of service business ▪ Optimization of supply chain	▪ Automation and digital services ▪ Alternative drive technologies	▪ Leading in environmental services ▪ Developing new markets	▪ Bauer construction process ▪ Digital products and technologies

OUR ASPIRATION

We give the best for our **customers and partners**.

Our **long-term orientation** makes us a successful and profitable company.

We are a **responsible employer** for our people.

PASSION for PROGRESS

KELLER

The World Leader in Geotechnical Solutions

Our Expertise

Vibro Stone Columns

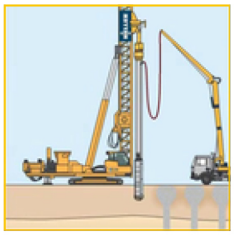
Vibro Concrete Columns

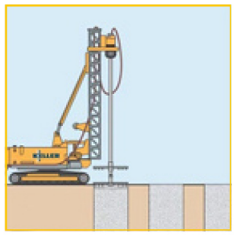
Deep Soil Mixing

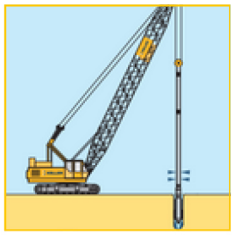
Vibrocompaction

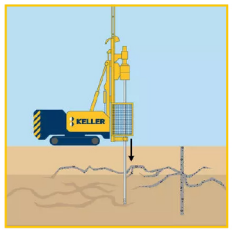
Grouting

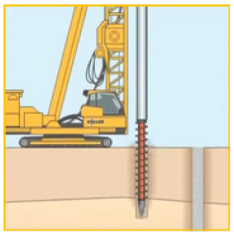
Rigid Inclusions

Our Projects

East Java Multipurpose Terminal

Mines of Bahodopi Block 2 & 3

Jogja - Bawen Toll Road

Klang Valley MRT

Probolinggo - Banyuwangi Toll Road

Scan Here

PT Keller Ground Indonesia

Address : Gedung Graha Kencana Lt. 7, Unit B-I
Jalan Raya Perjuangan No. 88 Kebon Jeruk
Jakarta Barat 11530, Indonesia

Website : www.keller.com

Email : info@keller.co.id

Phone : +62 21 5366 0778 | Fax: +62 21 5366 0779

ORIENTAL SHEET PILING | ArcelorMittal

All Your Foundation Needs

Oriental Sheet Piling

ArcelorMittal is the world's leading steel and mining company, with 160 thousand employees of 134 nationalities in more than 60 countries and steelmaking operations in 16 countries.

Oriental Sheet Piling, part of the ArcelorMittal group, is a leading provider of steel sheet piling and foundation solutions in Asia. With a strong local presence across Southeast Asia and China, OSP is dedicated to meeting local requirements and ensuring compliance with regional standards. Our commitment is reflected in our impressive project track record, demonstrating our ability to deliver high-quality solutions tailored to the specific needs of each market.

E-Catalogue

Contact Us

Manyar Smelter Desalination Plant
East Java, Indonesia
Type 3 JIS Sheet Piles

Darul Hana River Wall
Kuching Malaysia
OZ16A Cold Formed Sheet Piles

Ular River
North Sumatera, Indonesia
OT 22 Cold Formed Sheet Piles

Tano Ponggol, Lake Toba
North Sumatera, Indonesia
OZ36 Cold Formed Sheet Piles

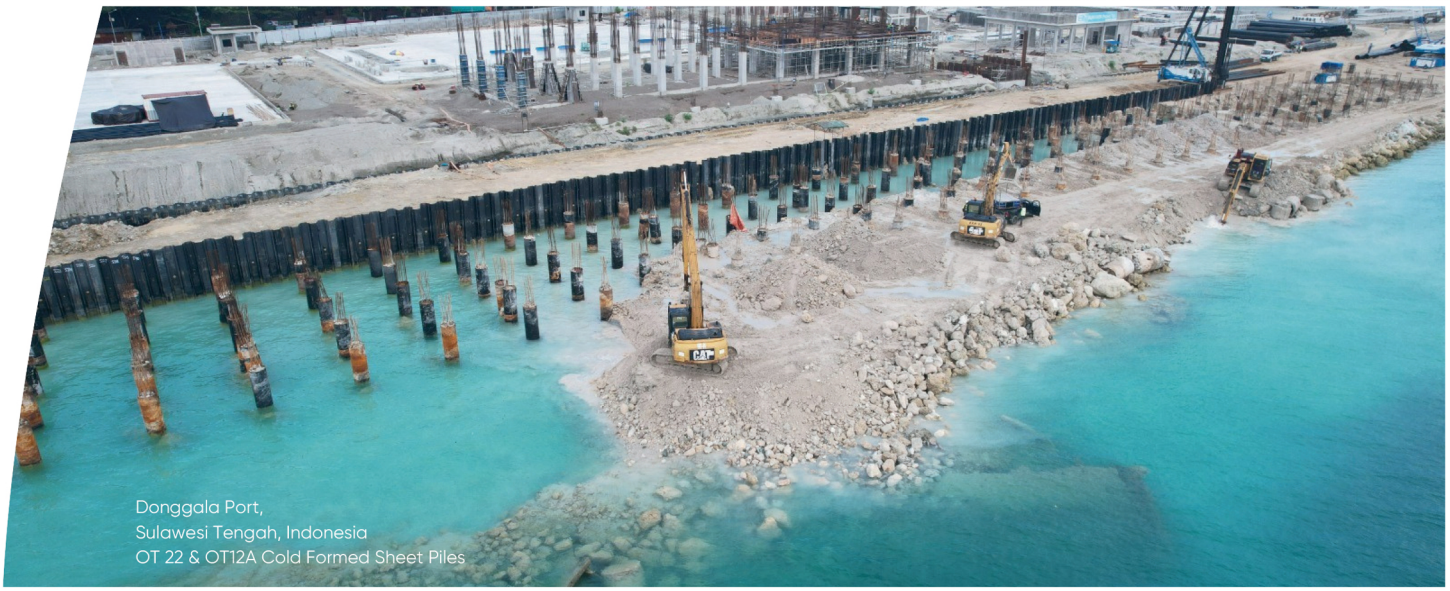

Donggala Port,
Sulawesi Tengah, Indonesia
OT 22 & OT12A Cold Formed Sheet Piles

Rapid Concrete Columns

Solutions for Faster and Reliable Housing.

Menard offers alternative foundation solutions using **Rapid Concrete Columns** (RCC), a faster and more efficient alternative to traditional piling, designed specifically for residential developments.

Rapid Concrete Columns (RCC) eliminates common drawbacks of piles such as low productivity and spoil generation, while still delivering the same soil compaction and strength performance.

Items	Conventional Pile	Rapid Concrete Columns (RCC)
Production	• The installation of Bored pile usually ranging from 60-100 m/shift/rig • The installation of Driven Pile usually ranging from 100-120 m/shift/rig	• **Fast installation**, with fewer steps and less equipment
Load Intensity	• High-strength concrete, typically fc > 35 Mpa • Designed to receive 100% load design	• Low to medium-strength mortar, ranging between 15-25 Mpa • **Designed to receive 100% load design**
Installation	• While it can reach a depth of >30m, bored pile requires supporting equipment for installation e.g. casing • Driven Pile has standard fabricated length of 12m and requiring joints for extension tp greater depth	• RCC can be **installed up to >30m without joint connections** or additional supporting equipment
Impact on Adjacent Structure	• Bored pile requires spoil disposal area and may affect nearby facilities • Driven pile with hammer generates vibration to surrounding existing structure during installation	• RCC is installed using displacement auger, producing **no vibration** and minimal disturbance to nearby structures
Spoil & Pollution	• Installation of pile, using continuous auger method, generates a lot of soil spoils	• Displacement method produces minimal to **no spoil**, keeping site conditions clean and low-impact • **Reduced carbon footprint** due to less concrete and zero spoil handling.

Contact Us

BUT Menard Geosystems

Indonesia@menard-asia.com

(+62) 021 2782 5507

ISO 9001 Quality Management Systems CERTIFIED
ISO 14001 Environmental Management CERTIFIED
ISO 45001 Occupational Health and Safety Management CERTIFIED

OUR PRODUCTS & SERVICES :

GSRW | GeoFrame | Geomembrane | GI-Tube | Geocell | GI-Drain (PVD) | PHD | Silt Protector | Geotextile | GI-Bag | Geogrid | Gabion | Erosion Mat | HDPE Pipe | GCL | Geocomposite | GBRW

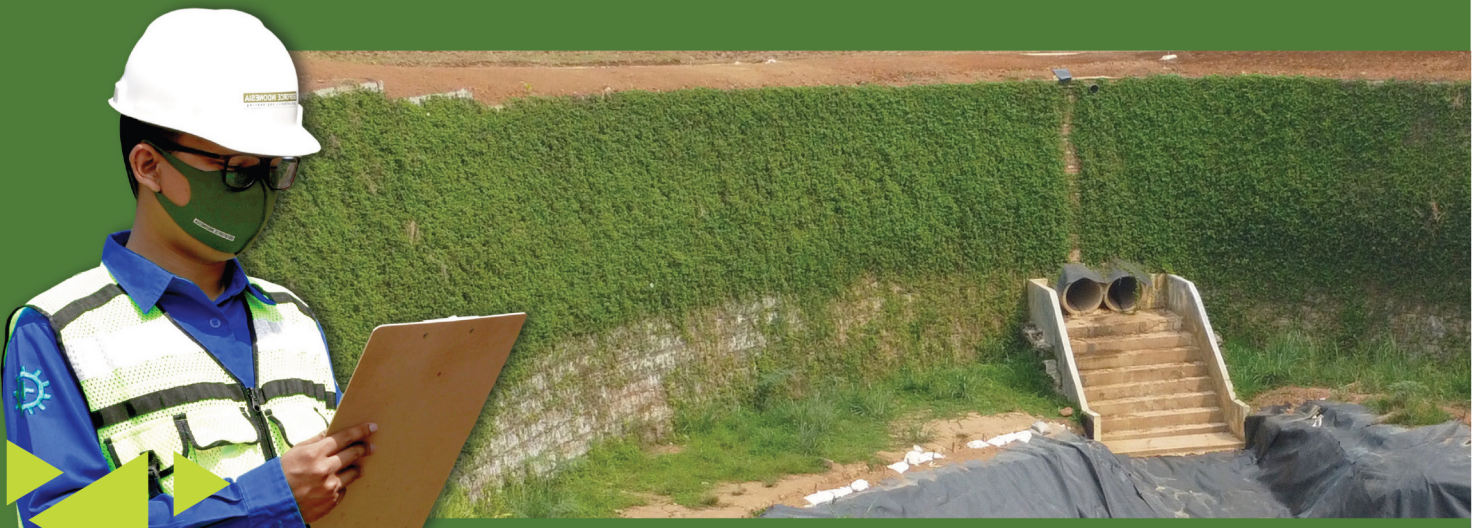

PT GEOFORCE INDONESIA

Head Office : Wisma GKBI Lt. 39, Suite 3901 Jl. Jend. Sudirman No. 28, Jakarta 10210
Operational Office : Jl. Penjernihan 1 No. 12B, Bendungan Hilir, Jakarta 10210
Email : info@geoforce-indonesia.com | Web : www.geoforce-indonesia.com
Phone : +62 21 - 5795 1342 | Fax : +62 21 - 5737534 | Whatsapp : +62 811 902 268

Geoforce Indonesia @geoforceindonesia Geoforce Indonesia

SCAN HERE